What is the future for Central Asian endorheic lakes? A water balance model for Shortandy Lake, Burabay National Nature Park, Kazakhstan

Baigaliyeva Marzhan

Thesis submitted to The University of Nottingham
for the degree of Doctor of Philosophy

December 2020

Abstract

Lakes are recognised as having a high sensitivity to environmental change and human interventions. This is particularly the case with endorheic lakes due to the fact that their water volume is not controlled by outflow from a river outlet. Most of the endorheic lakes are formed in dry, *i.e.* in arid or/and semi-arid regions. Central Asia occupies one-third of the arid area of the world, where lakes are a valuable source of freshwater for irrigation and daily usage.

This thesis investigates the reasons for the lake volume decline in Shortandy Lake; one of the endorheic lakes located in Burabay National Nature Park (BNNP) in Northern Kazakhstan. BNNP was established in order to preserve and restore the unique landscape of the region, which plays an important role in ecologic, scientific and recreational dimensions. The Park consists of a number of endorheic lakes, in which water volumes have been fluctuating during the last century. However, the reasons for the current trends in water volume reduction in the Burabay lakes system remain unexplored.

This PhD project develops and validates a new water balance model for Shortandy Lake that is built from fundamental hydrological relationships. The water level and volume of the lake is estimated monthly using estimates of daily open water and grass evaporation, snowmelt and rainfall-induced runoff from observed climate variables available from the State Hydro-meteorological agency. Crucially, it also incorporates estimates of anthropogenic water abstraction.

The water balance model is applied to assess future water volume changes under changing future climate scenarios. The analysis reveals new information on the potential impacts of regional climate fluctuation as well as allowing assessment of the impact of past and future water management strategies in the Shortandy Lake catchment.

Acknowledgements

I want to express my sincere gratitude and thanks to numerous people and organisations for their support and help without which this research would not have been possible.

First of all, I would like to thank my supervisors Dr. Nick Mount, Prof. Simon Gosling and Prof. Suzanne McGowan, for their support, guidance and patience over the last four years. Secondly, I would like to acknowledge Nazarbayev University for their financial support and School of Geography staff (University of Nottingham) for creating an excellent research environment.

Special thanks go to my mom for being there for me and her great support and encouragements throughout this PhD journey.

Table of Contents

Abstract ii
Acknowledgements iii
List of Figures viii
List of Tables xvii
Chapter 1 Introduction 1
1.1 Research aims and objectives 4
Chapter 2 Literature Review Part I 8
2.1 Water scarcity and water management in Central Asia 8
2.1.1 Water resources in Central Asia 10
2.1.2 Water scarcity and mismanagement in Central Asia 12
2.2 Modelling the effects of climate change and lake level dynamics 15
2.2.1 Past climate in semi-arid Central Asia and lake response 15
2.2.2 Climate variation 21
2.2.3 Future climate 26
2.3 Previous research on the Burabay area 29
2.3.1 Historic hydrological changes in Burabay lakes 30
2.3.2 Regional climate and Burabay lakes water level fluctuation 31
2.3.3 Historical water regime 35
2.4 Summary 38
Chapter 2 Literature Review Part II 42
2.5 The water balance of endorheic lakes 42
2.5.1 Key hydrological drivers of endorheic lake water balance 44
2.5.2 Development of a water balance model for endorheic lakes 46
2.5.3 Complexity of water balance models 47
2.6 Quantification of water balance components 48
2.6.1 Water volume and lake level/area/volume assessment (ΔV) 49
2.6.2 Output variables 57
2.6.3 Input variables 62
2.6.4 Groundwater flux 69
2.7 Summary 71
Chapter 3 Study area 74
3.1 Overview of Burabay National Nature Park 74
3.1.1 Hydrology of BNNP 76
3.1.2 Geology of BNNP 79
3.1.3 Hydrogeology of BNNP 81
3.1.4 Land cover and vegetation 86
3.1.5 Anthropogenic impacts 88
3.2 Overview of Shortandy Lake 91
3.2.1 Shortandy Lake and its catchment 91

3.2.2 Regional climate 95
3.2.3 Air temperature 96
3.2.4 Precipitation 100
3.3 Summary 102
Chapter 4 Methodology 104
4.1. Conceptual water balance model 104
4.2 Data requirements 107
4.2.1 Data introduction 112
4.3 Quantifying lake volume (ΔVt) 117
4.3.1 GIS volumetric model development 117
4.3.2 GIS volumetric model application 118
4.3.2 Interpolation of bathymetry survey data 121
4.4 Output variables 124
4.4.1 Open water evaporation (EO) 124
4.4.2 Evapotranspiration from vegetation 130
4.4.3 Anthropogenic impact - Water abstraction $Wabs$ 136
4.4.4 Snow sublimation ($Esub$) 137
4.5. Input variables 138
4.5.1 Snowmelt Runoff Model (SRM) model development ($Qsnow, Qrain$) 138
4.6 Groundwater model, $Gi - GO$ 156
4.6.1 Groundwater flux estimated by measured water levels (i) 156
4.6.2 Water balance approach (ii) 157
4.7 Summary 158
Chapter 5 Results – Water balance model 161
Chapter 5.1 Results - Output variables 161
5.1.1 Estimation of Open water evaporation (Eo) 161
5.1.2. Evapotranspiration from vegetation 164
5.1.3 Results - Water abstraction ($Wabs$) 168
5.1.4 Snow sublimation ($Esub$) 169
5.1.5 Summary – Relative contribution of outflow variables 171
5.2 Results - Input variables 173
5.2.1. Estimation of snowmelt runoff $Qsnow$ 173
5.2.2 Estimation of rainfall-runoff $Rrain$ 183
5.2.3 Summary – Relative contribution of input variables 187
5.3 Groundwater model ($Gi - Go$) 190
5.3.1 Results - Groundwater flux (i) 190
5.3.2 Water balance approach (ii) 192
5.3.3 Results – Groundwater models comparison 193
5.4. Results – Reconstruction of water volume dynamics 195
5.5 Input and output variables and volume dynamics 196
5.5.1 General relationship between input and output 196

5.5.2 Interannual changes in net flux 198
5.6 Model validation 204
5.6.1 Lake level-area-volume relationship 204
5.6.2. Results – Model validation 208
5.7 Sensitivity analysis 210
5.7.1. Model sensitivity analysis 210
5.7.2 Model parameterisation 212
5.7.3 Results – Sensitivity analysis 212
5.7.4 Summary – Model sensitivity analysis 222
5.8 Summary 223
Chapter 6 Future climate modelling 227
6.1 Description of future climate models 227
6.1.1 Historical modelling 228
6.1.2 Future climate and emission scenarios 228
6.2 Supplementary model for future water balance 236
6.2.1 Lake ice freezing and ice break-up model development 236
6.2.2 Model variables and parameters 237
6.2.3 Break-up model description for climate modelling and evaluation 239
6.2.4 Freeze-up model description for climate modelling and evaluation 239
6.3 Water balance computation for future climate modelling 241
6.4 Results - Future climate model 242
6.4.1. Air temperature 242
6.4.2 Precipitation 248
6.4.3 Input variables in future climate 254
6.4.4 Output variables in future climate 256
6.4.5 Water volume fluctuation 263
6.5 Summary 270
6.6 Role of anthropogenic impact 272
6.6.1 Role of anthropogenic impact in the past 272
6.6.2 Role of anthropogenic impacts in the future 275
6.7 Summary 281
Chapter 7 Discussion 282
7.1 Water balance model 282
7.2 Implications of anthropogenic impact and water management 283
7.3 Uncertainties and limitations 290
7.4 Summary 295
Chapter 8 Conclusion 296
8.1 Introduction 296
8.2 Summary of the Main Findings 296
8.3 Research Conclusions 301
8.4 Suggestions for Future Research 302

8.4.1 Groundwater flux 302
8.4.2 Water balance modelling for other Burabay lakes 303
8.4.3 Input and Output estimations 303
References 305
Appendix A – Water balance calculation spreadsheet 324
Appendix B – Evaporation modelling 325
Appendix C – Snow sublimation modelling 330
Appendix D – Runoff Modelling 332
Appendix E – Groundwater modelling 334
Appendix F - Interannual changes in net flux 340
Appendix G – Future Climate Modelling 356

List of Figures

Figure 1. 1 The variation of water level in Ulken Shabakty Lake from 1946 to 1957 3

Figure 1. 2 A schematic workflow of the project 5

Figure 2. 1 Central Asia countries and their boundaries 10

Figure 2. 2 Lake area reduction of the Aral Sea 1960-2011 13

Figure 2. 3 Long-term water level fluctuation of Lake Balkhash 14

Figure 2. 4 Mean annual temperature (a) and total annual precipitation trend in the Aral Sea in 1960-2018 20

Figure 2. 5 Mean annual air temperature changes in Central Asia 22

Figure 2. 6 Distribution of horizontal wind field at 850hPa for years with increased (a) and decreased (b) precipitation over the semi-arid and arid regions 23

Figure 2. 7 Spatial distribution of precipitation trend over Kazakhstan and west regions of China 24

Figure 2. 8 River system one in the Burabay area during the 18th Century 32

Figure 2. 9 River system two during the 18th Century and terraces on the south shore of Shortandy Lake 33

Figure 2. 10 Water level fluctuation in Burabay lakes from 1945-1965 36

Figure 2. 11 The lake level variation in 2008-2015 in the three lakes of Burabay area 38

Figure 2. 12 Water balance components for any lake 43

Figure 3. 1 Burabay National Nature Park boundaries, lakes and settlements 75

Figure 3. 2 Burabay National Nature Park 76

Figure 3. 3 Burabay National Nature Park and the largest lakes and lake catchment boundaries 78
Figure 3. 4 Hydrogeology map for the BNNP..... 80
Figure 3. 5 Geologic cross-section and groundwater wells located in the Shortandy catchment 85
Figure 3. 6 Mixed forest in the Shortandy watershed during winter 2015 87
Figure 3. 7 Mixed forests formed in highland areas (between Burabay and Ulken Shabakty lakes) 87
Figure 3. 8 Total number of tourists visited BNNP park from 2004-2011 89
Figure 3. 9 Water supply construction in Burabay during summer 2019 91
Figure 3. 10 Shortandy Lake catchment..... 93
Figure 3. 11 Shortandy Lake levels and 3D map of the Shortandy catchment .. 94
Figure 3. 12 Gravel southeast shore of Shortandy Lake 95
Figure 3. 13 Mean monthly air temperature variation in the Shortandy catchment 97
Figure 3. 14 Mean monthly temperature fluctuation and mean annual temperature in the Shortandy catchment from 1986-2016..... 98
Figure 3. 15 Shortandy Lake ice coverage during the 31st of March 2018 99
Figure 3. 16 Total annual precipitation (mm) according to cold and warm seasons from 1986 to 2016..... 102

Figure 4. 1 Conceptual water balance model for Shortandy Lake..... 106
Figure 4. 2 Water balance modelling steps for warm (red) and cold (blue) seasons 107
Figure 4. 3 A schematic flow chart representing the derivation of GIS-based water level-area-volume relationship of Shortandy Lake 117
Figure 4. 7 The schematic chart on estimation evaporation losses in the Shortandy catchment 132

Figure 4. 8 Leaf Area Index (LAI) estimated from MOD15A2H for July 2013 for the Shortandy catchment 136
Figure 4. 9 Schematic chart on SRM model requirements..... 140
Figure 4. 10 Land cover map for the Shortandy catchment 143
Figure 4. 11 Snow cover detection using NDSI method in grass areas of Shortandy watershed by 31 of March 2016 148
Figure 4. 12 Snow accumulation and depletion in forest and grassland in the Shortandy catchment during winter-spring season 2012-2013..... 149

Figure 5. 1 Shortandy Lake ice-releasing and air temperature dynamics 163
Figure 5. 2 Total annual potential open water evaporation of Shortandy Lake 164
Figure 5. 3 Potential reference evapotranspiration ($Epet$) in July 166
Figure 5. 4 Comparison of evapotranspiration model outcomes with CGIAR-CSI Global Potential Evapotranspiration (Global-PET) geospatial dataset for the Shortandy catchment 168
Figure 5. 5 Total annual surface and groundwater abstraction $(Wabs)$ from Shortandy Lake 169
Figure 5. 6 Total annual snow sublimation $(Esub)$ from the lake surface during cold-seasons from 1986 to 2016..... 170
Figure 5. 7 Relative contribution and mean values of output variables estimated between 1986 and 2016 in the Shortandy catchment 172
Figure 5. 8 Total annual cold-season precipitation ($Psnow$) and mean air temperature of cold-seasons 175
Figure 5. 9 Averaged degree-day factor estimated for forest and grass areas of the Shortandy catchment during the snowmelt seasons from 1986 to 2016 .. 176
Figure 5. 10 Mean annual snow water equivalent (SWE) and annual SCA ratio of a snowpack accumulated in the forest by snowmelt season (green line) and total annual snow precipitation (grey column) 178

Figure 5. 11 Snow water equivalent (SWE) of a snowpack accumulated in grassland and SCA ratio of grassland during cold-seasons in Shortandy..... 178
Figure 5. 12 Total duration of seasonal snowmelt in the forest (green) and grassland (grey) plotted with the mean air temperature from 1986 to 2016 in the Shortandy catchment 180
Figure 5. 13 Seasonal runoff volume estimated by the SRM model and SWE in snowpack accumulated in the forested area of the Shortandy catchment from 1986 to 2016 182
Figure 5. 14 Total seasonal snowmelt runoff and estimated deviation of the runoff volume (Dv) between computed and measured discharge produced in the Shortandy catchment 183
Figure 5. 15 Total annual warm-season precipitation, where $Prain$ is was estimated based on $tcrit \geq 0$ 185
Figure 5. 16 Total monthly warm-season precipitation distribution throughout the year (blue chart) and total monthly warm-season precipitation distribution in years with excessive rainfall events or when monthly warm precipitation was higher than evapotranspiration losses ($Prain > Eact$), where error bars show a standard deviation 186
Figure 5. 17 Total monthly rainfall-runoff ($Qrain$) produced in the Shortandy catchment occurred from 1986 to 2016 187
Figure 5. 18 Relative contribution and mean values of input variables estimated from 1986 to 2016 in the Shortandy catchment..... 188
Figure 5. 19 Groundwater flux ($Gi - Go$) estimated by the regional model..... 191
Figure 5. 20 Total annual groundwater flux ($Gi - Go$) (i) estimated by the regional model 192
Figure 5. 21 Total annual groundwater flux ($Gi - Go$) (ii) by the water balance approach 193
Figure 5. 22 Groundwater flux modelling results 194

Figure 5. 23 Water volume dynamics of Shortandy Lake simulated using the water balance model 196
Figure 5. 24 Total annual net balance plotted with the total annual water volume dynamics of Shortandy Lake from 1986 to 2016 197
Figure 5. 25 The total annual input and output values in mm, where inflow are: $Prain$, $Psnow$, $Rsnow, Rrain$ and output variables are: $Esub$, Eo, $Eact$, $Wabs$ and $Gi - Go$ is the groundwater flux 200
Figure 5. 26 Shortandy Lake area and water level dynamics, where A_L is lake area identified by Landsat TM for 1986 (blue line) and 2016 (red line), and water level (white lines) is observed measurements on water levels 206
Figure 5. 27 Water volume dynamics based on the observed daily lake level measurements, where errors bars show annual standard deviation 207
Figure 5. 28 Validation of water volume simulation by using two groundwater models against water volume by measured water levels 209
Figure 5. 29 Total annual open lake evaporation estimated based on wind speed sensitivity analysis, where σ is an average standard deviation estimated based on ±25% variations in wind speed 213
Figure 5. 30 Total annual open lake evaporation estimated based on relative humidity sensitivity analysis, where σ is an average standard deviation estimated based on ±25% variations in relative humidity 214
Figure 5. 31 Total annual open lake evaporation estimated based on air temperature sensitivity analysis, where σ is an average standard deviation estimated based on ±25% variations in air temperature 214
Figure 5. 32 Total annual input to the lake estimated based on precipitation sensitivity analysis, where σ is an average standard deviation estimated based on ±25% variations of precipitation and runoff 215
Figure 5. 33 Sensitivity analysis of lake volume dynamics based on the variations of wind speed parameter, where Initial model shows lake volume dynamics with initial wind speed values in open water evaporation model 216

Figure 5. 34 Sensitivity analysis of lake volume dynamics based on the variation of relative humidity parameter, where Initial model shows lake volume dynamics with initial relative humidity values in open water evaporation model 217
Figure 5. 35 Sensitivity analysis of lake volume dynamics based on the variation of air temperature, where Initial model shows lake volume dynamics with initial air temperature values in open water evaporation model 217
Figure 5. 36 Sensitivity analysis of lake volume dynamics based on the variation of precipitation, where Initial model shows lake volume dynamics with initial precipitation values 218
Figure 5. 37 Change in annual groundwater flux based on the variation in wind speed (u) parameter 220
Figure 5. 38 Change in annual groundwater flux based on the variation in relative humidity (RH) parameter 220
Figure 5. 39 Change in annual groundwater flux based on the variation in air temperature (T) parameter 221
Figure 5. 40 Change in annual groundwater flux based on the variation in precipitation (P) parameter 221
Figure 5. 41 Lake volume dynamics derived from Initial model, where errors bars show standard deviation of the lake volume values obtained from a one-by-one sensitivity analysis with four selected model parameters 222
Figure 5. 42 Mean annual proportion of water balance input and output variables from 1986 to 2016 225

Figure 6. 1 Mean annual air temperature for Burabay National Nature Park based on historical GFDL model, from 1971 to 2005 230
Figure 6. 2 Mean annual air temperature for Burabay National Nature Park based on historical IPSL model, from 1971 to 2005 231
Figure 6. 3 Mean annual air temperature for Burabay National Nature Park based on RCP2.6 GFDL model, from 2006 to 2100 232

Figure 6. 4 Mean annual air temperature for Burabay National Nature Park based on RCP2.6 IPSL model, from 2006 to 2100 233
Figure 6. 5 Mean annual air temperature for Burabay National Nature Park based on RCP6.0 GFDL model, from 2006 to 2100 234
Figure 6. 6 Mean annual air temperature for Burabay National Nature Park based on RCP6.0 IPSL model, from 2006 to 2100 235
Figure 6. 7 Comparison of predicted ice break-up dates with observed records on annual Shortandy Lake ice decay 239
Figure 6. 8 Comparison of predicted freeze-up model with observed records on annual Shortandy Lake ice formation 240
Figure 6. 9 Computation process of future climate modelling for Shortandy Lake 241
Figure 6. 10 Mean annual air temperature based on GFDL for Shortandy Lake 244
Figure 6. 11 Mean annual air temperature based on GFDL for Shortandy Lake 244
Figure 6. 12 Mean annual air temperature based on IPSL Shortandy Lake..... 245
Figure 6. 13 Mean annual air temperature based on IPSL for Shortandy Lake 245
Figure 6. 14 Mean monthly air temperature projected for the Shortandy catchment from 2006-2100 based on RCP2.6 and RCP6.0 protocols by two GCM models and observed historical mean monthly air temperature observed from 1986 to 2016 247
Figure 6. 15 Total annual precipitation based on RCP2.6 GFDL model from 1971 to 2100 and historical precipitation pattern observed in the Shortandy catchment from 1986 to 2016..... 249
Figure 6. 16 Total annual precipitation based on RCP6.0 GFDL model from 1971 to 2100 and historical precipitation pattern observed in the Shortandy catchment from 1986 to 2016..... 249
Figure 6. 17 Total annual precipitation based on RCP2.6 IPSL model from 1971 to 2100 and historical precipitation pattern observed in the Shortandy catchment from 1986 to 2016..... 250

Figure 6. 18 Total annual precipitation based on the IPSL model under RCP6.0 from 1971 to 2100 and historical precipitation pattern observed in the Shortandy catchment from 1986 to 2016 250
Figure 6. 19 Mean monthly amount of precipitation based on future climate models from 1971-2100 and historical observed precipitation in the Shortandy catchment (1986-2016)..... 253
Figure 6. 20 Mean input variables estimated based on climate models for the period of 1986-2016 and historical relative contribution to the lake water balance in 1986-2016 estimated using the observed climate data 255
Figure 6. 21 Mean input variables estimated based on climate models for the period of 2006-2100 and historical relative contribution to Shortandy Lake from 1986-2016..... 255
Figure 6. 22 Total annual open lake evaporation (Eo) based on RCP2.6 GFDL model (1971-2100) and open lake evaporation of Shortandy Lake estimated using observed climate data from 1986 to 2016 258
Figure 6. 23 Total annual open lake evaporation (Eo) based on RCP6.0 GFDL model (1971-2100) and open lake evaporation of Shortandy Lake estimated using observed climate data from 1986 to 2016 258
Figure 6. 24 Total annual open lake evaporation (Eo) based on RCP2.6 IPSL model (1971-2100) and open lake evaporation of Shortandy Lake estimated using observed climate data from 1986 to 2016 259
Figure 6. 25 Total annual open lake evaporation (Eo) based on RCP6.0 IPSL model (1971-2100) and open lake evaporation of Shortandy Lake estimated using observed climate data from 1986 to 2016 259
Figure 6. 28 Mean output variables estimated based on climate models for the period of 2006-2100 and output variables of the lake estimated using observed climate data from 1986-2016..... 262

Figure 6. 29 Water volume (level) fluctuation based on the future climate models (1971-2100) plotted with a historical water volume of the lake (1986-2016) estimated using the lake water balance model..... 265
Figure 6. 30 Lake area reduction, where future climate models estimate the lake reduction from 1971 to 2100, and the historical lake area is estimated using the lake water balance model from 1986 to 2016 269
Figure 6. 31 The lake volume dynamics, where the blue line shows water volume estimated by measured lake levels, ... 274
Figure 6. 32 Water volume dynamics of Shortandy estimated using the GFDL climate model based on the water abstraction restrictions ($0.5x10^6m^3$ of water per year) and without anthropogenic water abstraction from 1971 to 2100 ... 277
Figure 6. 33 Water volume dynamics of Shortandy estimated using the IPSL climate model based on current water abstraction restrictions ($0.5x10^6m^3$ of water per year) and without anthropogenic water abstraction from 1971 to 2100 278
Figure 6. 34 The lake volume dynamics of Shortandy Lake estimated using two GCM models without water abstraction restrictions 280

Figure 7. 1 Mean total water volume changes of Shortandy Lake and total seasonal snowmelt runoff produced from the lake catchment and total seasonal snow precipitation from 1986 to 2016 286
Figure 7. 2 Ice-cover duration in Julian days modelled for Shortandy Lake based on the GFDL (red) and the IPSL (grey) from 2006 to 2099..... 287

List of Tables

Table 2. 1 Summary of historical climate fluctuations and endorheic lakes response. 17

Table 2. 2 Major periods of regional climate fluctuation and the hydrologic response of Burabay lakes 35

Table 2. 3 Water balance components, quantification methods and modelling approaches 52

Table 3. 1 Morphometric characteristics of main lakes of Burabay National Nature Park 77

Table 3. 2 Dynamics of recreational facilities in Burabay area 89

Table 3. 3 Monthly mean air temperature analysis for cold and warm seasons months according to Schuchinsk weather station from 1986 to 2016,..... 100

Table 4. 1 Summary of the data requirements for Shortandy water balance model 109

Table 4. 2 Shortandy water balance model data availability and regional climate records collected for the model..... 114

Table 4. 3 Deviation from the mean in total water volume estimated using three interpolation methods for the total water volume of Shortandy Lake 122

Table 4. 4 Comparative analysis on open water evaporation of Shortandy Lake in 2013 based on monthly (Eo) and daily (Eo daily) estimations 130

Table 4. 5 Snow cover area changes during snowmelt season 2013 simulated by two models for degree-day factor. 152

Table 5. 1 The maximum crop coefficient kc,max for deciduous forest..... 165

Table 5. 2 Sensitivity classes..... 211

Table 5. 3 Sensitivity Index estimated for selected model parameters 218

Table 6. 1 Description of each variable required for ice formation and decay models based on the Canadian model (Shuter, 2013)..... 237
Table 6. 2 Parameters required in freeze-up and break-up model 238
Table 6. 3 Monthly mean air temperature difference ($\Delta Tmean$) estimated as the difference between historical monthly $Tmean$(1971-2005) and mean air temperature projected by RCP2.6 and RCP6.0 by two GCM models from 2006-2100 248
Table 6. 4 Regression analysis on the temporal trend of precipitation patterns in the Shortandy catchment. 252
Table 6. 5 Regression analysis between the total annual input of Shortandy water balance and four input variables estimated with the future climate models 256
Table 6. 6 Regression analysis on the temporal trend of open lake evaporation based on future climate projections..... 261
Table 6. 7 Regression analysis between the total annual output of Shortandy Lake water balance and three variables estimated with the future climate models 263

Chapter 1 Introduction

Lakes have been recognised as a highly sensitive for any environmental changes and interventions (Micklin, 2007, Petr, 1992, Street-Perrot and Harris, 1985, Harris, 1994). This is particularly true for endorheic lakes due to the fact that the water level of these lakes is not controlled by an outlet. Endorheic lakes are driven by components of the hydrologic cycle which are linked to climate and human activity. Therefore, they have been studied as a 'proxy indicator' of climate change (Mason et al, 1991). Most endorheic lakes are found in dry areas with less precipitation than evaporation, specifically in semi-arid and arid climates. Consequently, falling levels and reduction in surface area of endorheic lakes are closely interconnected with changes in land cover (deforestation, land desertification), water shortage, water pollution, biodiversity losses and vegetation degradation. In addition, freshwater from endorheic lakes has been used as a source for agriculture, domestic and industrial needs.

Central Asia occupies one-third of the arid lands of the world, where the number of lakes exceeds 6000 with a total area of 12.3 thousand km^2, where most of them are endorheic lake systems (Savvaitova and Petr, 1992). Over the last six decades, most endorheic lakes in the Central Asian region have faced desiccation (Aral Sea, Balkhash, Bosten, Ebinur etc.) and some of them have even disappeared (Manas, Lop Nur) (Micklin, 1988, Savvaitova and Petr, 1992, Bai et al., 2011). The Aral Sea is the most well-known and dramatic example, where the water level of the lake has fallen by 23m, and water volume decreased by 90% (Micklin, 2007). In addition, Lake Balkhash, which is one the largest endorheic lakes of Central Asia, has experienced desiccation due to the dam construction (water volume decreased to 20%, whereas water level decreased from 344m (1910) to its lowest recorded minimum level of 340m in 1985 (Propastin, 2012), where natural inflow to the basin was disturbed by dam construction. This intervention affected both the quality and quantity of water which has entered to

the lake, specifically, water salinity rose from 2.23 to 2.75 gl^{-1} during the 1970-1980s, and has been correlated with a decline in fish productivity (carp landing reduced to one of six of original value) (Petr, 1992).

In general, major endorheic lakes of Central Asia have received significant attention from environmental researchers around the globe (Propastin, 2012, O'Hara, 2010). However, there are a number of smaller water bodies, such as Burabay and Ulken Shabakty lakes, that stayed unexplored. Meanwhile, there is evidence that water levels of these lakes have fluctuated, which raises a serious warning considering the future of the Burabay area.

Burabay National Nature Park (BNNP) is an exceptional and notable place in the middle of the steppe and has been one of the major tourist attractions in Kazakhstan for years, with a highly specific pine and birch forest growing over a set of exceptional granitic cliffs. There are nearly 30 lakes in the park, among the biggest ones are Ulken Shabakty Lake, Shortandy Lake and Burabay Lake. BNNP was established in order to preserve and restore the unique landscape of the region, which plays an important role in ecological, scientific and recreational dimensions.

Most BNNP lakes are recognised as endorheic lakes. The only exception is Burabay Lake, which receives inflowing water from two tributaries. This lake used to overflow into the Ulken Shabakty Lake, which has the biggest catchment in Burabay area, but its outflow is limited and regulated by a dam now. The Ulken and Kishi (large and small) Shabakty lakes used to be one lake; however, surface water connection has been strongly modified by natural water level changes during the last decades.

Previous research on BNNP lakes conducted during the Soviet Era established that lake levels were declining at an average rate of 14-17cm per year (Figure 1.1.) (Uryvayev, 1959, Korde, 1951). Soviet researchers hypothesised that potential reasons for water volume decrease in most lakes was climate, where a decrease in snow that resulted in a decline of melted water inflow to the lakes were

established. In addition, changes in water discharge rates caused by dam construction, and water abstraction for water supply to a nearby settlement were identified (Korde, 1951, Shnitnikov, 1973, Uryvayev, 1959). After the collapse of USSR, the water circulation within Burabay lakes along with changes in regional climate last 60 years remain unexplored, except shot-term hydrological studies (Yapiyev et al., 2017).

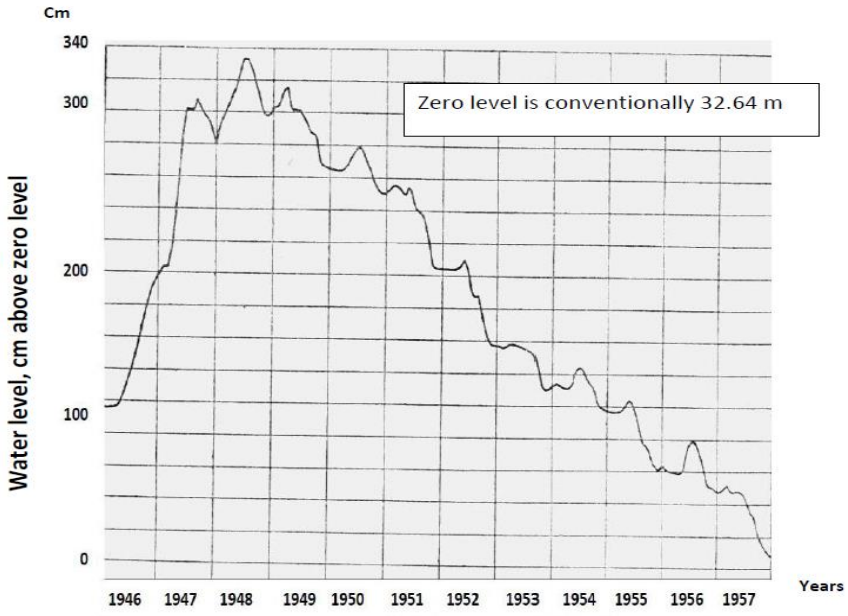

Figure 1. 1 The variation of water level in Ulken Shabakty Lake from 1946 to 1957 (Uryvayev, 1959)

Aside from the hydrologic and climate perspective, there is a need to assess anthropogenic disturbances to the Burabay area. Surface lake and groundwater from Burabay lakes have been widely used for water supply. The situation becomes more complicated considering that the government of Kazakhstan has targeted the Burabay National Nature Park to be upgraded as an international tourist area with additional investments for the construction of numerous resorts around these lakes (Ministry of Industry and New Technologies of the Republic of Kazakhstan, 2014). However, this initiative may promote further lake level reductions as well as deterioration of water in Burabay lakes and may have a negative impact on the regional ecosystem of northern Kazakhstan. Specifically,

the touristic expansion will raise the demand for freshwater for daily needs and recreation purposes as well as changes in land cover and land use.

1.1 Research aims and objectives

Central Asian endorheic lakes are highly sensitive from a hydrological point of view. The effect of climate change and human activity in Central Asia have already been recorded in the past as well as water managements problems which affected water resource in this region. In addition, future trends indicate that water availability and water related problems may severely worsen in the next decades (Lioubimtseva and Henebry, 2009a). Throughout the thesis, Shortandy Lake was selected as the case study to investigate the long-term lake level decline, which has been observed in most lakes located in BNNP area. Extensive reading on existing literature on Burabay lakes has shown groundwater interaction between Burabay and Ulken Shabakty. However, groundwater level records were not publicly available, thus it turned into a challenging task development of an accurate water balance for these lakes. Literature review on Shortandy lake could not confirm a significant groundwater interaction with the lake (Chapter 3.1.3), so made possible to establish a water balance model without groundwater levels. Hence, the main aim of the project is to understand the mechanisms of the water cycle and to quantify the water balance of Shortandy Lake in order to establish a magnitude of confirmed sensitivity of this hydrological system to changing climate as well as to understand the role of anthropogenic impacts and water management strategies accepted for the lake.

In this regard, *the main aim of this project is to assess the reasons for the observed dynamics of Shortandy Lake from 1986 to 2016 and the likely implications of projected climate change for future dynamics*. A schematic workflow follows (Figure 1.2) research questions and objectives for this PhD project.

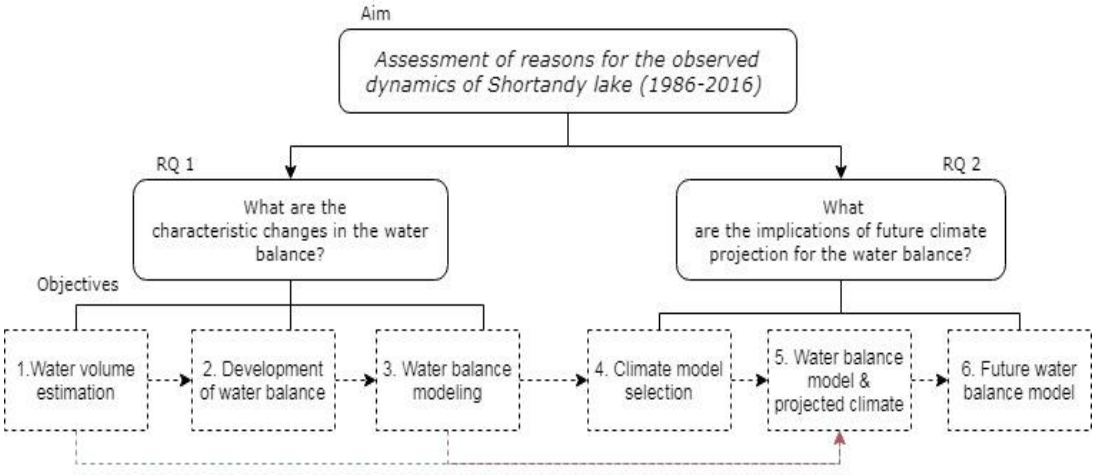

Figure 1. 2 A schematic workflow of the project

In order to achieve the aim, it is crucial to understand desiccation dynamics in Shortandy Lake catchment, and it is necessary to identify how the relationship between input and output variables have fluctuated/changed from 1986 to 2016.

Research Question 1: What are the characteristic changes in the water balance of Shortandy Lake over the three decades?

Water balance components of Shortandy Lake since the most recent research on water circulation has been conducted in the 1950s remain unexplored. Therefore, first of all, the water volume dynamics of Shortandy Lake over the 30 years is required. The water depth-volume relationship was estimated using a GIS-based volumetric model (Objective 1).

Secondly, to assess the sensitivity of Shortandy Lake to climatic fluctuations, it is crucial to identify and quantify the dynamics of the main regional hydrological drivers thought to have determined the water balance of Shortandy Lake. Objective 2 will address the following tasks:

In order to identify key hydrologic drivers of water balance for endorheic lake systems, a literature review on previous research for endorheic lakes will be conducted. By identifying the sensitivity of various endorheic lakes and their water balances, it will be possible to derive key regional drivers and the parameters that represent them, will be presented (Objective 2.1). After that, data availability of, and/or gaps in, records of key water balance parameters in the study area will

audited and collated (Objective 2.2). For identified gaps in parameter observations, options for generating data from proxies/simulations and create records will be examined (Objective 2.3).

An accurate and up-to-date quantification of water balance with numerical models optimised for Shortandy Lake is one of the most important prerequisites for the planning of sustainable development within the area. Thus, it necessary to develop a water balance model that represents the relationships between hydrological drivers and water volume dynamics in Shortandy Lake over thirty years. In order to accomplish this task, the following objective will be addressed (Objective 3):

A literature review on modelling approaches used to model water balance in (endorheic) lake systems globally and regionally will be conducted (Objective 3.1). The assessment of the potential of different modelling approaches in the context of Shortandy Lake will assist in selecting modelling approach(es) best suited to the case study (Objective 3.2). Consequently, a water balance model for Shortandy Lake will be developed (Objective 3.3). After that, the developed water balance model using historical data (three decades) of regional hydrologic drivers will be run. Water balance model outcomes will be validated against the water volume dynamics estimated by measured water levels and GIS volumetric model obtained in Objective 1 (Objective 3.4).

The development of water balance for three decades with the identified main regional hydrological drivers controlling the water budget of Shortandy, will establish future water changes under changing future climate. Therefore, the second research question is expressed as follows:

Research Question 2: What are the likely implications of projected climate futures for the water balance of the Burabay lakes?

In order to answer this question, there is a need to quantify the future dynamics of main regional hydrological drivers of the Shortandy water balance under climate change scenarios (Objective 4). Thus, it is necessary to choose projected climate scenarios available for Central Asian region and employ rainfall simulators/global

hydrology impact models (or similar) to simulate changes to key, regional water balance parameters (identified from Objective 2 and Objective 3) impacting the lake. Three decades of the field-observed data is assumed to be sufficient to project hundred years forward the lake level response to the future climate, where climate scenarios will provide a robust basis for the model.

Secondly, applying water balance model developed for Shortandy Lake (Objective 3) and the data generated for future climate dynamics (Objective 4), the likely impacts of the future dynamics of the water balance of the lake will be modelled/simulated (Objective 5). Lastly, by using model outputs, it will be possible to evaluate the role of anthropogenic impact and water management strategies accepted for Shortandy Lake in the past and in the future (Objective 6). The following assessment will assist in generating a strategy and recommendation for managing the future water balance of Shortandy Lake, thus informing environmental sustainability within the Burabay region.

Chapter 2 Literature Review Part I

The literature review aims to investigate endorheic lakes, particularly in semi-arid and arid regions of Central Asia. This chapter consists of two parts: Part I intends to study historical endorheic lakes fluctuations in response to natural and anthropogenic stressors; Part II addresses the development of water balances for endorheic lakes.

This section of the thesis explores the water volume reduction in major endorheic lakes of the region in order to understand the sensitivity of such lakes system to the changing climate as well as water management policies and strategies. Water management problems and water scarcity in Central Asia are addressed in Section 2.1. Section 2.2 examines the past climate fluctuation in conjunction with the water level reduction in major endorheic lakes of Central Asia, such as the Aral Sea, Lake Balkhash, Chany Lake and the Caspian Sea during the last century. Future climate predictions developed for Central Asia are examined regarding the implications to the future water levels of endorheic lakes (Section 2.2.3). Section 2.3 addresses previous research conducted at Burabay lakes so that changes in the regional climate and water level response to them could be understood. Section 2.5 focuses on reviewing of various hydrological approaches used to investigate water circulation in endorheic lakes. This part of the literature review aims to identify key hydrologic drivers of water balance for endorheic lakes and to evaluate various approaches in the development of water balance models.

2.1 Water scarcity and water management in Central Asia

Growing population and increased freshwater usage due to human demands are now evident in different parts of the world. Fundamental water purposes are increasingly conflicted where, on the one hand, it is essential part of environment, but on the other hand, it is used as a commodity or economic resource (O'Hara, 2010, Oki and Kanae, 2006). The increasing world population (2.5 billion in 1950 to 7 billion in 2011), in which urban population has grown rapidly from 746 million

in 1950 to 3.9 billion in 2014 (Nations, 2014) has been associated with more freshwater extraction and significant reduction of natural habitat. As a result, many places are at risk in terms of the health of aquatic ecosystems and the natural habitat (Postel and Carpenter, 1997, Covich, 1993). The world population is projected to peak in 2064 at 9.7 billion with further reduction to 8.8 billion in 2100 (Vollset et al., 2020). Therefore, finding ways to satisfy humanity's need for fresh water without damaging the natural ecosystem and life-support functioning of freshwater systems has been recognised as one of the most vital and critical challenges of the 21st century.

The global hydrological cycle produces several times more freshwater per year than is necessary to sustain the current world population (Postel, 2000). Due to uneven water distribution in time or space, a great proportion of it is not accessible for a great proportion of the population. Specifically, it is estimated that 2.3 billion people will be living in areas with severe water scarcity, especially North and South America, and Central Asian countries by 2050 (OECD, 2012). Here, Central Asia is a good example where most lakes are recognized as endorheic lake system. In semi-arid and arid climate conditions, water bodies of Central Asia deliver a scattered but valuable source of fresh water for the environment and human welfare. Central Asia occupies one-third of the arid area of the world (Chen, 2008) and comprises the nations such as Uzbekistan, Tajikistan, Kyrgyzstan, Kazakhstan, Mongolia and the northwest part of China (Lioubimtseva et al., 2005, Lioubimtseva and Henebry, 2009b) (Figure 2.1).

In Central Asia, rivers and lakes are a major source of freshwater for irrigation and human daily usage. Importantly, endorheic lakes are very sensitive to climate change and anthropogenic influences, largely because they do not drain into bigger water bodies (i.e. they have no outflow) (Bai, 2010, Mason, 1994). The water inflow to endorheic lakes comes from precipitation and small rivers; the major loss is evaporation, water consumption by people and, to a lesser extent, groundwater discharge. The absence of regulating outlets leads to evaporative

concentration of solutes and subsequent water quality deterioration (Micklin, 1988, Zhang et al., 2015).

Endorheic lakes studied as a vital proxy of both, in global and regional climate variations (Mason et al. 1994). However, Uzbekistan, Tajikistan, Turkmenistan, Kyrgyzstan and Kazakhstan were developed as highly dependent on farming during the existence of the Soviet Union. After collapse of the Soviet Union, economic development of these counties were highly dependent on agriculture sector. As a results, these countries have the highest per capita water usage in the world where, for example, an average Turkmen person consumes four times more water than a US citizen, and 13 times more than average Chinese consumer (Varris, 2014).

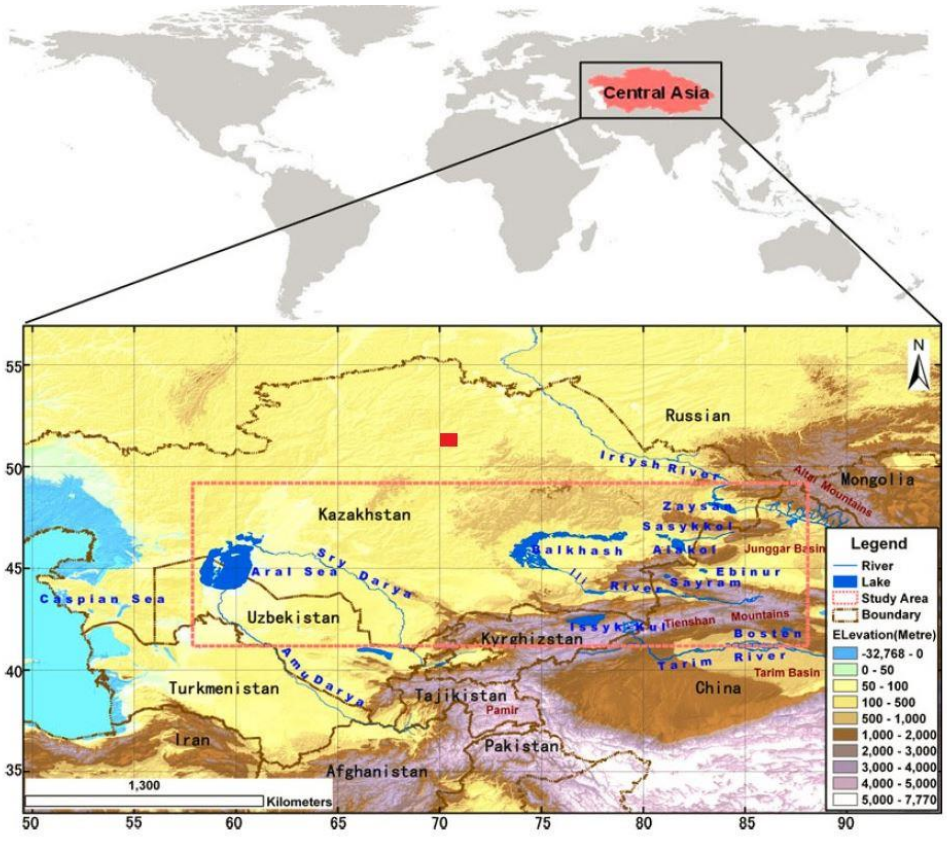

Figure 2. 1 Central Asia countries and their boundaries

where red rectangle shows study area i.e. Burabay area (Bai et al., 2011)

2.1.1 Water resources in Central Asia

Central Asia is a region which is situates from the Caspian Sea in the west to

Mongolia and China in the east, including Afghanistan and Iran in the south and Russia in the north. This region has an arid and continental climate, where the great proportion of the region is steppe and desert, and only the southern, eastern and north-eastern borders are located in the high mountains (Pamir and Tian Shan). Endorheic lakes are the major source of fresh water in arid Central Asia. However, water management and water availability have become one of the main concerns in the context of economic development or/and instability. Water security is strongly associated with geopolitical tendencies, including the collapse of the USSR in 1991 (O'Hara, 2010). Economic development in the newly formed independent countries of Central Asia was heavily dependent on agriculture. Expansion of agriculture in arid Central Asia was associated with the expansion of irrigation where access to water had become a barrier towards the social and economic well-being of countries. Currently, around 40% of the total population of Central Asia relies directly or indirectly on the agricultural sector (WARMAP, 1996) and 90% of the territory of countries such as Tajikistan, Uzbekistan and Turkmenistan energy needs come from hydropower (GWP, 2014). All these countries are facing water scarcity, and increasing demand for water due to growing population and economies, as well as increasing risk of water conflict among the different water consumers.

In the Central Asia region, the environmental integrity of endorheic lakes is compromised due to mismanagement, economic instability, lack of expertise, and lack of cooperation among Central Asian Republics (O'Hara, 2010). Consequently, the largest endorheic lakes such as Aral, Balkhash, Ebinur lakes have deteriorated and become shallower with devastating implications for the regional ecosystem (soil degradation, water quality deterioration), natural habitat (biodiversity loss). The outcomes and consequences of water management of Central Asia during the Soviet era are clearly illustrated in the Aral Sea example, also described as 'a water management disaster' (Micklin, 1988). The Aral Sea and its drainage area occupy about 1.8×10^6 km^2 and encompass Kazakhstan, Uzbekistan,

Turkmenistan, Afghanistan, Tajikistan, Turkmenistan, and Iran. The well-known rapid deterioration of the Aral Sea due to the uneven distribution of water alongside agricultural intensification over the 70 years under Soviet rule (from 1922 to 1990).

2.1.2 Water scarcity and mismanagement in Central Asia

Many hydrological systems have been modified humans globally (Goudie, 2019). Because of a wide range of factors, planetary-scale changes in the occurrence of water and land have occurred. Globally, the total area of about 173,000 km^2 has been converted to land, whereas 115,000 km^2 has been converted to water during 1985-2015 (Donchyts et al., 2016). The hydrologic systems of Central Asia have undergone significant changes throughout the last decades.

The Aral Sea shrinking remains as the most catastrophic example of water mismanagement within the CA region. The first significant water level changes in the Aral Sea were recorded in the early 1960s. Alterations were associated with water abstraction from the lake tributaries which resulted in a dramatic water level reduction by 23m (from 53.41m to 30m) when the lake area shrunk to 73% and water volume decreased by 90% (from 1089 km^3 to 108 km^3), which affected the ecological portfolio of the entire Central Asia. Expanding irrigated agriculture decreased the inflow from two tributaries (Amu Darya and Syr Darya), especially when the agricultural area increased dramatically from 5 million to 7.9 million hectares between 1965 and 2000 (Micklin, 2007). Consequently, the lake lost an annual recharge of 809 mm between 1960-1970 and 304 mm during 1970-1985 (Micklin, 1988).

During the mid-eighteenth century until the 1960s, the net flux was remarkably stable. The water balance of the Aral Sea was in long-term equilibrium with a maximum variation of the lake level of less than one meter (Micklin, 2007). The significant water abstraction from the lake tributaries caused a dramatic water

level decline during 1965-2006 (Figure 2.2). One of the serious environmental implications was a vast salt layer accumulation on exposed sediments (Lioubimtseva, 2014). Since 1975, this salt crust led to salt/dust storms and contaminated adjacent areas which were used for pasture and agriculture. It was estimated that almost 43 million tons of salt per year were carried from the Sea to nearby territories and deposited as aerosols by rain and dew over 150-200x10^3 km^2 (Micklin, 1988).These changes inevitably damaged agriculture and diminished its productivity along with the penetration of salt to deeper layers of soils.

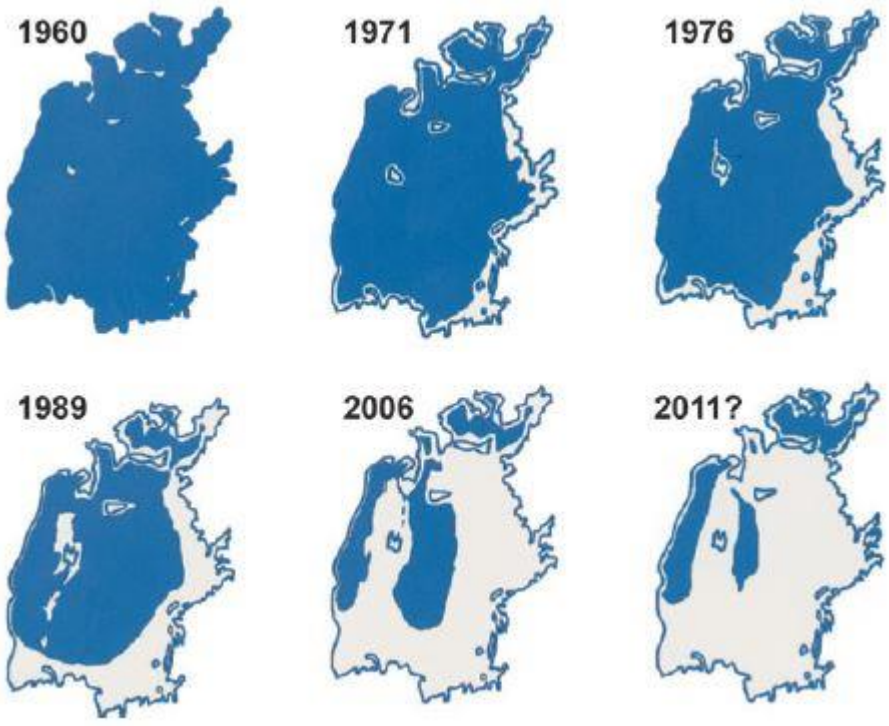

Figure 2. 2 Lake area reduction of the Aral Sea 1960-2011

(Micklin, 2007)

A similar example of significant water level reduction from this region is Lake Balkhash. Lake Balkhash is the second largest endorheic lake within Central Asia and situated in the arid southern part of Kazakhstan. The water level of the lake declined considerably between 1970 and 1985, due to the reduction in one of the inflow tributaries (the Ili River) caused by the construction of the Kapchagay Reservoir. The dam on the River Ili was closed in autumn 1969, and the Kapchagay

Reservoir behind it then started to fill. The Kapchagay Reservoir has not been permitted to reach full supply water-level as it was subsequently recognised that complete filling would diminish runoff to the lake, and as a result would have devastating implications for the water level in Balkhash. Significant proportions of Lake Balkhash water are used for irrigation in the Ili Delta. Nevertheless, the water supply for domestic and industrial needs is relatively small (0.2-0.3 km^3 annually), and by contrast, these losses in the delta during floods, before the creation of the Kapchagay Reservoir were estimated to be 2-7 km^3 per year (Petr, 1992) (Figure 2.3).

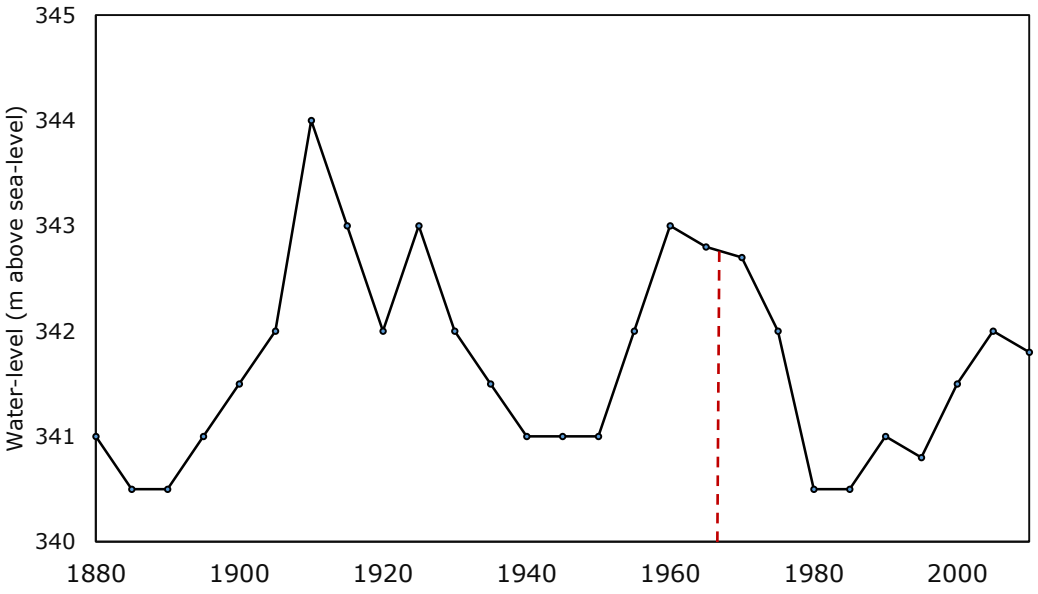

Figure 2. 3 Long-term water level fluctuation of Lake Balkhash

where the red line indicates the period after dam construction on the Ili River and water levels in 1880-1990 Petr (1992) and in 1991-2010 from Propastin (2012)

It is clear that the lake levels were considerably affected by the dam construction in 1969, which decreased the total annual inflow from tributaries to the lake by roughly 15% (Petr, 1992). In addition, the dam construction may have affected the wet period (1948-1960) when the lake did not reach the previous lake levels of 344m observed in 1910.

Lake Balkhash is another example of human-made alteration of the natural water cycle of the lake watershed. The dam construction affected both the quality and

quantity of water in the lake. Falling water-levels of Lake Balkhash have caused an increase in the mean salinity of the basin (Petr, 1992). This increase has been associated with a reduction in aquatic productivity, particularly in fisheries. Groundwater abstraction and extensive agriculture irrigation have worsened the lake shallowing process.

To sum up, Central Asian countries are facing water scarcity and increasing demand for water due to growing population and economies. Water management problems in this region have risen since the 1960s in the biggest endorheic lake systems, such as Aral and Balkhash. The rapid expansion of irrigated agriculture has led to significant disturbances to natural water cycle. Anthropogenic water abstraction from the main tributaries of the Aral Sea and Lake Balkhash have diminished the annual water inflow and, as a result, have caused the dramatic deterioration of the biggest endorheic lakes system within the region. Moreover, the following examples highlight the sensitivity of endorheic lakes to the disturbance of their natural water cycle.

2.2 Modelling the effects of climate change and lake level dynamics

The following section investigates the extent to which the water level of endorheic lakes responds to climate variation. Section 2.2.1 examines water level dynamics and the past climate variation in semi-arid regions of Central Asia. Section 2.2.2 addresses climate variation in semi-arid and arid regions of Central Asia, whereas Section 2.2.3 explains how climate (temperature, precipitation) is likely to change under the changing future climate.

2.2.1 Past climate in semi-arid Central Asia and lake response

Many studies have investigated water fluctuations in the major endorheic lake systems of Central Asia (Petr, 1992, Micklin, 2007, Matsuyama and Kezer, 2009, Vasil'Ev et al., 2006). Most of the previous research focuses on local basin and lake level variation as a response to changing climate or human interventions. The fluctuation of water levels in lakes of west Asia during the 19th and 20th centuries

shows a regional cyclical variation between dry and wet periods (21-40 years). However, conclusions are based on generalised water level trends, without considering site-specific features of the lakes such as hydrogeology, precipitation regime and anthropogenic impact. Bai et al. (2011) analysed lake area dynamics using satellite imagery with annual precipitation variations using Asian Precipitation-Highly-Resolved Observational Data Integration Towards Evaluation (APHRPDITE) of the Water Resources. It was identified that the water levels of most endorheic lakes in Central Asia have fluctuated during the last century, and in most lakes levels have significantly decreased (e.g. Caspian Sea, Aral, Balkhash). In contrast, increasing water level dynamics were observed in high-altitude lakes (e.g. Zaysan, Sayram, Alakol, Sasykkol lakes), due to the increasing pattern in annual precipitation.

In most Soviet literature dedicated to endorheic lakes, researchers apply "dry" and "wet" terms. Yet, these terms are not clearly defined. In many cases, dry/wet periods are associated with a deviation of total annual precipitation from the long-term mean. Previous water balance studies based on *in-situ* observations of Central Asian endorheic lakes demonstrate that most of the dry periods were characterised by the reduction of overall P_{sum} by 30-40% and anomalies associated with the seasonal snowmelt runoff (Shnitnikov, 1970b, Gangopadhyaya et al., 1966, Uryvayev, 1959, Shnitnikov, 1973). By contrast, wet years were predominantly driven by increased precipitation during warm seasons and increased seasonal snowmelt runoff.

Shnitnikov (1970b) studied Central Asian lakes in order to establish long-term climate fluctuations in this region. He concluded that most endorheic lakes fluctuate with a periodicity of every 20-40 years, where wet periods interchanged with a gradual decline over two decades, with a substantial decrease in moisture and ten years of water volume reduction.

However, based on sediment core analysis, the decreasing water level dynamics in the majority of Central Asian lakes may have started earlier (Tarasov, 1996,

Lebedyev, 1928). Numerous studies indicate that the regional climate has been changing over many thousands of years with the overall reduction in moisture over the vast majority of the Central Asian territory (Tarasov, 1996, Kes et al., 1993, Lebedyev, 1928, Micklin, 2010). The climatic variations and the rapid development of agriculture have gradually influenced the development of the river network (Boomer et al., 2000).

There is some evidence that humidity in the Aral basin remained higher for a long period during the 14th and 15th centuries (Shnitnikov, 1973). Then, major changes to hydrologic water circulation occurred in this region during the 19th century (Bruckner, 2000, Shnitnikov, 1970a), when the lake level reached its lowest for that epoch by 1880 (Bruckner, 2000). The significant water reduction was due to droughts which occurred between 1810 and 1820 and repeated between 1856 and 1870 (Shnitnikov, 1973). These droughts were associated with the reduced precipitation across the entire Central Asian territory (Bruckner, 2000).

Interestingly, besides the Aral Sea, many other endorheic lakes became shallower during the 19th century including the Caspian Sea (Micklin, 1973), Lake Balkhash (Matsuyama and Kezer, 2009), Lake Chany, and Lake Issyk-Kul (Shnitnikov, 1973).

Table 2. 1 Summary of historical climate fluctuations and endorheic lakes response.

Sources: 1 Shnitnikov (1973), 2 Matsuyama and Kezer (2009), 3 Bruckner (2000), 4 Petr (1992), 5 Grave (1970), 6 Vasil'Ev et al. (2006)

Hydrological period	**Years**	**Lake**	**Lake response**
Dry	1810-1820	Aral	Water level decline to 3m[1]
	1870-1890	Balkhash	Water level decline to 10m; ≈346m (first half of 18th century) ≈338m (by 1890)[2]
	1861-1875	Chany	Disconnection of Chany, Abyshkhan, Chebakly and other smaller lakes (P<150mm)[1]
	1880-1911	Issyk-Kul	The lake level decreases to 4m by 1880[1];
Wet	1890-1915	Chany	Lake level increase to 1.5m driven by precipitation (P>380mm)[3]
			Lake level increase (from 341m to 344m)[4]

	1900-1910	Balkhash	
Dry	1919-1948	Chany	Lake level decrease to 2.75m[1]
	1929-1965	Caspian Sea	Water level decrease to 3m[5]
	1910-1940	Balkhash	Lake level drop 3m (from 344m to 341m)[4]
Wet	1948-1950	Chany	Rapid water increase to ≈1.75m[6]
	1948-1960	Balkhash	Lake level increase (from 341m to 344m)[4]
Dry	1951-1958	Chany	Lake level reduction to 1.5m[6]

It is clear that droughts had occurred in the 19th century had significant implications for water levels of most lakes located in this region (Table 2.1). According to Shnitnikov (1973), the water balance of these lakes was mainly affected by reduced precipitation and overall aridization of the Central Asian region. Research on long-term precipitation variation in the Lake Balkhash basin confirms that there were negative precipitation anomalies from 1872 to 1950 (Matsuyama 2009).

Negative precipitation anomalies occurred in the 1940s and 1950s with a 30% decrease in total annual precipitation (from 150 mm to 100mm for the Aral Sea; 170mm versus 128mm for Balkhash; 300mm versus 250mm for Issyk-Kul) for arid areas. In contrast, the negative precipitation trend was more pronounced for semi-arid lakes with a considerable reduction by 40% (from 375mm-160mm for Chany lake (Shnitnikov, 1973); 506mm versus 283mm Shortandy Lake (Kokshetau weather station).

Since 1960, the hydrological response and the magnitude of changes in the aforementioned lakes were distinctive. In many cases, it was difficult to separate climatic changes from anthropogenic impact, as local water management regulations predominately influenced the natural water cycle. For example, the lake level dynamics of Lake Balkhash show human intervention to its natural water cycle. Table 2.1 shows, the amplitude of change in Lake Balkhash levels ranged

between ±3m during dry and wet periods, with a roughly 30 year periodicity.

Recent research on Lake Balkhash shows positive water volume response over the last decades (Propastin, 2012, Matsuyama and Kezer, 2009). Propastin (2012) analysed precipitation records from regional weather station as well as lake level records from satellite altimetry observations. Based on these findings, the positive lake level dynamics were driven by the upward trend in warm-season precipitation during the 1990s. Specifically, annual precipitation has increased to 11.06mm $year^{-1}$ (+3.66% from long-term mean annual), whereas air temperature has changed +0.08°C $year^{-1}$ between 1993 and 2010 (with 1% and 5% significance respectively). Duan and Bastiaanssen (2013) research confirms a positive precipitation trend in 2003-2015 for Lake Balkhash. In addition, the maximum lag in response to precipitation of the Lake Balkhash occurs with a postponement of 1-2 years. Overall, the lake level strongly correlated with precipitation and air temperature.

Similar but more dramatic water level changes in the Aral Sea were observed in the early 1960s. The water balance of the Aral was clearly modified by human intervention. Expanded irrigated agriculture has dramatically reduced inflow from two tributaries (Section 2.1.1). As well as anthropogenic water abstraction, drying-out of the Aral was accompanied by increases in summer and winter temperatures of 1.5°-2.5°C (Chub, 2000) with the highest temperature changes occurring in April and May (4°-5°C since 1960 (Small el, 2001). Yang et al. (2020) studied Aral Sea water volume and their potential driving factors based on MODIS and long-term hydrological data. Based on these findings, precipitation and temperature are among factors that affected long-term water level reduction in the lake (Figure 2.4). However the dominant factor was a long-term extensive water abstraction from the lake tributaries, which diminished annual inflow to the lake.

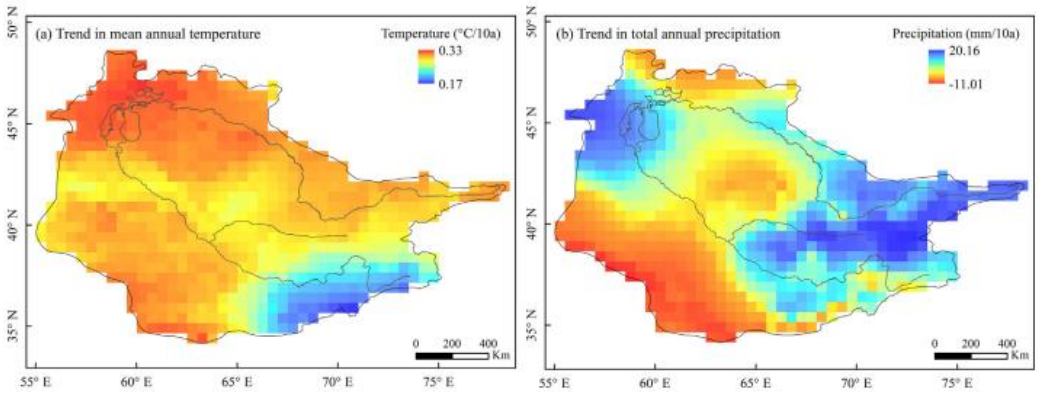

Figure 2. 4 Mean annual temperature (a) and total annual precipitation trend in the Aral Sea in 1960-2018

(Yang et al., 2020)

Water level dynamics of the Caspian Sea and Chany Lakes differed from the previous examples. For instance, the biggest endorheic lake, the Caspian Sea, where water level decreased by 3m during the dry 1930s (Table 2.1) reversed this decreasing trend by the end of 1970s. The positive lake level response was associated with a considerable increase in runoff recharging the Volga river basin. The water balance remained positive (+131mm $year^{-1}$) in 1978-1995, followed by another recession by -67mm $year^{-1}$ in 1996-2015. Recent water balance studies (Chen et al., 2017) revealed that the water reduction from 1996-2005 was due to reduced precipitation and runoff (≈50mm and ≈90mm, respectively). However, since then, surface water evaporation has been the dominant driver of water level recession between 2006 and 2015, which exceeds losses from the Volga basin.

Chany Lake is located in the West Siberian Plain, where water circulation has been modified significantly during the 19^{th} century. During this dry period, the Chany water basin (composed of Abyshkhan, Chebakly lakes and other smaller basins (Shnitnikov, 1973) has shown disconnection. Water levels reduced in Chany Lake during the dry period of 1920-1945 (Table 2.1) and recovered its water level during the wet 1950s (Vasil'Ev et al., 2006). Despite lake level fluctuations after the 1950s, the overall water volume of the lake remained unchanged by 2000.

This following section shows past climate fluctuation in the Central Asian region and lake responses to them. Significant transformations in regional hydrology

have occurred during the 19th century (Brukner, 2000). Climate variation, as well as water volume fluctuation, are evident in most Central Asian endorheic lakes considered in this section. Specifically, the dry period in 1920-1940 was typical for this region which led to significant decreases in the level of most endorheic lakes of Central Asia. However, after the 1960s, the hydrologic behaviour of these lakes has become increasingly distinctive as the natural water balances of Central Asian lakes have been significantly modified by human intervention.

2.2.2 Climate variation

The Central Asian region is continental with an arid and semi-arid climate. The region is a transitional zone between mid-high latitudes and the equator, in the Northern Hemisphere (Wang et al., 2010). In the south, arid regions are dry (precipitation<250mm annually), with warm and moist summers and relatively warm winters (Lioubimtseva and Henebry, 2009b). In the north, semi-arid regions are characterised by cold winters and greater annual precipitation (precipitation>300mm annually).

Climate studies over Central Asia show that mean annual air temperature has increased during the twentieth century (Lioubimtseva et al., 2005, Lioubimtseva and Henebry, 2009a, Chub, 2000, Chen et al., 2009). The rate of increase of the annual mean temperature is 0.18°C per decade (Chen et al., 2009), with a greater increasing trend (0.28°C per decade) in 1977-2001 (Jones and Moberg, 2003) (Figure 2.5). Based on Jones and Moberg (2003) findings, the following increasing trend in arid Central Asia was of greater magnitude than in other regions of the Northern Hemisphere (0.074°C per decade). The most notable warming patterns in Central Asia were established during cold-seasons (Lioubimtseva and Henebry, 2009a, Jones and Moberg, 2003).

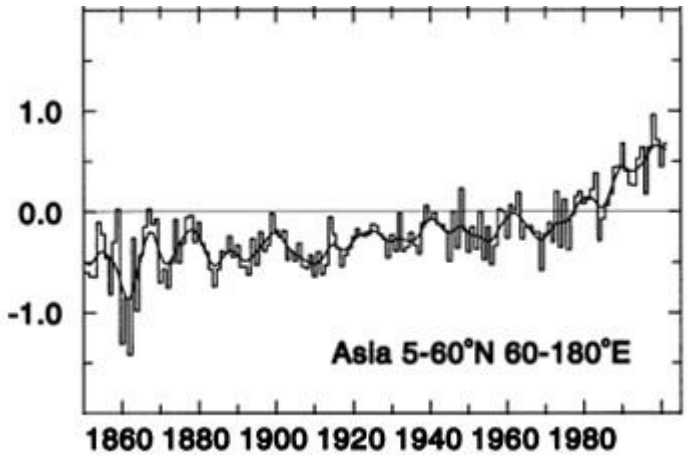

Figure 2. 5 Mean annual air temperature changes in Central Asia

Jones and Moberg (2003)

According to paleoclimate and archaeological studies, the climate over the Central Asian region has undergone many changes that could repeat under a future changing climate. Lioubimtseva (2003) assumed that, based on early-to-mid Holocene reconstructions, the arid region of Central Asian (the Aral Sea, Issyk-Kul) received more moisture as a result of the expected southward shift of air masses and potential intensification of westerly cyclones.

The territory of Central Asia is influenced by mid-latitude westerlies from the west as well as by Asian monsoon circulation coming from the east (Chen et al., 2010). More frequent precipitation is delivered from depressions which form over the Mediterranean region, migrate north-eastwards, and regenerate over the Caspian Sea. Chen (2008) showed that a wet monsoon in Asia correlated with decreased moisture over Central Asia during the early Holocene, whereas the decreased influence of the monsoon corresponded with a wet period during the mid- and late Holocene. Specifically, strong Asian monsoon transports a strong warm and moist airstream from the west Pacific Ocean, which by the wind fields favor an increase in precipitation over semi-arid regions (Figure 2.6).

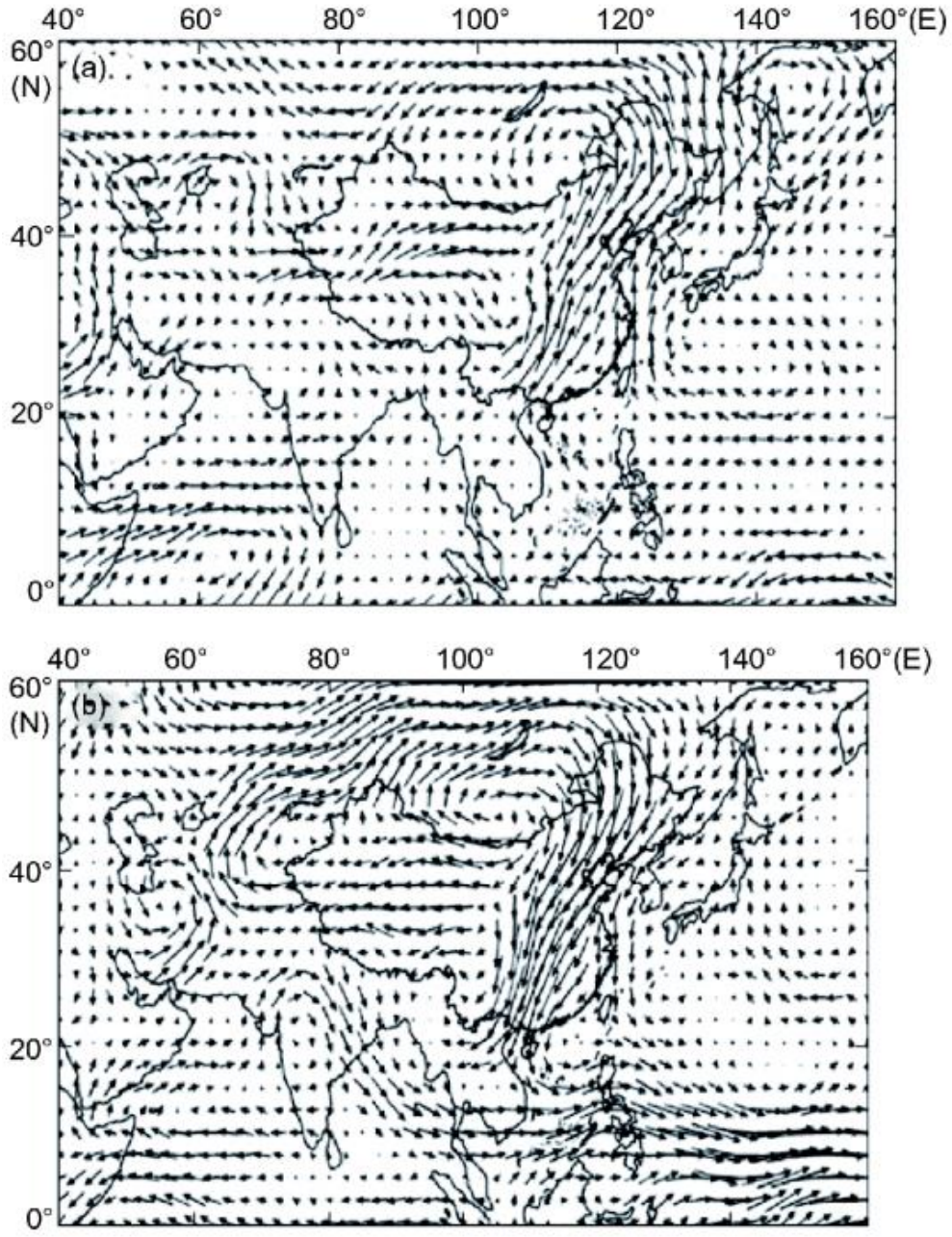

Figure 2. 6 Distribution of horizontal wind field at 850hPa for years with increased (a) and decreased (b) precipitation over the semi-arid and arid regions

(Liu et al., 2018)

Over the twentieth century, the climate over Central Asia has become warmer, with a considerable change in the distribution of precipitation (Wang et al., 2010) and the overall expansion of semi-arid regions over arid areas (Chen et al., 2011). Air temperature and precipitation anomalies over Central Asia correlate positively with the westerly index since the 1980s (Liu et al., 2018). In contrast, the influence of the Asian monsoon has become weaker (Wang, 2001), which is one

of the reasons for warmer and wetter conditions during recent years (Bai et al., 2010). Recent studies indicate an increasing trend of precipitation over 64% of Central Asian area during 1901-2013, especially over Northern Kazakhstan and in most parts of the Tianshan Mountains in 1951-2013, whereas a considerable reduction was observed in the south-west regions (the Aral Sea region) (Figure 2.7) (Hu et al., 2017).

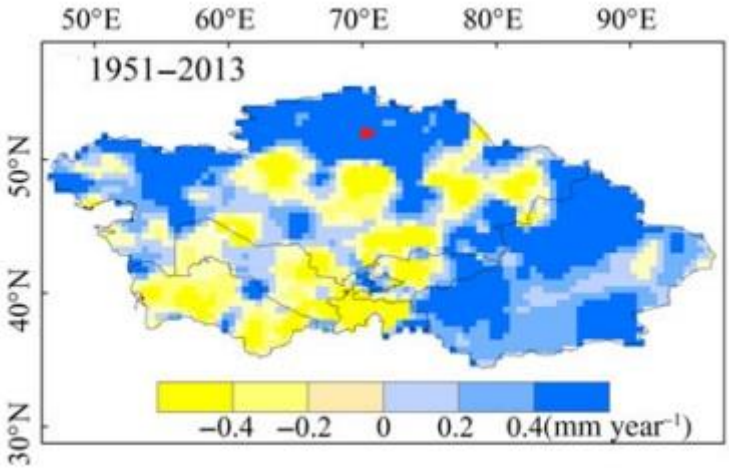

Figure 2. 7 Spatial distribution of precipitation trend over Kazakhstan and west regions of China

where red rectangle shows study area i.e. Burabay area (Hu et al., 2017)

Precipitation changes over the Central Asian region were also influenced by latitudinal shifts of the cyclonic circulation and position of the Siberian high, which predominantly affects winter precipitation (Lioubimtseva, 2003). Atlantic sea surface anomalies and associated North Atlantic Oscillation (NAO) over central Siberia affect both surface air temperate and precipitation and thus influence snow accumulation (Ye, 2001). Over the last six decades, the NAO pattern has gradually changed from the most extreme and persistent negative phase in the 1960s to the most positive phase during the late 1970s to the middle of 1980s (Lioubimtseva, 2014, Robinson and Frei, 2000). However, this trend has recently changed again with decreasing snow cover during the 1990s.

Significant decreases in snow-cover have been observed over the previous century across semi-arid regions of Central Asia (Brown, 2000, Ye et al., 1998, Micklin,

1973, Lioubimtseva and Henebry, 2009b). Reduced winter precipitation is associated with an air temperature increase during the spring months, which increases the proportion of rainfall and conversely decreases the proportion of snow (Brown, 1997, Clark et al., 1999). Eurasian mid-latitudes have become warmer, with stronger trends in March and April (2.8°C and 2.3°C respectively) (Brown, 2000), resulting in a transformation of solid precipitation to rainfall. As a result, snow accumulation and snow cover have substantially decreased to 20% (Brown, 2000).

Long-term reduction in spring snow cover shows stronger sensitivity to air temperature in mid-latitude Eurasia than other snow-dominated regions. This is because of the greater continentality of Eurasia (Foster et.al., 1983). It is the biggest continent and land surface, and consequently has a greater potential to influence climate. Lioubimtseva et al. (2014) suggested that a gradual increase of winter temperature during the past century could be explained by the general spatial shift in atmospheric circulation in the region. The increasing winter/spring mean temperature trend in Central Asia is likely to result from the declining influence of the Siberian High since the 1970s which is linked to increased precipitation during warm-seasons (Panagiotopoulos et al., 2005).

Ye et al., (1998) analyzed snow depth data collected during 1936-1983 for the region between 50°-70°N and 30°-140°E. Although the winter accumulation trend was positive throughout the higher latitudes (higher 60°N), a substantial decreasing trend for the area around 50°N latitude was established. According to Ye (1998), snow depth has been decreasing to 0.23 cm $year^{-1}$ or 0.8% per decade (Ye et al., 1998). This spatial distribution of winter precipitation changes may be explained by the combined effect of air temperature and regional topography of the region. Low-lying areas in this latitude (50°-70°N and 30°-140°E) are relatively warmer and the higher temperature may result in lower snow precipitation versus rainfall (Ye and Mather, 1997). The following trend has been observed in Canada over the last four decades of the 20^{th} century, where winter

precipitation increased in high altitudes, whereas for lower-elevation areas the opposite trend was observed (Karl et al., 1993).

Further research on historical winter precipitation analysis shows anomalies for October, March and April months over the Eurasian region (40°-60°N and 20°-90°E) in 1915-1997. These months are known as the transitional period between cold and warm seasons in the Northern Hemisphere. According to Brown (2000) there was no significant long-term change in solid precipitation, but a considerable reduction in spring snow cover, particularly in April. Linear regression analysis showed that these changes were associated with a considerable increase in temperatures during March and April air temperature of +2.5°C (100 yr^{-1}). Interestingly, this temperature increase has been observed in the spring (Bonsal and Prowse, 2003) along with considerable spring runoff reduction in the continental Canadian prairie region over the last century (Zhang et al., 2001).

2.2.3 Future climate

Climate change is generally expected to intensify the global water cycle as a result of changes in hydrologic variables such as precipitation and temperature (Huntington, 2006). Future climate simulations for the Central Asian territory assume that air temperature is likely to increase. As discussed above, winter temperatures have been widely affected during the last century.

According to multi-model simulations discussed in the IPCC Fourth Assessment Report (IPCC, 2007), the temperature will increase by a median of 3.7°C by 2099. Several studies of future climate scenarios produced by the Atmospheric Ocean Global Climate Models (AOGCMs) used by the IPCC (Lioubimtseva and Henebry, 2009b) are available for the Central Asian region. Despite some uncertainties, i.e. coarse resolution of AOGCM (250-600 km), these models are in a good agreement, suggesting that air temperatures will increase in arid regions of Central Asia (Aral territory, Issyk-Kul). Annual temperature under A1F1[1]-AIM and A1B[1]-MES IPCC

[1] A1 – storyline and scenario family indicates a future world of fast economic development, population growth that peaks in mid-century and declines thereafter and rapid development

SRES scenarios (Nakicenovic et al., 2000, Manning et al., 2013) predicts an increase in air temperature above 4°C by 2080 for northern regions of Central Asia and 2-3°C for mountainous areas (Tien Shan and Tibetan Plateau).

For snow-dominated areas, climate variation in the 20th century has already led to alterations in the timing of seasons, snowpack coverage and water volume available from snowmelt runoff (Stewart et al., 2005b). These variables are closely related to seasonal variability and change from year to year. The sensitivity of winter precipitation to air temperature affects snow accumulation, and as a result, snowmelt induced runoff, whereas rapid temperature changes promote glacial melting and affect spring influence the timing of runoff (Barnett et al., 2005). The potential future impacts in snowmelt-dominated catchments may include a reduction in snowpack volume and earlier onset of melting (Dibike and Coulibaly, 2005, Merritt et al., 2006).

Seasonal air temperature distribution under A1B emission scenario differs across seasons, but higher temperatures are predicted for cold seasons. Similar findings based on IPCC, yet under A1B (Manning et al., 2013) for the whole of Central Asia show that winter temperatures (December, January and February) will significantly increase to 5-8°C, primarily affecting Northern Kazakhstan by 2100. Regional future climate modelling on Lake Baikal confirms that under a 1% increase in CO_2 the winter temperature will rise to 4.8°-9.3°C for the northern Asian region by 2070-2100 (IPCC, 2001). The consequence for Lake Baikal will be that ice cover duration may decline by 15-28 days (Todd and Mackay, 2003) or the lake surface may remain unfrozen up to 2 months longer than the present (Shimaraev et al., 2002).

Heterogeneity of the Central Asian region creates spatial variability with contradictory precipitation trends throughout the area. As a result, future

---

of technologies. The A1 develops into different groups that defines alternative directions developed in the energy system, where A1F1-fossil intensive; A1B balanced usage, where similar improvement rates apply to all energy supply as well as sustainable usage (IPCC, 2007).

projections of precipitation show high discrepancies depending on regional topography and land use (Manning et al., 2013, Lioubimtseva, 2014). Most General Circulation Models (GCM) indicate a reduction in rainfall during warm seasons across Central Asia (Christensen and Benestad, 2007). Yet, the simulations based on AOGCM show the discrepancies between future projections for arid (territory occupied by south of Caspian Sea, Aral Sea, Lake Issyk-Kul) and semi-arid (Lake Balkhash, Chany Lake, Burabay Lake) regions are significant. Most climate projections predict a slight decrease in annual precipitation rate ~1mm/day by 2050 with a stronger trend for the western and southwestern region and contradictory increasing precipitation trend ~1 mm/day in the northern and eastern parts of Central Asia (Lioubimtseva and Henebry, 2009a). The IPCC simulations confirm that the arid regions of Central Asia are likely to continue the aridization process, whilst western parts, i.e. the semi-arid area (east from longitude 70°E) will receive slightly more precipitation by the end of this century. According to HadCM3, ECHAM4, 5, CSIRO-Mk3 and CGCM3 models under AOGCM/SRES, the changes in air temperature will be the major factor influencing the entire Central Asian region. Precipitation over the Aral region will increase insignificantly; specifically, snow will increase to +4%, but decrease during the warm season (-13%) (Lioubimtseva, 2014). By contrast, Meleshko (2004) predicts an increase in summer precipitation in the northern part of Central Asia, i.e. for the semi-arid region (Meleshko, 2004). Models under AOGCM show that precipitation is likely to increase for the European Russia and Central Siberian region. Regional-scale modelling of GCM indicates contradictory precipitation patterns over Asia (Manning 2013). An increasing trend primarily covers northern Kazakhstan, with an opposite trend for Lake Balkhash and Tien Shan areas.

Most future global climate models predict less snow accumulation in snow-dominated regions (Barnett et al., 2005). In contrast, most regional climate models show opposing patterns in winter precipitation distribution all over Central Asia. However, the overall precipitation trend is predicted to increase for semi-

arid areas of Central Asia (Christensen and Benestad, 2007, Panagiotopoulos et al., 2005). It is explained by a decline in the strength of the Siberian High since the 1970s which has caused milder than normal air temperature conditions and, as a result, intensification of rainfall instead of snow. This declining trend is neither well-explained nor understood in the literature. Future climate circulation model projections suggest a negative correlation between the intensity of the Siberian High and increases of greenhouse gases until 2100 (Mackay et al., 2006). For example, a positive relationship between increased air temperature and hydrological inflow into Lake Baikal was identified. A positive hydrological response will be due to warm-season precipitation, where rainfall is expected to increase by 5-10% resulting in increasing lake inflow by the same proportion (Shimaraev et al., 2002). According to the AOGCM models, precipitation is expected to increase in northern regions. The precipitation distribution shows an increase of 25mm in the south, whereas, in Northern Kazakhstan, a more considerable increase up to 100mm annually by 2070-2100 is predicted.

Yet, the relative contributions of these factors to climate changes over Central Asia are unclear. Most GCM models do not allow to examine future climate changes in small watersheds due to topographical heterogeneity and great seasonal variability of the Central Asian regions. In addition, a limited understanding of the mechanism of changing climate over this region makes difficult to evaluate future implications of changing climate to endorheic lakes.

2.3 Previous research on the Burabay area

Most hydrologic studies on the Burabay lakes were conducted during the Soviet era. Most research over that period was focused on understanding water availability, directed to water supply for nearby settlements, as well as for agricultural needs. Water balance studies were conducted only by Uryvayev, based on field observation between 1953-1955, with limited analysis on regional climate fluctuation (Uryvayev, 1959). Studies over the Burabay area conducted

by Shnitnikov (1970b), (1970a) were focused on lake level fluctuation as a response to climate variation in Western Siberian over the 20th century. Zemlyanicyna (1970) research established the groundwater interactions between Burabay, Ulken Shabakty and Maibalyk lakes. Following interaction between these lakes is confirmed by hydrogeologic survey by Posokhov (1947) and *in-situ* measurements of water levels conducted Muraveiskij (1936) in 1927.Konshin (1951) studied sediment cores of Burabay, Ulken Shabakty and Kishi Shabakty, who confirmed that these three lakes used to be one lake system, yet which surface water had been separated in 1888 according to Uspenskij (1948).

There are several paleohydrological investigations available for Burabay area. The first such investigation was conducted by Korde during the 1940s (Korde, 1951) and focused on Burabay, Ulken Shabakty, Maibalik and Svetloe lakes. Together with more recent studies using paleomorphometric analysis, it was possible to reconstruct the maximum water levels of Burabay Lake (Tarasov (1996). It was revealed that the strong floods had influenced the Burabay area over the Quaternary period, which in turn resulted in higher lake level and developed river systems.

2.3.1 Historic hydrological changes in Burabay lakes

Burabay lakes have experienced two big floods and at least three lake level reduction process accompanied by increased water salinity during the Quaternary period (Korde, 1951). Most of the lakes of Northern Kazakhstan and in the Burabay area were formed in regions with developed river systems which are now shallowing or have already disappeared (Kassin, 1931, Gerasimov and Markov, 1939). However, these river systems were replete during the wet periods of the Quaternary (Lebedyev, 1928, Laptyev, 1940). For example, Lebedyev (1928) showed that Chagly Lake (an endorheic lake located north-west from Shortandy) was previously connected with the Irtysh River via the Kamyshylovka River (which

disappeared in 1768). According to Laptyev (1940), Burabay lakes were previously connected by a stronger river network. Figure 2.8 and 2.9 illustrate river system described by Lapteyev, where current endorheic lakes such as Koturkul, Burabay and Ulken Shabakty were previously linked to one river system. Shortandy Lake was drained by another river system, the Kylshakty River during the 18th century as confirmed by three terraces on the lake that provide evidence of former high water levels (Dravert, 1930) (Figure 2.9).

2.3.2 Regional climate and Burabay lakes water level fluctuation

The overall tendency towards drying out over the last three centuries started at the end of the 19th century (end of the 1880s). Observations over Burabay lakes indicate regional climate variation over the last two centuries. For example, the surface disconnection in the one lake system, currently three separate lakes (Maibalik, Ulken Shabakty and Kishi Shabakty) is associated with prolonged droughts during the 19th Century (Phorsh, 1970, Shnitnikov, 1957). Ulken Shabakty and Maibalik became disconnected during dry climatic conditions in the early 19th century, yet Maibalik remained connected with Kishi Shabakty. Subsequently, these lakes become endorheic following another dry period between 1865 and 1880 (Uspenskij, 1930, Uspenskij, 1948). Interestingly, a similar shallowing process occurred at Chany Lake (Section 2.2.1) during the same period[2].

[2] In Chany Lake area this arid period showed disconnection in one lake system composed from Abyshkhan, Chebakly lakes and other smaller basins. SHNITNIKOV, A. 1970a. *Semi Arid Lakes of USSR,* Leningrad, USSR, USSR Reseach Academy.

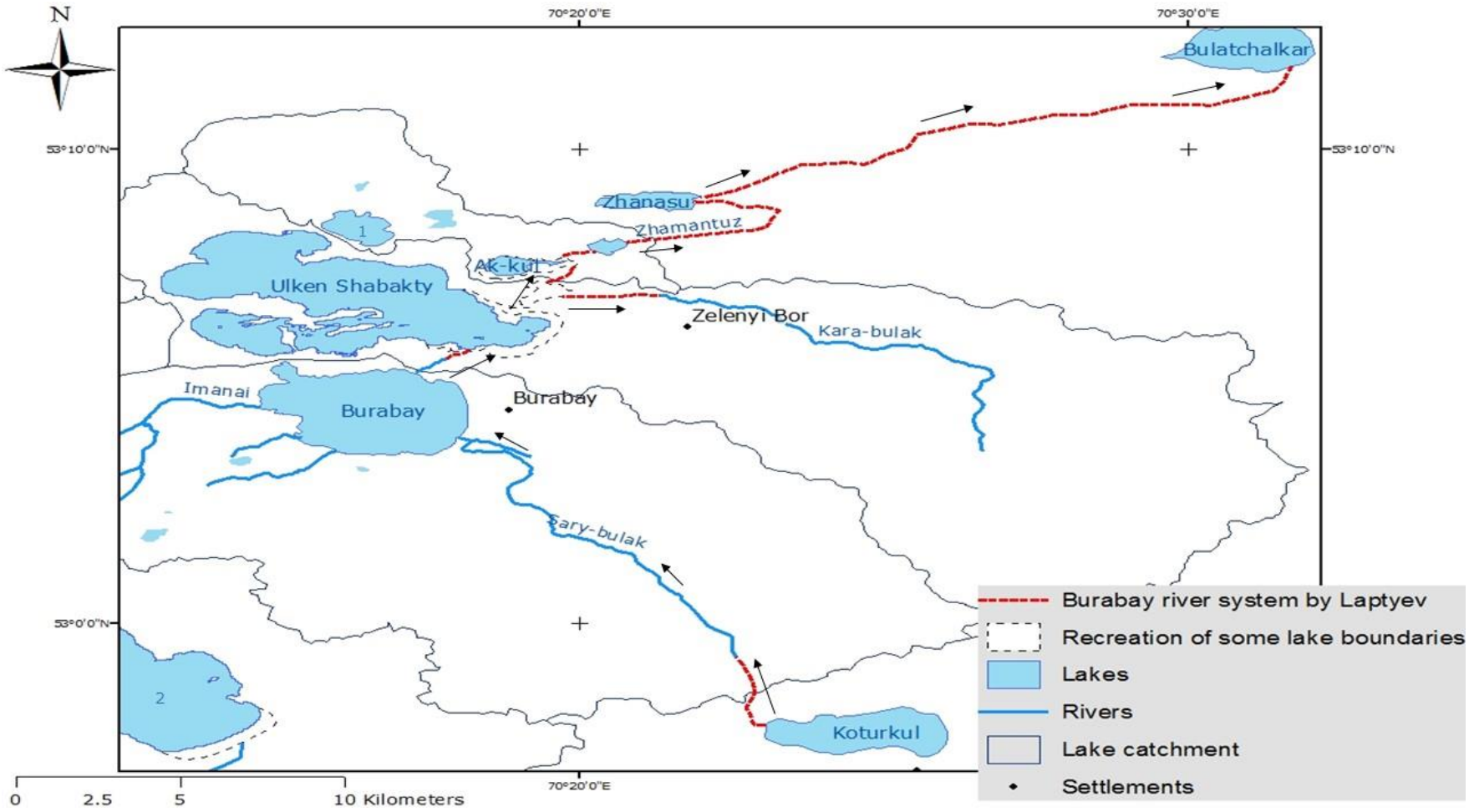

Figure 2. 8 River system one in the Burabay area during the 18th Century

where 1-Maibalik Lake and 2-Shortandy Lake (Laptyev, 1940)

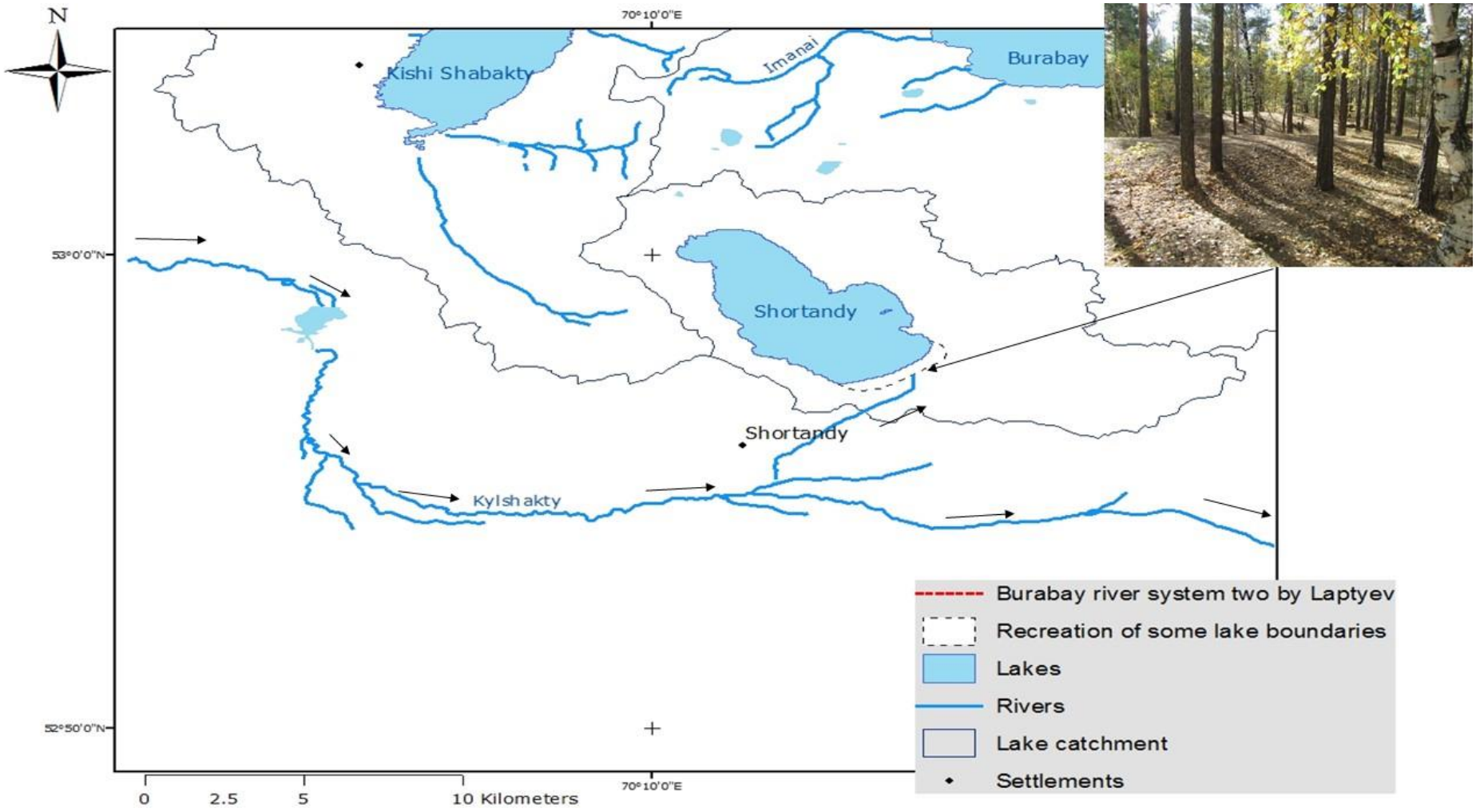

Figure 2. 9 River system two during the 18th Century and terraces on the south shore of Shortandy Lake

From Laptyev (1940) and picture from a field trip in September 2012

Shnitnikov (1973) suggested that water levels of most Burabay lakes are responsive to precipitation and temperature anomalies during warm-seasons. Lake level fluctuations in the Burabay area between 1936 and 1968, was found to be caused by higher temperatures during summer months (June, July and August) (mean temperature 16°C in 1936-1968 versus 13.6°C in 1888-1930 (Zemlyanicyna, 1970).

The drought events in the 1930s and 1940s resulted in further aridization of the Burabay area (Uspenskij, 1930, Posokhov, 1947). This period is defined as "severe drought" in the literature for the entire Burabay area and is reflected in water level decreases in all Burabay lakes (Shnitnikov, 1957). Although lakes levels were not measured, there is some evidence of this drought. For example, Tseeb (1940) established that Shortandy Lake water level decreased from terraces on the south shoreline. Uspenskij (1930) and Posokhov (1947) examined lake response by measuring the surface water distance between the newly-formed Kishi Shabakty and Maibalik.

It clear that most lakes in the Burabay area were highly responsive to the observed series of dry periods in the 20th century. Water salinity also changed in response to climate variability. Gorshenin (1927) highlights three major reasons for salinisation of West Siberian lakes: groundwater connectivity, conditions of their formation and climatic changes. However, Korde (1951) concluded that groundwater is located deeper than most water bodies, and therefore, most lakes in the Burabay area are fed from surface runoff. Consequently, water salinity tends to be driven by surface runoff intensity, which is a function of regional climate (Korde, 1951).

Phorsh (1970) studied climate variation in the Burabay area by analysing the historic water salinity of Maibalik Lake. The decreasing water level was accompanied by increasing water salinity in most Burabay lakes including Maibalik and Kishi Shabakty Lakes, whereas Ulken Shabakty Lake water mineralisation does not correlate with climatic variations due to complex morphometry on the

lake bottom, and small bays and islands which disturbs water mixing and creates localised water conditions.

The drought in 1920 significantly transformed hydrological water circulation in the Burabay area (Table 2.2). For example, the dry period in 1929-1940 resulted in water level reduction in most Burabay lakes. Table 2.2 summaries that the 19th and early 20th centuries were marked with prolonged droughts, and as a result were accompanied with water volume reduction in most lakes which in turn transformed the water circulation in Burabay area.

Table 2. 2 Major periods of regional climate fluctuation and the hydrologic response of Burabay lakes

	Years	**Lake response**
dry	Early 19th Century	Surface water disconnection between Ulken Shabakty and Maibalik (Shnitnikov, 1957)
dry	1865-1880	Maibalik Lake disconnection from Kishi Shabakty (Uspenskij, 1930, Uspenskij, 1948)
stable	1913-1925	Stable water salinity (Phorsh, 1963)
dry	1929-1940	Ulken Shabakty and Shortandy lakes became endorheic, where the water level of Shortandy dropped to 2m (Dravert, 1930, Korde, 1951, Shnitnikov, 1970a, Tseeb, 1940); considerable increase in water salinity in Maibalik (from 9.1g/L in 1925 to 15.76g/L) and Kishi Shabakty lakes (1.97 g/L in 1929 to 2.66 g/L 1940) (Posokhov, 1955, Uspenskij, 1948)
wet	1941-1947	The highest water level recorded in the 20th century by that time (Zemlyanicyna, 1970) Significant decrease in water salinity in Maibalik (from 11.76 g/L in 1947 versus 15.76 g/L in 1940) (Phorsh, 1970)
dry	1951-1958	Increase in water salinity in Maibalik (from 11.8g/L to 18.1g/L in 1959) (Phorsh, 1963, Phorsh, 1970)
wet	1958-1965	Less intensive than during the 1940s due to warmer summer (Zemlyanicyna, 1970)

2.3.3 Historical water regime

Historical analyses show that Burabay lakes water levels have different hydrologic responses under the same regional climatic conditions. The wet period between 1959 and 1965 caused a less marked water level increase than the previous wet period in the 1940s. Burabay Lake has open drainage and is supplied by many rivers including the Sary-Bulak River and receives plentiful water from forested swamps and mountainous areas. This lake level was almost stable over wet and dry periods, whereas endorheic lakes, such as Ulken Shabakty and Maibalik

fluctuated with different magnitudes, with Ulken Shabakty Lake having the greatest deviation (Figure 2.8). Burabay Lake outflows through the Gromatukha River which delivers excessive water from Burabay to Ulken Shabakty during wet years. Therefore, during dry periods the outflow was negligible, consequently causing a significant reduction of the water level in Ulken Shabakty (Uryvayev, 1959). Figure 2.10 shows that endorheic lake water levels decreased significantly during the dry period from 1950 to 1958. Subsequently, there was a rapid level increase to almost 2m by 1965. In contrast, the water level of Burabay Lake, which is an open lake, was predominantly stable over the period.

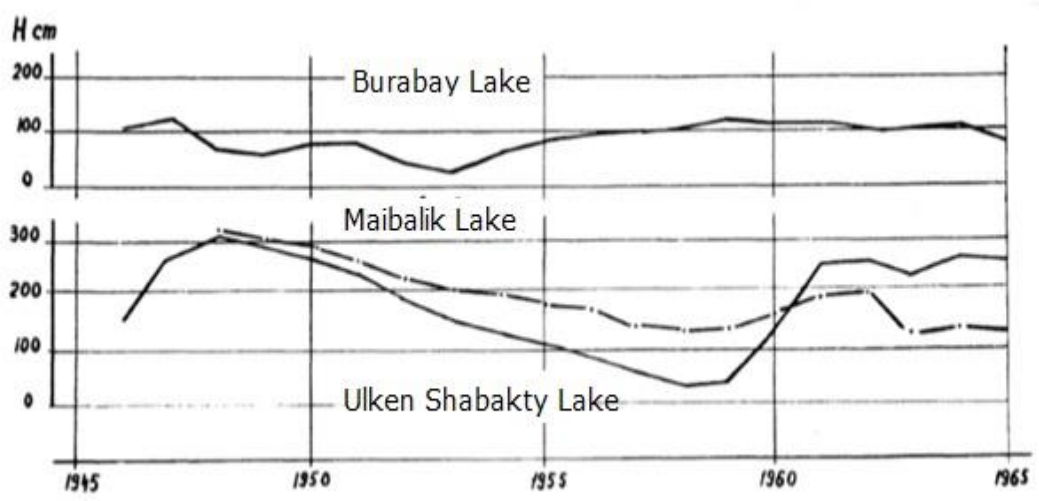

Figure 2. 10 Water level fluctuation in Burabay lakes from 1945-1965 (Shnitnikov, 1968)

The historical amplitude of Burabay lakes is within the range of 5.0–5.5 m, but it was higher in some lakes of the Burabay area (Shnitnikov, 1970a). For example, lake level variation to 6.4m and 6.7m was observed in Shortandy and Ulken Shabakty, respectively. The greatest water level decrease in these lakes was explained by the additional anthropogenic water abstraction from these lakes, where Shortandy and Ulken Shabakty lakes were used extensively as the major lakes for water supply (Shnitnikov, 1970a).

There were two water balance studies conducted for Burabay Lake. The first water balance research for these lakes was conducted by Uryvayev based on field

observation from 1955-1956. This research was mainly focused on the evaluation of water resources in Northern Kazakhstan for agricultural water supply (Uryvayev, 1959). The findings revealed that the water inflow of Burabay lakes is driven by seasonal snowmelt runoff, which proportionally fluctuated from season to season and consequently resulted in water level variation from 1-6m. This deviation in water levels was recognised as a typical amplitude for major lakes in Northern Kazakhstan. Water balance investigations on endorheic lakes in Northern Kazakhstan based on two years of the field observation (from 1955 to 1957) revealed that most water comes from watershed runoff (50-60% of the annual water budget) and 28-35% was from precipitation which falls on the lake surface. Water outflow depended on surface and groundwater interactions, but open water evaporation ranged from 60 to 80% of total annual water losses. Recent water balance studies conducted from 2011 to 2013, established a considerable water volume reduction in Burabay (Figure 2.11), Ulken Shabakty and Shortandy lakes (Yapiyev et al., 2017). Based on this study, the water level reduction in Burabay lakes was driven by the lake evaporation with a minor influence of anthropogenic water abstraction. Yet, this conclusion is based on a short-term observations conducted in 2011-2013, after the water policy accepted in 2010 (more in Section 3.1.5), thus cannot explain a long-term water reduction in Burabay lakes.

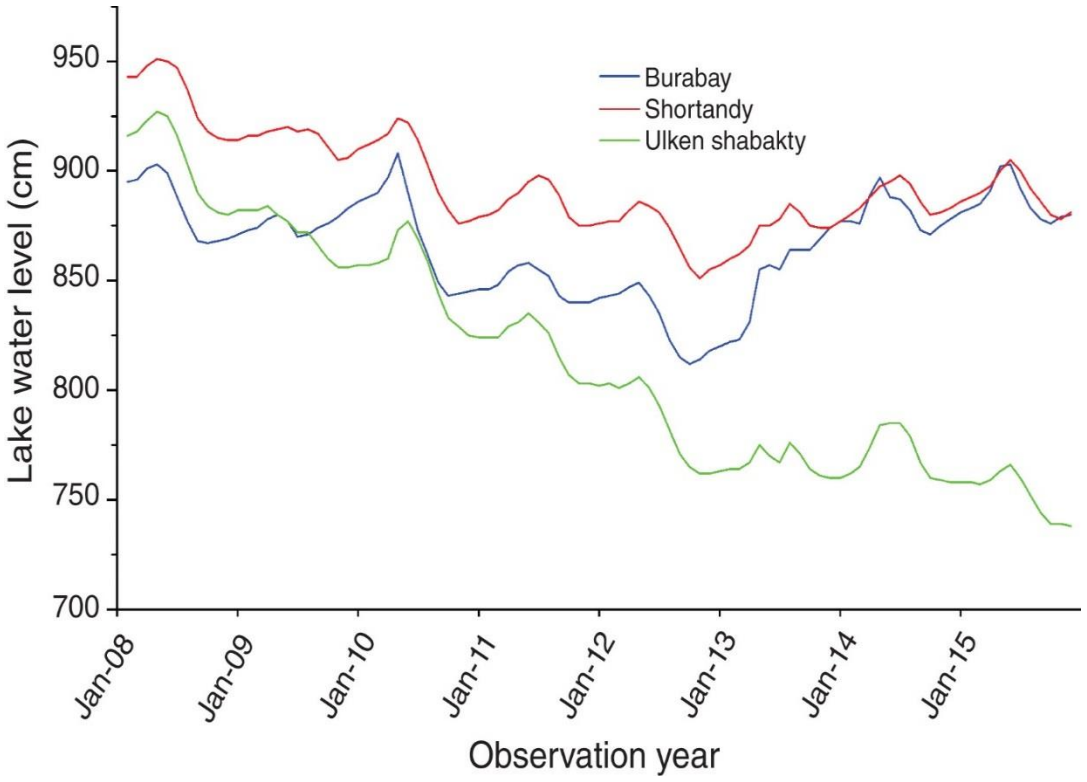

Figure 2. 11 The lake level variation in 2008-2015 in the three lakes of Burabay area (Yapiyev et al., 2017)

2.4 Summary

The literature review reveals that most lakes in Central Asia have fluctuated over the past centuries. Water level of most endorheic lakes of Central Asia region was highly responsive to variability in air temperature and annual precipitation. However, significant water level reduction in most Central Asian lakes was driven to human activity and changes in water management policies in the past. Lake level variability could be explained as follows:

1. Negative precipitation anomalies were evident during the 19th century and continued until the 1950s. The significant reduction in precipitation resulted in considerable changes both to lake levels, and the entire water circulation in the Central Asian region. Prolonged droughts have considerably influenced river systems in the Burabay area (Figure 2.8, 2.9).
2. Reduction of annual precipitation in 1920-1940 affected most lakes in this region, including Burabay lakes (Section 2.3), resulting in disconnection of

lakes from their tributaries (e.g. Shortandy and Ulken Shabakty lakes). Wet periods occurred during 1950s were insufficient to restore river system in Burabay area.

3. Since 1960, the water volume fluctuation of Central Asian lakes was distinctive since the natural water balance of most lakes has been significantly modified by human intervention (Aral, Balkhash lakes). In semi-arid regions, despite high-frequency inter-annual water level fluctuations in lakes such as Chany and Balkhash, most lake levels increased after the 1970s, which were driven by an increasing trend in warm-season precipitation (Propastin, 2012). In arid regions for lakes such as the Caspian Sea and the Aral Sea, this trend was the opposite. Overall, in Central Asia, climate has become warmer (during the winter months) and wetter (during summer months) (Section 2.2).
4. Hydrological investigations over endorheic lakes located in the Burabay area are sparse, and previous water balance studies were based on short-term (2-3 years) observations during the 1950s and the 2010s.

The twentieth century was marked with an increasing precipitation trend for semi-arid regions of Central Asia, yet with a reduction of snow cover due to an increasing trend in air temperature during spring months for mid-latitudes regions of Eurasia (Brown, 2000). Atlantic sea surface anomalies and associated North Atlantic Oscillation (NAO) over central Siberia affect both surface air temperate and precipitation. The literature review shows that over the last decades, the NAO pattern has gradually changed from the most extreme and persistent negative phase from the early 1910s until the 1950s which resulted in a water level reduction in most lakes of Central Asia. However, this trend changed to the most positive phase during the late 1970s (Lioubimtseva, 2014, Robinson and Frei, 2000, Hu et al., 2017). The positive period had distinctive monsoonal signatures due to the weakening of Asian monsoon circulation (Chen, 2008), which led to increased rainfall during the warm-seasons. As a result, positive water dynamics

have been observed in most regions of Kazakhstan (except south-west regions). Severe droughts during the 1900s-1930s in Central Asia were also common in the Canadian Prairie regions and affected these lakes. These years were marked as the 'dust bowl' and resulted in considerable water level reduction. The similar conditions with a significant reduction in moisture were observed in 1961-1988 (Bonsal and Regier, 2007). Consequently, the drought events occurring over the specified periods were not general for Central Asia but may signify anomalies in cyclonic activities prevailing at this latitude (50°N).

Previous short-term water balance studies (3-4 years) have established the main drivers of water circulation for Burabay lakes. The water balance components are common for most of the endorheic lakes in this area. The main variables of water inflow were runoff produced by snowmelt, warm-season precipitation on the lakes surface and groundwater recharge. The outflow variables were open water evaporation and water abstraction (KazHydroMet, 2014). However, these studies were inadequate to explain a long-term water reduction in Burabay lakes.

Future climate models suggest that air temperature will increase up to 4°C by 2080 for the northern regions, affecting cold seasons more significantly. Warming will be common across the entire region, yet for Northern Kazakhstan, a more considerable air temperature increase to 5-8°C is predicted during the winter months. A considerable decline of snowpack volume (Mote et al., 2005, Stewart et al., 2005b) and early snow-thaw seasons and lake ice-break-up (Adam and Hamlet, 2009, Stewart et al., 2005b) are predicted by 2100 in the Northern Hemisphere, with the greater magnitude of change in mid-latitude Eurasian regions (Brown, 2010). Future cold and warm precipitation distribution show controversial patterns. Barnett (2005) findings showed a general decreasing tendency in snow proportion. Propastin (2012) and Matsuyama and Kezer (2009) indicate that winter precipitation will significantly reduce for semi-arid areas and rainfall will be driving force for positive water balance dynamics. By contrast, Manning (2013) and Christensen (2007) findings confirm the overall pluvial

tendency by increasing the proportion of both warm and cold seasons precipitation in the 21st century, yet by increasing proportion of snow precipitation.

Topographical heterogeneity of the region creates spatial variability in precipitation trends throughout the area. Future projections of precipitation show high discrepancies for the Central Asian region due to the sparse climate observations as well as regional topography, land use etc. Positive water balance dynamics remain for semi-arid lakes in the 21st century, while further aridization for lakes in the arid regions is likely to occur.

Chapter 2 Literature Review Part II

According to UNESCO (1979), half of the globe is already facing aridity. Endorheic lakes which serve as a scattered but valuable source of fresh water for the environment and human welfare have fluctuated historically in response to changing climate as well as anthropogenic impact (Section 2.2). The dramatic water volume reduction which occurred in major Central Asian endorheic lakes has resulted in environmental problems (Lioubimtseva et al., 2005, Micklin, 1988), water problems related to transboundary water management (O'Hara, 2010), and overall water scarcity in most Central Asian countries. Future climate projections have established that climate in Central Asia is likely to become warmer and wetter. Section 2.2 shows that lake level decline of many endorheic lakes of Central Asia remain unexplained. In many cases, the major constraint in modelling hydrological processes for Central Asian lakes is to separate climatic changes from human intervention. Sparse observations and limited data availability (Biskop et al., 2012) increase the complexity of modelling water balance components. Additionally, the hydrological regime of semi-arid water basins is highly variable (Wheater et al., 2007). Therefore, the following section of the literature review will focus on the development of water balances for endorheic lakes. Specifically, the review aims to identify: i) key hydrological drivers of water balance for endorheic lakes; ii) input data requirements (parameters) needed to model them; iii) various approaches in the development of water balance models.

2.5 The water balance of endorheic lakes

There are many depressions within the continents which have no connection to the ocean. Under appropriate weather conditions, runoff water accumulates within these depressions to form endorheic lakes (Szesztay, 1974). As a result, endorheic lakes differ from exorheic lakes, in that the water level of exorheic lakes is more stable (Harris, 1994), whereas endorheic lakes' water level is highly dependent on balance between inflowing water sources and water losses. For example,

Section 2.3 showed that the water level of Burabay Lake (an exorheic lake) was largely stable, by regulating its outflow to Ulken Shabakty Lake during dry/wet periods.

The water balance of lakes is an important part of environmental studies, and lakes can provide valuable information on regional climate and ecosystem functions. Despite the difference between exorheic and endorheic lakes, Figure 2.12 demonstrates the main components of a water balance for any lake and the interdependency of inflow and outflow components.

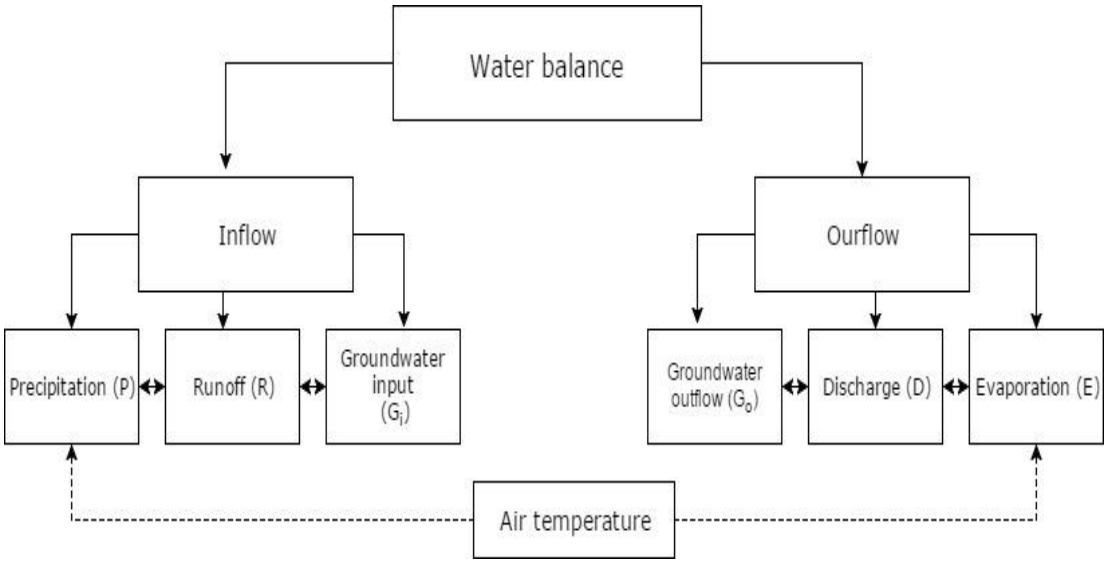

Figure 2. 12 Water balance components for any lake

The inflow and outflow relationship in water balance modelling is expressed in Equation 2.1. Based on the equation, the change of in lake storage (V) within the specified time scale (t) is explained by the difference between input and output variables per unit time (Street-Perrot and Harrison, 1985):

$$\frac{\Delta V}{t} = (P + R + G_i) - (D - E - G_o) \qquad \text{Eq.2.1}$$

where:

Input variables: P - precipitation which falls on a lake surface, R – river inflow and runoff produced in the watershed area excluding the lake surface, and G_i- groundwater inflow;

Output variables: D - discharge from the lake, E - open lake evaporation, and G_o - groundwater outflow.

Since Eq.2.1 describes any water basin, some modifications for endorheic lake systems are required. Endorheic lakes lack an outlet, i.e. D=0 and so in many long-term water balance investigations, the G_i and G_o values are simplified and estimated as groundwater flux or $G_i - G_o$ (Szesztay, 1974, Mason et al., 1994, Street-Perrot and Harris, 1985, UNESCO, 1974). So, the water balance equation for endorheic basins could be re-written as follows:

$$\frac{\Delta V}{t} = P + R - E + (G_i - G_o) \qquad \text{Eq.2.2}$$

2.5.1 Key hydrological drivers of endorheic lake water balance

Natural factors such as atmospheric circulation and regional geologic features of a catchment are common drivers of lake level changes. Numerous studies have been devoted to regional climate investigations by analysing lake level dynamics (Harris, 1994, Szesztay, 1974, Mason et al., 1985). This response is particularly marked for endorheic lakes as the water level is tightly linked to the monthly balance between input and output components.

Key variables in water balance modelling:

i) Based on the water balance equation for endorheic lakes, lake area (A_L) variation has a large impact on $\frac{\Delta V}{t}$ prediction and affects the overall accuracy of estimations. The magnitude of lake level-volume fluctuation in a specific lake area depends on the relationship between A_L and lake level-volume relationship. The fractional change in a level-volume-area relationship depends on the basin shape and lake bathymetry (Mason et al., 1994, Huybers et al., 2016). In addition, E and P values are function of A_L and, as a result errors in estimation of A_L will in turn affect the overall accuracy of the water balance modelling. Therefore, the accurate estimation of lake area-level-volume relationship is critical for water

balance studies (Szesztay, 1974, Harris, 1994).

ii) Lake evaporation and precipitation values are a function of A_L which also have great importance for water volume changes. Based on Section 2.2 and 2.3, in most cases, lake evaporation is the major sources of output in most endorheic lakes, whereas precipitation is the major driving source of input variables. For example, excessive P will be accompanied by increased runoff and decreased open water evaporation (Szesztay, 1974). Therefore, the relationship between these variables influence how lakes levels change and can amplify lake responses

iii) Runoff is available from both rainfall and spring snow-melt. The value is derived from the lake catchment (excluding the lake surface);

iv) Surface water (SW) and groundwater interaction (GW) is another factor which needs to be established (Gilfedder et al., 2012). Specifically for arid and semi-arid lakes where the SW and GW interaction is complicated by pumping water for population needs and irrigation, surface water diversions which could significantly change the flow regimes of SW and GW (McCallum et al., 2013, Tian et al., 2015)

v) Anthropogenic impacts, e.g. inflow loss due to dam construction or water abstraction (Szesztay, 1974). Human impacts have been successfully integrated into water balance models by quantifying water abstraction or evaluating the implications of land-use change on runoff values (Petr, 1992, Micklin, 2007, Leira and Cantonati, 2008).

Based on Section 2.2 and 2.3 water level of endorheic lakes is a function of the balance between three processes: precipitation on the lake surface (P), runoff to the lake produced from the catchment (R) and evaporation from the lake surface (E). Aside from natural reasons, anthropogenic alterations of the natural water cycle components can affect the water balance equilibrium of endorheic lakes. Previous water balance studies of level decline in Central Asian lakes showed the great influence of human activity on the water balance of endorheic lakes (Section

2.1.2). Therefore, anthropogenic impacts which include land-use change, water abstraction, and inflow regulation should be integrated into a water balance model.

2.5.2 Development of a water balance model for endorheic lakes

Water balance models vary in terms of complexity, particularly with temporal resolution (annual, monthly, and daily), data requirements and parameters they require. For example, physically-based models (SWAT, MODFLOW, MIKESHE etc.) are complex regarding structure and data requirements and can be applied for obtaining accurate results for a wide range of applications. On the other hand, simple models which have a smaller range of applications show adequate results at greatly reduced cost with less data input (Jiang et al., 2007). The choice between simple and physically-based approach is primarily related to the purpose for which such models are to be applied. The selection of an appropriate model for particular hydrologic assessment, thus, is based on many criteria (Gleick, 1987), where data availability has become one of the main factors (Ng and Marsalek, 1992, Biskop et al., 2012).

Conceptual water balance models have been successfully applied for reconstruction of the hydrology of lake basins (Bracht-Flyr et al., 2013, Haghighi and Klove, 2015, Crapper et al., 1996). This approach has been widely used to model regional water balance in the past, using past lake level fluctuations recognised from the paleo record of geomorphological features or/and analysis of sediment cores (Aebly and Fritz, 2009, Street-Perrot and Harris, 1985, Kutzbach, 1980, Tarasov, 1996).

The physical characteristics of endorheic lakes predetermine the input and outputs of the water balance equation, where water level and area tend to fluctuate signifying dynamic components. Most lake modellings investigate individual lakes or small lake systems and water volume responses to changes in air temperature, precipitation fluctuations (Propastin, 2012, Shnitnikov, 1973,

Van der Kamp et al., 2008). In many water balance studies the impact of climate change on endorheic lake systems was explored by establishing E/P relationships which indicated moisture conditions in arid and semi-arid regions for different epochs (Mason et al., 1985, Mason et al., 1994, Szesztay, 1974, Shnitnikov, 1973). The relationship between water balance components has been established through long-term comparative analysis of chemical water composition and water level fluctuation (Phorsh, 1970, LaBaugh et al., 1997, Legesse et al., 2004). In addition, water balance models have been used for both long and short term hydrological studies (Thornthwaite, 1948, Mason et al., 1994, Street-Perrot and Harris, 1985, Uryvayev, 1959) as well as seasonal intra-annual lake variation (Song et al., 2014).

Water balance modelling has been used in quantification of historical global water balance components (Mather, 1969, UNESCO, 1974), Szesztay, 1974; Mather 1969; Legates and McCabe, 2005), runoff (Van der Camp et al., 2002); Blackburn et al., 1991; (Bengtsson and Malm, 1997), soil moisture and land use (Jong and Kachanoski, 1987, Van der Camp, 2013); irrigation and water abstraction (McCabe and Wolock, 1992; Pieter et al., 2013)

2.5.3 Complexity of water balance models

The water balance can be established for waterbodies of any size, but the complexity of computation depends greatly on the extent of the study. The complexity of water balance modelling of lakes tends to increase with increases in the catchment area (Chapman, 1974). This is due to the increasing complexity of accurate measurements or estimates of the variables required to estimate water balance components, such as water volume, precipitation on the lake surface, and open evaporation.

In order to solve the water balance equation, it is necessary to measure or estimate all the water balance components by utilizing independent models. Computations and estimations of water balance components inevitably involve

errors due to limitations in the various approaches applied. The discrepancy of water balance is explained as a residual term of the water balance equation and includes errors in the estimations of the water balance components, including those variables that were neglected or not taken into consideration by the particular form of the equation being utilised (Chapman, 1974). Alternatively, water balance models are used in combination with isotope analysis (Gibson et al., 2020, Gibson et al., 2016) in order to establish lake water inflow (Gibson et al., 2002), outflow and evaporation fluxes (Skrzypek et al., 2015, Gibson and Reid, 2014) based on isotope compositions.

In many studies, water balance components are not obtained by direct measurements or estimations, where a component may be predicted as a residual term in the water balance equation (Winter, 1981). It means that the term includes the balance discrepancy, and as a result, which includes the unknown components and errors.

2.6 Quantification of water balance components

A model is an idealized representation of the catchment conditions and is subject to simplifications, yet assumptions must be reasonable. In-situ measurements of each water balance component provide a complete understanding of the inflow and outflow relation, and as a result, lake storage changes. However, in reality, (i) direct measurements are often not available due to lack of observation or absence of weather stations; (ii) in some cases, observed data is incomplete, and it is difficult to reconstruct water circulation in the lake and the lake catchment (e.g. water level measurements, precipitation); (iii) the data quality is poor or unknown; (iv) direct measurements are conducted but with limited public access. The aforementioned data-limitations are common for most lakes in the Central Asian region, which in turn discourages long-term hydrological investigations. Therefore, in water balance studies, a great variety of hydrological modelling approaches which aim to estimate water budget components have been

developed. Data-intensive physical-based modelling is inapplicable in most cases due to the data scarcity. Therefore, the application of conceptual models with some simplification is the only option for modelling data-sparse study areas. There are numerous conceptual water balance models which effectively modelled water level variation in endorheic lake (Yihdego and Khalil, 2017, Dinka et al., 2014, Chiew, 2010).

Present-day research indicates the importance of remotely sensed techniques in water balance studies. This section attempts to review existing modelling methods to quantify key hydrological drivers of endorheic lake water balance (Section 2.6), as well as a possible application of remotely sensed products when data is unavailable or sparse.

2.6.1 Water volume and lake level/area/volume assessment (ΔV)

The change in lake area or volume is an important variable in water balance studies of lakes. A particular change in water volume within a certain time frame gives a quantified measure of the inflow and outflow relation described by the water balance equation (Section 2.5). The estimation of lake volume requires measured water levels and water surface area and bottom features. Traditionally, lake volume is estimated using benchmarked observations on water levels and bathymetry mapping (Table 2.3).

Lake levels records are primarily observed by a local weather station. The following variable can be measured by in-situ gauging stations installed near the lakes, weirs and sluices. In areas where these data are unavailable, it is possible to use satellite products with an accuracy of 10cm.

Lake bathymetry. The contemporary bathymetric survey establishes the underwater profile of a waterbody. The objective of this survey is to gain a quantitative analysis of the depth and determine the physical properties of the bottom features. The data is used to create a bathymetric map and calculate the water volume of a lake. Based on the bathymetric map, it is possible to establish

the level-volume-area relationship. The total lake water volume could be estimated using one of these relationships.

In climate research, lakes have been assessed throughout monitoring changes in lake area (Harris, 1994, Mason et al., 1994, Szesztay, 1974) where bathymetry data is unavailable. By using the development of satellite products, historical lake level, and area relations have been established via remote sensing techniques. Various types of remotely sensed products may be used for surface water detection at a range of spatial and temporal resolutions. Satellite imagery has successfully been used to estimate lake surface areas (Liebe et al., 2005, Li et al., 2007, Bai et al., 2011). Furthermore, various techniques are aimed to classify and extract water basins (Song and Zheng, 2012), and specific index-based approaches are also available for water surface area estimation (McFeeters, 1996, Xu, 2006). The sensitivity analysis conducted in accuracy measurements of remotely sensed capabilities showed accuracy of 1% in the lake area and 0.1m in lake level which is less than in-situ observations over water level (Mason et al., 1991, Harris et al., 1992);

Remotely sensed techniques have been widely used to establish both long term and short-term measurements, such as seasonal variations of lake water levels (Alsdorf et al., 2001, Calmant et al., 2008, Sima and Tajrishy, 2013, Duan and Bastiaanssen, 2013). Remote sensing data has provided valuable global information on endorheic lakes for multiple lake investigation (Harris, 1994) since the late 1970s, although satellite radar altimeter products are available since the middle of the 1990s. The main advantage of remote sensing is that it offers consistent historical surface area sampling with limited resolution; for example, early products of LandSat-1 could only provide a resolution of 80m. Previous research on historical lake area mapping established that waterbody classification using Landsat 5 could provide roughly 82% of accuracy (Frazier and Page, 2000). Temporal resolution is one of the major limitations in remotely sensed lake area detection. Satellite-based sampling varies from 10 to 35 days compared with daily

in situ water level measurements. Furthermore, high-resolution altimeter databases have recently become available. For instance, ICESat (since 2003) and SENTINEL-3 (since 2016) are inapplicable for long-term historical analysis. Thus, in many lake investigations, satellite altimetry and imagery data are used in combination. For example, the Aral Sea monthly water volume variation was modelled using a digital bathymetry model and lake levels derived from TOPEX/Poseidon (Crétaux et al., 2005). Similarly, TOPEX/Poseidon altimetry derived water level data for Lake Dongting (China) was converted to water-level-storage which was estimated from remotely sensed water levels and ground-based water storage (Zhang et al., 2006). Landsat has been successfully applied to establish the water area-level-volume relationship in the Fengman Reservoir (China) using in-situ measured water levels and surface lake area (Peng et al., 2006).

Validation. In-situ measured water levels have been successfully used to validate water volume predictions estimated by the water balance model (Kite, 1981, Tetzlaff and Adams, 1983). The following method is appropriate for individual lake water balance research rather than generalised global lakes water investigation (Mason et al., 1994).

Table 2. 3 Water balance components, quantification methods and modelling approaches

Water balance component	Dependency factor	Role in water balance	Quantification	Modelling
1. Lake volume quantification (ΔV)	Geologic settings	Numerical relation between input and output variables	1.1 Lake volume: Bathymetry maps available from bathymetry survey; 1.2 Lake area: Remotely sensed products using optical and radar sensors; Index-Based approaches (NDWI) and land-use classification techniques. 1.3 Lake level: In-situ gauging stations; Satellite radar and laser altimeters (GRLM, ICESat-GLAS, RLH, SENTINEL-3)	Lake volume-level-area relationship
Input variables				
2. Precipitation falling to the lake surface (P)	Controlled by macroscale atmospheric and orographic factors (terrain)	A direct driving force for surface hydrology process, such as runoff, soil and groundwater storage and water discharge. The main importance of water balance is to establish variability and structure in precipitation pattern from time-scale. Also, it is needed space-time distribution field i.e. spatial and temporal patterns (orographic conditions)	In-situ direct measurements at the lake; Gauges near the lake; Data from weather station; Most accurate, however sparsely spread over; Ground-based satellite measurements: Satellite products based radar/radiometer system: Global Precipitation Measurement (GPM) available from 2000 to present; Satellite remote sensing. The sensors can be classified into the following categories: Visible/Infra-Red (VIS/IR) sensors on geostationary (GEO) and low Earth orbit (LEO): Griffith-Woodley, GEO operational Environment Satellite	Calculation methods can be divided into two classes: 1. Weight average of the measured values: 1.1 Arithmetic Average 1.2 Thiessen Polygons 1.3 Isohyetal 2. surface-fitting methods – measured values to estimate the precipitation at points in the area of a catchment: - Statistical: based on principle minimising estimation variances (interpolation errors) - Deterministic: based on mathematical criteria. 2.1 "eyeball" Isohyetal method 2.2 Optimal Interpolation/Kriging

			(GEOS) Precipitation Index (GPI), the Convective/Stratiform technique Passive microwave sensors on LEO satellites: Special Sensor Microwave/Imager (SSMI), TRMM, Advanced MW Scanning Radiometer for the Earth Observation System (AMSR-E); Active microwave sensors on LEO: GPM databases including NOAA, TRMM, GPM core observatory.	2.3 Conventional hypsometric 2.4 Algorithmic hypsometric
3. Runoff (Q)	Rainfall and melt intensity; Snowmelt, orographic conditions of a catchment, i.e. geomorphology;	Seasonally variable. Important to establish season in which runoff occurs and the degree to which runoff is concentrated in that season. Snow contributes proportionally more to runoff than rainfall (Lawrence, 2002). A fraction of snow and water equivalent of snow are a strong function of elevation (velocity, solar radiation) and vegetation cover (canopy interception)	3.1 Direct measurements of runoff - Point measurements using flumes, weirs, and current meters; 3.2 Snowpack measurements: In-situ measurements: snow stakes; Snow survey (most accurate); Snow pillows; Acoustic gages; Radioactive gages (remote as well); Remote measurements: airborne microwave and radar; satellites. Snowmelt measurements: lysimeters, snow pillows, gages and pans 3.3 Remotely sensed snow measurements: - LandSat and Normalized Difference Snow Index (NDSI) every 16-18 days with resolution-15-30m;	3.1 Empirical models (metric model) – consider only the information from the existing data without considering the features and processes of hydrological systems. Unit hydrograph, regression, correlation models, artificial network and fuzzy regression. 3.2 Conceptual models – represent physical elements in a catchment using semi-empirical equations and model parameters are assessed through field-data and calibration. Stanford Watershed Model IV (Crawford and Linsley, 1966), HBV model, SRM TOPMODEL

			- MODIS MOD10_L2 and MYD10_L2 every day with 500m resolution; AVHRR – every day with 1.1km; HRVIR - every 26 days 20m;	3.3 Physically based model – including the principles of physical processes. The hydrological processes of water circulation are represented by finite difference equations. SHE or MIKE SHE model, SWAT, PRSM.
Outflow fluxes				
4. Lake Evaporation (E)	Solar radiation, temperature, humidity, wind. Physical parameters: salinity, water depth, area and temperature.	Evaporation that occurs from an open water surface in the absence of advection and heat storage. Lake evaporation is computed free-water evaporation to account for the advection and heat storage effects on a lake (Lawrence, 2002)	4.1 Water balance approach Using the water balance equation. May cause uncertainty and rely on the measurement accuracy of water balance components. Provide rough calculation, yet accuracy increase as Δt increases; 4.2 Energy-balance (shortwave radiation, longwave radiation, water-advected energy, change in stored energy) for waterbodies energy can transfer: precipitation, groundwater and surface inflows, and ground-water and surface water outflows; Energy balance provides better results for the study period longer than a week, with a maximum accuracy approaching ±5% of mean evaporation (Harbeck, 1954). This approach is being considered as the best method for lake evaporation estimation for small lakes (Rosenberry et al., 1993). However, the most useful applications of the energy balance approach are combination with the mass-transfer method 4.3 Comparative method (evaporation pans) 4.4 Eddy-correlation is the most direct method of estimation; Requires high-quality instruments and most applicable for short time period estimation. 4.5 Mass-Transfer Approach (uses wind speed air vapour pressure); Useful for lake evaporation estimates during a given time period which the independent variables have been measured at a representative location. Difficult to apply this method for	
Evapotranspiration (E_{pet})	Solar radiation, temperature, humidity, wind and soil moisture.	Evapotranspiration is the loss from the soil both by evapotranspiration from the soil and by transpiration from the leaves		

			naturally heated water bodies, due to no climatic data on surface water temperatures, and which are difficult to model 4.6 Combination Approach "Standard" hydrological method for determining open lake evaporation (Lawrence, 2002) derived by Penman (1948). This method combines the energy needed to sustain evaporation and empirical description of the diffusion mechanism by which energy is removed from the surface water vapour. Performed well in comparative studies for open- lake evaporation (Winter et al., 1995). Could be applied for evaporation determining both from measured data and in the future simulation modelling (Lawrence, 2002) - Pan-Evaporation less heat-storage capacity, lacking surface and groundwater inputs and outflows, exposed to the sun and air. It was found that annual lake evaporation can probably be estimated within 10-15% by applying an annual coefficient to pan evaporation (Harbeck, 1954) 4.7 Remote sensed products: SEBAL – remotely sensed surface temperature, surface reflectivity and NDVI data and based on energy balance method; SEBS – determines physical parameters (albedo, emissivity, temperature, vegetation cover from spectral reflectance and radiance measurements; determines evaporation fraction based on energy balance; METRIC - derived from SEBAL and computes evapotranspiration values by Penman-Monteith combination equation. Accuracy between daily lysimetric observation and METRIC showed 5% (Kalma et al., 2008); ALEXI – uses low-temporal, high-spatial-resolution surface temperature and vegetation cover information from aircraft or satellite imagery (Landsat, ASTER, MODIS) to disaggregate ALEXI flux estimates obtained from high-temporal, low-spatial resolution (5-10 km) GOES data down to 30-300m;

			GLEAM- satellite-sensor product which estimates daily evaporation at a global scale with 0.25-degree spatial resolution and utilizes Priestley and Taylor evaporation model. The validation of daily values with an average correlation coefficient of R=0.84 and monthly R=0.94 ETLook – estimated evaporation and transpiration based on energy balance data derived from combined optical and passive microwave sensors; Global-PET – dataset provide high-resolution (30 arc seconds) global raster climate data which is estimated by FAO-PM (Allen, 1998) with albedo 0.23.
Groundwater flux			
5. Groundwater storage ($G_i - G_o$)	Recharge rate-climate driven, spatial distribution- Geology (Lithology, Stratigraphy, Structure) – hydraulic conductivity Topography – flow system (local, regional, intermediate) Geoology+topography produce a wide range of possible flow-net	Stable component of the hydrologic cycle. Lakes are almost always sites of ground-water discharge. Main features: Porosity-percentage of the total volume of a rock which is represented by voids; Permeability-soil features (soil texture and structure/soil moisture);	6.1 A field-oriented - approach – requires either installation of shallow piezometers in the vicinity of a lake or the application of seepage meters installed on the bottom of the lake. The method measures hydraulic conductivity and hydraulic head, and hydraulic gradient and seepage meters are used for quantitative water balance studies; 6.2 Numerical modelling – this approach is used to quantify flow between a reservoir and a groundwater system; simulation tool for analysing the response of the groundwater system response to stressors; predictive tools for future conditions simulations MODFLOW (McDonald and Harbaugh, 1988) (RES1) (Fenske et al., 1996) three-dimensional finite-difference modular groundwater flow model; GSFLOW (USGS) – coupled Groundwater and Surface-water FLOW model based on the integration of the PRMS-V and MODFLOW-2005; 6.3 Water balance approach – the most common method in estimating groundwater flux to lake volume. This method is based on quantifying the lake volume and other balance components independently, so that groundwater flux can be estimated through the water balance equation.

2.6.2 Output variables

In water balance modelling, output variables are described as the major source of water losses from lake systems. In most water balance modelling for endorheic lakes, output variables are described as follows: lake evaporation, evapotranspiration from the catchment, groundwater outflow and water abstraction.

Evaporation is the major component in the water balance of a catchment, lake or reservoir, and for some groundwater systems. This is particularly true in the endorheic lake system as their water budgets are tightly linked to climate variables, where water evaporation is a major flux.

This section of the thesis addresses background theory and models to estimate output variables for water balance modelling. Lake evaporation models will be studied comprehensively in terms of climate data requirements, modelling accuracy as well as existing approaches for determination of gaps in parameters observation.

2.6.2.1 Lake evaporation (E_o)

In most water balance studies of lakes, open water evaporation is one of the most important variables which influences water volume changes directly. Accurate representation of endorheic lake water balance can be achieved when all variables are accurately quantified. However, the estimation of open water evaporation from lakes is a difficult task.

The evaporation rate is largely controlled by the available energy and the way water vapour diffuses into the atmosphere. The available energy is a combination of the amount of heat stored in the water and the net radiation at the basin surface. The net radiation ($\mathrm{R_n}$) is the amount of energy captured by the water basin, and it has a great impact on annual evaporation losses. $\mathrm{R_n}$ is the difference between the incoming net shortwave radiation ($\mathrm{R_{nS}}$) and outgoing net longwave radiation ($\mathrm{R_{nL}}$). $\mathrm{R_{nS}}$ is the function of incoming solar radiation (($\mathrm{R_s}$) and reflection

coefficient or albedo (α).

Therefore, the surface albedo is an important variable influencing lake evaporation features. Various factors can influence albedo, such as the reflection coefficient of the lake bottom (for shallow lakes), the proportion of direct to diffuse solar radiation, and the turbidity of the water. In most cases, the value of 0.08 is suggested for open water albedo (Shuttleworth, 1993) and 0.23 for grass evapotranspiration (Allen, 1998). However, the open water albedo value may be altered, especially regarding lake depth because of the possibility of reflectance from a shallow/deep bottom (Finch and Calver, 2008).

Traditionally, evaporation losses have been calculated using meteorological records from available weather stations located within the study area. Several approaches have been developed for lake evaporation quantification with different complexity, instrument and data requirements. These methods include budget estimations (Tab.2.3, 4.1 and 4.2), comparative methods (4.3), the aerodynamic method (4.4), and mass transfer (4.5).

Evaporation pan instruments are commonly used for direct evaporation measurements from lakes. However, they have uncertainties associated with the size (10-20% error) (Gangopadhyaya et al., 1966), construction material (10% error) (Richter, 1966), insulation (15-35% error) (Neuwirth, 1973) and colour (7-17% error) (Gangopadhyaya et al., 1966) of pans. The commonly used above ground Class A pan measurements are often affected by wind and thermal regimes of lakes (Winter, 1981). Insulated evaporation pans have been improved by combining pan measurements with the energy budget equation, although it requires incoming and reflected solar radiation data.

Among evaporation estimation methods, the energy balance approach is considered to have better accuracy (error of 10% for seasonal average and 15% for monthly values) for estimating evaporation losses over longer timescales on small lakes for monthly water loss calculations (Rosenberry et al., 2007, Winter, 1981, Winter et al., 2003). This method estimates three major energy fluxes: (i)

solar and (ii) atmospheric radiation which have the largest inputs to lakes, and (iii) long-wave radiation emitted from the water surface. However, energy balance models require large input data and equipment-based measurements. Energy balance combination models (Penman, Priestley-Taylor) have been introduced to develop a lake evaporation model which provides accurate estimates as the energy balance approach (Rosenberry et al., 2007, Winter et al., 1995).

The original Penman equation (Penman, 1948), and subsequent modifications, have been widely used to calculate both potential open water evaporation and evapotranspiration produced by vegetation under various climatic conditions (Shuttleworth, 1993). This method is the most advanced resistance-based model of evaporation modelling.

$$\mathrm{E_{PEN}} = \frac{\Delta}{\Delta+\gamma} * \frac{\mathrm{R_n}}{\lambda} + \frac{\gamma}{\Delta+\gamma} * \frac{6.43\,(\mathrm{f_u})\mathrm{D}}{\lambda} \qquad \text{Eq.2.6.2.1}$$

where:

$\mathrm{E_{PEN}}$ - Potential evaporation (mm/day);

$\mathrm{R_n}$- Net radiation at the surface (MJ/m^2/d);

Δ - Gradient of the saturated vapor pressure curve (kPa/°C). A physically-based gradient of saturated vapour pressure, which is not only a function of temperature. Saturated vapour pressure is a pressure which is in equilibrium with its liquid, specifically the maximum pressure possible for water vapour at a given temperature;

γ - Psychrometric coefficient (kPa/°C). It is a site-specific constant for each location.

λ - Latent heat of vaporisation, which is the energy required for water evaporation (MJ/kg);

f_u - Wind function which is equivalent to $a_u - 0.38 + 0.54u$, where original Penman a_u=1 (m/sec).

The term $\frac{\Delta}{\Delta+\gamma} * \frac{\mathrm{R_n}}{\lambda}$ is the evaporation equivalent of the net flux density of radiant energy to the surface, the so-called the "radiation term". The second $\frac{\gamma}{\Delta+\gamma} * \frac{6.43\,(\mathrm{f_u})\mathrm{D}}{\lambda}$

term is the "aerodynamic term".

Although the Penman method eliminates the measurements of water-surface temperature, the main disadvantage of the Penman equation (Eq.2.6.2.1) is that specific instruments are required to measure net radiation and vapour pressure deficit. Direct measurements of evaporation (pan measurements) are not always available in many areas due to the expensive cost of equipment and monitoring. Thus, evaporation estimation methods based on climatic data are common and applied in many hydrological and irrigation applications (Linacre, 1993, Valiantzas, 2006). Such methods represent different empirical equations which vary from simple formulations to complex methods such as the physically-based combination method of Penman developed by Valiantzas (Valiantzas, 2013, Valiantzas, 2006) (see more in Section 4.4.1).

Rosenberry et al. (2007) compared different modelling approaches for the estimation of lake evaporation. Based on this study, Penman (1948) and Priestley-Taylor results showed accuracy close to those obtained by the accurate energy-balance approach. The Penman method was sensitive to wind speed, where results overestimated with a 10% decrease in wind speed. According to this study, the Priestley-Taylor had small standard deviations from energy balance values and a lack of seasonal bias. Lhomme (1997) studied the empirical value of the Priestley-Taylor coefficient (1.26) which is explained as "the evaporation from a horizontally uniform saturated surface". Based on this paper, this coefficient predicts that the drier a region the higher the coefficient. On the other hand, this formulation gives no support to the complementary relationship, which appears to be physically unrealistic at equilibrium condition.

Winter et al. (1995) compared 11 different methods for small lakes. The comparative analysis included mass transfer and combination methods equations validated against energy balance method for 22 months of evaporation measurements over five years. The combination method of Penman (1948), Priestley (1972) and de Bruin and Keijman (1979) results had small standard

deviations from energy balance values and a lack of seasonal bias. However, these models require measurements of heat storage which can be estimated from water-temperature profiles which are commonly unavailable in many lakes.

Satellite products for evaporation flux estimates are temporally and spatially variable due to the satellite overpass schedule and frequent cloud cover. Therefore, remote sensing products have been widely used to validate evaporation measurements or estimated values of evaporation fluxes (Xiong et al., 2010, Kalma et al., 2008). Numerous evapotranspiration models have been developed (Tab. 2.3 section 4.7) such as SEBAL (Bastiaanssen et al., 1998) and SEBS (Su, 2002), ALEXI (Anderson et al., 2004), METRIC (Allen et al., 2007), GLEAM (Miralles et al., 2010), ETLook (Bastiaanssen et al., 2012) which are based on the energy balance. Most satellite-based products estimate evapotranspiration through the determination of land surface physical parameters such as albedo, temperature, vegetation cover, land use/cover and soil parameters. The comparison analysis of remotely sensed products versus ground-based measurements of evapotranspiration shows an average root mean relative square error of 15-30% (Kalma et al., 2008).

2.6.2.2 Anthropogenic impact

Anthropogenic impacts have the potential to indirectly and directly influence water quantity and the natural water regime of a hydrological system. Previous research on endorheic lakes indicates that indirect impacts to the hydrologic cycle can result from land-use changes which include deforestation, urbanization etc. Indirect human intervention associated with deforestation has already affected seasonal runoff in Central Asian lakes (Tan et al., 2018).

Rising demand for freshwater, as well as water scarcity in arid regions, have affected water volume of endorheic lakes directly. Direct impact can result from water diversions, withdrawals and discharges, and from dams (flow regulation and water storage) and anthropogenic abstraction from surface and groundwater.

Most examples of anthropogenic water abstraction from Central Asian lakes were demonstrated in Section 2.1.2 and Section 2.2. In many cases, the direct anthropogenic impact can be evaluated by acquiring water abstraction values from local water agencies during the study period (Yapiyev et al., 2017). The indirect impact has been established by long-term evaluation of runoff inflowing to and/or infiltration losses (Micklin, 2010, Propastin, 2012).

2.6.3 Input variables

In water balance modelling, input variables are described as the major driving source of lake volume. For endorheic lakes, input variables are described as follows: direct precipitation to the lake surface, runoff produced from the catchment and groundwater inflow.

Section 2.2 showed that in most cases, the volume of endorheic lakes is tightly linked to fluctuations in annual moisture, where precipitation is the major component of the water cycle in any water basin. This section of the thesis addresses background theory and models to estimate input variables for water balance modelling. Precipitation (Section 2.6.3.1) and runoff (Section 2.6.3.2) models will be studied comprehensively in terms of climate data requirements, modelling accuracy as well as existing approaches in determination of gaps in parameters observation.

2.6.3.1 Precipitation to lake surface (P)

Precipitation falling directly onto the lake surface is measured by establishing rain gauges over the lake (Table 2.3). In order to provide accurate spatial and temporal variability of precipitation distribution, more than one rain gauge is usually required, especially over large water basins. For many endorheic lakes, especially small lakes, these measurements are lacking. This is especially true for lakes located in remote semi-arid and arid regions of Central Asia. Where direct measurements of precipitation are not available, indirect methods can be used

(Table 2.3). Gauged data from single or several available nearby locations may be transferred by interpolating the data around the lake (Table 2.3) (Wale et al., 2009).

Table 2.3 explains methods and approaches which have widely applied in estimating precipitation falling directly to the lake surface. Data obtained from the local weather stations are generally considered to provide good information on precipitation. However, some factors should be considered prior to their application. For, example, problems may arise from the relocation of weather stations from one place to another (Burnash and Farrell, 1979) or from weather stations in locations that are remote from the water surface, which can create a considerable error in rainfall estimation (Winter, 1981)

Error and associated uncertainties in sampling precipitation data are functions of rain-gauge network density, duration of precipitation and the size of the lake (Winter, 1981). Regionalized point gauge data may significantly underestimate rainfall intensity which resulted in a reduction of simulated runoff in the mid-size Walnut Gulch watershed (Arizona) (Michaud and Sorooshian, 1994). Linsley and Kohler (1951) studied an intense (55 stations) rain-gauge network installed across a 570km^2 area in Ohio and established that intensive rainfall up to 250mm has an average error of 18% based on single gauge observations, 12 % when two gauges are used and less than 3% if 18 stations are utilized. However, errors decline substantially over longer time periods relative to single-event based analyses. For example, Winter (1981) established that average sampling error could be less than 5 % for the seasonal rainfall assessment even in sparsely-gauged areas.

Remotely sensed products (Table 2.3, Section 2.4, 2.5) have been widely used in lake precipitation modelling. Satellite precipitation data such as the Tropical Rainfall Measuring Mission (TRMM) has been successfully used for water balance investigations for large lakes (Deus et al., 2013, Khan et al., 2011). For example, the TRMM combined product was validated against ground-truthed data for Manyara Lake. However, a recent paper (Guo et al., 2015) examined the spatial

error structure of eight precipitation models derived from remotely-sensed algorithms and compared with a ground-truthed database (APHRODITE) over the Central Asian region. Two years of precipitation observations were overestimated by all models (except PERSIANN) over the Aral Sea and surrounding areas. The remotely sensed models such as PERSIANN, adjusted PERSIANN, CMORPH, and TRMM have been applied for precipitation modelling in wet periods over the Caspian Sea coastal region (Katiraie-Boroujerdy et al., 2013). All three models underestimated precipitation, whereas CMORPH performed poorly for Central Asia. Remotely sensed precipitation models, exhibit great spatial and temporal variability over the Central Asian territory (Malsy et al., 2015). Moreover, seasonal analysis established inaccurate predictions of winter precipitation, especially for areas with high elevation.

In most cases, satellite-based precipitation data should be calibrated against local observations. In areas without gauges over a water surface, it is impossible to conduct a good calibration process. As a result, the associated uncertainties and errors are not well understood. Recent accuracy evaluation of satellite-derived precipitation observations has established large uncertainties in magnitude and variability at multiple time-scales (Sun et al., 2018). It was estimated that the deviation could reach up to 300mm in the calculated magnitude of annual precipitation, even among the same product groups. Moreover, the satellite precipitation dataset is limited by the short length of the record, where most of the high-resolution products provide data from 2000 (GPM, PERSIANN, CMORPH, etc.).

2.6.3.2 Surface runoff (Q)

Surface runoff can be an important contributor to the inflow of lakes in many regions. This is true in the case of endorheic lakes with no inflowing rivers, where the surface runoff is a major source of surface water contributing to lake volume (Winter, 1981). Some drainage area contributes directly to the lake independent

of the number of sub-basins draining into a lake via streams.

Runoff modelling simulates the transformation of incoming precipitation to outgoing streamflow. It also estimates losses to the atmosphere, temporary storage, lag and attenuation as water is routed by pathways over and through the ground. In many parts of the world, seasonal and short term variation in runoff is associated with rainfall variability (Q_{rain}). Yet, in areas at latitudes above 40°N, precipitation falls as snow seasonal snowpack accumulates during cold-seasons (Masuda et al., 1993). In such areas runoff depends on melting water available during the thaw season or $\mathrm{Q_{snow}}$. In case of endorheic lakes in Central Asia, seasonal runoff accounts for a major source of annual water inflow contributing to water basins (Uryvayev, 1959, Shnitnikov, 1973, Yapiyev et al., 2017). In most cases, timing of the seasonal runoff affects snowpack depth accumulated during cold-seasons and as a result amount of water inflowing to lakes through seasonal runoff.

Surface runoff produced from the watershed can be estimated by ground-based measurements of runoff after intense rainfall and/or during the snowmelt season (Table 2.3, Section 3.1). Although direct estimates are more accurate (<5% of error), these measurements are often unavailable. Furthermore, the lack or poor coverage of rain-gauges prevent accurate estimation of rainfall and snowmelt depth. For instance, poor gauge coverage (less than 50% of the total area of the catchment) was a major challenge in establishing total water inflow to Lake Tana (Wale et al., 2009) and Lake Victoria (Kizza et al., 2011) from upstream sub-catchments.

Runoff models are equations that were developed to describe runoff as a function of the various parameters used for describing watershed characteristics. These models range from simple regression and other empirical approaches (Table 2.3, Section 3.1), through to conceptually-based models (3.2) with one or more stores connected by hydrological pathways, to complex physical-based models which include equations for all hydrological processes. Most black-box models are

lumped where a lake catchment is considered as a single spatial unit. In contrast, physically-based models are distributed, where a lake catchment is disaggregated into zones or cells. Conceptual models can be either lumped or distributed.

Two major inputs are required for all runoff models, which are rainfall/snowpack records and drainage area. Besides these variables, watershed features such as soil properties, land cover and vegetation types, catchment topography, soil moisture content and groundwater characteristics are also required.

Catchment-scale response to precipitation has been widely used for simulating and predicting runoff and streamflow since the 1950s. Many hydrological models such as the conceptual Stanford Watershed Model (Crawford and Linsley, 1966), the SSARR model (Rockwood, 1964), and the USDA HL-74 model (Holtan et al., 1975) have been improved so that they can simulate most of the hydrological processes within a watershed. The following models are primarily based on a modified version of the simple water balance with two major differences. Firstly, they are dynamic models, simulating runoff with a temporal resolution ranging between days, months and years. Secondly, they take temporal changes occurring in the catchment into consideration by utilising routing coefficients and storage variables to delay the movement and storage of water within a watershed. These models include a considerable number of fitting parameters developed for storage, drainage, routing and vegetation cover. The calibration process requires in-situ records of daily discharge, evaporation, and infiltration features.

Sophisticated computer-based physical models (Table 2.3, Section 3.3) simulate runoff in a mathematically idealised representation of the real phenomena. They do not require extensive hydrological and meteorological records for calibration, but the evaluation of a large number of parameters which are used for physical characteristics of the watershed are needed (Abbott et al., 1986). Furthermore, physically-based models require a large number of data, such as soil characteristics, moisture content, and geology data. Moreover, it is not possible to modify equations embedded into these models by users, and such models

require high processing ability compared to others.

The SWAT model has been successfully used for long-term runoff prediction (Borah and Bera, 2003, Setegn et al., 2008). However, runoff estimations can be inaccurate in regions with poor rain-gauge representation in the simulated basin or sub-basin (Bouraoui et al., 2005, Cao et al., 2006). Moreover, SWAT prediction accuracy can be considerably affected by the lack of model calibration (Bosch et al., 2004), or insufficient calibration and validation periods (Muleta and Nicklow, 2005).

Runoff produced by snowmelt (Q_{snow}) is routed by the same pathways as rainfall, so snowmelt runoff models basically are rainfall-runoff models with extra routines added to store and subsequently melt precipitation that falls as snow (Ferguson, 1999). However, some extra procedures have to be included in runoff models for cold regions. Thus snowmelt models have to include the following procedure at each time-step:

- Extrapolate climate data such as the relation between temperature and precipitation to the snowpack, in order to
- Estimate snowmelt at different points;
- Integrate snowmelt over the area of the snowpack so that the total volume of new meltwater can be simulated.

Snowmelt runoff models utilise depletion of snow cover over time and derived from the snow-cover area. This is due to varying snow accumulation in various land cover types and elevation, and thus melt rate can vary where some areas transition from snow sooner than others, although any fresh snow during spring-thaw causes temporary expansion of a snowpack (Ferguson, 1999). Detailed snow accumulation, melt processes will be further explained in Section 4.3.

Ferguson (1999) compared widely applied snowmelt models with the main focus on seasonal snowmelt simulations performed by Hydrologiske Byráns Vattenbalansavdelning model (HBV) and Snowmelt Runoff Model (SRM) to conclude that simple regression models have been replaced by conceptual or

physically-based models which account for the influence of topography on snow cover and melt features. In addition, this study shows that more complex structured models do not necessarily predict runoff better. For instance, physically-based models which require a large amount of data could be affected by calibration problems due to spatial variability.

By contrast, SRM (temperature-index) and HBV (energy balance) models could perform accurate estimates, and each model can be performed in many simpler or more complex ways, depending on data availability (Ferguson, 1999). Snow-runoff modelling accuracy depends on landcover type; for example, the energy balance has better results in open (unforested) watersheds with considerable climatic variations, whereas for heavily forested watersheds the temperature-index model shows better results (Anderson, 1976). The SRM model has attracted many researchers to model snow-melt induced runoff in areas with data scarcity. The model has widely applied for seasonal snow-melt runoff estimations. For example, when the SRM was applied to a number of basins in China, including rivers in Tianshan Mountains (Ma and Cheng, 2003) and Qinghai Lake in the Tibetan Plateau (Zhang, 2014), the model performed well for snowmelt water volume quantification. (Harshburger, 2012) applied the SRM successfully to generate short-to-medium-term snowmelt predictions in three melt-dominated basins in Idaho, USA.

Unfortunately, there are no direct satellite measurements available for runoff from specific water basins, but this value can be estimated from water balance components such as precipitation, air temperature, soil moisture, water storage and evapotranspiration. These variables can be independently modelled by satellite-based products or/and using a dataset from available local weather stations.

Surface runoff estimates require catchment-based rainfall-runoff estimation and studies on runoff depth prediction in ungauged catchments. The Prediction in Ungauged Basins (PUB) initiative was set up to help improve understanding of

hydrological processes in data-sparse catchments. The PUB assists in improving the basin-scale responses of rainfall-runoff and snowmelt-induced runoff prediction. The following initiative is addressed in Hrachowitz et al. (2013) and Blöschl et al. (2013), providing a broad review of research progress and existing challenges in runoff modelling.

2.6.4 Groundwater flux

Groundwater flux is usually the most difficult water balance variable to quantify due to extensive and expensive instrument requirements. There are three main methods for lake groundwater flow evaluation: field-based (6.1), numerical (6.2) and water balance (6.3) approaches (Table 2.3). In the field-based approach, measured values have been successfully utilized with the Darcy equation to quantify groundwater recharge (Rhinaldo-Lee and Anderson, 1980) and to infer potential pathways for groundwater storage. Ground-based measurements provide reliable measurements of groundwater and solute flux (Shaw and Prepas, 1990, Belanger and Mikutel, 1985, Brock et al., 1982). However, this method is only applicable at the local scale, and previous studies have shown that extrapolation of point-based measurements of groundwater variables obtained from seepage meters to the entire lake basin will generate inaccurate estimates (Brock et al., 1982, Cherkauer and Nader, 1989). In addition, there are some uncertainties associated with geological map boundaries and water table maps (Winter, 1981). The quality and accuracy of such maps could be affected by poor quality and quantity of control points. So, in-situ groundwater quantification needs extensive instrument-based field observations to characterize groundwater flux from all hydro stratigraphic units.

The numerical approach (Table 2.3, Section 6.2) provides valuable information on the controlling parameters and processes, forcing the lake groundwater-flow system. The first application of numerical models aimed to simulate steady-state regional flow patterns in hypothetical layered aquifers (Freeze and Witherspoon,

1966, Freeze and Witherspoon, 1967). Such models have the advantage of representing three-dimensional groundwater flow in heterogeneous catchments. However, most of the early numerical modelling studies are limited to hypothetical scenarios (Winter, 1978a, Winter, 1978b, McBride and Pfannkuch, 1975). This generalization is explained by the lack of detailed ground-measured data necessary to characterise spatial and temporal variability in a lake-catchment. Such models have been successfully utilized to provide an understanding of groundwater storage under various hydrological conditions (Rhinaldo-Lee and Anderson, 1980, Anderson and Munter, 1981) in small watersheds.

Computer-based numerical models (Table 2.3, Section 6.2) have been widely used for surface and groundwater interaction simulations in various sized-watersheds (Zhou and Li, 2011). These models were developed to describe flow systems and simulate the effects of land-use change on groundwater. However, because hydrogeological data is limited for many lakes, the development of sophisticated three-dimensional models is difficult. Successful application of such models requires the availability of high-resolution time-series data and the development of a good conceptual hydrological model.

The water balance approach (Table 2.3, Section 6.3) is the most common method of evaluating the sources of nutrients and water volume entering and leaving a lake. This approach is based on a calculation of the water balance components to a lake and ignores the spatial variability of the physical components of the catchment (Crowe and Schwartz, 1985). The water balance approach has advantages over the previously mentioned approaches, as it estimates the net contribution of groundwater to the hydrologic balance of a lake with limited field data.

Alternatively, the groundwater storage in lakes can be estimated when the transient stable hydrogen and oxygen isotope composition of water are established or if the stable composition of inflowing and outflowing water is known (Craig and Gordon, 1965). In recent studies have been utilises a combination with

isotopic data to estimate annual lake water balance (Gibson et al., 2016, Gibson et al., 2020). This method is based on lake inflow, outflow and evaporation rates as well as the isotopic composition of inflow, outflow and evaporation fluxes.

Therefore, in many water balance investigations, the following assumptions are common:

1. Groundwater has an insignificant contribution to the total lake volume or is completely ignored (Mason et al., 1994, Shnitnikov, 1973);
2. Only the groundwater flux value estimated as the difference between $G_i - G_o$ (Rhinaldo-Lee and Anderson, 1980, Uryvayev, 1959);
3. Either groundwater inflow or groundwater outflow is set to zero to allow the other to be estimated (Karnauskas and Anderson, 1978, Cook et al., 1977).

The water balance method may be coupled with others, such as environmental stable isotope techniques, to identify the groundwater inflow and outflow quantitatively (Kluge et al., 2012, Gurrieri and Furniss, 2004, Nachiappan et al., 2002). However, the isotopic approach requires long-term field sampling measurements and reflects the proportional distribution among water balance components for the investigated hydrological period.

The application of remotely sensed products in groundwater modelling is limited. This is because satellites mainly capture water balance components on the surface or to a very limited depth under the ground (soil moisture content). Thus, the current application of remotely sensed data is to measure relevant surface water balance components or to support information for groundwater modelling. Satellite-driven soil moisture measurements have been widely used in groundwater models, and also can be used for runoff modelling to calibrate groundwater estimations (Sutanudjaja et al., 2014, Jackson, 2002).

2.7 Summary

The following section of the literature review aims to explore existing approaches in the water balance models for endorheic lakes. Section 2.5 explains the

development of water balance models/equations for endorheic lakes identifying key hydrological drivers (Section 2.5.1) and application of water balance models in various hydrological assessments (Section 2.5.2).

Section 2.6.2 describes evaporation methods which range from fairly accurate methods that require sophisticated instrument measurements to relatively simplified methods developed for open lake flux estimations. Many evaporation modelling approaches require large data requirements which, in most cases, are unavailable for Central Asian lakes, such as mass balance and bulk transfer methods. Combination equations are the most widely used methods for evaporation flux estimations. They are practically applicable for lake studies as they require input data available from local weather stations. Since the simplified method of combination approaches have been introduced, accurate physically-based methods have become possible for remote areas with sparse data availability.

Aside from lake evaporation, anthropogenic impact is another output variable which must be considered when modelling endorheic lakes water balance. Section 2.1.2 and 2.2 explained that bigger lakes in Central Asia have deteriorated since the 1960s when direct human intervention was the major driving force for lakes level decline.

Section 2.6.3 reviews existing methods in the quantification of input variables. Great variability in precipitation measurements and remotely sensed products involve a wide range of uncertainties. In the Central Asian region, due to the sparse gauge network, the calibration of satellite products is difficult, whereas in-situ point measurements provide reliable data for precipitation modelling for small lakes.

Runoff modelling methods have different data requirements, temporal resolution, computational routine and calibration requirements. Physically-based models require many parameters and calibration which, in most cases, are unavailable and cannot be measured routinely in endorheic lake modelling. Conceptual

distributed models can provide accurate results with lower data demands and easier calibration routines.

Finally, Section 2.6.4 explores existing methods in the estimation of groundwater flux. Groundwater flux is the most difficult water balance component to estimate, which requires extensive and expensive field measurements. In-situ groundwater level measurements provide a reliable estimation of groundwater flux, yet in most cases, these data are unavailable for public use. Numerical models require high-resolution time-series data and a good conceptual hydrological model. For areas where groundwater levels are unavailable, the water balance approach could be applied.

Chapter 3 Study area

This chapter aims to introduce the study area by giving site-specific information which is critical to understand the water cycle in this specific area. First of all, Burabay National Nature Park itself, the importance of the Park for Kazakhstan, and its uniqueness will be addressed in Section 3.1. Regional hydrology, geologic and hydrogeologic settings of the Park will be briefly described in Section 3.1.1 and Section 3.1.2 respectively. Vegetation and land cover features of the Park will be described, with a greater focus on Shortandy Lake catchment (Section 3.1.3). In addition, recent rapid tourism development in the Burabay area will be explained in Section 3.1.5.

Shortandy Lake and its catchment will be studied more comprehensively in terms of physical characteristics of the basin and hydrogeologic features (Section 3.2). It should be noted that the information available from the literature and governmental reports regarding hydrogeology and anthropogenic impact assessment is given for the entire Park. As a result, these sections address more general patterns for the entire Burabay area. Furthermore, regional climate fluctuation will be analysed using meteorological records available only from the Shortandy Lake catchment. Water balance components, such as air temperature and precipitation, will be investigated by splitting into cold and warm seasons.

3.1 Overview of Burabay National Nature Park

BNNP was established in 2000 and, supervised by the Administration of Presidential Affairs, it represents a part of a unique natural system in Northern Kazakhstan. The BNNP is located in Burabay County, 258 km away from Astana, where the county town is Shortandy with a population of roughly 50,000. The total area of the BNNP is 1295 km^2 (Figure 3.1). BNNP is a forested area with more than 800 different species of plants and 305 animal species occupy this area (Nugmanova, 2013). In Shortandy, the majority of forest area are represented by

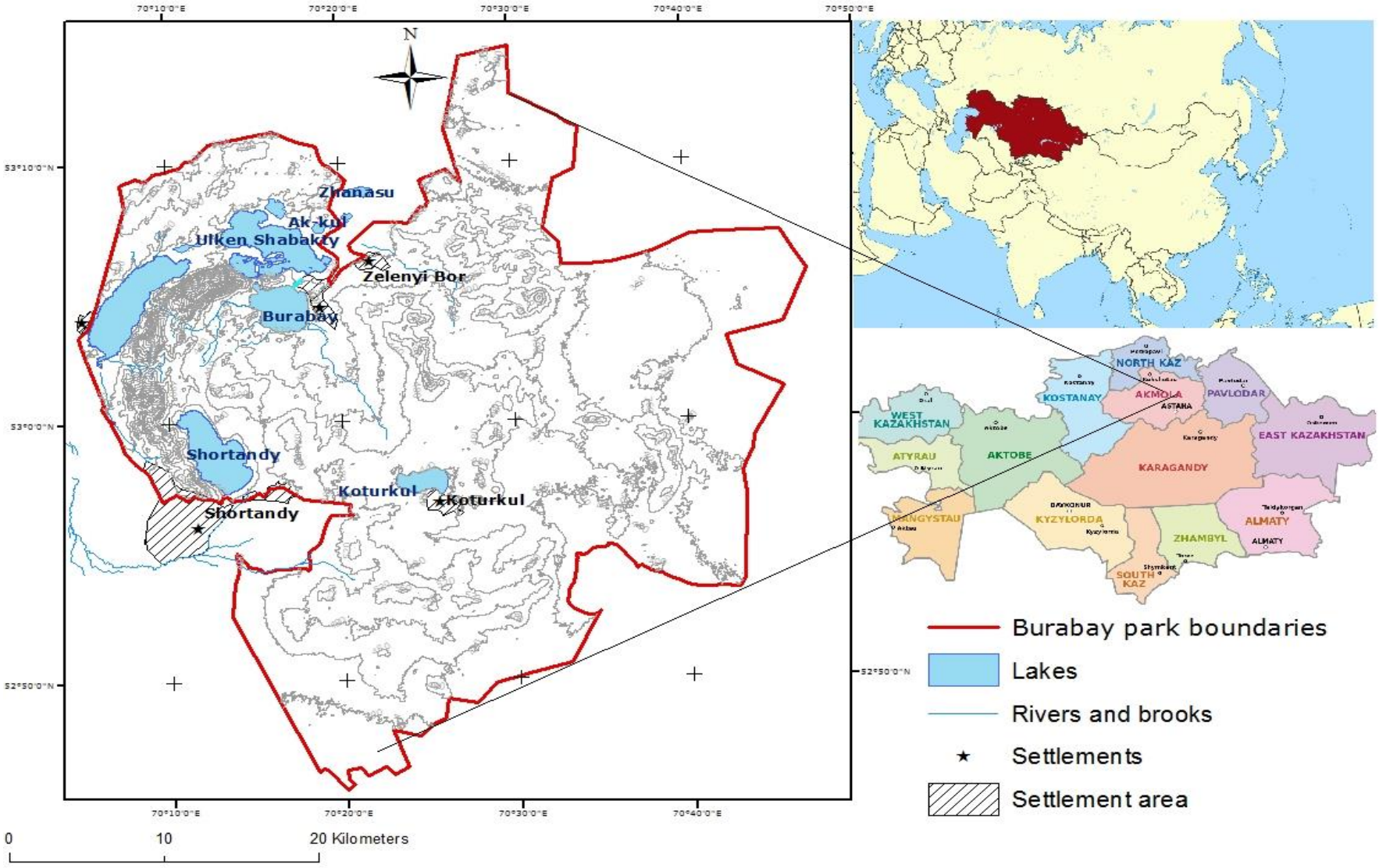

Figure 3. 1 Burabay National Nature Park boundaries, lakes and settlements

Scots pine (*Pinus sylvestris*) and mixed birch (*Betula pendula*, *B. pubescens).*

BNNP consists of several different sized water bodies distributed around the Park. Among the biggest ones are Ulken and Kishi Shabakty lakes, Kotyrkol, Zhukei, Shortandy and Burabay lakes (Table 3.1. and Figure 3.1 and 3.2). Shortandy Lake occupies nearly 17 km^2 and is one of the deepest lakes in the Park. Burabay Lake has a rounded shape, and the lake surface area is roughly 10 km^2. These two lakes are the most visited places within BNNP.

Figure 3. 2 Burabay National Nature Park

Ulken Shabakty Lake (left) and Burabay Lake (right)

3.1.1 Hydrology of BNNP

General characteristics of BNNP lakes. BNNP area consists of nearly 30 lakes in the territory of the Park including the eight biggest: Ulken Shabakty, Kishi Shabakty, Shortandy, Burabay, Zhukey, Kotyrkol, Tekekol and Maybalyk (Table 3.1. and Figure 3.3). The distribution of lakes is predetermined by local relief, and the geological structure of the area. The input part of the water balance of the lakes comprises the spring inflow of snowmelt that comes from the lake catchment

area and atmospheric precipitation. The output part of the water balance is evaporation from the lake surface as the majority of water bodies are terminal. The river network is sparse and consists only of small rivers, springs and temporary channels. Most rivers and streams are fed by melting snow during spring, and they cease during dry and prolonged summers.

The lakes have a mostly tectonic origin and are at 301-446 meters above sea level. The largest length of the lakes is 5-9 km (except Kishi Shabakty), the width is 2-5 km. BNNP lakes are relatively shallow; the average depth of most lakes does not exceed 5m; where Ulken Shabakty (14.4m) and Shortandy (13.5m) lakes are the deepest basins. Most of them, except Burabay Lake, is endorheic. Water in most BNNP lakes is fresh (Hydrocarbonate), except Maybalyk and Kishi Shabakty (Table 3.1).

Table 3. 1 Morphometric characteristics of main lakes of Burabay National Nature Park

(The source of data: [1]LANDSAT 5 and 8 imagery, August 1986 and 2016 respectively, [2]Budnikova, 2006, [3]KazHydroMet, 2007)

Lake	Catch. area (km^2)	Lake Area[1], (km^2) 1986-2016	Lake Length[2] (km)	Lake Width[2] (km)	Average depth[2] (m)	Salinity[3]
Burabay	162.4	9.4-10.2	4.6	3.2	3.2	fresh
Ulken Shabakty	160.7	20.6-18.5	8.3	5.1	14.4	fresh
Kishi Shabakty	147.7	17.5-16.9	13.7	2.6	6.3	low salinity
Shortandy	69.2	16.2-14.9	6.5	3.3	13.5	fresh
Kotyrkol	27.4	-	3.4	1.6	4.2	fresh
Zhukey	22.1	-	5.5	5.1	3.9	low salinity

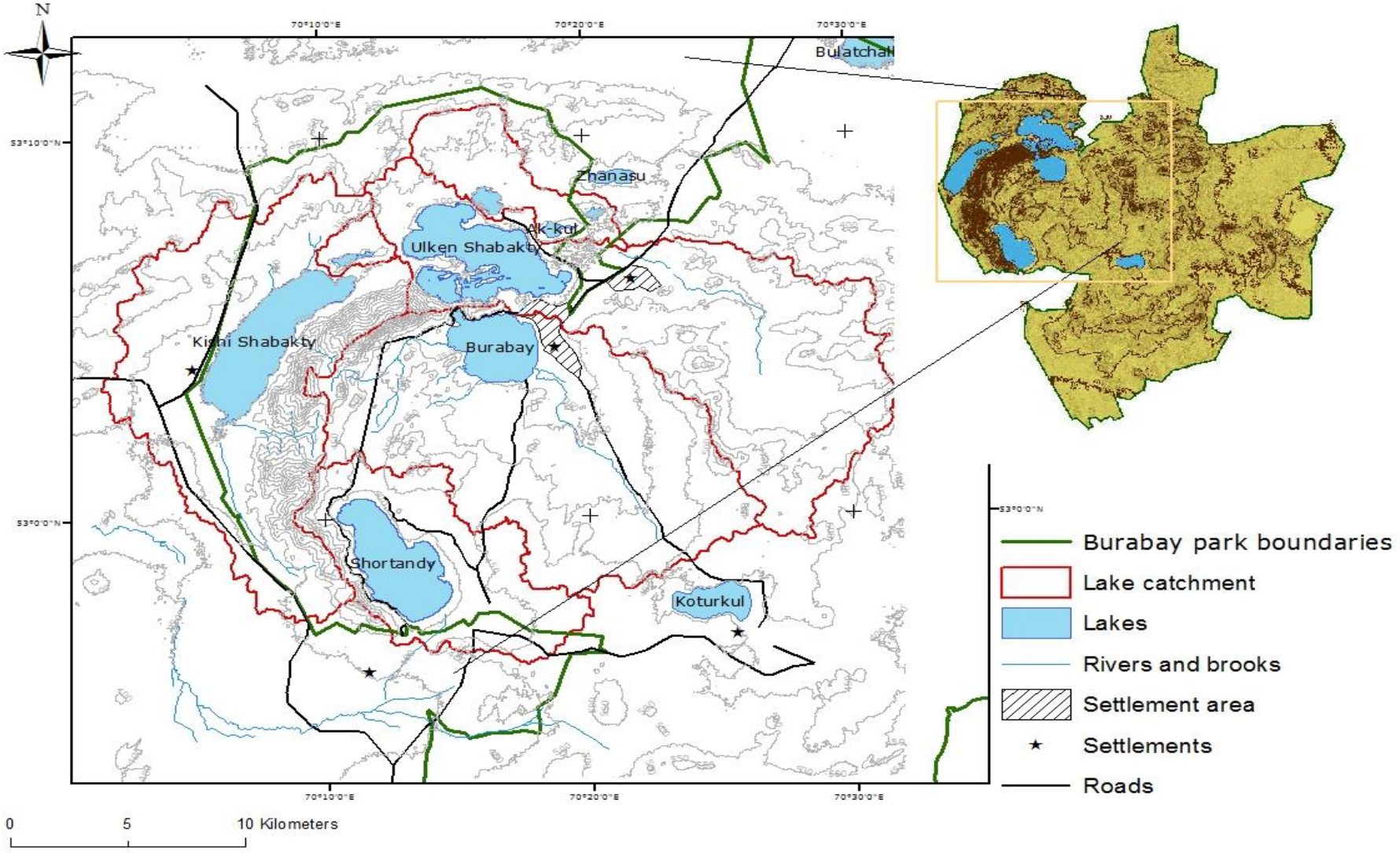

Figure 3. 3 Burabay National Nature Park and the largest lakes and lake catchment boundaries

3.1.1.1 The seasonal and intra-annual water regime of BNNP lakes

Seasonally, the lowest annual lake level is observed towards the end of the warm season (September-October), whereas the highest water level occurs after the cold season (April-May) due to the sharp influx of water from seasonal snowmelt. Most endorheic lakes in Burabay region have stable levels during cold seasons when the lakes surfaces are fully covered with ice. Yet, there are some lakes which fluctuate over this season signifying substantial groundwater inflow (Uryvayev, 1959).

Despite intra-annual water level variation, the water level regime is characterised by so-called wet/dry periods which form a multiyear level variation that is typical for Northern Kazakhstan. The lake level variation is defined by a considerable increase in water level for 1-3 years and a progressive decrease, during dry periods which sometimes results in complete drying of water bodies. Multi-year lake level variation is accompanied with the block of years with increased/decreased precipitation. According to KazHydroMet reports, during wet years with extensive precipitation, inflow could increase by 5-8 times, whereas during dry years the outflow was twice as higher than inflow (Budnikova et al., 2010).

The various lakes in the Burabay area have very different hydrological status (Figure 3.3). Section 2.3. shows that regional climate fluctuations have affected entire water regime in the Burabay area. Previous research on climate fluctuations and water level variation has established an inter-connection through surface and groundwater for Burabay, Ulken Shabakty, Kishi Shabakty and Maybalyk lakes which used to be one lake system (Section 2.3). In addition, Koturkul Lake is located slightly further away, and it is used to be a part of this hydrological system (Figure 3.3). The lake was disconnected from the Saribulak river (which inflows to Burabay Lake), although a wetland area still seems to connect the lake and the river through groundwater. Burabay Lake used to overflow into the Ulken Shabakty Lake, but its outflow is limited and regulated by a dam now.

3.1.2 Geology of BNNP

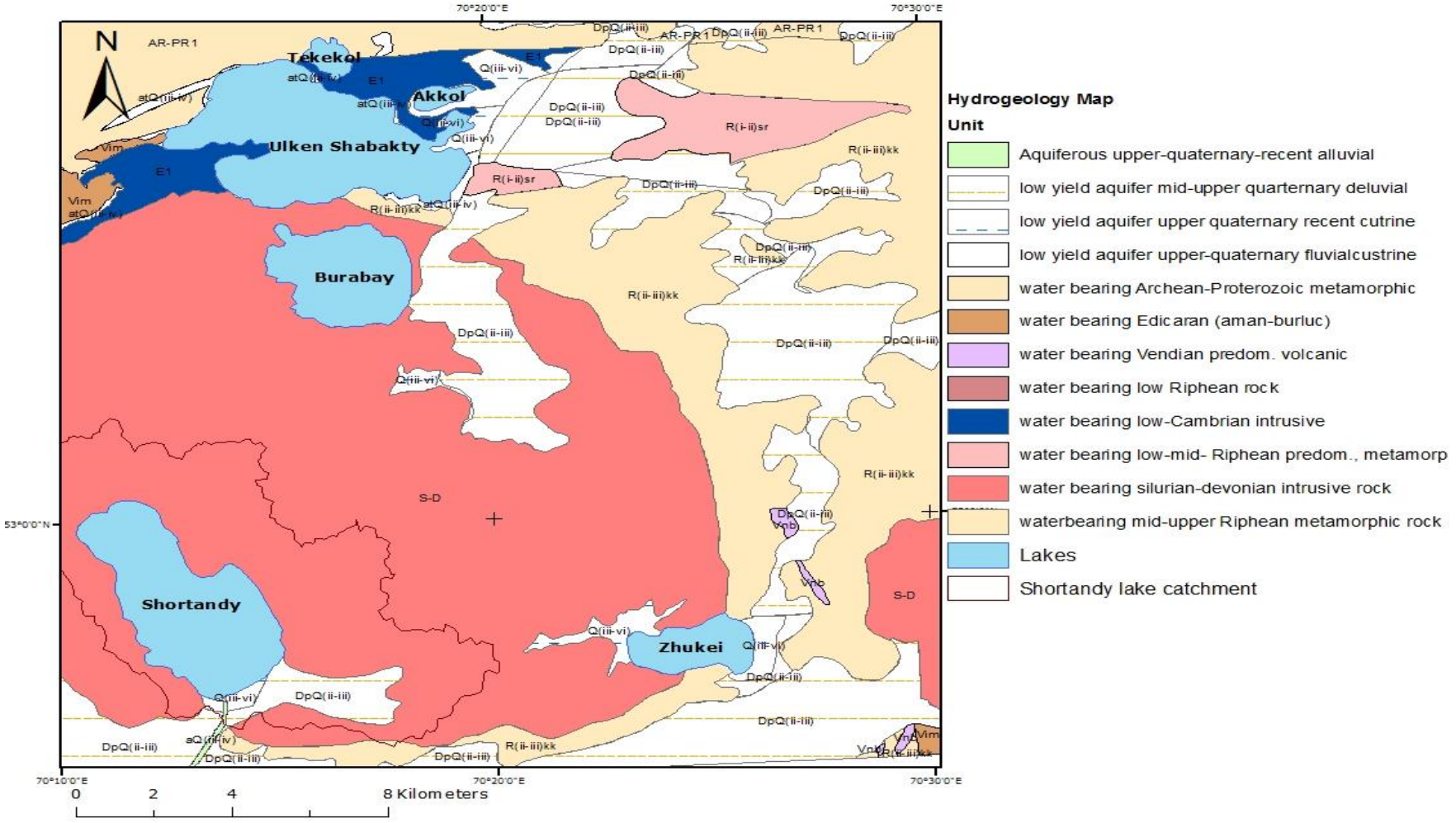

Figure 3. 4 Hydrogeology map for the BNNP

(Kirilenko, 2011)

North Kazakhstan consists of two large geomorphological structures: the West Siberian Plain in the north and the Kazakhstan Uplands in the south. The park area has terrain that is common in both kinds of structures, specifically flat steppe and forested mountains. This part of the country is characterised by erosive-tectonic and denudation highlands and mounded hills. Hilly and mountainous terrain surrounds a granite and intrusive massif that occupies the central area of the Park (Figure 3.4). An arched rocky ledge of hills, consisting of a strip about 20km long with an average width of 2.5km, extends north of the Shortandy settlement. The highest peak of the area is Kokshetau mountain, which is 947m a.s.l. towering between lakes Ulken Shabakty and Burabay (Figure 3.7). The terrain was formed during the early-middle Pleistocene, and it is believed that the formation process is ongoing due to the overall tectonic rise of the territory (KazHydroMet, 2006).

Erosive-tectonic depressions mainly occupy the west part of BNNP, and at the lowest depressions, Burabay lakes were formed. The deepest lakes, such as Ulken Shabakty and Shortandy, were formed due to tectonically lowered blocks and the intersection of fault zones. Burabay Lake has small rocky islands and peninsulas.

3.1.3 Hydrogeology of BNNP

In BNNP park, areas with an elevation of 400-600m a.s.l. have favourable conditions for groundwater formation. Predefined by hydro-geologic settings, the Park territory is the main area of groundwater recharge. Groundwater storage of the Burabay area recharges mainly through atmospheric precipitation, more specifically by snow. Due to frequent blizzards and snow redistribution, the major proportion of snow accumulates in forested areas of BNNP. In the case of Shortandy, the catchment is mainly covered by boreal forest (Section 4.5.1), where a significant amount of snow accumulates during cold-seasons, which eventually recharges groundwater storage by the end of snow-thaw seasons.

3.1.3.1 Hydrogeologic characteristics of Shortandy Lake catchment

Subsurface flow is mostly driven by snowmelt infiltration from March to May (KazHydroMet, 2007). Due to the primary recharge of groundwater by snowpack thickness accumulated during winters and the early spring period, water is usually fresh, especially in areas of fractured rocks (KazHydroMet, 2007). These zones are especially favourable for the formation of fresh fractured water.

Surrounding geologic settings are crucial for groundwater flow. Homogenous geological structure of Shortandy catchment may signify that groundwater flow to lakes is concentrated on the littoral zone (Kirilenko, 2011). The littoral zone alter the movement and processing of material flowing into the lake through surface runoff and groundwater influencing the physical and biological processes in this zone and the rest of the lake ecosystem (Peters and Lodge, 2009). Lakes lower in the landscape tend to have larger and more productive littoral zones. In the case of Shortandy, the hypsometric position of the lake catchment is located in 384m a.s.l. which is mid-elevation among Burabay lakes (Figure 3.11).

The hydrogeologic settings of Burabay lakes have a similar structure, where late Silurian Devonian intrusive rocks (S-D) are the most widespread, covering 88% of the total area of the Shortandy catchment (Figure 3.4). The geologic structure of Shortandy is represented by granites, and these deposits accumulate water for the surrounding aquifers. The vadose zone thickness is roughly 4.5-6m (Kirilenko, 2011). Water unloads along the sides of river valleys, streams and lakes.

Low yield mid-upper Quaternary diluvial deposits (DpQ(ii-iii) are located in the large valleys, which cover nearly 10% of the total area of the catchment in low-lying depressions and on the slopes. Slopes are covered by sandy loam soils and gravel, with thickness around 3-4m, whereas clays, sandy loams and sandy-gravel layers are developed on the plains (KazHydroMet, 2005). Parent soils are mostly heavy brown and loess-like loams with tertiary saline clays underneath (Uryvayev, 1959). In the mountainous areas, soils are represented by gravel and friable fragmented weathering products. The low permeability of loams contributes to surface runoff formation, but limits groundwater recharge. Lakes beds and local

groundwater have very good connectivity owing to the high permeability of the fractured zone (Kabiyev, 1997). Shallow groundwater provides water for pine forest transpiration, especially during dry summers. (KazHydroMet, 2007). The role of the upper quaternary recent alluvial material of the former river-bed (Figure 3.4) is limited due to the disconnection occurred in Shortandy Lake when the lake level dropped below the threshold of 408m (Korde, 1951). Therefore, according to Kirilenko (2011), the river-bed does not contribute to the lake volume.

Data on the hydrogeologic settings is insufficient for a full description of the hydrogeological system in Burabay area. Previous research on Burabay lakes focused on a hydrogeologic survey of the area with limited information on groundwater storage and groundwater interconnection of these lakes.

3.1.3.2 Groundwater formation and recharge

The lake catchment receives an average annual precipitation of about 335 mm[3] (Section 3.5.2). In comparison with the long-term precipitation averages, the Shortandy catchment gets more rainfall than the Burabay lake catchment (315mm[4]) and Kokshetau (300mm[5]) due to the higher hypsometric position (384m) of the catchment. This amount of precipitation generates sufficient surface runoff to feed the lake during snowmelt periods, and the permeability of intrusive rock also allows water to percolate and recharge the groundwater. Figure 3.5 shows four groundwater abstraction wells, which are penetrating the aquifer.

Groundwater levels fluctuate during seasons, where the maximum level is reached by April-June (Kirilenko, 2011). The rapid groundwater increase occurs at the beginning of the snowmelt season. For example, in 2001, the groundwater level reached the maximum level by a rapid increase to 2.8m (from 4.26m to 1.5m)

[3] Based on Schuchinsk weather station records from 1934-2006
[4] Based on Burabay weather station records from 1981-2006
[5] Based on Kokshetau weather station records from 1934-2006

between 14-30th of April (16 days) (Kirilenko, 2011). After the snowmelt season, a gradual water decline is ongoing by the end of warm-season (October) and reaches the lowest level during the winter. Although the major proportion of precipitation falls during warm seasons, the contribution to groundwater recharge is insignificant due to transpiration losses by forests and surface flow (KazHydroMet, 2007). Therefore, summer rainfall does not contribute to groundwater recharge. However, there are some years when groundwater level increases twice per year, specifically after the snowmelt season and in August during wet years (Kirilenko, 2011). The summer groundwater level increase is mainly driven by heavy rains which occur in July (Section 3.2.4).

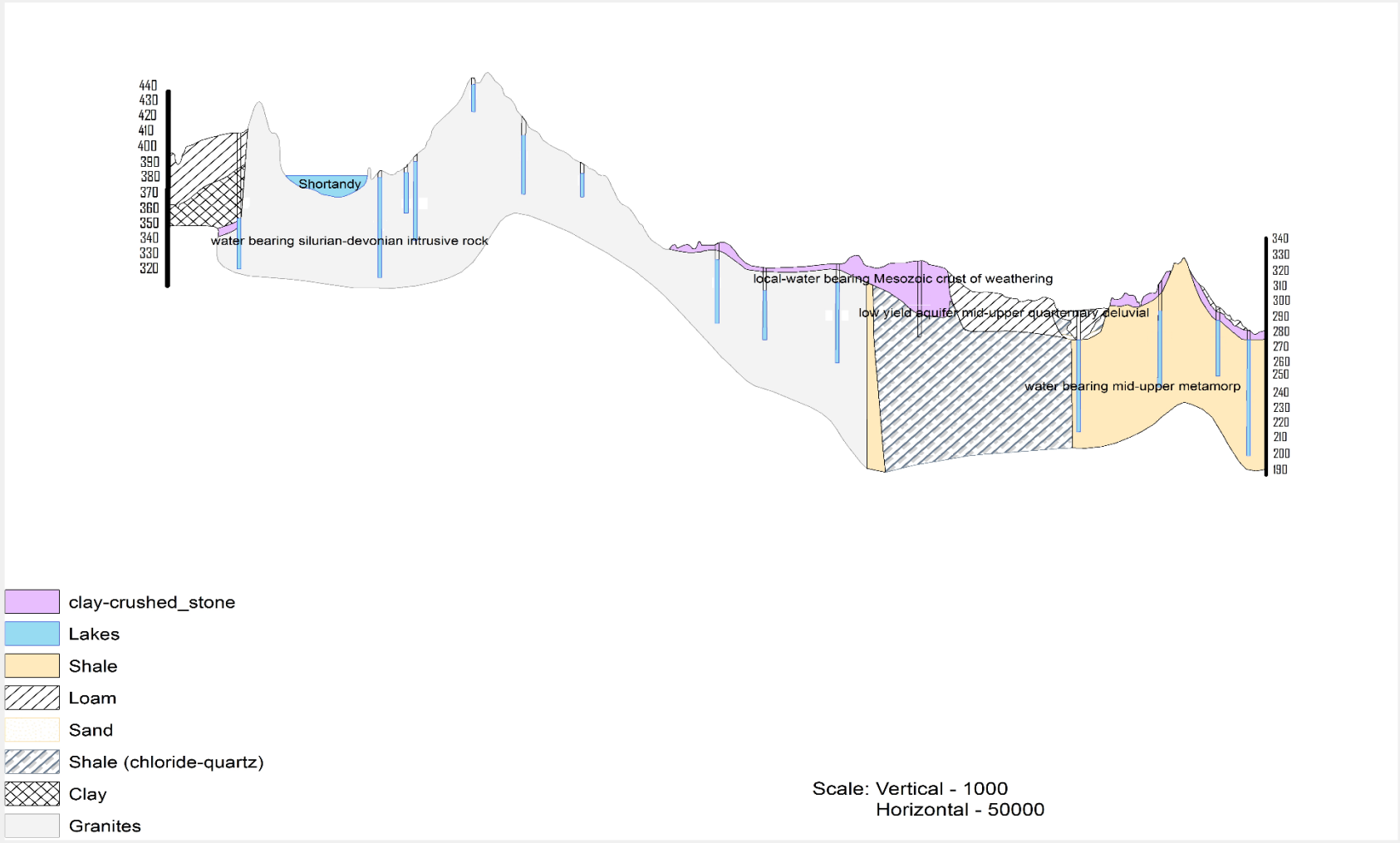

Figure 3. 5 Geologic cross-section and groundwater wells located in the Shortandy catchment

(GeoByte, 2014)

3.1.4 Land cover and vegetation

In the Burabay area, vegetation cover is mainly represented by boreal forest with the following tree species in the region: pine (65%), birch (31%), aspen (3%), various shrubs (1%) (Figure 3.6) (Nugmanova, 2013). Pine forests are mainly formed on mountains and hilly areas, while mixed forests (pine and birch) (Figure 3.6 and 3.7) are formed on quartz schists. Steppe and flat ridges along with denudation plains are equally represented with pine, birch and aspen species. Among the most forested areas are Shortandy, Burabay watersheds, where Shortandy is mostly occupied with pine forest (Figure 3.5), and the Burabay watershed is covered by pine and birch trees (Figure 3.6) (KazHydroMet, 2014). Based on historical records, the Shortandy area was occupied with almost 85% with boreal forest during the 1950s (Uryvayev, 1959). Kremenetski (1997) studies of the postglacial development of Kazakhstani forest, identified that pine forest was formed around 5200BP in this area. According to this study, there is no change in forest cover of BNNP has been detected by 1997. As a result, it was concluded that vegetation cover remained undisturbed. However, it should be noted that the following conclusion had been made before the establishment of BNNP and rapid tourism developments (Section 3.1.5). Therefore, the land cover change after the development of BNNP remain unexplored.

Figure 3. 6 Mixed forest in the Shortandy watershed during winter 2015

Figure 3. 7 Mixed forests formed in highland areas (between Burabay and Ulken Shabakty lakes)

3.1.5 Anthropogenic impacts

During the USSR epoch, human activity in the Burabay area developed in the following direction: agricultural, forestry, recreational and urban expansion. Agricultural lands with pastures mainly occupy the Kishi Shabakty and Ulken Shabakty catchments. Figure 3.2 and 3.3 shows that some of the lake catchment lying outside the National Park, *i.e.*, Kishi Shabakty and Zhanasu lakes. According to KazHydroMet, water and soil in the Kishi Shabakty catchment have been negatively affected by adjacent agricultural lands, which is not under the protection of the national park.

Burabay and Shortandy lakes were major tourist destinations, and the Shortandy settlement was the biggest in this area. The first recreational building in the Burabay Lake area was founded in 1910, whereas in Shortandy it was by 1927. The development of tourism in Burabay area was intensified by the end of the 20th century due to the increasing interest in diverse and unique natural landscapes of Burabay area. Transport accessibility and affordability of the Burabay area promoted an expansion of tourism and high demand during warm-seasons. In 1971, the government of Kazakhstan signed another agreement on further development of tourism in Burabay area allowing construction of resort and recreation facilities within the Park territory. Among these anthropogenic factors, the recreational impact has the most significant effect on the transformation of natural landscapes and ecological state of Burabay region (KazHydroMet, 2007).

According to the Agency for Statistics in Kazakhstan, it was revealed that the number of tourists in Burabay rose significantly, for example from 12,101 people in 2005 to 118,600 in 2011 (Ministry of Industry and New Technologies of the Republic of Kazakhstan, 2014). This rapid trend is explained by Burabay area development in term of tourist facilities and amenities, as well as the rapid development of the newly-formed capital city- Astana. The population growth in

Astana has accelerated the tourism growth in Burabay area over the last two decades.

There were nearly 350 recreation facilities registered within the Park by 2011 (Ministry of Industry and New Technologies of the Republic of Kazakhstan, 2014). It is clear from Table 3.2 that the number of hotels increased significantly from 2007 to 2011, where the number of hotels had been increasing to 77% annually.

Table 3. 2 Dynamics of recreational facilities in Burabay area

	2007	2008	2009	2010	2011
Hotels and resorts	26	31	50	135	166
Cafes and restaurants	28	47	314	269	189
Other	3	3	3	3	3
Total	57	81	367	407	358

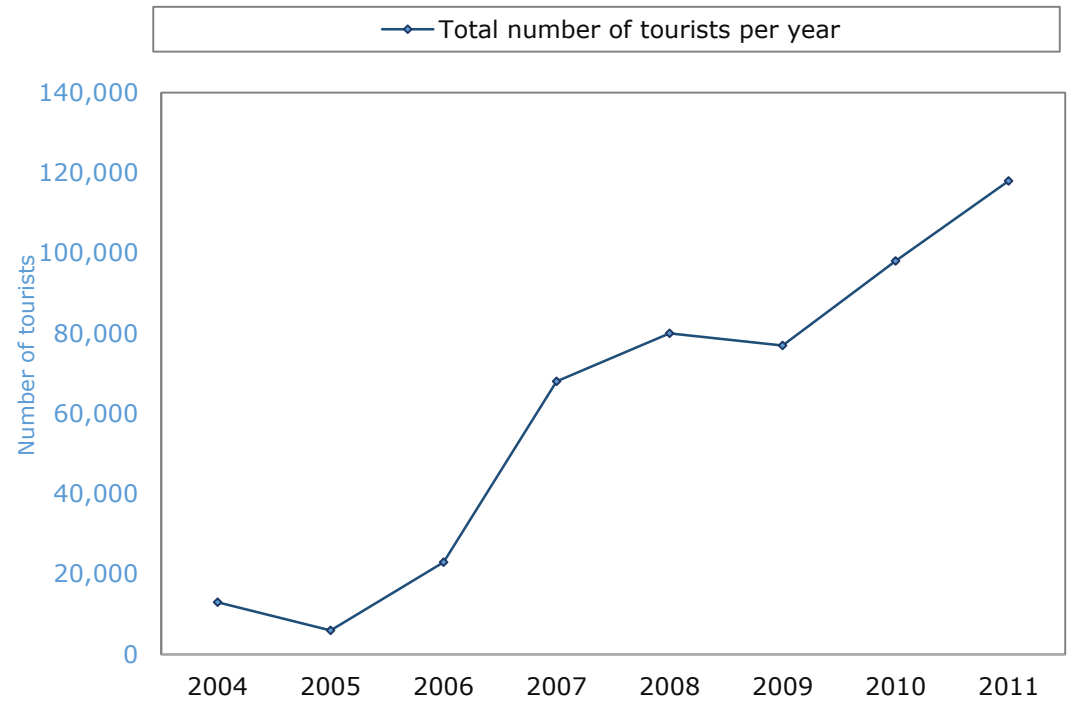

Figure 3. 8 Total number of tourists visited BNNP park from 2004-2011

(Ministry of Industry and New Technologies of the Republic of Kazakhstan, 2014)

The increasing number of recreational facilities within Burabay and Shortandy lakes have expanded visitor numbers during warm seasons (Figure 3.8). According to the authorities, the number of tourists has been increasing by 16% per year (Ministry of Industry and New Technologies of the Republic of

Kazakhstan, 2014). Figure 3.8 shows that the total quantity of visitors to the Burabay area increased considerably from 2004 to 2011. There was a noticeable increase from 2006 when the annual number of tourists increased by four times in comparison with previous years. It should be noted that the recreation development of the Park focusses around Burabay and Shortandy lakes, where most recreational facilities are distributed.

Water abstraction has been established by using pumping stations located in Shortandy, Ulken Shabakty, Kishi Shabakty, Burabay, and Katarkol lakes, where Shortandy Lake water was used with to a greater extent (Kirilenko, 2011). According to the water balance studies conducted during the 1950s (Uryvayev, 1959), the freshwater resources in these lakes were adequate to fulfil local settlement needs for water.

Since the establishment of the Park in 2000, the rapid development of Burabay area in terms of recreational facilities created a higher demand for water, especially during warm periods. The tourist activity on BNNP lakes has been higher than during the USSR period. Shortandy and Burabay settlements, as well as numerous resorts located in their watersheds, stayed without sufficient public water supply. Water supply for touristic development was fulfilled by surface and groundwater abstraction from the lakes. Subsequently, declining water levels of Shortandy and Ulken Shabakty lakes raised awareness about the future of Burabay lakes. As a result, the government has restricted water abstraction to 0.5 million m^3 per year from Shortandy Lake since 2010.

Nowadays, ground and surface water abstraction from lakes does not exceed the threshold given by the government. Furthermore, Shortandy and Burabay settlements are provided by the centralised water supply from Kokshetau (Figure 3.9). Although the accepted restriction for water abstraction, unauthorised water abstraction from the lakes remains one of the biggest issues for the Park authorities.

Figure 3. 9 Water supply construction in Burabay during summer 2019

3.2 Overview of Shortandy Lake

In order to understand water cycle in the Shortandy catchment, physical characteristics, basin hydrology and land cover change will be investigated. Regional climate settings, with the main focus on the fluctuation of water balance components from 1986 to 2016 will be further addressed.

3.2.1 Shortandy Lake and its catchment

Shortandy Lake (former name - Schuchye) (52°59′N, 70°13′E, 398m a.s.l.) catchment is hydrologically isolated from the rest of the area (Figure 3.10). It is a tectonic lake which lies at the foot of Kokshetau mountain ridge and extends north-west to south-east. The lake was formed at the beginning of the Holocene in an aeolian depression (Tarasov, 1996). The catchment area is 69.15 km^2, which has an elongated shape with a surface area is around 14.7km^2, where the lake length is 6.5km, and width is 3.3km (based on bathymetry survey conducted in

2014) (Figure 3.11).

The bottom of the lake is cone-shaped. The bottom topography of the lake has the following depth: 7% of the lake bottom is nearly 2m, from 2m to 5m - 16%, from 5m to 10m - 35%, and over 10m - 42% of the total surface area. The lake depth rises close to the lake shores from the south and west. These shores are well forested, with rock outcrops in some places, terminating almost vertically to the basin's edge. The northern and eastern shores of the catchment are flat, sandy and covered with pine forest.

The lake surface is open, without vegetation. In the central part of the lake, the sediments are represented by grey clay. The Northern and eastern shores are sandy, with gravel in the southeast (Figure 3.12). Despite the presence of sandy-gravel, from a depth of 1.0-1.5m, the lake bed is strongly silted.

Shortandy Lake is an endorheic lake. The Kylshakty River formerly drained the lake until 1920 (Kirilenko, 2011). The disconnection occurred when the lake level dropped below the threshold of 408m (Korde, 1951). However, as a result of water abstraction for the Shortandy settlement during dry periods of the 1920s (Section 2.3), the flow into Kylshakty had ceased by November 1930. According to historical records, the highest level of Shortandy was observed (not measured) in 1841, when the Shortandy settlement was founded (KazHydroMet, 2014).

Shortandy Lake level fluctuated over the 20th century, with an overall declining trend. According to water level observations, the lake level was at 397.5m with a water volume of 265 $10^6 m^3$ in 1942 and 1958 (Shnitnikov, 1942), at 395.2 m in 1961 (Kirilenko, 2011) and 391.1m in 2001 (Murtazin, 2005). Bathymetry surveys conducted in Shortandy Lake by Uryvayev (1959) and the recent bathymetry survey conducted in 2014 indicate that the maximum depth of the lake dropped from 31m to 23m from 1956 to 2013.

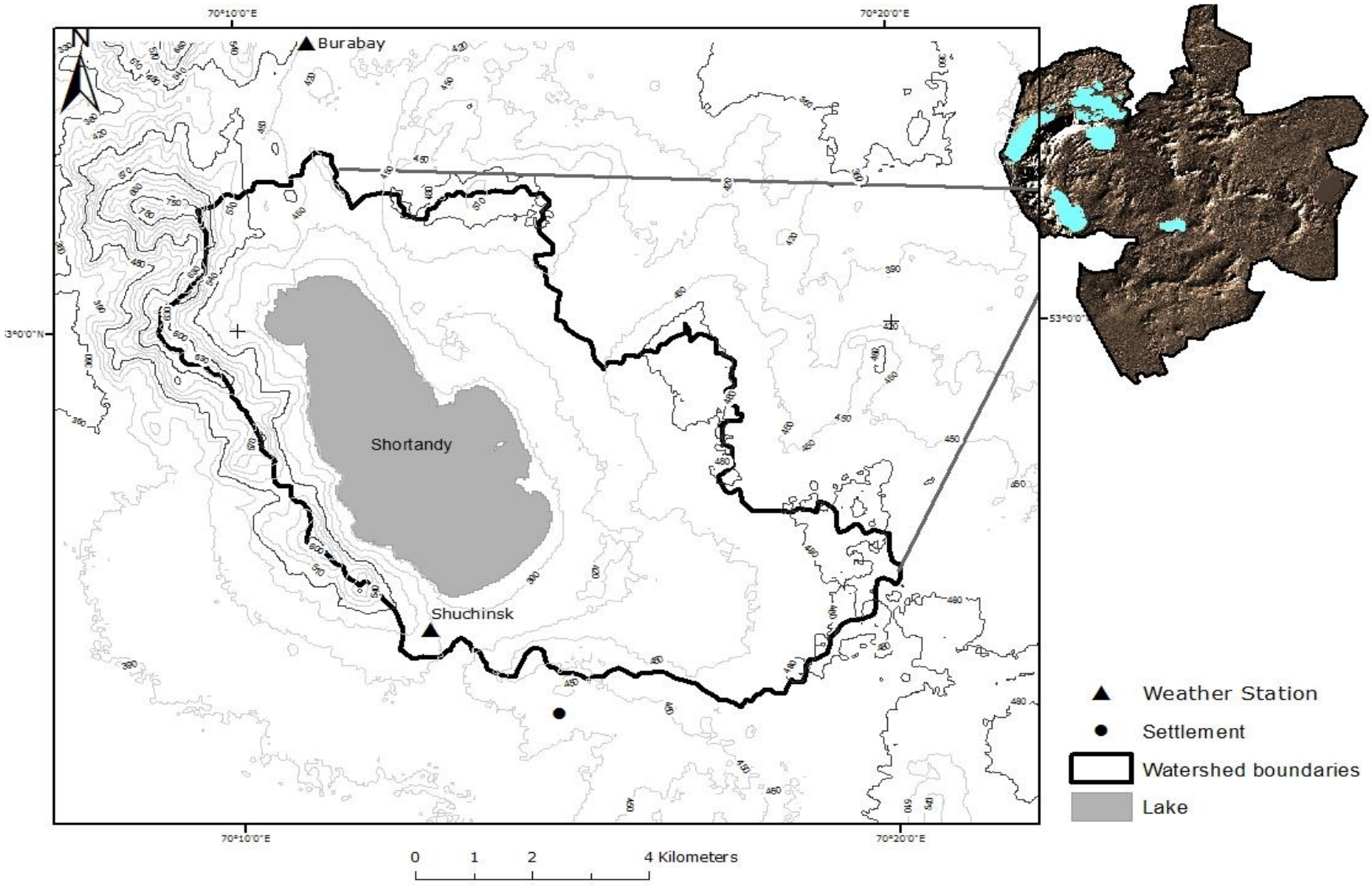

Figure 3. 10 Shortandy Lake catchment

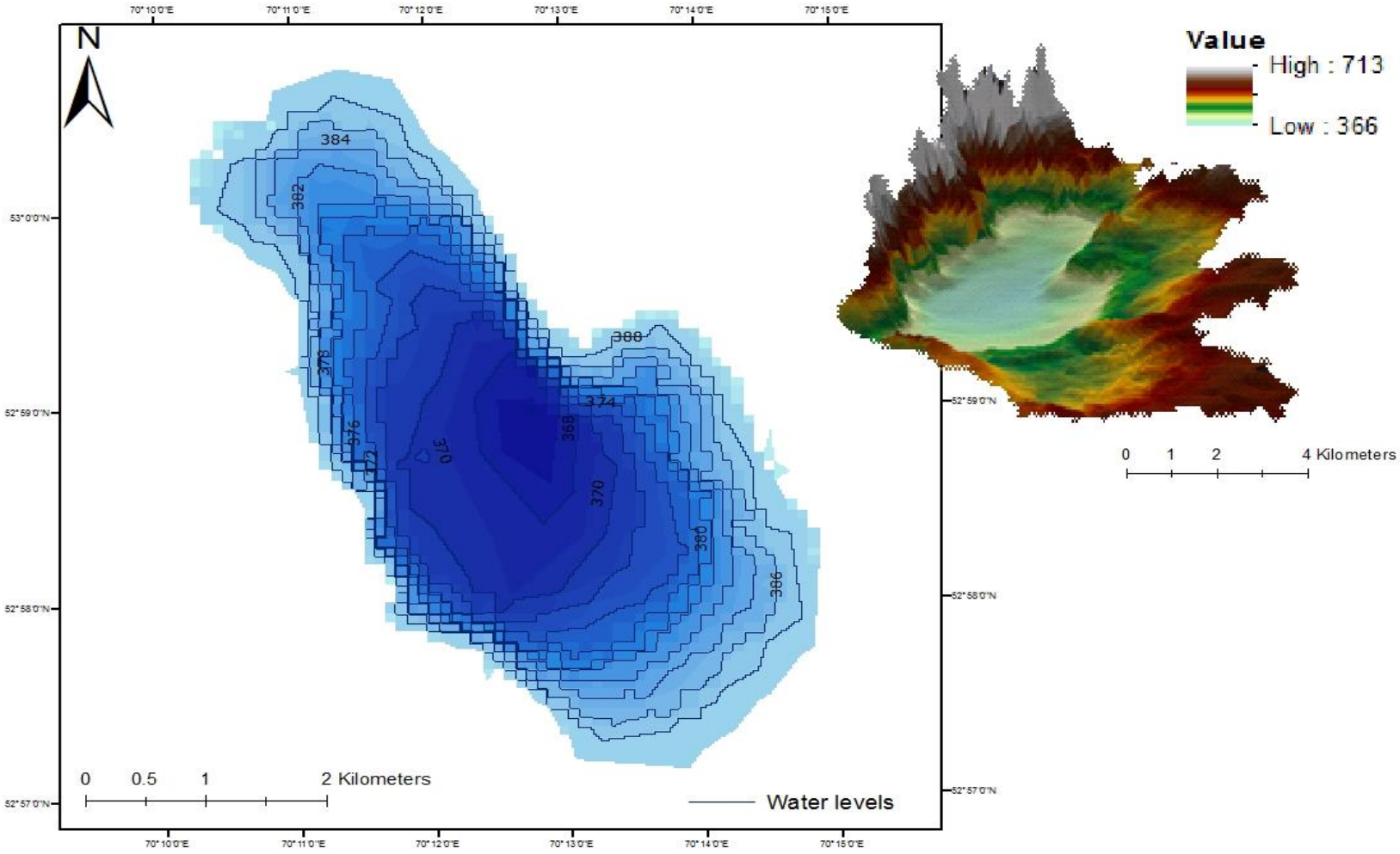

Figure 3. 11 Shortandy Lake levels and 3D map of the Shortandy catchment

where left figure shows lake depths (water level), and right figure shows catchment elevation above mean sea level

Figure 3. 12 Gravel southeast shore of Shortandy Lake

(GeoByte, 2014)

3.2.2 Regional climate

Central Asia has continental climate conditions, where the northern part of the region has the greatest deviation in the air temperature between seasons (Manning et al., 2013). In Northern Kazakhstan with a low oceanic influence, winter seasons are cold with an extensive snow cover, whereas summers are usually dry and warm. Therefore, the precipitation and air temperature regimes are largely controlled by land-surface water exchange processes, and one might expect specific rainfall patterns, with significant control by regional land-use and water management strategies (Lioubimtseva et al., 2005).

Cold seasons in Shortandy are influenced by the west Siberian anticyclone which brings steady freezing temperatures. Extensive winters (up to 6 months) in this area are associated with snowfall, snow accumulation and subsequent snowmelt during the spring. Winters are characterised by reduced solar radiation as a result of dense clouds and misty weather conditions (KazHydroMet, 2005). The winter

season typically lasts from November to March.

The warm season is controlled by a land-surface air mass that drives cyclones of arctic masses and monsoon air masses from the Atlantic Ocean. These processes have a great impact on the precipitation regime in this region. As a result of the latitudinal circulation, which brings intensification of cyclonic activity, precipitation sharply increases in this particular region, especially during the summer months. The invasion of northern air masses causes precipitation and unstable weather. Moreover, droughts events are frequent in this region. It is explained by frequent intrusions of dry air masses from Arctic and Siberia and their subsequent intense warming and drying effect. The next section of the thesis will consider cold and warm seasons separately in terms of air temperature (Section 3.2.3) and precipitation regime (Section 3.2.4) in the Shortandy area.

3.2.3 Air temperature

Shortandy area, which is located in the north of Kazakhstan, has a continental climate with different climate conditions that govern the hydrological process. In this project, the regional climate examines in terms of seasonality by dividing it to cold and warm seasons. According to KazHydroMet analysis on air temperature observation (1950-2000), the period of actively growing vegetation is around 195 days, when the temperature is higher than 0°C (Budnikova et al., 2010).

Mean annual temperature during the warmest month (July) is roughly 18.7°C, whereas the temperature during the coldest month (January) is -15.9°C (Figure 3.13). The maximum temperature ranges between +39-42°C; by contrast, the lowest temperature was -52-54°C. Annually, monthly temperature deviation is 3.8-3.9°C during the cold season, whereas it is only 1.5-1.6°C during the warm period. It shows an inter-annual variation in cold seasons and relatively stable temperature during warm seasons.

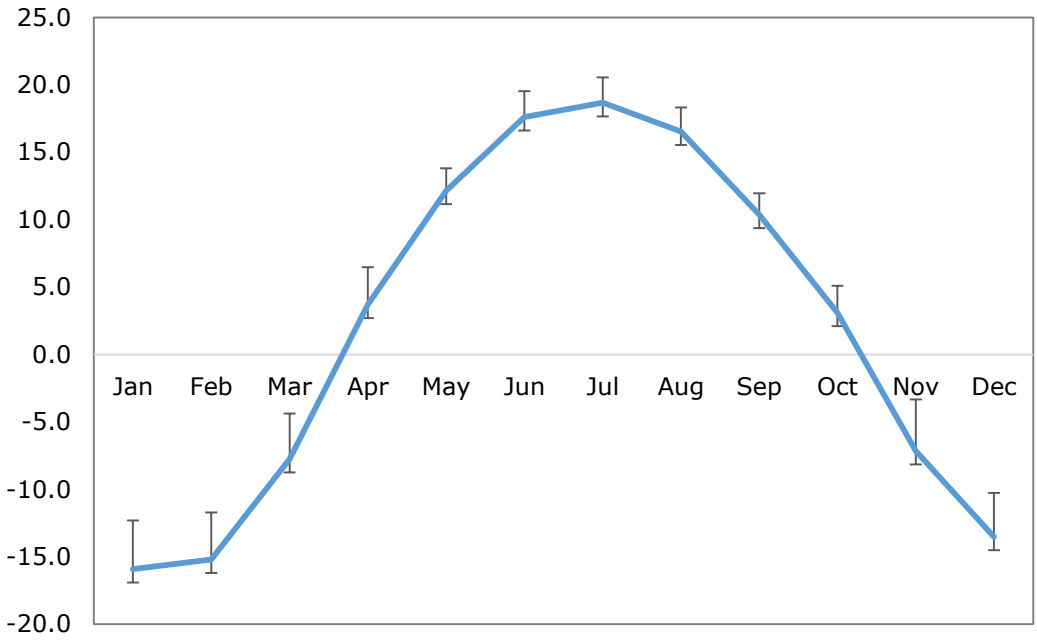

Figure 3. 13 Mean monthly air temperature variation in the Shortandy catchment

Data obtained from Schuchinsk and Kokshetau weather stations during 1986-2015, where error bars represent a standard deviation

3.2.3.1 Cold seasons

The cold season in Shortandy starts in late October and lasts until mid-April. This season is defined as a continuous season with air temperature below zero, with prolonged cloudiness (55-65%), strong winds and blizzards. Mean monthly temperature of the coldest month (January) fluctuates from -15°C to -19°C. However, air temperature is characterised by the frequent interannual variation, with discrepancies of up to ±7-8°C. For example, mean monthly air temperature of January and February during cold years could reach -22-25°C (February 1994 and January 2006 respectively), whereas in some years temperature of these months barely reaches -8°C, as in 2002 (Figure 3.14).

Despite air temperature variation, ice covers Shortandy during the cold season. According to KazHydroMet records of ice formation and decay in the Shortandy Lake catchment, the freezing-up process begins around November with full ice coverage by December (KazHydroMet, 2014). Depending on air temperature deviation from season to season, lake ice thickness ranges from 60-70cm during

warm winters (2003, 2008 2012 and 2014) and more than 1m (2003, 2004, 2011, 2012 and 2015) during cold winters.

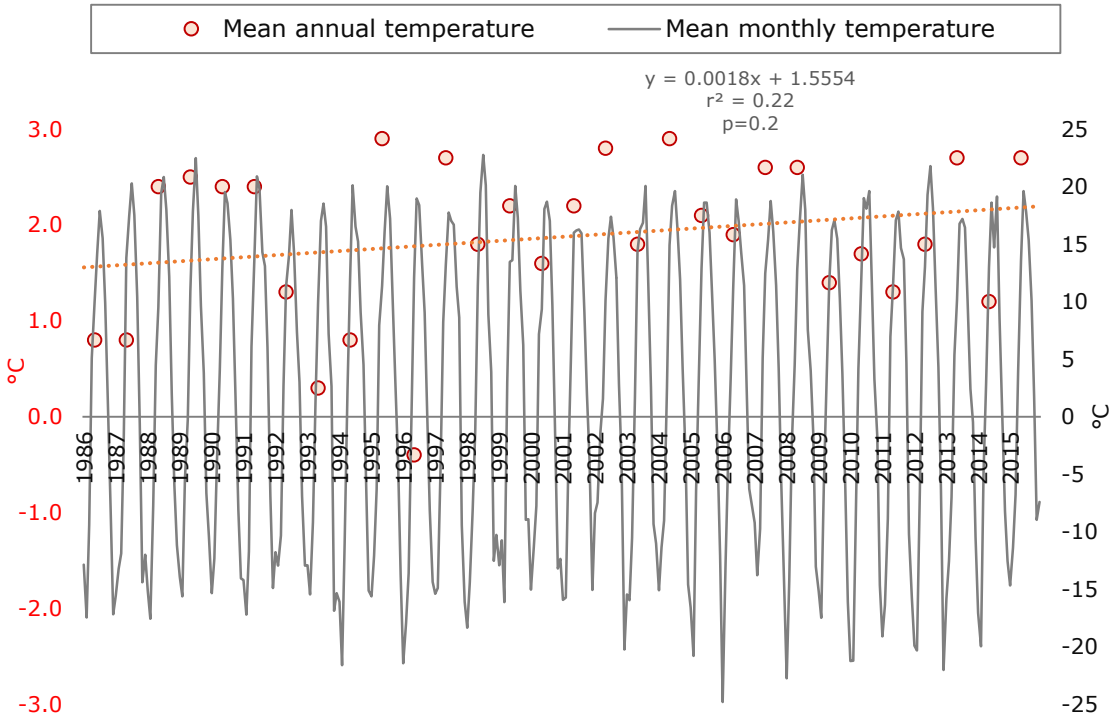

Figure 3. 14 Mean monthly temperature fluctuation and mean annual temperature in the Shortandy catchment from 1986-2016

(Based on Schuchinsk weather station)

During cold seasons, Shortandy Lake remains fully covered with ice (Figure 3.15), producing minimal losses only from snow sublimation from the lake surface. Ice break-up begins when persistent mean daily temperatures are above zero. According to historical observations, Shortandy Lake surface is released from the ice within 12 to 40 days between April and May.

The gradual seasonal transition from the warm to the cold season starts in August, and this trend becomes more pronounced from September to October, when the temperature falls to roughly 6-9°C, with a further decrease from October to November for 9-10°C. As a result, the cold season sets in the second half of October.

Figure 3. 15 Shortandy Lake ice coverage during the 31st of March 2018

3.2.3.2 Warm seasons

The warm season in Shortandy arrives around March-April, when the mean air temperature is above 0°C. In March temperature frequently fluctuates from rapid warming to freezing temperature. As a result, both snowmelt and snow accumulation can occur in this month. Mean air temperature increases rapidly and reaches 10-12°C deviation between March and April, with further increase in May to 9-10°C. By contrast, inter-annual air temperature variation during the summer period is less pronounced. According to KazHydroMet observations, the deviation in the summer month temperature is roughly +3-5°C (KazHydroMet, 2006).

Table 3.3 shows temperature analysis based on cold and warm seasons recorded in Shortandy from 1986 to 2016 (Table 3.3). Monthly temperature analysis illustrates that the upward temperature trend was more pronounced for November, March and April (+4°C, +3.5°C and +2.5°C respectively) although January was colder by -3.5°C. Interestingly, within the warm season month, the warmest month-July was colder for 2°C from 1986 to 2016.

Table 3. 3 Monthly mean air temperature analysis for cold and warm seasons months according to Schuchinsk weather station from 1986 to 2016,

where Δt is temperature variability within the study period

Cold season air temperature changes		
Month	Temperature change (1986-2016)	Δt (°C)
November	-9°C - -5°C	+4
December	-13.8°C – 13.8°C	0
January	-14.5°C - -18°C	-3.5
February	-14.9°C - -15.1°C	-0.2
March	-9.5°C - -6°C	+3.5
April	2.5°C - 5°C	+2.5
Total cold season	+1.1	
Warm season temperature changes		
May	11.8°C – 12.8°C	+1
June	17.6°C – 17.6°C	+0.2
July	19.8°C – 17.8°C	-2
August	16.1°C - 17°C	+0.9
September	10°C – 10.8°C	+0.8
October	2.9°C – 3.3°C	+0.4
Total warm season	+0.2	

3.2.4 Precipitation

3.2.4.1 Cold season precipitation

Mean winter precipitation fluctuates between 60-80 mm per season, which is about 20-30% of total annual precipitation (Figure 3.16). Snow cover establishes annually with full coverage of the catchment, during five months, reducing to 4 months over abnormally warm winters. Snow coverage and further snow accumulation start after 2-3 weeks of snow around the 5th-15th of November. Snow accumulation lasts over the entire cold season. However, strong winds in the

Burabay area result in snow redistribution from grassland to more vegetated areas (Uryvayev, 1959).

Based on the snowpack surveys conducted by KazHydroMet, snow accumulation varies in different land cover types, for example in grasslands, snow depth barely reaches 0.3-0.40m per season, whereas in forested areas snowpack depth exceeds 1.2m. According to KazHydroMet, forest-canopy controls on snow accumulation due to frequent snowstorms and blizzards (Kirilenko, 2011). During dry years, snow precipitation decreases significantly with the snowpack depth to less than 0.6m in the forested area and less than 0.2m in grasslands. Conversely, in wet years, snow depth in forests reaches 2m and roughly 0.5-0.8m in grasslands.

Snowmelt duration process varies in Shortandy as it is a function of air temperature and overall snowpack thickness accumulated over that season. First snow thaw occurs during the first or second week of March. However, in almost 45-50% of winters in Shortandy, early thaw follows with frost that sustains snow coverage and conversely leads to further snow accumulation. In most cases, full snow cover disappearance occurs by the 20th of April, but in some cases, snow cover lasts until mid-May.

3.2.4.2 Warm season precipitation

Warm seasons have the greatest proportion of total annual precipitation, where more than 70% precipitation falls as rainfall during spring and summer (Figure 3.16). The maximum values of precipitation recorded from 1986 to 2016 in Shortandy were in July 1993 and 1990 with more than 183 mm and 192mm respectively. Over these years, half of the total annual proportion fell during July month. Similar events with more than 100mm occurred in July of 1994, 1999, 2007, 2005, 2009, 2013 and 2014. Most of the effective precipitation during these years was produced as a result of a few flashflood events, i.e. due to high-intensity rainfall. For example, in the wet summer of 1990, there was roughly 40 mm and

68mm of rainfall on 9 and 25 July respectively, with a total monthly precipitation of 192mm. Nonetheless, summer months in Shortandy are generally dry.

Other warm months, such as June and August, receive 10-15% of the total annual precipitation. However, during dry years, these two months were recorded as the driest, when precipitation values barely reached 10 mm (Figure 3.16), or in some cases, i a total drought was recorded (e.g. in 1997).

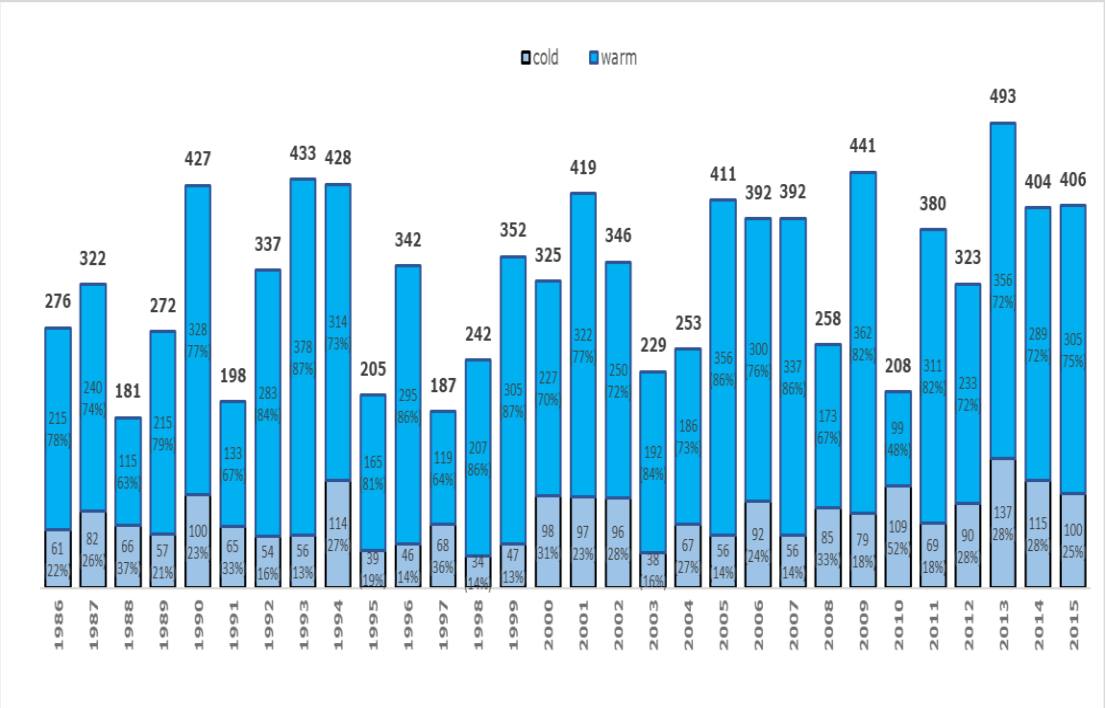

Figure 3. 16 Total annual precipitation (mm) according to cold and warm seasons from 1986 to 2016

based on the Schuchinsk weather station

3.3 Summary

This introduction to the study area reflects the uniqueness of the area, as well as the great importance of the Park in terms of socio-economic development and recreation needs of Kazakhstan (Section 3.1). This part of the thesis aimed to explain the physical characteristics of Burabay area and lakes catchment, which predetermine water balance components of these lakes. The hydrologic and hydrogeologic features of the BNNP lakes as well as groundwater storage recharge were examined.

Since the establishment of the Park, the rapid expansion in tourism was identified.

The tourist development in Shortandy and Burabay lakes has been more remarkable since the 2000s. Numerous resorts located in Shortandy and Burabay have relied on surface and groundwater abstraction from the lakes before the restriction policy came into force in 2010. The lake catchment was considered extensively in terms of the physical characteristics of the basin and hydrogeologic settings (Section 3.2.1). Regional drivers (temperature and precipitation) of Shortandy water balance were analysed for cold and warm seasons separately (Section 3.2.3 and 3.2.4).

Chapter 4 Methodology

This chapter details the methodology of a single lake model developed to understand water fluxes in Shortandy Lake. Firstly, the conceptual water balance model, which demonstrates the relationship between the lake volume with input and output variables is presented. Then, the water balance equation, which expresses the relationship between identified water balance variables, will be presented. The data requirements for the developed model will be listed in Section 4.2. After that, the GIS-based model for establishing lake area-volume-level relationship in Shortandy Lake will be explained. The hydrological models used for quantification of output and input variables will be explained in Section 4.4 and Section 4.5, respectively. Lastly, the groundwater inflow and outflow modelling approaches will be described in Section 4.6.

4.1. Conceptual water balance model

Endorheic lakes have a limited drainage basin that retains water and permits no outflow through rivers. Section 2.5 shows that input and output variables for a lake rely on the physical characteristics of the lake as well as on the local climatic, hydrologic and geologic settings of the water body and its catchment.

In this project, the first research question aims to detect characteristic changes within the water balance of Shortandy Lake from 1986 to 2016. Therefore, to understand water circulation in the Shortandy catchment, a conceptual water balance model was developed (Figure 4.1). This conceptual model was used as the fundamental point for defining the critical model components. The relationship between the model components was then specified using the mathematical expression given in Equation 4.1. *The water balance equation explains the relationship between input and output variables which predetermines volumetric response in Shortandy Lake.*

The model estimates water balance components of Shortandy Lake on a monthly basis. Here, groundwater flux expressed as $G_i - G_o$, could be a part of either input or output varying from year to year. Consequently, the water balance equation is described as follows:

$$\frac{\Delta V}{t} = \overbrace{P + Q_{rain/snow}}^{\text{Input}} - \overbrace{E_{sub} - E_O - E_{pet} - W_{abs}}^{\text{Output}} + (G_i - G_O)$$

Eq.4.1

where:

ΔV – Change in storage, million m^3;

t – Time, month;

Input variables:

P – Precipitation, (mm/month) where:

P_{snow}– Cold-season precipitation, when mean temperature is below 0;

P_{rain} – Warm-season precipitation, when mean temperature above 0.

Q_{rain} – Rainfall-runoff, mm/month;

Q_{snow} – Seasonal snowmelt runoff, mm/month;

Output variables:

E_{sub} – Snow sublimation, mm/month;

E_O – Potential open water evaporation, mm/month;

E_{act} – Actual evapotranspiration, mm/month;

W_{abs} – Water abstraction from surface and ground, mm/month;

$G_i - G_o$ – Groundwater flux, mm/month.

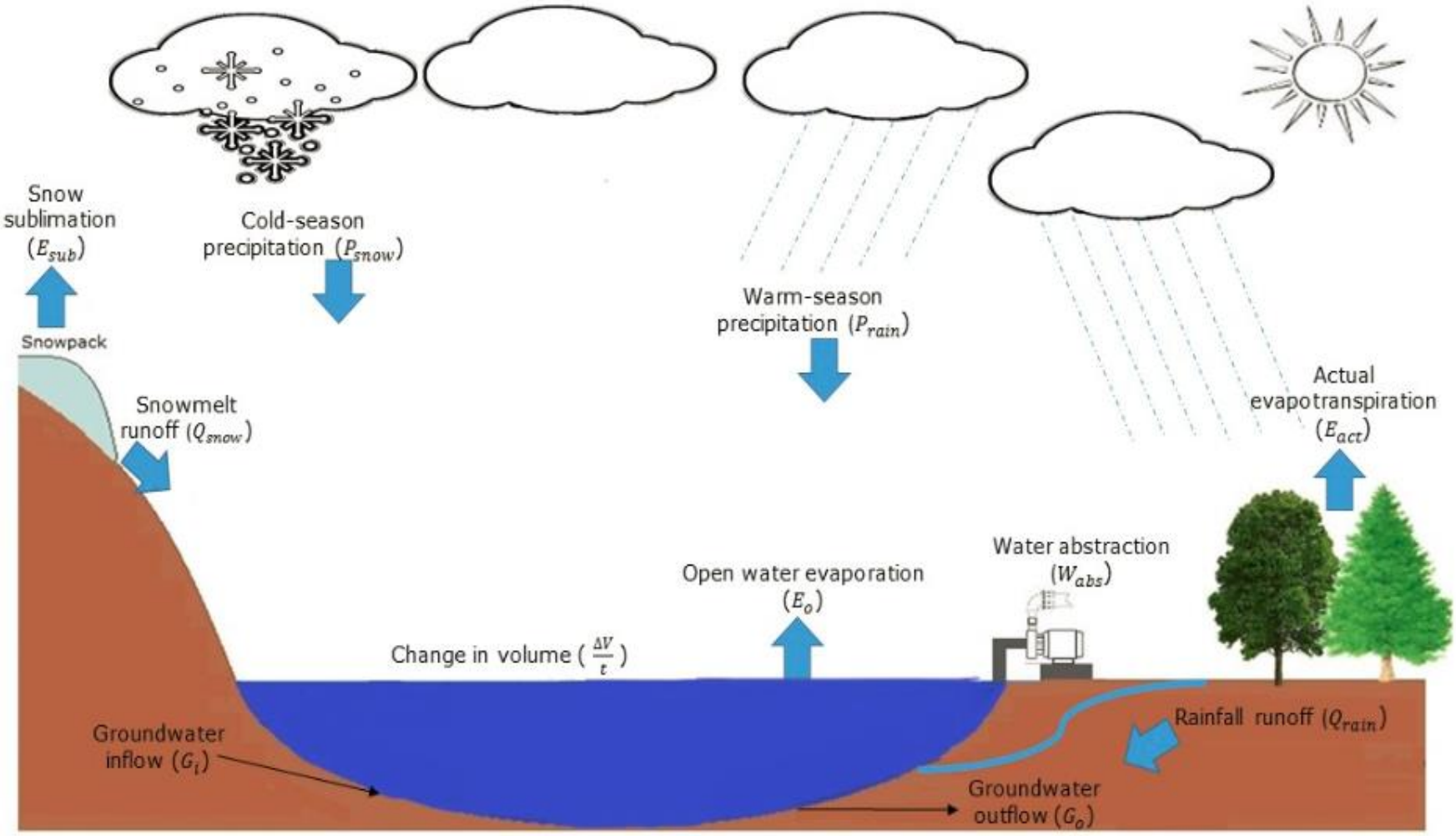

Figure 4. 1 Conceptual water balance model for Shortandy Lake

The water balance estimations were accomplished using Excel spreadsheet. Water balance components as well as modelling approaches change according to seasonality in the Shortandy catchment. The single lake model was developed in accordance with seasonal changes in Shortandy. Therefore, the modelling routine was conducted separately for warm and cold seasons (Fig. 4.2). According to the lake water balance model, monthly values of P and E are the functions of the lake area (A_L), whereas Q_{rain}, Q_{snow} and E_{act} variables depend on the lake catchment area (A_{catch}) minus A_L. Here, the historical lake area in 1986 was estimated using Landsat products, whereas further lake areas were established by GIS-based construction of a depth-volume (Section 4.3) based on the lake volume changes estimated using Equation 4.1.

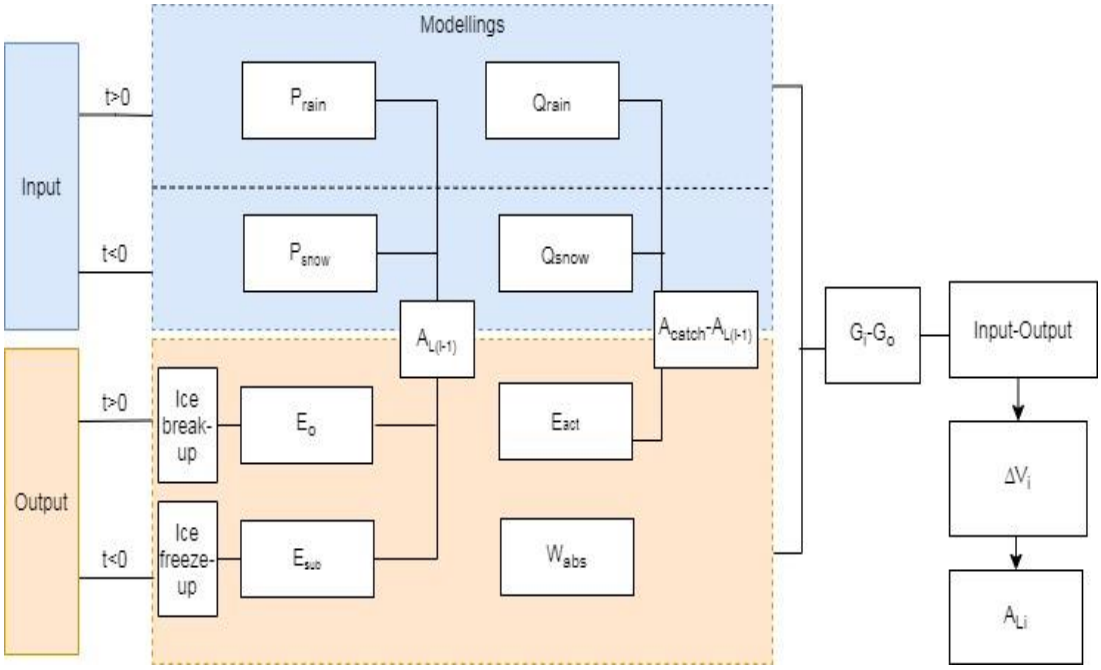

Figure 4. 2 Water balance modelling steps for warm (red) and cold (blue) seasons

where P_{rain} is warm-season precipitation, P_{snow} is cold-season precipitation, Q_{rain} is a rainfall-runoff, Q_{snow} is a snowmelt runoff and $G_i - G_o$ is a groundwater fluxon the lake surface, A_{catch} is Shortandy Lake catchment, $A_{L(i-1)}$ is lake area of the previous month, E_o is open lake evaporation, W_{abs} is water abstraction from the lake, E_{act} evapotranspiration from the catchment, E_{sub} is snow sublimation, ΔV_i is water volume change and A_{Li} is lake area corresponding to ΔV_i and t is mean air temperature

4.2 Data requirements

The literature review chapter shows that the complexity of hydrological modelling fundamentally depends on data availability. The data required for a

single lake model developed for Shortandy Lake was reflected in Table 4.1. Selected models utilise climate variables, which in most cases, are available in most weather stations. However, analysis of data requirements revealed gaps in observations.

Lake evaporation and runoff models require a large number of parameters. In the evaporation model, the required measured solar and extraterrestrial radiation was unavailable at Shortandy area. Thus, alternative equations for filling observational gaps were proposed for each model (Table 4.2). However, some parameters could not be established for the lake, such as heat storage required for the net radiation in the lake evaporation model. Thus, the model is simulated without this parameter, and associated uncertainties will be further discussed in Chapter 7. Furthermore, in some cases, the required data were obtained using remotely sensed products. For instance, Leaf Index Area (LAI) for actual evapotranspiration was estimated by MODIS, whereas the lake area was estimated by Landsat products.

Most runoff models require the following parameters: rainfall and melt intensity, orographic conditions and geomorphologic settings of a catchment and runoff coefficient from historic runoff measurements. In this project, these parameters are unknown due to the sparse observations. Therefore, these parameters for runoff modelling were obtained using empirical equations suggested by Martinec (2008). Furthermore, seasonal runoff simulations require snow cover area index (SCA) derived from a depletion curve of the snow coverage (Bavera et al., 2012, Butt and Bilal, 2011). In most research, SCA index is established using remotely sensed data such as MODIS or Landsat.

Both groundwater inflow and outflow computations require extended knowledge of porosity, hydraulic conductivity and permeability, which include an understanding of soil structure as well as soil moisture conditions. In some cases, groundwater storage is estimated by measured groundwater levels (Johansson, 1987). Yet, none of the given parameters is available for the Shortandy water

Table 4. 1 Summary of the data requirements for Shortandy water balance model

Model	Parameters and derivation	Source / climate variable	Resolution
1. Water volume change in time, $(\Delta \boldsymbol{V}/\boldsymbol{t})$	Lake bathymetry	Contour map; depth measurements	Variable
	Lake area (A_L)	Remote sensed products	Monthly
Output variables			
2. Lake evaporation, $(\boldsymbol{E_o})$ Simplified Penman equation developed by Valiantzas (2006)	Net Radiation (R_n): - Solar radiation, (R_s), - Reflection coefficient or albedo, (α), - Water temperature profile.	Measured sunshine hours (n), minimum air temperature (T_{min}), maximum air temperature (T_{max})	Daily
	The slope of the saturation, (Δ);	Minimum air temperature (T_{min}), maximum air temperature (T_{max})	Daily
	Vapour pressure deficit, (D): - Saturation vapour deficit, (e_s), - Actual vapour pressure, (e_a).	Relative humidity (RH), minimum air temperature (T_{min}), maximum air temperature (T_{max})	Daily
	Wind function, (f_u)	Wind speed measured at 2m above the surface, (u_2)	Daily
	Lake area (A_L)	Remotely sensed products	Monthly
3. Evapotranspiration from vegetation, $(\boldsymbol{E_{act}})$ FAO-56 Penman (Allen, 1998)	Air humidity: - Saturation vapour deficit, (e_s), - Actual vapour pressure, (e_a);	Minimum air temperature (T_{min}), maximum air temperature (T_{max}), dew-point temperature (T_{dew})	Daily
	Radiation: - Solar radiation, (R_s), - Extraterrestrial radiation, (R_A), - Reflection coefficient, (albedo) (α) - Relative shortwave radiation, (R_{so}), - Net radiation: - Net solar radiation, (R_{ns}), - Net longwave radiation, (R_{nl}).	Measured sunshine hours (n), minimum air temperature (T_{min}), maximum air temperature (T_{max})	Daily

	Wind speed	Wind speed measured at 2m above the surface, (u_2)	Daily
	Crop coefficient, (k_c): - LAI - Leaf Area Index, - trees height (h), -wind speed.	Minimum relative humidity, (RH_{min}), wind speed at 2m, remotely sensed product or ground-proved data (for LAI)	Monthly
	Catchment area without lake area (A_{catch})	Lake area (A_L)	Monthly
4. Water abstraction, $(\boldsymbol{W_{abs}})$	Surface water abstraction	Actual water volume intake	Monthly
	Groundwater abstraction	Actual water volume intake	Monthly
5. Snow sublimation, $(\boldsymbol{E_{sub}})$	Vapour pressure deficit, (VPD)	Mean vapour pressure deficit	Monthly
Input variables			
6. Precipitation, $(\boldsymbol{P_{snow}})(\boldsymbol{P_{rain}})$	Precipitation on lake surface	Rain gauges or weather station measurements or remotely sensed data	Monthly
	Air temperature	Mean air temperature, (T_{mean})	Monthly
	Lake area, (A_L)	GIS-based model, remotely sensed products	Monthly
7. Runoff model, $(\boldsymbol{Q_{snow}})$ $(\boldsymbol{Q_{rain}})$	Snow cover Area, (SCA)	Depletion curve of the snow coverage	Daily
	Degree-day factor, (α)	Mean air temperature (T_{mean}), snow density (ρ_{snow})	Daily
	Temperature lapse rate, (γ)	Mean air temperature, (T_{mean}), altitude	Catchment based
	The critical temperature, (t_{crit})	Mean air temperature, (T_{mean})	Daily
	Runoff coefficient, (r_{Sn})	Ratio of the measured precipitation to the measured runoff	10-day/half-season
	Time lag, (L)	Weather station altitude, hypsometric elevation zone	Catchment based

	Recession coefficient, (k)	Measured historical averages	Catchment based
	Basin or zone area	Area-elevation curve	Every 500m
Groundwater flux			
8. Regional groundwater model (i), $\boldsymbol{G_i - G_o}$	Lake volume at the beginning and by the end of the cold-season	Water level/volume measurements	Daily/monthly
	Total water volume abstraction during the cold-season	Actual water volume intake	Monthly
	Water content from snowpack, (h)	Snowpack measurements	10-days/monthly
9. Water balance approach (ii), $\boldsymbol{G_i - G_o}$	Measured or computed water balance variables	Variables from Equation 4.1	Annual
	Annual water volume changes	Water level or volume measurements	Annual

balance model. Therefore, the groundwater flux is simulated by the regional model, which requires the establishment of the lake volume before and after cold-seasons. Consequently, daily lake level records were obtained from the local weather station.

4.2.1 Data introduction

The required climate data was obtained from Schuchinsk (N52°95.00' E70°21.70'') weather station at an altitude-433m a.s.l. Schuchinsk weather station has operated since 1935 and has long-term climate records. The weather station is located on the south-west coast less than 5km away from the lake (Figure 3.10). The lake catchment is relatively small (69.15km^2) and air temperature, precipitation, and relative humidity were utilised without interpolation. Moreover, the temperature lapse rate (γ) used in runoff estimation was excluded from simulations (Section 4.5.1.3.4).

In open lake evaporation and actual evapotranspiration models measured solar radiation (R_s) and extraterrestrial radiation (R_A) were derived from empirical equations. For example, R_A was estimated as a function of latitude and seasonality in the Shortandy catchment (Appendix B). Solar radiation depends on the relative sunshine duration $\frac{n}{N}$ (Appendix B), expressed as the cloudiness ratio of the atmosphere. This ratio was estimated from the actual measured sunshine hours (n), and the maximum possible duration of daylight hours. Both evaporation models require a wind speed measured at 2m above the ground surface (u_2), whereas in Schuchinsk weather station the sensor was installed at 10m height (Section 4.4.2). Therefore, the wind function was corrected empirically in accordance with the model requirements (Appendix B).

The SRM model, which is used for snowmelt runoff modelling is sensitive to the degree-day factor and snow cover area (Martinec, 2008). Snow cover maps for the deciduous forest were derived from regional snowpack measurements obtained from the snowpack measurements conducted by KazHydroMet agency.

Here, *in-situ* based snowpack measurements give more accurate temporal resolution and snow-cover distribution for small catchments in comparison with remotely sensed products (Martinec, 2008). Snow density which is required for degree-day factor, was also obtained from snow surveys conducted by KazHydroMet agency (Table 4.2).

Finally, to determine the lake volume changes every month ($\frac{\Delta V}{t}$), a GIS-based model was constructed. This model estimates the lake area-volume-level-water relationship in Shortandy using a bathymetry survey from the lake as well as the estimated lake area (Section 4.3). Daily water level records were used to estimate the lake volume changes (Section 4.3) to evaluate the performance of the lake water balance model. Moreover, the lake level measurements were utilised to estimate groundwater flux by two different approaches explained in Section 4.6

Table 4. 2 Shortandy water balance model data availability and regional climate records collected for the model

Model parameters	Data	Year	Source	Form of data	Notes
Water Balance Model					
GIS volumetric model					
Bathymetry	Lake Shortandy	2014	Field trip (Institute of Geography)	Vector	Resolution 30 m
DEM	Elevation features	2016	SRTM DEM	Raster	Resolution 30 m
Lake area detection	Lake area series	1976 1986	Landsat 1 Landsat TM	Raster	Resolution 80m Resolution 30m
Evaporation modelling					
	Temperature (T_{max}) (T_{min}), °C	1986-2016	Schuchinsk weather station	Daily time series	KazHydroMet observations
	Wind speed (u_2), m/s	1986-2016	Schuchinsk weather station	Daily time series	KazHydroMet observations
Solar Radiation	Measured bright sunshine hours (n), hours	1986-2016	Schuchinsk weather station	Daily time series	KazHydroMet observations
	Relative humidity RH, %	1986-2016	Schuchinsk weather station	Daily time series	KazHydroMet observations
Snow sublimation	Humidity deficit, (HD), g/m	1986-2016	Schuchinsk weather station	Daily time series	KazHydroMet observations
Snow Runoff Modelling					

	Precipitation, mm	1986-2016	Schuchinsk weather station	Daily time series	KazHydroMet observations
SCA	Land use classification	1986-2009; 2010-2016	LandSat	Raster	Resolution 30 m
Degree-day factor	Mean temperature, °C	1986-2016	Schuchinsk weather station	Daily time series	KazHydroMet observations
SWE (Snow Water Equivalent)	Snowpack measurements	1986-2016	KazHydroMet reports	10 days/month	Snow measurement has been done for forested and grass areas separately;
	Snow density	1986-2016	KazHydroMet reports	10 days/month	
Groundwater modelling					
Snow depth	Snowpack measurements	2002-2016	Schuchinsk weather station	Ten days per month	Snowpack measurements, which was formed on the lake surface
	Water levels	2003-2016	KazHydroMet reports	Daily	
Water abstraction					
Water abstraction	Surface and groundwater abstraction, m^3	1986-2014	Astana Su Arnasy	Monthly averages	
Ice freeze-up and break-up model					
	Observed date of lake freezing and ice break-up	1986-2002 and 2003-2016	Schuchinsk weather station	Daily	
30-day running average	Mean temperature, °C	2006-2099		Daily time series	Based on climate scenarios and models

Validation					
	Water levels (Shortandy)	2003-2016	KazHydroMet reports	Daily	

4.3 Quantifying lake volume ($\frac{\Delta V}{t}$)

A bathymetric survey in Shortandy Lake was conducted during the 1950s and then in 2014 (Chapter 2). However, the long-term water volume dynamics of the lake remain unidentified. Therefore, the water volume dynamics for Shortandy Lake from 1986 to 2016 with a monthly time step was established. GIS-based construction of the depth-volume relationship was performed to achieve this.

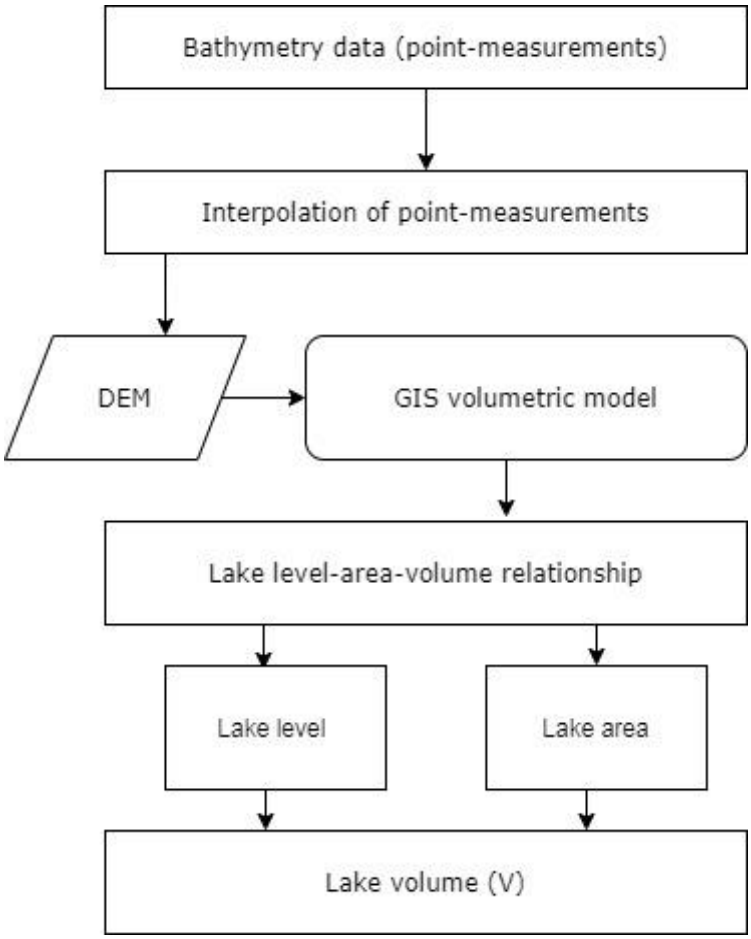

Figure 4. 3 A schematic flow chart representing the derivation of GIS-based water level-area-volume relationship of Shortandy Lake

where DEM is digital elevation model of the catchment

4.3.1 GIS volumetric model development

Figure 4.3 illustrates the derivation of the lake level-area-volume relationship of Shortandy Lake. The GIS volumetric model utilises a Shuttle Radar Topography Mission Digital Elevation Model (i.e. SRTM DEM) and bathymetry map of Shortandy

Lake. The lake bathymetry is based on *in-situ* measurements of the lake depths, which was collected by Nazarbayev University and the Institute of Geography (Kazakhstan) in October 2014 using a motorboat, Lowrance LNS 480 echosounder with 10cm accuracy, and single-frequency GPS Leica SR 20. The bathymetry survey for Shortandy, used 20 transverse profiles, with a total length of about 50 km, and 360 depths were measured.

4.3.2 GIS volumetric model application

After interpolation of the bathymetry data, a continuous bottom surface of Shortandy Lake was obtained. The catchment topography was simulated by the SRTM DEM product from August 2016 with a 30-meter resolution (Table 4.2). This elevation model was merged with the interpolated bathymetry map. Subsequently, a continuous digital elevation model for the whole catchment, including the bottom features of the lake was established (Figure 4.5).

Polynomial regression analysis between the lake volume and lake surface area was performed. Here, the lake volume (independent variable) and lake area (dependent variable) were modelled as 4^{th}-order polynomial in water volume and the produced regression was significant correlation (r^2=0.98, p<0.0001). GIS-based construction of the depth-volume relationship in Shortandy Lake indicates that in 1986 the lake area of 17.1 km^2 corresponded to the total lake volume of approximately 222.1x$10^6$$m^3$. The established lake area and volume are the first step in solving the water balance equation. Further monthly relation between input and output variables of the lake water balance, explained in Equation 4.1, was then transformed into an area-volume relationship using the GIS volumetric model.

Figure 4.4 shows that the relationship between the lake area and water volume is non-linear. For example, the lake bathymetry indicates that when the lake area is bigger than 12km^2 shallow areas of the lake become water-filled. Therefore in this range, any changes in the lake volume result in a considerable change in the lake

area within the given range of the lake area. In contrast, A_L<12km^2 coincides with the deepest areas of Shortandy Lake, where changes in the lake volume would result in smaller changes in the lake area. Therefore, the Shortandy Lake volume-area response is non-linear, depending on the lake level. The GIS volumetric model sensitivity and related uncertainties in estimates will be further addressed in Section 7.3.

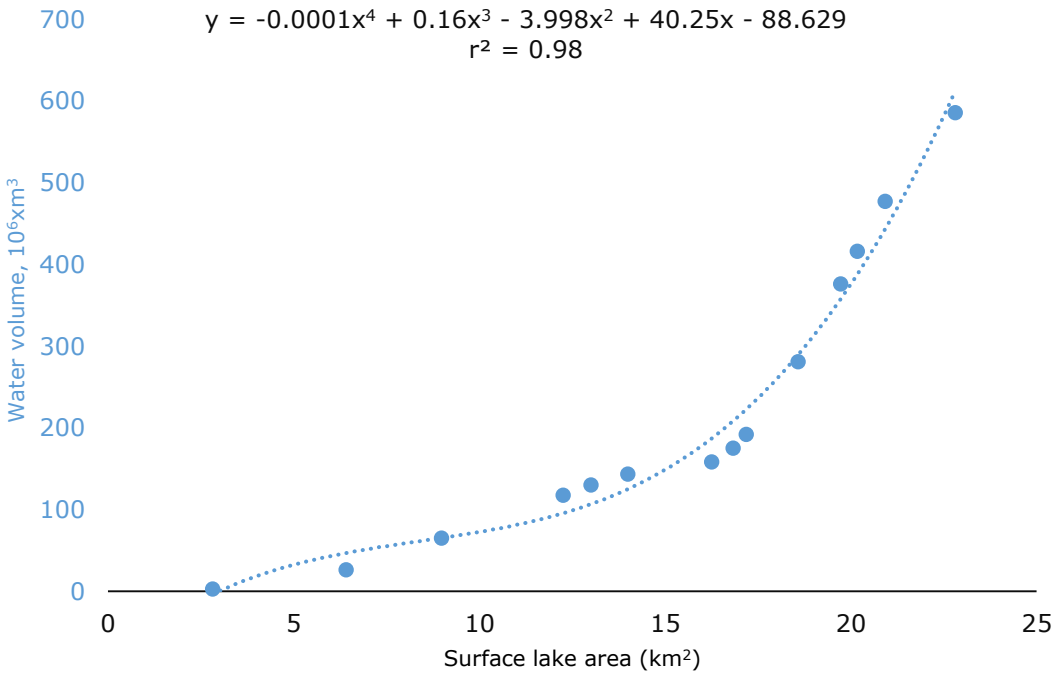

Figure 4. 4 Water volume and surface lake area relationship established for Shortandy Lake based on the IDW interpolation method

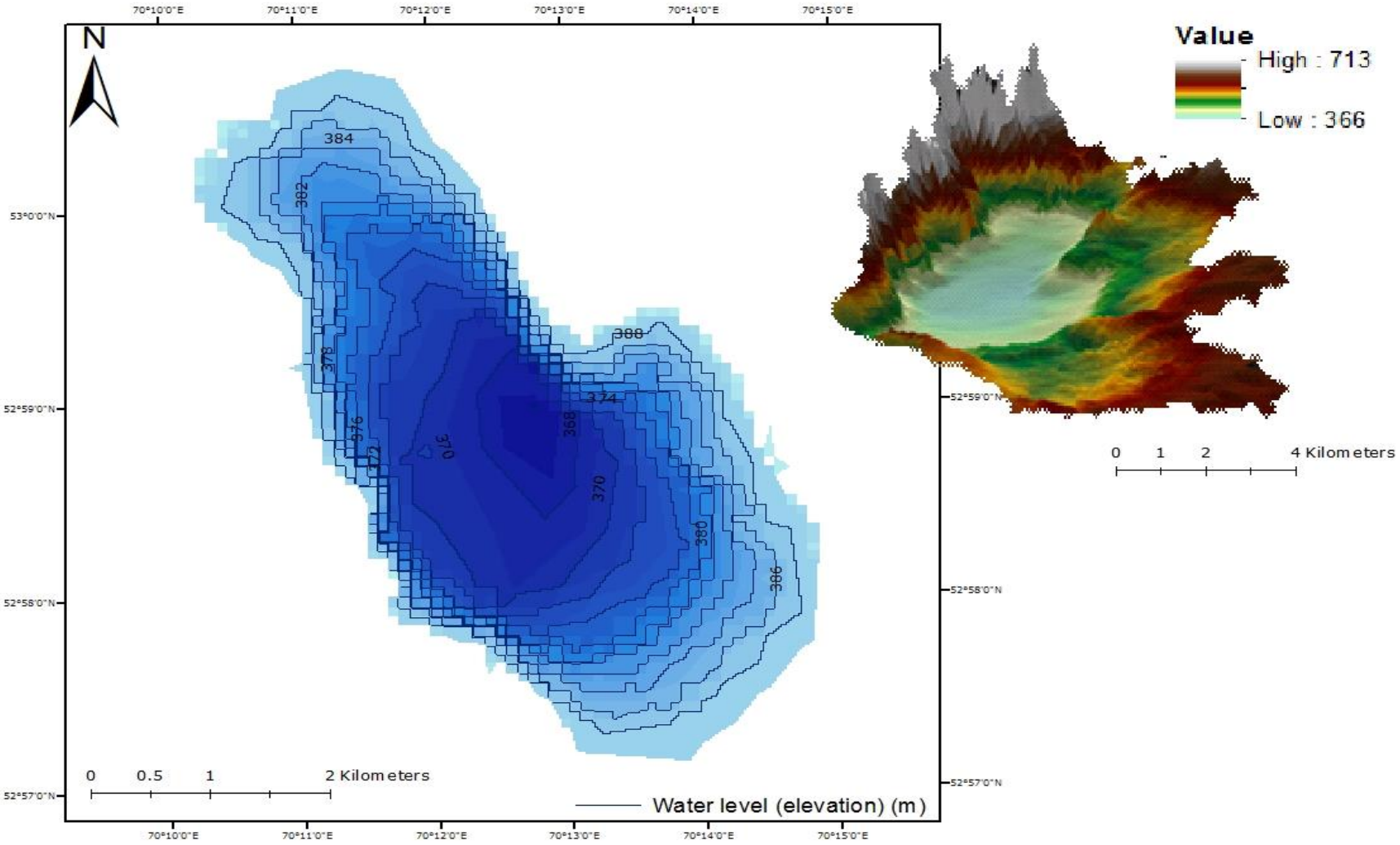

Figure 4. 5 Shortandy Lake levels and 3D map of the Shortandy catchment

where left figure shows lake depths (water level), and right figure shows catchment elevation above mean sea level

4.3.2 Interpolation of bathymetry survey data

To generate a digital elevation model of the lake bottom, it was necessary to estimate values of the deepest bottom areas where data was not collected directly. The selection of an appropriate interpolation method is crucial, as minor inaccuracies in monthly water volume estimates can generate a significant error in annual water balance estimation. Since there is no "best" extrapolation method for bathymetry data, and due to the absence of consistent findings of spatial interpolator performance (Li et al., 2005, Tan and Xu, 2014), several interpolation methods were tested and compared.

There three interpolation methods which have been widely used for topographic, bathymetric and geophysical studies (Burrough, 1986, Burrough et al., 2014, Siljeg et al., 2015, Watson, 1992, McCauley and Engel, 1997). In this study, three interpolation methods were applied using ArcMap 10.2 and then obtained results were compared. Two deterministic methods were used: Triangulated Irregular Network (TIN) and Inverse Distance Weighting (IDW), where both techniques have been applied for effective surface representation for various applications such as visualisation and visibility analysis (Mitas and Mitasova, 1999, De Floriani and Magillo, 1999). The TIN method is considered as the most straightforward and basic linear version, yet the least accurate (Franke, 1982, Nielson, 1993, Renka and Cline, 1984), which depends on the development of a triangular network based on the sample's spatial location. The IDW is recognised as an exact interpolator, which predicts non-sampled attribute values based on the spatial distance of measured points from these non-sampled points (Burrough et al., 2014). One geostatistical method, Ordinary Kriging, was applied. The ordinary kriging method is useful when estimating z values (depth) or to interpolate values for grid cells of a specific size for quantitative modelling (Burrough et al., 2014). The main strength of this interpolation is the statistical quality of its prediction and the ability to predict the spatial distribution of

uncertainty. Moreover, it was seen as the most effective tool for interpolation of bathymetry data (Siljeg et al., 2015).

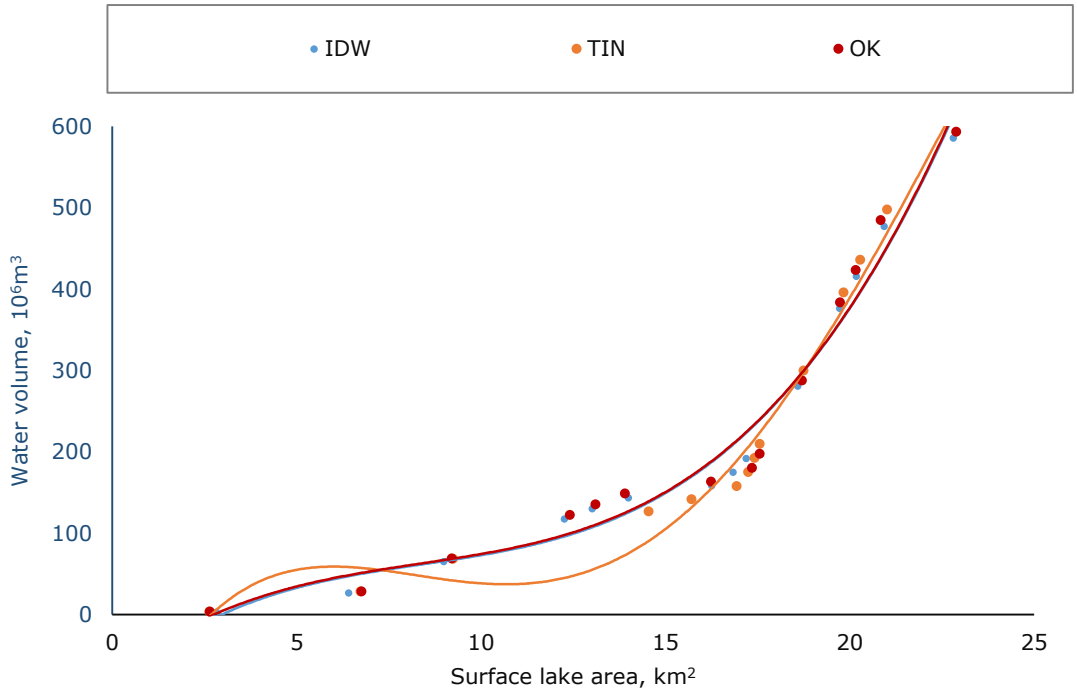

Figure 4. 6 The lake area and water volume relationship established using bathymetry survey interpolated by three approaches

where Triangulated Irregular Network (TIN), Inverse Distance Weighting (IDW), and Ordinary Kriging (OK)

Table 4. 3 Deviation from the mean in total water volume estimated using three interpolation methods for the total water volume of Shortandy Lake

where Triangulated Irregular Network (TIN), Inverse Distance Weighting (IDW), and Ordinary Kriging (OK), V_{total} *is the total lake volume*

Lake	Interpolation method		
	TIN	IDW	OK
V_{total} (m^3x10^6)	200.6	222.1	222.3
Deviation from the mean total water volume (m^3x10^6)	-14.4	7.1	7.3
r^2	0.98	0.98	0.97

Table 4.3 and Figure 4.6 compare the main outcomes from the interpolation of bathymetry data using the three approaches. The lake area-volume relationship

was established using polynomial curve which is used for nonlinear relationship, for example analysing gain and losses in water volume (Fan, 1996). The water volume which was estimated using the lake area in 1986 ranges from 200.6x$10^6$$m^3$ to 222.3x$10^6$$m^3$ in total, with a standard deviation of 12.4x$10^6$$m^3$ and root mean square error (RMSE) of 10.2 x$10^6$$m^3$. The IDW and Ordinary Kriging methods produced similar estimates of the water volume, and the standard deviation of Ordinary Kriging falls within the range of RMSE. By contrast, the highest deviation was produced by TIN (-14x10^6 m^3 from the mean total), which predicted the lowest water volume among the methods used. The volume predicted by the IDW interpolation method showed satisfactory results in both r^2 and RMSE. Therefore, the GIS-volumetric model will be established based on bathymetry data interpolated by the IDW method for further predictions of Shortandy Lake water volume.

Lake area (A_L)

Remotely sensed products have been widely applied for lake surface detection (Mason et al., 1994, Bai et al., 2011, Savvaitova and Petr, 1992, Micklin, 1988). Therefore, the historical lake area in 1986 was established by Landsat 5-TM with a 30-meter resolution during the ice-free period.

The Landsat data was downloaded from USGS GLOVIS, and images were processed with ArcMap 10.2 software. The lake area was established using the Normalized Difference Water Index (NDWI), which is used to identify and extract the water surface from Landsat products (McFeeters, 1996). NDWI index was estimated as follows:

$$NDWI = \frac{Green - NIR}{Green + NIR}$$

where:

$Green$ - Visible green light;

NIR - Near-infrared radiation.

4.4 Output variables

The lake water balance model estimates warm-season output variables as follows: potential open water evaporation (E_O) and reference crop evapotranspiration (E_{act}) models. A simplified version of the Penman equation was used for open water evaporation (Valiantzas, 2006). For evapotranspiration losses, the FAO Penman-Monteith model was applied (Allen, 1998). Here, open water evaporation is estimated as the flux produced from a particular lake area. Evapotranspiration is loss produced from the lake catchment by vegetation that would affect effective runoff-rainfall events. The evaporation losses in the Shortandy catchment were estimated on a daily basis. The only output variable in cold-season months is snow sublimation (E_{sub}), estimated through the regional model. In addition, anthropogenic impact (W_{abs}) was assessed using water abstraction records from the lake during the study period.

4.4.1 Open water evaporation ($\mathrm{E_O}$)

Evaporation is a collective term which includes evaporation from lakes and reservoirs, and from soil surfaces and vegetation. The definitions, time steps, and input parameters related to evaporation losses throughout the literature may vary and, in some cases, can be difficult to define (McMahon et al., 2013). To avoid the confusion around the terms in literature, the concept of "potential open water evaporation" developed by Shuttleworth (1993) was used for the estimation of Shortandy Lake evaporation flux. This term is defined as follows:

Potential open water evaporation is the quantity of water evaporated per unit time from an idealised, extensive free water surface under existing atmospheric conditions.

In this project, open lake evaporation is the losses from Shortandy Lake during warm-season months, where the warm-season is defined as a period when the lake surface is free from ice cover. Records on ice formation and decay were obtained from KazHydroMet and will be analysed in Chapter 5.

Derivation of the model. Open water evaporation estimates use a simplified version of the classic Penman equation (Penman, 1948) develop by Valiantzas (2006) for potential evaporation flux estimations. This simplified approach of potential evaporation has been successfully applied in semi-arid catchments (MacDonald et al., 2012, McMahon et al., 2012) and water balance studies of endorheic lakes with limited data requirements (Niedda and Pirastru, 2013, Vainu and Terasmaa, 2014)

The original classic Penman equation requires direct measurements on net radiation, R_n vapor pressure deficit, D, *which in Shortandy case was unavailable*. In this simplified approach, these parameters were obtained empirically, so that the simplified approach for Penman developed by Valiantzas (2006) could be expressed as follows:

Eq. 4.4.1.

$$E_O \approx 0.051\,(1-\alpha)R_S\sqrt{T} + 9.5 - 2.4\left(\frac{R_S}{R_A}\right)^2 + 0.048(T+20)(1-\frac{RH}{100})(a_u - 0.38 + 0.54u)$$

where:

E_O- Potential open water evaporation (mm day^{-1});

α – Surface albedo, for open water is 0.08 (Allen, 1998, Shuttleworth, 1993) ;

R_S- Solar Radiation calculated (MJ m^2 day^{-1});

RH- Relative humidity (%);

u - Wind speed (m s^{-1});

a_u - Wind function, for original Penman is equal to 1;

R_A- Extraterrestrial radiation[6];

T- Temperature (°C) estimated as follows:

Eq. 4.4.1a

$$T = \frac{T_{max} + T_{min}}{2}$$

where:

T_{max} - Daily maximum air temperate, (°C);

T_{min}- Daily minimum air temperate, (°C);

The estimation of R_n and D is established on the "standard" calculation sequence recommended by Shuttleworth (1993) and Allen et al. (1998). Based on this procedure, R_n for Shortandy Lake was derived from solar radiation (R_S) and the reflection coefficient (α). Furthermore, the derivation of vapour pressure deficit (D) was estimated using T_{max}, T_{min} and relative humidity (RH) (Appendix B). Based on Valiantsaz (2006), the accuracy of the model is equivalent to the Penman 1963 equation. In addition, the application of the mean of the minimum and maximum daily temperatures produces an error of 0.4°C and 0.8°C of annual temperature, which may produce overestimation in evaporation (Tait and Zheng, 2007)

4.4.1.1 Parameters for open water evaporation

Reflection coefficient or albedo(α)

One of the variables within lake evaporation modelling is net radiation ($R_{n)}$ which is a function of shortwave albedo (Section 2.6.1). Albedo depends on transient features, such as the direction of the solar beam and the proportion of diffuse radiation, yet it also changes with the surface capacity to reflect solar radiation (Shuttleworth, 1993). Albedo varies during the day, season, altitude and cloud cover. There are several methods developed to estimate the albedo, but they

[6] For radiation parameters (R_S, R_A) estimation see Appendix B.

require extensive measurements of radiation and air humidity that were unavailable for Shortandy Lake. Shuttleworth (1993) established plausible values for daily shortwave albedo values for various land cover types, where the *open water surface* value is equivalent to *0.08* (dimensionless), which is applied in most estimations. As a result, open lake evaporation in Shortandy Lake was estimated with albedo recommended by Shuttleworth (1993).

Wind function (u)

This wind function is commonly applied for the estimation of water evaporation losses in small lakes, ponds and reservoirs (Shuttleworth, 1993). Simplified open water evaporation offers two methods of computation, i.e. when wind speed is known or not given. The average value of u=2 m s^{-1} is suggested for simplification, where data is sparse or unavailable (Allen, 1998). However, open water evaporation models which include measured wind velocity, give more accurate estimations (Section 2.6.1) (Shuttleworth, 1993, Valiantzas, 2006).

The original wind function suggest by Penman (1948), where the wind (u) is measured at 2m above the ground, is described as the following expression:

$$f_U^{(1)} = 1 + 0.536u \qquad \text{Eq. 4.4.1b}$$

Later findings (Penman, 1956) suggest reducing the original wind function by replacing with the following expression:

$$\mathrm{f_U^{(2)}} = 0.5 + 0.536\mathrm{u} \qquad \text{Eq. 4.4.1c}$$

However, the wind function stated above tends to overestimate evaporation for large lakes by approximately 10-15% (Shuttleworth, 1993). Linacre (1993) suggested reducing the value of the wind by introducing the following equation:

$$\mathrm{f_U^{(3)}} = 0.54\mathrm{u} \qquad \text{Eq. 4.4.1d}$$

The following wind function is recommended and recognized as the standard approach for estimating evaporation from larger lakes (>10km^2) (Valiantzas, 2006). The simplified open water evaporation (Valiantzas, 2006) in conjunction

with reduced wind function suggested by Linacre (1993) is in a good agreement with the original Penman model (R^2=0.997) (Valiantzas, 2006). Thus, in Shortandy Lake, evaporation flux was estimated by the $f_U^{(3)}$ wind function.

Net radiation (R_n)

Net radiation takes into account the changes in the heat stored in the lake and advected energy due to inflows and outflows of water. The heat storage of lakes affects the surface energy flux when these lakes tend to continue heating up during hot months and release it as latent heat during colder months which causes seasonal changes in evaporation losses. The seasonal evaporation flux can be significantly affected by the heat-storage capacity of the lake, which is primarily determined by its depth (Finch and Hall, 2005). Therefore, it is crucial to reconsider the general concept behind the definition of potential open-water evaporation. In many cases, this term refers to shallow lakes, ponds and reservoirs. However, the definition of "shallow" is not well-defined in literature. For example, McMahon (2013) defines shallow lakes as basins with an average of 2m in depth. The situation is different if a lake becomes thermally stratified. Stratification occurs in large, deep lakes, which produces the time lag between net radiation and the evaporation rate.

In many models for deep lakes, evaporation flux models are estimated using open-water models for shallow basins but are corrected with changes in heat storage and water-advected energy. In many cases, it is accomplished by calibrating the Penman equation by incorporating the heat capacity of the water layer with the daily water temperature (Keijman, 1974) or with mean monthly water temperature profile (Vardavas and Fountoulakis, 1996, Kohler and Parmele, 1967). Moreover, CRLE model (Complementary Relationship Lake Evaporation Model) (Morton, 1983) transforms outcome from shallow-lake based models, but it requires the average depth and the concentration of total dissolved solids.

Based on Section 3.2.1, the mean depth of Shortandy Lake is about 15m and thus cannot be classified as shallow. However, evaporation models for a deep lake were inaccessible for Shortandy Lake modelling due to the limited data availability. As explained in Section 4.2, the standard weather data records were only available for this project with no measurements for lake water temperature which is required for most deep lake evaporation models. Thus, no correction for heat storage of Shortandy Lake was applied. According to Finch and Hall (2005), lakes with a mean depth of about 15m as Shortandy Lake, produce a lag of about one month between net radiation and evaporation flux. This will result in the model overestimating the evaporation during springs due to the increased net radiation, and conversely underestimate evaporation during autumns (See more in Chapter 7).

Temporal resolution and model parameters

The simplified approach of Penman estimates the net radiation as the difference between incoming net shortwave radiation and outgoing net longwave radiation using solar and extraterrestrial radiation. Therefore, solar radiation is an important variable in evaporation flux simulation. Specifically, the modelling approach and temporal resolution of modelling have a significant influence on the accuracy of the estimations.

In this project, the monthly and daily computation of R_s were compared. Comparative analysis of the temporal resolution of R_s revealed that the deviation between averaged monthly R_s^1 versus daily R_s^2 can be insignificant. However, temporal resolution *may generate a significant difference in total annual evaporation* (Table 4.4). Table 4.4 indicates that differences between monthly and daily estimations may generate a difference of more than +150 mm year^{-1} in the total lake evaporation of Shortandy Lake. As a result, monthly and daily estimation of open water evaporation indicates that the simplified equation of Penman (Valiantzas, 2006) is sensitive to the temporal resolution of solar radiation.

An additional correction for the open lake evaporation model was made for the wind function. The original wind function (Eq. 4.4.1) was substituted by the reduced value of the wind i.e. $f_u^{(3)}$ (Eq.4.4.1d). Comparative analysis between original and reduced wind function for evaporation flux from Shortandy Lake coincides with Cohen's conclusion that the original wind function shows higher values of open water evaporation for large lakes (Cohen, 2002). *Consequently, in this project, E_o was established using Eq. 4.1 with the reduced wind function $f_u^{(3)}$* (Eq. 4.4.1d) on a daily basis.

Table 4. 4 Comparative analysis on open water evaporation of Shortandy Lake in 2013 based on monthly (E_o) and daily (E_o daily) estimations

where R_s^1 is monthly solar radiation and R_s^2 is averaged monthly values from daily solar radiation. E_o daily is open water evaporation with corrected wind function based on Linacre (Linacre, 1993) with the reduced value of the wind function, $f_u^{(3)}$=0.54*u Eq.4.4.1d

Month	Monthly E_o		Total monthly E_o daily	
	R_s^1, (MJ m^2 day^{-1})	E_o, mm	R_s^2, (MJ m^2 day^{-1})	E_o daily, mm
May	24.5	164	20.3	121
June	26.1	207	25.2	173
July	22.3	164	19.6	147
August	18.9	134	17	107
September	14.8	84	12.6	61
October	8.4	35	6.5	17
Total	18.4	**789**	16.9	**626**

4.4.2 Evapotranspiration from vegetation

The water balance model estimates evaporation losses produced by the catchment during warm-season months. The following variable is critical for estimating effective runoff which contributes the lake volume after excessive rainfall events.

The evaporation losses produced in the Shortandy catchment were estimated by utilisation of the concept of reference crop evapotranspiration model developed by Allen (1998).

Reference crop evapotranspiration is the evaporation flux from a hypothetical reference crop, well-watered with height=0.12m, surface resistance=70 s m^{-1}, and albedo=0.23.

Derivation of the model. The Penman-Monteith model is commonly utilised to estimate evaporation from vegetated areas. The most widely applied and considered as the "standard" method in hydrological and water management applications is FAO-56 Penman (Allen, 1998).

In this project, the evaporation losses from the Shortandy catchment were modelled according to the steps illustrated in Figure 4.7. The FAO-56 Penman model consists of the following steps: i) estimation of potential crop evapotranspiration (E_{pet}) and ii) estimation of the crop coefficient (k_c). E_{pet} estimates the evaporating feature under certain climate conditions, at a particular area and time and neglects soil factors and crop characteristics. After determining E_{pet} , evapotranspiration loss produced in a certain crop type could be established using k_c.

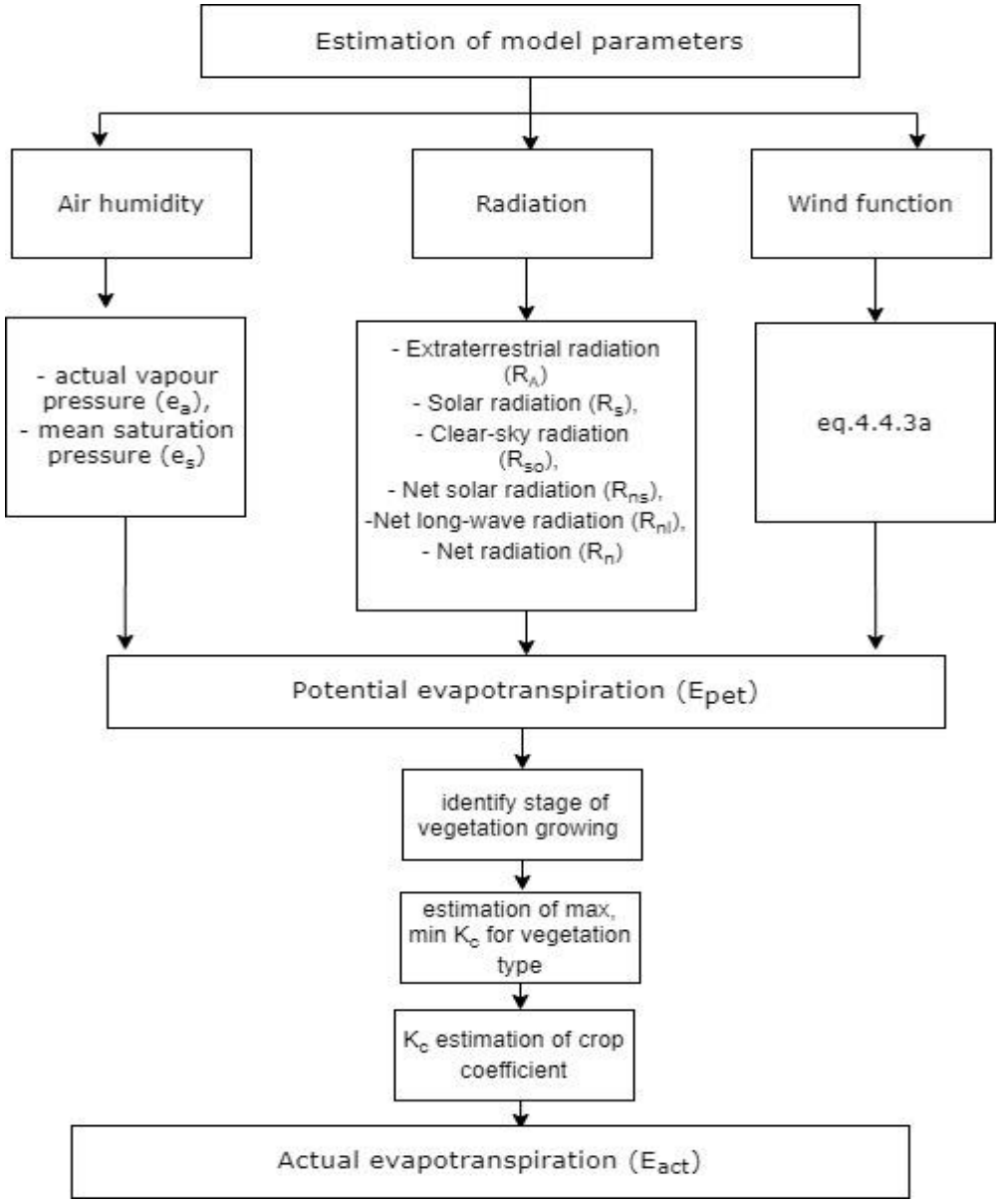

Figure 4. 4 The schematic chart on estimation evaporation losses in the Shortandy catchment

The FAO-56 Penman-Monteith is a physically-based approach, which estimates evapotranspiration losses with the incorporation of both physiological and aerodynamic parameters. The original formula is described as follows:

$$E_{pet} = \frac{0.408\Delta(R_n - G) + \gamma \frac{900}{T+273} u_2 (e_s - e_a)}{\Delta + \gamma(1 + 0.34u_2)} \quad \text{Eq. 4.4.2}$$

where:

E_{pet}- Potential reference evapotranspiration, mm day;

R_n - Net radiation at the vegetated surface (MJ m^{-2} day)[7];

G - Soil heat flux density (MJ m^{-2} day)[2];

T - Mean daily temperature (°C);

u_2- Wind speed at 2m height (m s^{-1});

e_S - Saturation vapour pressure (kPa)[2];

e_a - Actual vapour pressure (kPa)[2];

$e_S - e_a$- Saturation vapour pressure déficit (kPa);

Δ slope vapour pressure curve (kPa °C^{-1})[2];

γ – psychrometric constant (kPa °C^{-1})[2].

where wind function (u_2) is the wind velocity measured at 2 m above the surface (m s^{-1}) :

$$u_2 = u_z \frac{4.87}{\ln(67.8z - 5.42)} \qquad \text{Eq. 4.4.2a}$$

where

u_2- Wind speed at 2m above the ground surface (m s^{-1}),

u_z - Measured wind speed at z m above the ground surface (m s^{-1}),

z - Height of measurement above the ground surface (m)

Parameters from Equation 4.4.2 are derived with the help of a direct empirical relationship. All variables within the equation were obtained from the air temperature difference, wind speed and humidity data. Air humidity parameters such as the actual vapour pressure and mean saturated pressure for the lake catchment were derived by utilisation of daily T_{min} and T_{max}.

4.4.2.1 Actual evapotranspiration E_{act}

[7] The estimation procedure of vapor pressure and radiation variables is reflected in Appendix B

Based on FAO-56 Penman, most of the climate effects are incorporated in the E_{pet} estimation. Thus, E_{pet} represents an index of evaporation demand, whereas the crop coefficient (k_c) changes predominantly with the specific vegetation type characteristics and only to a limited extent with climate (Allen, 1998). According to FAO-56, actual evapotranspiration estimation is described as follows:

$$E_{act} = E_{pet} * k_c \qquad \text{Eq.4.4.2.1}$$

where

E_{act} - Actual evapotranspiration of a catchment (mm day^{-1}),

E_{pet} - Potential reference evapotranspiration (mm day^{-1}),

k_c - Crop coefficient (dimensionless).

In this study, evapotranspiration from vegetation was generalised, *i.e.* was estimated for only forested areas of the Shortandy catchment. The uncertainties of this generalisation and potential error in evapotranspiration will be further addressed in Chapter 7.

4.4.2.2 Parameters for actual evapotranspiration

The crop coefficient is a parameter which indicates the regional terrestrial water availability, dry or wet conditions, as well as crop water stress (Anderson, 2012). Consequently, the following ratio is affected by vegetation growing stage during the warm-season, vegetation type, soil features and conditions, vegetation height and Leaf Index Area (LAI).

Because of variations in evapotranspiration during the different growing stages, the k_c ratio for a specific vegetation type will change over the developing period. According to the model, three values of k_c are required depending on the crop development stage: initial stage, mid-season stage and late-season stages.

Shortandy Lake catchment is characterised as a forested area, where vegetation species are predominantly deciduous trees (Section 3.1.4). Furthermore, the evapotranspiration model is required to estimate the losses from rainfall-induced

runoff produced in the lake catchment during excessive rainfall events. In this model, the soil moisture content is neglected but assumes that sufficient water is available. Based on climate data for the Shortandy Lake catchment, excessive rainfall events occur during July months, thus with sufficient water available for soil. Furthermore, the k_c index is required to estimate for July, which is *the mid-season of the growing stage*.

The crop coefficient for Shortandy Lake catchment was estimated by utilising an equation for natural vegetation during the mid-season (Allen, 1998) as follows:

$$k_c = k_{c,min} + (k_{c,max} - k_{c,min})(1 - e^{-0.7LAI}) \quad \text{Eq.4.4.2.2}$$

Where:

k_c - Crop coefficient, dimensionless;

$k_{c,min}$ - The minimum crop coefficient for the deciduous forest, dimensionless;

$k_{c,max}$ - The maximum crop coefficient for the deciduous forest, dimensionless;

LAI - Leaf Area Index, ratio.

where $k_{c,max}$ described as follows:

$$k_{c,max} = k_{c,min} + [0.04(u_2 - 2) - 0.004(RH_{min} - 45)](\frac{h}{3})^{0.3} \quad \text{Eq.4.4.2.2a}$$

where:

u_2 - Wind speed measured 2 m above the ground surface, m s^{-1};

RH_{min} - Relative humidity, %;

h - Mean maximum tree heights, m.

$k_{c,max}$ - Parameter estimated by Eq.4.4.2.2a is an adjusted parameter for semi-arid climates suggested by Allen (1998), where 0.1< h<10m and 20%<RH_{min}<80%. In addition, $k_{c,min}$ value is equivalent to 0.9, as recommended for deciduous forest (Allen, 1998). h value was taken from the field observations (Budnikova et al., 2010), and it is equivalent to 9 m on average.

Another parameter required for $k_{c,max}$ estimations was Leaf Area Index (LAI). LAI is defined as the amount of leaf area per unit ground area. The LAI for the

Shortandy catchment was identified using land cover map (Section 4.5.1.1.1) and by the MOD15A2H[8] product (Myneni et al., 2015), which is an 8-day composite dataset with 500-meter resolution. For example, the averaged LAI index for July 2013 was equal to 6.5 (Figure 4.8) for the lake catchment.

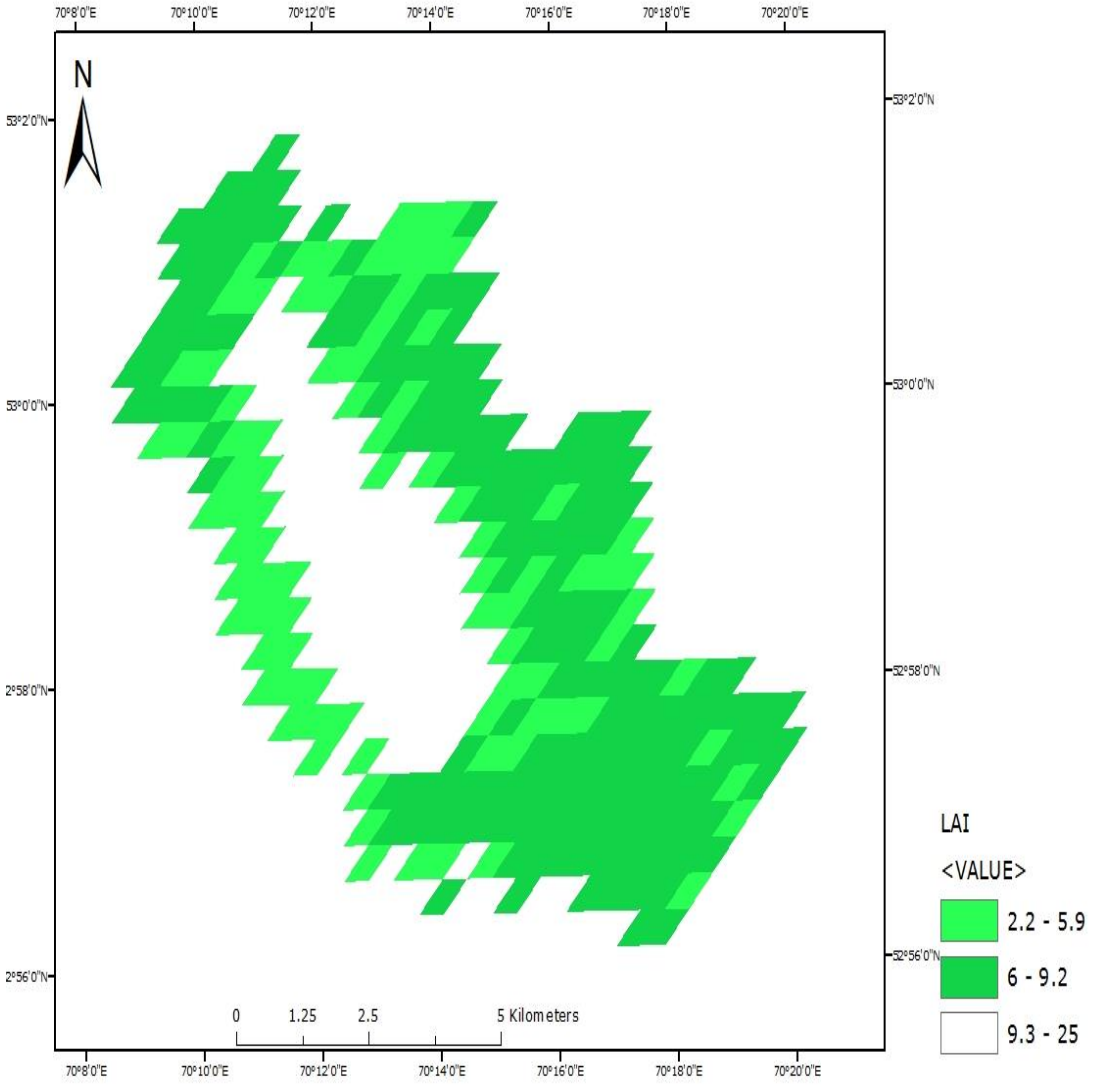

Figure 4. 5 Leaf Area Index (LAI) estimated from MOD15A2H for July 2013 for the Shortandy catchment

4.4.3 Anthropogenic impact - Water abstraction W_{abs}

[8] MOD15A2H - Moderate Resolution Imaging Spectroradiometer (MODIS) product which is combined Leaf Area Index and Fraction of Photosynthetically Active Radiation (FPAR).

Previous studies indicate that human activity has the potential to affect endorheic lakes indirectly and directly in terms of water quantity (Section 2.1.2.). Thus, the hydrological cycle parameters can be represented in a water balance model by including anthropogenic components which affect the physical balance. Section 3.1.5 shows the BNNP has significantly accelerated in terms of tourist development over the study period. In the Burabay area, water supply for human needs of the nearby settlements has been implemented by the surface and groundwater abstraction since the establishment of the Shortandy settlement in 1850 until the water restriction policy, which was implemented in 2010.

In the single lake model, the total monthly surface and groundwater abstraction (W_{abs}) values from the lake, were incorporated. The water abstraction values were obtained from the Water Supply Agency in Shortandy – Burabay Su Arnasy, from 1989 to 2016 and will be presented in Chapter 5.

4.4.4 Snow sublimation (E_{sub})

Snow sublimation is a loss of water produced by the snowpack to the environment. Thus, changing snowpack accumulation and sublimation may affect both the timing (Stewart et al., 2005a) and the amount of water (Barnhart et al., 2016), which contributes to the lake volume. Sublimation occurs when the total pressure of the atmosphere is less than the vapour pressure of the compound, and when melting has not occurred.

In this project, the snow sublimation model aims to estimate monthly losses from Shortandy Lake during cold-season months (Section 4.1). Similarly, with the open lake evaporation model, ice formation and decay records in Shortandy were obtained from the KazHydroMet agency. The snowpack losses from the lake catchment during the snowmelt seasons are incorporated in the snowmelt runoff model (Section 4.5). Therefore, snow sublimation estimates from the lake catchment were excluded to avoid double-counting.

As reflected in Section 2.6, snow sublimation is difficult to obtain by direct measurements (Raleigh et al., 2013) which have never been conducted in the lake catchment. Thus, to estimate snow sublimation from Shortandy Lake, the regional model developed by Semenov (1990) was applied. The following expression for snow sublimation estimation was developed specifically for Northern Kazakhstan (Semenov, 1990). The model was established using correlation analysis between air humidity and snow ablation in the region. The correlation coefficients derived from a long-term observation (10-years) over the stated above parameters during the 1980s by KazHydroMet (KazHydroMet, 2014). So that, losses for snow sublimation are estimated as follows:

$$E_{sub} = n(0.35VPD - 0.06) \quad \text{Eq. 4.4.4}$$

where:

E_{sub} - Monthly snow sublimation from the lake surface, (mm);

n - Number of days that month;

VPD - Mean monthly vapour pressure deficit, (kPa).

4.5. Input variables

Input variables in the water balance are: P_{snow} P_{rain} - precipitation falling directly onto the lake surface, runoff produced from the lake catchment during seasonal snowmelt (Q_{snow}) and runoff produced from extensive rainfall events (Q_{rain}). Daily *precipitation and mean air temperature values* were obtained from Shuchinsk weather station from 1986 to 2016.

4.5.1 Snowmelt Runoff Model (SRM) model development (Q_{snow}, Q_{rain})

Seasonal snow accumulation and melt processes play an essential role in maintaining the global water balance (Goodison 1999; Immerzeel 2010). Section 3.4.2.1 indicates that mean winter precipitation contributes only 20-30% of the total annual precipitation in Shortandy. Literature review findings show that

warm-season precipitation comprises the highest proportion of total annual precipitation, but has an insignificant contribution to the lake due to the evaporation losses (Yapiyev et al., 2017, Uryvayev, 1959). Unlike warm-season precipitation, the snow that accumulates during cold months, which is only affected by minimal losses for snow sublimation, thus may have a significant contribution to the lake volume.

Seasonal snowmelt runoff and rainfall-runoff have never been measured in the Shortandy catchment. The Shortandy water balance model, therefore, utilises the Snowmelt Runoff Model (SRM) for estimation of runoff produced by both snow-melt and rainfall events. Based on Section 2.6, distributed hydrological models provide a relationship between snowpack accumulation and snow-thaw processes. However, these models require a large amount of input data and parameterisation. By contrast, conceptual semi-distributed runoff models require a manageable amount of data and parameters, and are more applicable for areas with limited observations. The model simulates the relationship between precipitation and air temperature by taking into account catchment-specific parameters (Martinec, 1975).

The SRM is a semi-distributed, temperature index, hydrological model that can be used to simulate daily catchment runoff and to forecast snowmelt and rainfall. It was developed and first applied in Switzerland with further development in collaboration with the US Agricultural Research Service.

The minimal set of parameters required to run SRM simulations have attracted researchers to study areas where station observations are limited and sparse (Figure 4.9). The model is applicable for both large and small basins and is designed to simulate and forecast seasonal runoff where snowmelt is a major runoff factor. Specifically, the SRM has been applied in over 100 basins in 29 countries, with a catchment area from 1 to over 900 000 km^2 (Martinec, 2008). The SRM model has been applied to catchments with various elevation ranges and simulations ranging from one melt-season to 10-year period. Examples of SRM

application in the Central Asian area with semi-arid and arid conditions are in Uzbekistan and Kyrgyzstan (Baumgartner et al., 2001) and China (Li, 2008, Abudu et al., 2012). According to the model application for a mountainous area in China, the model accuracy was within the range of $R^2 \approx 0.79\text{-}0.9$ of the Nash-Sutcliffe coefficient. The SRM simulation for snow-dominated regions of Uzbekistan and Kyrgyzstan performed with $R^2 = 0.81\text{-}0.87$ for the one melt-season discharge computation.

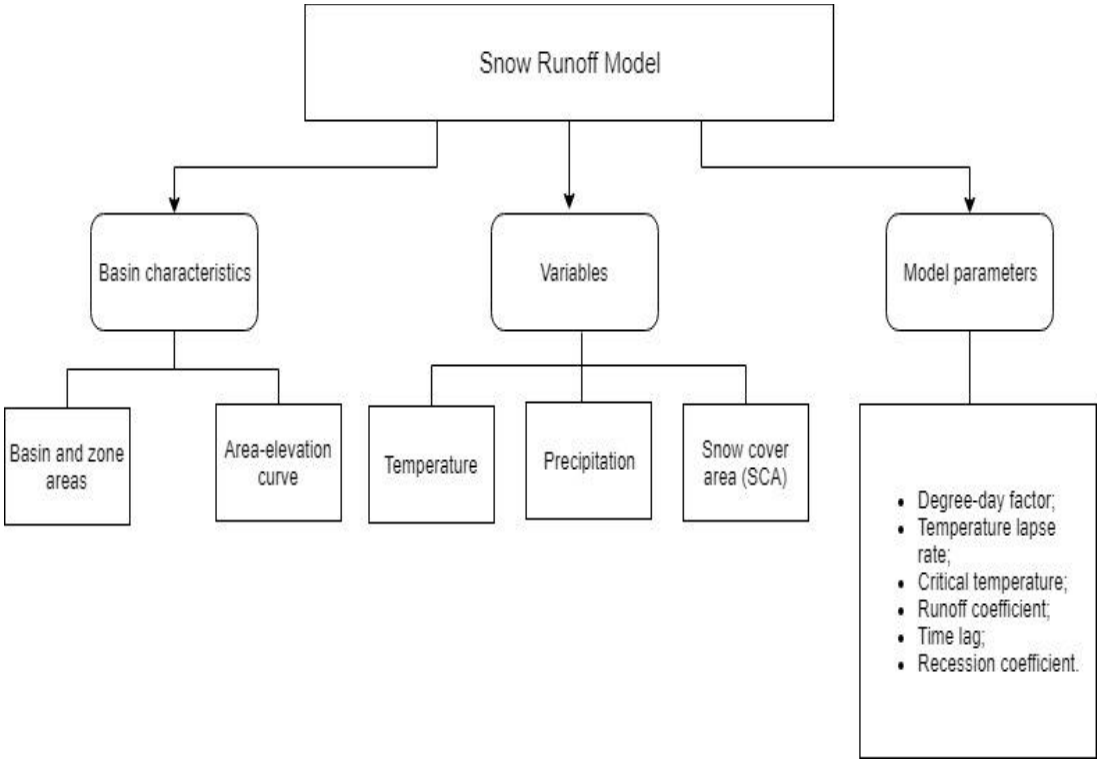

Figure 4. 6 Schematic chart on SRM model requirements

In this study, daily snowmelt in the Shortandy watershed was calculated according to the following equation:

$$Q_{n+1} = [c_{sn} * \propto_n \ (T_n + \Delta T_n) * SCA * A * 0.116] * (1 - k_{n+1}) + (Q_n \, k_{n+1})$$

Eq. 4.5.1

and if rain runoff:

$$+[\, c_r P_n A * 0.116] * (1 - k_{n+1}) + (Q_n \, k_{n+1})$$

where:

Q_{n+1} - Average daily discharge ($m^3\ s^{-1}$);

c_{sn} - Snow runoff coefficient;

α_n - Degree-day factor (cm $°C^{-1}$ day^{-1}) indicating the snowmelt depth from one degree-day;

T_n - Number of degree-days above the base of 0°C (°C day);

ΔT - Adjustment by temperature lapse rate;

SCA - Ratio of the snow-covered area to the total area;

c_{rn} - Rainfall-runoff coefficient;

P_n - Precipitation on n day, (mm);

A - Area of the zone or basin (km^2);

k_{n+1} - Recession coefficient indicating the decline of discharge in a period without snowmelt;

n - Sequence of days during the discharge estimation period;

0.116 is the conversion factor from cm km^2 day^{-1} to $m^3\ s^{-1}$.

4.5.1.1 Basin characteristics

The area-elevation curve of the basin is required to determine the altitude difference for the extrapolation of temperature. According to the model requirements, when the elevation range of the basin exceeds 500m, there is a need to divide given watershed into elevation zones. In the case of Shortandy, there is no need to create elevation zones, as the lowest elevation equals to 388m and the highest 713m above sea level (Figure 4.3.2)**.** Therefore, the runoff model for Shortandy was developed depending upon land cover types instead, due to various snow cover accumulation and melt condition properties.

4.5.1.1.1 Land cover change

According to KazHydroMet records, the snowpack measurements in the Shortandy catchment was conducted based on three land cover types. The land cover types

were generalised as: i) forest, ii) grassland iii) lake area. Therefore, in this project, changes in these particular land cover types were examined from 1986 to 2016. The land cover types were established to model snow cover distribution within the catchment required for the model parameter, *i.e.* snow cover area (SCA). In addition, land cover map was also used for evapotranspiration modelling (Section 4.4.2.2) specifically for estimation of LAI parameter. Urban areas (with less than <5 km^2) were classified as grassland due to the absence of the snowpack measurements at the Shortandy settlement. Here, the assumption was that the snow accumulation and melting processes in urban and grassland cover types are similar. Therefore, Shortandy land cover classification is based on the estimation of proportional changes in the total areas within these three land cover types.

Each land cover type was evaluated by image classification using the ArcGIS Spatial Analyst extension within ArcMap software. Landsat products during the ice-free season were classified using the Supervised classification method. The signature files, which identify the classes and their statistics were created based on three land cover types.

According to the land cover classification, forest area has reduced from 45.7km^2 in 1986-2009 to 39.9km^2 by 2010 within the Shortandy catchment, whereas grassland area has expanded from 6.7km^2 to 12.5km^2over the period (Figure 4.10).

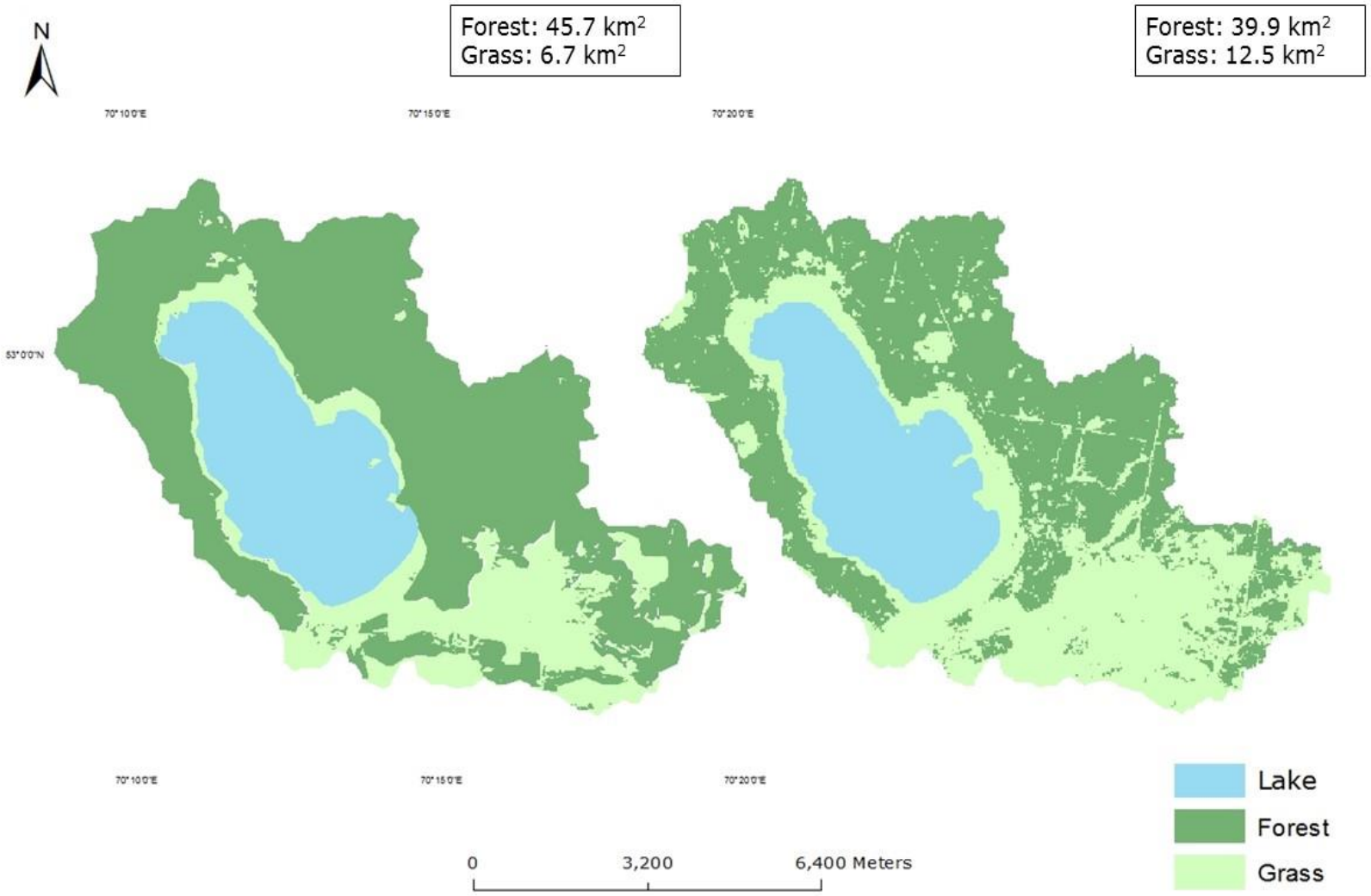

Figure 4. 7 Land cover map for the Shortandy catchment

where the left figure shows the land cover map for the period of 1986-2009 and the right figure shows a land cover map from 2010-2016

Subsequently, the original SRM Equation 4.5.1 was re-written to consider land cover types, *i.e.* for forest and grassland areas in the Shortandy catchment (Figure 4.9) Therefore, total daily runoff produced by snowmelt in the lake catchment was estimated with the following expression:

$$Q_{n+1} = c_{nF}[\propto_{Fn} (T_n + \Delta T_n) SCA_F * A_F * 0.116]$$
$$+ c_{nG}[\propto_{Gn} (T_n + \Delta T_n) SCA_G * A_G * 0.116] * (1 - k_{n+1}) + Q_n k_{n+1}$$

Eq. 4.5.2.

where indices F and G refer to forest and grassland respectively.

Land cover classification evaluates proportional changes in forest and grassland areas of the Shortandy catchment. The total area of each land cover type was used to estimate the overall snowmelt runoff values produced in a specific area. Moreover, the shapefiles produced were utilised in snow cover area detection addressed in Section 4.5.1.2.1.

4.5.1.2 Model variables

In the SRM model, there are three variables which need to be measured:

- Temperature;
- Precipitation;
- Snow-covered area (SCA).

Based on the model, in basins with a great elevation range (>500m), air temperature and precipitation vary and it is required to interpolate these values by hypsometric altitudes of the respective zones. In the case of Shortandy, relatively low relief variation (388m-713m) of the catchment allows modelling of the lake catchment as a single zone. Here, air temperature is an important variable for the estimation of the daily snowmelt depths, which is estimated by the degree-day factor (α). In this project, the daily mean temperature measured from the single local weather station was used.

The critical temperature is used to determine whether a precipitation event will be considered as rainfall when ($T \geq T_{CRIT}$) or as new snow ($T \leq T_{CRIT}$). At the point when the precipitation occasion is classified as snow, its delayed effect on runoff is modelled variously depending on whether it falls over a snow-covered or snow-free area of the catchment. The new snow that falls over the existing snow-covered territory is considered to be a part of the seasonal snowpack, and its proportion contributes to the depletion curve of the snow coverage. Whereas, the new snow falling over the territory without snow-cover is considered as precipitation to be added to snowmelt, with this effect delayed until the following day is sufficiently warm to create melting.

In this project, snow depth and density changes were taken from observed snowpack measurements obtained from KazHydromet. Due to periodicity of the measurements, in some cases, snow-cover was modelled by the SRM model, where snow depletion would be estimated as the relationship between precipitation and air temperature. At the Shortandy catchment, T_{CRIT} is equal to 0°C.

4.5.1.2.1 Snow cover area (SCA)

SCA is a ratio of the snow-covered area to the total area, where values of 1 indicate complete snow coverage, and 0 equals no snow. The SCA ratio is an important variable in SRM. The depletion curve of snow coverage should be established daily, where the SCA ratio could be derived from ground observations, aircraft photography, and satellite images. Terrestrial observation can be used for small basins (Martinec, 2008), whereas satellite images are more applicable to larger basins.

Here, the RS techniques such as microwave images are difficult to interpret, and low resolution makes passive microwave sensors applicable only for large watersheds or global snow cover mapping. By contrast, optical images may provide an accurate observation on a cloud-free day. Snow cover detection

methods on optical images include unsupervised and supervised classification methods, spectral mixture analysis, and the MODIS snow-mapping algorithm.

The Normalized Difference Snow Index (NDSI) is widely used for snow cover area detection. The fundamental idea of using optical sensors for snow mapping is that snow has a different spectral reflectance. Specifically, snow reflectance is highly responsive between visible (green) and shortwave infrared (SWIR), at 0.66 and 1.6 micrometres. The NDSI controls the variance of two bands, and its equation defines as follows:

$$NDSI_{TM} = \frac{(\rho_{green} - \rho_{SWIR1})}{(\rho_{green} + \rho_{SWIR1})} \quad \text{Eq. 4.5.3}$$

Values of NDSI which are lower than 0.4, typically indicate the presence of snow. The accuracy of RS derived snow mapping methods is considerably higher for non-forested than forested areas (Wang et al., 2018) because tree height increases the complexity of an image by masking snow on the ground and affecting the spectral reflectance of snow. This is especially true for evergreen forests, where tree canopy disturbs the detection of snow underneath and so RS methods fail to detect snow cover accurately.

Section 4.5.1.1.1 shows that the Shortandy catchment is dominated by deciduous forest where grassland area is only 6.7 km^2 from the total area of the catchment (52.4 km^2 excluding the lake area). Thus, the RS techniques were used to estimate snow cover area in grasslands, whereas snow mapping in forests required a different approach.

The satellite-based snow cover area provides spatial information on snow/no snow, which is sensitive to changes in the snow amount. In many cases, the time interval between the subsequent satellite images becomes too long for snow-thaw detection. As a result, the depletion curve, which should be derived from daily measurements of snow coverage, could be distorted by occasional snowfalls. These anomalies, such as blizzards are common in the Shortandy catchment

(Murtazin, 2005) and, as a result, RS derived products provide unrealistic snow coverage.

Snow water equivalent (SWE) data derived from snowpack surveys provide reliable information on snow coverage with better temporal resolution than the RS products. SWE defines as the amount of liquid water that would be obtained upon complete melting of the snowpack per unit ground surface area. SWE (mm) can be calculated from snow depth (m), snow density and water density. The snowpack measurements dataset (KazHydroMet) was available for the cold-seasons from 1986 to 2016. Snow surveys were conducted with 10-15 days periodicity for grassland and forested areas separately within the Shortandy catchment. Maximum, minimum and average snow depths and snow density were measured during winter seasons (Table 4.2).

In the SRM model, the SCA depletion curve should have a daily temporal resolution during the melt season, where the main challenge is to establish the SCA ratio. (Martinec, 1960). In order to avoid errors caused by satellite images, the short-lived snow cover from occasional spring snowfalls were ignored. In such cases, when the spatial resolution of actual point snow measurements was insufficient, the estimation of new snow was accounted for based on the relation between precipitation and temperature, where $T_{CRIT} \leq 0℃$.

For Shortandy, a snow depletion curve was established from the relationship between point-measured SWE and computed degree-day factors (Fig 4.11). An assumption was made regarding the SCA modelling in forests, where the SWE=100mm with roughly 0.3 kg m^3 snow density, it would be equal to 100% of snow coverage or 1.0 value of SCA ratio. Further snow cover area reduction simulation was based on degree-day factor values, where the snow-cover area decrease was estimated as a linear function of SWE and degree-day factor (snowmelt depth) which results in the SCA reduction in the following day. This calculation carried on until SWE was 0 and with persistent $T_{mean} > 0$, which is equivalent to no snow and end of the snowmelt season. To validate the following

estimations, the day where it was modelled SCA=0 or no-snow, was compared with satellite images if they were available.

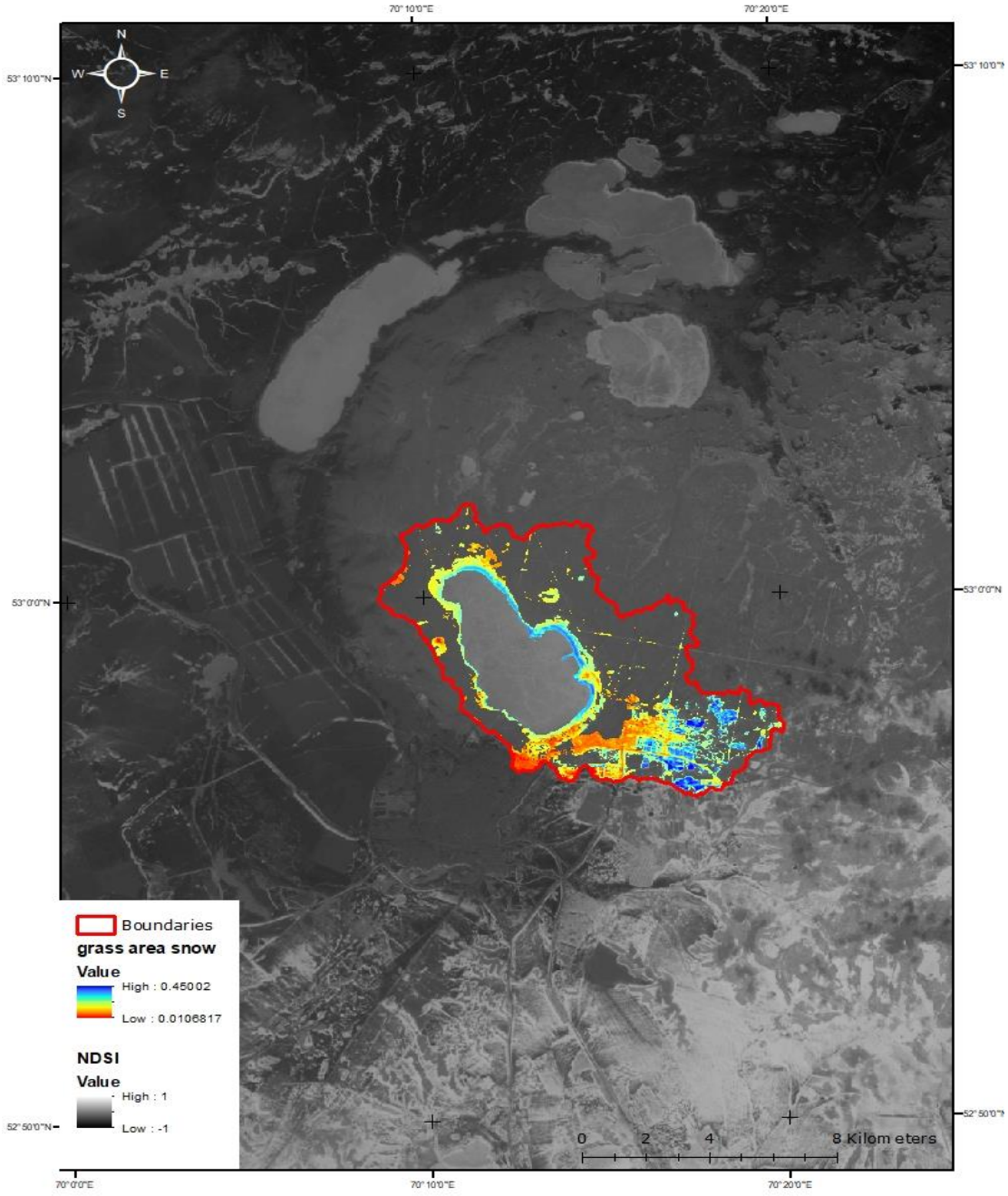

Figure 4. 8 Snow cover detection using NDSI method in grass areas of Shortandy watershed by 31 of March 2016

Blue colour corresponds to values >0.4 micrometers which indicate the presence of snow, and the red line shows the Shortandy catchment boundaries

A similar computation procedure was used for grasslands, and, snow coverage was validated with the NDSI, where this method was helpful for snow identification

(Figure 4.10). For example, the SCA ratio was established using SWE and degree-day factor for both land cover types during the cold-season in 2013 (Figure 4.12). The findings indicate that SCA simulated by SWE would disappear by the 19th of April or SCA=0. The following date was compared with the calculated NDSI, which also showed "no-snow" conditions (obtained in 17-25 April 2013). Furthermore, it was critical to validate snow cover ratio in grasslands due to the frequent snowstorms and snow redistribution over the catchment on this land cover type. A snowstorm occurred toward the end of the melt-season April in 2013, which resulted in snow redistribution and re-accumulation in grassland twice (14th and 16th of April). Due to these storms, the SCA ratio rose from 0 on the 13th of April to 0.7 by 17th of April (Figure 4.12) and then newly formed snow cover disappeared by 20th of April.

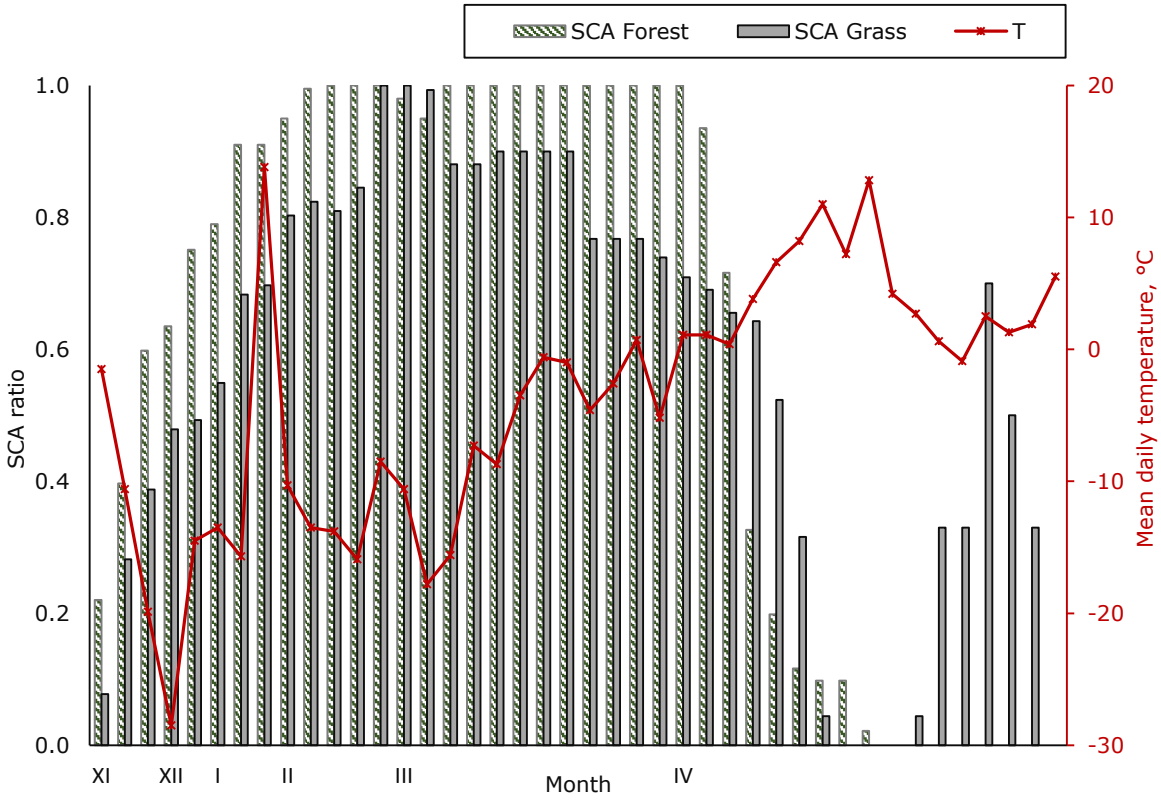

Figure 4. 9 Snow accumulation and depletion in forest and grassland in the Shortandy catchment during winter-spring season 2012-2013

where the end of snowmelt season corresponds to 19th of April and SCA is estimated snow cover area

4.5.1.3 Model parameters

4.5.1.3.1 The degree-day factor (α)

The empirical degree-day factor or melt coefficient is incorporated in most models used to simulate or predict snowmelt runoff (Lawrence, 2002). The parameter converts the number of degree-days into snowmelt depth produced. The degree-day method is widely used because the air temperature is a good measure of energy flux, and consequently, it is an easy variable to measure, extrapolate and predict. In the SRM model, α is calculated from the following equation (Martinec, 1960):

$$\alpha_{original} = 1.1 \frac{\rho_s}{\rho_w} \qquad \text{Eq. 4.5.4a}$$

where:

α - Degree-day factor (cm°C^{-1} day^{-1});

ρ_S - Snowpack density (kg m^3);

ρ_w - Water density (kg m^3).

Snowmelt depth is a function of α and daily air temperature, where $T > 0$℃. The degree-day factor is not constant throughout the snow-melt season. According to the Eq. 4.5.4a, the snow density is an index showing snow properties which promote snowmelt. Specifically, it increases when snow ripens, and solar radiation becomes more intensive.

There are several approaches for α estimations. The value varies with latitude, elevation, slope inclination, land cover, and time of year. Ideally, α has to be calculated empirically for a given catchment. In the SRM model, degree-day factor is estimated using snow density properties for all elevation zones disregarding land cover types. However, snow density changes throughout the melt season, but it is also a fraction of land cover type and snow albedo (Lawrence, 2002).

In this study, the original degree-day factor equation of SRM model (Eq.4.5.4a) was replaced by a degree-day factor regarding land-cover types in Shortandy. For forest:

$$\alpha_{Fn} = 10.4 \frac{\rho_{Fs}}{\rho_w} - 0.7 \quad \text{Eq. 4.5.4b}$$

for grassland,

$$\alpha_{Gn} = 19.6 * \frac{\rho_{Gs}}{\rho_w} - 2.39 \quad \text{Eq. 4.5.4c}$$

where:

α_{Fn} - Degree-day factor for forest (cm°C^{-1} day^{-1});

ρ_{Fs} - Snowpack density in forest (kg m^3);

α_{Fn} - Degree-day factor for grassland (cm°C^{-1} day^{-1});

ρ_{Gs} - Snowpack density in grassland (kg m^3).

Introduced equations for degree-day factors aim to improve seasonal snowmelt runoff estimations. According to Kuusisto (1980), the degree-day factor changes based on the land cover type. For example, a rapid increase in this factor is more pronounced on grassland than in the forest, which is explained by the larger effect of solar radiation on grass (Kuusisto, 1980). Furthermore, these findings highlight the importance of snow density for degree-day factor estimations, as it represents several factors affecting snowmelt, such as snow albedo and higher liquid water content.

In order to compare the degree-day factor computed by Eq. 4.5.4a against equations 4.5.4b and 4.5.4c, the spring snowmelt modelling in 2013 was validated against remotely sensed LandSAT8. Our findings show that snowmelt runoff simulated by degree-day factor estimated through equations for forest and grassland (4.2.4b and 4.2.4) would give "no snow-cover" end of melt-season by 18 April (Table 4.5), showing the SCA=0. The following findings correspond with

the SCA ratio modelled through SWE (Figure 4.11) and Landsat images (obtained between 17.04.2013 and 25.04.2013). By contrast, the original degree day factor simulation showed quicker snow thaw for five days, i.e. 13 April in a forested area. Consequently, in this study, the snow runoff model utilises the degree-day factor developed for grassland and forest areas, *i.e.* using Equation 4.5.4b and 4.5.4c.

Table 4. 5 Snow cover area changes during snowmelt season 2013 simulated by two models for degree-day factor.

α_F – degree-day factor modelled by Eq.4.5.4b; $\alpha_{original}$- degree-day factor modelled Eq.4.5.4a

Month	Date	T_{mean}, °C	d_{snow}, cm	ρ_{snow}, kg m^3	α_F	$\alpha_{original}$	$SCA_{\alpha F}$	$SCA_{original}$
March	29	0.7	57	0.32	1.8	2.5	1.0	1.0
	31	-7.1	55	0.32	0.0	0.0	1.0	1.0
April	4	1.1	55	0.34	3.1	4.1	1.0	1.0
	5	1.1	54	0.34	3.1	4.1	1.0	1.0
	6	0.4	-	0.34	1.1	1.5	1.0	1.0
	7	3.8	-	0.34	10.8	14.2	1.0	1.0
	8	6.6	-	0.34	18.7	24.7	1.0	1.0
	9	8.2	-	0.34	23.3	30.7	1.0	1.0
	10	11	41	0.36	33.5	43.6	1.0	1.0
	11	7.2	-	0.36	21.9	28.5	0.9	0.5
	12	12.8	-	0.36	39.0	50.7	0.7	0.2
	13	4.2	-	0.36	12.8	16.6	0.3	0.0
	14	2.7	-	0.36	8.2	10.7	0.2	
	15	0.6	-	0.36	1.8	2.4	0.1	
	16	-0.9	-	0.36	0.0	0.0	0.1	
	17	2.5	-	0.36	7.6	9.9	0.1	
	18	1.3	-	0.36	4.0	5.1	0.0	

4.5.1.3.2 The recession coefficient, (k)

The recession coefficient is a critical parameter of SRM as $(1-k)$ is the proportion of the daily meltwater production, which directly appears in the runoff. The recession coefficient (k) can be obtained using historical daily streamflow measurements. The coefficient is used during the periods with a decrease in discharge or with no snowmelt or rainfall,

In particular, the coefficient variability in relation to the actual discharge on day n by the discharge on day n+1 where recession coefficient is equal to $(k = \frac{Q_n+1}{Q_n})$. Since, the main focus is on k values that are less than 1, *i.e.* when the streamflow on day n+1 is less than the streamflow on day n. This coefficient is not constant and tends to increase as the magnitude of the stream discharge grows so that the SRM model requires x and y coefficients to estimate the recession coefficient on day n+1 using the magnitude of the simulated discharge on day n:

$$k_{n+1} = x * Q_n^{-y}$$

Eq. 4.5.5

Constants x and y are required for the estimation of recession coefficient, which can be estimated using the pair of recession coefficient (k_1, k_2) corresponding to Q_1 and Q_2. Thus, k_1, k_2 can be calculated by taking log using the following expression:

$$\log k_1 = \log x + y \log Q_1$$

$$\log k_2 = \log x + y \log Q_2$$

Eq. 4.5.5a

In this study, the discharge range is equal to Q_1=1 $m^3 sec^{-1}$ and Q_2=10.4 $m^3 sec^{-1}$, and x=0.83 and y=-0.488 were established using the Eq.4.8.5a. According to runoff modelling for the Shortandy catchment, on average the k coefficient was within the range of 0.2-1.0, where the lowest coefficient is established at the start - increasing to 1.0 towards the end of the melt season.

4.5.1.3.3 Runoff coefficient (c_{Sn}), (c_{rn})

The snow runoff coefficient range (c_{Sn}) and rainfall coefficient (c_{rn}) are used to estimate the percentage snowmelt and percentage of precipitation that contribute to the lake discharge. Ideally, they should be estimated as a ratio of measured precipitation and the measured runoff on a long-term basis. The actual runoff measurements have never been conducted for the Shortandy basin. However, the runoff coefficient could be adjusted without *in-situ* measurements, *i.e.* by adjusting daily discharge estimates if there is general under or over prediction (Martinec, 1994).

For Shortandy snowmelt runoff simulation, at the beginning of the snow-melt period, losses were assumed to be minor. This is due to the minimum effect of evaporation from the snow-covered surface and the c_{Sn}value is near 1.0 (Martinec, 1986). After that, when the growing season starts, more losses must be expected due to evapotranspiration and interception, so that the runoff coefficient declines. Thus, the c_{Sn}value was approximately from 1.0 to 0.5. The c_{rn} value which estimates losses for evapotranspiration during warm-season rainfall-runoff was replaced by E_{act} (Section 4.4.3) in order to avoid double counting.

4.5.1.3.4 Temperature lapse rate (γ)

The temperature lapse rate is the rate at which air temperature varies with altitude. In the SRM model, this parameter is required when weather stations at different altitudes are available. Consequently, in the SRM model, it should be determined for a single basin or each zone with a different rate. Runoff modelling for Shortandy is based on a single zone due to the altitude range in the catchment (Section 4.2.2). According to the model requirements, the lapse rate parameter could be ignored if the temperature station is located near the mean elevation of the basin (Martinec, 2008). This generalisation also excludes potential error produced by extrapolation of air temperature, which might both over-or-under predict the air temperature within the catchment. In the case of Shortandy, the only station available within the catchment is Schuchinsk weather station. It is

situated at the altitude of 433m, which is about 10m lower than the mean elevation of the Shortandy catchment (444m). Consequently, the temperature lapse rate parameter was ignored in runoff modelling.

4.5.1.3.5 The accuracy assessment of SRM

The accuracy assessment of the model is evaluated by the utilisation of the Nash-Sutcliffe determination coefficient (R^2) and volume difference (D_V) which are estimated using the following expressions:

$$R^2 = 1 - \frac{\sum_{i=1}^{n}(Q_i - Q_i')^2}{\sum_{i=1}^{n}(Q_i - \bar{Q})^2} \quad \text{Eq. 4.5.6}$$

where:

Q_i- Measured daily discharge, ($m^3\ s^{-1}$);

Q_i' - Computed daily discharge, ($m^3\ s^{-1}$);

$\bar{Q}$ - Average measured discharge of the given snowmelt season, ($m^3\ s^{-1}$);

n - Number if daily discharge values.

The deviation of the runoff volumes (D_v):

$$D_V = \frac{V_R - V_R'}{V_R} * 100 \quad \text{Eq. 4.5.6a}$$

where

D_v - Deviation of the runoff volume, %;

V_R - Measured seasonal runoff volume;

V_R' - Computed seasonal runoff volume.

Positive values of D_v indicates that simulation underestimates seasonal runoff proportion, whereas negative shows overestimation.

4.6 Groundwater model, $G_i - G_O$

Groundwater inflow and outflow from lakes is the most challenging water balance component to predict. Most groundwater models require field-based measurements on groundwater level and parameters such as soil thickness, hydraulic conductivity aquifer transmissivity, porosity etc. Previous research on Burabay lakes (Section 2.3.3) shows a limited understanding of the groundwater settings in the Shortandy catchment. The last comprehensive research into groundwater levels (Shnitnikov, 1970a) was more focused on Burabay, Ulken Shabakty, and Maybalyk lakes and establishment of groundwater connectivity between them. Yet, the groundwater interaction between these lakes and Shortandy Lake has not been established yet.

Groundwater level measurements of Shortandy Lake are not accessible for public and research purposes. Furthermore, limited knowledge of hydro-geologic settings of the catchment makes most numerical and computer-based models inapplicable for groundwater storage simulation in Shortandy.

In this project, two methods were used to estimate groundwater flux. The first approach estimates groundwater flux using water level measurements during cold-season months (i). The second approach estimates groundwater interaction through the water balance model explained in this chapter (ii). Both model outcomes will be compared and validated with the observed water volume dynamics in the lake in Chapter 5.

4.6.1 Groundwater flux estimated by measured water levels (i)

The regional groundwater model requires measured lake levels at least monthly records during the cold-season months. Here, an assumption was made regarding the groundwater input and output relationship that could be quantified more accurately only during the cold-season months, *i.e.* when the lake surface is fully covered with ice. Accurate estimation of the lake losses during warm-seasons is difficult, depending on data availability and measurement accuracy of input and

output variables. However, according to Uryvayev (1959), the water balance of cold-season months gives a better understanding of groundwater interactions with the lake.

Water balance studies conducted by Uryvayev on Burabay lakes were based on long-term climate observations (40 years) and were validated during the field trips from 1954-56. Based on these observations, a groundwater flux equation developed specifically for endorheic lakes of the Burabay region was introduced, which is described as follows:

$$G_i - G_o \approx V_{b.w} - V_{e.w.} + h_s - \sum_{cold} W_{abs}$$

Eq. 4.6.1

where

$G_i - G_o$ - Annual groundwater inflow and outflow, ($m^3 10^6$);

$V_{b.w}$ - Lake volume before winter, ($m^3 10^6$);

$V_{e.w.}$ - Lake volume at the end of winter, ($m^3 10^6$);

h_s - Water content from snow packs formed on the lake surface by the end of winter, ($m^3 10^6$);

$\sum_{cold} W_{abs}$- Total water abstraction during the cold-season, ($m^3 10^6$).

The following equation of groundwater flux is based on a water balance model developed for the cold season. The assumption is based on the relation between G_i and G_o a being constant during the year. The following simple empirical expression utilises the volumetric difference in the lake before and after the cold season. Lake volume was estimated using the GIS volumetric model (Section 4.3). h_S value was computed by snowpack measurements on the lake with a snow density of 0.35 kg m^3.

4.6.2 Water balance approach (ii)

The second approach for groundwater flux estimation is the water balance method. Based on this method, where groundwater flux is estimated by solving

Equation 4.1. *i.e.* by identifying the difference between ΔV and input and output variables. In the Shortandy groundwater model, the groundwater flux is estimated as the difference between groundwater inflow (G_i) and groundwater outflow (G_o) or $G_i - G_o$ which is assumed to alter water volume.

As in most water balance studies, the delay between precipitation and runoff is difficult to establish (Hutchinson, 1957), and so, it was ignored in the Shortandy water balance model. Consequently, recalling the Eq.4.1, the annual groundwater flux could be expressed by the following equation:

$$(G_i - G_O) = (V_{begin} - V_{end}) - (\sum P + \sum R_{\frac{rain}{snow}} - \sum E_{sub} - \sum E_O - \sum E_{act} - \sum W_{abs})$$

Eq. 4.6.2

where

$(G_i - G_O)$ - Annual groundwater flux, (10^6 m^3);

$(V_{begin} - V_{end})$ - Annual measured water volume changes, (10^6 m^3);

$\sum P$ - Total annual precipitation fell on the lake surface, (10^6 m^3);

$\sum R_{\frac{rain}{snow}}$ - Total runoff produced from the lake catchment during snowmelt season and excessive rainfall events, (10^6 m^3);

$\sum E_{sub}$ - Total annual snow sublimation from the lake surface, (10^6 m^3);

$\sum E_O$ - Total annual open lake evaporation, (10^6 m^3);

$\sum E_{act}$ - Total annual actual evapotranspiration, (10^6 m^3);

$\sum W_{abs}$ - Total annual water abstraction from both surface and groundwater, (10^6 m^3).

4.7 Summary

This chapter explains the methodology of the single lake model developed for Shortandy Lake. A conceptual water balance model which explains the relation between input and output variables was presented. Furthermore, the water balance equation (Eq.4.1.) presented in Section 4.1, explains the inter-relation

between identified water balance variables which predetermines water volume changes on a monthly basis.

Section 4.2 shows data requirements for the water balance studies, by which gaps in observations were identified. The alternative solutions for inconsistency in the dataset was discussed and presented in Section 4.2.1.

Section 4.3 explains the methodology applied for the reconstruction of water volume dynamics in Shortandy Lake over the study period. The GIS-based model, which was used for the construction of depth-volume relationship, was explained. The model is based on interpolated data from bathymetry survey and remotely sensed SRTM DEM and Landsat products.

Section 4.4 describes hydrological models selected for the quantification of output variables. For warm-season evaporation modelling, a simplified approach for the Penman equation developed by Valiantzas (2006) for the lake evaporation, whereas FAO-56 Penman model (Allen, 1998) for evapotranspiration losses produced by vegetation were selected. Cold-season lake losses were quantified using a regional model for snow sublimation. In addition, the anthropogenic impact was incorporated into the water balance model by obtaining both surface and groundwater abstraction every month from Shortandy.

Section 4.5 explains methods for quantification of input variables of Shortandy Lake. SRM model was selected for both runoff simulations, *i.e.* for seasonal snowmelt runoff and rainfall-runoff. The model is a conceptual, degree-day, hydrologic model which simulates daily runoff, and to forecast snowmelt and rainfall with limited climate data. SRM requires only daily air temperature and precipitation measurements, thus the model was applicable for Shortandy water balance studies. The model parameters were quantified and explained in Section 4.5.1.3.

Groundwater flux was estimated using two approaches, specifically, estimated through measured water levels (i) and by utilizing the water balance approach

developed for Shortandy Lake (ii) (Section 4.6). Model outcomes will be compared and validated with the measured water levels in Chapter 5.

Chapter 5 Results – Water balance model

The results chapter presents findings from a single lake model developed to examine water balance variables in Shortandy Lake. Firstly, the key findings of the quantification of input and output variables of the water balance model will be addressed. The model parameters, which are required to simulate/estimate water balance variables, will be discussed. Furthermore, the dynamics of each water balance component during the study period will be assessed.

The reconstructed water volume dynamics of Shortandy Lake will be compared with the annual relationship between input and output variables. The relative contribution of input and output variables will be examined annually so that the relationship between hydrological drivers and water volume dynamics can be explained. The historical water volume dynamics of the lake estimated by measured water levels will be analysed. Moreover, Shortandy Lake volume dynamics will be compared with the lake volume estimated using measured lake levels. Finally, model findings and model performance will be evaluated.

Chapter 5.1 Results - Output variables

This section of the thesis aims to address how the output variables of the lake water balance fluctuated during the study period in Shortandy Lake. Specifically, the warm season output variables were modelled as follows: evaporation from the lake surface during warm seasons was estimated by the open lake evaporation (E_o), and evapotranspiration from the lake catchment (E_{act}) which affects effective runoff. The only cold-season output variable was snow sublimation (E_{sub}), which is the loss from the lake surface during cold-seasons. The volume of water abstracted from the lake was supplied throughout the study period from records obtained from water supply authorities in Shortandy.

5.1.1 Estimation of Open water evaporation (E_o)

5.1.1.1 Results - Lake ice-break-up

Lake evaporation is one of the major output variables in the water balance of endorheic lakes (Rosenberry et al., 2007, Van der Kamp et al., 2008). Air temperature is the major parameter which affects evaporation flux. In Shortandy, the temperature analysis shows (Section 3.4.1.2) that warm-season mean temperature increased by +1.1°C from 1986 to 2016. The following trend was observed in the mean temperature during November, March and April (+4°C, +3.5°C and +2.5°C respectively). The temperature changes over these months affect seasonal lake ice decay (March, April) and formation (November), changing the duration of lake freezing. In many cases, variability in the duration of lake freezing has been identified as a primary indicator of climate change (Brown and Duguay, 2010). In this study, the ice break-up dates were used to identify the beginning of the warm season, i.e. when open lake evaporation losses need to be quantified.

The lake ice break-up dates and changes in the mean monthly air temperature of March and April in Shortandy Lake are shown in Figure 5.1. Correlation analysis shows a significant and strong negative relationship between the lake ice break-up dates and the air temperature deviation of April and March (r=-0.78 and $p<0.001$).

The patterns in the lake ice-off indicate a temporal trend with a weakly negative relationship during the study period (r=-0.47, $p<0.05$). The lake ice-off dates fluctuated over the period with a standard deviation of 7 days, and a mean of 126 Julian day, corresponding to 6th of May during 1986-2004. Based on the ice decay patterns in Shortandy Lake, the decreasing trend was more noticeable since 2005, where ice-free conditions in Shortandy were observed on the 120th Julian day or 30th of April.

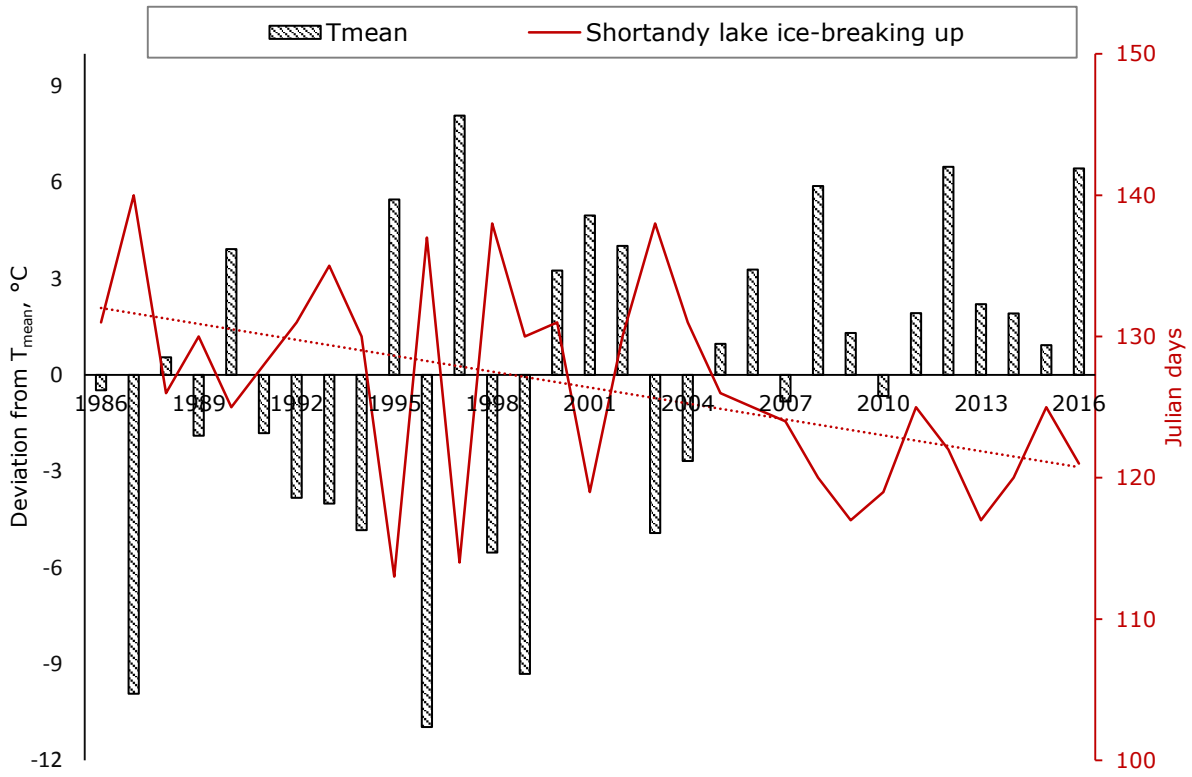

Figure 5. 1 Shortandy Lake ice-releasing and air temperature dynamics

where dates were reflected as Julian days, and T_{mean} is the mean air temperature deviation of April and May from historical averages observed from 1986 to 2016

5.1.1.2 Results – Open water evaporation (E_o)

The open water evaporation modelling established the annual evaporation losses produced by Shortandy during warm seasons from 1986 to 2016. The temporal evaporation trend fluctuated over the observed period (r=0.3 and *p*=0.08), with an average of 611mm year^{-1} and a standard deviation of 54mm.

The polynomial curve on open lake evaporation losses shows two periods with different evaporation patterns (Figure 5.2). For example, the lake evaporation flux during the period of 1986-2005 remained stable (r=0.04 and *p*=0.37) with a total annual average of 594 mm year^{-1}. However, after the lowest peak of about 543mm during 1999 and 2002, the overall pattern evolved into an upward trend. From 2006 to 2016, a significant positive moderate trend in the lake evaporation was established (r=0.4 and *p*<0.05). Specifically, annual E_o increased on average from 594mm (1986-2005) to 682mm per year, with a maximum value of 707mm in 2010.

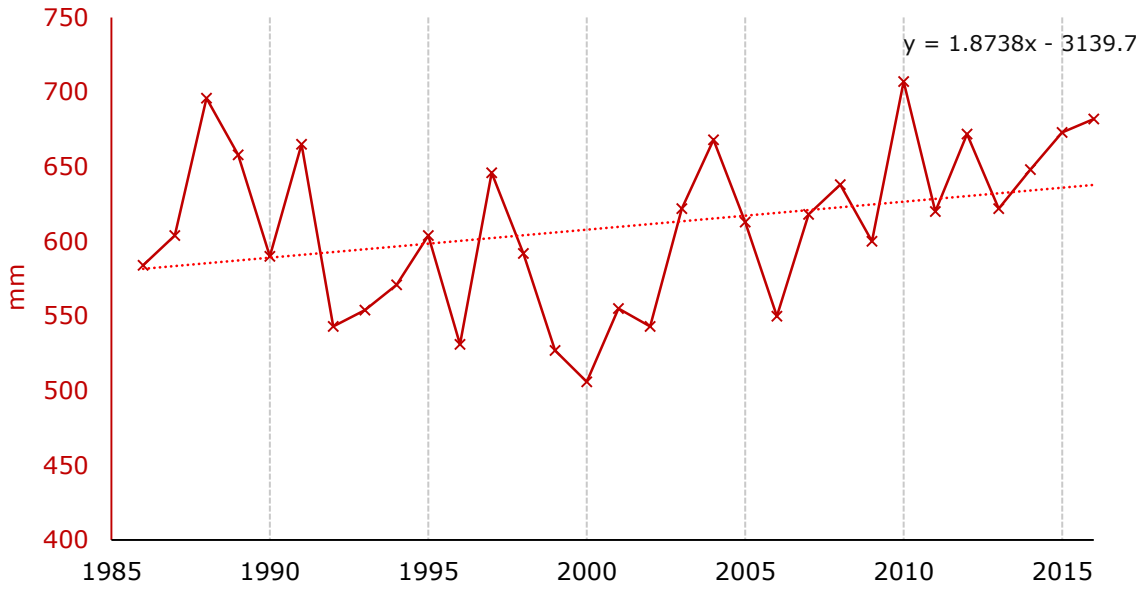

Figure 5. 2 Total annual potential open water evaporation of Shortandy Lake

5.1.2. Evapotranspiration from vegetation

The water balance model requires the estimation of evaporation losses produced by the catchment during warm season months. The following variable is critical to the simulation of effective runoff which contributes to the lake water volume after excessive rainfall events. The warm season months are relatively dry in the Shortandy area when the net balance is negative or $P_{rain} < E_{act}$. However, based on the local precipitation records, excessive rainfall events when monthly precipitation was higher than evaporation losses from the lake surface i.e. $P_{rain} > E_{act}$. These events occurred only in July during the following years: 1990, 1993, 1994, 2007, 2009, 2013 and 2014 (Chapter 3.4.2.2). Therefore, to estimate the water volume, which contributed to the lake volume during such events, the evapotranspiration flux was modelled for July months over the years mentioned above.

The FAO Reference crop evaporation model was selected to estimate evapotranspiration from the vegetated surface in Shortandy. This modelling consists of the following steps: i) estimation of potential crop evapotranspiration (E_{pet}) and ii) estimation of the crop coefficient (k_c). The first step of the modelling

estimates the effect of local climate conditions which define evaporation losses in the lake catchment (Allen, 1998). After that, the establishment of a crop coefficient adjusts the first step computations to the particular vegetation evapotranspiration needs (Section 4.4.3.1). The first step of the modelling was accomplished by solving Equation 4.4.3. The crop coefficient was estimated from the vegetation type, height and the LAI (Eq. 4.4.3.2). Subsequently, actual evapotranspiration losses were estimated by multiplying E_{pet} and k_c (Eq.4.4.3.1).

5.1.2.1 Results – Crop coefficient (k_c)

The lake catchment is predominantly occupied by deciduous forest (≈88%-75% in 1986-2009 and 2010-2016 respectively). As a result, the crop coefficient was estimated for this vegetation type. The model parameters, the maximum crop coefficient (k_{max}) and crop coefficient (k_c) (Eq.4.4.3.2a and Eq.4.4.3.2. respectively) fall within the range of 0.8 and 0.9 (Table 5.1). Similar values of k_{max} and k_c are explained due to the deciduous forest exhibiting substantial stomatal control due to reduced aerodynamic resistance (Allen et al., 2007).

Table 5. 1 The maximum crop coefficient $k_{c,max}$ for deciduous forest

using Eq.4.4.3.2a and crop coefficient (k_c) for a mid-season stage for growing vegetation by Eq.4.4.3.2 in the Shortandy catchment.

Years	$k_{c,max}$	k_c
1990	0.94	0.94
1994	0.80	0.80
2007	0.82	0.82
2009	0.86	0.86
2013	0.84	0.84
2014	0.83	0.83

The standard crop coefficient recommended for evapotranspiration estimates in a deciduous forest is equal to 1 (Allen, 1998). The k_c factor estimated for Shortandy is slightly lower (0.8-0.9) than the crop coefficient suggested by Allen (1998). However, it should be noted that the k_c values were computed for the period when the monthly net balance was positive or $P_{rain} > E_{act}$. Therefore, the reduced k_c

established for the Shortandy catchment confirms the assumption of Allen (1998), that crop coefficient could be reduced for large forests with well-watered soil condition.

5.1.2.2. Results - Actual evapotranspiration (E_{act})

Chapter 4.4.2 indicates that the vegetation evapotranspiration is estimated by multiplying potential evapotranspiration (E_{pet}) and the crop coefficient (k_c) factor, where E_{pet} is a function of climate and k_c is a function of a vegetation type. Overall, the average E_{act} in July was 95mm with a standard deviation of 10mm (Figure 5.3)

By comparing E_{pet} and E_{act} outcomes, the vegetation losses for deciduous forests estimated by climate variables only, were higher than adjusted estimations using k_c (Figure 5.3). Specifically, E_{pet} tends to overestimate for roughly 10-15% per month in the Shortandy catchment. These results coincide with the literature review findings that potential evapotranspiration tends to overestimate water loss from a vegetated surface in comparison with the crop corrected actual evapotranspiration (Lianglei Gu, 2017).

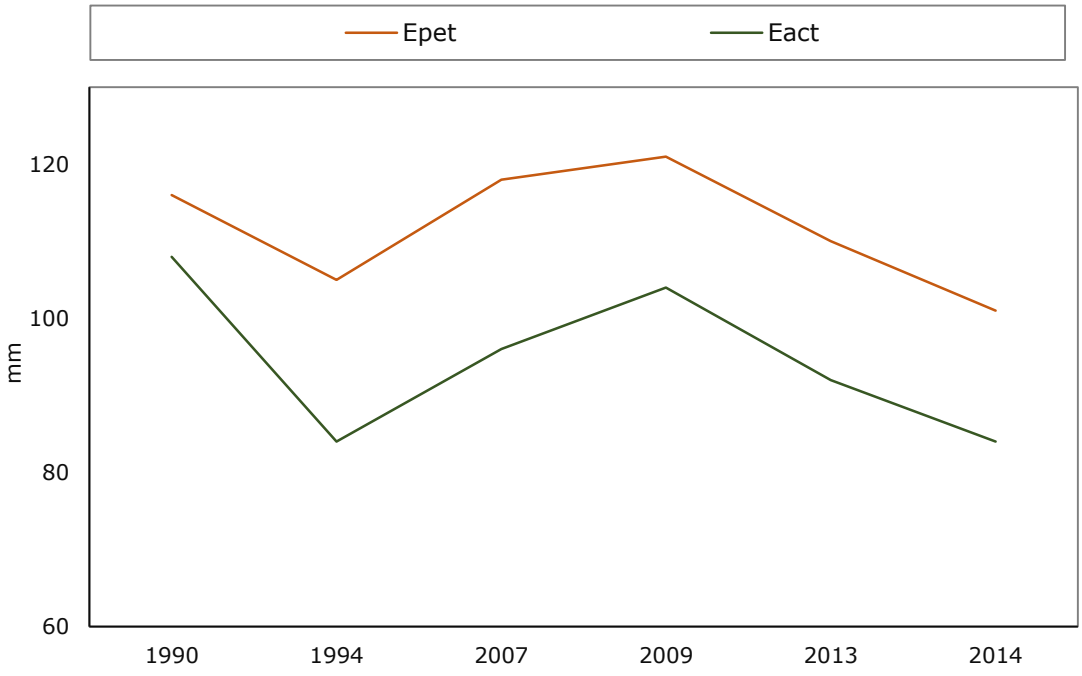

Figure 5. 3 Potential reference evapotranspiration (E_{pet}) in July

estimated by Equation 4.4.3 and actual monthly evapotranspiration (E_{act}) estimated by Equation 4.4.3.1 for months when $P_{rain} > E_o$ for the Shortandy catchment

5.1.2.3. Results – Validation of evapotranspiration

Remote sensing products have been widely applied to validate actual measurements or computed values of evaporation losses (Xiong et al., 2010, Kalma et al., 2008). In the case of Shortandy, the evapotranspiration measurements were unavailable for this study. Therefore, Global Potential Evapotranspiration (*Global-PET*) geospatial datasets (at 30 arc second resolution) were used to compare the evapotranspiration model outcomes. The Global-PET provides potential evapotranspiration estimates based on a new version of the Worldclim dataset. The evapotranspiration estimates derive from the satellite-derived data on the minimum and maximum temperature, solar radiation, water vapour pressure and wind speed (Trabucco and Zomer, 2018). These parameters were used to estimate monthly 30-year averages of potential evapotranspiration using the FAO model. In this study, the Global PET values for Shortandy catchment were abstracted using catchment boundaries in ArcMap 10.2 software. By doing this, the satellite-derived evapotranspiration values were compared with evapotranspiration estimated using field-observed data from the regional weather station.

Figure 5.4 compares monthly averages of evapotranspiration losses estimated as E_{act} (Eq.4.4.3.1) and values estimated by the Global-PET database. Correlation analysis indicates a significant very high positive relationship between E_{act} and Global-PET estimation of evapotranspiration losses for the Shortandy catchment (r=0.97 and p<0.001). Based on the Global-PET, the average historical total annual evapotranspiration flux was 695mm, and total mean monthly losses in July was 149mm from 1970 to 2000 (Fig. 5.4 and Appendix B). By contrast, the total annual actual evapotranspiration losses (estimated by Eq.4.4.3.1) in Shortandy from 1986-2016 was on average equal to 625mm annually and 138mm in July. It

is clear that E_{act} outcomes show both monthly and annual values, roughly 10% lower than the global Global-PET dataset. However, it should be noted that Global-PET estimates potential evapotranspiration, whereas in this study the evapotranspiration losses were corrected by the integrated crop coefficient (k_c) and adjusted to a specific vegetation type. Therefore, the comparison analysis demonstrates the potential error of the using the potential evapotranspiration model without crop type adjustment.

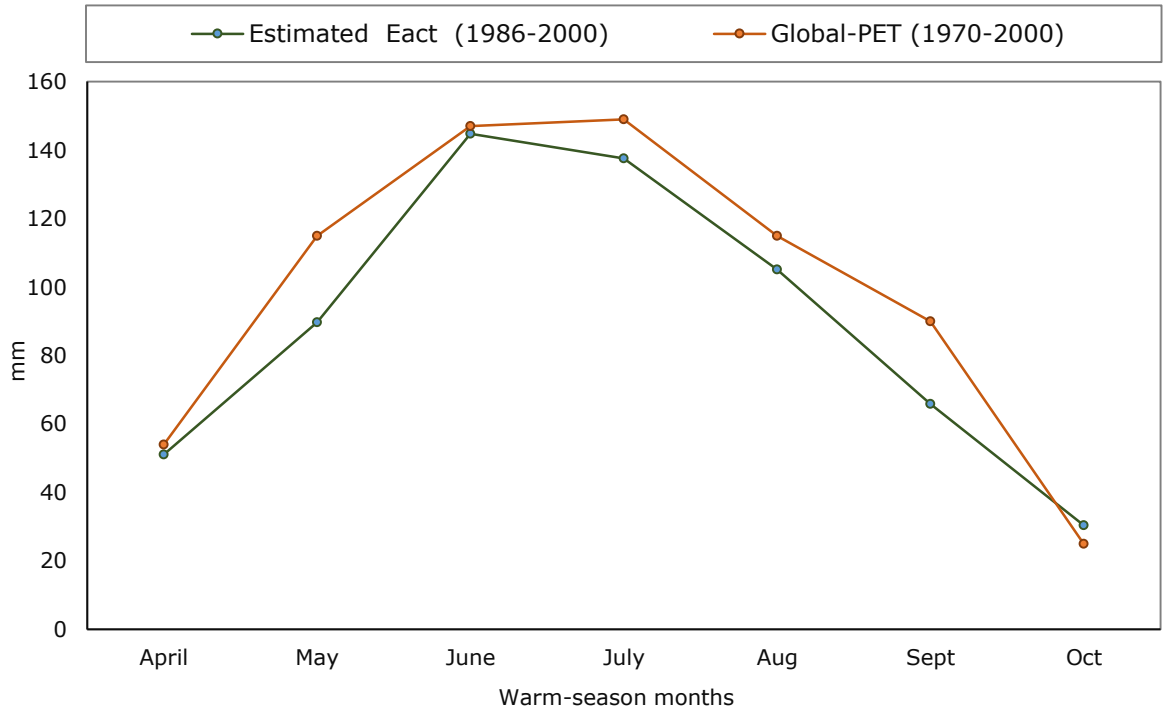

Figure 5. 4 Comparison of evapotranspiration model outcomes with CGIAR-CSI Global Potential Evapotranspiration (Global-PET) geospatial dataset for the Shortandy catchment where modelled E_{act} by FAO-56 Penman-Monteith (green line) in 1986-2016 and remotely sensed CGIAR-CSI (orange line) data are reflected as monthly averages of evapotranspiration losses in 1970-2000

5.1.3 Results - Water abstraction (W_{abs})

The water balance of Shortandy estimates anthropogenic impact by monthly water volume abstraction through surface and groundwater abstraction from the lake. It should be noted that based on the water agency - Burabay Su Arnasy, the water abstraction records exist *only* for the period of 1989-2016 for Shortandy Lake. Quantitatively data on water abstraction from the lake are not available for 1986-

1988. However, according to the authorities, the water abstraction during that period was insignificant (Telegenova G., personal communication, 26 April 2015). According to the government water agency records, the water volume abstraction was, on average, more than 4.4 $x10^6m^3$ per year which is the equivalent of a > 274mm reduction in lake depth between 1989 and 1993. Maximum water abstraction was recorded in 1989, at more than $5.5x10^6m^3$ (340mm) (Fig.5.5). Since 1996, the water abstraction from Shortandy was approximately $1.6x10^6m^3$ per year, until the government instated a policy to reduce water abstraction from the lake to *no more than $0.5x10^6m^3$ million m^3 annually in 2010 (around 30mm)*. Overall, the total water volume abstracted from the lake during the study period was equal to $51.4x10^6m^3$, where water abstraction on average was roughly $2.31x10^6m^3$ of water annually.

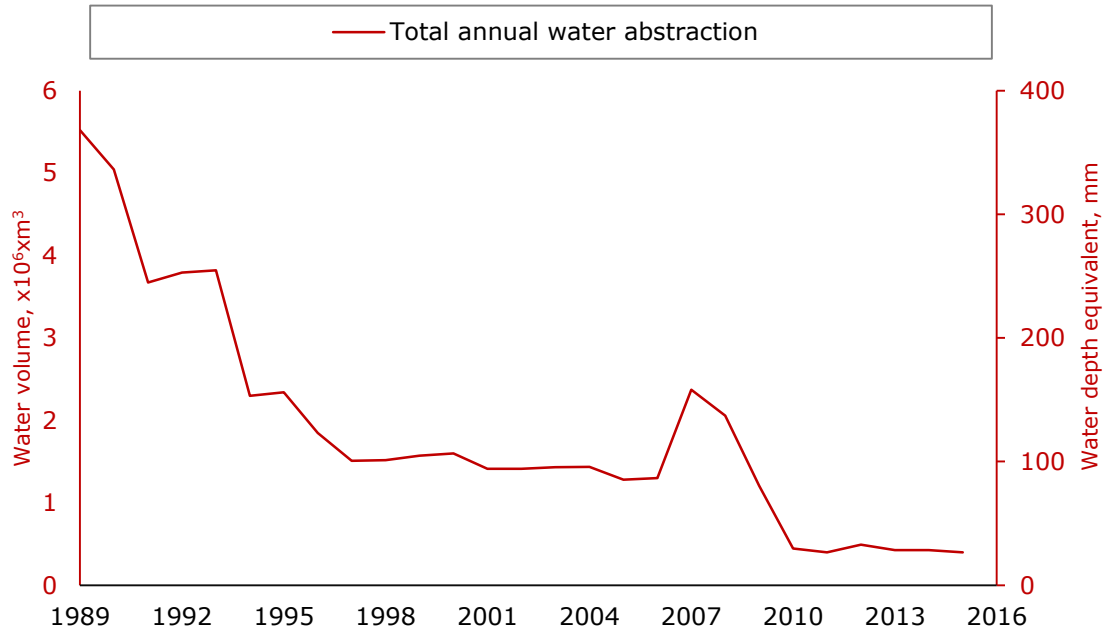

Figure 5. 5 Total annual surface and groundwater abstraction (W_{abs}) from Shortandy Lake according to Water Supply Agency in Shortandy – Burabay Su Arnasy from 1989 to 2016

5.1.4 Snow sublimation (E_{sub})

Snow sublimation and water abstraction are the only variables within the Shortandy water balance model, which estimates lake water losses produced

during the cold-season months. According to Strasser et al. (2008) and Barnhart et al. (2016), in the cold climate, when lake evaporation is equal to 0, snow sublimation is the only variable that affects snowpack properties, and as a result, affects seasonal runoff. The snow sublimation model was estimated using the regional model developed by Semenov (1990) specifically for endorheic lakes of North Kazakhstan.

Figure 5.6 shows the total monthly snow sublimation from a lake surface during cold-seasons. Temporal correlation analysis indicates a slight increase in the snow sublimation (r=0.4, p<0.05). Notably, the averaged cold season water loss from the lake surface was roughly 20mm during 1986-1999, whereas the following value increased to 25mm per season in 2000-2015. The monthly distribution of snow sublimation during cold seasons shows that Shortandy Lake produced more losses during the ice formation (November) and ice decay (March) months (6.3mm and 7.4mm respectively) (Appendix C). By contrast, the minimum losses of 2.6 and 3.3mm occurred in mid-winter months, i.e. January and December, which corresponds to the coldest annual air temperature for Shortandy Lake (Chapter 3.4.1).

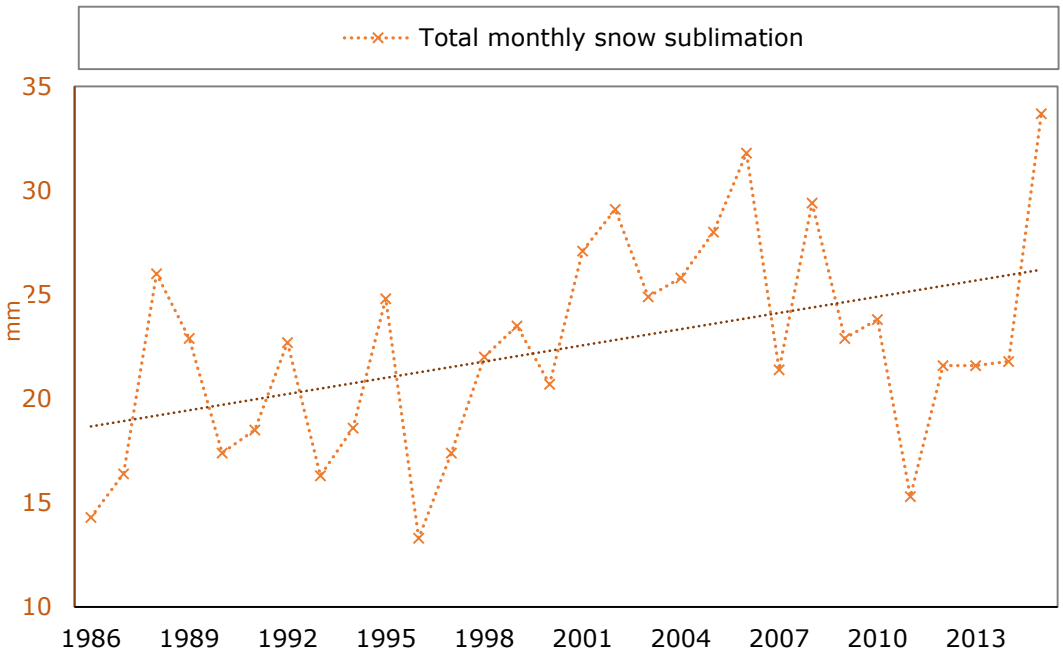

Figure 5. 6 Total annual snow sublimation (E_{sub}) from the lake surface during cold-seasons from 1986 to 2016

5.1.5 Summary – Relative contribution of outflow variables

This section of the thesis explains the main results obtained from the quantification of the output of variables of Shortandy Lake. The temporal regression indicates that the total annual outflow variables of the lake water balance remained stable during the observed period (r=0.02, *p*=0.9). The total annual water loss from Shortandy Lake, on average was equivalent to 812mm year^{1} with a standard deviation of 184mm.

The relative contribution of outflow variables of the lake water balance model from 1986 to 2016 is summarised in Figure 5.7. Key findings outline that lake evaporation is the major flux of water losses in Shortandy Lake. Specifically, the lake evaporation flux proportion was around 78% of the annual lake losses, which is on average equivalent to 611mm from 1986 to 2016. Conversely, the minimum loss was produced during cold-seasons, which is the snow sublimation. The snow sublimation proportion was about 3% (19mm) of the annual average. Anthropogenic water abstraction from the lake added, on average, 12% which is equal to 105mm of additional water loss.

To sum up, the output variables modelling reveals the following findings:

- The lake evaporation model indicates a slight increase in open water evaporation (E_o) in 2006-2016. Based on the air temperature analysis and the lake ice-cover timings, this upward trend could be influenced by the extended ice-free season in Shortandy Lake. It is clear that the warm season temperature has changed insignificantly by +0.2°C. Therefore an increasing trend in the lake evaporation flux *by roughly 30mm could be affected by extended ice-free season of roughly 7-12 days over the observed period*;

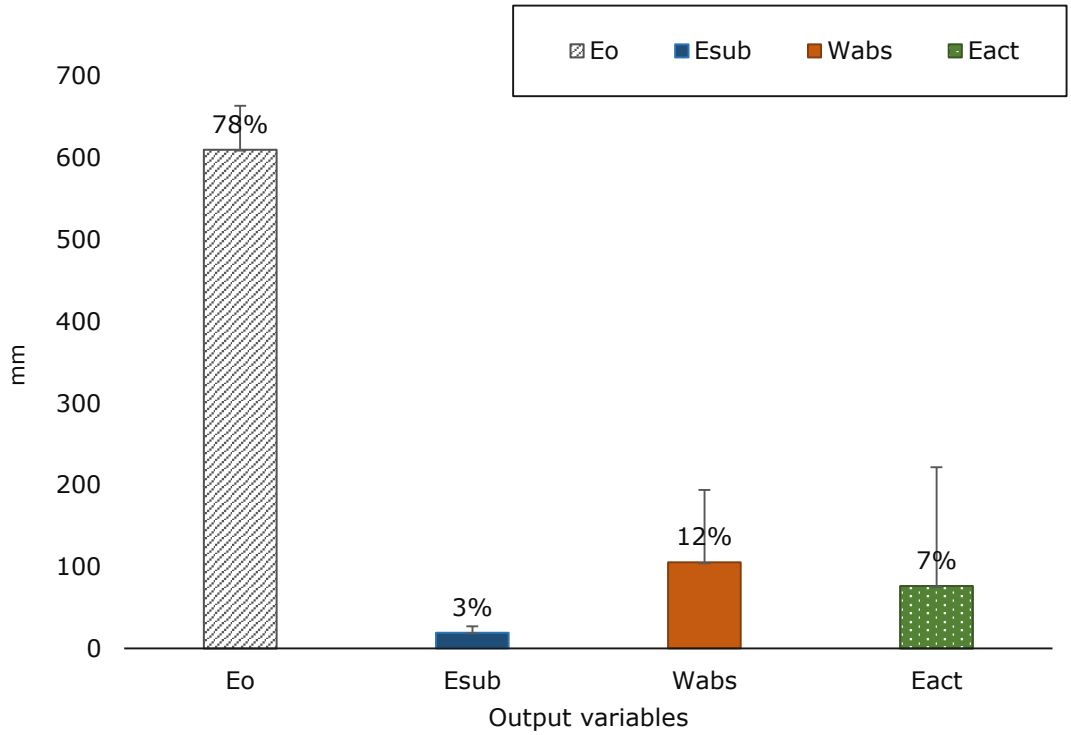

Figure 5. 7 Relative contribution and mean values of output variables estimated between 1986 and 2016 in the Shortandy catchment

where E_o is open lake evaporation, E_{sub} is a snow sublimation, W_{abs} is an anthropogenic water abstraction, E_{act} is actual evapotranspiration and error bars represent a standard deviation

- Grass evapotranspiration was modelled using the FAO Penman-Monteith approach with crop coefficient (k_c) so that actual evapotranspiration was computed (E_{act}). The model results were compared with remotely sensed Global-PET database, where a significant and very strong positive relationship was established between estimated E_{act} and remotely sensed evapotranspiration for Shortandy (r=0.97 and p<0.001);
- Using water abstraction values from the local water supply agency, it was identified that water abstraction exceeded 150 mm annually in 1989-2009 until water abstraction restriction in 2010;
- The snow sublimation model reveals a minor increase in the losses from snow cover since 2000. However, the proportion of snow sublimation was a minor component of the total annual outflow variables of Shortandy Lake.

5.2 Results - Input variables

This section of the thesis addresses how input variables of the lake water balance fluctuated during the study periods in Shortandy Lake. Input variables change based on air temperature when daily $t > 0$ counts as warm-season precipitation (P_{rain}) and $t < 0$ as a cold season precipitation (P_{snow}). Similarly, the runoff modelling varies, where seasonal snowmelt runoff is Q_{snow} and Q_{rain} is runoff produced by excessive rainfall events. The transitional period between liquid and solid phases of precipitation was estimated using the SRM model. In Shortandy, this period occurs in October-November and March-April. Snow and rainfall proportion accounted based on the relation between daily temperature and precipitation recordings. This section of the thesis reflects the key findings of the input variables modelling estimated between 1986 and 2016.

5.2.1. Estimation of snowmelt runoff $\mathrm{Q_{snow}}$

The SRM hydrological model simulates snowmelt runoff by utilising the degree-day factor (α), critical temperature (t_{crit}), runoff coefficient (c_{Sn}), and recession coefficient (k). These parameters vary during snowmelt season depending on hydro-meteorological conditions as well as snow properties accumulated in the catchment.

In SRM, the snow runoff coefficient is used to estimate the percentage snowmelt and percentage of precipitation that contributes to the lake discharge. A c_{Sn} coefficient within the range of 1.0-0.5 is applied to adjust the inflow discharge with overestimations, which is tested using accuracy assessment. Similarly, the critical temperature is applied to determine whether precipitation is snow or rain ($t_{crit} < 0$ the precipitation is snow, and $t_{crit} \geq 0$ is rain). The recession coefficient from the daily meltwater production was estimated daily (Appendix D). On average k coefficient falls within the range of 0.2-1, where the lowest coefficient is established at the start - increasing to 1.0 towards the end of the melt season.

5.2.1.1. Results SRM Variable – Temperature and Precipitation during cold-seasons

In SRM snowmelt runoff modelling, it is necessary to utilise ground-measured cold-season precipitation i.e. P_{snow}, and daily mean air temperature (T_{mean}). Figure 5.8 shows the average mean temperature during the cold-seasons and the total annual cold-season precipitation. According to the results, the temporal trend in the mean air temperature during the cold-seasons remained unchanged over the study period (r=0.2, *p*=0.22). The air temperature was on average equal to -9.3°C, and the standard deviation was 1.5°C. By contrast, temporal correlation analysis indicates a significant but weak positive trend in snow precipitation, (r=0.41, *p*=0.02), with an average value of 84mm and standard deviation of 25mm.

In 1988 and 1989, the snow precipitation was slightly lower than the historical average (70mm and 68mm respectively) until 1990, when the snow precipitation rose to 101mm. The maximum values of cold-season precipitation were recorded in 2001 (123mm), 2013 (147mm) and 2014 (140mm). In contrast, the lowest values were established in 1996 with 49mm, in 2004 with 48mm as well as in 2006 and 2009 (53mm and 63mm respectively). However, the snow precipitation was above the historical average (84mm) since 2010.

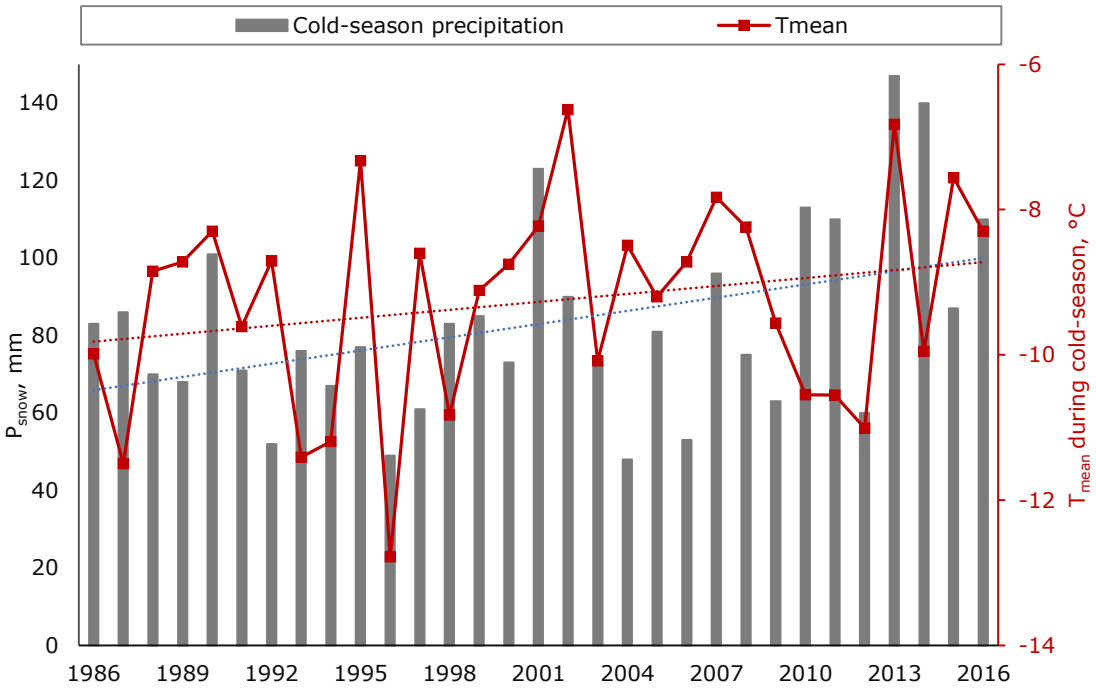

Figure 5. 8 Total annual cold-season precipitation (P_{snow}) and mean air temperature of cold-seasons

where P_{snow} is snow precipitation, and the air temperature was estimated for November, December, January, February, March and April

5.2.1.2. Results SRM Parameter - Degree-day factor (α)

Kuusisto (1980) long-term study over variability of degree-day factor established that forest canopy decreases the degree-day factor on the average by 0.16mm°C^{-1}d^{-1}. Section 4.5.1.1.1 showed that Shortandy catchment is dominated by boreal forest. Therefore, the degree-day factor is computed for forest (α_F) and grass areas (α_G) separately (Equation 4.5.4b and Equation 4.5.4c, respectively). This factor is a function of snow density which changes throughout the cold-season. Figure 5.9 shows that the degree-day factor estimated for forest area (α_F) was lower than for the grassland (α_G). The degree-day factor was on average within the range of 2.2-3.0 for forest and 3.1-3.9 for grass area, where α_G variability was higher than α_F (0.7 and 0.4 respectively). In SRM, the degree-day factor parameter is used to convert the number of degree-days into snowmelt depth (Martinec, 1960). Consequently, a lower degree-day factor produces lower

snowmelt depth. Therefore, based on Figure 5.9, *the snow cover thaw process was slower for a forest than in grassland*.

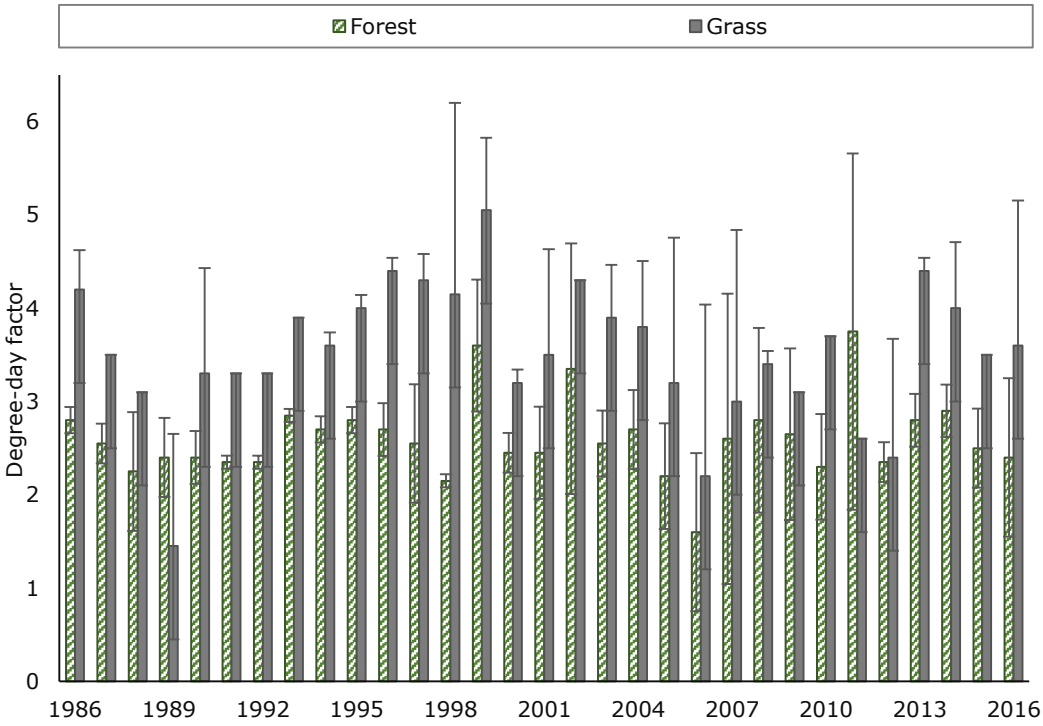

Figure 5. 9 Averaged degree-day factor estimated for forest and grass areas of the Shortandy catchment during the snowmelt seasons from 1986 to 2016

5.2.1.3 Results SRM Parameter – Snow cover area (SCA)

The SCA ratio is an important variable required for SRM simulations. In literature, snow-mapping have been successfully implemented using SWE changes during snowmelt season and remotely sensed products (Stigter et al., 2017, Dawson et al., 2018). In this study, the SCA ratio was derived from the relationship between point-measured SWE and computed degree-day factor (Chapter 4.5.3). The following ratio falls within the range of 0.0 for "no snow-cover" and 1.0 or "full snow-cover" (Martinec, 1986).

According to the findings, in most cases, the ratio was equal to 1.0 in forested areas, which means that Shortandy forests were primarily fully covered with snow during the cold-seasons (Fig. 5.2.1.3). The lowest SCA was equal to 0.39 and 0.51 in 1988 and 1989 respectively.

In general, the lower SCA ratio and SWE in forest corresponds with the reduced P_{snow} observed in Shortandy. Specifically, full snow-coverage was not reached in those years, when P_{snow} <70mm (Figure 5.10). The highest peaks of the SWE coincide with P_{snow} in the following years: 1990, 2001, 2010, 2013 and 2014. However, based on statistical analysis, a weak and non-significant correlation between P_{snow} and the SWE in forests was established (r=0.3, *p*=0.07). Based on the graph, increasing dynamics in P_{snow} since 2010 did not correspond with the SWE dynamics. Furthermore, in comparison with the historical proportion of snow precipitation, SWE of snowpack in the forest was noticeably higher. For example, in 1995 with only 67mm of P_{snow}, the SWE reached the maximum value of 232mm. By contrast, with an increase of snow precipitation after 2010, SWE response was lower.

Overall, SWE in forests fluctuated considerably (standard deviation ≈47), yet the overall trend remained stable during the study period (r=-0.03, *p*=0.88), and SWE was on average equal to 127mm during the cold-seasons.

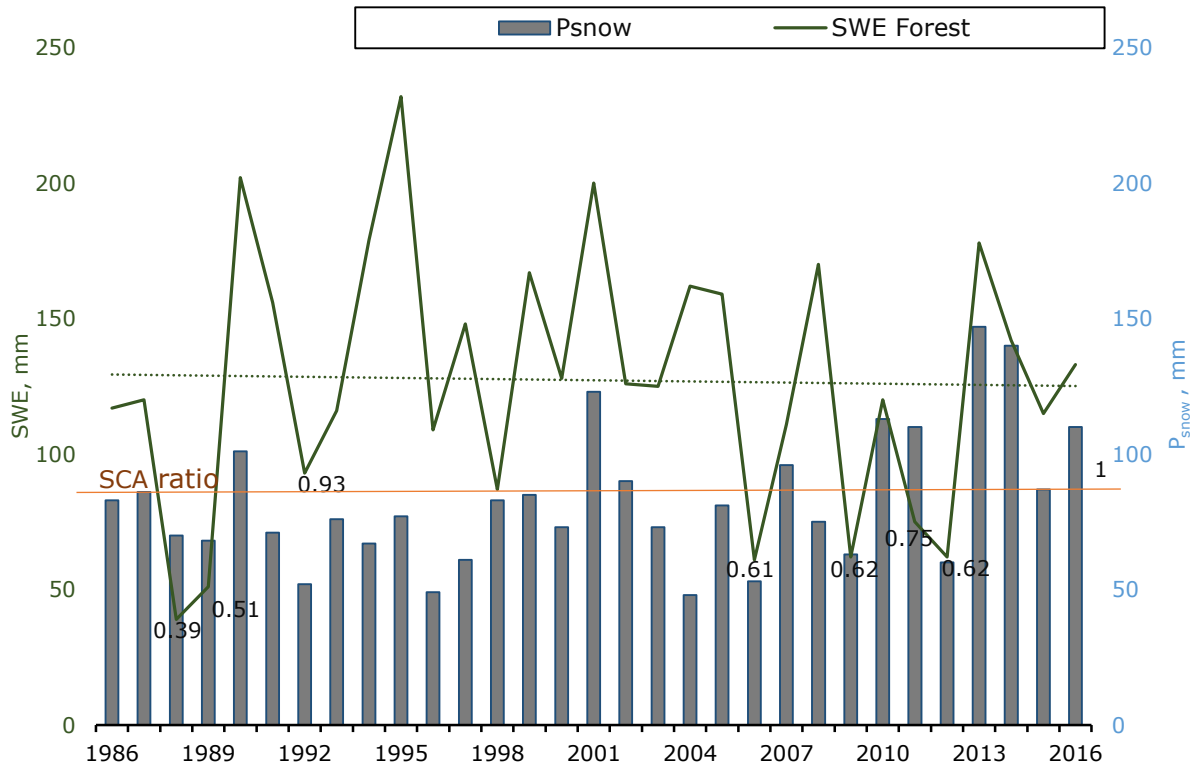

Figure 5. 10 Mean annual snow water equivalent (SWE) and annual SCA ratio of a snowpack accumulated in the forest by snowmelt season (green line) and total annual snow precipitation (grey column)

It is clear from Figure 5.11 that full snow coverage was infrequent in grasslands compared with forested areas in Shortandy. The lowest SCA ratio established for grassland is different from the lowest values recorded for the forest. For example, the lowest SCA ratio simulated for grassland in 1998 and 2002 (SCA≈0.2), whereas this ratio was equivalent to 0.9 and 1.0 for forests respectively, indicating a significant snow coverage difference between forest and grassland. The regression analysis between SCA estimated for forest and grassland indicates a non-significant correlation between ratios (r=0.07 and p=0.72).

Unlike the forested area of Shortandy, a significant weak positive correlation between SWE in grass and snow precipitation was established (r=0.36, p=0.047). The overall temporal trend in SWE in grassland remained stable during the study period (r=0.1, p=0.5) with an average of 62mm annually.

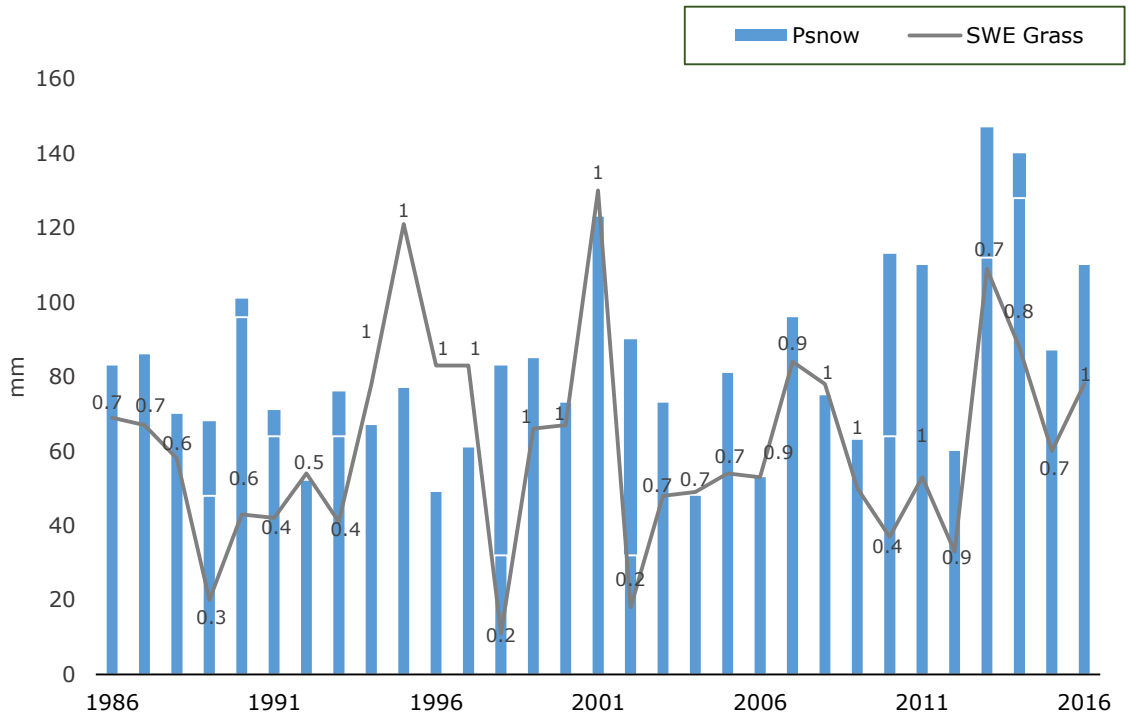

Figure 5. 11 Snow water equivalent (SWE) of a snowpack accumulated in grassland and SCA ratio of grassland during cold-seasons in Shortandy

Overall, the snow accumulated in the forest was significantly higher than in grassland (127mm and 62mm). Snow coverage in the grassland was variable, whereas in forested areas the snow accumulation was constant and provided a significant snow coverage every year during the simulated period. The difference in snowpack formation in forest and grassland is associated with various snow density features (Chapter 5.2.1.2), where snow cover in grassland is more sensitive to radiation and due to the higher effect of wind (Adams, 1976, Kuz'min, 1963). Furthermore, since grassland accumulates shallow snow cover, the snowpack is more sensitive to winter rainfall events, which result in a quicker melting in grassland than in forest (Adams, 1976).

Snow cover modelling shows that interpretation of the SCA ratio in the understanding of cold-season variation is less informative than SWE. Key findings of this section show that SWE is more sensitive to changes in snowfall precipitation than the SCA ratio. By contrast, SCA is more sensitive during the spring arrival due to the quick response of the snowpack albedo.

5.2.1.4 Results SRM model outcomes

The snowmelt runoff modelling shows that seasonal runoff in Shortandy is tightly linked to the seasonal amount of snowfall, snowpack accumulation and areal distribution throughout the catchment. Figure 5.12 illustrates the snowmelt process duration in forest and grassland plotted with the mean air temperature during the snow-thaw in Shortandy. The duration of the snow-thaw season was on average 22 days in the forest and 14 days in grassland. On average, the melt season occurred by 28th of March and ended by 19th of April at the Shortandy catchment. The overall trend shows a significant reduction in snowmelt duration by 12 days (r=0.5, p<0.001) during the study period. Furthermore, snowmelt duration in the forested area at the Shortandy catchment was driven T_{mean} and SWE, where the snowmelt duration shows a significant moderate negative relationship between T_{mean} (r=-0.6, p<0.001) and significant weak positive

relationship with SWE (r=0.4, p<0.05). In contrast, the relationship between snowmelt duration in grassland was statistically significant with the air temperature only (r=0.61, p<0.001).

To sum up, air temperature during the spring months controls melt-season duration in forested and grassland areas. SWE and snow precipitation was non-linear since 2010, where an increasing trend in snow precipitation was reflected in a lower response of SWE. In the forested area, snowmelt duration was reduced during the study period, which could potentially affect snowpack properties in Shortandy. Moreover, the non-linear relationship between P_{snow} and SWE could be explained by increasing losses from snow sublimation during the 2000s (Section 5.1.4).

The following section of the thesis reveals that the mean air temperature during the cold-seasons remained stable (-9.3°C) (Chapter 5.2.1.1). However, the start of seasonal snow-thaw indicates that T_{mean} fluctuation has reduced the snowmelt process duration in the forested area.

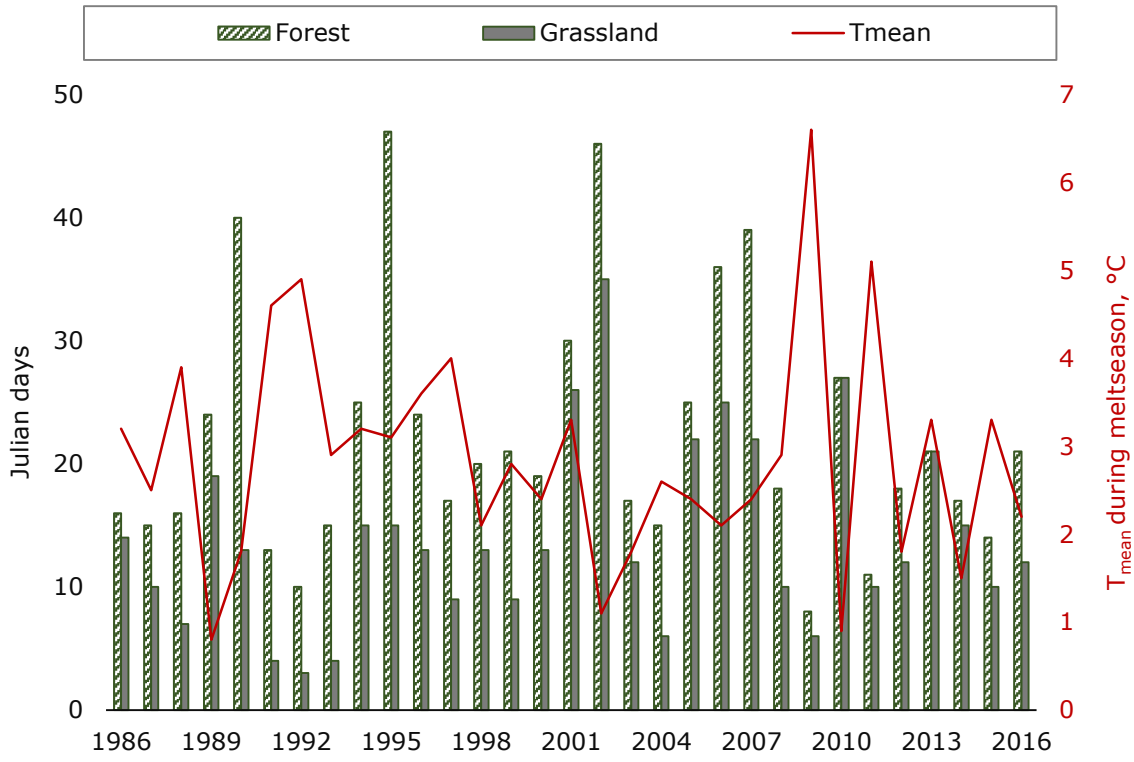

Figure 5. 12 Total duration of seasonal snowmelt in the forest (green) and grassland (grey) plotted with the mean air temperature from 1986 to 2016 in the Shortandy catchment

5.2.1.5 Results – Snowmelt runoff estimations

Snowmelt runoff remained unchanged during the study period (r=0.1, p=0.5), with, on average, 248mm of water contributed to the lake volume annually. Regression analysis on snowmelt runoff shows a significant moderate positive relationship (r=0.6, p<0.05) with SWE (r=0.6, p<0.05) and snowmelt duration (r=0.6, p<0.05). According to the model outcomes, runoff produced by snowmelt varies from year to year with a standard deviation of 122mm. The interannual variation in seasonal runoff shows 2-3 years of reduced snowmelt runoff. For example, the lowest runoff simulated in 1988 and 1989, with R_{snow} was four times less than the historical average (less than 60mm of the lake depth) and in 1998 and 2010 with a lower magnitude (68mm and 90mm).

In Shortandy, a decreasing trend in snowmelt runoff was followed by a rapid increase for 1-3 years. For example, the highest peak of runoff was in 2002 with more than 182 mm (around $9x10^6 m^3$ of water volume). Interestingly, the highest peak of simulated runoff discharge did not coincide with the highest SWE values (Figure 5.13). For example, in 2002, the maximum SWE was equal to 158mm at the beginning of the snowmelt season, which is not the maximum value over the observed period in Shortandy. However, a long snowmelt season (46 days) occurred in 2002, and relatively low mean air temperature (1.1°C) resulted in re-accumulation of snow coverage in April.

To sum up, runoff modelling shows that the snowmelt process in Shortandy is driven by SWE in snowpack and snowmelt duration. SWE was significantly higher in a forested area in comparison with grassland. Key findings indicate that trends in snow precipitation and SWE was non-linear, where SWE reduction could be affected by quicker snow thaw during the observed period. These findings concur with the literature, where significant SWE and reduction of snowmelt duration was estimated for the cold regions of the Northern Hemisphere (Brown, 2000, Brown and Mote, 2009, Räisänen, 2008, Déry and Brown, 2007). Moreover, lower snow

precipitation in Shortandy during the 1980s and 1990s corresponds to Brown (2000), where a significant snow cover reduction was established for Eurasian mid-latitude areas (40°-60°N) due to the increasing air temperature (1.26°C 100yr^{-1}) and long-term decrease in SWE during April.

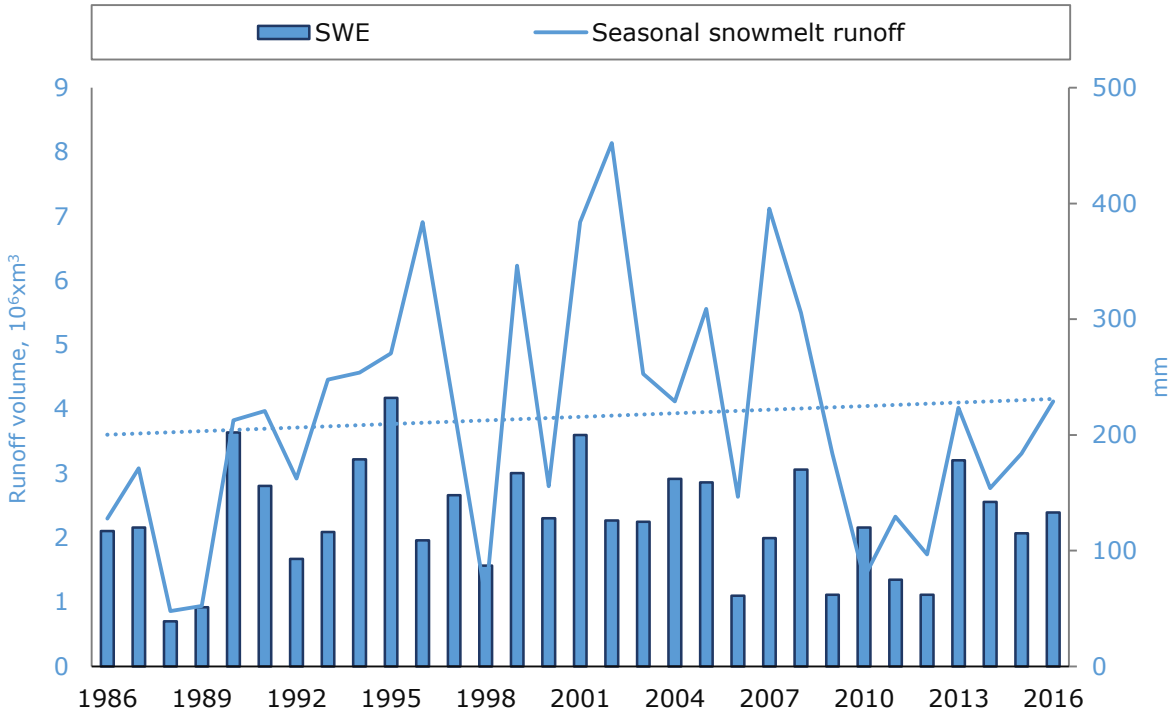

Figure 5. 13 Seasonal runoff volume estimated by the SRM model and SWE in snowpack accumulated in the forested area of the Shortandy catchment from 1986 to 2016

5.2.1.6 Results – Snowmelt Runoff Model accuracy assessment

Figure 5.14 illustrates seasonal runoff produced in the Shortandy catchment from 1986 to 2016 and the seasonal deviation in runoff volumes (D_V) which is estimated using measured and computed discharge and average Nash-Sutcliffe determination coefficient (R^2). D_V estimation (Figure 5.14) was used to adjust the runoff simulations with overestimates using c_{Sn} coefficient.

The accuracy assessment results illustrate that the average R^2 was equal to 0.97 while the volume difference between computed and measured volume shows on average 1.3% of underestimation of a seasonal runoff during the period. Based

on SRM performance for runoff predictions in the Shortandy watershed, the lowest determination coefficient (≈0.89 and 0.91) was established for years with the minimum runoff values in 1988 and 1989 respectively.

It is difficult to compare SRM performance on the Shortandy catchment for seasonal runoff predictions with other SRM simulations. The model has not been evaluated on small lake catchments (>50 km^2) with an altitude range less than 500m, i.e. with only one elevation zone for 30 years of runoff simulations.

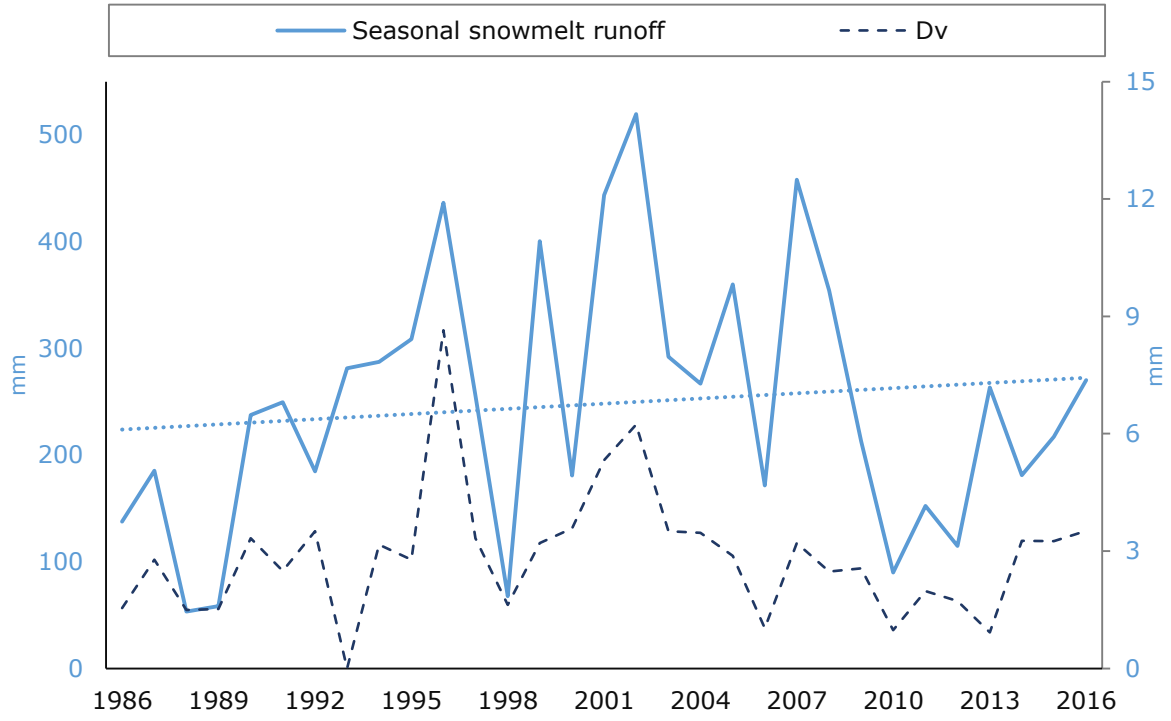

Figure 5. 14 Total seasonal snowmelt runoff and estimated deviation of the runoff volume (D_v) between computed and measured discharge produced in the Shortandy catchment

5.2.2 Estimation of rainfall-runoff R_{rain}

In this study, the SRM model was used to estimate both seasonal snowmelt as well as runoff produced by excessive rainfall events. In SRM, the runoff coefficient is used to estimate the percentage of precipitation that contributes to the lake discharge (Chapter 4.5.4). The critical temperature parameter was applied to determine whether precipitation is snow or rain ($t_{crit} < 0$ the precipitation is snow,

and $t_{crit} \geq 0$ is rain). The recession coefficient was estimated daily, which transforms daily rainwater to runoff produced from the catchment (Appendix D). Based on Pilgrim et al. (1988), the arid and semi-arid regions are in fragile hydrological balance. The hydrologic behaviour of the catchments can be modified by prolonged sequence of wet or dry periods. In semi-arid regions, rainfall is highly variable, in both time and space comparing to those occurring in regions with a more humid climate.

In this model, the balance between precipitation and evapotranspiration is evaluated. This assumption has been successfully applied for estimation rainfall-runoff in arid and semi-arid regions (Cirilo et al., 2020, Love et al., 2010, Zhang et al., 2016). The following relationship characterises the response of a catchment to rainfall, in terms of production of runoff versus interception, transpiration and evaporation of water, where evaporation processes and interception play a controlling role in runoff generation (Love et al., 2010). Based on the local precipitation records, the excessive rainfall events occurred in July during the following years: 1990, 1993, 1994, 2007, 2009, 2013 and 2014. In fact, the total monthly precipitation was higher than evapotranspiration losses from the catchment or $P_{rain} > E_{act}$ (Chapter 5.1.2.2), whereas for other years warm-season precipitation and evaporation relation was negative or $P_{rain} < E_{act}$. In addition, years with excessive rainfall months were compared with the monthly lake levels changes, which confirmed excess water contributing the lake volume (further discussed in Section 5.6). Therefore, to estimate the water volume which contributed to the lake volume during such events, the SRM model was used to estimate Q_{rain} in the month of July over the years mentioned above.

5.2.2.1 Rainfall Precipitation P_{rain}

The warm season precipitation pattern shows year-to-year variation, where the total annual rainfall proportion was on average 256 mm year^{-1} with a standard

deviation of 80mm. Temporal correlation indicates no significant change in warm-season precipitation during the study period (r=0.26, *p*=0.17).

Figure 5.15 illustrates the lowest values of rainfall occurred in 2010, 1988 and 1992 when P_{rain} was two times lower than the historical average. In contrast, the maximum proportion of rainfall fell in 1990, 1993, 1994, 2007, 2009, 2013 and 2014.

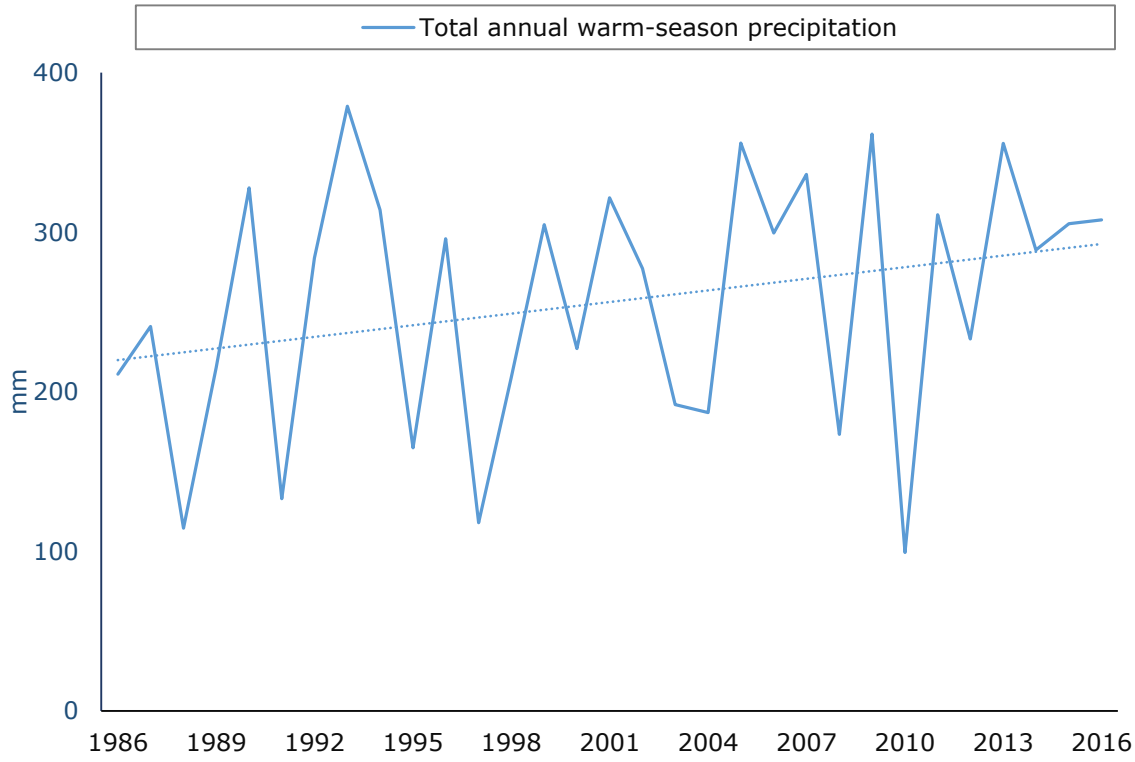

Figure 5. 15 Total annual warm-season precipitation, where P_{rain} is was estimated based on $t_{crit} \geq 0$

Figure 5.16 compares the monthly distribution of the total mean annual warm-season proportion with years when excessive rainfall events occurred. It is clear from the graph that the major proportion of warm-season precipitation fell during July. During the study period, the annual proportion was 31% on average (79mm), whereas in wet years, when $P_{rain} > E_o$, P_{rain} in July it was almost 44% (149mm) of the total annual. The lowest proportion corresponds to April (7-6%) and the autumn months (September and October) with 9-7% of the total annual proportion.

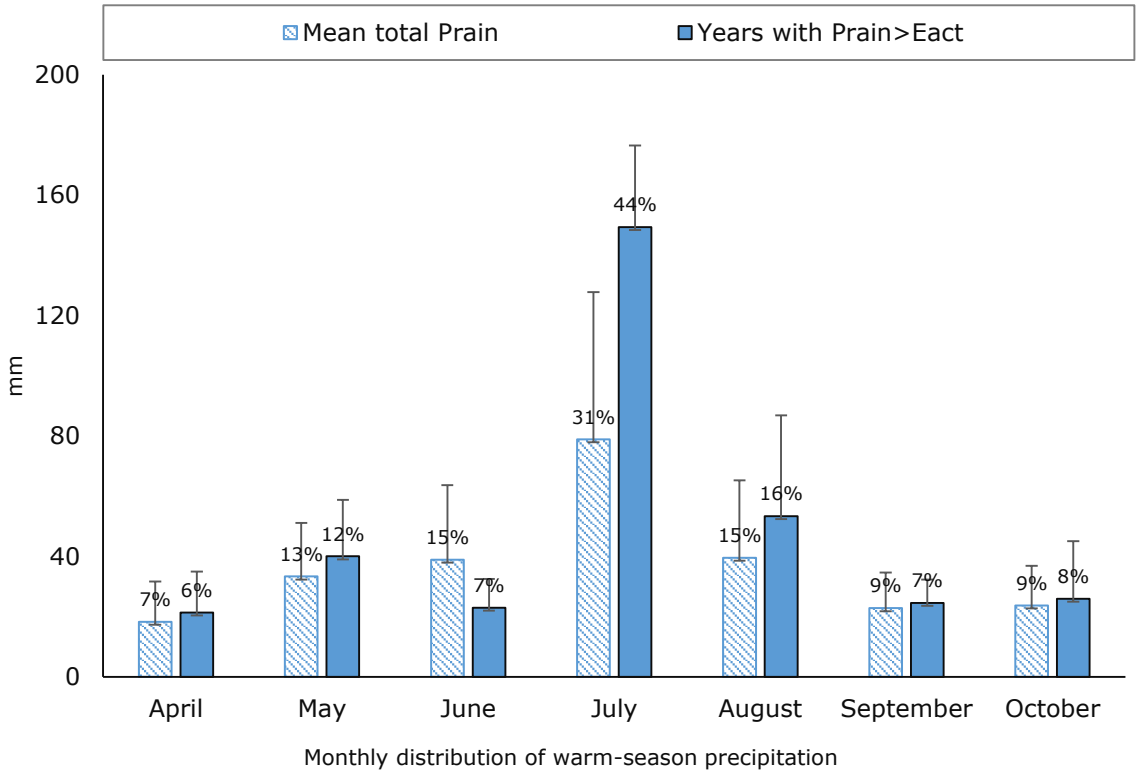

Figure 5. 16 Total monthly warm-season precipitation distribution throughout the year (blue chart) and total monthly warm-season precipitation distribution in years with excessive rainfall events or when monthly warm precipitation was higher than evapotranspiration losses ($P_{rain} > E_{act}$), where error bars show a standard deviation

5.2.2.2 Results – Rainfall-runoff

Figure 5.17 summarises the total monthly rainfall-runoff produced in the lake catchment. In 1990 and 1993, the rainfall-induced runoff proportion was higher than 600mm per month. However, after the lowest Q_{rain} value estimated in 1994, the runoff proportion decreased and was less than 450 mm.

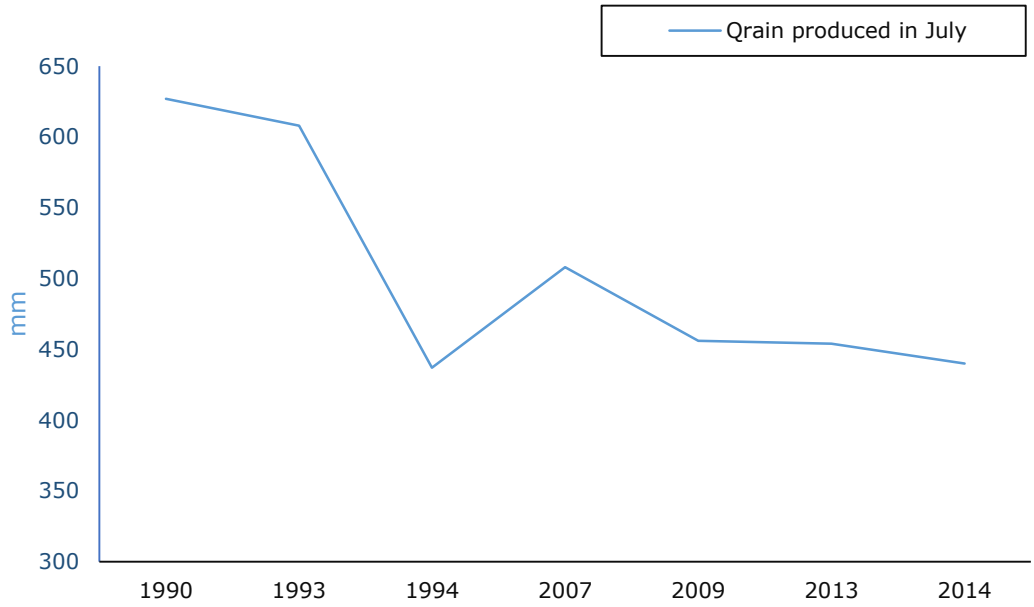

Figure 5. 17 Total monthly rainfall-runoff (Q_{rain}) produced in the Shortandy catchment occurred from 1986 to 2016

5.2.3 Summary – Relative contribution of input variables

The input variables show variation from year to year, with a standard deviation equal to 324mm and the mean total annual input of 702mm. Temporal trend in the total annual input of the Shortandy water balance remained stable from 1986 to 2016 (r=0.3 and *p*=0.107).

The relative contribution of input variables during the study period was reflected in Figure 5.18. The key findings show that water input was predominantly driven by precipitation falling during the warm season, where the total annual input contribution to the lake volume was equal to roughly 37%, which is on average 256mm from 1986 to 2016. Seasonal snow-runoff contributed to the lake volume every year and was approximately 35% of the total annual input with a standard deviation of 217mm. Cold-season precipitation (P_{snow}) was equal to 13% or 84mm on average during the study period. Rainfall-induced runoff was only 9% (114mm) of the total annual input proportion during the study period, with the highest standard deviation of 217mm. However, it should be noted that the Q_{rain} contribution to the annual water balance when there were excessive rainfall events

(when $P_{rain} > E_{act}$) was higher (on average 41%) (Chapter 5.6); however, such events occurred six times during 30 years of simulations.

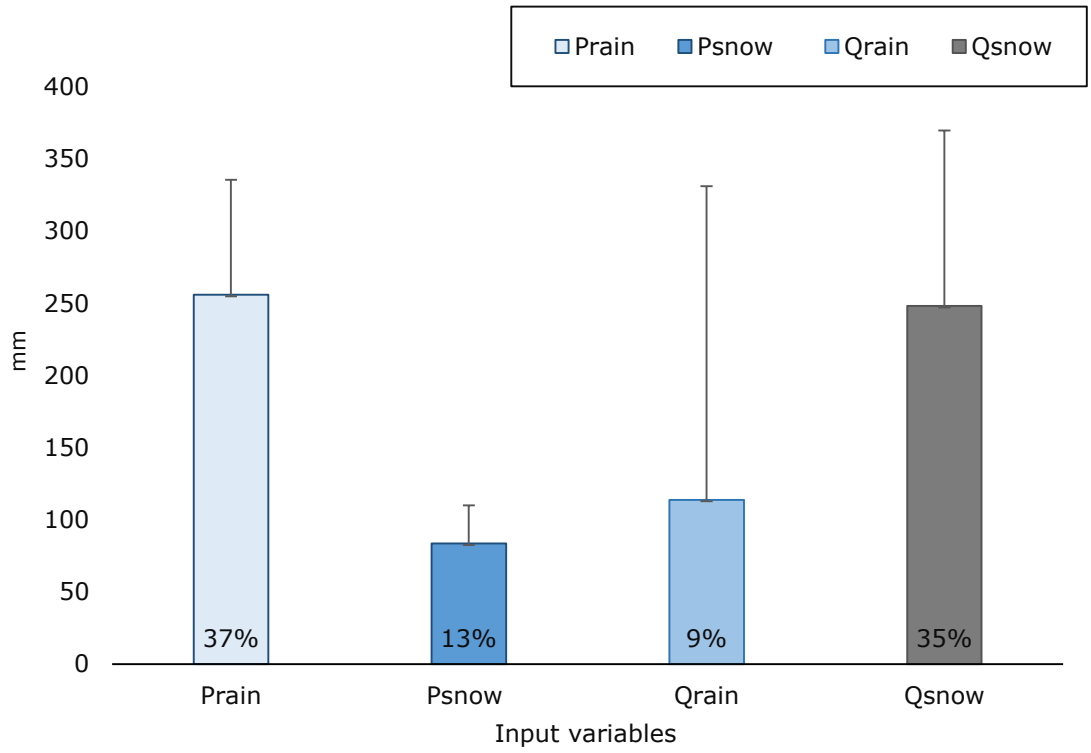

Figure 5. 18 Relative contribution and mean values of input variables estimated from 1986 to 2016 in the Shortandy catchment

where P_{rain} is warm-season precipitation, P_{snow} is cold-season precipitation, Q_{rain} is a rainfall-runoff, Q_{snow} is a snowmelt runoff and error bars represent standard deviation

To sum up, input variable modelling revealed the following findings:

- Based on snowmelt runoff modelling, the spring season is highly variable in the Shortandy area with regards to the snow accumulation and distribution over the catchment. The air temperature also affects the melt-season duration. The runoff modelling shows that snowmelt processes in Shortandy were driven by SWE in snowpack and snowmelt duration
- The SCA parameter in the SRM model shows great variation over the cold-season. The SCA ratio, as well as SWE, was higher in the forest than in grassland. Moreover, the degree-day factor (α) simulation showed that the snow-thaw processes were on average eight days slower in the forested area than in grassland;

- The runoff simulations show interannual variations. The runoff modelling shows great variability in rainfall, especially during warm-seasons;
- Key findings indicate a step-change in snow precipitation and SWE since 2006, where SWE reduction could be affected by air temperature changes during cold-season months. The nature of the non-linear relationship between snow and SWE in this particular region will be further addressed in Chapter 7;
- The accuracy assessment on SRM model results showed underestimation of seasonal runoff, where the lowest coefficient of determination was established for years with the lowest seasonal runoff predictions in the Shortandy catchment.

5.3 Groundwater model ($G_i - G_o$)

In this study, the groundwater flux was estimated using two different approaches. The first approach estimates the groundwater flux through measured water levels of the lake during the cold-season months (i) and second, the water balance approach, which estimates groundwater flux using the water balance equation (ii). Results will be compared and validated with measured water levels.

5.3.1 Results - Groundwater flux (i)

The regional groundwater model established by Uryvayev (1959) utilises measured lake levels during the cold season. In this model, the cold season is defined as months when the lake surface was frozen, i.e. fully covered with ice. Therefore, the lake volume difference calculated by the measured lake levels at the start and by the end of the cold season month was required.

The groundwater inflow and outflow relationship in Shortandy based on the groundwater model (i) was reflected in Figure 5.19. The parameters used for this model are shown in Appendix E. The groundwater flux was estimated for cold-season months, i.e., from November to March within the observed period in Shortandy Lake (Figure 5.19). Furthermore, the negative groundwater flux was established in November (-0.2×10^6 m^3), whereas the highest proportion of groundwater inflow occurred during January (0.2×10^6 m^3).

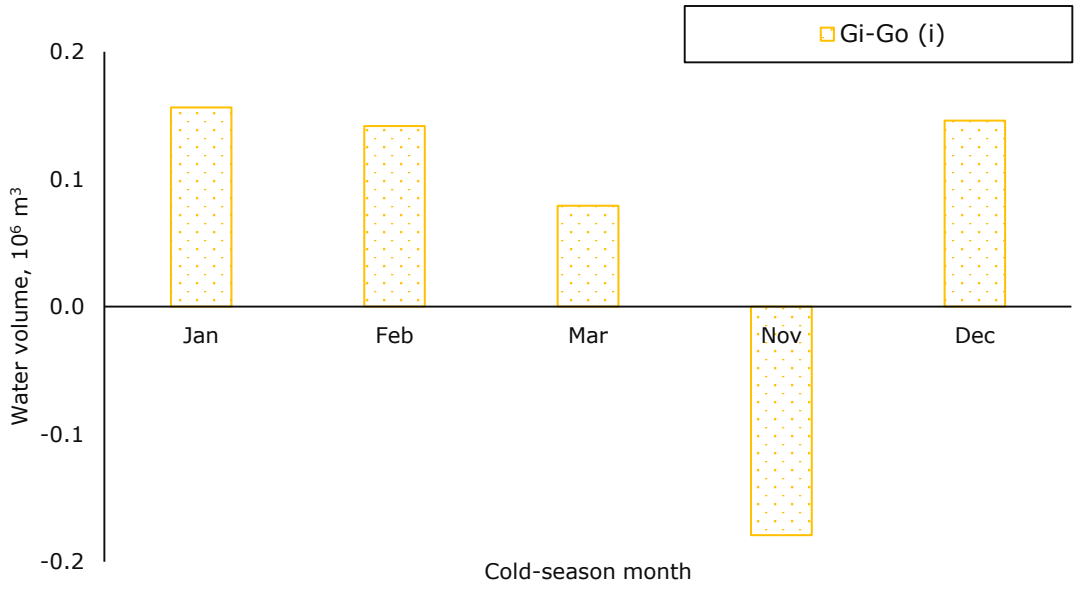

Figure 5. 19 Groundwater flux ($G_i - G_o$) estimated by the regional model using measured water levels during cold-season months

The total annual groundwater storage estimated by measured water levels is illustrated in Figure 5.20. The highest negative $G_i - G_o$ was estimated for 1997 and 2007, with approximately -1.1x10^6 m^3 and -1.6x10^6 m^3 of water outflowing from the lake volume (71mm and 102mm of the lake depth respectively). By contrast, the most positive groundwater flux was established in 2010 and 2016. According to this model, groundwater contributed 2.1x10^6 m^3 (135 mm) and 2x10^{6}m^3 (130mm) to the lake volume during these years. Overall, the groundwater flux established by measured water levels was equal to *+0.29x10^{6}m^3 on average (annual)* during the period.

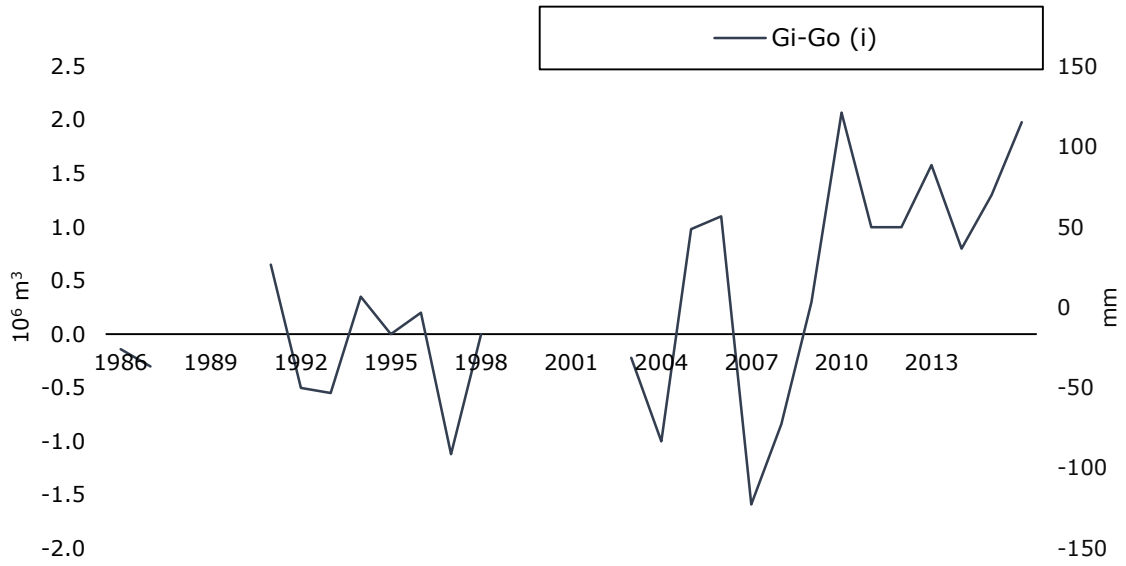

Figure 5. 20 Total annual groundwater flux ($G_i - G_o$) (i) estimated by the regional model using measured water levels during cold-season months

5.3.2 Water balance approach (ii)

The water balance approach estimates the groundwater flux as is the difference between input and output variables of the water balance. Similarly to the previous groundwater model, this model requires measured water level of the lake ($V_{begin} - V_{end}$) so that water volume changes during the year could be established (Appendix E). The lake levels were converted into volumetric water changes using the GIS-based volumetric model.

According to the model, the relationship between groundwater inflow and outflow on average was equal to $0.16 \times 10^6 m^3$ (Figure 5.21). The highest positive groundwater flux was simulated for years 2010 and 2016 with a water volume contribution with $2.3 \times 10^6 m^3$ and $3.3 \times 10^6 m^3$, which is equivalent to 219mm and 153mm of the lake depth respectively. In 2007 and 2008, the most negative groundwater flux with -1.5×10^6 and -1.4×10^6 was established.

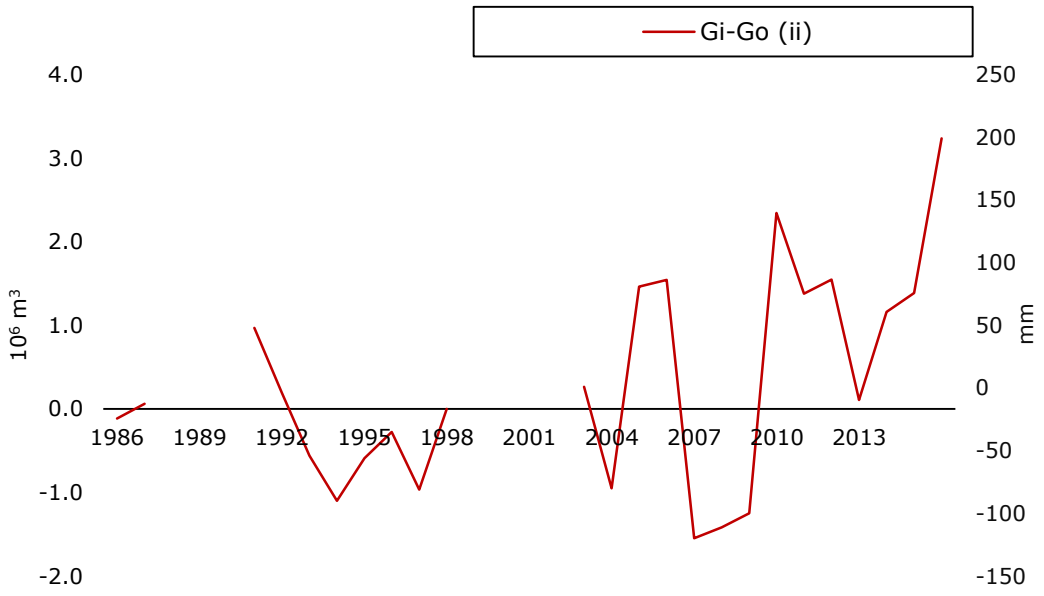

Figure 5. 21 Total annual groundwater flux ($G_i - G_o$) (ii) by the water balance approach

5.3.3 Results – Groundwater models comparison

Two groundwater model outcomes are compared in Figure 5.22. *The key findings of groundwater modelling show that groundwater flux* was positive*,* where the average $G_i - G_o$ was +0.29x10^{6}m^3 estimated by the regional model (i) and +0.16x10^{6}m^3 when estimated by the water balance approach (ii). The groundwater predictions produced by the models show similar trends, especially between 2003 and 2011, illustrating similar patterns in groundwater flux. Predicted groundwater storage by regional model highly correlates with groundwater storage estimated with water balance model (r=0.84, p<0.001).

The results indicate that there is a clear relationship between Shortandy Lake volume and groundwater flux (Figure 5.22). When the lake volume is relatively high as it was during the 1980s and 1990s, the groundwater relation was negative. However, the positive response in groundwater flux with considerable inflow was established since 2010, when the lake volume reached the lowest level during the study period. This relationship was also reported by Uryvayev (1958), who stated that significant groundwater recharge stabilises water level fluctuations by recharging lakes when they reach their minimal water level. The estimation of

groundwater flux in Shortandy Lake demonstrates that groundwater flow changes in response to fluctuations in surface lake levels.

Major discrepancies between the models were computed for 1994 and 2013. Specifically, in 2013, according to the regional model (i), the groundwater flux was positive and equivalent to $1.6 \times 10^6 m^3$, whereas the water balance approach (ii) predicted only $+0.1 \times 10^6 m^3$, generating more than one million m^3 of water discrepancy between the models. The following deviation between model outcomes could result from an underestimation of groundwater inflow during warm-season months. Specifically, the highest discrepancy corresponds with years when P_{rain} was higher than the historical average, i.e. exceeded 350mm.

Overall, the groundwater flux on average was positive over the study period. Yet, the groundwater recharge was insignificant, on average less than $0.3 \times 10^6 m^3$.

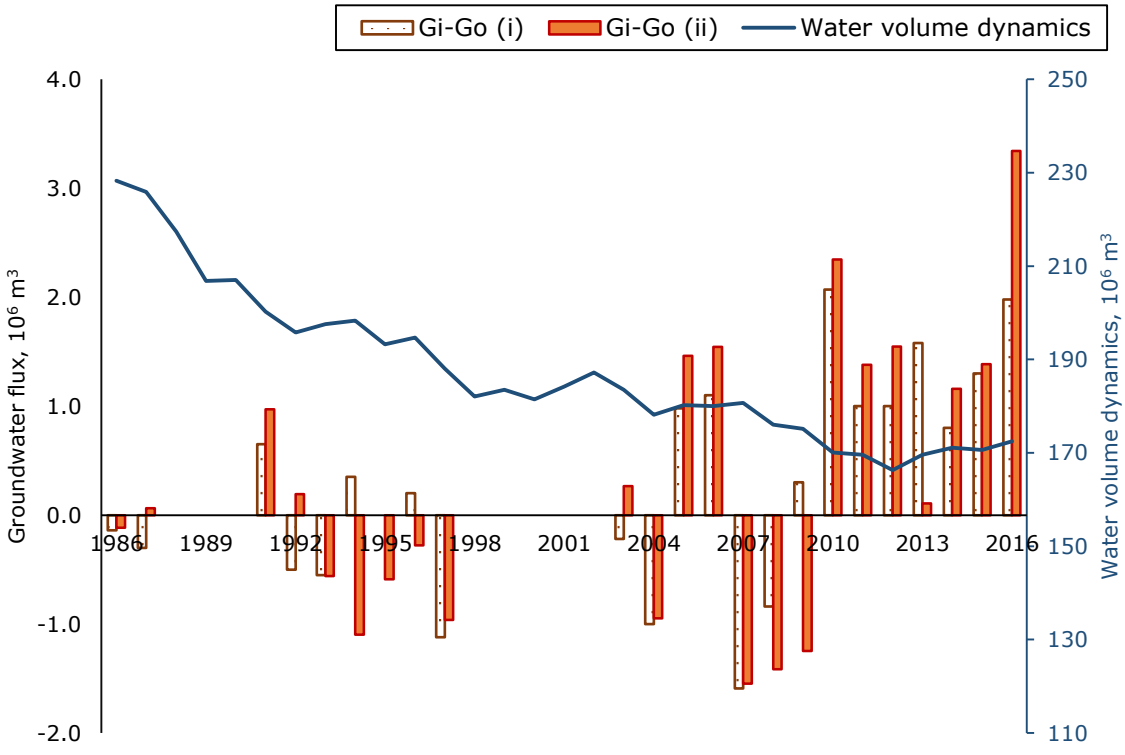

Figure 5. 22 Groundwater flux modelling results

where $G_i - G_o$ the water level is a groundwater model estimated by the regional model developed by Uryvayev (1959); $G_i - G_o$ water balance is estimated by Shortandy water balance model expressed by Eq.4.1

5.4. Results – Reconstruction of water volume dynamics

The water volume dynamics were reconstructed using the GIS volumetric model and Landsat for estimation of the lake area-level-volume relation (Section 4.3). Further water volume change was estimated as the difference between input and output variables expressed in Equation 4.1. *The lake water balance model reveals a significant water volume reduction in the lake from 1986 to 2016* (r=-0.93, p<0.001). Specifically, the water volume declined significantly from 231.7x$10^6$$m^3$ in 1986 to 172.5x$10^6$$m^3$ by the end of 2016 based on the relation between the water balance variables.

It is clear from the graph (Figure 5.23) that the overall water volume dynamic was negative over the observed period, where "dry" years with roughly 3-4 years periodicity were replaced with 1-2 "wet" years. The most rapid and dramatic water volume decrease occurred from 1986 to 1992. Despite some inter-annual water volume fluctuations, with positive water volume dynamics (1992-1996; 2002; and 2005-2009), the overall trend was to decrease for Shortandy Lake. However, since 2013, the water volume trend turned positive after the lowest peak simulated in 2012 (about 166.3x$10^6$$m^3$) and rose to 172.5x$10^6$$m^3$ by 2016.

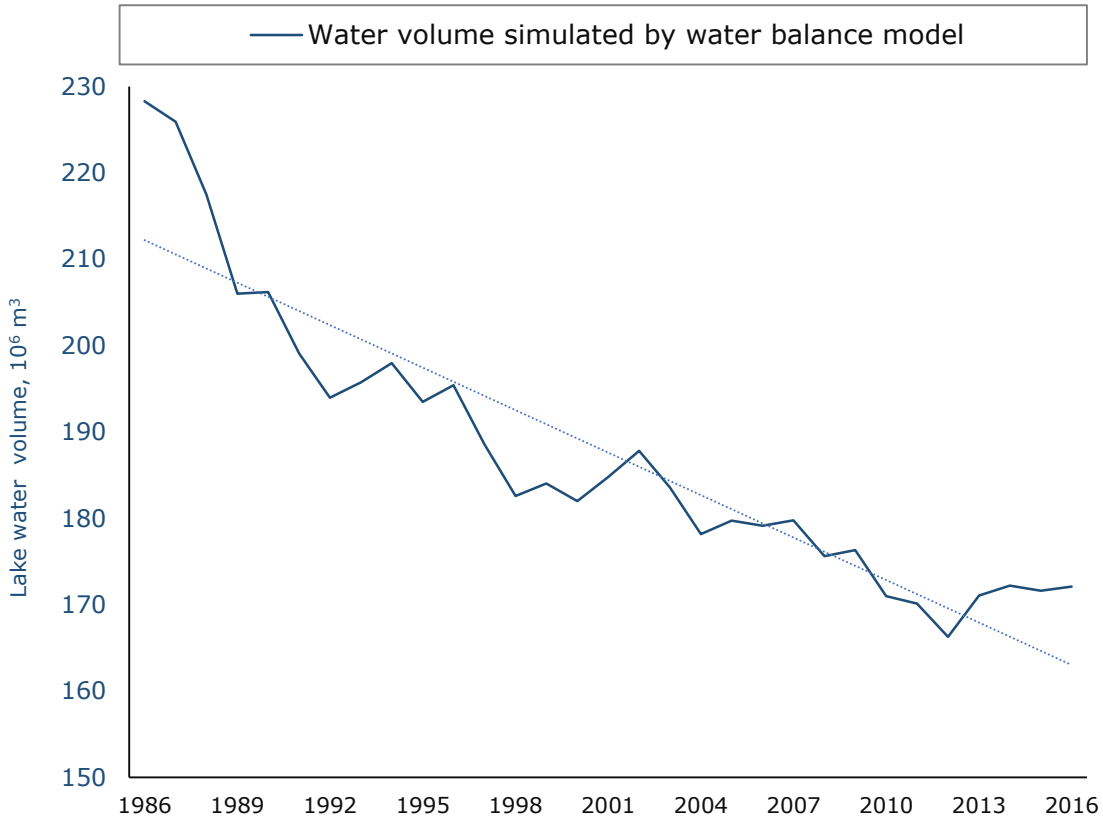

Figure 5. 23 Water volume dynamics of Shortandy Lake simulated using the water balance model

5.5 Input and output variables and volume dynamics

According to the lake water balance model (Eq.4.1), the relationship between input and output predetermines volumetric changes in the lake ($\frac{\Delta V}{t}$). This section of the thesis addresses the relative contribution of input and output variables during the study period. Furthermore, the relation between input and output variables or I-O will be examined, so that identified water volume patterns can be explained.

5.5.1 General relationship between input and output

The relation between annual input and output variables, as well as the water volume dynamics of Shortandy, are reflected in Figure 5.24. It is clear from the graph that *the overall net balance was negative, with -95mm* difference on average from 1986 to 2016.

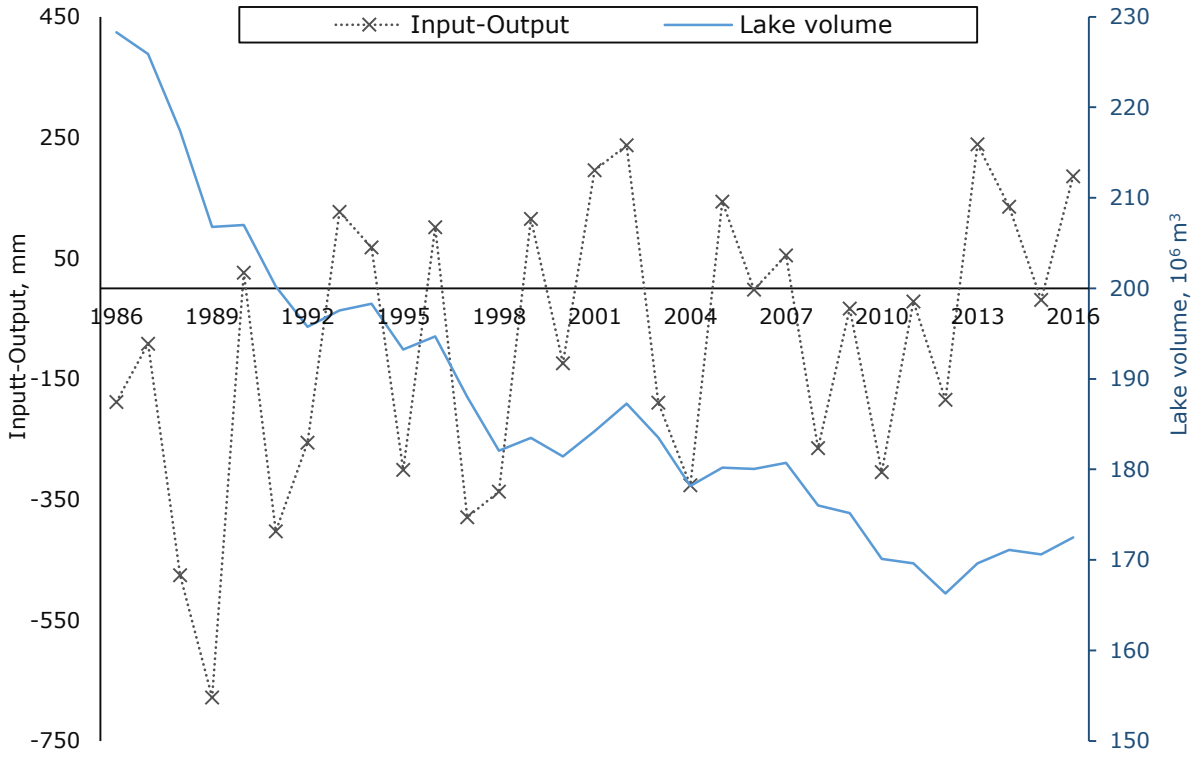

Figure 5. 24 Total annual net balance plotted with the total annual water volume dynamics of Shortandy Lake from 1986 to 2016

The input and output relationship of the water balance variables show a series of years with the negative net balance or "dry" periods and years with a positive relationship or "wet" periods. For example, dry periods occurred by the end of the 1980s and then repeated during the 2000s. Such inter-annual changes between dry and wet periods have been previously observed in the Burabay lakes (Shnitnikov, 1970a, Uryvayev, 1959).

The negative water balance trend was primarily established during the 1980s and 1990s. The most negative net balance was estimated for 1988, 1989 and 1991 when the outflow proportion was as twice as high than inflow variables (-476mm, -678mm and -403mm respectively). By contrast, years with the positive water balance contributed to the lake volume with less than 115mm on average during the 1980s and 1990s.

To sum up, *the inflow and outflow relationship of Shortandy water balance was predominately negative during the study period*. The negative relationship in water balance variables, which resulted in the negative water volume response

occurred during the 1980s and 1990s with a greater magnitude than it was established after the 2000s. Furthermore, the positive water balance tendency has become more frequent since 2000 with a greater contribution to the lake volume. For example, the highest positive relation was established for 2002 and 2013, with more than 230mm annually.

5.5.2 Interannual changes in net flux

The year-by-year analysis of the input-output variables shows a negative water balance in the 1980s (Figure 5.25 and Appendix F). In 1986, 1987 and 1988, the water balance was driven by warm-season precipitation (more than 46% of the annual water input), whereas lake evaporation was the main flux of the lake losses (98%). However, in 1988 the decreasing magnitude of the lake volume was higher than 1986-1987.

Based on Chapter 5.5.1 findings, in 1989, a negative relationship of -678mm between inflow and outflow resulted in the most negative ΔV within the study period. The relative contribution of the variables shows that more than half of the total annual water input was driven by P_{rain}(64%) with the reduced snowmelt runoff in comparison with 1986 and 1987 (17% and 33-35% respectively) (Appendix F). By contrast, the total annual outflow proportion increased considerably due to the water abstraction from the lake, which was equal to 34%. It is clear from Figure 5.25 that the series of dry years occurred from 1986 to 1992. Despite 1990, the total annual precipitation over these years was only 247mm on average, which is less than the historical average ($P_{sum} < 332$mm), where in 1988, P_{sum} was the lowest from 1986 to 2016 (181mm). By contrast, the lake output variables, specifically the lake evaporation was higher (≈653mm) than the historical average established for Shortandy Lake ($E_o > 611$). Since 1989, the balance between input and output variables had become more negative due to the additional anthropogenic water abstraction from the lake. The proportion of the water abstraction from the lake was within the range of 25%-34% of total annual

water output from the lake during 1989-1992. Consequently, the net negative water balance established by the end of the 1980s and early 1990s resulted in *the massive water volume decline from 228.3x10^{6}m^3 in 1986 to 195.8 x10^{6}m^3 in 1992.*

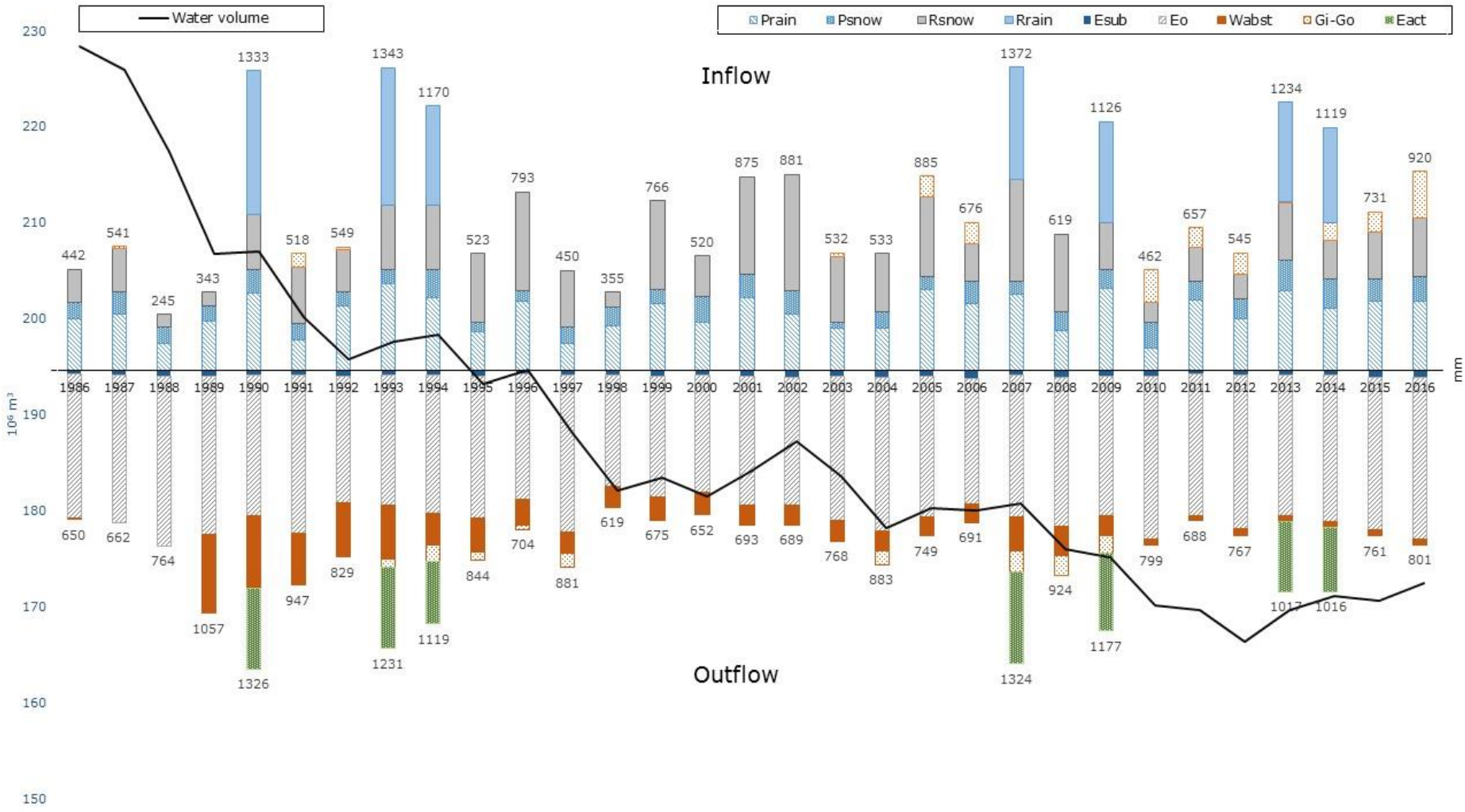

Figure 5. 25 The total annual input and output values in mm, where inflow are: P_{rain}, P_{snow}, R_{snow}, R_{rain} and output variables are: E_{sub}, E_o, E_{act}, W_{abs} and $G_i - G_o$ is the groundwater flux

In 1990, a positive water volume response was established. Specifically, the positive water balance was driven by increased warm-season precipitation and rainfall-induced runoff during July, which was 49% of the total annual input. The years with a similar water balance repeated in 1993, 1994, 2007, 2009, 2013 and 2014, when the lake volume was predominantly driven by excessive rainfall events in July (Figure 5.25, Appendix F).

In 1993 and 1994, a positive water volume response in Shortandy Lake was established (Figure 5.25). During these years, the total annual P_{sum} was 432mm, whereas the lake evaporation was lower than the historical average of Shortandy (588mm year^{-1}) (Appendix F). The increased warm-season precipitation resulted in summer R_{rain}, however, the water produced from excessive runoff events had an insignificant contribution to the lake volume. For example, the positive water balance was only 68mm in 1993. This is explained by high grass evaporation during warm seasons which diminished the effective runoff to the lake. Subsequently, the lake volume during this wet period increased only by 2.6x10^{6}m^3 (from 195.8 x10^{6}m^3 to 197.6 x10^{6}m^3).

In 1995, 1997 and 1998, the series of dry years repeated in Shortandy. The water volume decline was considerable, specifically from 198x10^{6}m^3 in 1994 to 182x10^{6}m^3 in 1998. In comparison with the dry period which occurred in the 1980s and early 1990s, the total annual P_{sum} was even lower (≈212mm year^{-1}), yet the lake evaporation was on average 614 mm per year. However, the later dry period resulted in less volume reduction due to the reduced water abstraction from the lake. Figure 5.25 illustrates than the water abstraction from Shortandy Lake was reduced by 10% (from 25%-34% in 1989-1993 to 13-14% in 1997-1998) (Appendix F).

From 1999 to 2002, the water volume of the lake recovered from 182x10^{6}m^3 to 187.2x10^{6}m^3 in 2002. In comparison with the earlier wet period, the later period was driven by an increased proportion of the seasonal snowmelt runoff. The

annual P_{sum} was on average equal to 358mm, whereas the lake evaporation remained lower than the historical average (533 mm year^{-1}).

It could be noted from Figure 5.25, during the period from 1997 to 2006, the water volume fluctuation was less notable than for the earlier period. The water volume change was equal to -3.5x10^{6}m^3. Furthermore, according to Figure 5.25, the input and output values remained low, where a negative relation between input and output variables was only -67mm.

In 2007 and 2009, a positive water volume response in Shortandy Lake was established. This period was similar to the wet period that occurred in 1990, 1993 and 1994, yet the later wet period had no contribution to the lake volume. In 2007, the relation between input and output variables was positive, giving only 0.7x10^{6}m^{3,} whereas, in 2009, this balance turned negative (-0.9x10^{6}m^3). In comparison with earlier wet periods with a similar water balance, the negative relation between input and output occurred due to the decreased proportion of R_{snow} in 2009 (Figure 5.25).

During the dry period of 2010-2012, the water volume reached the lowest peak during the study period (Figure 5.25). The following dry period was driven by a significant reduction in the total annual precipitation (as well as in R_{snow}), whereas the lake losses were higher than the historical average (≈611mm) approximately 690 mm year^{-1}. Furthermore, the groundwater flux was positive, with the relative contribution of 34%-19% of the total annual input proportion (Appendix F).

Since 2013, the relation between input and output remained positive (except 2015), and the lake volume rose from 166.3x10^{6}m^3 in 2012 to 172.5x10^{6}m^3 by 2016. The net positive water volume response was driven by R_{rain} in 2013 and 2014 (Figure 5.25). Despite the total annual input being identical in years 1993, 1994, 2007 and 2009, the contribution to the lake volume over this period was greater. This pattern is explained by the overall reduction of output proportion due to the decrease in anthropogenic water abstraction since 2010.

To sum up, the water volume trend was negative over the observed period, where dry periods repeated on average with 3-4 years periodicity replacing with 1-2 wet years. During the wet years driven by warm-season precipitation, the positive water volume response was on average equal to 88mm or $1.1x10^6m^3$ annually, where the highest positive ΔV was estimated for 2013 ($3.3x10^6m^3$). In contrast, the negative response was established only in 2009 ($-0.9x10^6m^3$). A significant increase in the inflow variables for years with flash flood events during summer *made little contribution to the lake volume due to the losses from evapotranspiration.* Yet, in 2013 and 2014 greater contribution to the lake volume was established. Although the evapotranspiration proportion was higher in 2013-2014 than during the 1990s (33%-30% and 29% respectively), the proportion of the anthropogenic water abstraction reduced significantly (from 20% to 4%). *Consequently, the positive water balance response was driven by the lower annual proportion of output variables.*

Nonetheless, the positive water balance response was also observed in 1996, 1999, 2001, 2002 and 2005 (Figure 5.26). In comparison with the years driven by the warm-season runoff, the water balance of these years was driven by seasonal snowmelt-runoff. The relative contribution of the R_{snow} was more than 50% (except 2005). Interestingly, the snow precipitation contribution was minor during these years. Yet, this proportion of snow produced a significant amount of snowmelt runoff, which was the major driving force of the water balance. The increased proportion of snowmelt runoff during these years contributed to the annual lake volume on average with 158mm or 2.14 $x10^6m^3$ of water. Consequently, *the magnitude of the positive lake response was greater during the years which were driven by snowmelt runoff than by warm-season rainfall-runoff.*

5.6 Model validation

In this project, Shortandy Lake volume estimated using the lake water balance model is validated with the lake volume based on the observed lake level measurements. The water level-area-volume relationship was established by utilisation of the GIS volumetric model explained in Section 4.3. In this section, Shortandy Lake volume dynamics were estimated with the observed lake levels and lake area detected by Landsat images.

5.6.1 Lake level-area-volume relationship

Lake area (A_L) dynamics

The lake level measurements exclude the earlier period (from 1986 to 2002) so that the lake area from 1986 was identified by a remotely sensed product, i.e. Landsat TM. It was determined that Shortandy Lake area was equal to 17.3km^2 which corresponds to a lake level of 392.3m and the lake volume of 231.7x10^{6}m^3 in 1986 (Figure 5.26). The lake area of Shortandy reduced to 15.7km^2 by 2016 which corresponds to a lake volume of 174.9x10^{6}m^3 and a lake level 388.9m. Therefore, Shortandy Lake *level decreased by roughly 3.3m, whereas the lake area decreased by 1.5 km^2 from 1986 to 2016*.

Lake volume (ΔV) dynamics

Figure 5.27 shows that the water volume of Shortandy decreased significantly from 2003 to 2016. The most noticeable water volume reduction occurred from

2007 and 2012 when the lake volume dropped from $183x10^6m^3$ to a minimum value of $168x10^6m^3$. However, it is clear from the chart that the trend has become positive since 2013, and the water volume increased to approximately $2.5x10^6m^3$ by 2016.

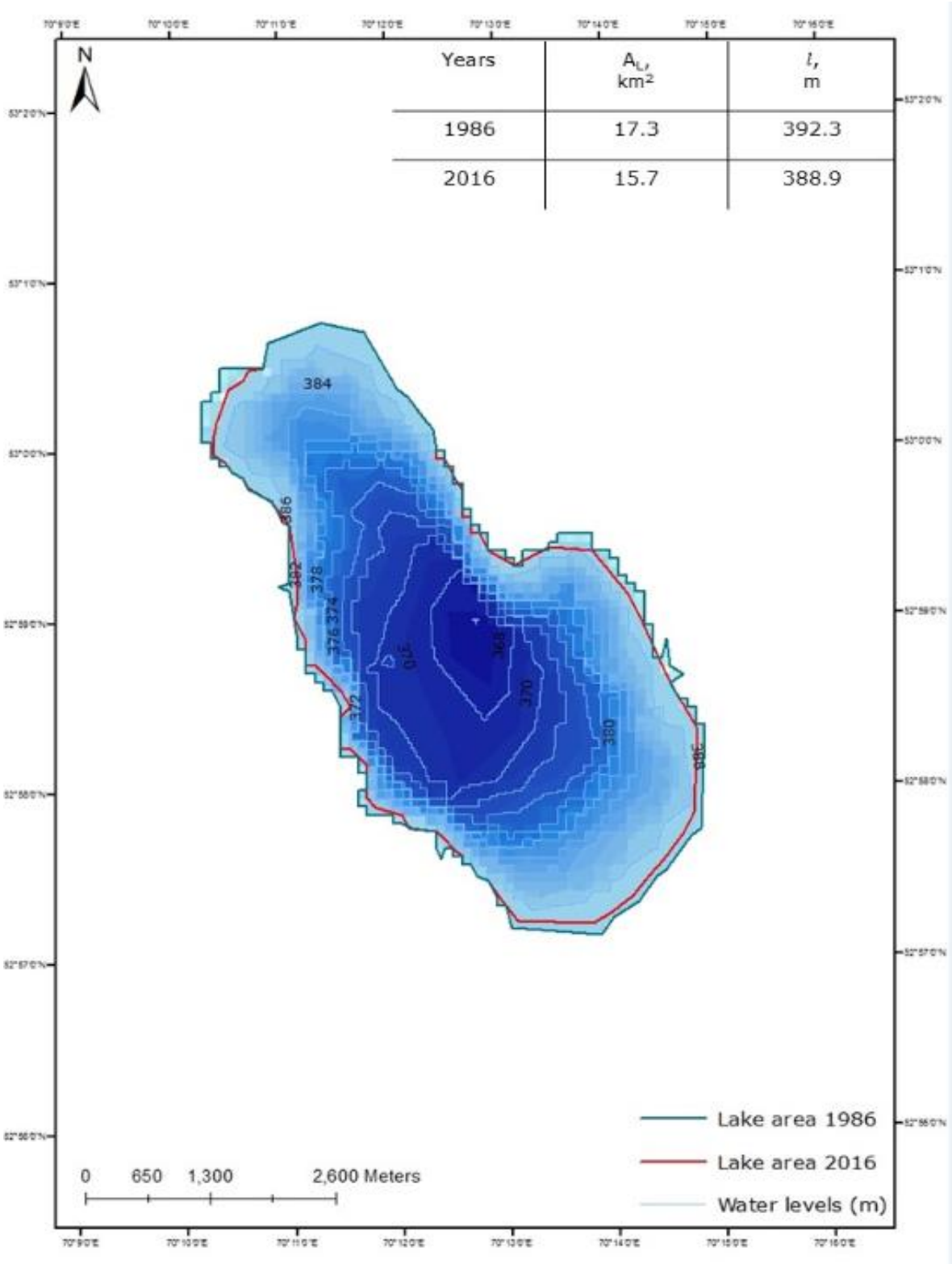

Figure 5. 26 Shortandy Lake area and water level dynamics, where A_L is lake area identified by Landsat TM for 1986 (blue line) and 2016 (red line), and water level (white lines) is observed measurements on water levels

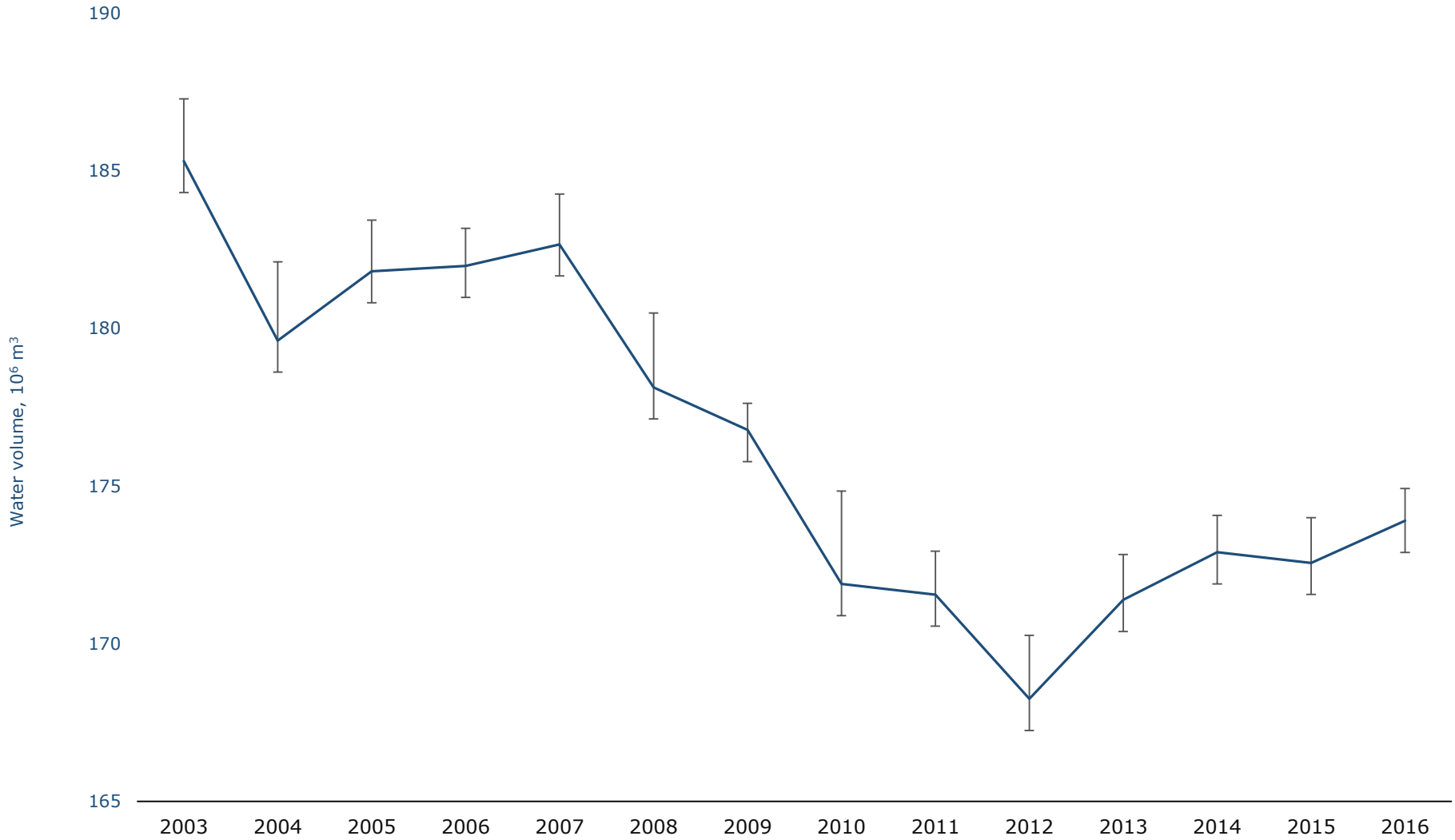

Figure 5. 27 Water volume dynamics based on the observed daily lake level measurements, where errors bars show annual standard deviation

5.6.2. Results – Model validation

Annual water volume dynamics were computed by using the water balance model with the regional groundwater model (i) and the groundwater model (ii), which estimates groundwater flux by the water balance model (Chapter 5.3). Although a difference of $0.13x10^6m^3$ was established between these models, (Chapter 5.3.3.), a controversial pattern for some years of water balance predictions was identified (1994, 2013). Thus, both model outcomes were validated against the water volume calculated by observed levels.

The water volume patterns simulated by both models were statistically highly significant (r=0.99) with the water volume obtained by measured lake levels (Figure 5.28). However, the lake volume simulated using the groundwater predicted by the water balance model (ii) showed a higher correlation coefficient with the observed lake volume in comparison with the regional groundwater model (i) (r=0.999, $p<0.001$ and r=0.989, $p<0.001$). The discrepancy between the observed and simulated water volume by the groundwater model (ii), on average, is equal to $1.8\ x10^6m^3$, where *the water balance model underestimates observed total volume*. However, the water volume estimated by the regional groundwater (i) model showed less deviation in the total annual water volume predictions. On average, the discrepancy between the measured and observed water volume showed an underestimation of $1.6x10^6m^3$, which is less than 10% of the total lake volume. Interestingly, according to the water balance predictions using the regional groundwater model (i) *the deviation between simulated and observed water volume was minimal during the years of 2009-2010 and 2013-2014 which corresponds to the period with the summer flashflood events.*

Overall, both models show a high correlation with the observed water volume fluctuation, underestimating water volume changes to 10% of the total lake volume than the observed water volume dynamics in Shortandy Lake.

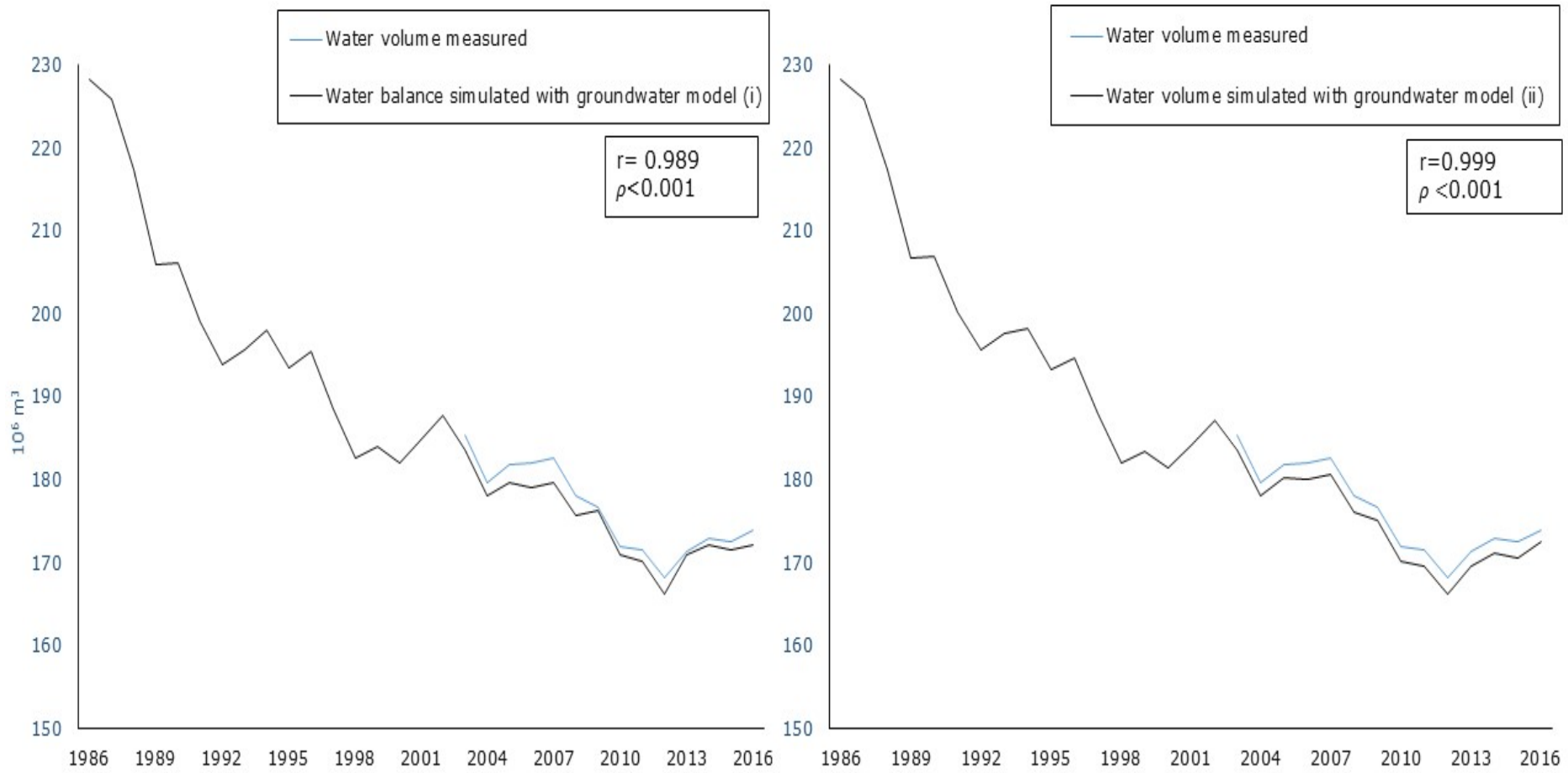

Figure 5. 28 Validation of water volume simulation by using two groundwater models against water volume by measured water levels

where water volume was simulated by the regional groundwater model (i) (left figure) and water volume simulation using water balance approach for groundwater flux (ii) (right figure)

5.7 Sensitivity analysis

The influence of hydrological and climate parameters can be analysed, and their significance to the water balance can be studied using a sensitivity analysis (SA). This type of analysis involves the systematic variation of one or more model parameters while the others are held unchanged. In this section, four model parameters are studied to evaluate their influence on the water volume of Shortandy Lake and reveal model sensitivity. The parameters of interest are (1) air temperature, (2) precipitation, (3) wind speed and (4) relative humidity. The last two parameters are included in this analysis as they are embedded in the open water evaporation model (Section 4.4.1), which is the major source of the lake output. Therefore, these parameters were included to identify their significance to the lake evaporation model.

The following section of the thesis aims to study the sensitivity of the water balance model developed for Shortandy Lake. The SA of the model was structured as follows:

1. Open lake evaporation model (Section 4.4.1) based on SA for the three model parameters (air temperature, wind and relative humidity) (Section 5.7.3.1);
2. SA of the input model based on precipitation parameter (Section 5.7.3.2);
3. The SA of the lake volume to variations in the selected model parameters;
4. Variations in groundwater flux.

5.7.1. Model sensitivity analysis

Any hydrological modelling study should include a sensitivity analysis to assess the possible values to assign to the parameters and the qualitative and/or quantitative variations in the output of an associated model (Devak and Dhanya, 2017, Vemuri et al., 1969). Critical examination of the relationships between model inputs and outputs is fundamental to recognise any possible flaws in model

structure and formulation, provide guidance for model order reduction and parameterisation, and assess available observations contents. Therefore, SA methods assist in identifying the parameters that have a major impact on model outputs. SA varies in multiple shapes and sizes and is defined in many ways, ranging from the simple local 'one at a time' approach (Hamby, 1994) to the complex variance-based global method (Saltelli et al., 2010, Song et al., 2015). For the developed water balance model for Shortandy Lake, SA was conducted based on a 'one at a time approach'. This approach is based on assumptions of model linearity (Saltelli and Annoni, 2010). Referring to Section 4.1, the change in storage is assumed to be a linear function of the relationship between input and output variables. Furthermore, the one at a time method has been widely applied in hydrological studies as it is simple to implement and easy to interpret (Saltelli and Annoni, 2010, Song et al., 2015). In this method, by changing one input parameter from the selected sensitive parameters at a time while keeping the other parameters constant, the changes in output value can be determined.

The sensitivity of the model was assessed using the Sensitivity Index (Lenhart et al., 2002), which has been successfully utilised in the evaluation of hydrological models (Abdulla et al., 2009, Saharia and Sarma, 2018, Tegegne et al., 2019). The Sensitivity Index (I) describes as follows:

$$I = \frac{(y_2 - y_1)/y_0}{2\Delta x/x_0} \qquad \text{Eq.5.7.1}$$

Where y_0 is the initial model output estimated with an initial x_0 of the parameter x. In the SA, this initial parameter value is varied by $\pm\Delta x$ yielding $x_1 = x_0 - \Delta x$ and $x_2 = x_0 + \Delta x$ with corresponding values y_1 and y_2. The derived Sensitivity Index can be interpreted based on the following table:

Table 5. 2 Sensitivity classes

Class	*Index*	*Sensitivity*
I	$0.00 \leq \lvert I \rvert < 0.05$	Small to negligible
II	$0.05 \leq \lvert I \rvert < 0.20$	Medium
III	$0.20 \leq \lvert I \rvert < 1.00$	High
IV	$\lvert I \rvert \geq 1.00$	Very high

5.7.2 Model parameterisation

According to Section 4.1, the relationship between input and output variables predetermines volumetric response in the lake. Lake storage calculations (Eq.4.1) primarily are based on measurements of *air temperature*, which governs output variables (E_O, E_{act}) and *precipitation* which controls input variables (P_{snow}, P_{rain}, R_{rain}, R_{snow}). Therefore, SA aims to assess these parameters. Furthermore, Linacre (1993) pointed out that the accuracy of the Penman formula for lake evaporation (Penman, 1948) depends on measurements of wind (u) and relative humidity (RH) parameters. Therefore, these parameters are included in SA to evaluate the following models: open lake evaporation and evapotranspiration from vegetation.

The simplest way to accomplish a sensitivity analysis is to use ±10% of the initial value (x_0) frequently found in the literature (Hamby, 1994, Ray et al., 2015, Binder et al., 1997). Concurrently, future projections of precipitation for the Central Asian region show high discrepancies for both snowfall and rainfall values within the range of 20%-25% (Section 2.2.3). Therefore, the relative width of the ranges is taken into consideration by varying initial value or Δx by ±10%, ±15%, ±20% and ±25%, which can substantially improve the effectiveness of sensitivity analysis for the hydrological model (Lenhart et al., 2002). In this study, the initial value of four selected parameters will be varied by ±10%-25%, where varied only one parameter at a time and kept others constant. After that, changes in the lake storage based on the SA will be then compared to the 'initial model', which is the lake storage estimations explained in Section 5.4.

5.7.3 Results – Sensitivity analysis

5.7.3.1. Evaporation model

Figure 5.29, 5.30 and 5.31 show total annual open lake evaporation variations based on SA for three parameters (wind speed, relative humidity and air

temperature, respectively). The main findings indicate the open lake evaporation model is more responsive to changes in air temperature among three selected parameters, with a standard deviation of 48mm. By contrast, less variation in open lake evaporation values showed wind parameter, with a standard deviation of 22 mm over the period.

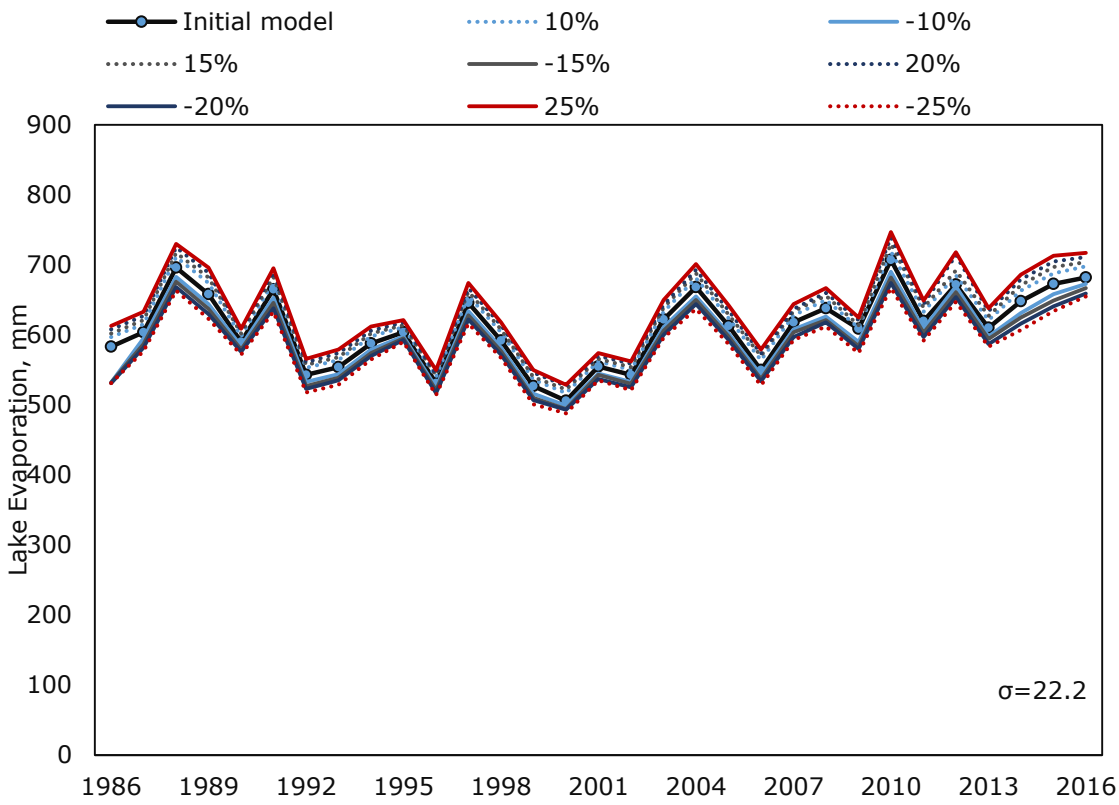

Figure 5. 29 Total annual open lake evaporation estimated based on wind speed sensitivity analysis, where σ is an average standard deviation estimated based on ±25% variations in wind speed

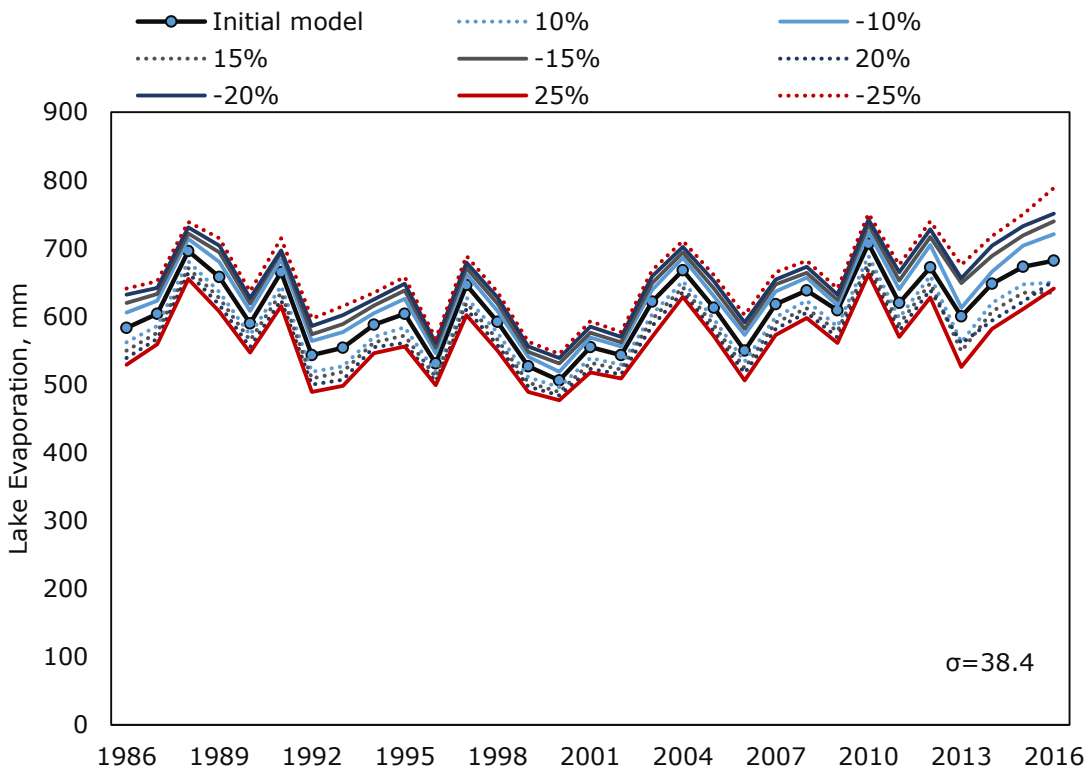

Figure 5. 30 Total annual open lake evaporation estimated based on relative humidity sensitivity analysis, where σ is an average standard deviation estimated based on ±25% variations in relative humidity

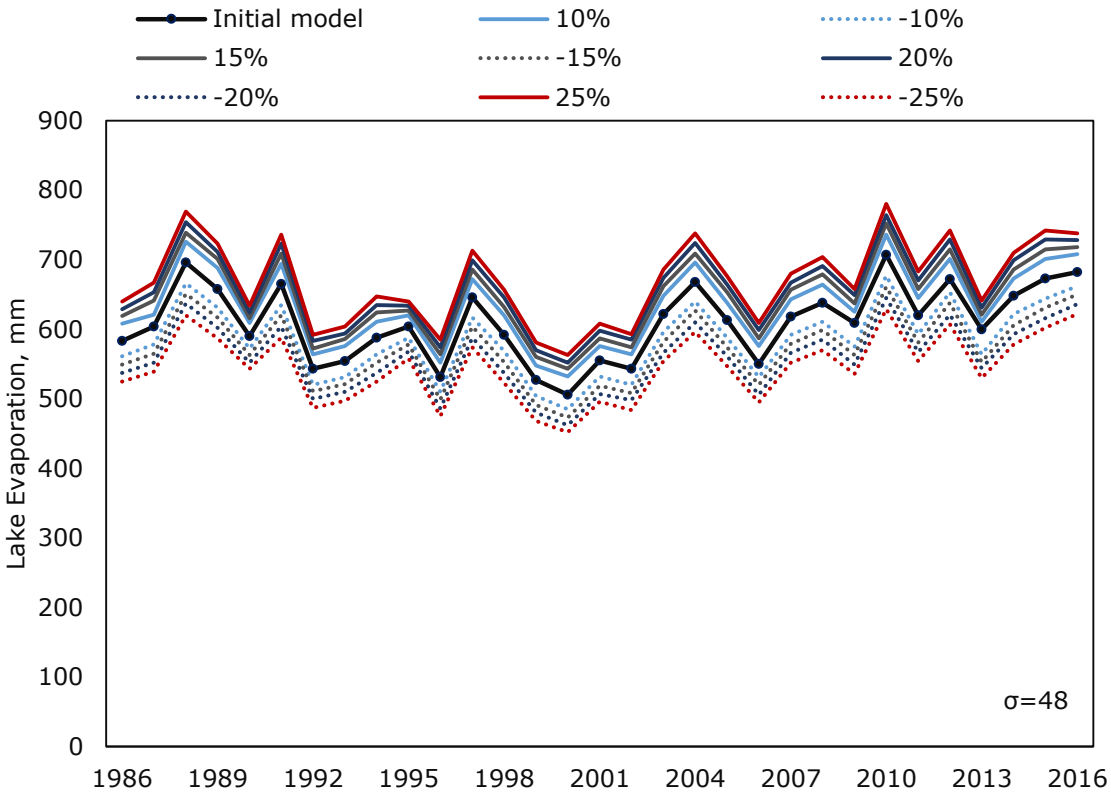

Figure 5. 31 Total annual open lake evaporation estimated based on air temperature sensitivity analysis, where σ is an average standard deviation estimated based on ±25% variations in air temperature

5.7.3.2 Precipitation and runoff modelling

Figure 5.32 shows that the SA of precipitation generates a great deviation from the initial model with a standard deviation of approximately 131 mm. According to Section 5.2, the Shortandy catchment is influenced by prolonged series of wet/dry periods, which is primarily driven by snowmelt/rainfall. Therefore, SA indicates that the lake volume is highly responsive to variations in input values. For example, wet years that occurred in 1990, 1993, 1993, 2007, 2009 and 2013 create greater derivation from the initial model affecting runoff values substantially (Figure 5.32).

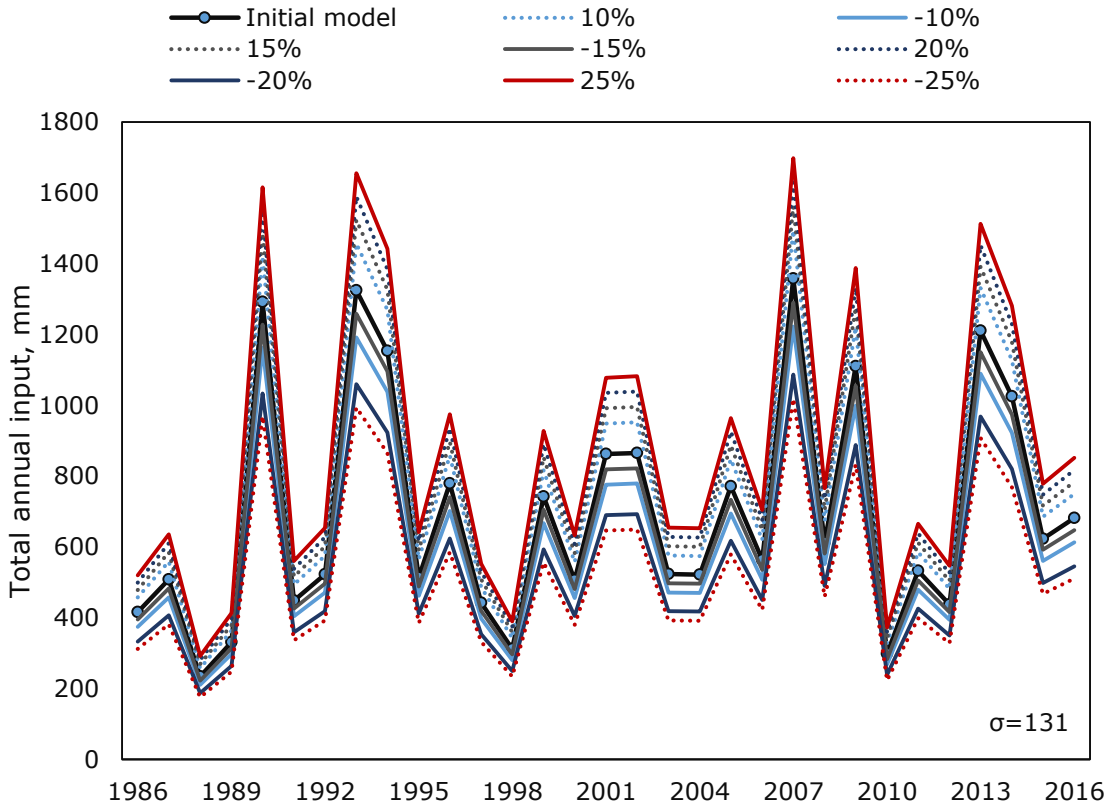

Figure 5. 32 Total annual input to the lake estimated based on precipitation sensitivity analysis, where σ is an average standard deviation estimated based on ±25% variations of precipitation and runoff

5.7.3.3 Lake volume and parameters

Figure 5.33 and Figure 5.34 show the SA of the lake storage variations based on wind speed and relative humidity parameters. The SA of the wind speed and

relative humidity parameters show relatively similar results. Specifically, the difference in the lake storage produced by variations in wind speed and relative humidity was within the range of $3.4x10^6m^3$ and $5.2\ x10^6m^3$ or 2%-3.1%, respectively. However, Figure 5.35 and Figure 5.36 indicate that the difference of lake storage was greater for air temperature, and the greatest difference was established for precipitation parameter. For example, the SA of the initial model and air temperature parameter indicates the difference of around $7.6x10^6m^3$ of the water volume, which is 4.5% difference. By contrast, a difference of $20.5x10^6m^3$ or 12% from the initial model is established for the precipitation parameter.

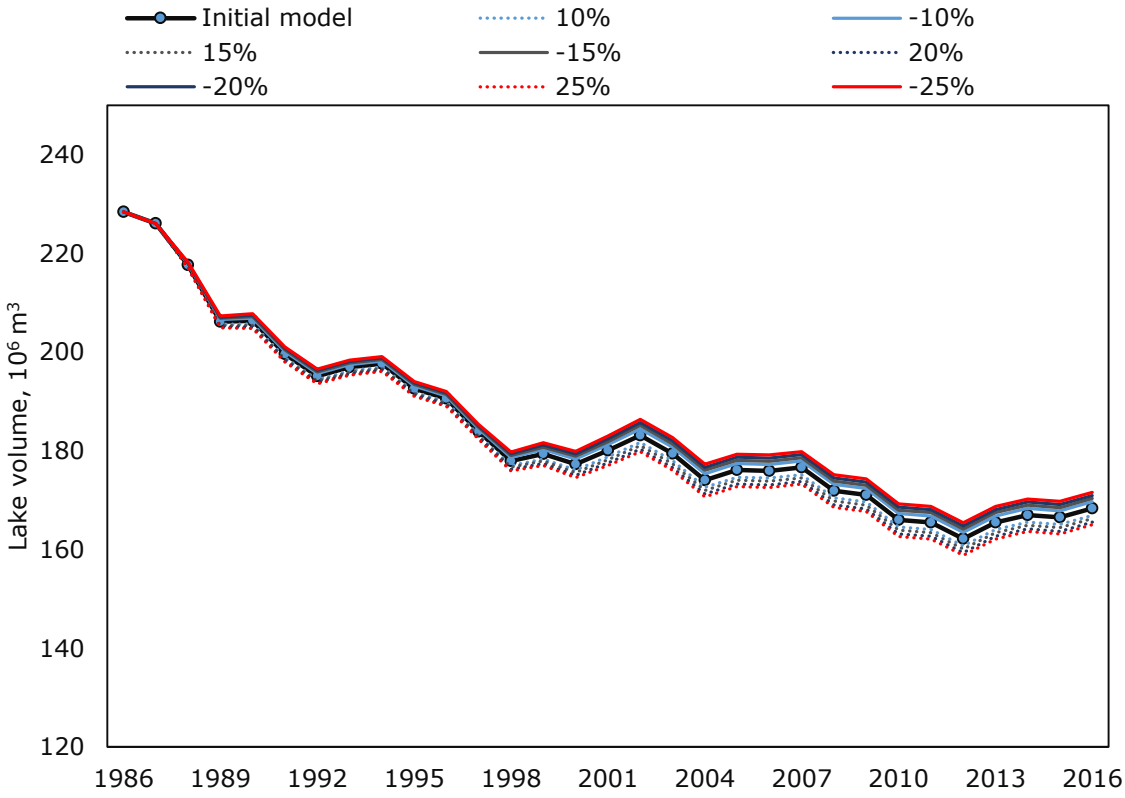

Figure 5. 33 Sensitivity analysis of lake volume dynamics based on the variations of wind speed parameter, where Initial model shows lake volume dynamics with initial wind speed values in open water evaporation model

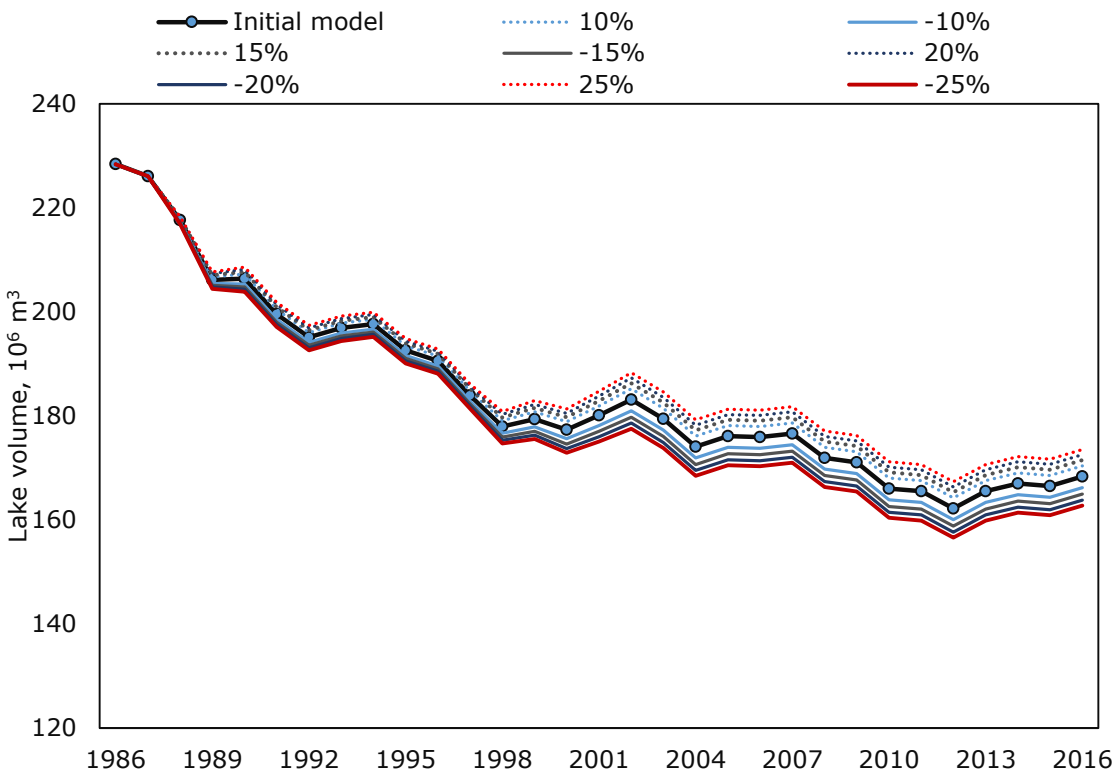

Figure 5. 34 Sensitivity analysis of lake volume dynamics based on the variation of relative humidity parameter, where Initial model shows lake volume dynamics with initial relative humidity values in open water evaporation model

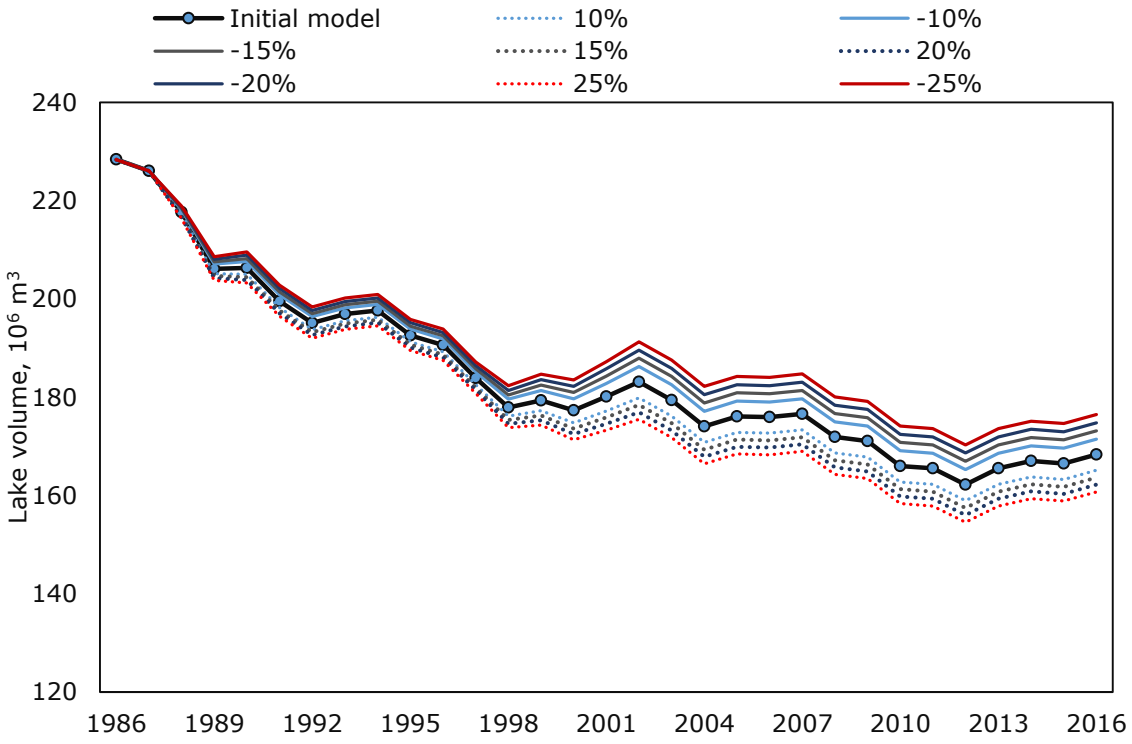

Figure 5. 35 Sensitivity analysis of lake volume dynamics based on the variation of air temperature, where Initial model shows lake volume dynamics with initial air temperature values in open water evaporation model

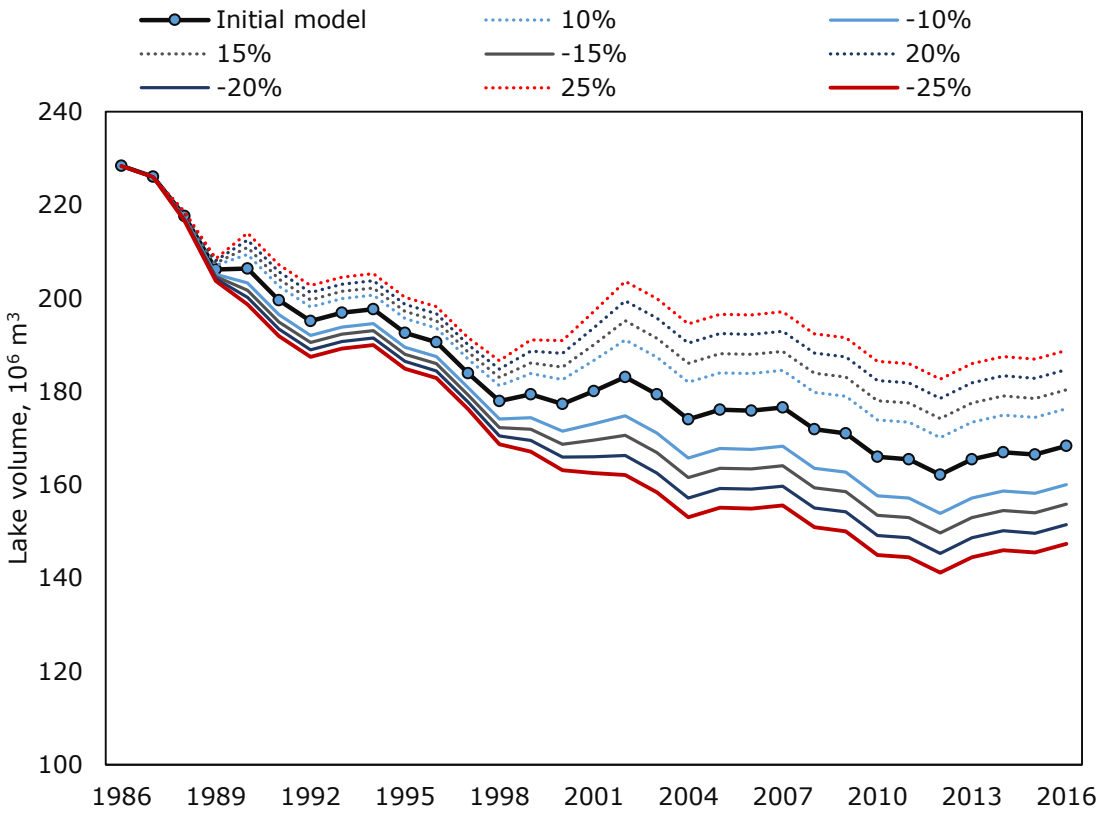

Figure 5. 36 Sensitivity analysis of lake volume dynamics based on the variation of precipitation, *where Initial model shows lake volume dynamics with initial precipitation values*

Table 5.3 shows SI indexes estimated for the selected model parameters. Based on the main results of the SA, the developed model for Shortandy Lake shows a negligible sensitivity for the four parameters when Δx is 10%. However, the model demonstrates *medium* sensitivity with 15%-25% variations in precipitation. The water balance model showed a small sensitivity to air temperature, yet with a variation up to 25% yields medium sensitivity. The tested wind and relative humidity parameters are of minor importance for the considered values of model output.

Table 5. 3 Sensitivity Index estimated for selected model parameters

	P	*T*	*u*	*RH*
10%	*I*	*I*	*I*	*I*
15%	*II*	*I*	*I*	*I*
20%	*II*	*I*	*I*	*I*
25%	*II*	*II*	*I*	*I*

5.7.3.4 Groundwater flux

Based on Equation 4.1, the developed model estimates groundwater flux by identifying the difference between ΔV and input and output variables, where ΔV derives from measured lake levels (Section 4.6.2). Therefore, variations of the selected parameters ultimately affect the groundwater flux. For example, temperature, wind and relative humidity parameters affect evaporation values and alter the output from the lake, whereas changes in precipitation influence input values.

In this section, groundwater flux was analysed as the difference between the initial values of $G_i - G_o$ and values estimated based on Δx. Figure 5.37 shows groundwater flux changes based on the SA of the wind speed. It is clear from the chart that Δu of ±25% alters initial groundwater flux within the range of ±0.5x10^{6}m^3 annually, which is the lowest variation in $G_i - G_o$ among selected parameters. The SA of RH and T parameters shows that these parameters affect groundwater storage by an almost identical amount of water, approximately ±1x10^{6}m^3.

In contrast, SA of the precipitation parameter revealed the greatest difference in the annual groundwater flux. Figure 5.40 shows the variation of $G_i - G_o$ from the initial values was within the range ±2.8 x10^{6}m^3. The highest variations in annual groundwater flux were particularly established for wet years, confirming the model sensitivity to precipitation.

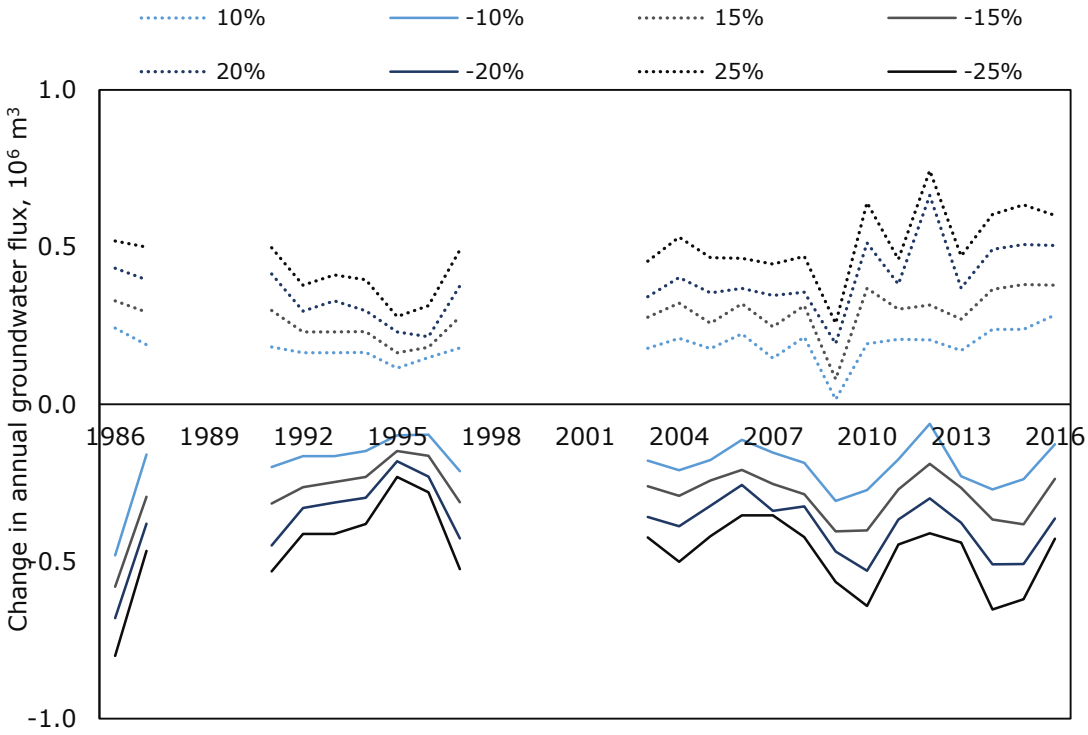

Figure 5. 37 Change in annual groundwater flux based on the variation in wind speed (u) parameter

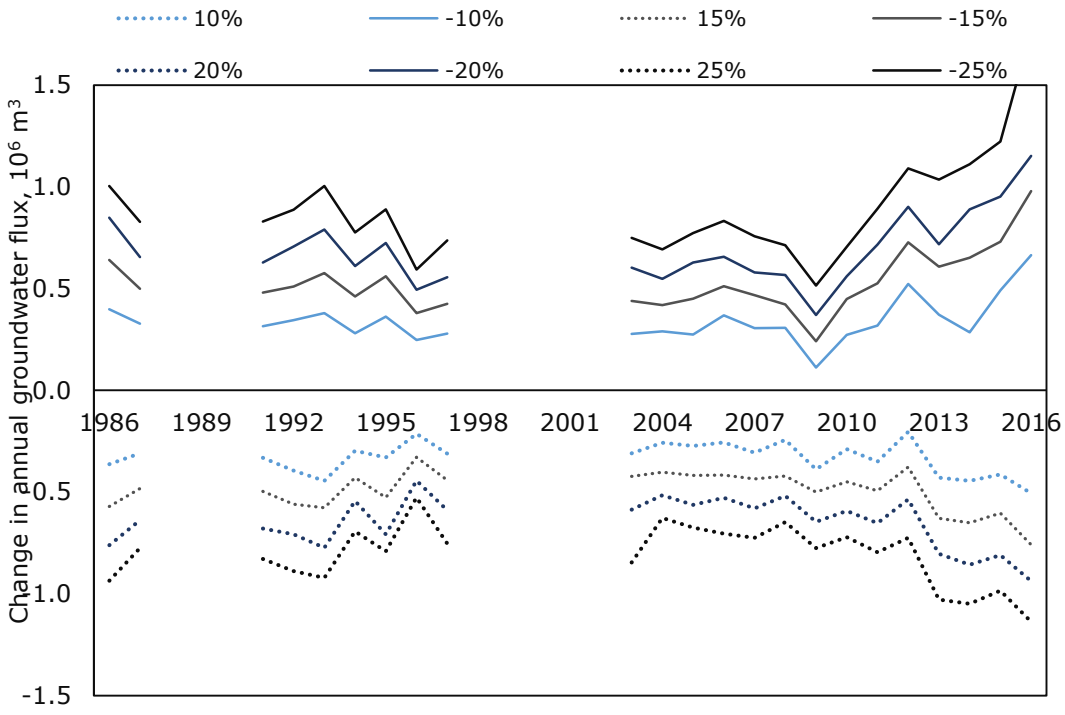

Figure 5. 38 Change in annual groundwater flux based on the variation in relative humidity (RH) parameter

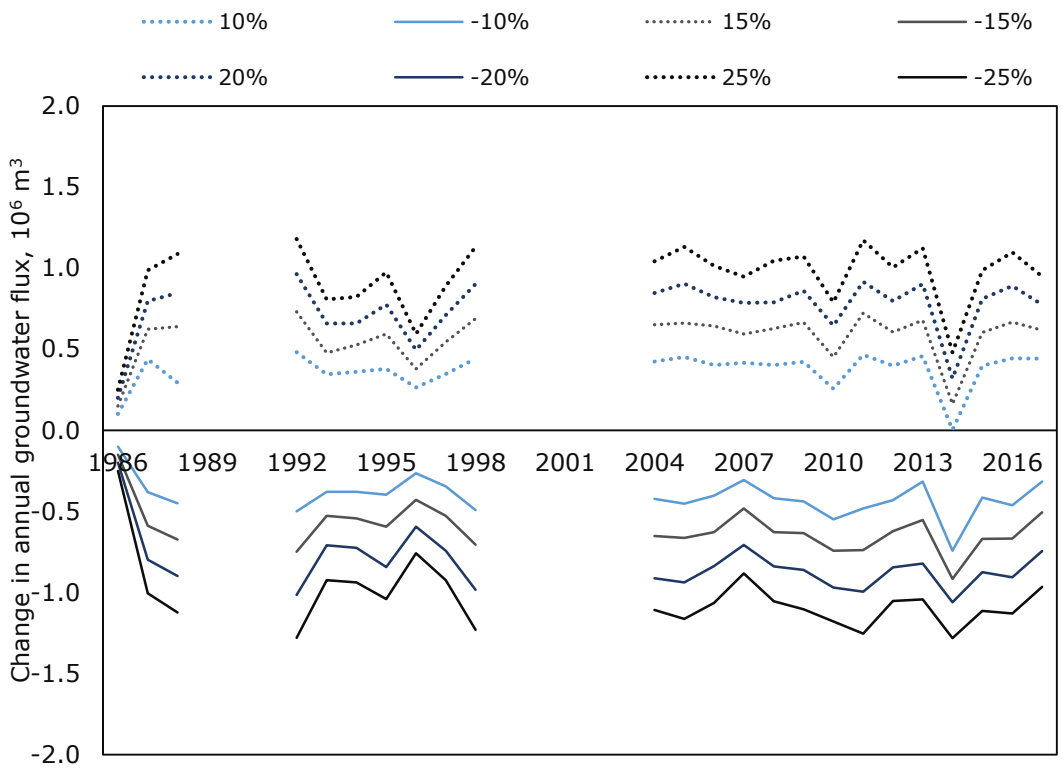

Figure 5. 39 Change in annual groundwater flux based on the variation in air temperature (T) parameter

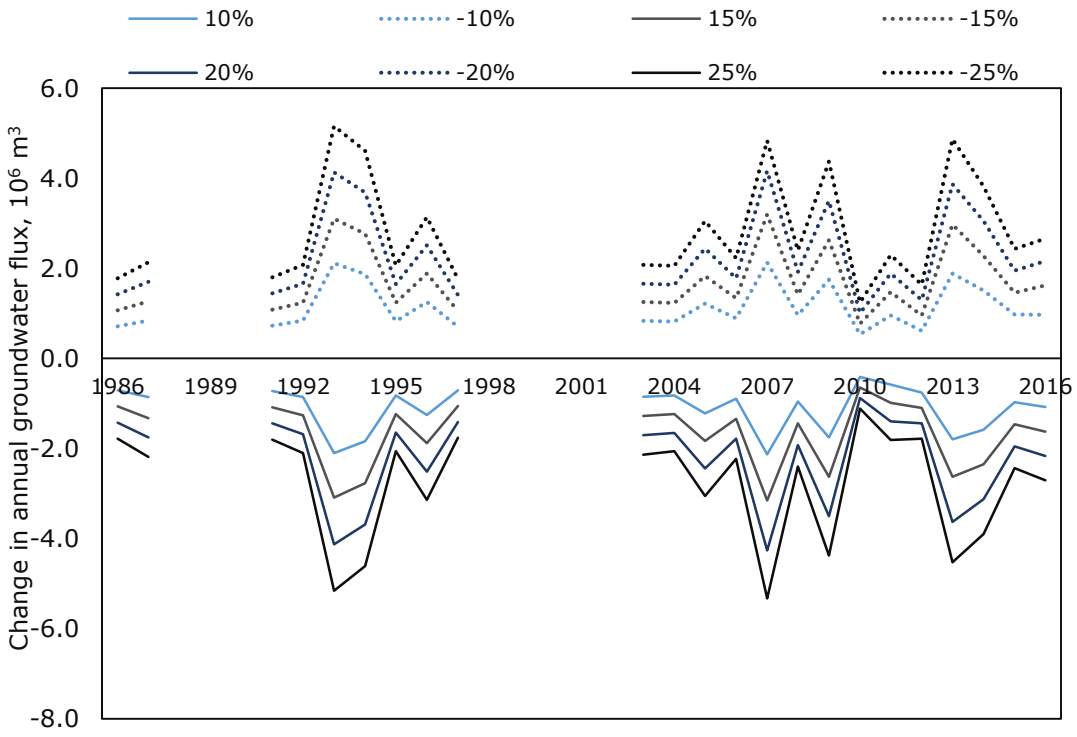

Figure 5. 40 Change in annual groundwater flux based on the variation in precipitation (P) parameter

5.7.4 Summary – Model sensitivity analysis

In this section, four model parameters were studied to evaluate model sensitivity as well as to define the key driver of lake level change for Shortandy Lake. Firstly, the SA indicates that the developed model shows negligible sensitivity when the variation of selected parameters is within the range of 10% (Section 5.7.3.3). However, the model is sensitive to precipitation when variation exceeds 10%. In this study, precipitation data is based on only one weather station records (Section 4.1). Therefore, precipitation records of Shortandy can be a subject of uncertainty due to the small number of rain gauges which results in a systematic error in the model parameters. Systematic errors in hydrological models may be present due to sparse coverage of rain gauges, and topographic effects may also induce a systematic error. Previous studies show that the following error in the observed precipitation data is about 10%-15% (Xu et al., 2006, Eriksson, 1983).

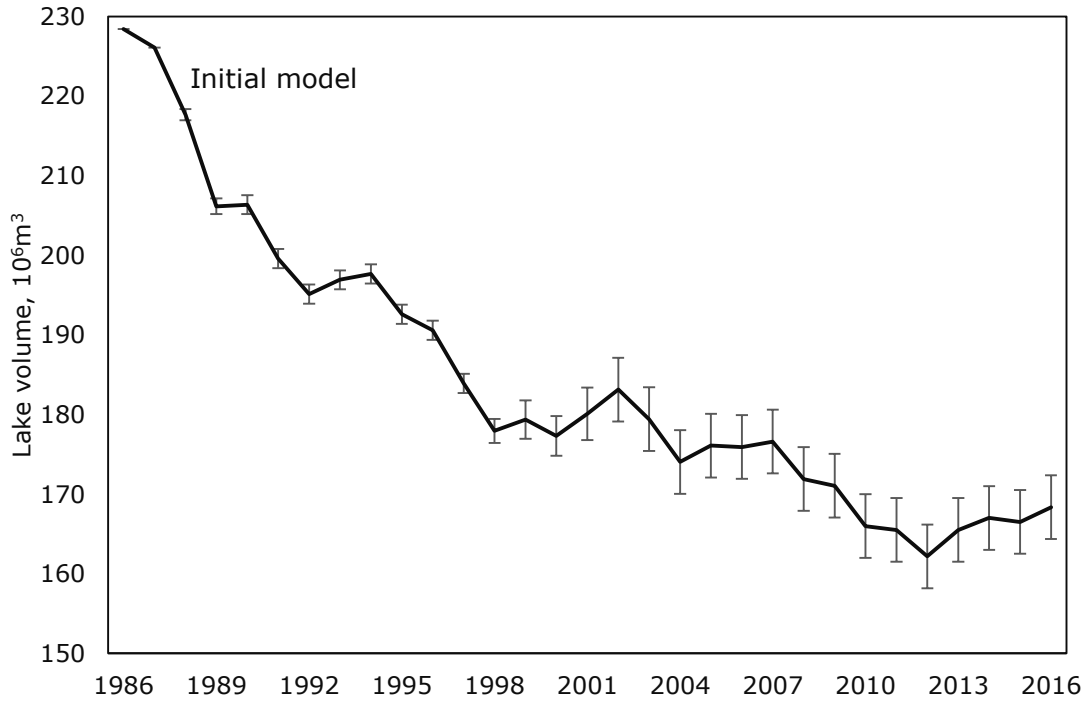

Figure 5. 41 Lake volume dynamics derived from Initial model, where errors bars show standard deviation of the lake volume values obtained from a one-by-one sensitivity analysis with four selected model parameters

The SA indicates that the lake volume is highly responsive to variations in precipitation, particularly for wet years, which affects runoff values. By contrast,

the model showed less sensitivity to air temperature, showing medium sensitivity with variation in T up to 25%, whereas wind and relative humidity were of minor importance for the model output. Therefore, the SA shows that precipitation is a key driver of the lake volume. The following conclusion is consistent with the conclusion that hydrological models are more sensitive to precipitation errors than to evaporation errors (Schaake and Liu, 1989, Xu et al., 2006).

Overall, regression analysis on the lake storage derived from the SA and the initial model outcomes were statistically highly significant (r=0.99, p<0.001 with a standard deviation of 8.6x10^{6}m^3), where the model could adequately reproduce the lake volume changes. Nevertheless, Figure 5.41 shows that the model sensitivity increases over time (number of modelling years). Specifically, the SA of the model illustrated a small difference in the initial model from 1986 to 1997. Since 1998, the standard deviation becomes greater, reaching the maximum value by 2002 (≈8.6x10^{6}m^3 or 5% from the total lake volume), which then remain unchanged until 2016 (Figure 5.41). This trend is associated with the model structure, *i.e.* the way components of the water balance were computed; specifically, groundwater flux, which was established as a function of measured lake levels. Unfortunately, lake level measurements were incomplete for the following years: 1988-1990 and 1998-2002; thus, no $G_i - G_o$ was established for these years. Consequently, these factors have affected model accuracy in the lake volume simulations during above mentioned years.

5.8 Summary

This chapter demonstrates key findings from the lake water balance model, which was developed to investigate the characteristic changes in the water balance of Shortandy Lake over the last three decades. Based on the model findings, the lake volume dynamics show a significant and highly negative temporal trend from 1986 to 2016 (r=-0.93, p<0.001). The relative contribution of input and output

variables were determined. The main findings of the water balance revealed that the relation between Input-Output was negative (-95mm on average), which resulted in the water volume reduction over the study period.

The inflow variables showed variation from year to year (standard deviation ≈ 324mm) where the highest deviation was established for Q_{snow} and Q_{rain} (112mm and 217mm respectively). The following conclusion corresponds with the historical water balance findings for Shortandy Lake established during the 1950s (Uryvayev, 1959).

Analysis of the relative contribution of input variables shows that warm-season precipitation (P_{rain}) and seasonal snowmelt runoff (Q_{snow}) contribute the greatest proportion to the lake volume (37% and 35% respectively) (Figure 5.42). By contrast, open lake evaporation was the major source of the losses during the study period (78%). In comparison with the historical water balance findings for the Northern Kazakhstan lakes, the seasonal snowmelt runoff contribution declined from 50% to 35% (Section 2.3.3), whereas warm-season precipitation increased by 2% (Uryvayev, 1959).

In most cases, dry periods were accompanied with lower annual precipitation, where the proportion of snowmelt runoff varied considerably, from 34% to 17%, as well as with an increased loss for the lake evaporation. These findings coincide with the previous water balance studies conducted in Burabay area, where most of the dry periods were characterised with the reduction of overall P_{sum} and anomalies associated with the seasonal snowmelt runoff (Shnitnikov, 1970b). Furthermore, dry years showed a decrease in the total annual precipitation by around 30% (from the historical average of 332mm year^{-1} to 226mm year^{-1}) in Shortandy.

The water balance had the greatest negative relation from 1988-1992, which resulted in the rapid and dramatic water volume decline (from 225.9x10^{6}m^3 in 1987 to 195.8 x10^{6}m^3 in 1992). Negative water balance, resulting in water volume

reduction occurred during the 1980s and 1990s at a greater magnitude than established after the 2000s.

Year-by-year analysis on the lake water balance model revealed the lowest total annual precipitation as well as an increase in the lake evaporation, which predetermined the *1980s and 1990s period as the driest period* within the study period. Furthermore, a declining trend of the water volume was exacerbated by allowing anthropogenic water abstraction, whose relative contribution was more than 25% of the total annual output variables.

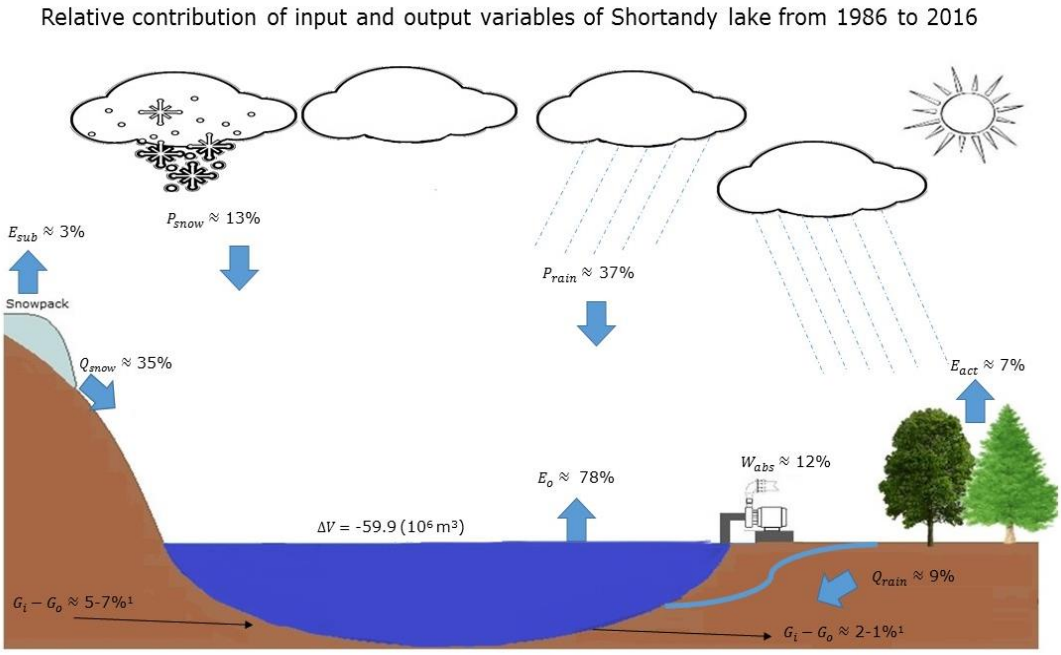

Figure 5. 42 Mean annual proportion of water balance input and output variables from 1986 to 2016

Since 2013, the relation between input and output was positive, which resulted in the water volume increasing. This following pattern is explained by the overall reduction of output proportion due to the decrease in anthropogenic water abstraction since 2010. Consequently, the positive water balance response was driven by the decreased annual proportion of output variables.

According to the water volume dynamics estimated through the water balance equation, a significant water volume reduction was established. The water volume simulated through the lake water balance model was compared with the water

volume simulated by observed water levels. A high statistical significance between simulated and observed water volume was established (r=0.999, p<0.001). The sensitivity analysis indicates that the developed model shows negligible sensitivity when the variation of model parameters is within the range of 10%, and the model could adequately reproduce the lake storage changes (Section 5.7.3). However, the model is sensitive to precipitation when variation exceeds 10%. Moreover, it was identified that the model sensitivity increases over time. Particularly, the overall model accuracy has been affected due to the lack of groundwater flux estimations in 1988-1990 and 1998-2002, which affected the lake storage simulations.

Chapter 6 Future climate modelling

According to the literature review (Section 2.2.3), endorheic lakes of Central Asia are most likely to be influenced by the changing future climate. The thirty years water balance modelling of Shortandy Lake illustrates the delicate relationship between input and output variables, indicating the sensitivity of endorheic lakes to any changes. However, little is known about how the future climate will affect the hydrological cycle of Shortandy Lake and Burabay area, in general. The main objectives of the following chapter of the thesis are: (1) to quantitatively examine input and output variables of the developed water balance model under a global temperature increase of 1.5°C-2°C; (2) to identify the likely implications of projected climate on Shortandy Lake volume fluctuation, (3) to evaluate the role of anthropogenic impact on Shortandy Lake based on future climate scenarios.

6.1 Description of future climate models

To assess future volume changes in Shortandy Lake, the main regional hydrological drivers were quantified. For this purpose, future change impacts were assessed within the broader framework outlined by Inter-Sectoral Impact Model Intercomparison Project (ISIMIP2b), which is a framework for projecting the impact of the changing climate on different sectors, including water resources, agriculture and ecosystems, for example. In general, ISIMIP is intended to examine future climate change by forcing various climate-impact simulations under identical climate and socio-economic input (Schellnhuber et al., 2014). Specifically, this projection allows assessment of the impact of historical warming related to pre-industrial reference levels. Secondly, it allows the assessment and comparison of different scenarios of global mean temperature increase (Frieler et al., 2017). Climate modelling for Shortandy Lake utilises historical impact simulations to calibrate outcomes from the future climate modelling under the

low-emission Representative Concentration Pathway-RCP 2.6 (Vuuren et al., 2011); and no-mitigation pathway-RCP 6.0 (Masui et al., 2011).

6.1.1 Historical modelling

Various external drivers, such as changing water management, land-use change, expansion of agriculture, etc. are integrated into ISIMIP2b. These factors have developed simultaneously with climate, improving future climate change predictions.

Historical simulation using a future climate model allows for cross-sectional assessments of when the changing climate signal becomes significant (Frieler et al., 2017). In ISIMIP, the historical simulations for future climate modelling could be conducted starting from the period of 1861. However, in this study, the historical water balance simulation begins from 1971. The year selection can be explained by the lake water balance model developed for Shortandy (Eq.4.1), which requires the established lake area/volume/level (Chapter 4.1). Due to the lack of historical lake level measurements, remotely sensed products were used for detection of the lake area, where for Shortandy Lake, the earliest available product was from 1970. Therefore, air temperature and precipitation data was obtained based on GFDL (Figure 6.1) and IPSL (Figure 6.2) models for the Shortandy catchment.

6.1.2 Future climate and emission scenarios

Future projections under the strong mitigation scenario are represented by RCP2.6, which represents global warming conditions consistent with achieving the 2°C goal of the Paris Agreement, signed in 2015 (Vuuren et al., 2011). The RCP2.6 was based on future changes in human influence and climate change under the strong mitigation scenarios. Based on the climate projection, the cumulative emission should be reduced by roughly 70%, and emissions must be reduced by 95% in 2100 in comparison with to baseline observational climate data (Vuuren et al., 2011). Particularly, the emission rate has to be reduced rapidly, by around

4% every year (Vuuren et al., 2011). Furthermore, greenhouse gas intensity should be improved from the present 5-6% to historical rates of 1-2% annually. In RCP2.6, CO_2 emissions from fossil fuel use are reduced by a combination of energy efficiency with an alternative renewable source of energy such as nuclear power, bioenergy, etc.

By contrast, RCP6.0 declares future projections for a no-mitigation scenario (Fricko et al., 2017). Based on RCP6.0, the cumulative emission needs to be reduced by 50% below baseline by 2100. Specifically, the following scenario is considering the reduction of most emissions by 2080, where a higher proportion of emissions are expected by 2050 and compensated by lower emissions afterwards (Vuuren et al., 2011). The mean global long-term, steady-state air temperature is expected to increase 4°C-4.9°C above the pre-industrial level (Masui et al., 2011).

Future climate modelling for Shortandy was performed under two GCMs from ISIMIP2b, specifically GFDL-ESM2M and IPSL-CM5A-LR based on RCP2.6 (Figure 6.3 and Figure 6.4 respectively) and RCP6.0 (Figure 6.5 and Figure 6.6 respectively) emission scenarios, including the historical period from 1971 to 2100. Both models simulate atmospheric circulation coupled with an oceanic circulation model as well as representation of land, sea and cryosphere interactions. GFDL and IPSL model the effect of the ocean response under various emission scenarios and climate change to ocean configuration (Dunne et al., 2012, Dufresne et al., 2013). Therefore, these models have been widely applied for future lake level changes (Beecham, 2015, Sahoo et al., 2013). These impact models include physical and biochemical data which provide first and secondary climate input data required for hydrologic modelling. Climate data was subtracted using coordinates of the catchment with 1km of spatial resolution.

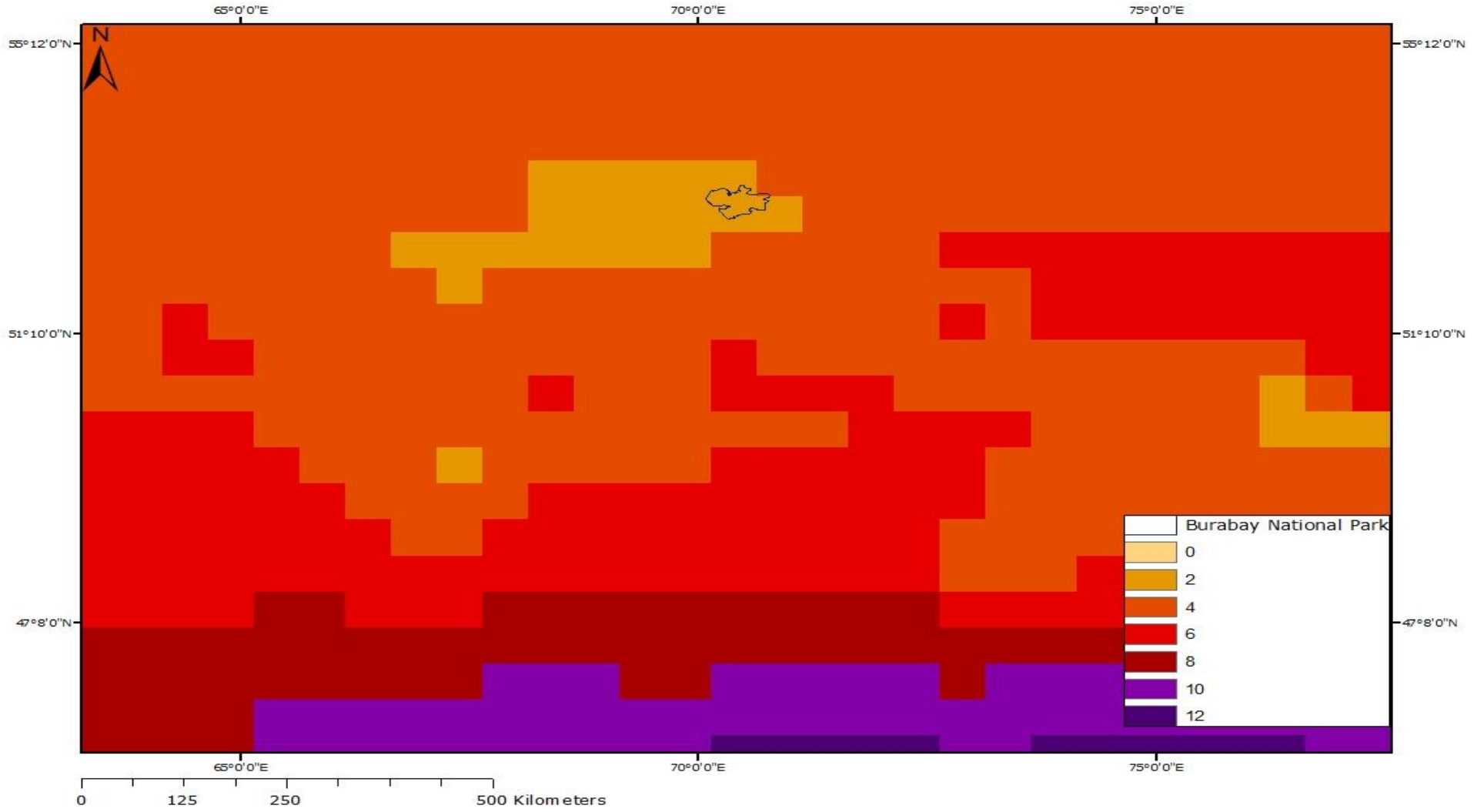

Figure 6. 1 Mean annual air temperature for Burabay National Nature Park based on historical GFDL model, from 1971 to 2005 where black line shows boundary of Burabay National Nature Park

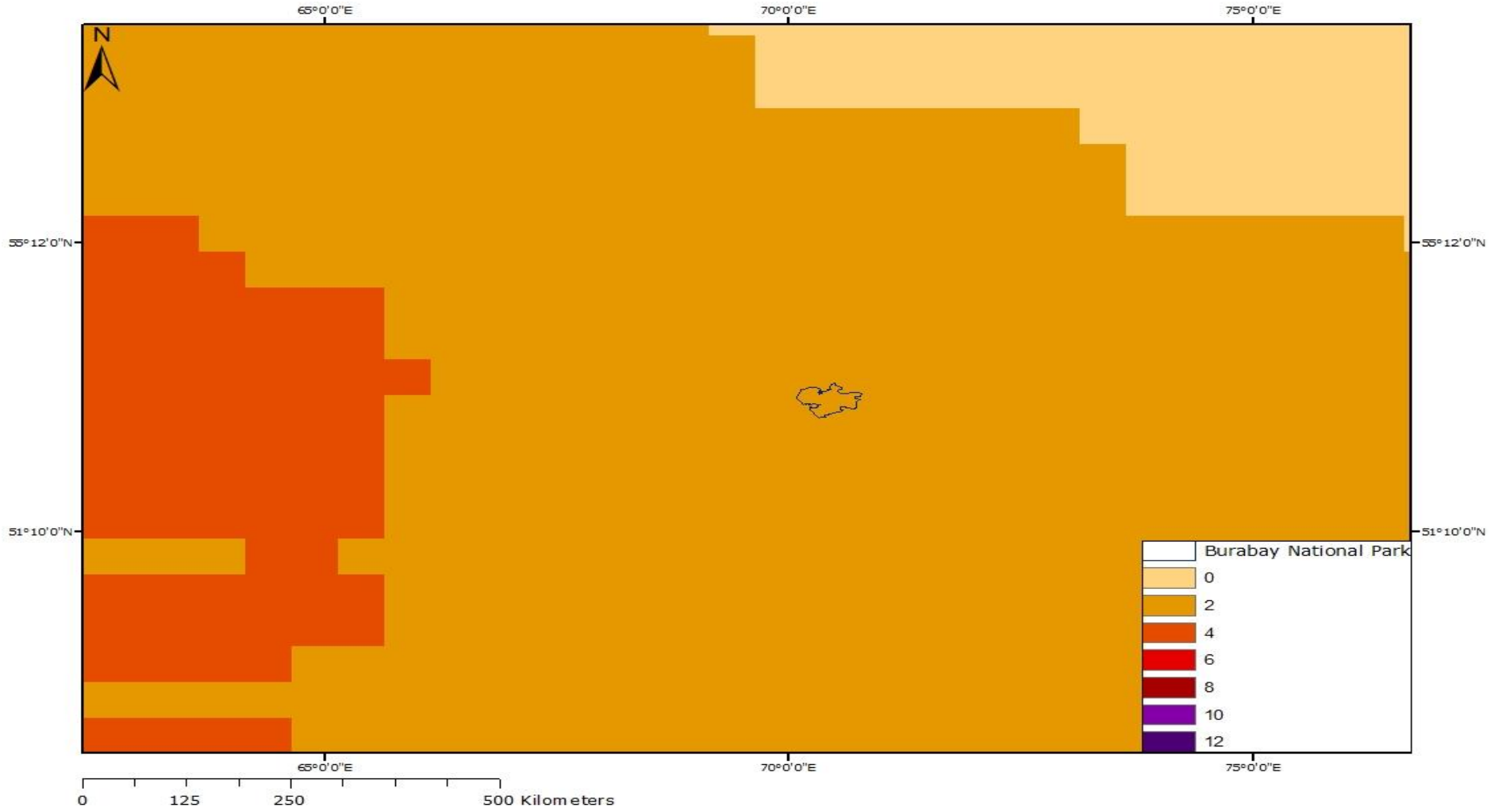

Figure 6. 2 Mean annual air temperature for Burabay National Nature Park based on historical IPSL model, from 1971 to 2005 where black line shows boundary of Burabay National Nature Park

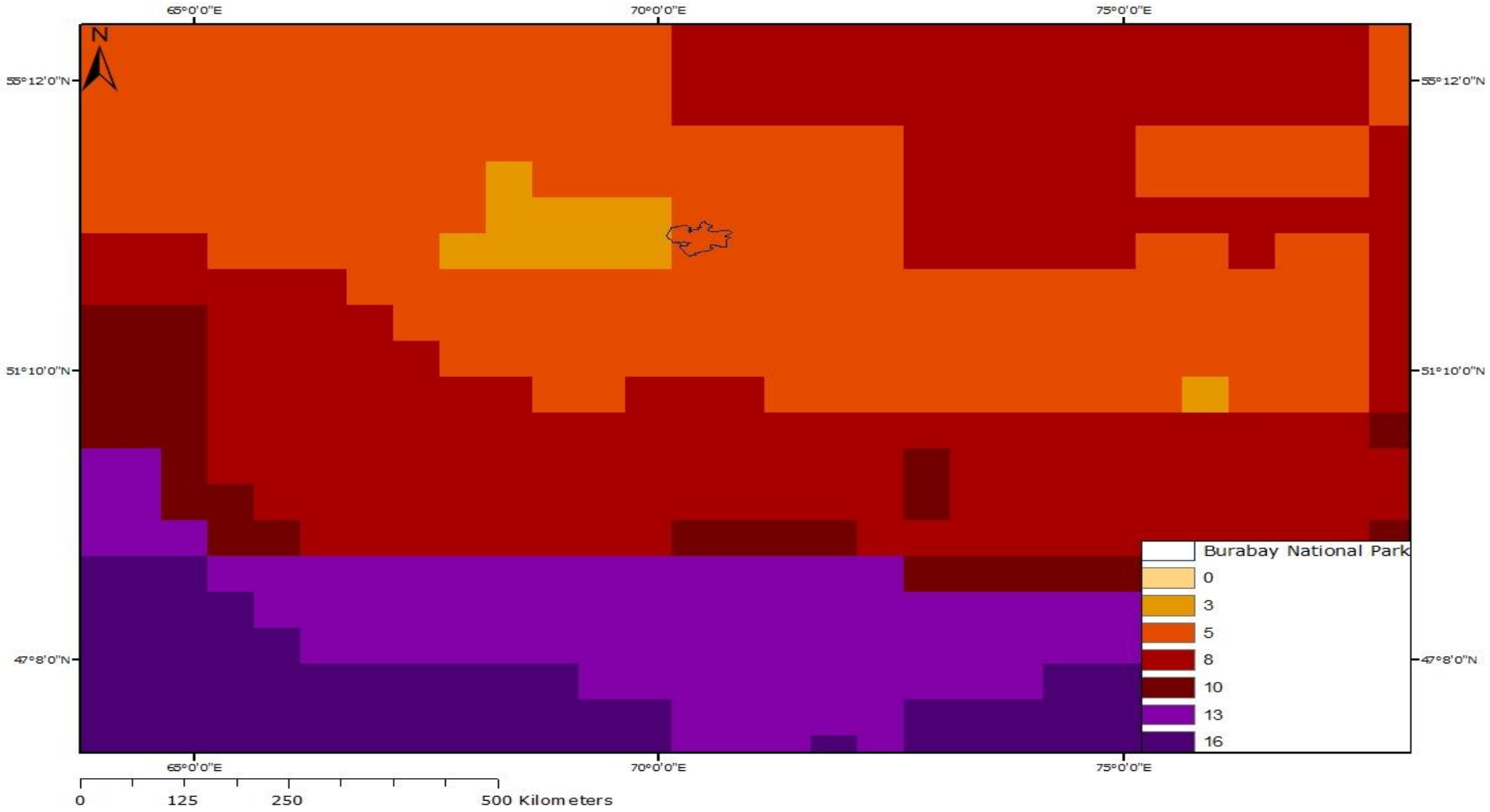

Figure 6. 3 Mean annual air temperature for Burabay National Nature Park based on RCP2.6 GFDL model, from 2006 to 2100 where black line shows boundary of Burabay National Nature Park

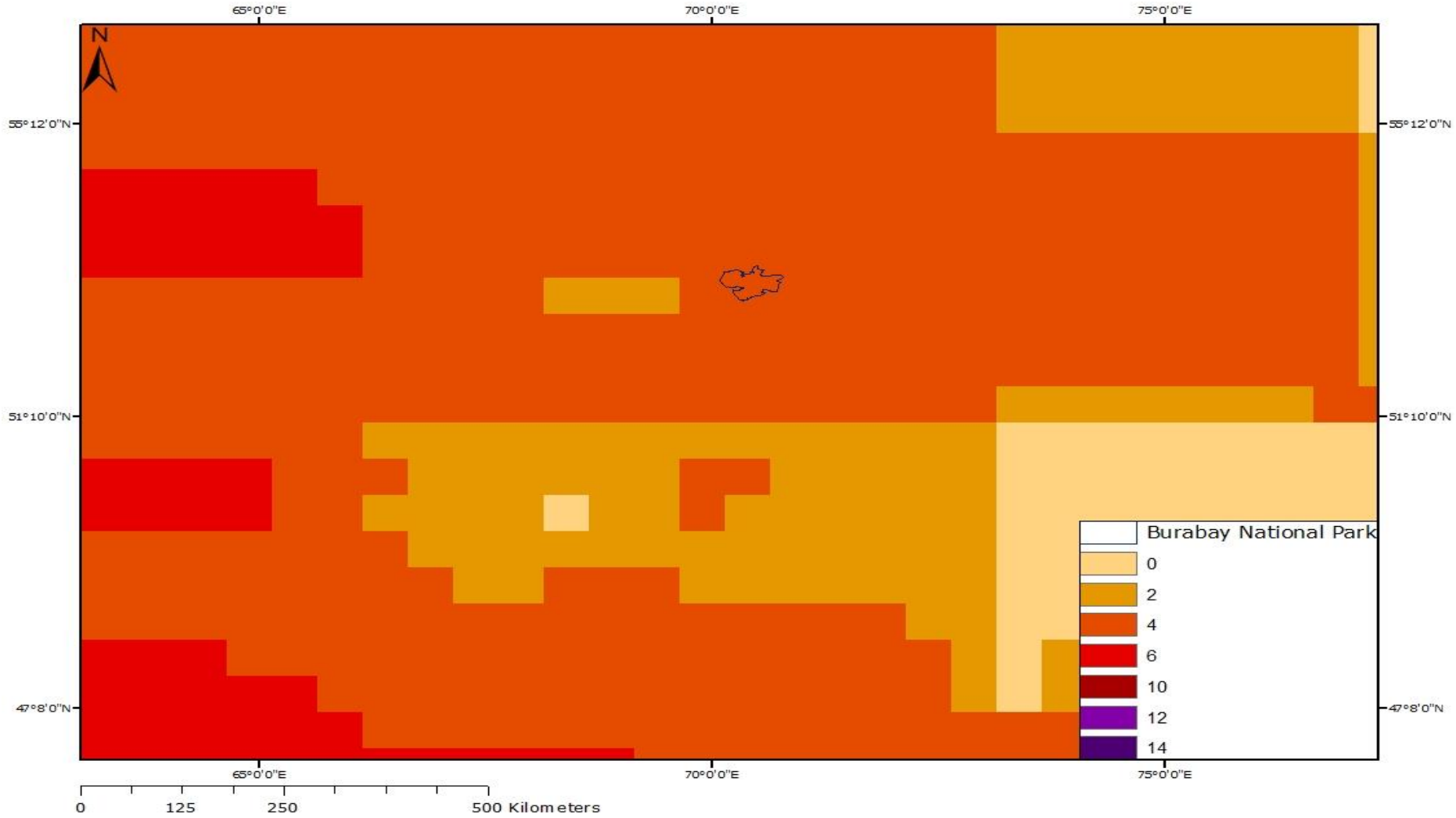

Figure 6. 4 Mean annual air temperature for Burabay National Nature Park based on RCP2.6 IPSL model, from 2006 to 2100 where black line shows boundary of Burabay National Nature Park

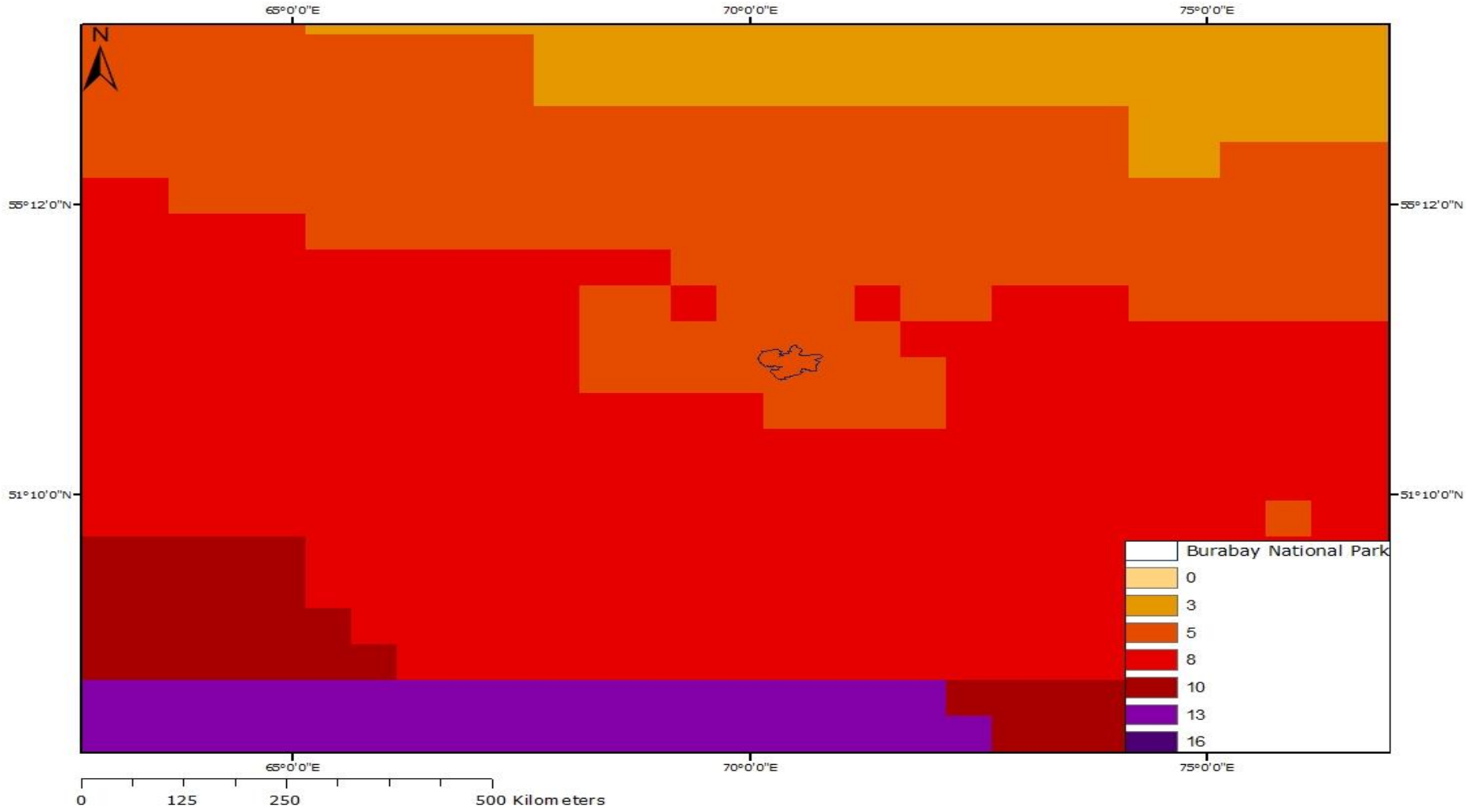

Figure 6. 5 Mean annual air temperature for Burabay National Nature Park based on RCP6.0 GFDL model, from 2006 to 2100 where black line shows boundary of Burabay National Nature Park

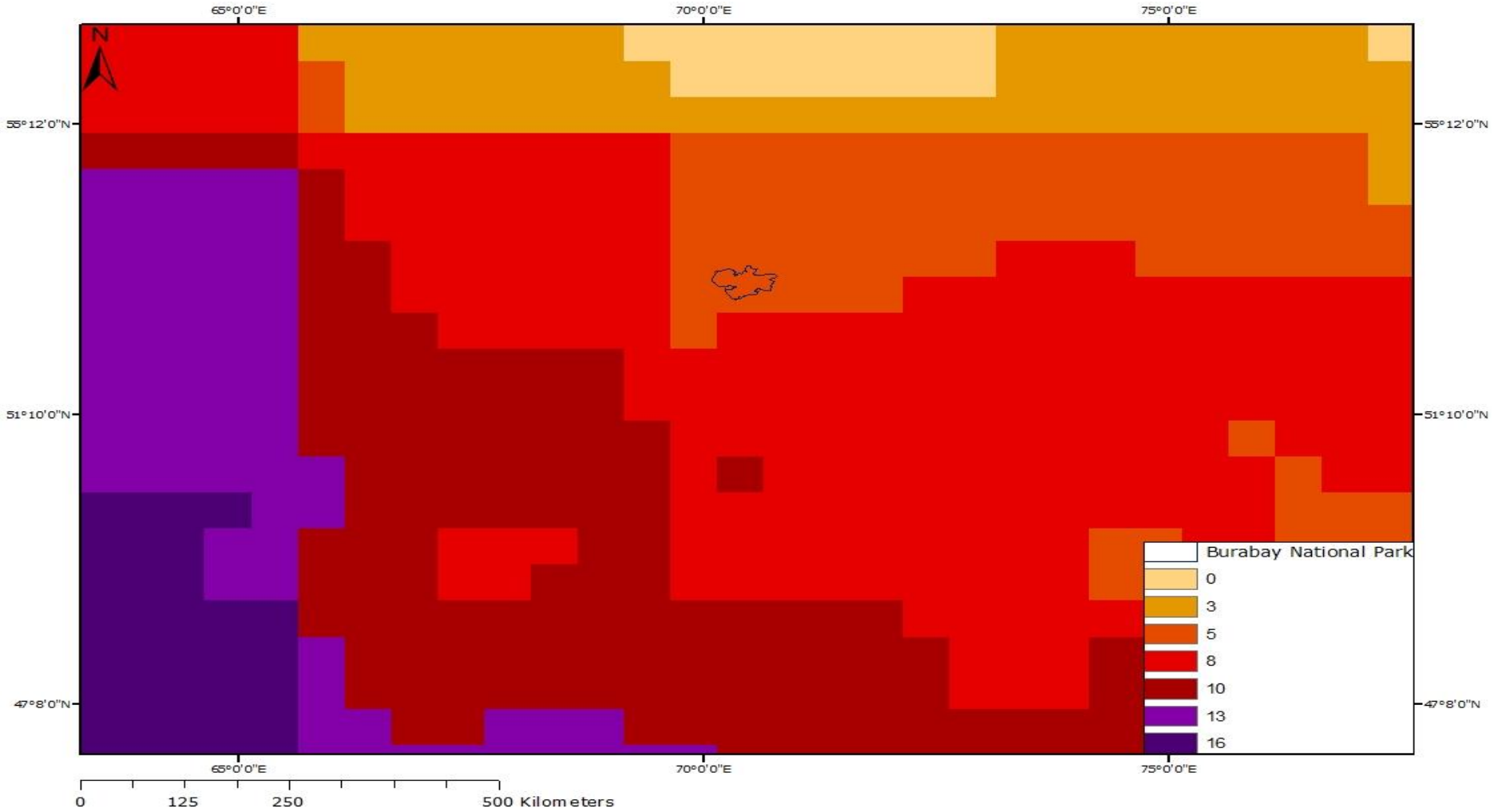

Figure 6. 6 Mean annual air temperature for Burabay National Nature Park based on RCP6.0 IPSL model, from 2006 to 2100 where black line shows boundary of Burabay National Nature Park

6.2 Supplementary model for future water balance

The lake water balance model developed for Shortandy Lake, utilises the daily records on the lake ice formation and decay obtained from Schuchinsk weather station used for the estimation of lake evaporation during warm-seasons. Chapter 5 outlines that open lake evaporation comprises 84% of the total annual outflow, whereas snow sublimation is only 1-2%.

Chapter 2.2.3 indicates that in warming global temperatures, snow-thaw and lake ice break-up periods are predicted to be quicker in the Northern Hemisphere, with a greater impact on mid-latitude Eurasian regions (Adam and Hamlet, 2009, Stewart et al., 2005a). Therefore, the lake ice-phenology modelling is required for the accurate estimation of the warm and cold season duration, which affects lake evaporation (E_o) and snow sublimation (E_{sub}). This section describes a simple empirical model which establishes the relationship between ice formation/decay and air temperature in Shortandy Lake.

6.2.1 Lake ice freezing and ice break-up model development

Empirical models for lake ice cover modelling are based on the methodology developed for Canadian lakes (Shuter, 2012) and adopted for Shortandy Lake due to similarities in the regional climate, hydrologic regime and landscape settings. These models were developed for Canadian lakes and applicable for endorheic lakes modelling to forecast future climate change impact on the timing of ice formation and decay during spring (Shuter, 2013). This model produced relatively similar results to more accurate, yet difficult well-grounded mechanistic models (Dibike et al., 2012), where the empirical model tends to overestimate ice break-up by 2.3 days more than the mechanistic model.

The model variables and parameters for the empirical equation were estimated for Shortandy Lake specifically. To evaluate the model performance, first of all, empirical equations were established based on model parameters estimated from

1991 to 2016. Subsequently, the model outcomes were compared with the observed lake freeze and break-up dates in Shortandy Lake. In the future climate model, the empirical equations were recalculated based on the model parameters estimated from 1971 to 2100.

6.2.2 Model variables and parameters

The model variables required for ice freeze-decay models are reflected in Table 6.1. Lake ice-freeze model variables (*ZERO_FL, AT_FL, ZERO_DAYS, ZERO_SP*) are estimated using the 30-days running average of the observed daily air temperature from 1986 to 2016. Whereas, in future climate simulations, the 30-days running average filter was applied from 1971 to 2100.

Table 6. 1 Description of each variable required for ice formation and decay models based on the Canadian model (Shuter, 2013)

Acronym with units	***Definition***	***Potential influence***
Freeze-up modelling		
ZERO_FL: Julian day	Julian date following the last day when the 30-day running average of local daily T>0°C	Consistent T<0°C is required for surface water to freeze
ANG_FL: degrees	Angular elevation of the Sun above the horizon at noon on ZERO_FL	Higher values are driven by higher ground-level radiation
AT_FL:°C	Mean air temperature for the 3-month where the central month contains ZERO_FL	Lower fall T will promote greater heat loss from the lake
Break-up model		
ZERO_DAYS: days	Number of days between ZERO_FL and ZERO_SP	Longer period with T<0°C will promote the growth of ice thickness

ZERO_SP: day, starting from 1 on 1 January	Julian date following the last spring date when the 30-day running average of local daily T<0˚C	No ice thickness growth at temperature>0˚C
ANG_SP:˚C	Angular elevation of the Sun above the horizon at noon on ZERO_SP	Higher values are driven by higher ground-level radiation

Computed model parameters were used to establish regression analysis (Table 6.2), which explains the relationship between air temperature and ice formation/decay in Shortandy Lake.

Table 6. 2 Parameters required in freeze-up and break-up model

where Zero_SP is Julian date, ANG_SP is degree, ZERO_FL is Julian date and AT_FL is °C

Year	Break-up		Freeze-up model	
	Zero_SP	**ANG_SP**	**ZERO_FL**	**AT_FL**
1991	111	47.14	321	-5.18
1992	113	43.05	314	-5.61
1993	116	44.2	311	-9.76
1994	113	43.21	317	-5.43
1995	102	39.31	315	-4.85
1996	125	46.64	308	-7.44
1997	101	39.16	321	-5.6
1998	125	47.04	-	-
2003	116	44.11	311	-5.9
2004	112	42.75	314	-4.63
2005	114	48.35	322	-3.49
2006	107	45.86	327	-3.88
2007	109	46.48	317	-5.03
2008	101	43.49	322	-3.52
2009	107	45.96	313	-6.14
2010	113	47.95	328	-4.93
2011	106	45.43	314	-7.04
2012	104	44.61	317	-8.07
2013	107	45.97	331	-7.9

2014	107	45.88	307	-6.71
2015	113	47.87	309	-4.83
2016	101	43.51	302	-0.017

6.2.3 Break-up model description for climate modelling and evaluation

The break-up dates obtained through the model were compared with observed dates of ice-decay in the lake. Figure 6.7 illustrates that the simulated break-up dates were significantly correlated with observed dates (r^2=0.92, n=22, p<0.001 and Nash-Cutcliffe =0.990), precision (as measured by the standard deviation of the observed-modelled difference) was ±2.9 days. Regression analysis on break-up model parameters established a simple regression equation for forecasting break-up dates in Shortandy Lake:

$$Break\ up = 19.87355 + 1.0613 * ZERO_{SP} - 0.28215 * ANG\_SP \qquad \text{Eq.6.2.2}$$

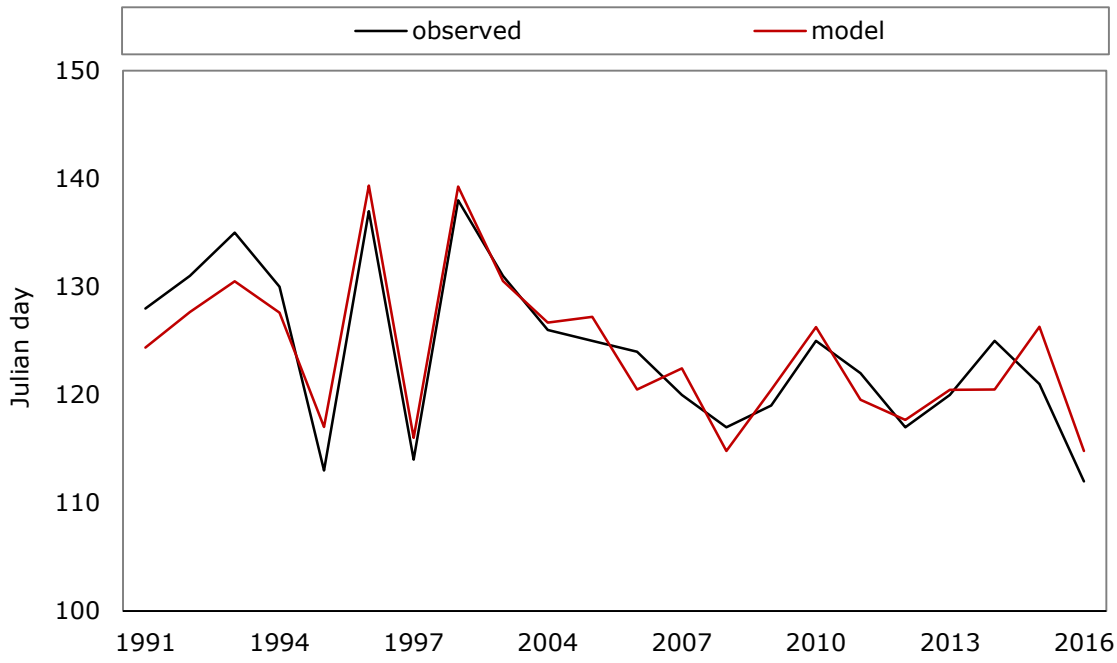

Figure 6. 7 Comparison of predicted ice break-up dates with observed records on annual Shortandy Lake ice decay

6.2.4 Freeze-up model description for climate modelling and evaluation

Similarly, simulated freeze-up dates were validated against observed ice-decay in Shortandy. The predicted freeze-up dates show significant correlation (Figure 6.8) with observed dates of lake freezing, where r^2=0.86, n=21, and p<0.001 Nash-Sutcliffe =0.992, with average overestimation of ice formation timing in Shortandy for three days, with standard deviation equivalent to ±4.4 days. Regression analysis of the lake freeze-up model parameters produced an equation to simulate ice freeze-up in changing climate conditions in Shortandy as follows:

$$Freeze\ up = 3.11858 + 1.036745 * ZERO_{FL} + 0.752455 * AT\_FL \qquad \text{Eq 6.2.2b}$$

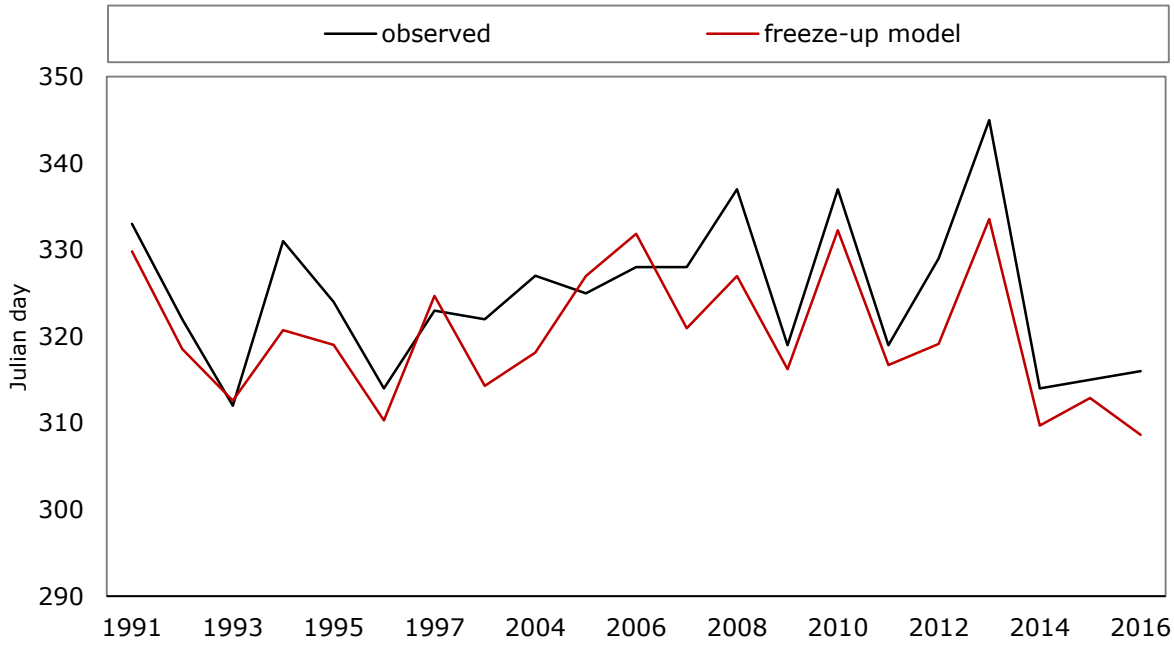

Figure 6. 8 Comparison of predicted freeze-up model with observed records on annual Shortandy Lake ice formation

The empirical equations obtained from a simple statistical analysis conducted for Shortandy Lake show significant correlation with observed data. The break-up model outcomes show a higher correlation for Shortandy with ±2.9 day in comparison with Canadian model outcomes, which is ±7.4 days for lakes in Canada. Yet, the freeze-up model validation shows wider error for the Shortandy correlation than the Canadian example, specifically ±4.4 days versus ±2.4 days,

respectively. Overall, the sensitivity of the water balance to the lake ice freezing and ice break-up is around ±7.3 days.

6.3 Water balance computation for future climate modelling

Climate projections from climate models were applied to the developed water balance described in Chapter 4. The computation routine for the future climate model is reflected in Figure 6.9, where E_{act} estimation was based on methodology explained in Section 4.4.2 and assumption mentioned in Section 5.1.2. In this modelling, water balance estimates are monthly. Future water volume changes were estimated using an Excel spreadsheet. Similarly, lake evaporation was estimated using an Excel spreadsheet, whereas seasonal snowmelt runoff estimations were transferred into MatLab code.

Based on the lake water balance equation (Eq.4.1), established lake area is required. Historical climate modelling starts from 1971, which means that the historical lake area and the lake volume were required for that period. To do so, the earliest LandSat-1 image with 80-meter resolution available for Shortandy (July 1976) was used.

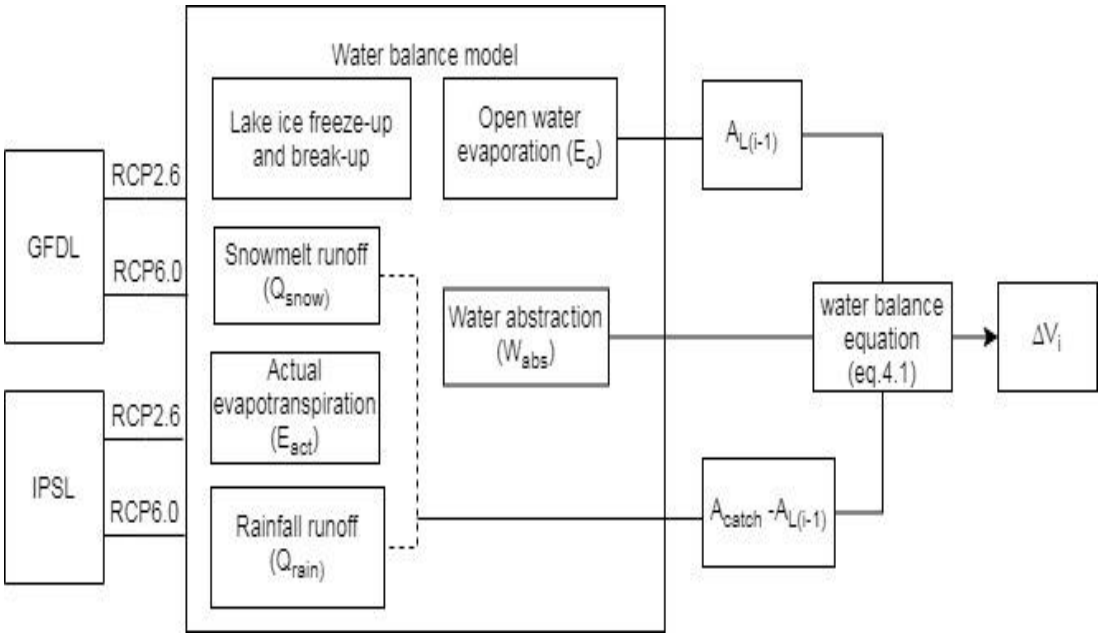

Figure 6. 9 Computation process of future climate modelling for Shortandy Lake

where $A_{L(i-1)}$ is the lake area of the previous month, A_{catch} is the catchment area, and ΔV_i is the water volume change

Water abstraction in the future climate model

Anthropogenic water abstraction in future climate modelling was incorporated into the lake water balance as follows:

- From 1989 to 2016, the lake water balance model utilises annual water abstraction values obtained from the Water Supply Agency in Shortandy – Burabay Su Arnasy, explained in Chapter 5.1.3;
- From 2016 to 2100, annual water abstraction was incorporated as a *constant value of* $0.5x10^6 m^3$ *of water* based on the current governmental water abstraction restrictions from Shortandy Lake.

Groundwater flux in the future climate model

According to the developed water balance model, the groundwater storage was estimated based on two approaches: (i) by measured water levels and (ii) throughout the established water volume of the lake and the difference between input and output variables. However, in future climate simulations, it is not possible to establish these model parameters so that these models were inapplicable. As a result, the groundwater storage *was excluded* from future climate simulations. The uncertainties of the exclusion of the groundwater storage will be further addressed in Chapter 7.

6.4 Results - Future climate model

6.4.1. Air temperature

Future climate modelling for Shortandy confirms the *air temperature increase* based on two GCM models in both emission scenarios, RCP2.6 and RCP 6.0. According to Figure 6.4, the minimum temperature increase is projected under GFDL RCP2.6 from 2°C of the historical average to 3.4°C from 2006-2100 (Figure 6.10) with the positive temporal trend r=0.18, p<0.001 and a standard deviation of 1.4. The GFDL model under RCP6.0 protocol predicts a higher temperature increase, specifically the average mean annual air temperature will rise from 1.9°C to 3.8°C (r=0.44, p<0.001 and standard deviation of 1.6) (Figure 6.11). Percent

bias analysis between GFDL two emission scenarios indicates that the mean air temperature will increase on average to 31% under RCP6.0, with the highest difference in 2080-2099 (123%) and lowest difference projected in 2040-2065 (16%).

IPSL under RCP2.6 predicts that the mean annual air temperature is expected to increase from 1.9°C to 4°C (where temporal relation shows r=0.38, p<0.001 and a standard deviation of 1.5) (Figure 6.12). The highest temperature increase is projected by IPSL under no-mitigation emission scenario (RCP6.0) by approximately 6°C by 2100 (Figure 6.13). There is a significant positive temporal relationship in air temperature for Shortandy area, r=0.67, p<0.001 and a standard deviation of 2.1. Percent bias analysis shows that under IPSL RCP6.0 the mean temperature will increase on average by 22% relatively to IPSL RCP2.6, with the highest difference in 2080-2099 (82%) and the negative difference (-1%) projected in 2020-2045.

Overall, percent bias analysis between the two GCM models indicated that the IPSL model predicts higher mean air temperature for Shortandy under both emission scenarios. Specifically, under RCP2.6, the mean air temperature is projected to be higher by 80% under IPSL, whereas under RCP6.0, the difference is around 93%.

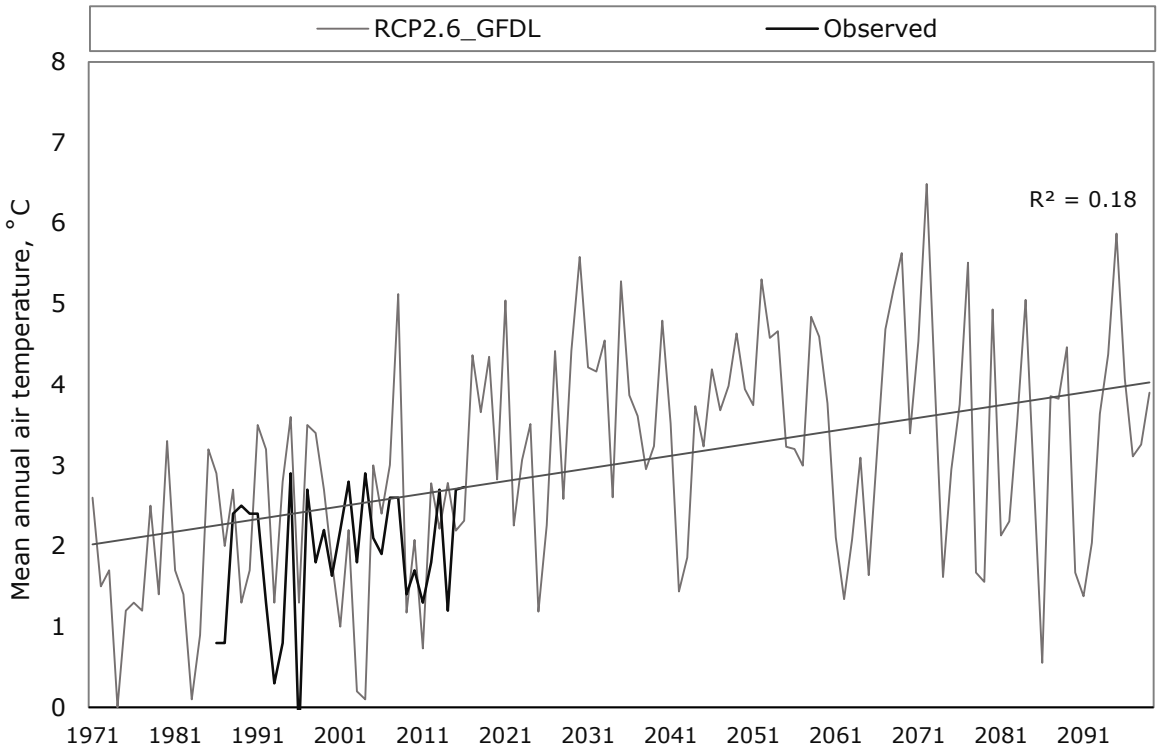

Figure 6. 10 Mean annual air temperature based on GFDL for Shortandy Lake

where the grey line shows linear regression based on RCP2.6 from 1971 to 2100; black line shows air temperature observed in Shortandy from 1986 to 2016

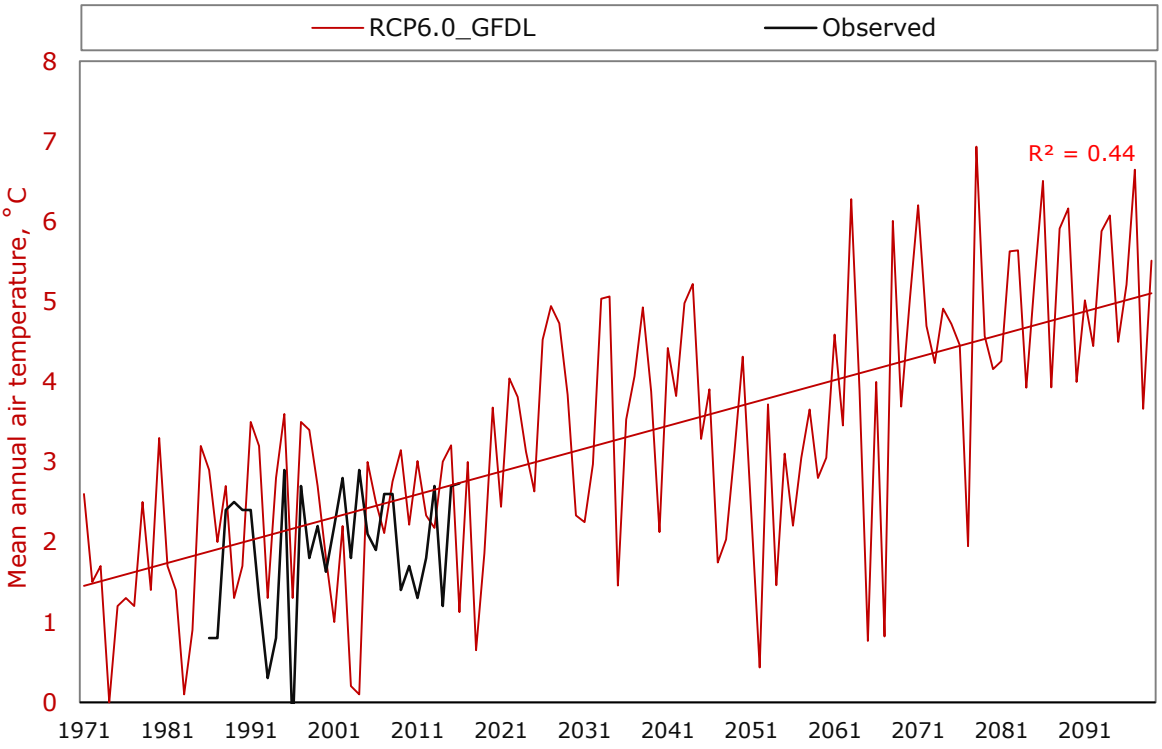

Figure 6. 11 Mean annual air temperature based on GFDL for Shortandy Lake

where the red line shows linear regression based on RCP6.0 from 1971 to 2100; black line shows air temperature observed in Shortandy from 1986 to 2016

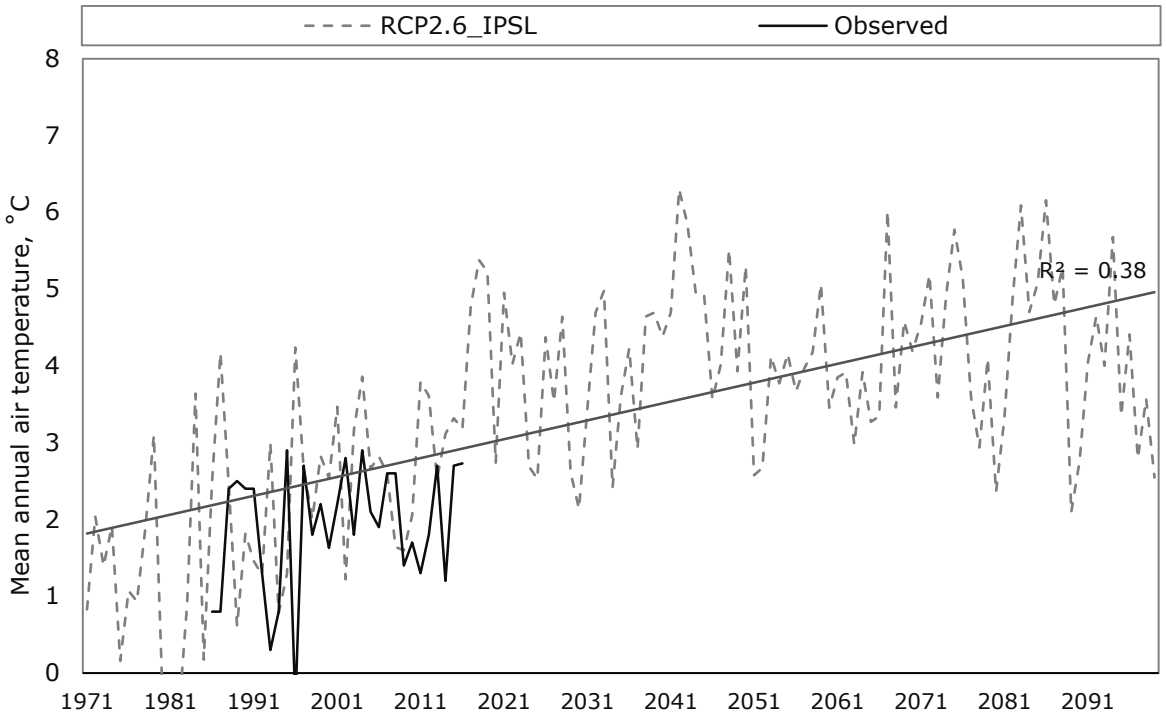

Figure 6. 12 Mean annual air temperature based on IPSL Shortandy Lake

where the grey dashed line shows linear regression based on RCP2.6 from 1971 to 2100; black line shows air temperature observed in Shortandy from 1986 to 2016

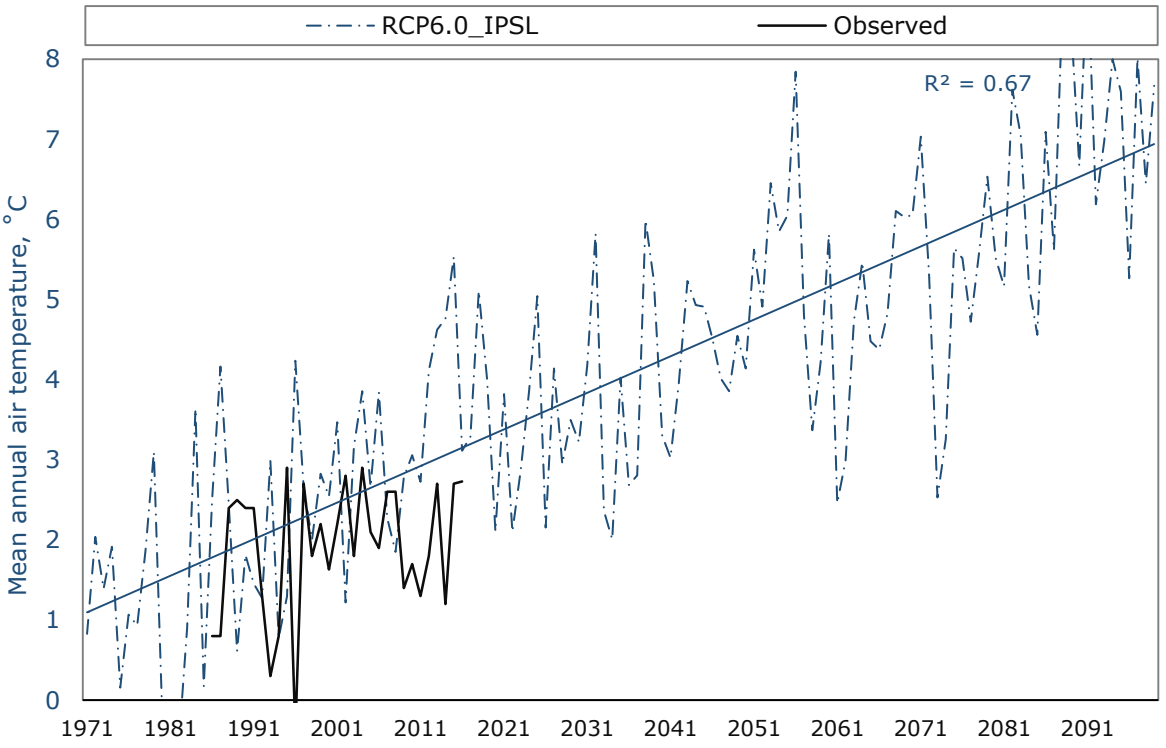

Figure 6. 13 Mean annual air temperature based on IPSL for Shortandy Lake

where the blue line shows linear regression based on RCP6.0 from 1971 to 2100; black line shows air temperature observed in Shortandy from 1986 to 2016

6.4.1.1 Monthly air temperature distribution

Figure 6.8 shows the mean monthly air temperature distribution projected from 1971 to 2100 and the mean monthly air temperature observed in Shortandy Lake from 1986 to 2016. Based on the GFDL model, the temperature increase is expected to influence *cold-season months with insignificant changes during warm season months (June, July, and August) with less than 1°C increase* (Table 6.3). The model predicts that the air temperature will increase for all cold season months, with the greater influence on DJM with more than 2.5°C increase by 2100 under both emission scenarios relative to the historical averages (15%-17%). By contrast, the IPSL model results agree with the GFDL under RCP6.0, specifically predicting warmer mean air temperature from December to March, with the highest temperature increase for February up to 3.7°C (+17%) and in April (+49%) under RCP6.0.

Furthermore, Figure 6.14 indicates that the mean air temperature differs significantly for cold-season months over the simulated period. Both climate models are in good agreement indicating a significant variation of air temperature predicted for DJF months under both emission-scenarios (standard deviation of higher than 4°C). The highest standard deviation was estimated for January and February under RCP6.0 IPSL and GFDL and for January (3.9°-4.5°C and 3.5°-4.5°C respectively). By contrast, the warm-season months (from May to October) temperature show less variation with 2.1°C-2.4°C based on GFDL and 2.5°C-2.6°C based on the IPSL model.

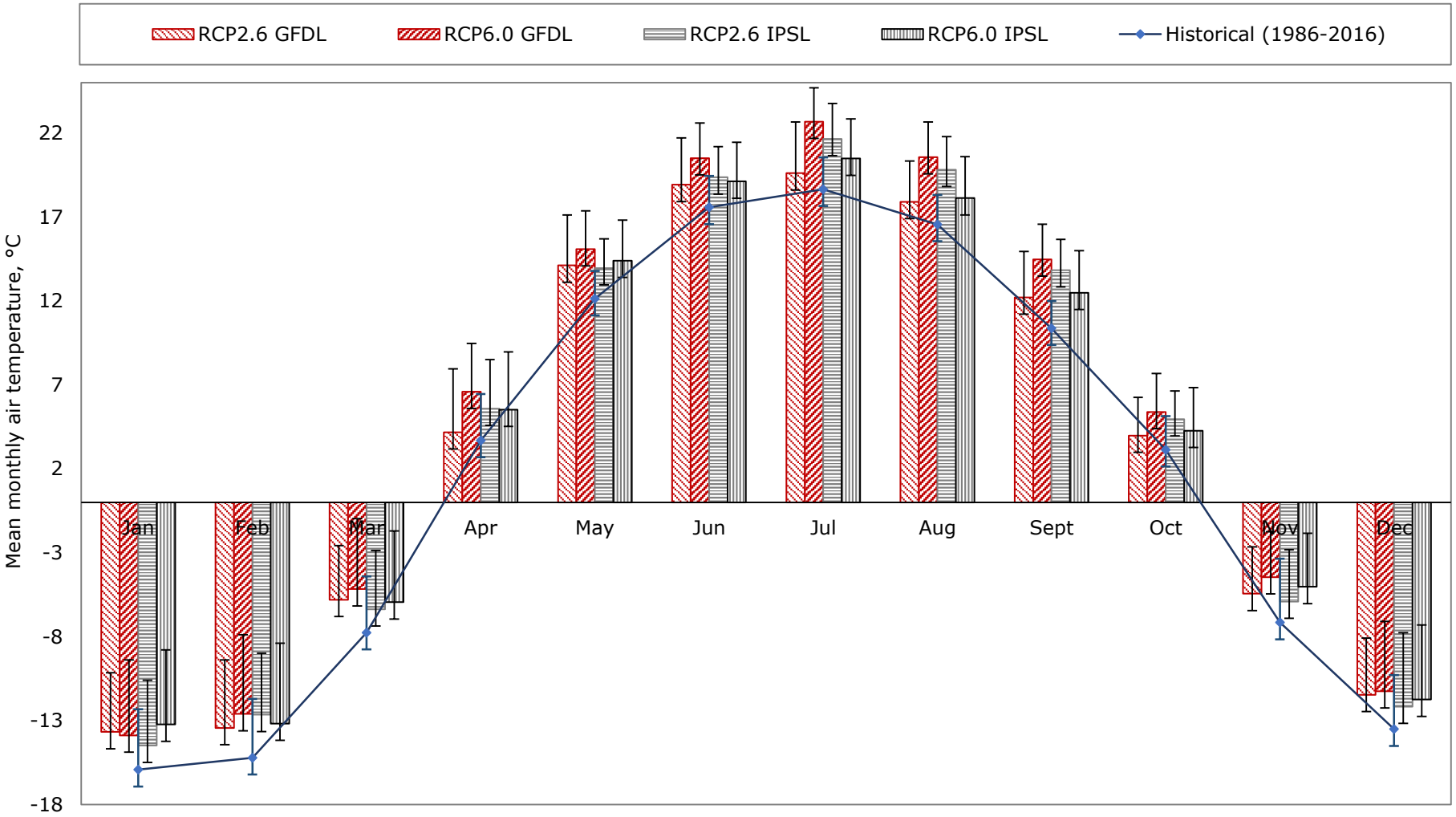

Figure 6. 14 Mean monthly air temperature projected for the Shortandy catchment from 2006-2100 based on RCP2.6 and RCP6.0 protocols by two GCM models and observed historical mean monthly air temperature observed from 1986 to 2016

where error bars show standard deviation

Table 6. 3 Monthly mean air temperature difference (ΔT_{mean}) estimated as the difference between historical monthly T_{mean}(1971-2005) and mean air temperature projected by RCP2.6 and RCP6.0 by two GCM models from 2006-2100

Model	ΔT_{mean}	Jan	Feb	Mar	Apr	May	Jun	Jul	Aug	Sept	Oct	Nov	Dec
GFDL	Historical and RCP2.6	3.8	2.1	2.6	1.6	1.3	0.0	-0.2	0.0	0.7	1.4	1.8	2.6
	Historical and RCP6.0	4.3	2.4	2.5	2.9	1.6	0.2	0.7	0.3	0.9	1.7	2.2	2.3
IPSL	Historical and RCP2.6	1.9	3.7	2.2	2.7	1.1	1.4	2.0	2.4	2.3	2.3	1.6	1.9
	Historical and RCP6.0	2.5	3.7	3.4	3.7	2.2	2.6	3.0	3.2	3.0	2.7	3.1	2.8

6.4.2 Precipitation

Although the simulated climate model output represents the general changes in climate, it is helpful to compare how future climate is likely to alter the precipitation regime in the catchment. Figure 6.15 and Figure 6.16 compares the GFDL model prediction for annual precipitation trends under both emission scenarios with the observed precipitation patterns at the Shortandy catchment. Based on the GFDL model, the total annual mean precipitation is likely to increase by 25%-26% (from 359mm to 449mm and 452mm) based on RCP2.6 and RCP6.0 respectively by 2100 (Figure 6.15 and Figure 6.16). Percent bias analysis indicates that the difference in precipitation between two emission scenarios is 6% on average, with the highest difference projected in 2060-2080 (around 12%).

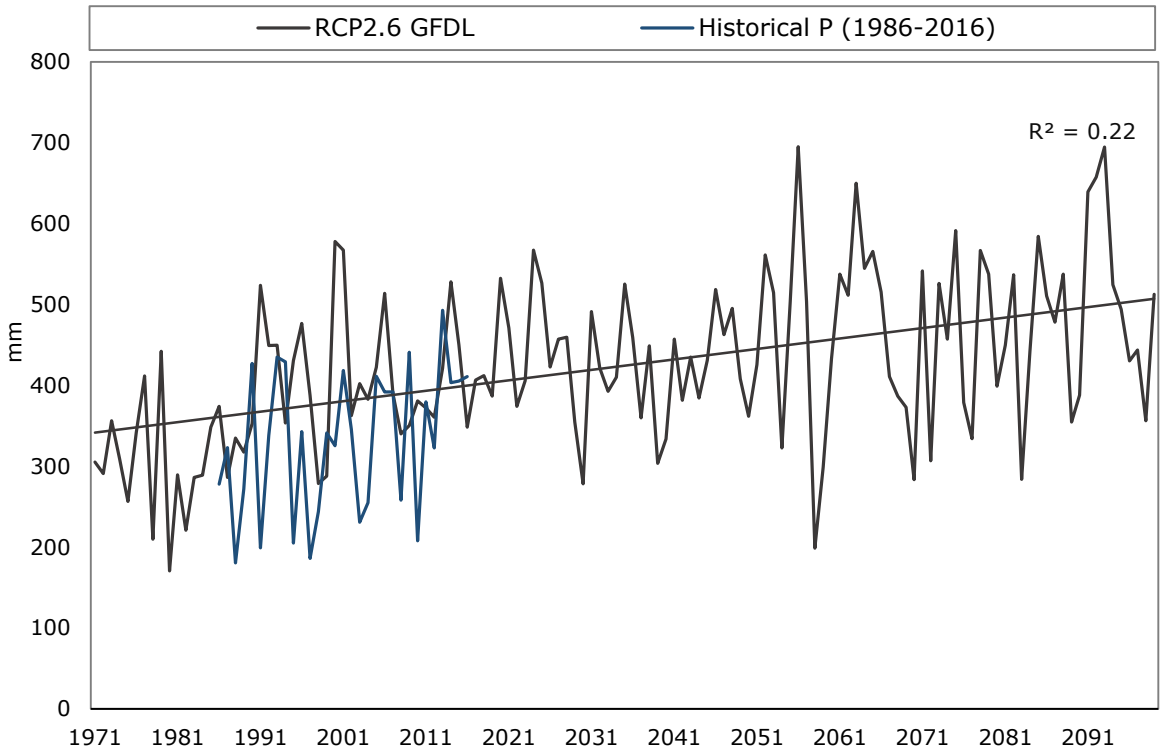

Figure 6. 15 Total annual precipitation based on RCP2.6 GFDL model from 1971 to 2100 and historical precipitation pattern observed in the Shortandy catchment from 1986 to 2016

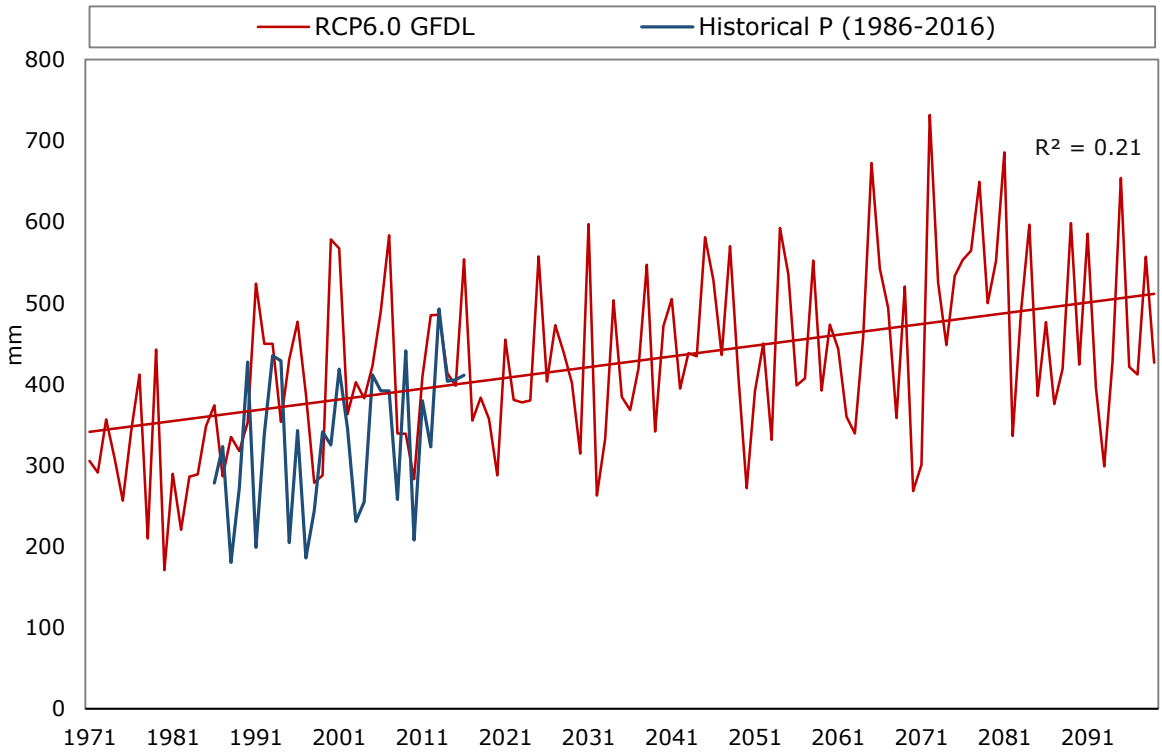

Figure 6. 16 Total annual precipitation based on RCP6.0 GFDL model from 1971 to 2100 and historical precipitation pattern observed in the Shortandy catchment from 1986 to 2016

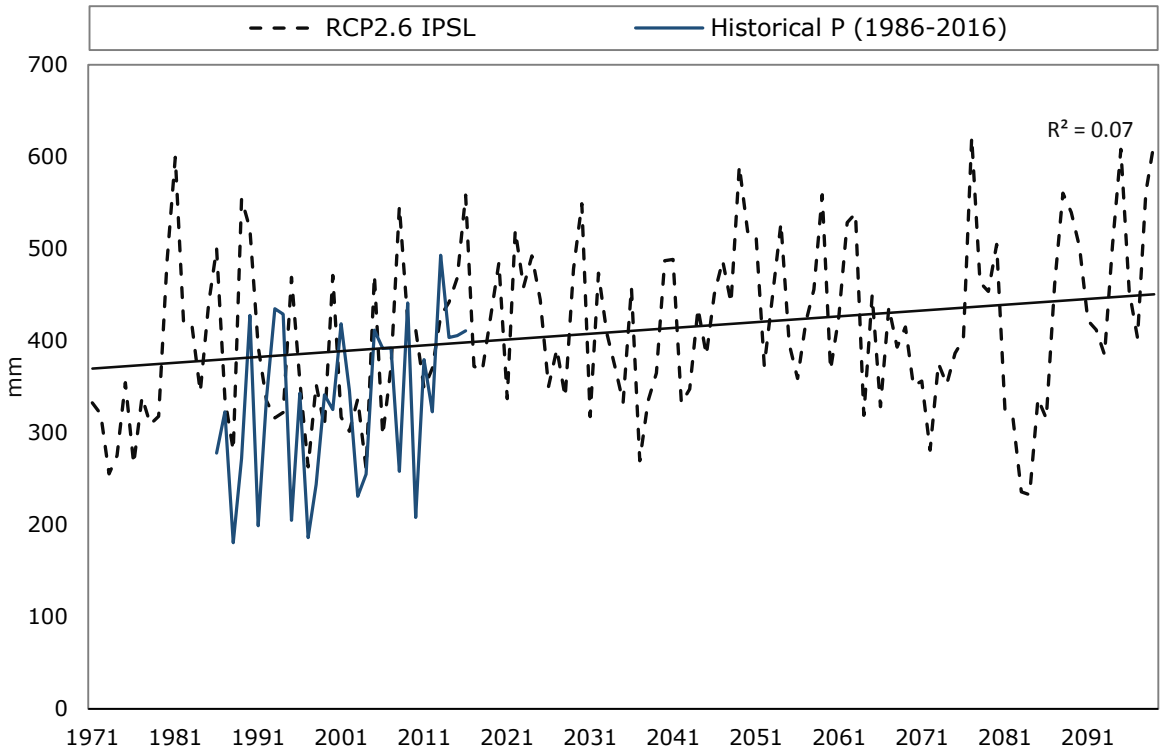

Figure 6. 17 Total annual precipitation based on RCP2.6 IPSL model from 1971 to 2100 and historical precipitation pattern observed in the Shortandy catchment from 1986 to 2016

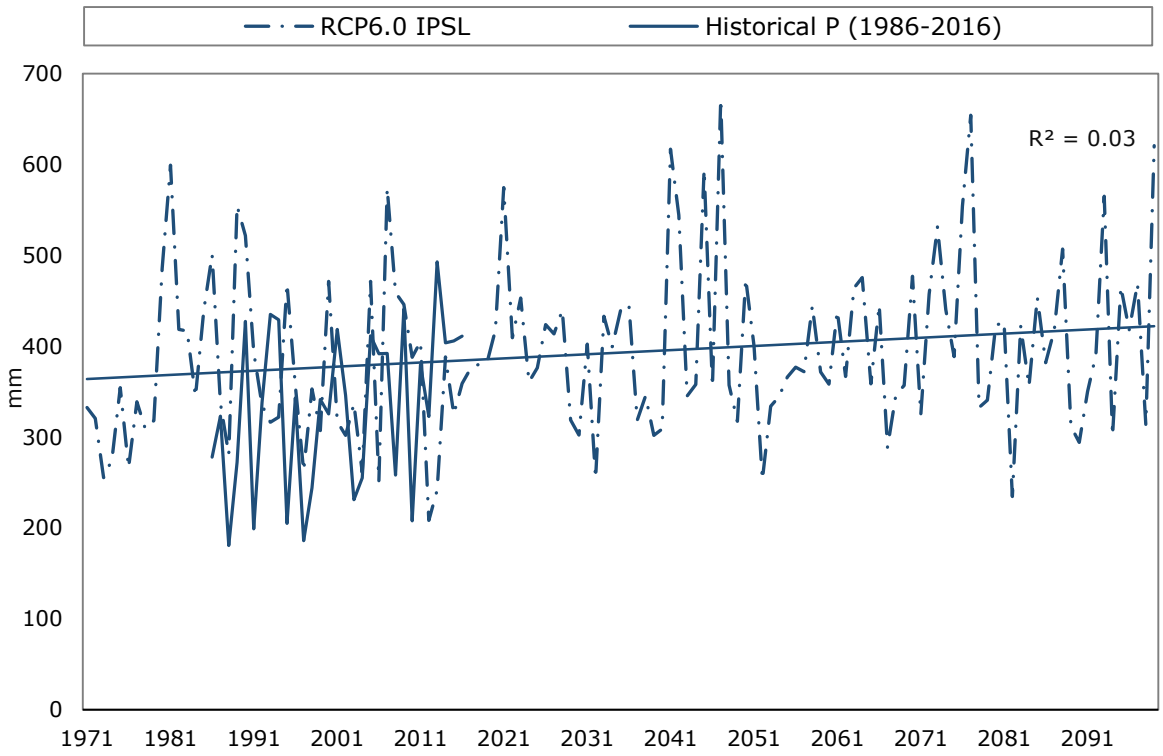

Figure 6. 18 Total annual precipitation based on the IPSL model under RCP6.0 from 1971 to 2100 and historical precipitation pattern observed in the Shortandy catchment from 1986 to 2016

By contrast, the IPSL model predicts less mean total annual precipitation compared with the GFDL model outcomes, with a lower determination coefficient (Table 6.4 and Figure 6.17 and 6.18). Specifically, the total annual mean precipitation is projected to increase by 15% and 8% (from 370 mm to 425mm and 401mm) based on RCP2.6 and RCP6.0 respectively.

Overall, percent bias analysis between the two GCM models indicates that the IPSL model predicts lower mean precipitation for Shortandy under both emission scenarios. Specifically, under RCP2.6, the mean precipitation is projected to be lower by 5% than GFDL, whereas, under RCP6.0, the difference is around 11%.

According to the observed precipitation records from 1986 to 2016, the mean total annual precipitation was equal to 332mm (Table 6.4). In comparison with the GCM predictions for the same period, the GFDL shows higher precipitation values by 30%-32% (402mm and 413mm based on RCP2.6 and RCP6.0 respectively), whereas the IPSL model shows 26%-21% of overestimation (391mm and 371mm based on RCP2.6 and RCP6.0 respectively).

Correlation analysis between the historical temporal trends in precipitation at Shortandy and precipitation trends projected by GFDL under RCP6.0 indicates positive moderate linear relationship ($r=0.32$, $p=0.08$) and weak positive relation with RCP2.6 GFDL ($r=0.19$, $p=0.3$) and RCP2.6 IPSL ($r=0.14$, $p=0.46$) and no correlation with RCP6.0 IPSL ($r=0.01$, $p=0.97$).

6.4.2.1 Monthly precipitation

Mean total monthly precipitation based on future climate modelling shows similar patterns to those observed in the Shortandy catchment from 1986 to 2016. Figure 6.19 shows that the precipitation patterns in August and September vary much less than during other months. Both models predict that the highest peak of precipitation will remain in July (≈72mm), but the mean monthly total value is projected to reduce by 14% and 3% based on IPSL and GFDL, respectively. GCM models indicate that the highest increase is projected to be during the cold-season

months. Specifically, in December and January, the proportion of precipitation is predicted to increase by 94%-98% respectively, whereas in February and November by 75%-81%.

Table 6. 4 Regression analysis on the temporal trend of precipitation patterns in the Shortandy catchment.

P_{mean} is the mean total annual of precipitation, where historical is related to the observed precipitation trend in Shortandy from 1986 to 2016, whereas future models are simulated for the period of 1971-2100

Model	P_{mean}, mm	r	p	Std. Dev
Historical (1986-2016)	332	0.38	<0.05	89
RCP2.6 GFDL	449	0.46	<0.001	104
RCP6.0 GFDL	452	0.46	<0.001	108
RCP2.6 IPSL	425	0.26	<0.05	90
RCP6.0 IPSL	401	0.18	<0.05	93

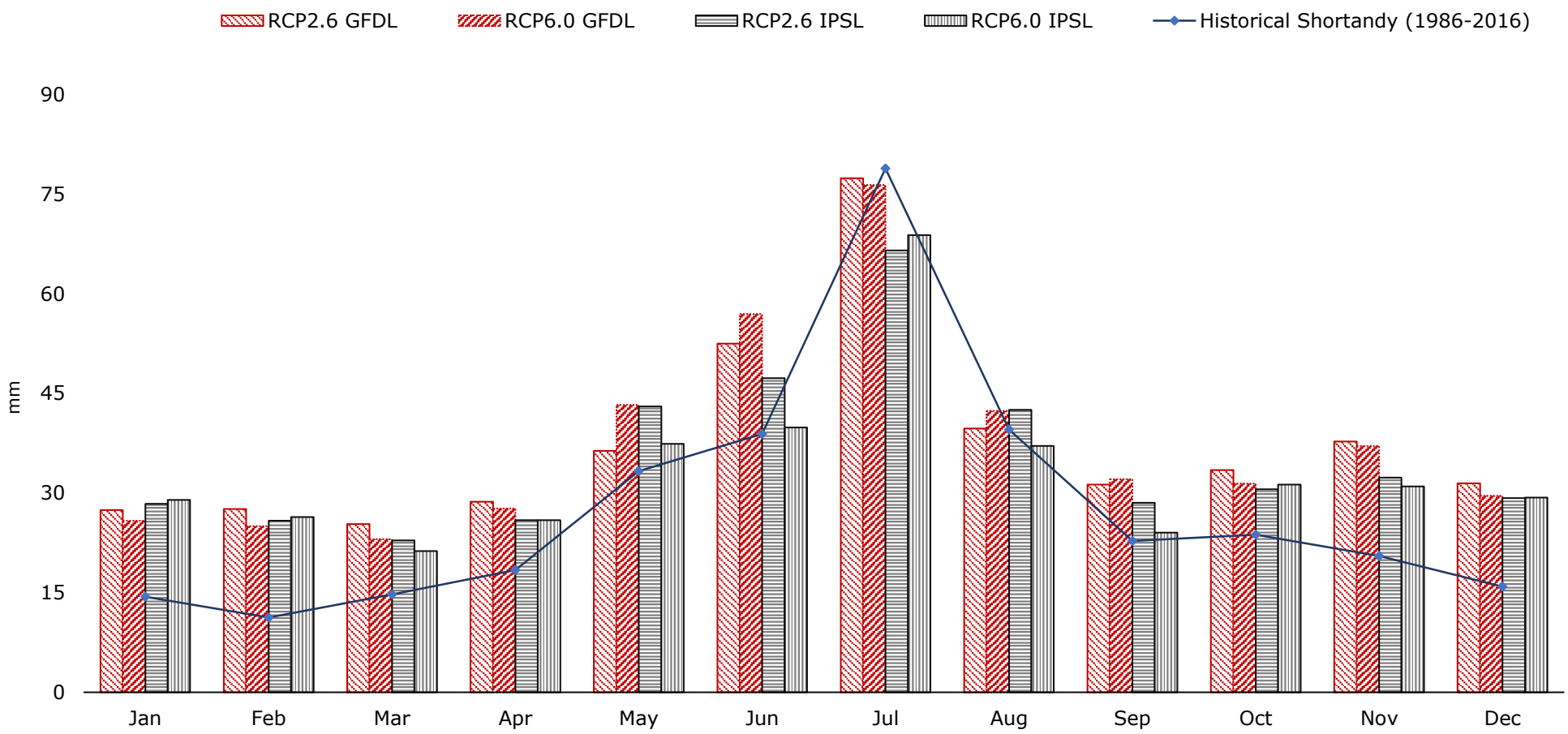

Figure 6. 19 Mean monthly amount of precipitation based on future climate models from 1971-2100 and historical observed precipitation in the Shortandy catchment (1986-2016)

6.4.3 Input variables in future climate

Figure 6.20 compares the relative contribution of input variables estimated using two GCM models and historical relative contribution to the lake using the observed climate data from the catchment. The graph shows that both model predictions of rainfall proportion were in agreement with the observed pattern in Shortandy area. However, the relative contribution of the seasonal snowmelt runoff to the water balance was less by 13%-15% in the IPSL and 17%-20% based on the GFDL. Moreover, both GCMs predict a higher contribution of snow precipitation by roughly 4%-8%.

Future climate modelling indicates that the highest proportion of input variables will remain as liquid precipitation (Figure 6.21). Specifically, four scenarios show a significant positive relationship between P_{rain} and the total annual input (Table 6.5). Similarly, snow precipitation is projected to increase from an historical average of 14% (84mm) to 19-20% (roughly 140-150mm) of the total annual input proportion.

Based on future climate models, runoff values vary, where the highest variation is projected for runoff produced during July months (Table 6.5). The key finding of future climate modelling shows that *runoff produced by rainfall (primarily in July) will make a greater contribution to the water volume of the lake due to the decreasing proportion of snowmelt runoff*. Four scenarios show that R_{rain} the proportion of the total annual water input will increase by 8%-13%. Despite the projected positive dynamics in snow precipitation, the relative contribution of R_{snow} to the annual lake volume is projected to decrease.

The pattern with the less snowmelt runoff and increased P_{snow} could be explained by the declining pattern in snow water equivalent (SWE) in the future climate models.

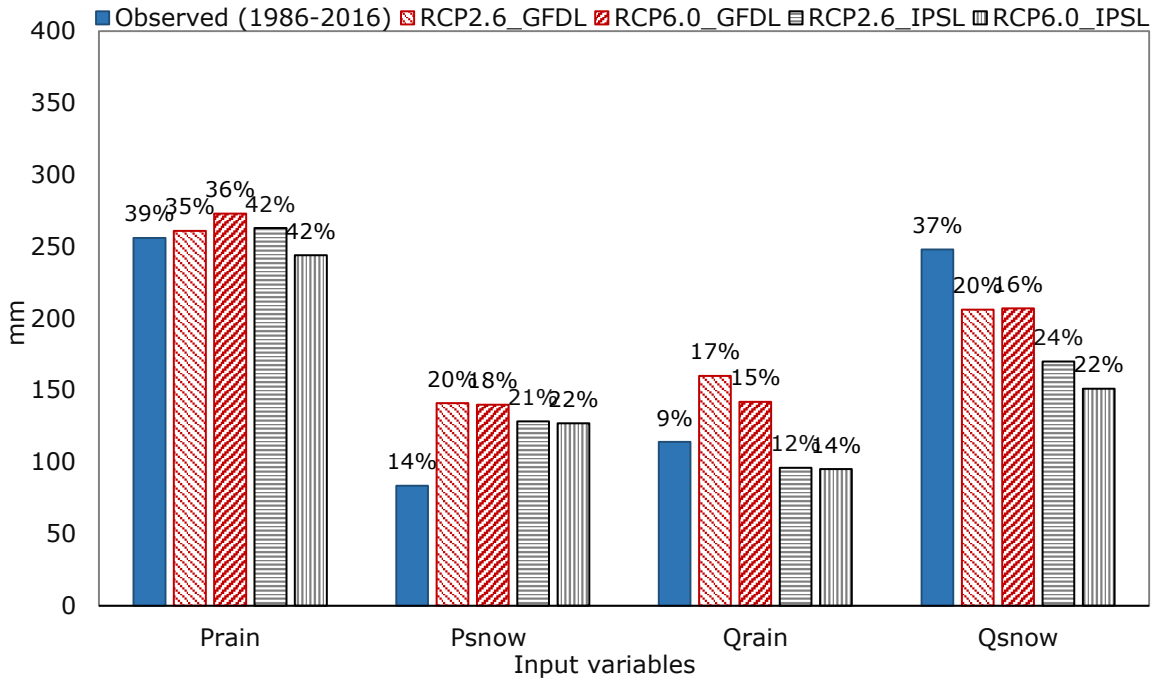

Figure 6. 20 Mean input variables estimated based on climate models for the period of 1986-2016 and historical relative contribution to the lake water balance in 1986-2016 estimated using the observed climate data

where P_{rain} is rainfall, P_{snow} is snow, Q_{rain} is rainfall-runoff, and Q_{snow} snowmelt runoff

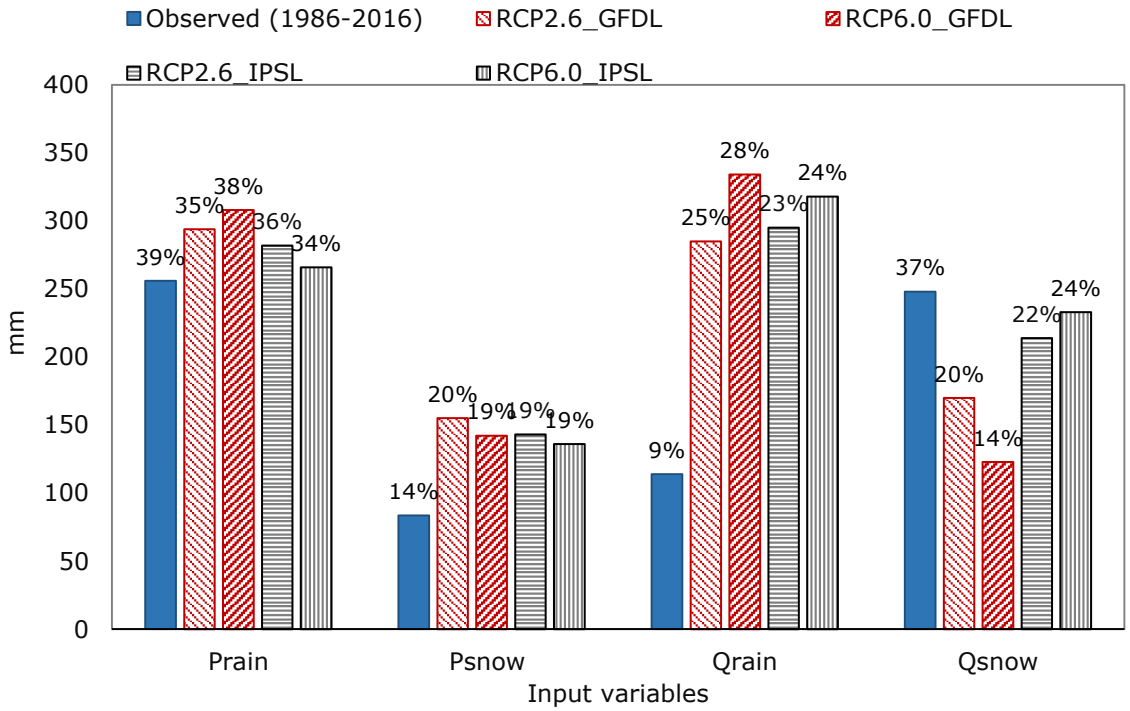

Figure 6. 21 Mean input variables estimated based on climate models for the period of 2006-2100 and historical relative contribution to Shortandy Lake from 1986-2016

where $P_{rain}$is rainfall, P_{snow} is snow, Q_{rain} is rainfall-runoff, and Q_{snow}snowmelt runoff

Table 6. 5 Regression analysis between the total annual input of Shortandy water balance and four input variables estimated with the future climate models

	rcp26 GFDL			**rcp6.0 GFDL**			**rcp2.6 IPSL**			**rcp6.0 IPSL**		
	r	p	std. dev	r	p	std. dev	r	p	std. dev	r	p	std. dev
P_{rain}	0.94	<0.001	89	0.95	<0.001	95	0.89	<0.001	79	0.95	<0.001	80
P_{snow}	0.39	<0.001	32	0.4	<0.001	33	0.4	<0.001	39	0.56	<0.001	29
R_{rain}	0.67	<0.001	307	0.63	<0.001	362	0.32	<0.05	429	0.5	<0.001	494
R_{snow}	0.01	<0.4	109	0.1	<0.4	113	0.18	<0.07	186	0.23	<0.05	233

6.4.4 Output variables in future climate

The open lake evaporation estimated using the future climate models in comparison with the historical values shows a higher correlation with the GFDL model outcomes (Figure 6.22), than the IPSL, where RCP2.6 showed r=0.47, p>0.05 and for RCP6.0, r=0.44, p>0.05. By contrast, both scenarios based on IPSL showed no correlation with the historical estimations (RCP2.6, r=0.19, p=0.3 and RCP6.0, r=0.25, p=0.17) (Figure 6.25 and Figure 6.26)

Future climate modelling with the GFDL model under RCP2.6 shows a weak positive temporal trend, where E_o will increase from the historical mean of 636mm to 697mm (Figure 6.22) and no statistical significance in the lake evaporation under RCP6.0 with an increase to 688mm (Figure 6.23 and Table 6.6). The following outcomes of the GFDL model could be explained by the air temperature trend (Chapter 6.4.1), where a warming trend predominantly affects cold season months with an insignificant temperature increase during the summer seasons (less than 1°C).

There is a moderate positive trend in the open lake evaporation based on RCP2.6 IPSL, where lake evaporation is projected to increase from the historical average of 609mm to 754mm (Figure 6.24 and Table 6.6). RCP6.0 IPSL model shows a higher regression coefficient, indicating a significant positive temporal trend with a mean value of 786mm of the lake evaporation during warm-seasons by 2100

(Figure 6.25 and Table 6.6). Overall, the highest proportion of the lake evaporation is projected to be produced during June and July, similarly as it was established during the historical period in 1986-2016(Figure 6.26). By contrast, the lowest values are estimated to be observed during April and October.

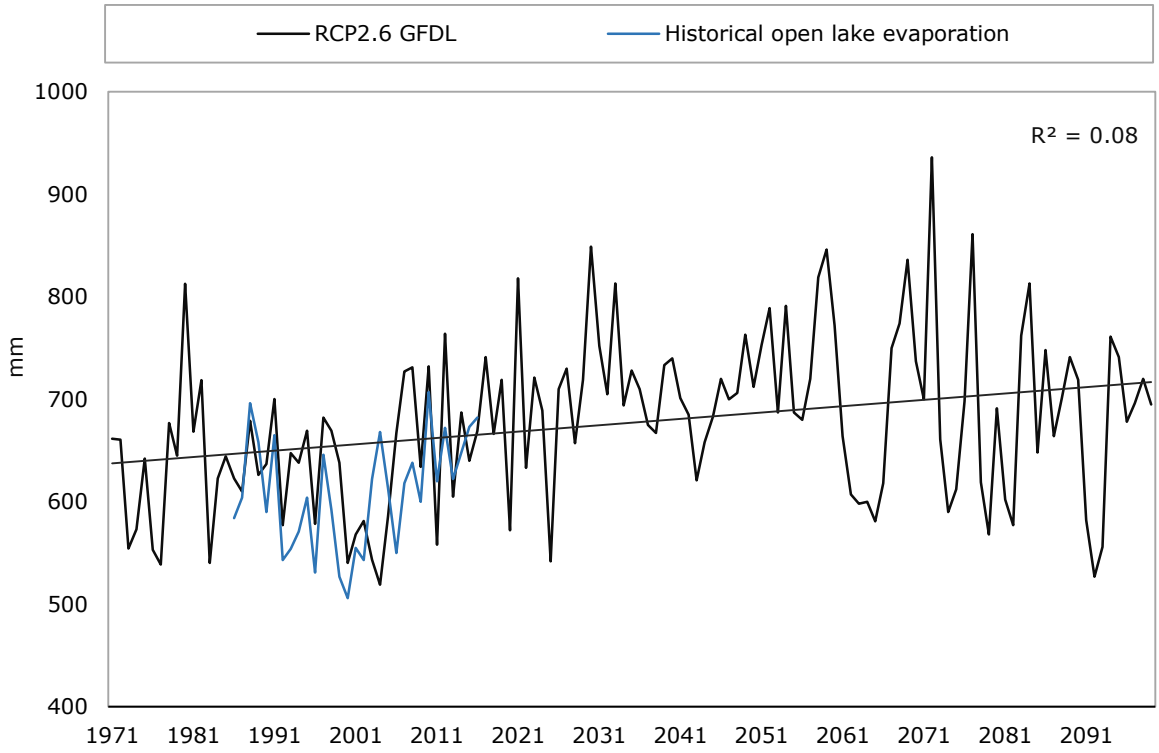

Figure 6. 22 Total annual open lake evaporation (E_o) based on RCP2.6 GFDL model (1971-2100) and open lake evaporation of Shortandy Lake estimated using observed climate data from 1986 to 2016

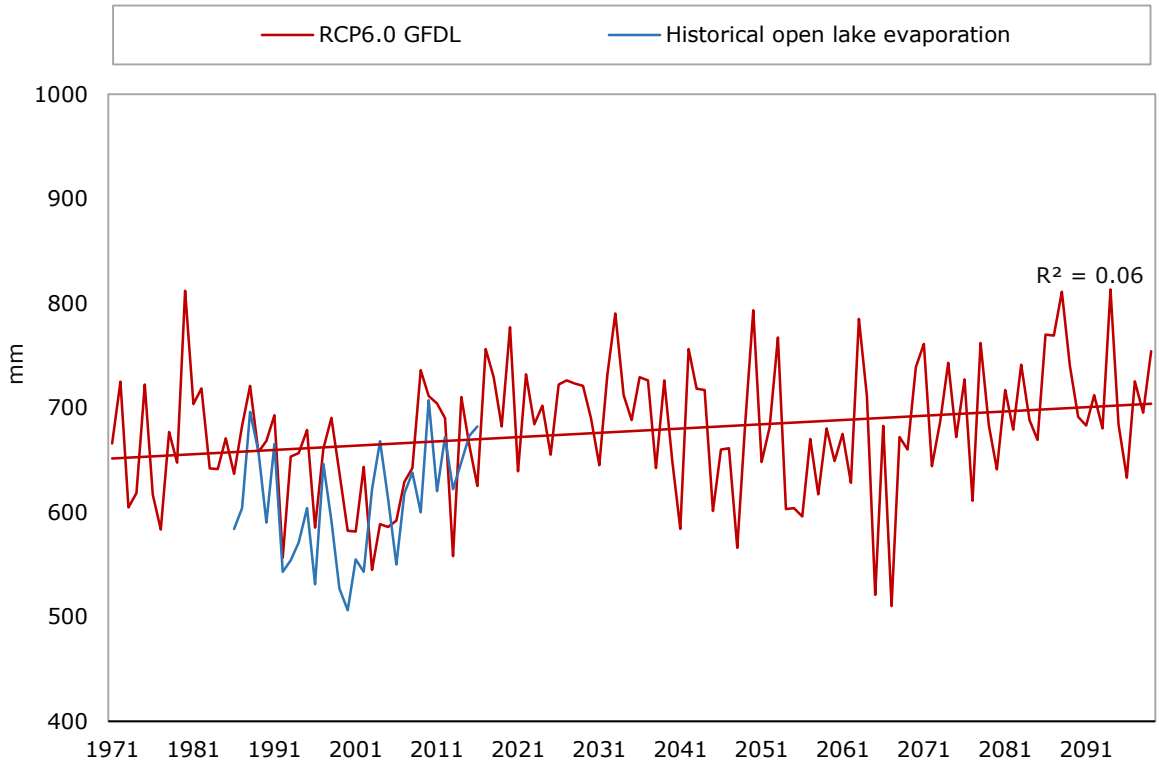

Figure 6. 23 Total annual open lake evaporation (E_o) based on RCP6.0 GFDL model (1971-2100) and open lake evaporation of Shortandy Lake estimated using observed climate data from 1986 to 2016

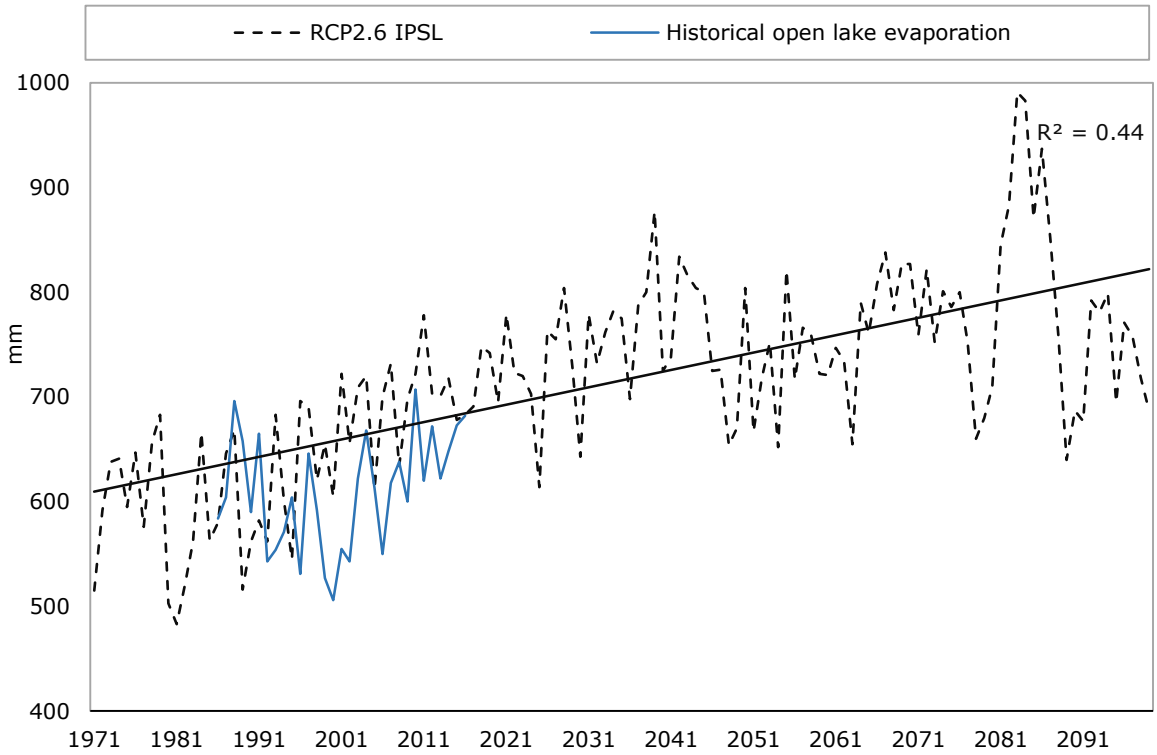

Figure 6. 24 Total annual open lake evaporation (E_o) based on RCP2.6 IPSL model (1971-2100) and open lake evaporation of Shortandy Lake estimated using observed climate data from 1986 to 2016

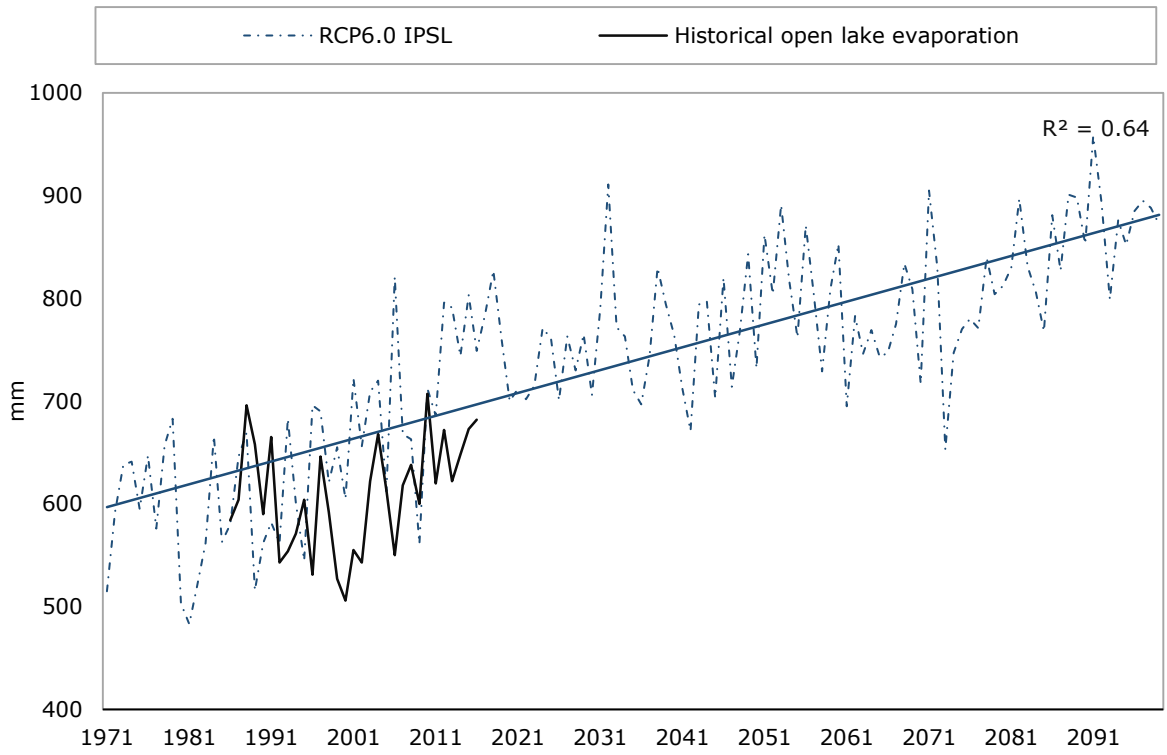

Figure 6. 25 Total annual open lake evaporation (E_o) based on RCP6.0 IPSL model (1971-2100) and open lake evaporation of Shortandy Lake estimated using observed climate data from 1986 to 2016

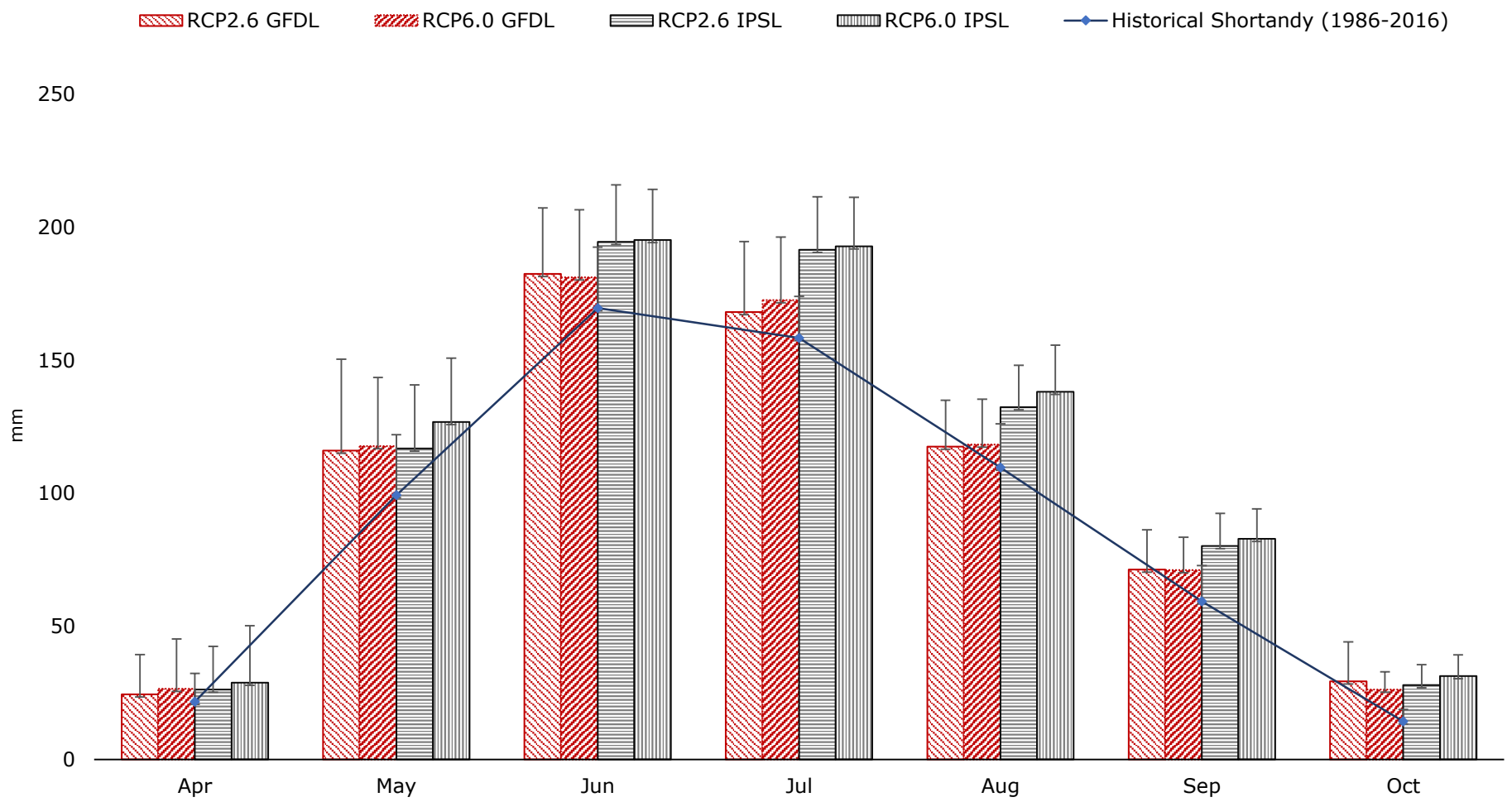

Figure 6.26 Mean monthly proportion of open lake evaporation based on future climate models from 1971-2100 and historical observed lake evaporation in the Shortandy catchment (1986-2016)

Table 6. 6 Regression analysis on the temporal trend of open lake evaporation based on future climate projections

E_o is the total mean value of Shortandy Lake evaporation, where historical is related to the estimated evaporation trend in Shortandy from 1986 to 2016, whereas future models are simulated for 2006-2100

Model	E_o, mm	r	p	Std. Dev
Historical (1986-2016)	609	0.31	0.08	54
RCP2.6 GFDL	697	0.21	<0.05	77
RCP6.0 GFDL	688	0.13	0.14	61
RCP2.6 IPSL	754	0.64	<0.001	71
RCP6.0 IPSL	786	0.77	<0.001	71

Figure 6.26 indicates that four scenario predictions of open lake evaporation are in agreement with the observed patterns in Shortandy Lake from 1986 to 2016, where GCMs overestimate by 5% (GFDL) to 9% (IPSL). However, evapotranspiration losses from the catchment were underestimated by 37mm from the historical mean value.

Future climate modelling shows that the open lake evaporation is likely to remain as the dominant source of water losses (Table 6.7). Figure 6.27 illustrates that the future climate models show similar results, where evapotranspiration loss (E_{act}) will vary less than for the historical period (1986 to 2016) with the standard deviation of 146 mm. However, the evapotranspiration loss is projected to decrease based on the IPSL model under both scenarios from the historical average of 77mm year^{-1} to 29mm year^{-1}. Chapter 6.4.2 outlines that the effective runoff is projected to occur during April, May, and October more frequently, with minimal losses for evapotranspiration from vegetation.

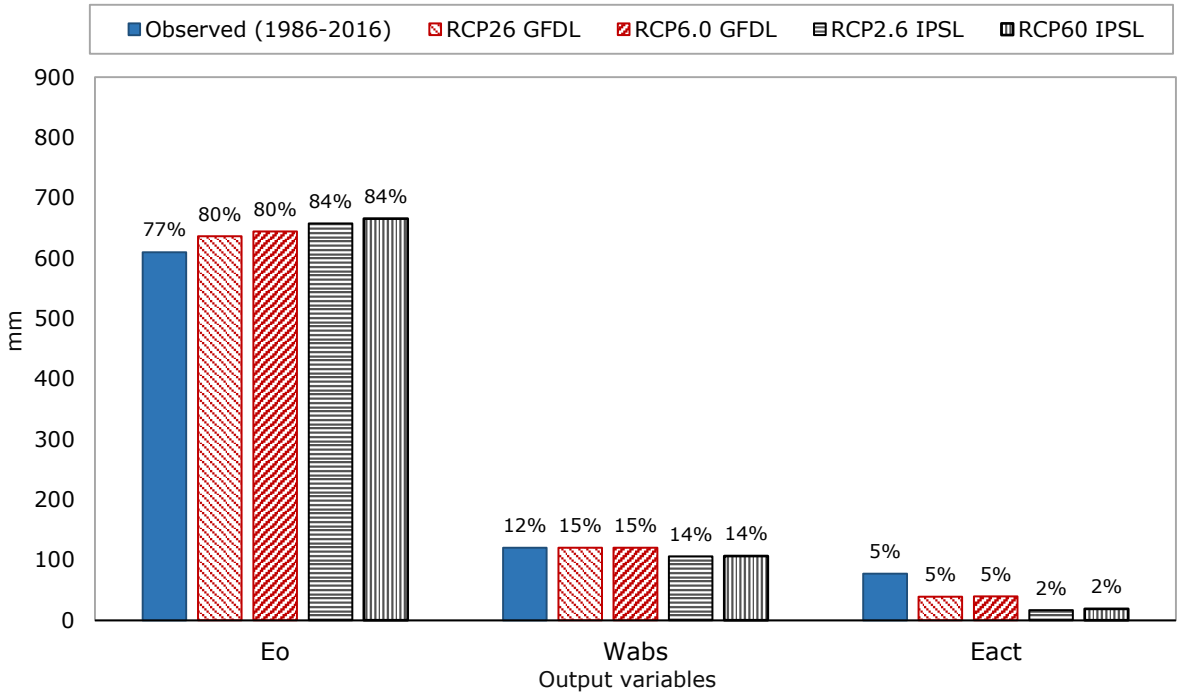

Figure 6. 27 Mean output variables estimated based on climate models from 1986 to 2016 for Shortandy Lake and output variables of the lake estimated using observed climate data from 1986-2016

where E_o is open lake evaporation, W_{abs} is water abstraction from the lake, E_{act} evapotranspiration from the catchment

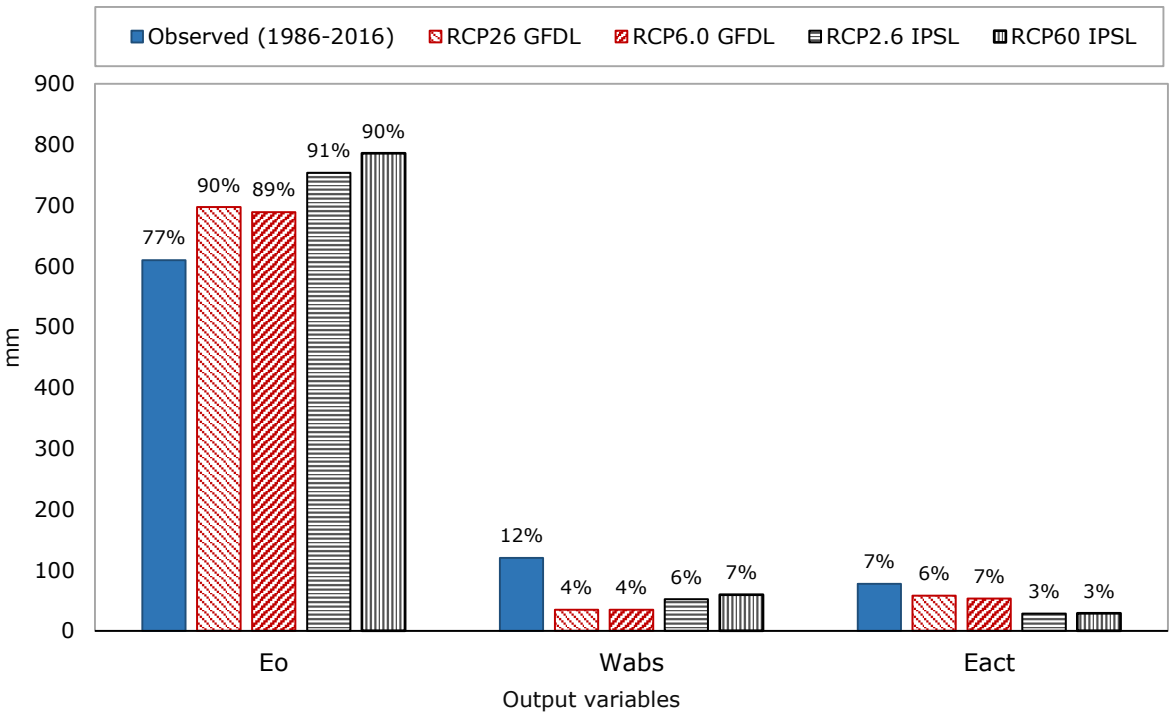

Figure 6. 26 Mean output variables estimated based on climate models for the period of 2006-2100 and output variables of the lake estimated using observed climate data from 1986-2016

where $E_o$is open lake evaporation, W_{abs} is water abstraction from the lake, E_{act} evapotranspiration from the catchment

Table 6. 7 Regression analysis between the total annual output of Shortandy Lake water balance and three variables estimated with the future climate models

	rcp26 GFDL			**rcp6.0 GFDL**			**rcp2.6 IPSL**			**rcp6.0 IPSL**		
	r	p	std. dev	r	p	std. dev	r	p	std. dev	r	p	std. dev
E_o	0.78	<0.001	73	0.47	<0.001	60	0.8	<0.001	71	0.85	<0.001	71
W_{abs}	0.18	0.08	19	0.35	<0.001	34	0.43	<0.001	21	0.43	<0.001	23
E_{act}	0.33	<0.001	49	0.48	<0.001	53	0.35	<0.001	40	0.36	<0.001	40

6.4.5 Water volume fluctuation

The rising awareness of how endorheic lakes respond to the changing future climate has received significant attention around the world (Angel and Kunkel, 2010, Shi et al., 2007). Figure 6.28 shows that *the decreasing pattern of the water volume of Shortandy* Lake *is likely to continue by 2100*.

GFDL model

Based on the GFDL model, the water volume of Shortandy is expected to decrease from 230x10^{6}m^3 to 149x10^{6}m^3 and 128x10^{6}m^3 under RCP2.6 and RCP6.0 respectively by 2100. The correlation analysis between the water volume predicted by the GFDL under RCP2.6 and RCP6.0 shows a strong positive correlation with the historical water volume changes in Shortandy Lake with r=0.90 and r=0.92, respectively. Both scenarios show similar declining water volume patterns until 2100.

Based on the RCP2.6 GFDL model, the main hydrological periods could be noticed, where the dry periods are as follows: 1980-1999, 2008-2023, 2025-2061 and 2068-2090. By contrast, years with positive water volume response: 2001-2007, 2061-2067 and 2091-2099. The years with positive water balance response show an increased proportion of precipitation and decreased losses in the lake evaporation. In comparison with the historical relative contribution to the lake volume during wet years, the total P and Q_{rain} are projected to increase, yet Q_{snow}

the contribution will be reduced. For example, Q_{rain} will be increased from the historical mean of 208mm to 569mm, whereas Q_{snow} will decrease from 229mm to 114mm by 2100 (Appendix F).

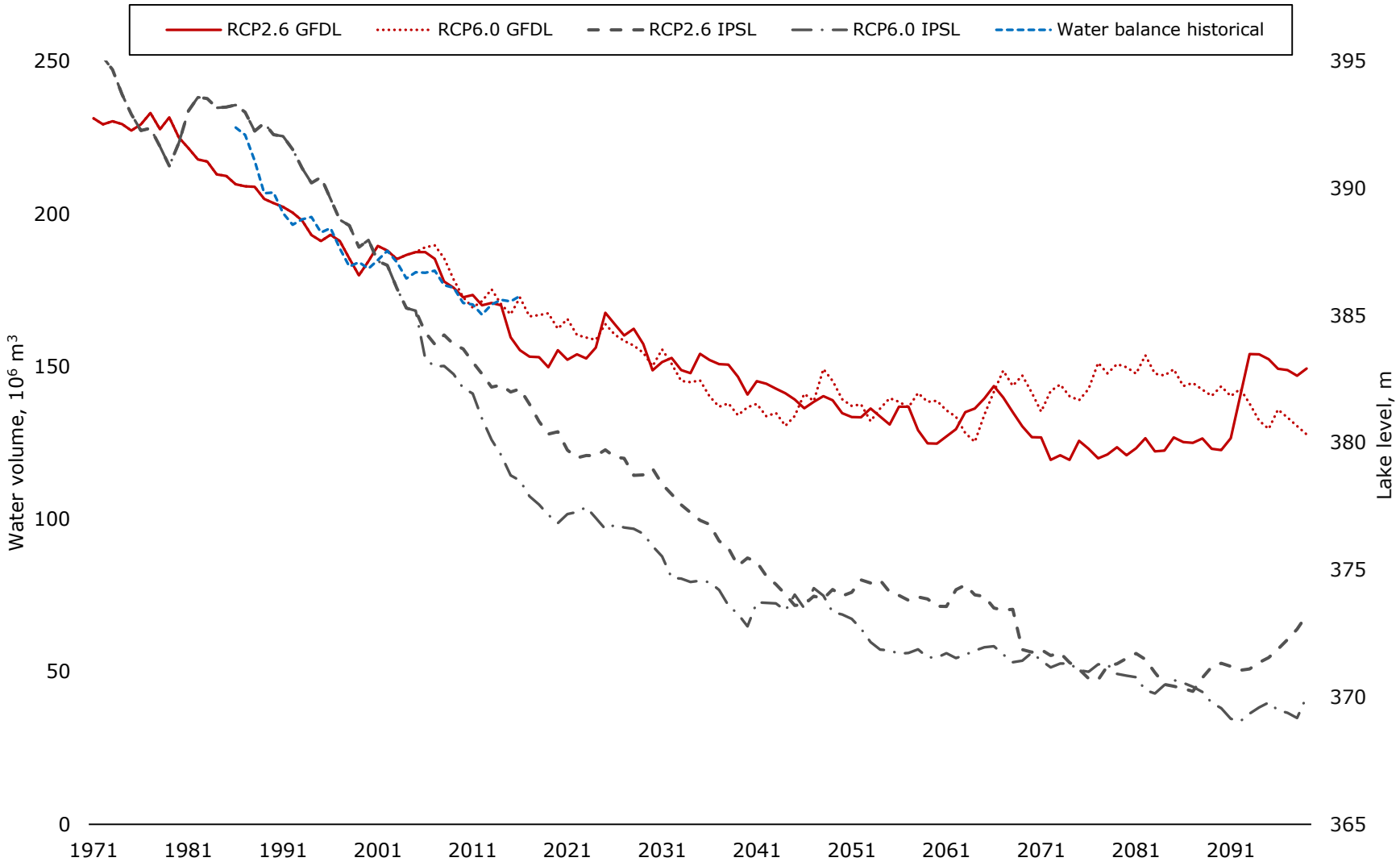

Figure 6. 27 Water volume (level) fluctuation based on the future climate models (1971-2100) plotted with a historical water volume of the lake (1986-2016) estimated using the lake water balance model

The RCP6.0 GFDL model predicts similar lake volume patterns. However, the dry period in 2008-2023 projected by RCP2.6 is projected to extend until 2044. Over the dry periods, a rapid increase in E_o and Q_{rain} whereas a considerable decrease in P_{snow} and Q_{snow} are expected. The major difference in water volume predictions between the two emission scenarios occurs in 2060. In 2065-2082, RCP6.0 GFDL predicts a positive water balance pattern due to the increased proportion of P_{rain} and R_{rain}.

By contrast, the wet period under the RCP2.6 is projected to be shorter (2061-2067). After 2068, the water volume shows negative patterns, due to the reduction in R_{snow} which will be replaced by Q_{rain}. However, the water volume is expected to increase significantly after 2085 based on the RCP2.6 GFDL model. The following pattern is predicted to be driven by a considerable increase in the rainfall-induced runoff events which are predicted during 2090-2100 (more than 700 mm annually). By contrast, the RCP6.0 predicts higher temperature, where the difference between two emission scenarios is projected to reach 123% (Chapter 6.4.1). Moreover, a significant reduction of annual runoff under RCP6.0 is projected in 2090-2100. Specifically, the snowmelt runoff is projected to diminish by four times in comparison with the historical average (from 222mm $year^{-1}$ to 57mm $year^{-1}$) and to a lesser extent in the rainfall-runoff (from 334mm $year^{-1}$ to 252mm $year^{-1}$).

The regression analysis on RCP2.6 GFDL water volume and water balance variables shows a significant positive relationship between P_{rain} P_{snow} and E_o, with r=0.72, p<0.001. By contrast, under the RCP6.0 significant positive relationships between water volume and water balance variables was established for P_{rain}, $E_o$and Q_{snow} with r=0.70, p<0.001. The following findings indicate that the air temperature increase projected by RCP6.0 GFDL during the cold-season months is likely to alter Shortandy water balance, where snow precipitation is likely to be replaced by more frequent rainfall events.

IPSL model

The water volume estimated using the IPSL model shows a correlation with historical water volume dynamics of Shortandy, r^2=0.92 for RCP2.6; and r^2=0.89 for RCP6.0. It is clear from the graph (Figure 6.24) that the water volume reduction of the lake with the IPSL model under both scenarios will be even more dramatic. Specifically, the total volume of Shortandy may reduce by three times by the end of 2090 to a volume of less than 42x$10^6$$m^3$ based on RCP6.0 if the mean annual temperature will increase by 6°C.

The water volume dynamics predicted by the IPSL show a continuous decreasing trend, where the water volume reduction, under the two emission scenarios, indicates similar volume patterns until 2010. In 2011-2041 and 2048-2069, a significant water volume deviation between RCP2.6 and RCP6.0 is predicted. The following difference is explained due to the increased temperature, which is predicted under the RCP6.0 IPSL from 2048-2099 and to a greater extent in 2080-2099 (p-bias ≈82%). The following period is projected to be accompanied by a decrease in Q_{rain} and Q_{snow} and higher annual lake evaporation (Appendix G).

Based on the RCP2.6 IPSL, the water balance relation is projected to be positive by 2090. The increasing water volume is projected to be driven by the increased precipitation, specifically by Q_{snow} and decreased lake evaporation. However, it should be noted that decreased lake evaporation is more important due to the smaller lake area A_L which minimises the lake losses during the warm-seasons (Figure 6.29). The implication of the reduced lake area and associated alteration to the shoreline will be addressed in Chapter 7.

Table 6.6 shows that the lake volume will be driven by E_o, P_{rain} and P_{snow}, with r=0.9, p<0.001, whereas under the RCP6.0 a significant positive relationship was established for E_o and P_{rain} with p<0.001 and Q_{snow} with p<0.05.

Comparing two GCM model outcomes, the IPSL model predicts higher air temperature and lower precipitation than GFDL at Shortandy area. Specifically, the difference in mean air temperature and precipitation is more than 80% and 5% under RCP2.6 respectively, and 93% and 11% under RCP6.0. Consequently,

this deviation in model predictions produced a considerable difference in the water volume simulations.

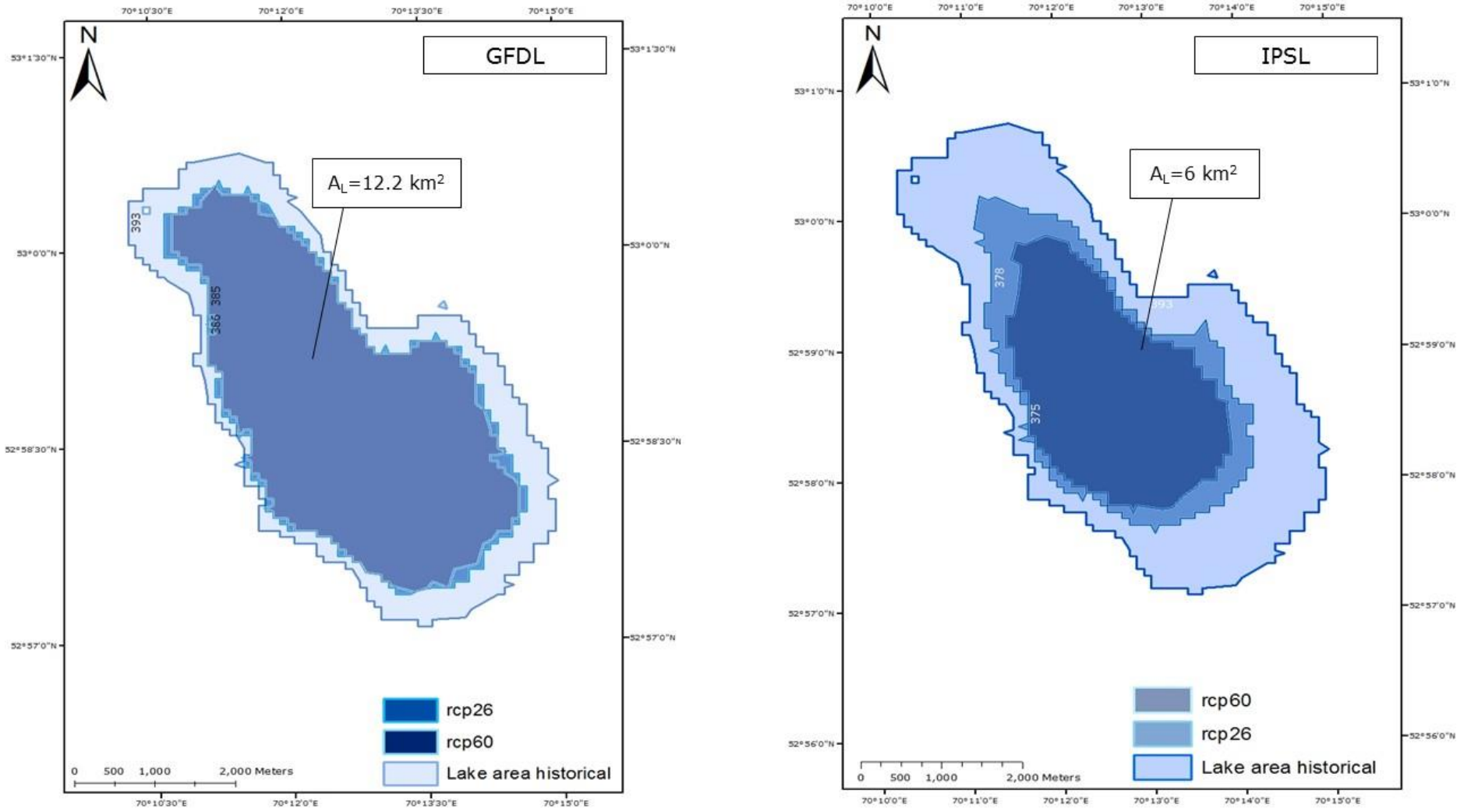

Figure 6. 28 Lake area reduction, where future climate models estimate the lake reduction from 1971 to 2100, and the historical lake area is estimated using the lake water balance model from 1986 to 2016

6.5 Summary

The future climate modelling chapter investigates how the input and output variables of Shortandy Lake will change under a global temperature increase of 1.5°C-2°C. The future climate modelling findings show that the mean air temperature in the Shortandy catchment is likely to increase, where:

- The GFDL model predicts that mean annual air temperature will increase from historical 2°C to 3.4°C under the low emission scenario (RCP2.6). By contrast, the higher emission scenario (RCP6.0) suggests an increase from 2°C to 3.8°C by 2100. Based on the GFDL, the temperature increase will alter cold-season months, specifically December, January and March, whereas warm-seasons are likely to be less influenced;
- The IPSL model predicts even higher temperature increases, where RCP2.6 suggests that a mean annual temperature increase from 1.9°C to 4.1°C, whereas RCP6.0 temperature predictions show an increase to 4.9°C. However, the IPSL model suggests that the temperature increase will be for both cold and warm seasons.

The GFDL model suggests that the mean annual precipitation will increase under both emission scenarios. The annual precipitation distribution shows that the major proportion of precipitation will be falling during warm-season months. Yet, according to both models, an increasing trend in air temperature is likely to affect sensitivity between air temperature and precipitation during cold-season months. However, the major discrepancy between GCM models is temperature and precipitation predictions, which controls the deviation in water volume predictions. For example, based on GFDL, the positive dynamics for snow precipitation and snowmelt runoff are projected to have a limited contribution to the lake volume. The key findings suggest that an increased P_{snow} will produce less snowmelt runoff due to the declining SWE in the future (Section 6.4.3). The following reduction in SWE could be affected by warmer air temperature during the cold-season months

suggested by the GFDL. By contrast, the IPSL model predicts less implications for cold-seasons under RCP2.6 and uniform temperature distribution throughout the period under RCP6.0. Thus, the IPSL model suggests higher spring runoff in comparison with the GFDL model and predicts higher Q_{snow}. The changes in SWE in warming temperature during the cold-season months will be further addressed in Chapter 7.2.

The major driving force for the lake losses will remain E_o. The IPSL model predicts that open lake evaporation will increase significantly under both RCPs, where an increase from 609mm to 754mm by RCP2.6 and from 609 to 786mm by RCP6.0 of the mean total annual lake evaporation.

The water volume patterns of Shortandy Lake illustrated in Section 6.4.5 show further water volume reduction under both emission scenarios by 2100. The lake volume trend under the IPSL model shows a dramatic water volume reduction, a less severe reduction under GFDL. Based on GFDL, the difference between RCP2.6 and RCP6.0 will be reflected in an increasing role of rainfall, open lake evaporation and warm-season runoff which will replace snowmelt runoff in the annual water balance of Shortandy Lake. Based on RCP2.6, the cold-season precipitation and snowmelt runoff are expected to decrease by two times by 2090, and by four times under RCP6.0 GFDL by 2065.

A significant air temperature increase (>4.1°C) suggested by RCP6.0 IPSL will result in a dramatic water volume reduction in Shortandy Lake by 2100. Water level lowering is projected to be driven by lower total annual precipitation as well as increased open lake evaporation. Moreover, under the RCP6.0, the contribution of snow precipitation and snowmelt-runoff is expected to be diminished by 2048.

In conclusion, Section 5.7 indicates that the developed model simulates the lake volume with around 5% accuracy, thus changes in precipitation and air temperature in the future inevitably will lead to further water volume reduction in Shortandy Lake by 2100.

6.6 Role of anthropogenic impact

Chapter 2 outlines that anthropogenic impact may indirectly and directly influence the water quantity and the natural water regime of a hydrological system. Indirect impacts on the hydrologic cycle can result from land-use changes which include deforestation, urbanisation, etc. Direct impact include water diversions, withdrawals, discharges, dams (flow regulation and water storage) and water abstraction. The developed water balance model for the historical period (1986-2016) takes into account both direct and indirect anthropogenic impacts on the water fluxes of Shortandy Lake. However, it is out of the scope of this chapter to investigate the uncertainties associated with the future climate forcing (see Council (2005). In contrast, the identification and quantification of the overall human pressures, *understanding exploitation or capturing the surface and groundwater abstraction from the lake are addressed.*

6.6.1 Role of anthropogenic impact in the past

To assess the role of anthropogenic impact within the water volume reduction of the lake, the anthropogenic load or W_{abs} was excluded from the developed water balance model. The dotted line shows the water volume dynamics if there had been no water abstraction from Shortandy from 1986 to 2016 (Figure 6.30). A key finding shows that despite the inter-annual water volume fluctuation, the lake volume *changes insignificantly over the three decades*.

By the end of the 1980s, there was a rapid lake volume decline from 228x$10^6$$m^3$ to 212 x$10^6$$m^3$ by 1992. The decreasing trend was followed by the water volume increase from 1993 to 1996. The lake water volume cycles between three or four-years of positive water volume changes followed by a similar negative water volume response. However, *Figure 6.26 indicates that the volume would reach the total lake volume of 223x$10^6$$m^3$ by 2013 and remained stable until 2016*. Consequently, the water volume fluctuation would be within the amplitude of ±15x$10^6$$m^3$ (or 1.5m of the lake level) if the water balance of Shortandy was

completely driven by regional climate only. Recalling Chapter 2.3 findings, the lake level amplitude of Shortandy Lake without anthropogenic impact corresponds with the historical amplitude of 1-3m of the water level change in Burabay lakes (Shnitnikov, 1970a).

Moreover, the total sum of the water volume abstraction is equivalent to $50x10^6m^3$ during 1986-2016. Interestingly, the discrepancy between water volume with and without water abstraction is approximately equal to cumulative water abstraction values. So, *the significant water volume reduction in Shortandy could be driven by anthropogenic water abstraction over the last 30 years*.

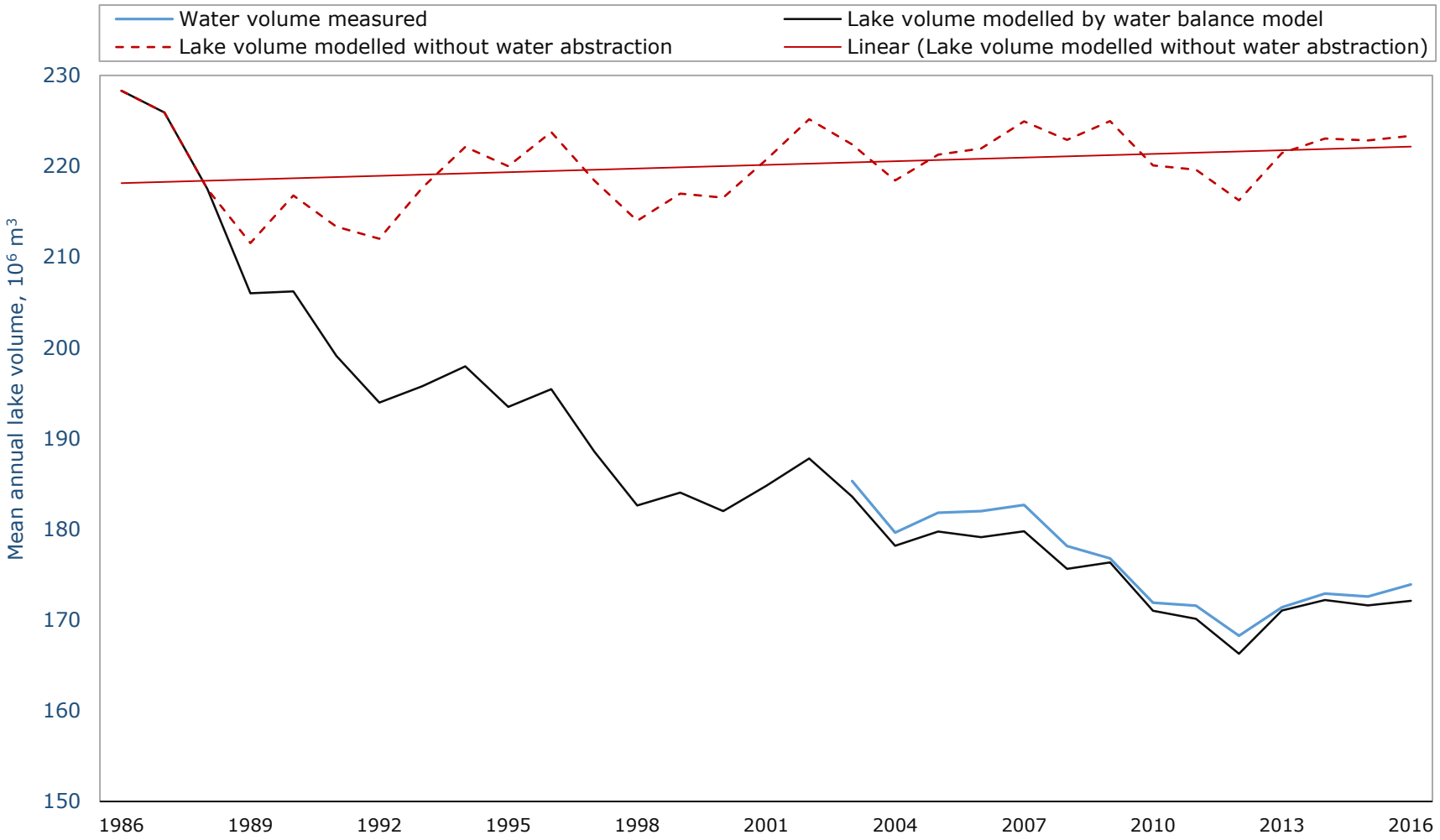

Figure 6. 29 The lake volume dynamics, where the blue line shows water volume estimated by measured lake levels, the black line is the lake volume simulated by the water balance model, and dotted lines show the water volume without water abstraction (W_{abs})

6.6.2 Role of anthropogenic impacts in the future

Shortandy Lake *volume without water abstraction*

The water volume dynamics under the future climate scenarios were examined based on the current water abstraction restrictions accepted for Shortandy Lake i.e. *less than 0.5x10^{6}m^3 of water per year*. Figures 6.27 and 6.28 compare the lake volume fluctuation with annual water abstraction from the lake with allowed 0.5 x10^{6}m^3 of water and the lake dynamics if the water abstraction was 0. The GFDL model under RCP2.6 and RCP6.0 emission scenarios predicts a significant water volume reduction (r=-0.8 and r=-0.87) (Figure 6.31). However, the water volume reduction magnitude is less than with the anthropogenic water abstraction, specifically the lake volume without abstraction is higher by +28%-27%.

The water volume dynamics simulated with the GFDL model show major periods with negative water balance relation; there are 1979-1999, 2007-2024, 2029-2058 and 2067-2090. By contrast, years with the positive water volume response 2001-2007, 2061-2067 and 2091-2099. The following periods with dry-and-wet conditions correspond with Burabay lakes level fluctuations at largely 20-40 year interval (Shnitnikov, 1970a).

According to the GFDL, the lake is predicted to reach the lowest lake volume by 2071. Specifically, the lake volume without human disturbance is equal to 170x10^{6}m^3 by 2071, whereas with anthropogenic water abstraction, the following threshold is projected to be reached by 2012. Nonetheless, an extended dry period during 2029-2058 and 2067-2090 years is likely to have a negative impact on Shortandy Lake even without anthropogenic impact. However, the positive water volume dynamics predicted by 2091 could bring back the lake volume established for 2040.

The lake volume projected by the IPSL model is in a good agreement with the GFDL (Figure 6.32), predicting a significant water volume reduction under both

RCP2.6 and RCP6.0 (r=-0.82 and r=-0.85, respectively). Section 6.4.5 outlines that the IPSL model predicts a monotonic negative net balance and without anthropogenic impact, the overall trend is projected to decrease. However, without water abstraction the lake volume is projected to be higher for +59%-69% based on RCP2.6 and RCP6.0 respectively.

However, Figure 6.28 shows that without anthropogenic impact, the lake area of around 6.5-7 km^2 would level off by 2050 and stay without considerable change until 2090 under both RCPs. The following steady lake volume/area patterns indicate that the lake has adapted to certain climate conditions, and the lake area has reached its equilibrium (Mason et al., 1994). Specifically, according to the lake bathymetry configuration (Figure 4.6), the deepest area of Shortandy Lake corresponds to the lake area of approximately 8-10 km^2. By contrast, the lake volume dynamics with anthropogenic water abstraction, the following equilibrium has not been reached, where the negative relation between input and output variables will result in the further lake level decline in Shortandy.

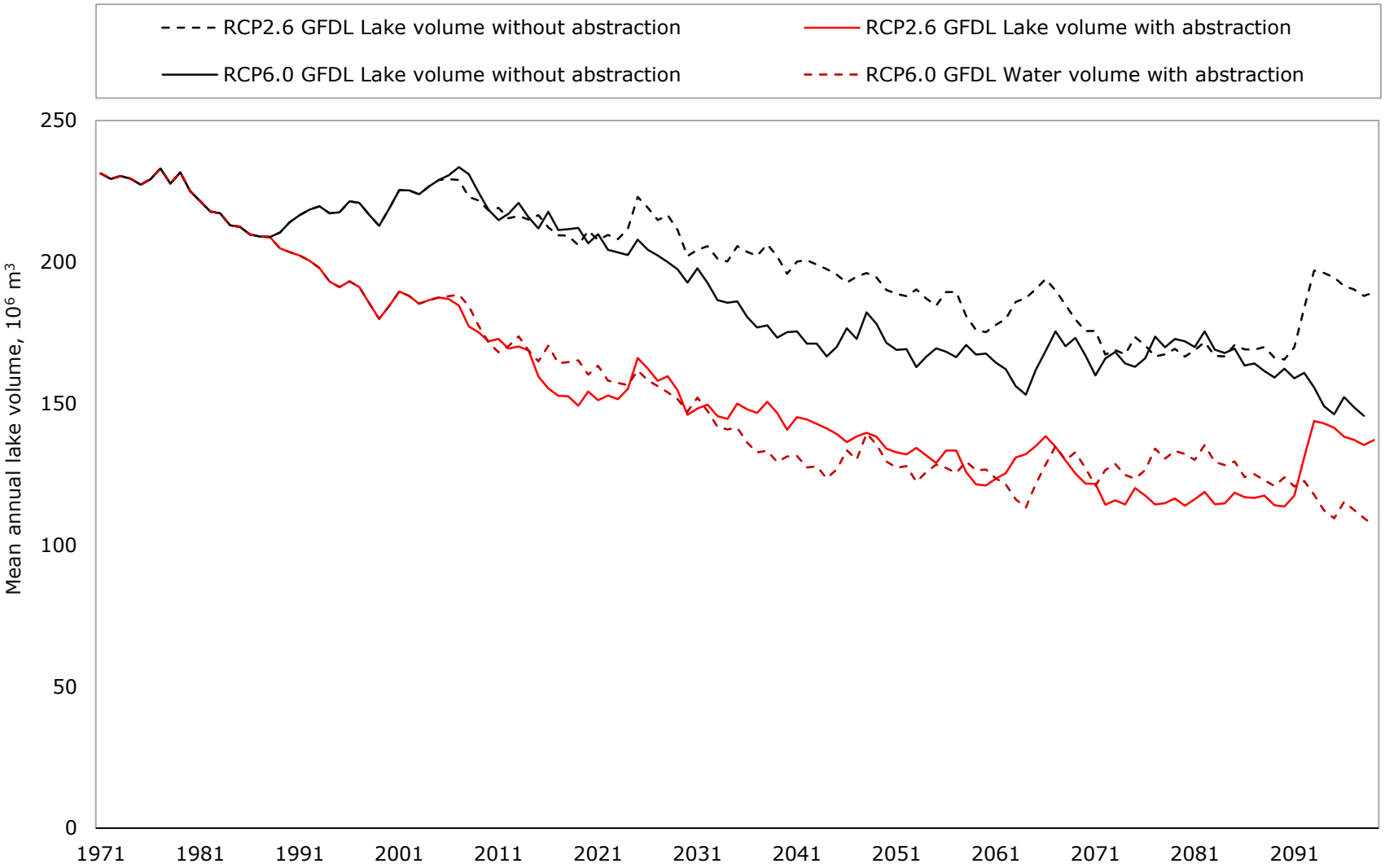

Figure 6. 30 Water volume dynamics of Shortandy estimated using the GFDL climate model based on the water abstraction restrictions ($0.5x10^6 m^3$ of water per year) and without anthropogenic water abstraction from 1971 to 2100

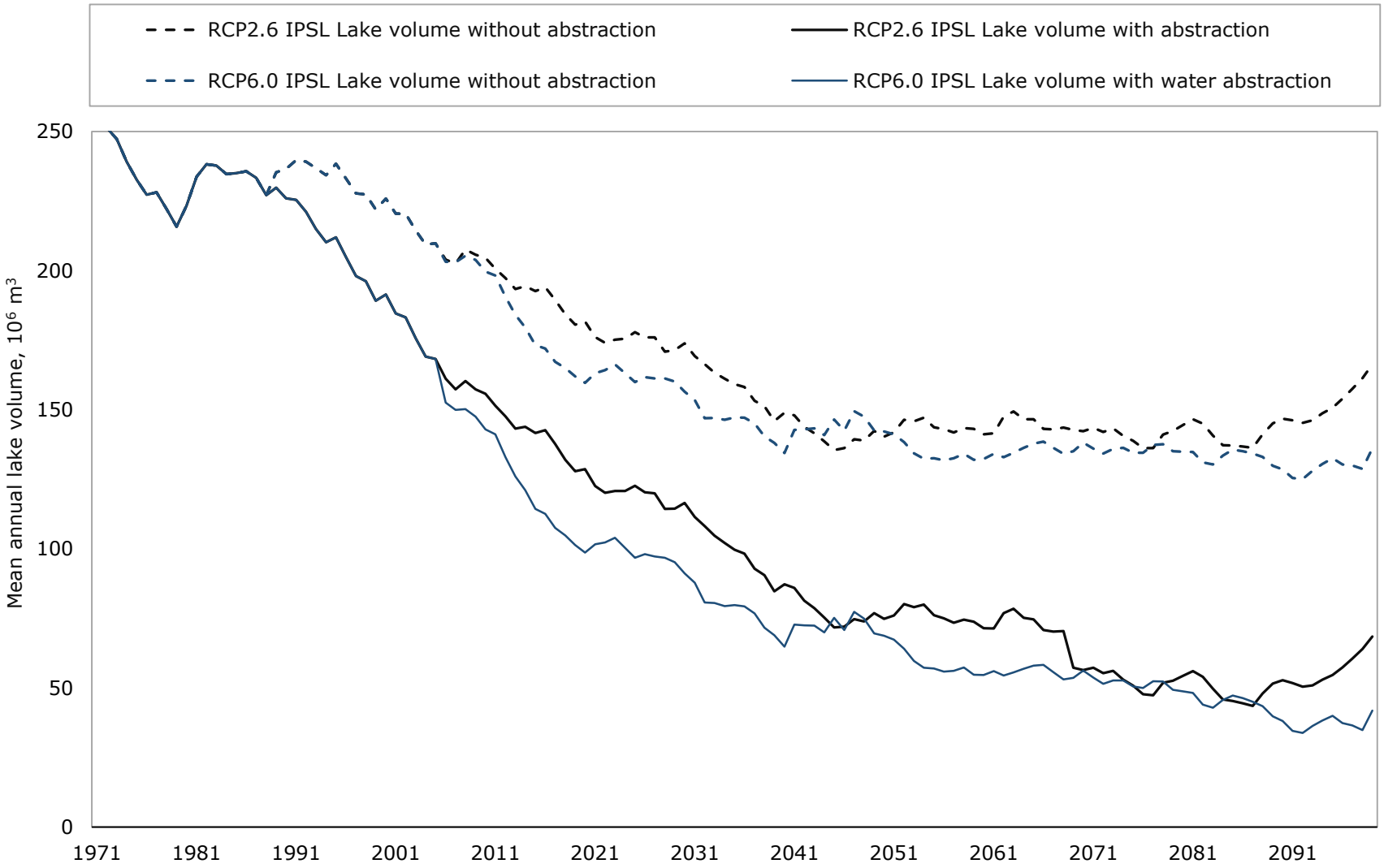

Figure 6. 313 Water volume dynamics of Shortandy estimated using the IPSL climate model based on current water abstraction restrictions (0.5x10^{6}m^3 of water per year) and without anthropogenic water abstraction from 1971 to 2100

6.6.2.1 The lake volume dynamics in the future without water policy

This section of the thesis examines the water volume dynamics without water abstraction restrictions for Shortandy Lake to reduce water abstraction from the lake in 2010. In this analysis, the developed single lake model and future climate were performed with the mean annual anthropogenic water abstraction from 1986 to 2009. Specifically, the annual mean water abstraction of $2.3x10^6m^3$ was applied.

Figure 6.29 shows the drastic consequences of a warmer future climate in conjunction with anthropogenic water abstraction from Shortandy Lake. Key findings indicate that under RCP2.6 GFDL, the mean annual temperature will increase by 1.5° in Shortandy area. As a result, the water volume could be shrunk by four times (r=0.96), whereas with the temperature increase by 1.9°C under RCP6.0 by five times (r=0.96).

However, the worst-case scenario is predicted by IPSL model. *The model findings show the total lake disappearance by 2076 under RCP2.6 and even earlier disappearance under RCP6.0 by 2071*. The Figure 6.33 illustrates that an increase of the mean annual temperature by 6°C (RCP6.0 IPSL) and insignificant increase in precipitation in conjunction with the past anthropogenic water abstraction could lead to the total disappearance of Shortandy by the 2070s.

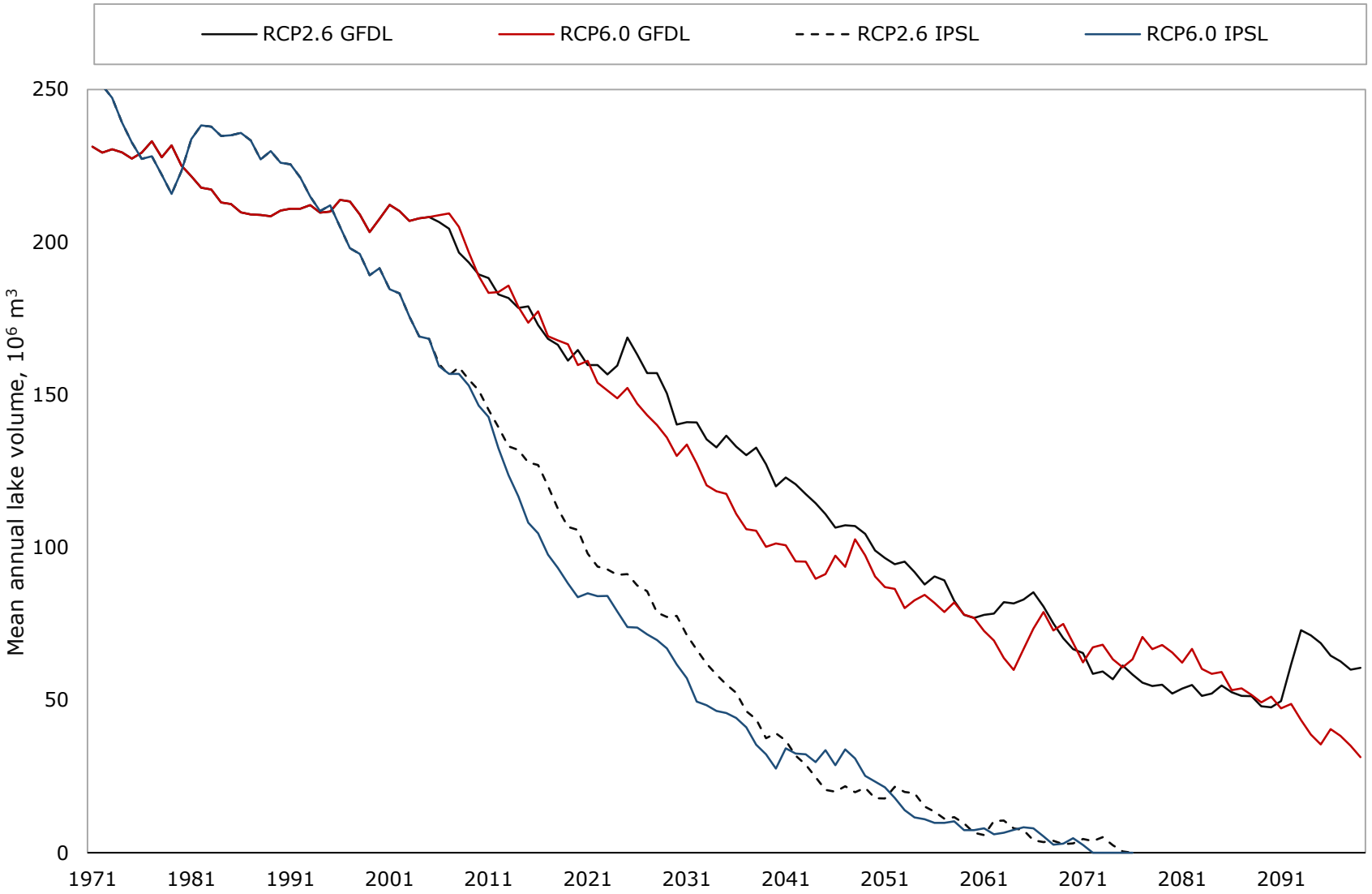

Figure 6. 32 The lake volume dynamics of Shortandy Lake estimated using two GCM models without water abstraction restrictions

6.7 Summary

This chapter of the thesis addresses how endorheic lakes are sensitive to changing future climate as well as human intervention. The developed water balance model shows that the role of anthropogenic water abstraction in Shortandy Lake volume reduction was critical. Furthermore, based on future climate projections, the shallowing-up process is expected to accelerate by the end of this century. The assessment of the future water volume dynamics has devastating implications, *i.e.* total lake disappearance without the governmental water policy accepted in 2010.

To sum up, the particular case of Shortandy Lake gives an understanding of water overexploitation and water scarcity in the Central Asian region. The developed water balance model captures how changing regional climate is likely to affect the lake volume in the future with the current water management strategies.

Chapter 7 Discussion

7.1 Water balance model

Since the 1880s, the negative anomalies in the precipitation trend have transformed the hydrological cycle in many Central Asian lakes (Matsuyama and Kezer, 2009, Bruckner, 2000). Chapter 2 findings indicate that the reduced pattern in precipitation started during the 19th century and continued until the 1950s in Central Asia. As a result, most lakes have faced a significant lake level reduction in this region, including Burabay lakes (Micklin, 1973, Shnitnikov, 1973, Uspenskij, 1948). Yet, numerous studies reported that the climate has become warmer and wetter during the last decades of the twentieth century and the first decades of the twenty first century over the north-west region of Central Asia (Matsuyama and Kezer, 2009, Propastin, 2012, Aji and Kondoh, 2006, Bai et al., 2011). The water volume reconstruction in Lake Balkhash shows that there was a positive lake volume trend in 1992-2010 due to the increase in precipitation so that the lake had reached its highest level by 2005 (Propastin, 2012). Furthermore, the positive lake volume response was observed in other Central Asian lakes, such as Urmia, the Aral Sea and Bosten lakes by 2013 (Liu et al., 2019, Tan et al., 2018). In contrast, the reconstruction of Shortandy Lake volume shows that the lake volume was persistently decreasing. The major finding of the study shows that the water volume reduction is likely to be *driven by anthropogenic water abstraction from the lake over the three decades*, *and without water abstraction, the lake volume would change insignificantly.*

Previous water balance studies for Burabay lakes (Shnitnikov, 1970a, Yapiyev et al., 2017, Uryvayev, 1959) were focused on short-term observations (2-4 years), which were inadequate to explain the long-term water level decline in these lakes due to interannual variability of the regional climate. Thus, the major contribution

of this study has improved understanding of the processes driving the water level decline in Shortandy Lake, which was achievable by reconstruction of a long-term (30 years) water balance of the lake. The developed model is the first attempt to model a long-term water volume/balance interaction with climate and anthropogenic impact in the Burabay area. The sensitivity analysis shows that the model adequately reproduces the lake storage changes with a standard deviation of around 5% from the total lake volume (Section 5.7.3).

The single lake model developed for Shortandy Lake shows that the anthropogenic water abstraction of on average 12% from the annual outflow can generate the significant water volume reduction in endorheic lake. Section 5.5.2 showed that the water abstraction from Shortandy Lake was 25%-34% in 1989-1993 and 13-14% in 1997-1998 from the annual outflow proportion. The cumulative water deficit due to the long-term water abstraction has resulted in a significant water level decline in the lake. The following conclusion disagrees with Yapiyev et al. (2017), whose studies concluded that the role of anthropogenic water abstraction in the water volume reduction of Shortandy Lake was minor.

The level reduction of Shortandy Lake is similar to the lake desiccation occurred in the Aral Sea, where anthropogenic impact contribution accounted around 77% for the lake level decline (Propastin, 2012). In case of Shortandy Lake, the water abstraction had 92% from the total water volume deficit ($51.5 \times 10^6 m^3$) and only 8% accounted for the natural lake level decrease.

7.2 Implications of anthropogenic impact and water management

Water scarcity and increasing demand for water due to the growing population and economies have become major reasons for the deterioration of most endorheic lakes in Central Asia since the 1960s. The water balance findings indicate that the regional climate *had a minor role in the decreasing lake water volume of Shortandy Lake relative to anthropogenic water abstraction over the*

three decades. Therefore, the shrinkage of Shortandy Lake is another example of the water mismanagement in the Central Asian region along with other endorheic lakes, such as the Aral Sea, Lake Balkhash, and Bosten Lake.

Water management and water availability have become one of the main concerns in the context of economic development or/and instability in Central Asian countries (O'Hara, 2010). For Kazakhstan, the implications of changing water volumes in the Burabay lakes are manifold. First of all, Section 3.1.5 shows that lakes and landscape of Burabay region have become the area that attracts many visitors. However, the decreasing trend in the lake volume will create unfavourable conditions for further development of tourism in the BNNP, which will negatively affect the economic situation in the region.

Historically, water abstraction from the Burabay lakes was only allowed for fulfilling the water needs of the nearby settlements and water supply of a few resorts located within the Park (with 2,000 visitors annually). According to hydrological studies conducted in the 1950s and 1960s (Uryvayev, 1959, Shnitnikov, 1970a) the freshwater resources in these lakes were sufficient to meet the water needs of local settlements. The creation of the BNNP was directed specifically to develop this area as the main tourist destination of Kazakhstan. Section 3.1.5 shows that there has been a rapid development of tourism in Burabay during the 2000s. The annual number of visitors increased tenfold by 2011 (Ministry of Industry and New Technologies of the Republic of Kazakhstan, 2014), which in turn has increased the demand for freshwater. Burabay lakes remained the major source of freshwater until 2010, where Shortandy, Burabay and Ulken Shabakty lakes were the major lakes for water abstraction in Burabay area (Section 3.1.5)(KazHydroMet, 2014). Since 2009, the widespread water level decline of the Burabay lakes raised a serious concern for the government of the country about the future of the BNNP lakes. Therefore the water policy accepted in 2010 has restricted water abstraction from the lakes. The water abstraction restrictions were only achievable by additional investments for centralised water

supply from the nearby settlement (Kokshetau). Nowadays, the maximum water abstraction is within the range of $0.5x10^6m^3$ $year^{-1}$ of Shortandy Lake, Burabay and Ulken Shabakty lakes and $0.3x10^6m^3$ $year^{-1}$ for Katarkol and Kishi Shabakty. However, according to KazHydroMet (2014), unauthorised water abstraction still remains a problem for the BNNP authorities.

The lack of accurate and up-to-date quantification of the water balance for more than six decades in Shortandy Lake has made it impossible to evaluate either present and future changes in the regional climate or water management strategies for these lakes. The major contribution of the single lake model developed for Shortandy Lake highlights that endorheic lake volume is sensitive to fluctuations in regional climate as well as to water management strategies/policies for these lakes. The water balance studies conducted by Uryvayev (1959) showed that water abstraction from the Burabay lakes was merely used for the nearby settlements. In addition, the interannual fluctuations in regional climate must be considered in the water management of Burabay lakes where, during dry periods, the water volume abstracted from the lakes should be ceased completely.

However Chapter 5.5.2 shows that the water abstraction from Shortandy was persistent, where the highest values of water abstraction (more than 25% from total annual outflow) corresponds with the driest periods within the study period. The dry periods at Shortandy occurred in 1988-1989, and 1998, which coincided with the negative phases of the West Pacific Oscillation released by ENSO over the northern Eurasia, and resulted in reduced snow precipitation (Popova, 2007) and subsequently affected the seasonal runoff in Shortandy during these years (Figure 7.1). However, the lack of understanding of the hydrological processes over the six decades in Burabay lakes has caused inadequate evaluation of water resources and massive water abstraction from the lake. Consequently, the negative net balance resulted in the significant lake volume decline in Shortandy Lake. Anthropogenic water abstraction increased the negative net balance of Shortandy

Lake during the 1980s and 1990s (Chapter 5.5.2). Therefore, the lake level could not recover fully, naturally, during the wet periods (1993-1994, 1999-2002, 2007, and 2009). The positive lake volume response was only observed after 2013 when the water abstraction was reduced to $0.5x10^6m^3$ annually.

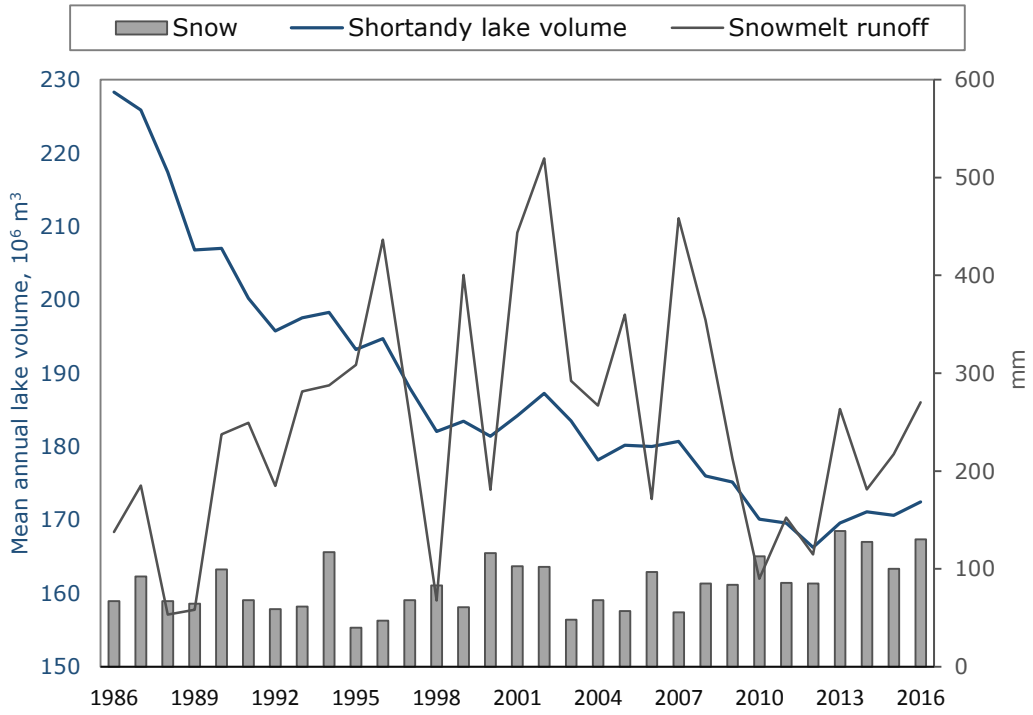

Figure 7. 1 Mean total water volume changes of Shortandy Lake and total seasonal snowmelt runoff produced from the lake catchment and total seasonal snow precipitation from 1986 to 2016

Recent studies indicate that the climate over the semi-arid and arid Central Asia is becoming warmer with an increasing precipitation trend (Liu et al., 2018, Huang et al., 2017, Lioubimtseva, 2014). The winter temperature anomalies over Central Asia and the West Siberian region during the last century were associated with the North Atlantic Oscillation (NAO) (Lioubimtseva, 2014, Popova, 2007, Livingstone, 1999). The NAO is recognised to have a significant impact on air temperature all over the Northern Hemisphere (Hurrell, 1996), controlling winter season precipitation over much of Eurasia, including Siberia (Hurrell and Loon, 1997, Brown and Duguay, 2010, Livingstone, 1999). Therefore, a strong winter NAO signal of warming climate established in most lakes of West Siberia also

affected the cold-season temperature in the Shortandy catchment (mean average +1.1°C). Future climate modelling results indicate that the regional climate in the Burabay area is likely to transform further towards warmer and wetter climate conditions. The upward trend in the cold-season temperature has resulted in earlier ice-free conditions in Shortandy lake since 2005 (Section 5.1.1). In the future warmer climate the ice-cover duration observed in Shortandy Lake is likely to further decrease (earlier ice-free conditions up to 20 days) by 2100 (Figure 7.5).

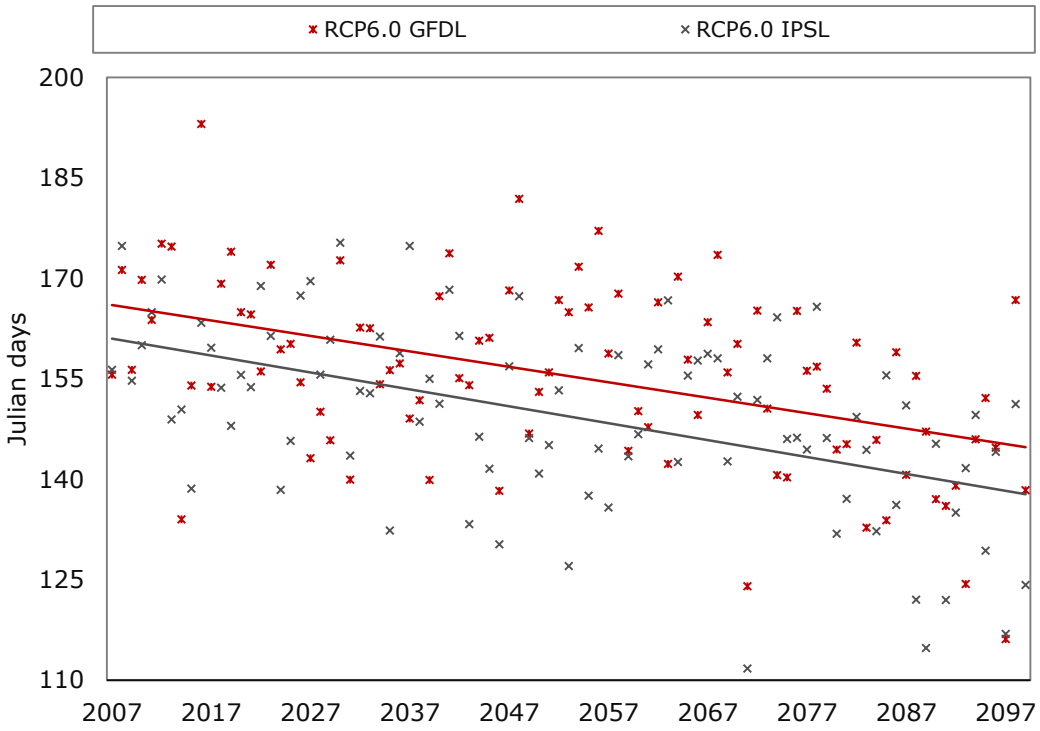

Figure 7. 2 Ice-cover duration in Julian days modelled for Shortandy Lake based on the GFDL (red) and the IPSL (grey) from 2006 to 2099

The following conclusion corresponds with other climate findings conducted for semi-arid regions of Central Asia, where climate is excepted to be warmer (during the winter months) and wetter (during summer months) (Section 2.2). Specifically, Section 6.4.1 shows that the air temperature increase (on average +2.5°C), suggested by both RCPs, is likely to alter the cold-season temperature. The warmer winter temperature and decreased SWE in snowpack characteristics in the Northern Hemisphere (Brown and Mote, 2009, Adam and Hamlet, 2009)

are likely to affect both snow accumulation and duration of cold-seasons, which in turn will decrease substantially Q_{snow} produced from the catchment (Section 6.4.3.). Warmer winters are likely to affect seasonal runoff, where rainfall-runoff will have a greater contribution to the annual water volume than snowmelt runoff by 2100 (Section 6.4.3).

In the context of the future changing climate, water management policies play a key role in the water volume changes of Shortandy Lake. Future climate modelling for Shortandy Lake shows that future water management strategies are critical in the water volume dynamics of the lake, when changing climate will have a greater impact on the lake water balance. In this study, multiple water abstraction scenarios were applied to evaluate various lake volume response (Section 6.6). The major findings of this project is that under water abstraction restrictions imposed on Shortandy Lake, which were implemented in 2010, were to be removed, the lake could disappear by 2076 under RCP2.6 (IPSL) or by 2071 under RCP6.0 (IPSL).

Although future climate change is predicted to reduce the lake volume of Shortandy, a significant decline in lake volume can be prevented by managing future water abstractions. Specifically, without water abstraction from Shortandy in the future, the water volume can be improved by 28%-27% (based on RCP2.6 GFDL and RCP6.0GFDL respectively) and 59%-69% (based on RCP2.6 ISPL and RCP6.0 IPSL respectively) relatively to the lake volume with the water abstraction (Section 6.6.2). Therefore, the water balance studies of Shortandy Lake should contribute to BNNP authorities in the future water management with taking into consideration changing future climate. Moreover, the key findings indicate that the current water management strategy for Shortandy Lake ($0.5x10^6 m^3\ year^{-1}$) is likely to have devastating implications for the lake volume in the future (Chapter 6.6.2). For example, under the present water abstraction policies, the lake area is projected to decrease from 11%-8% under RCP2.6 with GFDL and IPSL models respectively, whereas under RCP6.0 IPSL the lake area is likely to decrease by

three times (from 15.7km^2 to 5.9 km^2). Thus, the water abstraction from the lake should be further reduced or completely ceased.

The findings of the water balance modelling for Shortandy Lake raises a serious concern about other lakes in Burabay area. Besides the volume decline in Shortandy Lake, a significant water volume reduction has also been observed in other lakes within the BNNP. According to KazHydroMet (2014), a significant lake area reduction was reported in Ulken Shabakty Lake (-12%), Kishi Shabakty Lake (-21%), and the most dramatic lake area shrinkage in Maybalyk Lake (-40%). Continuous water abstraction was common in these lakes. Therefore the changing lake area in other lakes of Burabay area can also be affected by anthropogenic water abstraction. Future climate modelling for Shortandy Lake showed that the lake area is projected to decrease significantly (to 30%-60%) by 2100 under the present water abstraction policies (Section 6.4.5). Therefore, future regional climate change can have serious implications for smaller lakes in Burabay area (lake area >5km^2) or even total disappearance of lakes, such as Maybalyk, Katarkol, Tekekol and Akkol lakes. Consequently, future water management strategies and policies have a vital role in the future lake volume changes of the Burabay lakes.

7.3 Uncertainties and limitations

Many researchers noted that water balance modelling inevitably involves errors due to the limitations in the various approaches in estimating water balance components (Chapman, 1974, Winter, 1981). However, some model limitations should be addressed. The findings of this project highlight that the sparse *in-situ* measurements and limited data availability remain the biggest constrain in hydrologic modelling for Central Asian lakes. The sensitivity analysis of the model shows that the model is sensitive to precipitation (Section 5.7.4), which variation of higher than 15% affects the model accuracy. Unfortunately, the precipitation records of Shortandy is a subject of systematic error due to the limited number of rain gauges installed in this particular area. Therefore, data inaccessibility and sparse monitoring over main hydrological parameters affect the accuracy of the data-driven hydrological modellings in reconstructing a long-term regional climate variation in the Shortandy catchment.

As in most water balance studies, the interaction of the lake with groundwater is the most ambiguous factor of all (Winter, 1981). Due to the inaccessibility of groundwater level data, groundwater flux was estimated using the regional model for groundwater flux developed by Uryvayev (1959) and through solving the water balance equation (Section 4.6). The estimation of groundwater flux showed the lake and groundwater interaction, establishing the main periods when groundwater storage was considerable. Specifically, the groundwater flux was positive (annual total of +153mm) when the lake reached the lowest level in 2010, whereas groundwater outflow was highest (-100mm) after the slight water volume increase in 2007. Moreover, the comparative analysis of groundwater models shows that the regional model which estimates $G_i - G_o$ only during cold seasons, is likely to underestimate the groundwater flux (Chapter 5.3). The water balance

model indicates that lake-groundwater interaction occurs during summer months as well, especially during the years with excessive runoff-events.

Although the developed model could establish surface-ground water interaction in Shortandy Lake, the inaccessibility of the groundwater levels affected the overall model accuracy (Section 5.7.4). The sensitivity analysis of the model shows that water level measurements by which groundwater flux was estimated affected the model structure, and as a result, model accuracy in the long-term lake storage simulations.

More uncertainties are associated with groundwater flux in the future water balance modelling. This assumption was made based on the GeoByte (2014) survey on the groundwater storage in the Burabay area conducted in 2013. Specifically, a significant reduction of the groundwater resources in Burabay area was reported, where the groundwater storage contribution to Burabay lakes was estimated to be *no more than* $5.7x10^6m^3$ in 2013. It should be noted that in 2013, the precipitation value was the highest (493mm versus 332mm mean historical average) within the 30-years of observation, hence the groundwater storage may have been higher for that year compared to other years. In addition, research on groundwater storage in the future changing climate indicates that groundwater recharge is likely to decrease due to the combined effects of increasing evapotranspiration and reduction in runoff in arid and semi-arid regions (Havril et al., 2018, Ng et al., 2010). The only exception is the high-altitude areas where groundwater recharge is expected to increase as a result of extensive glacier melting (Kitabata et al., 2006, Dragoni and Sukhija, 2008). Nonetheless, the extensive scenarios provided by GCMs are seen as a provisional basis for analysis to be accomplished to understand the effects on groundwater of the changing climate (Ng et al., 2010, Dragoni and Sukhija, 2008). A detailed understanding of the geological structure of the entire Burabay area, as well as the use of complex models which take into account lake-groundwater interactions (groundwater

levels) would improve the accuracy of hydrological modelings and overall understanding of hydrological processes in Burabay area.

The single lake model developed for Shortandy Lake requires an accurate estimation of the lake area (A_L). Based on the water balance equation (Eq.4.1) inflow variables such as P_{rain} P_{snow} and the outflow variable E_o are functions of monthly lake area. The reconstruction of the depth-volume relationship was estimated using a GIS-based model (Section 4.3). The accuracy of this model and errors associated with the lake area estimations are dependent on the RS products resolution and bathymetric survey quality as well as its interpolation method selection. In this project, the GIS-based model is sensitive to changes that occur in A_L >10 km^2 or above 380m of the lake level, which is based on the lake bathymetry corresponding to the shallowest areas (Figure 4.6). Therefore within the given range, changes in lake volume would result in a considerable change in the lake area. In this project, A_L which is bigger than 10 km^2 was primarily calculated for the lake balance modelling in 1986-2016. However, model outcomes were statistically highly correlated with the observed lake level patterns (Section 5.6). In the future climate modelling, the smaller lake area is likely to produce less error in the lake volume-area relationship.

Lake evaporation was established without heat storage capacity, which is the required parameter for the net radiation in evaporation modelling of deep lakes. In deep lakes, heat storage influences the surface energy flux as deeper lakes tend to continue heating up during warm months and release it as latent heat during cooler months, causing seasonal changes in losses of evaporation. In this project, open lake evaporation utilises the concept which was developed for "shallow" lakes (surface albedo of 0.08) and without known heat storage (Section 4.4.1.1). The significant lake area-depth reduction projected by 2100, will decrease the heat storage capacity in Shortandy Lake. The shallowing process can substantially accelerate lake-air temperature interactions, for example, Small et al. (2001) established that changes in the lake area-depth of the Aral Sea in 1960-

1990, resulted in 5% of the increase in the net annual evaporation after the lake desiccation. Therefore, open lake evaporation modelling provides more accurate estimations of the reduced lake area-depth conditions predicted in the future climate modelling, rather than the estimations for 1986-2016. According to Linacre (1993), the fixed albedo of 0.08 may create 10% of overestimation of the deeper lake evaporation losses.

A similar error is related to the evapotranspiration model. A crop coefficient adjusting the model equation (Eq.4.4.2) based on vegetation types should be estimated for each land cover type separately. In this project, E_{act} was generalised and estimated as if the lake catchment was completely covered with forest. However, the catchment is covered with forest and grassland, with a greater proportion of forest area (≈88%-75% in 1986-2009 and 2010-2016 respectively). According to Allen (1998), the crop coefficient for grasslands during mid-season is roughly 0.85. The crop coefficient for forested areas of Shortandy was approximately within the range of 0.8-0.94 (Section 5.1.2.1), which is on average equal to 0.85. Therefore, the following generalisation is likely to produce an insignificant difference in evapotranspiration losses for the water balance estimation during 1986-2016. In the climate change impact assessment part of this study, evapotranspiration from vegetation was estimated as the fixed crop coefficient (0.9). In future climate modelling, uncertainties in estimations of evapotranspiration from the catchment are manifold, for example, changes in land use, soil moisture temperature etc.

Lastly, although there have been developments in advanced climate projection models, the extent of climate change remains largely unknown due to the uncertainties associated with climate models and greenhouse emission scenarios along with numerous complex feedback processes. In this study, two GCM models (out of 23) and two emission scenarios (out of 7) were utilised. Therefore, future climate modelling for Shortandy Lake shows estimates on how the regional climate (endorheic lakes specifically) is likely to be affected under 'low-emission' (RCP2.6)

and increased emission scenario (RCP6.0). However, it should be noted that other GCM models under different emission scenarios could have produced distinctive level changes in Shortandy Lake.

Future climate modelling for Shortandy indicates that a major discrepancy between GCM models is the winter temperature and precipitation predictions, where the IPSL model predicts a higher air temperature model and lower mean precipitation (Section 6.4). Specifically, wet periods which are primarily driven by excessive rainfall in July are projected to occur more often based on the GFDL model. Therefore, the lake volume simulations demonstrate a considerable difference in the water volume simulations. In addition, the sensitivity analysis of the model shows that the model outcomes becomes sensitive when precipitation variation exceeds 10% (Section 5.7.4). Therefore, the single lake model produces more accurate volume predictions with the IPSL model than with the GFDL. Specifically, the IPSL model predicts precipitation variation within the range of 5-11%, whereas the GFDL model suggests a variation of greater than 30%.

Chapter 2.2.2 shows that Shortandy area is located in the mid-latitude area, which is controlled by westerly circulation. For such areas, precipitation primarily falls during cold-season months (Chen et al., 2011). However, the NAO and ENSO are two important factors which influence the precipitation regime in this region, creating interannual and decadal variations in warm-season precipitation (Liu et al., 2018, Aizen and Melack, 2001). Based on Chen et al. (2011) and Huang et al. (2013) a cycle of 2-3 years of variation in precipitation pattern was established for North Kazakhstan, and 5-6 years for the southern regions of the country. Yet the understanding of the relationship between precipitation patterns and large scale atmospheric and oceanic systems in Central Asian region is limited (Huang et al., 2013, Mariotti, 2007, Randall and Fichefet, 2007), specifically in the simulation of the ENSO (Randall and Fichefet, 2007), which produces a great discrepancy in predicting future precipitation patterns.

7.4 Summary

This chapter of the thesis synthesises key findings of the thesis and explains the implications of the present and future volume fluctuations of Shortandy Lake. This study contributes to the understanding a fragile water balance of endorheic lakes highlighting the role of human intervention. Previous water problems in the Aral and Caspian Seas were related to transboundary water management, to solve which require cooperation between a number of countries (O'Hara, 2010). Key findings of this study highlight that water-related problems still exist in managing local water basins in Kazakhstan, where the water level decline in Shortandy is another example of mismanagement of water resources. In many cases, the water management problems are mainly due to the lack of up-to-date hydrological modelling which in turn result in overexploitation of water resources. The major findings of the project show that the future development of tourism in most Burabay lakes should be implemented with caution as further exploitation of water and land resources may have negative implications for Northern Kazakhstan and the sad repetition of the Aral Sea fate. The outcomes of this project will contribute to local authority communities for the planning of sustainable development not only in Shortandy but in the entire Burabay area.

Chapter 8 Conclusion

8.1 Introduction

The main contribution and novelty of this research lies in the investigation of problems related to a long-term water volume reduction occurred in one of the biggest lakes within the Burabay area - Shortandy Lake. The major contribution of the single lake model developed for Shortandy Lake highlights that endorheic lake volume is sensitive to fluctuations in regional climate as well as to water management strategies/policies for these lakes. The findings of this research will assist not only BNNP authorities in the future water management of Burabay lakes, but will also raise the awareness of the future of other endorheic lakes in Central Asian region. Endorheic lakes of Central Asia, such as the Aral Sea, the Caspian Sea, Lake Balkhash etc. received significant attention from environmental researchers around the globe (Propastin, 2012, O'Hara, 2010). However, a long-term water volume reduction in a number of smaller basins located in Burabay area, have stayed without attention. This research focuses on examining the potential reasons for the observed water volume dynamics of the lake, evaluation the likely impacts of the future dynamics of the water balance of the lake as well as assessment of water management strategies accepted for Shortandy. The following chapter presents the conclusion and main findings that arise from the study reported in this thesis.

Section 8.2 summaries this research by addressing its main outcomes around the research aim, questions and objectives stated in Chapter 1. Main findings and conclusions emerging from Chapter 5, 6 and 7 are presented in Section 8.3. Recommendation for future research are provided in Section 8.4.

8.2 Summary of the Main Findings

The conclusions identify the major topics within modelling of endorheic lakes that have been addressed in the previous chapters: analysis of water balance approach

to simulate water volume dynamics in endorheic lakes; and to evaluate the effect of regional climate and human activity on the changing water volume of endorheic lakes. Throughout the thesis, Shortandy Lake was selected as the case study to investigate the long-term lake level decline, which has been observed in most lakes located in BNNP area. Therefore, the overall aim of this project was to assess the reasons for the observed dynamics of Shortandy Lake from 1986 to 2016. In order to accomplish this aim two research questions and six research objectives were formulated. The following section of the thesis explains how successful this research was with respect to meeting these objectives.

Research Question 1: What are the characteristic changes in the water balance of Shortandy Lake from 1986 to 2016?

In order to answer Research Question 1, three research objectives were constructed:

Objective 1: The quantification of the water volume dynamics of Shortandy Lake over the 30 years.

The key findings of this objective showed a significant water volume reduction in the lake. Specifically, the water volume of Shortandy Lake declined significantly by 25% (from $231.7 \times 10^6 m^3$ in 1986 to $172.5 \times 10^6 m^3$) by the end of 2016. The reconstructed water volume provides valuable information about the lake volume dynamics in Shortandy Lake due to the water volume changes which were unknown since the 1960s.

Objective 2: The main regional hydrological drivers which determine the water balance of Shortandy Lake

In order to identify key hydrologic drivers of the water balance of Shortandy Lake, an extensive literature review on previous research for endorheic lakes was conducted. The literature review was predominantly focused on establishing the sensitivity of endorheic lakes to regional climate and human intervention with a particular interest in endorheic lakes of Central Asian region. Chapter 2 revealed the main regional hydrological drivers of Shortandy Lake based on the previous

research conducted for endorheic lakes both globally and regionally. The data required for the water balance modelling revealed gaps in observations (Section 4.2), which were filled using alternative equations and remotely sensed products. In the case of Shortandy, selected models for the single lake model utilises climate parameters (temperature, precipitation), which in most cases, are available in most weather stations.

Objective 3: The development of the water balance model for Shortandy Lake

The conceptual model was used as a fundamental point for defining the critical model components (Section 4.1). The relationship between the water balance variables was then specified using the mathematical expression (Equation 4.1). The hydrological models used for quantification of input and output variables were as follows:

Output variables:

- Open water evaporation (E_o) - the simplified approach for the Penman developed by Valiantzas (2006) (Chapter 4.4.1);
- Evapotranspiration from vegetation (E_{act}) - the FAO-56 Penman-Monteith approach (Allen, 1998) (Chapter 4.4.2);
- Snow sublimation (E_{sub}) – the regional model developed by Semenov (1990) (Chapter 4.4.4);

Input variables:

- Seasonal snowmelt runoff (Q_{snow}) and rainfall runoff (Q_{rain}) - Snowmelt Runoff Model (SRM) (Chapter 4.5.1);

The 30-years water balance modelling revealed that the overall net flux was negative (-*95*mm on average), which resulted in the water volume reduction over the study period. The key findings of the water balance modelling revealed that warm-season precipitation (P_{rain}) and seasonal snowmelt runoff (Q_{snow}) contribute the greatest proportion to the annual lake inflow (37% and 35% respectively), whereas the lake evaporation flux proportion had around 78% and anthropogenic water abstraction accounted 12% of the annual lake losses. The water balance

findings reveal valuable information on how regional climate as well as human activity have changed over the study period.

The water volume simulated through the water balance model was compared with the water volume simulated by observed water levels. A high statistical significance between simulated and observed water volume was established ($r=0.999$, $p<0.001$), where the discrepancy between the measured and observed water volume showed an underestimation of less than 10%.

The development of water balance model enabled future water volume fluctuation due to the changing future climate to be established. Therefore, the second research question was expressed as follows:

RQ2: What are the likely implications of projected climate futures for the water balance of Shortandy Lake?

To address this question, three research objectives were established:

Objective 4: The selection of future climate scenario for Shortandy Lake area

First of all, it was important to quantify potential dynamics of the key regional hydrological drivers of the water balance of Shortandy Lake under a global temperature increase of 1.5°C-2°C. In this study, future climate impacts were assessed using ISIMIP2b (Section 6.1) which is a framework for projecting the impact of the changing climate on different sectors, including water resources, agriculture and ecosystems. The climate data required to simulated water balance of Shortandy (Section 4.1) was obtained based on two GCMs *i.e.* GFDL and IPSL models for Shortandy catchment under two emission scenarios (RCP2.6 and 6.0) including the historical period from 1971 to 2100.

Objective 5: The future climate modelling for Shortandy Lake

The future climate modelling was based on the selected future climate scenario (Objective 5) and the single lake model developed for Shortandy Lake (Objective 3). The main findings show that the mean air temperature is likely to increase in the Shortandy catchment (Section 6.4.1). Specifically, the GFDL model suggests that the air temperature increase is likely to affect cold-season temperature,

whereas the IPSL shows that the temperature increase will be uniform throughout seasons. However, future precipitation dynamics show the discrepancy between GCM models, where the GFDL model shows an upward trend by 25%-26% (RCP2.6 and 6.0 respectively) and the IPSL suggests a negligible increase by 15%-8% (Section 6.4.2). The air temperature increase during winter months is likely to diminish the relative contribution of the seasonal snowmelt under RCP6.0, where rainfall runoff will make a greater contribution to the lake volume (Section 6.4.3). The future water volume dynamics show further water volume decrease under both emission scenarios, where IPSL model predicts a greater volume reduction by 2100 (Section 6.4.5).

Objective 6: The evaluation of the anthropogenic impact on the lake water volume

In order to assess the role of anthropogenic impact in the lake level decline of Shortandy Lake, the anthropogenic water abstraction (W_{abs}) was excluded from the water balance equation (Section 6.6). First of all, the following assessment was conducted for the past 30-years of water balance modelling. The major findings of the thesis indicate that the lake volume would change insignificantly without anthropogenic water abstraction (Section 6.6.1). Secondly, the present water management strategies accepted for Shortandy Lake were assessed under the changing future climate. The key findings illustrate that despite the overall declining water volume dynamics in the future, the lake volume can be improved by +27%-28% (RCP2.6 and RCP6.0 GFDL respectively) and 59%-69% (RCP2.6 ISPL and RCP6.0 IPSL respectively) by ceasing future water abstraction from the lake (Chapter 6.6.2). Lastly, the water volume dynamics without water abstraction restrictions accepted for the lake to reduce water abstraction from the lake in 2010 were assessed. Chapter 6.6.2.1 shows drastic consequences of a warmer future climate in conjunction with the previous anthropogenic water abstraction policies. Based on these findings, the total disappearance of Shortandy Lake would be predicted by 2071-2076 (RCP6.0 and RCP2.6 respectively).

8.3 Research Conclusions

- The development of water balance model for Shortandy Lake showed that the significant water volume reduction in the lake was driven by anthropogenic water abstraction from the lake from 1986 to 2016. Specifically, human activity caused around 92% of the total water volume deficit, whereas only 8% accounted for the natural lake level decrease (Section 7.1). The sensitivity analysis showed that the model could adequately reproduce the lake volume changes (Section 5.7) and showed that precipitation is a key driver of the lake volume.
- The future climate modelling indicates that under a global temperature increase of 1.5°C-2°C, the water volume of Shortandy Lake is likely to further decrease. However, the magnitude of the water volume reduction is highly dependent on the future water management, where in the absence of anthropogenic water abstraction, regional climate fluctuation is likely to account for 18%-33% (the GFDL and the IPSL respectively) of the water volume deficit by 2100 based on the low emission scenario (RCP2.6) or an even greater deficit of 45% under RCP6.0. However, the uncertainties regarding the future climate simulation is largely unknown due to the uncertainties associated with GCMs and greenhouse emission scenarios. In this study, GFDL and IPSL models produced a considerable difference in the future water volume dynamics due to the discrepancy in the future patterns of air temperature and precipitation during cold-season months.
- The lake level decline in Shortandy Lake demonstrates the extent to which endorheic lakes are sensitive to climate and human activity. In Central Asia, most endorheic lakes have experience a significant water level reduction, for example the Aral Sea, the Caspian Sea, Lake Balkhash, Issykol-Kul. In many cases, human disturbance to the natural water circulation was the driving force of the shallowing-up. The case study of

Shortandy Lake shows that direct (water abstraction) and indirect (land cover) anthropogenic impact have a central role in the lake level fluctuation. The main outcomes of this project highlight that the water-related problems still exist in managing local water basins in Kazakhstan, where the lake volume decrease in Shortandy is another example of mismanagement of water resources.

8.4 Suggestions for Future Research

In the following section areas for potential future investigation are reflected. The future research suggestions are relevant for hydrological modelling of endorheic lake systems and have a particular importance for the future research of Burabay lakes.

8.4.1 Groundwater flux

The major limitation of the developed model is the groundwater flux. The groundwater storage was established using the water balance equation (Equation 4.1) and through the measured water levels for the past water balance investigation. The inaccessibility of the groundwater levels affected the overall model accuracy (Section 5.7.4). Therefore, groundwater level measurements could substantially improve the model accuracy in the long-term lake storage simulations as well as improve the understanding on how future changing climate is likely to affect the lake volume. The measured groundwater levels would substantially improve the water balance estimates of those parameters which were neglected in the model. Specifically, the evaluation of losses for infiltration during snowmelt and rainfall runoff events as well as losses for evapotranspiration during the growing stages, which in this study was established using empirical equations (Section 4.4.2) or/and by calibrating estimates (Section 4.5.1). By establishing surface-groundwater interaction in the past, the future water level dynamics can be considerably enhanced, although the understanding of the future effects on groundwater

due to the changing climate in semi-arid areas is largely unknown. An extended understanding of the geological structure of the catchment, the use of comprehensive surface-groundwater models or isotopic analysis would improve the knowledge of how the groundwater storage affects the water volume dynamics of Shortandy Lake

8.4.2 Water balance modelling for other Burabay lakes

During the first year of the project, the aim was to develop water balance for the three lakes, including Burabay and Ulken Shabakty lakes. However, extensive reading on existing literature on Burabay lakes has shown that groundwater interaction between Burabay, Ulken Shabakty and Maybalyk lakes (Zemlyanicyna, 1970). Groundwater level records were not available for this project, thus it turned into a challenging task development of an accurate water balance for these lakes. However, the water balance modelling for other Burabay lakes can provide a valuable information on potential reasons for a large-scale lake level fluctuations occurring in most Burabay lakes.

Although Burabay and Ulken Shabakty lakes were beyond the scope of this project, the water balance model developed for Shortandy Lake is a fundamental template for other endorheic lakes of Burabay area. The water balance model can be improved for other Burabay lakes once groundwater levels as well as the hydraulic gradient between these lakes are established. The GIS-based volumetric model developed for Shortandy Lake can be similarly established for the mentioned above lakes for the depth-volume-area relationship. Due to the similar regional climate conditions, land use and vegetation cover in the BNNP, the input and output variables can be estimated using the methodology used for Shortandy Lake (Chapter 4).

8.4.3 Input and Output estimations

Lake evaporation. Lake evaporation is one of the major sources of losses during warm-seasons in endorheic lake systems. Therefore, the accurate

estimation of this variable may significant improve the overall precision of the modelling. In this study, the lake evaporation was established without heat storage capacity, which is the required parameter for the net radiation in deep lakes evaporation modelling. In the future, open lake evaporation can be substantially improved by calibrating the Penman equation by incorporating the heat capacity of the water layer with the daily or with mean monthly water temperature (Chapter 4.4). The inclusion of this parameters may substantially improve estimates of lake evaporation during spring (April, May) and autumn (September, October) months.

Precipitation and runoff. The precipitation records of Shortandy is a subject of systematic error and uncertainty due to the limited number of rain gauges installed in this particular area. An increased number of rain gauges would improve the quantification of input variables and, as a result, increase the overall accuracy of hydrological models.

Snowmelt and rainfall runoff other important variables within the water balance of endorheic lakes. In SRM, the runoff coefficient (c_{Sn}, c_{rn}) were used to estimate the percentage of snowmelt and rainfall runoff that contributed to the lake discharge. Due to the lack of actual measurements, these coefficients were calibrated using the methodology explained in Chapter 4.5.1.3.3. However, future field-based measurements on seasonal discharge or incorporation of soil moisture conditions to the SRM model can considerably enhance the runoff estimations.

References

ABBOTT, M. B., BATHURST, J. C., CUNGE, J. A., O'CONNELL, P. E. & RASMUSSEN, J. 1986. An introduction to the European Hydrological System — Systeme Hydrologique Europeen, "SHE", 1: History and philosophy of a physically-based, distributed modelling system. *Journal of Hydrology,* 87**,** 45-59.

ABDULLA, F., ESHTAWI, T. & ASSAF, H. 2009. Assessment of the Impact of Potential Climate Change on the Water Balance of a Semi-arid Watershed. *Water Resources Management,* 23**,** 2051-2068.

ABUDU, S., CHUNLIANG, C., SAYDI, M. & KING, J. 2012. Application of snowmelt runoff model (SRM) in mountainous watersheds: A review. *Water Science and Engineering,* 3.

ADAM, J. C. & HAMLET, A. F. A. L., D. P. 2009. Implications of global climate change for snowmelt hydrology in the twenty‐first century. *Hydrological processes,* 23**,** 962-972.

ADAMS, W. P. 1976. Areal differentiation of snow cover in east central Ontario. *Water Resources Research,* 12**,** 1226-1234.

AEBLY, F. & FRITZ, S. 2009. Palaeohydrology of Kangerlussuaq (Søndre Strømfjord), West Greenland during the last ~8000 years. *The Holocene,* 19.

AIZEN, E. M. & MELACK, J. 2001. Precipitation and atmospheric circulation patterns at mid-latitude of Asia *International Journal of Climatology,* 21**,** 535-556.

AJI, D. & KONDOH, A. 2006. The study on the dynamic change of water resources in Xinjiang by using GIS. *J. Japan Soc. Hydrol. & Water Resour.,* 19.

ALLEN, R., TASUMI, M. & TREZZA, R. 2007. Satellite-Based Energy Balance for Mapping Evapotranspiration With Internalized Calibration (METRIC) – Model. *Journal of Irrigation and Drainage Engineering,* 133.

ALLEN, R. G. P., L.S. RAES, D. SMITH, M. 1998. Crop evapotranspiration: guidelines for computing crop water requirements. *FAO Irrigation and Drainage Paper***,** 300.

ALSDORF, D., BIRKETT, C., DUNNE, T., MELACK, J. & HESS, L. 2001. Water level changes in a large Amazon lake measured with spaceborne radar interferometry and altimetry. *Geophysical Research Letters,* 28**,** 2671-2674.

ANDERSON, E. 1976. A point energy and mass balance model of a snow cover. U.S. National Oceanic and Atmospheric Administration.

ANDERSON, M. C., ALLEN, R. G., MORSE, A., AND KUSTAS, W. P 2012. Use of Landsat thermal imagery in monitoring evapotranspiration and managing water resources. *Remote Sens. Environment,* 122**,** 50-65.

ANDERSON, M. C., NORMAN, J. M., MECIKALSKI, J. R., TORN, R. D., KUSTAS, W. P. & BASARA, J. B. 2004. A Multiscale Remote Sensing Model for Disaggregating Regional Fluxes to Micrometeorological Scales. *Journal of Hydrometeorology,* 5**,** 343-363.

ANDERSON, M. P. & MUNTER, J. A. 1981. Seasonal reversals of groundwater flow around lakes and the relevance to stagnation points and lake budgets. *Water Resources Research,* 17**,** 1139-1150.

ANGEL, J. R. & KUNKEL, K. E. 2010. The response of Great Lakes water levels to future climate scenarios with an emphasis on Lake Michigan-Huron. *Journal of Great Lakes Research,* 36**,** 51-58.

BAI, J., CHEN, X., LI, J., YANG, L. & FANG, H. 2010. Changes in the area of inland lakes in arid regions of central Asia during the past 30 years *Springer,* 178**,** 247-256.

BAI, J., CHEN, X., LI, J., YANG, L. & FANG, H. 2011. Changes in the area of inland lakes in arid regions of central Asia during the past 30 years. *Environmental Monitoring and Assessment,* 178**,** 247-256.

BARNETT, T., ADAM, J. & LETTENMAIER, D. 2005. Potential impacts of a warming climate on water availability in snow-dominated region. *Nature,* 438.
BARNHART, T. B., MOLOTCH, N. P., LIVNEH, B., HARPOLD, A. A., KNOWLES, J. F. & SCHNEIDER, D. 2016. Snowmelt rate dictates streamflow. *Geophysical Research Letters,* 43**,** 8006-8016.
BASTIAANSSEN, W. G. M., CHEEMA, M. J., IMMERZEEL, W. W., MILTENBURG, I. & PELGRUM, H. 2012. Surface energy balance and actual evapotranspiration of the transboundary Indus Basin estimated from satellite measurements and the ETLOOK model. *Water Resources Research,* 48**,** W11512.
BASTIAANSSEN, W. G. M., MENENTI, M., FEDDES, R. A. & HOLTSLAG, A. A. M. 1998. A remote sensing surface energy balance algorithm for land (SEBAL). 1. Formulation. *Journal of Hydrology,* 212-213**,** 198-212.
BAUMGARTNER, M. F., SPREAFICO, M. & WEISS, H. W. 2001. Operational snowmelt runoff forecasting in the Central Asian mountains. *Remote Sensing and Hydrology,* 267**,** 66-71.
BAVERA, D., DE MICHELE, C., PEPE, M. & RAMPINI, A. 2012. Melted snow volume control in the snowmelt runoff model using a snow water equivalent statistically based model. *Hydrological Processes,* 26**,** 3405-3415.
BEECHAM, S., PIANTADOS J. 2015. *Water Resources in a Variable and Changing Climate,* Basel, Shu-Kun Lin.
BELANGER, T. V. & MIKUTEL, D. F. 1985. ON THE USE OF SEEPAGE METERS TO ESTIMATE GROUNDWATER NUTRIENT LOADING TO LAKES1. *JAWRA Journal of the American Water Resources Association,* 21**,** 265-272.
BENGTSSON, L. & MALM, J. 1997. Using rainfall-runoff modeling to interpret lake level data. *Journal of Paleolimnology,* 18**,** 235-248.
BINDER, C., SCHERTENLEIB, R., DIAZ, J., BADER, H. P. & BACCINI, P. 1997. Regional Water Balance as a Tool for Water Management in Developing Countries. *International Journal of Water Resources Development,* 13**,** 5-20.
BISKOP, S., KRAUSE, P., HELMSCHROT, J., FINK, M. & FLÜGEL, W. A. 2012. Assessment of data uncertainty and plausibility over the Nam Co Region, Tibet. *Adv. Geosci.,* 31**,** 57-65.
BLÖSCHL, G., SIVAPALAN, M., WAGENER, T., VIGLIONE, A. & SAVENIJE, H. E. 2013. *Runoff Prediction in Ungauged Basins: Synthesis across Processes, Places and Scales,* Cambridge, Cambridge University Press.
BONSAL, B. & PROWSE, T. 2003. Trends and Variability in Spring and Autumn 0 °C-Isotherm Dates over Canada. *Climatic Change,* 57.
BONSAL, B. & REGIER, M. 2007. Historical comparison of the 2001/2002 drought in the Canadian Prairies. *Climate Research,* 33**,** 229-242.
BOOMER, I., PLOTNIKOV, I. & WHATLEY, R. 2000. The paleolimnology of the Aral Sea: a review. *Quaternary Science Reviews,* 19**,** 1259-1278.
BORAH, D. & BERA, M. 2003. Watershed-Scale Hydrologic and Nonpoint-Source Pollution Models: Review of Mathematical Bases. *Transactions of the ASAE,* 46.
BOSCH, D., SHERIDAN, J., BATTEN, H. L. & ARNOLD, J. 2004. Evaluation of SWAT Model on a Coastal Plain Agricultural Watershed. *Transactions of the American Society of Agricultural Engineers,* 47.
BOURAOUI, F., BENABDALLAH, S., JRAD, A. & BIDOGLIO, G. 2005. Application of the SWAT model on the Medjerda river basin (Tunisia). *Physics and Chemistry of the Earth, Parts A/B/C,* 30**,** 497-507.
BRACHT-FLYR, B., ISTANBULLUOGLU, E. & FRITZ, S. 2013. A hydro-climatological lake classification model and its evaluation using global data. *Journal of Hydrology,* 486**,** 376–383.
BROCK, T. D., LEE, D. & ROBERT & JANES, D. 1982. Groundwater seepage as a nutrient source to a drainage lake; Lake Mendota, Wisconsin. *Water Research,* 16**,** 1255-1263.

BROWN, L. C. & DUGUAY, C. R. 2010. The response and role of ice cover in lake-climate interactions. *Progress in Physical Geography: Earth and Environment,* 34**,** 671-704.
BROWN, L. C. D., C. 2010. The response and role of ice cover in lake-climate interactions. *Progress in Physical Geography,* 34**,** 671-704.
BROWN, R. D. 1997. Historical variability in Northern Hemisphere spring snow covered area. *Ann. Glaciol.,* 25**,** 340-346.
BROWN, R. D. 2000. Northern Hemisphere Snow Cover Variability and Change, 1915-1997. *American Meteorological Society***,** 2339-2355.
BROWN, R. D. & MOTE, P. W. 2009. The Response of Northern Hemisphere Snow Cover to a Changing Climate. *Journal of Climate,* 22**,** 2124-2145.
BRUCKNER, E. 2000. Water level fluctuations in the Kirghiz steepe and fluctuations of rainfall in Russia since 1860. *In:* STREHR, N. & H., S. (eds.) *Eduard Bruckner-The sources and consequences of climate change and climate variability in historical times.* Netherands: Kluwer Academic Publishers.
BUDNIKOVA, T., MUSATAYEVA, G. & PLOKHIH, R. 2010. Report on integrated ecological studies of the Schuchinsk-Burabay resort area for the definition of the ways of sustainable development. Astana: The institute of Geography.
BURNASH, R. J. & FARRELL, R. L. 1979. Contamination in the hydrologic data base. *Proceedings of Engineers Foundation Conference, Improved Hydrologic Forecasting-Why and How.* American Society of Civil Engineers.
BURROUGH, P. 1986. *Principles of geographical information systems for land resources assessment,* New York, Oxford University press.
BURROUGH, P., RACHEL, A., LLOYD, M. & LLOYD, C. 2014. *Principles of Geographic Information Systems,* New York, Oxford University Press.
BUTT, M. J. & BILAL, M. 2011. Application of snowmelt runoff model for water resource management. *Hydrological Processes,* 25**,** 3735-3747.
CALMANT, S., SEYLER, F. & CRETAUX, J. F. 2008. Monitoring Continental Surface Waters by Satellite Altimetry. *Surveys in Geophysics,* 29**,** 247-269.
CAO, W., BOWDEN, W. B., DAVIE, T. & FENEMOR, A. 2006. Multi-variable and multi-site calibration and validation of SWAT in a large mountainous catchment with high spatial variability. *Hydrological Processes,* 20**,** 1057-1073.
CHAPMAN, T. 1974. Methods for water balance computation. *In:* SOKOLOV, A. (ed.) *A contribution to the International Hydrological Decade.* Paris: UNESCO.
CHEN, F. 2008. Holocene moisture evolution in arid central Asia and its out-of-phase relationship with Asian monsoon history. *Quaternary Science Reviews,* 27**,** 351-364.
CHEN, F., CHEN, J., HOLMES, J., BOOMER, I., AUSTIN, P., GATES, J., WANG, N., BROOKS, S. & ZHANG, J. 2010. Moisture changes over the last millennium in arid central Asia: a review, synthesis and comparison with monsoon region. *Quaternary Science Reviews,* 29**,** 1055-1068.
CHEN, F., HUANG, W., JIN, L., CHEN, J. & WANG, J. 2011. Spatiotemporal precipitation variations in the arid Central Asia in the context of global warming. *Science China Earth Sciences,* 54**,** 1812-1821.
CHEN, F., WANG, J., JIN, L., ZHANG, Q., LI, J. & CHEN, J. 2009. Rapid warming in mid-latitude central Asia for the past 100 years. *Front. Earth Sci.,* 3**,** 42-50.
CHEN, J., PEKKER, T., WILSON, C., TAPLEY, B., KOSTIANOY, A., CRETAUX, J. & SAFAROV, E. 2017. Long-Term Caspian Sea Level Change. *Geophysical Research Letters*.
CHERKAUER, D. S. & NADER, D. C. 1989. Distribution of groundwater seepage to large surface-water bodies: The effect of hydraulic heterogeneities. *Journal of Hydrology,* 109**,** 151-165.

CHIEW, F. H. S. 2010. Lumped Conceptual Rainfall-Runoff Models and Simple Water Balance Methods: Overview and Applications in Ungauged and Data Limited Regions. *Geography Compass,* 4**,** 206-225.

CHRISTENSEN, J. H., HEWITSON, B. , BUSUIOC, A. , CHEN, A. , GAO, X. , HELD, R. , JONES, R. , KOLLI, R. K. , KWON, W. K. , LAPRISE, R. , MAGANA RUEDA, V. , MEARNS, L. , MENENDEZ, C. G. , RÄISÄNEN, J. , RINKE, A. , SARR, A. , WHETTON, P. , ARRITT, R. , & BENESTAD, R., BENISTON, M. , BROMWICH, D. , CAYA, D. , COMISO, J. , DE ELIA, R. AND DETHLOFF, K. 2007. Regional climate projections , Climate Change, 2007: The Physical Science Basis. Contribution of Working group I to the Fourth Assessment Report of the Intergovernmental Panel on Climate Change. Cambridge.

CHUB, V. E. 2000. *Climate Change and its impact on the natural resources potential of the Republic of Uzbekistan,* Tashkent, Gimet.

CIRILO, J. A., VERÇOSA, L. F. D. M., GOMES, M. M. D. A., FEITOZA, M. A. B., FERRAZ, G. D. F. & SILVA, B. D. M. 2020. Development and application of a rainfall-runoff model for semi-arid regions. *RBRH,* 25.

CLARK, M. P., SERREZE, M. C. & ROBINSON, D. A. 1999. Atmospheric controls on Eurasian snow extent. *International Journal of Climatology,* 19**,** 27-40.

COHEN, S., IANETZ, A. STANHILL, G. 2002. Evaporative climate changes at Bet Dagan, Israel, 1964-1998. *Agric. Forest Meteorol.,* 111**,** 83-91.

COOK, D. G., MCCOMAS, M. R., WALLER, D. W. & KENNEDY, R. H. 1977. The occurrence of internal phosphorus loading in two small, eutrophic, glacial lakes in Northeastern Ohio. *Hydrobiologia,* 56**,** 129-135.

COUNCIL, N. R. 2005. *Radiative Forcing of Climate Change: Expanding the Concept and Addressing Uncertainties,* Washington, DC, The National Academies Press.

COVICH, A. 1993. Water and ecosystem,, pp. 40-55. *Water in crisis***,** 40-55.

CRAIG, H. & GORDON, L. I. 1965. Deuterium and oxygen 18 variations in the ocean and the marine atmosphere.

CRAPPER, P. F., FLEMING, P. M. & KALMA, J. D. 1996. Prediction of lake levels using water balance models. *Environmental Software,* 11**,** 251-258.

CRAWFORD, N. H. & LINSLEY, R. K. 1966. Digital Simulation in Hydrology: Stanford Watershed Model IV. *Technical Report 39.* Department of Civil Engineering, Stanford University.

CRÉTAUX, J.-F., KOURAEV, A. V., PAPA, F., BERGÉ-NGUYEN, M., CAZENAVE, A., ALADIN, N. & PLOTNIKOV, I. S. 2005. Evolution of Sea Level of the Big Aral Sea from Satellite Altimetry and Its Implications for Water Balance. *Journal of Great Lakes Research,* 31**,** 520-534.

CROWE, A. S. & SCHWARTZ, F. W. 1985. Application of a lake-watershed model for the determination of water balance. *Journal of Hydrology,* 81**,** 1-26.

DAWSON, N., BROXTON, P. & ZENG, X. 2018. Evaluation of Remotely Sensed Snow Water Equivalent and Snow Cover Extent over the Contiguous United States. *Journal of Hydrometeorology,* 19**,** 1777-1791.

DE BRUIN, H. & KEIJMAN, J. 1979. The Priestley-Taylor Evaporation Model Applied to a Large, Shallow Lake in the Netherlands. *Journal of Applied Meteorology - J APPL METEOROL,* 18**,** 898-903.

DE FLORIANI, L. & MAGILLO, P. 1999. Intervisibility on Terrains. *In:* LONGLEY, P., GOODCHILD, M. F., MAGUIRE, D. J. & RHIND, D. W. (eds.) *Geographic Information Systems: Principles, Techniques, Managament and Applications.* Wiley.

DÉRY, S. J. & BROWN, R. D. 2007. Recent Northern Hemisphere snow cover extent trends and implications for the snow-albedo feedback. *Geophysical Research Letters,* 34.

DEUS, D., GLOAGUEN, R. & KRAUSE, P. 2013. Water Balance Modeling in a Semi-Arid Environment with Limited in situ Data Using Remote Sensing in Lake Manyara, East African Rift, Tanzania. *Remote Sens.,* 5**,** 1651-1680.

DEVAK, M. & DHANYA, C. T. 2017. Sensitivity analysis of hydrological models: review and way forward. *Journal of Water and Climate Change,* 8**,** 557-575.

DIBIKE, Y. & COULIBALY, P. 2005. Hydrologic Impact of Climate Change in the Saguenay Watershed: Comparison of Downscaling Methods and Hydrologic Models. *Journal of Hydrology,* 307**,** 145-163.

DIBIKE, Y., PROWSE, T., BONSAL, B., RHAM, L. D. & SALORANTA, T. 2012. Simulation of North American lake-ice cover characteristics under contemporary and future climate conditions. *International Journal of Climatology,* 32**,** 695-709.

DINKA, M. O., LOISKANDL, W. & NDAMBUKI, J. M. 2014. Hydrologic modelling for Lake Basaka: development and application of a conceptual water budget model. *Environmental Monitoring and Assessment,* 186**,** 5363-5379.

DONCHYTS, G., BAART, F., WINSEMIUS, H. C., GORELICK, N., KWADIJK, J. & VAN DE GIESEN, N. 2016. Earth's surface water change over the past 30 years. *Nature Climate Change,* 6**,** 810-813.

DRAGONI, W. & SUKHIJA, B. 2008. Climate change and groundwater: a short review. *The Geological Society of London,* 288.

DRAVERT, P. A. 1930. *Mineralogy of Burabay area*, Zapadno Sib.geograph.obshestvo.

DUAN, Z. & BASTIAANSSEN, W. G. M. 2013. Estimating water volume variations in lakes and reservoirs from four operational satellite altimetry databases and satellite imagery data. *Remote Sensing of Environment,* 134**,** 403-416.

DUFRESNE, J.-L., FOUJOLS, M.-A., DENVIL, S., CAUBEL, A., MARTI, O., AUMONT, O., BALKANSKI, Y., BEKKI, S., BELLENGER, H., BENSHILA, R., BONY, S., BOPP, L., BRACONNOT, P., BROCKMANN, P., CADULE, P., CHERUY, F., CODRON, F., COZIC, A., CUGNET, D. & VUICHARD, N. 2013. Climate change projections using the IPSL-CM5 earth system model: from CMIP3 to CMIP5. *Climate Dynamics,* 40**,** 2123–2165.

DUNNE, J. P., JOHN, J. G., ADCROFT, A. J., GRIFFIES, S. M., HALLBERG, R. W., SHEVLIAKOVA, E., STOUFFER, R. J., COOKE, W., DUNNE, K. A., HARRISON, M. J., KRASTING, J. P., MALYSHEV, S. L., MILLY, P. C. D., PHILLIPPS, P. J., SENTMAN, L. T., SAMUELS, B. L., SPELMAN, M. J., WINTON, M., WITTENBERG, A. T. & ZADEH, N. 2012. GFDL's ESM2 Global Coupled Climate–Carbon Earth System Models. Part I: Physical Formulation and Baseline Simulation Characteristics. *Journal of Climate,* 25**,** 6646-6665.

ERIKSSON, B. 1983. Data ro¨rande Sverige nederbo¨rdsklimat normalva¨rden fo¨r perioden 1951–80. *SMHI Report 1983/3.* Norrko¨ping: Swedish Meteorological and Hydrological Institute.

FAN, J. A. G., I. 1996. *Local Polynomial Modelling and Its Applications: : From linear regression to nonlinear regression*, Chapman and Hall/CRC.

FENSKE, J. P., LEAKE, S. A. & PRUDIC, D. E. 1996. Documentation of a computer program (RES1) to simulate leakage from reservoirs using the modular finite-difference ground-water flow model (MODFLOW). *Open-File Report.* - ed.

FERGUSON, R. I. 1999. Snowmelt runoff models. *Progress in Physical Geography,* 33**,** 205-227.

FINCH, J. & CALVER, A. 2008. Methods for the quantification of evaporation from lakes. Oxford: World Meteorological Organizartion's Comissiom for Hydrology.

FINCH, J. W. & HALL, R. L. 2005. Evaporation from Lakes. *Encyclopedia of Hydrological Sciences.*

FRANKE, R. 1982. Scattered data interpolation:test of some methods. *Mathematics of Computation,* 38**,** 181-200.

FRAZIER, P. S. & PAGE, K. J. 2000. Water Body Detection and Delineation with Landsat TM Data. *Photogrammetric Engineering and Remote Sensing,* 66**,** 1461-1467.
FREEZE, R. A. & WITHERSPOON, P. A. 1966. Theoretical analysis of regional groundwater flow: 1. Analytical and numerical solutions to the mathematical model. *Water Resources Research,* 2**,** 641-656.
FREEZE, R. A. & WITHERSPOON, P. A. 1967. Theoretical analysis of regional groundwater flow: 2. Effect of water-table configuration and subsurface permeability variation. *Water Resources Research,* 3**,** 623-634.
FRICKO, O., HAVLIK, P., ROGELJ, J., KLIMONT, Z., GUSTI, M., JOHNSON, N., KOLP, P., STRUBEGGER, M., VALIN, H., AMANN, M., ERMOLIEVA, T., FORSELL, N., HERRERO, M., HEYES, C., KINDERMANN, G., KREY, V., MCCOLLUM, D. L., OBERSTEINER, M., PACHAURI, S., RAO, S., SCHMID, E., SCHOEPP, W. & RIAHI, K. 2017. The marker quantification of the Shared Socioeconomic Pathway 2: A middle-of-the-road scenario for the 21st century. *Global Environmental Change,* 42**,** 251-267.
FRIELER, K., LANGE, S., PIONTEK, F., REYER, C. P. O., SCHEWE, J., WARSZAWSKI, L., ZHAO, F., CHINI, L., DENVIL, S., EMANUEL, K., GEIGER, T., HALLADAY, K., HURTT, G., MENGEL, M., MURAKAMI, D., OSTBERG, S., POPP, A., RIVA, R., STEVANOVIC, M., SUZUKI, T., VOLKHOLZ, J., BURKE, E., CIAIS, P., EBI, K., EDDY, T. D., ELLIOTT, J., GALBRAITH, E., GOSLING, S. N., HATTERMANN, F., HICKLER, T., HINKEL, J., HOF, C., HUBER, V., JÄGERMEYR, J., KRYSANOVA, V., MARCÉ, R., MÜLLER SCHMIED, H., MOURATIADOU, I., PIERSON, D., TITTENSOR, D. P., VAUTARD, R., VAN VLIET, M., BIBER, M. F., BETTS, R. A., BODIRSKY, B. L., DERYNG, D., FROLKING, S., JONES, C. D., LOTZE, H. K., LOTZE-CAMPEN, H., SAHAJPAL, R., THONICKE, K., TIAN, H. & YAMAGATA, Y. 2017. Assessing the impacts of 1.5 °C global warming – simulation protocol of the Inter-Sectoral Impact Model Intercomparison Project (ISIMIP2b). *Geosci. Model Dev.,* 10**,** 4321-4345.
GANGOPADHYAYA, M., HARBECK, G., NORDENSON, T., OMAR, M. & URYVAYEV, V. 1966. Measurements and Estimation of Evaporation and Evapotranspiration. World Meteorological Organization.
GEOBYTE 2014. Report on Hydrogeologic survey for Schuchinsko-Borovskaya Kurortnaya Zona. GeoByte.
GERASIMOV, I. P. & MARKOV, K. K. 1939. *Glacial period on USSR territory*, Intitute of Geography.
GIBSON, J., BIRKS, S., YI, Y., MONCUR, M. & MCEACHERN, P. 2016. Stable isotope mass balance of fifty lakes in central Alberta: Assessing the role of water balance parameters in determining trophic status and lake level. *Journal of Hydrology: Regional Studies,* 6**,** 13-25.
GIBSON, J. & REID, R. 2014. Water balance along a chain of tundra lakes: A 20-year isotopic perspective. *Journal of Hydrology,* 519**,** 2148-2164.
GIBSON, J. J., PREPAS, E. E. & MCEACHERN, P. 2002. Quantitative comparison of lake throughflow, residency, and catchment runoff using stable isotopes: modelling and results from a regional survey of Boreal lakes. *Journal of Hydrology,* 262**,** 128-144.
GIBSON, J. J., YI, Y. & BIRKS, S. J. 2020. Watershed, climate, and stable isotope data (oxygen-18 and deuterium) for 50 boreal lakes in the oil sands region, northeastern Alberta, Canada, 2002–2017. *Data in Brief,* 29**,** 105308.
GILFEDDER, M., RASSAM, D. W., STENSON, M. P., JOLLY, I. D., WALKER, G. R. & LITTLEBOY, M. 2012. Incorporating land-use changes and surface–groundwater interactions in a simple catchment water yield model. *Environmental Modelling & Software,* 38**,** 62-73.
GLEICK, P. H. 1987. The development and testing of a water balance model for climate impact assessment: Modeling the Sacramento Basin. *Water Resources Research,* 23**,** 1049-1061.

GORSHENIN, K. P. 1927. *West Siberian soils of the chernozem zone,* Geographic Society, Zapiski Zapadnoi Sibiri.
GOUDIE, A. S. 2019. *Human Impact on the Natural Environment: Past, Present and Future,* Hoboken, NJ, USA, Wiley Blackwell.
GRAVE, M. K. 1970. What should be the level of the Caspian? : Izvestiya Akademii Nauk SSSR.
GUO, H., CHEN, S., BAO, A., HU, J., GEBREGIORGIS, A., XUE, X. & ZHANG, X. 2015. Inter-Comparison of High-Resolution Satellite Precipitation Products over Central Asia. *Remote Sens.,* 7**,** 7181-7211.
GURRIERI, J. T. & FURNISS, G. 2004. Estimation of groundwater exchange in alpine lakes using non-steady mass-balance methods. *Journal of Hydrology,* 297**,** 187-208.
HAGHIGHI, A. & KLOVE, B. 2015. A sensativity analysis of the water level response to chnages in climate and river regimes. *Limnologica,* 51**,** 118-130.
HAMBY, D. M. 1994. A review of techniques for parameter sensitivity analysis of environmental models. *Environmental Monitoring and Assessment,* 32**,** 135-154.
HARBECK, G. 1954. Water-loss investigations: Lake Hefner studies. Washinghton: U.S. Geological Survey Professional Paper 269.
HARRIS, A. R. 1994. Time Series Remote Sensing of Climatically Sensitive Lake. *Remote Sensing Environment,* 50**,** 83-94.
HARRIS, A. R., MASON, I. M., BIRKETT, C. M. & MANSLEY, J. A. 1992. Lake Remote Sensing for Global Climate Research. *European International Space Year Conference 1992: Space in the Service of the Changing Earth.* Munich.
HARSHBURGER, B. J., WALDEN, V.P., HUMES K.S., MOORE B.C., BLANDFORD, C.M, RANGO, A. 2012. Generation of Ensemble Streamflow Forecasts Using an Enhanced Version of the Snowmelt Runoff Model. *Water Resour. Resour Assoc.,* 48**,** 643-655.
HAVRIL, T., TÓTH, Á., MOLSON, J. W., GALSA, A. & MÁDL-SZŐNYI, J. 2018. Impacts of predicted climate change on groundwater flow systems: Can wetlands disappear due to recharge reduction? *Journal of Hydrology,* 563**,** 1169-1180.
HRACHOWITZ, M., SAVENIJE, H. H. G., BLÖSCHL, G., MCDONNELL, J. J., SIVAPALAN, M., POMEROY, J. W., ARHEIMER, B., BLUME, T., CLARK, M. P., EHRET, U., FENICIA, F., FREER, J. E., GELFAN, A., GUPTA, H. V., HUGHES, D. A., HUT, R. W., MONTANARI, A., PANDE, S., TETZLAFF, D., TROCH, P. A., UHLENBROOK, S., WAGENER, T., WINSEMIUS, H. C., WOODS, R. A., ZEHE, E. & CUDENNEC, C. 2013. A decade of Predictions in Ungauged Basins (PUB)—a review. *Hydrological Sciences Journal,* 58**,** 1198-1255.
HU, Z., ZHOU, Q., CHEN, X., QIAN, C., WANG, S. & LI, J. 2017. Variations and changes of annual precipitation in Central Asia over the last century. *International Journal of Climatology,* 37**,** 157-170.
HUANG, J., LI, Y., FU, C., CHEN, F., FU, Q., DAI, A., SHINODA, M., MA, Z., GUO, W., LI, Z., ZHANG, L., LIU, Y., YU, H., HE, Y., XIE, Y., GUAN, X., JI, M., LIN, L., WANG, S., YAN, H. & WANG, G. 2017. Dryland climate change: Recent progress and challenges. *Reviews of Geophysics,* 55**,** 719-778.
HUANG, W., CHEN, F., FENG, S., CHEN, J. & ZHANG, X. 2013. Interannual precipitation variations in the mid-latitude Asia and their association with large-scale atmospheric circulation *Chinese Science Bulletin,* 58**,** 3962-3968.
HUNTINGTON, T. G. 2006. Evidence for intensification of the global water cycle: Review and synthesis. *Journal of Hydrology,* 319**,** 83-95.
HURRELL, J. W. 1996. Influence of variations in extratropical wintertimeteleconnections on Northern Hemisphere temperatures. *Geogr Phys Research Letters,* 23**,** 665-668.

HURRELL, J. W. & LOON, V. 1997. Decadal variations in climateassociated with the North Atlantic Oscillation. *Climate Change,* 36**,** 301-326.
HUTCHINSON, G. E. 1957. *A treatise on limnology / G. Everlyn Hutchinson,* New York : London, New York : Wiley

London : Chapman & Hall.
HUYBERS, K., RUPPER, S. & ROE, G. H. 2016. Response of closed basin lakes to interannual climate variability. *Climate Dynamics,* 46**,** 3709-3723.
IPCC 2001. Climate Change 2001: The Scientific Basis. *In:* REPORT, W. G. C. T. T. I. T. A. (ed.).
IPCC, W. 2007. Climate change 2007: Contribution of Working Group I to the Fourth Assessment Report of the Intergovernmental Panel on Climate Change. *In:* SOLOMON, S., MANNING, M., CHEN, Z., MARQUIS, M., AVERYT, K. B., TIGNOR, M. & MILLER, H. L. (eds.). Cambridge, UK.
JACKSON, T. J. 2002. Remote sensing of soil moisture: implications for groundwater recharge. *Hydrogeology Journal,* 10**,** 40-51.
JIANG, T., CHEN, Y., XU, C.-Y., CHEN, X., CHEN, X. & SINGH, V. 2007. Comparison of Hydrological Impacts of Climate Change Simulated by Six Hydrological Models in the Dongjiang Basin, South China. *Journal of Hydrology,* 336**,** 316-333.
JOHANSSON, P.-O. 1987. Estimation of groundwater recharge in sandy till with two different methods using groundwater level fluctuations. *Journal of Hydrology,* 90**,** 183-198.
JONES, P. D. & MOBERG, A. 2003. Hemispheric and Large-Scale Surface Air Temperature Variations: An Extensive Revision and an Update to 2001. *Journal of Climate,* 16**,** 206-223.
KABIYEV, E. 1997. The laws of groundwater regime formation in the steppe zone of Northern Kazakhstan. *HYdrogeology***,** 27.
KALMA, J. D., MCVICAR, T. R. & MCCABE, M. F. 2008. Estimating Land Surface Evaporation: A Review of Methods Using Remotely Sensed Surface Temperature Data. *Surveys in Geophysics,* 29**,** 421-469.
KARL, T. R., GROISMAN, P. Y., KNIGHT, R. W. & HEIM, R. R. 1993. Recent variation of snow cover and snowfall in North America and their relation to precipitation and temperature variations. *J. Climate,* 6**,** 1327-1344.
KARNAUSKAS, R. J. & ANDERSON, M. P. 1978. Ground-Water Lake Relationships and Ground-Water Quality in the Sand Plain Province of Wisconsin—Nepco Lake. *Groundwater,* 16**,** 273-281.
KASSIN, N. G. 1931. *Short geologic description of North East Kazakhstan*, Tr. Vses. geolog-razv. ob'edinenie.
KATIRAIE-BOROUJERDY, P.-S., NASROLLAHI, N., HSU, K.-L. & SOROOSHIAN, S. 2013. Evaluation of satellite-based precipitation estimation over Iran. *Journal of Arid Environments,* 97**,** 205-219.
KAZHYDROMET 2006. Development of predictive models on the ecologic condition of Shuchinsk-Burabay resort territory. Almaty.
KAZHYDROMET 2007. Development of predictive models on the ecologic condition of Shuchinsk-Burabay resort territory. Final Report. Almaty.
KAZHYDROMET 2014. Conducting research to comprehensively address the issue of increasing volume (level) and water quality of lakes in Schuchinsk-Burabay resort territory. Almaty: KazHydrMet.
KEIJMAN, J. Q. 1974. The estimation of the energy balance of a lake from simple weather data. *Boundary-Layer Meteorology,* 7**,** 399-407.
KES, A. S., MAMEDOV, E. D., KHONDKARYAN, S. O. & TROFIMOV, G. N. 1993. Plains of Northern Central Asia during the Late Pleistocene and Holocene: stratigraphy and paleogeography. *In:* VELICHKO, A. A. (ed.) *Evolution of landscapes and climates of Northern Eurasia.* Moscow: Nauka.
KHAN, S., ADHIKARI, P., HONG, Y., VERGARA, H., ADLER, R., POLICELLI, F., IRWIN, D., T, K. & OKELLO, L. 2011. Hydroclimatology of Lake Victoria

region using hydrologic model and satellite remote sensing data. *Hydrology and Earth System Sciences,* 15.
KIRILENKO, S. I., ZHUKOV, Y.C., MITROFANOV, M.A. 2011. Report on groundwater exploitation in BNNP park, Northern Kazakhstan. Petropavlsk: Ministry of Geology and Ministry of Industry and Technologies of the Republic of Kazakhstan.
KITABATA, H., NISHIZAWA, K., YOSHIDA, Y. & MARUYAMA, K. 2006. Permafrost Thawing in Circum-Arctic and Highlands under Climatic Change Scenario Projected by Community Climate System Model (CCSM3). *SOLA,* 2**,** 53-56.
KITE, G. W. 1981. Recent changes in level of Lake Victoria. *Hydrological Sciences Journal,* 26**,** 233-243.
KIZZA, M., RODHE, A., XU, C.-Y. & NTALE, H. K. 2011. Modelling catchment inflows into Lake Victoria: uncertainties in rainfall–runoff modelling for the Nzoia River. *Hydrological Sciences Journal,* 56**,** 1210-1226.
KLUGE, T., VON ROHDEN, C., SONNTAG, P., LORENZ, S., WIESER, M., AESCHBACH-HERTIG, W. & ILMBERGER, J. 2012. Localising and quantifying groundwater inflow into lakes using high-precision 222Rn profiles. *Journal of Hydrology,* 450-451**,** 70-81.
KOHLER, M. A. & PARMELE, L. H. 1967. Generalized estimates of free-water evaporation. *Water Resources Research,* 3**,** 997-1005.
KONSHIN, V. D. 1951. Comperative analysis of sediment cores of Burabay lakes *Science Academy of the USSR,* 5**,** 81-95.
KORDE, N. V. 1951. The history of Burabay National Park lakes in Northern Kazakhstan. *The Laboratory of Sapropel Deposits of the Academy of Science of the USSR,* V.
KREMENETSKI, C. V., TARASOV, P.E., CHERKINSKY, A.E. 1997. Postglacial development of Kazakhstan pine forest. *Geogr Phys Quatern,* 51**,** 391-404.
KUTZBACH, J. 1980. Estimates of past climate at PaleoLake Chad, North Africa, based on a hydrological and energy balance model. *Quaternary Research,* 14**,** 210-233.
KUUSISTO, E. 1980. On the Values and Variability of Degree-Day Melting Factor in Finland. *Nordic Hydrology,* 11**,** 235-242.
KUZ'MIN, P. O. 1963. Snowcover and Snow Reserves *Gidrometeorologicheskoe Izdatel'stvo***,** 99-105.
LABAUGH, J., WINTER, T., ROSENBERRY, D., SCHUSTER, P., REDDY, M. & AIKEN, G. 1997. Hydrological and chemical estimates of the water balance of a closed-basin lake in north central Minnesota. *Water Resources Research - WATER RESOUR RES,* 33.
LAPTYEV, S. P. 1940. *Hydrology and hydrochemistry of Burabay*.
LAWRENCE, S. 2002. *Physical Hydrology,* Illinois, Waveland Press.
LEBEDYEV, P. N. 1928. *Short hydrogelogic description of Kazakhstan*, Mat. komissiya po eksp. issl.
LEGESSE, D., VALLET-COULOMB, C. & GASSE, F. 2004. Analysis of the hydrological response of a tropical terminal lake, Lake Abiyata (Main Ethiopian Rift Valley) to changes in climate and human activities. *Hydrological Processes,* 18**,** 487-504.
LEIRA, M. & CANTONATI, M. 2008. Effects of water-level fluctuations on lakes: An annotated bibliography. *Hydrobiologia,* 613**,** 171-184.
LENHART, T., ECKHARDT, K., FOHRER, N. & FREDE, H. G. 2002. Comparison of two different approaches of sensitivity analysis. *Physics and Chemistry of the Earth, Parts A/B/C,* 27**,** 645-654.
LHOMME, J. P. 1997. A THEORETICAL BASIS FOR THE PRIESTLEY-TAYLOR COEFFICIENT. *Boundary-Layer Meteorology,* 82**,** 179-191.
LI, X.-Y., XU, H.-Y., SUN, Y.-L., ZHANG, D.-S. & YANG, Z.-P. 2007. Lake-Level Change and Water Balance Analysis at Lake Qinghai, West China during Recent Decades. *Water Resources Management,* 21**,** 1505-1516.

LI, X. W. M. W. 2008. Snowmelt runoff modelling in an arid mountain watershed, Tarim Basin, China. *Hydrological processes,* 22**,** 3931-3940.
LI, Z., ZHU, Q. & GOLD, C. 2005. *Digital Terrain Modelling,* London, CRC Press.
LIANGLEI GU, Z. H., JIMIN YAO, GENHOU SUN 2017. Actual and Reference Evapotranspiration in a Cornfield in the Zhangye Oasis, Northwestern China. *Water,* 9.
LIEBE, J., VAN DE GIESEN, N. & ANDREINI, M. 2005. Estimation of small reservoir storage capacities in a semi-arid environment: A case study in the Upper East Region of Ghana. *Physics and Chemistry of the Earth, Parts A/B/C,* 30**,** 448-454.
LINACRE, E. T. 1993. Data sparse estimation of potential evaporation using a simplified Penman equation. *Agric. Forest Meteorol,* 64**,** 225-237.
LIOUBIMTSEVA, E. 2003. Arid Environments. *In:* SHAHGEDANOVA, M. (ed.) *Physical geography of Northern Eurasia.* Oxford: Oxford Press.
LIOUBIMTSEVA, E. 2014. Impact of Climate Change on the Aral Sea and Its Basin. *In:* MICKLIN, P. (ed.) *The Aral Sea.* Springler-Verlag Berlin Heidelberg: Springer Earth System Sciences.
LIOUBIMTSEVA, E., COLE, R., ADAMS, J. & KAPUSTIN, G. 2005. Impacts of climate and land-cover changes in arid lands of Central Asia. *Journal of Arid Environments,* 62**,** 285-308.
LIOUBIMTSEVA, E. & HENEBRY, G. 2009a. Climate and environmental change in arid Central Asia: Impacts, vulnerability, and adaptations. *Journal of Arid Environments 73* 73**,** 963-977.
LIOUBIMTSEVA, E. & HENEBRY, G. 2009b. Climate and environmental change in arid Central Asia: Impacts, vulnerability, and adaptations. *Journal of Arid Environments,* 73**,** 963-977.
LIU, H., CHEN, Y., YE, Z., LI, Y. & ZHANG, Q. 2019. Recent Lake Area Changes in Central Asia. *Scientific Reports,* 9**,** 16277.
LIU, Y., WU, C., JIA, R. & HUANG, J. 2018. An overview of the influence of atmospheric circulation on the climate in arid and semi-arid region of Central and East Asia. *Science China Earth Sciences,* 61**,** 1183-1194.
LIVINGSTONE, D. M. 1999. Ice break-up on southern Lake Baikal and its relationship to local and regional air temperatures in Siberia and to the North Atlantic Oscillation. *Limnology and Oceanography,* 44**,** 1486-1497.
LOVE, D., UHLENBROOK, S., CORZO-PEREZ, G., TWOMLOW, S. & VAN DER ZAAG, P. 2010. Rainfall–interception–evaporation–runoff relationships in a semi-arid catchment, northern Limpopo basin, Zimbabwe. *Hydrological Sciences Journal,* 55**,** 687-703.
MA, H. & CHENG, G. 2003. A test of Snowmelt Runoff Model (SRM) for the Gongnaisi River basin in the western Tianshan Mountains, China. *Chinese Science Bulletin,* 48**,** 2253-2259.
MACDONALD, R. J., BYRNE, J. M., BOON, S. & KIENZLE, S. W. 2012. Modelling the Potential Impacts of Climate Change on Snowpack in the North Saskatchewan River Watershed, Alberta. *Water Resources Management,* 26**,** 3053-3076.
MACKAY, A. W., RYVES, D. B., MORLEY, D. W., JEWSON, D. H. & RIOUAL, P. 2006. Assessing the vulnerability of endemic diatom species in Lake Baikal to predicted future climate change: a multivariate approach. *Global Change Biology,* 12**,** 2297-2315.
MALSY, M., AUS DER BEEK, T. & FLÖRKE, M. 2015. Evaluation of large-scale precipitation data sets for water resources modelling in Central Asia. *Environmental Earth Sciences,* 73**,** 787-799.
MANNING, B., MULLER, A., STARKE, M., MARKENSCHLAGER, C., MAO, W. Y. & ZHI, X. F. 2013. Dynamical downscaling of climate change in Central Asia. *Global and Planetary change,* 110**,** 26-39.
MARIOTTI, A. 2007. How ENSO impacts precipitation in southwest central Asia. *Geophysical Research,* 34.

MARTINEC, J. 1960. The degree-day factor for snowmelt runoff forecasting. IAHS: IUGG General Assembly of Helsinki, IAHS Commission of Surface Waters,.
MARTINEC, J. 1975. SNOWMELT - RUNOFF MODEL FOR STREAM FLOW FORECASTS. *Nordic Hydrology,* 6**,** 145-154.
MARTINEC, J., RANGO, A. AND ROBERTS, R. 1994. Snowmelt runoff model (SRM) user's manual. *In:* BAUMGARTNER, M. F. (ed.). Bern: Department of Geography, University of Bern.
MARTINEC, J., RANGO, A. AND ROBERTS, R. 2008. Snowmelt Runoff Model (SRM) User's Manual. *USDA Journada Experimental Range.* Las Cruces, USA: New Mexico State University.
MARTINEC, J. R., A. 1986. PARAMETER VALUES FOR SNOWMELT RUNOFF MODELLING. *Journal of Hydrology,* 84**,** 197-219.
MASON, I., HARRIS, A. R., BIRKETT, C. M., CUDLIP, W. & RAPLEY, C. 1991. Remote sensing of lakes for the proxy monitoring of climate change. *16th Ann. Conf. Remote Sensing Society.*
MASON, I., RAPLEY, C., STREET-PERROT, F. & GUZKOWSKA, M. 1985. ERS-1 Observation of Lakes for lakes for climate research. Starburg, May 1985, pp: Proc. EARSeL/ESA Symposium.
MASON, I. M., GUZKOWSKA, M. A. J., RAPLEY, C. G. & STREET-PERROTT, F. A. 1994. The response of lake levels and areas to climatic change. *Climatic Change,* 27**,** 161-197.
MASUDA, K., MORINAGA, Y., NUMAGUTI, A. & ABE-OUCHI, A. 1993. The annual extent of snow cover extent over the northern hemisphere as revealed by NOAA/NESDIS satellite data. *Geographical Reports.* Tokyo.
MASUI, T., MATSUMOTO, K., HIJIOKA, Y., KINOSHITA, T., NOZAWA, T., ISHIWATARI, S., KATO, E., SHUKLA, P. R., YAMAGATA, Y. & KAINUMA, M. 2011. An emission pathway for stabilization at 6 Wm−2 radiative forcing. *Climatic Change,* 109**,** 59.
MATHER, J. 1969. Average climatic water balance data of the continents. *Climatology* 19**,** 29-40.
MATSUYAMA, H. & KEZER, K. 2009. Long-term Variation of Precipitation around Lake Balkhash in Central Asia from the End of the 19th Century. *SOLA,* 5**,** 73-76.
MCBRIDE, M. & PFANNKUCH, H. 1975. Distribution of seepage within lakebeds. *U.S. Geological Survey Journal of Research,* 3**,** 505-512.
MCCALLUM, A. M., ANDERSEN, M. S., GIAMBASTIANI, B. M. S., KELLY, B. F. J. & IAN ACWORTH, R. 2013. River–aquifer interactions in a semi-arid environment stressed by groundwater abstraction. *Hydrological Processes,* 27**,** 1072-1085.
MCCAULEY, J. D. & ENGEL, B. A. 1997. Approximation of noisy bivariate traverse data for precision mapping. *Transactions of the American Society of Agricultural Engineers,* 40**,** 237-245.
MCDONALD, M. & HARBAUGH, W. 1988. *A Modular Three-Dimensional Finite-Difference Ground-Water Flow Model*, USGS.
MCFEETERS, S. K. 1996. The use of the Normalized Difference Water Index (NDWI) in the delineation of open water features. *International Journal of Remote Sensing,* 17**,** 1425-1432.
MCMAHON, T., PEEL, M., LOWE, L., SRIKANTHAN, R. & MCVICAR, T. 2012. Estimating actual, potential, reference crop and pan evaporation using standard meteorological data: a pragmatic synthesis. *Hydrology and Earth System Sciences Discussions,* 9**,** 11829-11910.
MCMAHON, T. A., PEEL, M. C., LOWE, L., SRIKANTHAN, R. & MCVICAR, T. R. 2013. Estimating actual, potential, reference crop and pan evaporation using standard meteorological data: a pragmatic synthesis. *Hydrol. Earth Syst. Sci.,* 17**,** 1331-1363.
MELESHKO, V. P. 2004. Anthropogenic climate change in Northern Eurasia in the 21st Century. *Russian Meteorol Hydrology Journal,* 7.

MERRITT, W. S., ALILA, Y., BARTON, M., TAYLOR, B., COHEN, S. & NEILSEN, D. 2006. Hydrologic response to scenarios of climate change in sub watersheds of Okanagan basin, British Columbia. *Journal of Hydrology,* 326**,** 79-108.

MICHAUD, J. D. & SOROOSHIAN, S. 1994. Effect of rainfall-sampling errors on simulations of desert flash floods. *Water Resources Research,* 30**,** 2765-2775.

MICKLIN, P. 1973. Dimensions of the Caspian Sea Problem. *Soviet Geography,* 13**,** 589-603.

MICKLIN, P. 1988. Dessication of the Aral Sea: A water management disaster in the Soviet Union. *Science,* 241**,** 1170-1176.

MICKLIN, P. 2007. The Aral Sea Disaster. *The annual Review of Earth and Planetary Sciences,* 35**,** 47-72.

MICKLIN, P. 2010. The past, present, and future Aral Sea. *Lakes & Reservoirs: Research and Management,* 2010**,** 193-213.

MINISTRY OF INDUSTRY AND NEW TECHNOLOGIES OF THE REPUBLIC OF KAZAKHSTAN 2014. System plan for the development of the resort area in Burabay. Astana: Ministry of Industry and New Technologies of the Republic of Kazakhstan.

MIRALLES, D., HOLMES, T., DE JEU, R., GASH, J., MEESTERS, A. & DOLMAN, H. 2010. Global land-surface evaporation estimated from satellite-based observations. *Hydrology and Earth System Sciences Discussions,* 7.

MITAS, L. & MITASOVA, H. 1999. Spatial interpolation. *In:* LONGLEY, P., GOODCHILD, M. F., MAGUIRE, D. J. & RHIND, D. W. (eds.) *Geographical Information Systems: Principles, Techniques, Management and Applications.* Wiley.

MORTON, F. I. 1983. Operational Estimates of Lake Evaporation *Journal of Hydrology,* 66**,** 77-100.

MOTE, P. W., HAMLET, A. F., CLARK, M. P. & LETTENMAIER, D. P. 2005. DECLINING MOUNTAIN SNOWPACK IN WESTERN NORTH AMERICA*. *Bulletin of the American Meteorological Society,* 86**,** 39-50.

MULETA, M. & NICKLOW, J. 2005. Sensitivity and Uncertainty Analysis Coupled With Automatic Calibration for a Distributed Watershed Model. *Journal of Hydrology,* 306**,** 127-145.

MURTAZIN, E. Z. 2005. Development of forecasting model of ecological situation of the Schuchinsk-Burabay resort zone. Kokshetau: KazHydroMet.

MYNENI, R., KNYAZIKHIN, Y. & PARK, T. 2015. OD15A2H MODIS/Terra Leaf Area Index/FPAR 8-Day L4 Global 500m SIN Grid V006 [Data set]. *In:* DAAC, N. E. L. P. (ed.).

NACHIAPPAN, R. M., KUMAR, B. & MANICKAVASAGAM, R. M. 2002. Estimation of subsurface components in the water balance of Lake Nainital (Kumaun Himalaya, India) using environmental isotopes. *Hydrological Sciences Journal,* 47**,** S41-S54.

NAKICENOVIC, N., ALCAMO, J., DAVIS, G. & VRIES, B. 2000. IPCC special report on emissions scenarios, IPCC special reports Cambridge, UK.

NATIONS, U. 2014. Revision of World Urbanization Prospects. Department of Economic and Social Affairs.

NEUWIRTH, F. 1973. Experiences with Evaporation Pans at a Shallow Steppe Lake in Austria. *Hydrology of Lakes, Helsinki Symposium.* International Association of Hydrological Sciences.

NG, G.-H. C., MCLAUGHLIN, D., ENTEKHABI, D. & SCANLON, B. R. 2010. Probabilistic analysis of the effects of climate change on groundwater recharge. *Water Resources Research,* 46.

NG, H. Y. F. & MARSALEK, J. 1992. Sensitivity of Streamflow Simulation to Changes in Climatic Inputs. *Hydrology Research,* 23**,** 257-272.

NIEDDA, M. & PIRASTRU, M. 2013. Hydrological processes of a closed catchment - lake system in a semi - arid Mediterranean environment. *Hydrological Processes,* 27.
NIELSON, G. 1993. Scattered data modeling. *Computer Graphics and Applications,* 13**,** 60-70.
NUGMANOVA, V., CHUNTONOVA, L., ZAKENAYEVA, O. 2013. Chronicle of Nature 2012. Burabay: Burabay National Nature Park Administration.
O'HARA, S. 2010. Central Asia's Water Resources: Contemporary and Future Management Issues. *International Journal of Water Resources Development* 16**,** 423-441.
OECD 2012. Global Environmental Outlook's Baseline Scenario. OECD Environment Directorate and the PBL Netherlands Environmental Assessment Agency.
OKI, T. & KANAE, S. 2006. Global Hydrological Cycles and World Water Resources. *Science,* 313**,** 1068.
PANAGIOTOPOULOS, F., SHAHGEDANOVA, M., HANNACHI, A. & D.B., S. 2005. Observed trends and teleconnections of the Siberian High: A recently declining center of action. *Journal of Climate,* 18**,** 1411-1422.
PENG, D., GUO, S., LIU, P. & LIU, T. 2006. Reservoir Storage Curve Estimation Based on Remote Sensing Data. *Journal of Hydrologic Engineering,* 11.
PENMAN, H. L. 1948. Natural evaporation from open water, bare soil and grass. *Proceedings of the Royal Society of London. Series A. Mathematical and Physical Sciences,* 193**,** 120-145.
PENMAN, H. L. 1956. Estimating evaporation. *Eos, Transactions American Geophysical Union,* 37**,** 43-50.
PENMAN, H. L. 1963. Vegetation and Hydrology. *Soil Science,* 96**,** 357.
PETERS, J. A. & LODGE, D. M. 2009. Littoral Zone. *In:* LIKENS, G. E. (ed.) *Encyclopedia of Inland Waters.* Oxford: Academic Press.
PETR, T. 1992. Lake Balkhash, Kazakhstan. *International Journal of Salt Lake Research,* 1**,** 21-46.
PHORSH, T. B. 1963. *Hydrochemical characteristics of lakes in Northern Kazakhstan,* Leningrad, AN USSR.
PHORSH, T. B. 1970. Inter-century fluctuations in water salinity and ionic composition of water in semiarid lakes. *Lakes of the Semiarid zone of the USSR. Inter-century fluctuation of lakes in Kazakhstan.* Leningrad: Nauka.
PILGRIM , D., CHAPMAN, T. & DORAN, D. 1988. Problems of rainfallrunoff modelling in arid and semiarid regions. *Hydrological Sciences Journal,* 33**,** 379-100.
POPOVA, V. 2007. Winter snow depth variability over northern Eurasia in relation to recent atmospheric circulation changes. *International Journal of Climatology,* 27**,** 1721-1733.
POSOKHOV, E. V. 1947. Characteristics of Maybalyk Lake. Alma-Ata: Nauka KazASSR.
POSOKHOV, E. V. 1955. *Saline lakes of Kazakhstan,* Leningrad, AN USSR.
POSTEL, S. 2000. Entering an era of water scarcity: The challenges ahead. *Ecological applications,* 10**,** 941-948.
POSTEL, S. & CARPENTER, S. 1997. Freshwater ecosystem service,. *Nature's services:societal dependence on natural ecosystems***,** 195-214.
PRIESTLEY, C. H. T., R.J. 1972. On the assessment of surface heat flux and evaporation using large scale parameters. *Mon. Weather Review,* 100**,** 81-92.
PROPASTIN, P. 2012. Patterns of Lake Balkhash water level changes and their climatic correlates during 1992-2010 period. *Lakes & Reservoirs: Research and Management,* 17**,** 161-169.
RÄISÄNEN, J. 2008. Warmer climate: less or more snow? *Climate Dynamics,* 30**,** 307-319.

RALEIGH, M. S., LANDRY, C. C., HAYASHI, M., QUINTON, W. L. & LUNDQUIST, J. D. 2013. Approximating snow surface temperature from standard temperature and humidity data: New possibilities for snow model and remote sensing evaluation. *Water Resources Research,* 49**,** 8053-8069.

RANDALL, D. & FICHEFET, T. Climate models and their evaluation. 2007.

RAY, S., MUKHERJEE, J. & MANDAL, S. 2015. Chapter 13 - Modelling nitrogen and carbon cycles in Hooghly estuary along with adjacent mangrove ecosystem. *In:* PARK, Y.-S., LEK, S., BAEHR, C. & JØRGENSEN, S. E. (eds.) *Developments in Environmental Modelling.* Elsevier.

RENKA, R. J. & CLINE, A. K. 1984. A triangle-based C^1 interpolation methos. *Rocky Mountain Journal of Mathematics,* 14**,** 223-237.

RHINALDO-LEE, M. B. & ANDERSON, M. P. 1980. High water levels in ground-water dominated lakes-- a case study from northwestern Wisconsin. *Ground Water.*

RICHTER, D. 1966. Results of Comparison Measurements Made with Floating Pans on Lake Stechlin. *Hydrology of Lakes and Reservoirs, Symposium of Garda.* International Association of Scientific Hydrology.

ROBINSON, D. A. & FREI, A. 2000. Seasonal Variability of Northern Hemisphere Snow Extent Using Visible Satellite Data. *The Professional Geographer,* 52**,** 307-315.

ROSENBERRY, D., WINTER, T. & LIKENS, G. 2007. Comparison of 15 Evaporation Methods Applied to a Small Mountain Lake in the Northeastern USA. *Journal of Hydrology,* 340**,** 149-166.

ROSENBERRY, D. O., STURROCK, A. & WINTER, T. 1993. Evaluation of the energy budget method of determining evaporation at William Lake, Minnesota, using alternative instrumentation and study approachs. *Water Resources Research,* 29**,** 2473-2483.

SAHARIA, A. M. & SARMA, A. K. 2018. Future climate change impact evaluation on hydrologic processes in the Bharalu and Basistha basins using SWAT model. *Natural Hazards,* 92**,** 1463-1488.

SAHOO, G. B., SCHLADOW, S. G., REUTER, J. E., COATS, R., DETTINGER, M., RIVERSON, J., WOLFE, B. & COSTA-CABRAL, M. 2013. The response of Lake Tahoe to climate change. *Climatic Change,* 116**,** 71-95.

SALTELLI, A. & ANNONI, P. 2010. How to avoid a perfunctory sensitivity analysis. *Environmental Modelling & Software,* 25**,** 1508-1517.

SALTELLI, A., ANNONI, P., AZZINI, I., CAMPOLONGO, F., RATTO, M. & TARANTOLA, S. 2010. Variance based sensitivity analysis of model output. Design and estimator for the total sensitivity index. *Computer Physics Communications,* 181**,** 259-270.

SAVVAITOVA, K. & PETR, T. 1992. Lake Issyk-kul, Kirgizia. *International Journal of Salt Lake Research,* 1**,** 21-46.

SCHAAKE, J. & LIU, C. Development and application of simple water balance models to understand the relationship between climate and water resources. New Directions for Surface Water Modeling Proceedings of the Baltimore Symposium, 1989.

SCHELLNHUBER, H. J., FRIELER, K. & KABAT, P. 2014. The elephant, the blind, and the intersectoral intercomparison of climate impacts. *Proceedings of the National Academy of Sciences of the United States of America,* 111**,** 3225-3227.

SEMENOV, V. A. 1990. *Arid rivers discharge,* Moscow, Gydrometeoizdatelstvo.

SETEGN, S., SRINIVASAN, R. & DARGAHI, B. 2008. Hydrological Modelling in the Lake Tana Basin, Ethiopia Using SWAT Model *The Open Hydrology Journal,* 2**,** 49-62.

SHAW, R. D. & PREPAS, E. E. 1990. Groundwater-lake interactions: II. Nearshore seepage patterns and the contribution of ground water to lakes in central Alberta. *Journal of Hydrology,* 119**,** 121-136.

SHI, Y., SHEN, Y., KANG, E., LI, D., DING, Y., ZHANG, G. & HU, R. 2007. Recent and Future Climate Change in Northwest China. *Climatic Change,* 80**,** 379-393.
SHIMARAEV, M. N., L.N., K. & V.N., S. 2002. Manifestation of global climatic change in Lake Baikal during the 20th century. *Doklady Earth Sciences* 383A**,** 288-291.
SHNITNIKOV, A. 1957. Variability of the general humidity of the continents of the Nortern Hemisphere. *Notes of geographic society.* Leningrad: Nauka.
SHNITNIKOV, A. 1970a. *Semi Arid Lakes of USSR,* Leningrad, USSR, USSR Reseach Academy.
SHNITNIKOV, A. 1973. Water balance variability of lakes Aral, Balkhash, Issyk-Kul and Chany. *Hydrology of Lakes,* 109**,** 130-140.
SHNITNIKOV, A. V. 1970b. Vliyanie vnitrivekovoi izmenchivosti uvlazhnennosti basseinov ozer na razvitie ix depresii. *In:* SHNITNIKOV, A. V. (ed.) *Ozera semiaridnoi SSSR.* Leningrad: Nauka.
SHUTER, B. 2012. The role of winter phenology in shaping the ecology of freshwater fish and their sensitivities to climate change. *Aquatic sciences,* v. 74**,** pp. 637-657-2012 v.74 no.4.
SHUTER, B. M., C. FUNG, S. 2013. Empirical models for forecasting changes in the phenology of ice cover for Canadian lakes. *Canadian Journal of Fisheries and Aquatic Sciences,* 70**,** 982-991.
SHUTTLEWORTH, W. J. 1993. Evaporation. *In:* MAIDMENT, D. R. (ed.) *Handbook of Hydrology.* New York: McGraw-Hill.
SILJEG, A., LOZIC, S. & SILJEG, S. 2015. A comparison of interplation methods on the basis of data obtained from bathymetric survey of Lake Vrana, Crotia. *Hydrology and Earth System Science,* 19**,** 3653-3666.
SIMA, S. & TAJRISHY, M. 2013. Using satellite data to extract volume–area–elevation relationships for Urmia Lake, Iran. *Journal of Great Lakes Research,* 39**,** 90-99.
SKRZYPEK, G., MYDŁOWSKI, A., DOGRAMACI, S., HEDLEY, P., GIBSON, J. J. & GRIERSON, P. F. 2015. Estimation of evaporative loss based on the stable isotope composition of water using Hydrocalculator. *Journal of Hydrology,* 523**,** 781-789.
SMALL, E. E., GIORGI, F., SLOAN, L. C. & HOSTETLER, S. 2001. The Effects of Desiccation and Climatic Change on the Hydrology of the Aral Sea. *Journal of Climate,* 14**,** 300-322.
SONG, C., HUANG, B., KE, L. & RICHARDS, K. S. 2014. Seasonal and abrupt changes in the water level of closed lakes on the Tibetan Plateau and implications for climate impacts. *Journal of Hydrology,* 514**,** 131-144.
SONG, X., ZHANG, J., ZHAN, C., XUAN, Y., YE, M. & XU, C. 2015. Global sensitivity analysis in hydrological modeling: Review of concepts, methods, theoretical framework, and applications. *Journal of Hydrology,* 523**,** 739-757.
SONG, X. D. & ZHENG, J. X. 2012. Comparison of artificial neural networks and support vector machine classifiers for land cover classification in Northern China using a SPOT-5 HRG image. *International Journal of Remote Sensing,* 33**,** 3301-3320.
STEWART, I. T., CAYAN, D. R. & DETTINGER, M. D. 2005a. Changes toward Earlier Streamflow Timing across Western North America. *Journal of Climate,* 18**,** 1136-1155.
STEWART, I. T., CAYAN, D. R. & M.D., D. 2005b. Changes toward Earlier Streamflow Timing across Western North America. *Journal of Climate,* 18**,** 1136-1155.
STIGTER, E. E., WANDERS, N., SALORANTA, T. M., SHEA, J. M., BIERKENS, M. F. P. & IMMERZEEL, W. W. 2017. Assimilation of snow cover and snow depth into a snow model to estimate snow water equivalent and snowmelt runoff in a Himalayan catchment. *The Cryosphere,* 11**,** 1647-1664.

STRASSER, U., BERNHARDT, M., WEBER, M., LISTON, G. E. & MAUSER, W. 2008. Is snow sublimation important in the alpine water balance? *The Cryosphere,* 2**,** 53-66.
STREET-PERROT, F. & HARRIS, A. R. 1985. Lake levels and climate reconstruction, in Paleoclimate Analysis and Modelling. *Wiley***,** 291-340.
SU, Z. 2002. The Surface Energy Balance System (SEBS) for estimation of turbulent heat fluxes. *Hydrol. Earth Syst. Sci.,* 6**,** 85-100.
SUN, Q., MIAO, C., DUAN, Q., ASHOURI, H., SOROOSHIAN, S. & HSU, K.-L. 2018. A Review of Global Precipitation Data Sets: Data Sources, Estimation, and Intercomparisons. *Reviews of Geophysics,* 56**,** 79-107.
SUTANUDJAJA, E. H., VAN BEEK, L. P. H., DE JONG, S. M., VAN GEER, F. C. & BIERKENS, M. F. P. 2014. Calibrating a large-extent high-resolution coupled groundwater-land surface model using soil moisture and discharge data. *Water Resources Research,* 50**,** 687-705.
SZESZTAY, K. 1974. Water balance and water level fluctuations of lakes. *Hydrological Science Bulletin,* 19**,** 73-84.
TAIT, A. & ZHENG, X. 2007. Analysis of the spatial interpolation error associated with maps of median annual climate variables. *NIWA, Wellington*.
TAN, C., GUO, B., KUANG, H., YANG, H. & MA, M. 2018. Lake Area Changes and Their Influence on Factors in Arid and Semi-Arid Regions along the Silk Road. *Remote Sens.,* 10.
TAN, Q. & XU, X. 2014. Comparative Analysis of Spatial Interpolation Methods: an Experimental Study. *Sensors & Transducers,* 165**,** 155-163.
TARASOV, P. E. 1996. Lake status records from the former Soviet Union and Mongolia: documentation of the second version of the database. *Paleoclimatology Publications Series Report #5.* World Data Center -A for Paleoclimatology.
TEGEGNE, G., KIM, Y.-O., SEO, S. B. & KIM, Y. 2019. Hydrological modelling uncertainty analysis for different flow quantiles: a case study in two hydro-geographically different watersheds. *Hydrological Sciences Journal,* 64**,** 473-489.
TETZLAFF, G. & ADAMS, J. 1983. Present-Day and Early-Holocene Evaporation of Lake Chad. *In:* STREET-PERROTT, A., BERAN, M. & RATCLIFFE, R. (eds.) *Variation in the Global Water Budget.* Dordrecht: Springler.
THORNTHWAITE, C. W. 1948. An Approach toward a Rational Classification of Climate. *Geographical Review,* 38**,** 55-94.
TIAN, Y., ZHENG, Y., WU, B., WU, X., LIU, J. & ZHENG, C. 2015. Modeling surface water-groundwater interaction in arid and semi-arid regions with intensive agriculture. *Environmental Modelling & Software,* 63**,** 170-184.
TODD, M. C. & MACKAY, A. W. 2003. Large-Scale Climatic Controls on Lake Baikal Ice Cover. *Journal of Climate,* 16**,** 3186-3199.
TRABUCCO, A. & ZOMER, R. 2018. Global Aridity Index and Potential Evapo-Transpiration (ET0) Climate Database v2. CGIARCSI.
TSEEB, J. J. 1940. *Undersatnding lakes in Northern Kazakhstan and fisheris*, Uch. zap. Orlovsk.gos.pedad. inst.
UNESCO 1974. Survey on water balance of lakes and reservoirs of the world. Paris, France: UNESCO.
URYVAYEV, V. 1959. Surface water resources of virgin lands. Kokshetau region of Kazakh SSR. Leningrad.
USPENSKIJ, A. P. 1930. Chemical water analysis of six lakes in Burabay area. Omsk: VGO department.
USPENSKIJ, A. P. 1948. Water salinity fluctuation in Burabay lakes over 10 years. Omsk: VGO department.
VAINU, M. & TERASMAA, J. 2014. Changes in climate, catchment vegetation and hydrogeology as the causes of dramatic lake-level fluctuations in the Kurtna Lake District, NE Estonia. *Estonian Journal of Earth Sciences,* 63**,** 45-61.

VALIANTZAS, J. D. 2006. Simplified versions for the Penman evaporation equation using routine weather data. *Journal of Hydrology,* 331**,** 690-702.
VALIANTZAS, J. D. 2013. Simplified forms for the standardized FAO-56 Penman–Monteith reference evapotranspiration using limited weather data. *Journal of Hydrology,* 505**,** 13-23.
VAN DER CAMP, G., HAYASHI, M. & GALLEN, D. 2002. Comparing the hydrology of grassed and cultivated catchments in the semi-arid Canadian prairies. *HYDROLOGICAL PROCESSES,* 17**,** 559-575.
VAN DER KAMP, G., KEIR, D. & EVANS, M. 2008. Long-term water changes in closed-basin lakes of the Canadian Prairies. *Canadian Water Resources Journal,* 33**,** 23-38.
VARDAVAS, I. & FOUNTOULAKIS, A. 1996. Estimation of lake evaporation from standard meteorological measurements: Application to four Australian lakes in different climatic regions. *Ecological Modelling,* 84**,** 139-150.
VARRIS, O. 2014. Curb vast water use in central Asia. *Nature's services:societal dependence on natural ecosystems,* 514**,** 27-29.
VASIL'EV, O., SAVKIN, V. & SAPRYKINA, Y. 2006. Analysis of water level fluctuations in Lake Chany. *Doklady Earth Sciences - DOKL EARTH SCI,* 407**,** 446-449.
VEMURI, V., DRACUP, J. A., ERDMANN, R. C. & VEMURI, N. 1969. Sensitivity analysis method of system identification and its potential in hydrologic research. *Water Resources Research,* 5**,** 341-349.
VOLLSET, S. E., GOREN, E., YUAN, C.-W., CAO, J., SMITH, A. E., HSIAO, T., BISIGNANO, C., AZHAR, G. S., CASTRO, E., CHALEK, J., DOLGERT, A. J., FRANK, T., FUKUTAKI, K., HAY, S. I., LOZANO, R., MOKDAD, A. H., NANDAKUMAR, V., PIERCE, M., PLETCHER, M., ROBALIK, T., STEUBEN, K. M., WUNROW, H. Y., ZLAVOG, B. S. & MURRAY, C. J. L. 2020. Fertility, mortality, migration, and population scenarios for 195 countries and territories from 2017 to 2100: a forecasting analysis for the Global Burden of Disease Study. *The Lancet,* 396**,** 1285-1306.
VUUREN, D., STEHFEST, E., ELZEN, M., KRAM, T., VLIET, J., DEETMAN, S., ISAAC, M., KLEIN GOLDEWIJK, K., HOF, A., MENDOZA BELTRAN, A., OOSTENRIJK, R. & VAN RUIJVEN, B. 2011. RCP2.6: Exploring the possibility to keep global mean temperature increase below 2°C. *Climatic Change,* 109**,** 95-116.
WALE, A., RIENTJES, T. H. M., GIESKE, A. S. M. & GETACHEW, H. A. 2009. Ungauged catchment contributions to Lake Tana's water balance. *Hydrological Processes,* 23**,** 3682-3693.
WANG, H. 2001. The weakening of the Asian monsoon circulation after the end of 1970's. *Advances in Atmospheric Sciences,* 18**,** 376-386.
WANG, J., CHEN, F., JIN, L. & BAI, H. 2010. Characteristics of the dry/wet trend over arid central Asia over the past 100 years. *Climate Research,* 41**,** 51-59.
WANG, X., WANG, J., CHE, T., HUANG, X., HAO, X. & LI, H. 2018. Snow Cover Mapping for Complex Mountainous Forested Environments Based on a Multi-Index Technique. *IEEE Journal of Selected Topics in Applied Earth Observations and Remote Sensing,* PP**,** 1-9.
WARMAP. Water resources management and agricultural production in the Central Asian Republics. Water resources management in Central Asia, 1996 Tashkent.
WATSON, D. F. 1992. *Contouring: a guide to the analysis and display of spatial data.*, Oxford.
WHEATER, H., SOROOSHIAN, S. & SHARMA, K. D. 2007. *Hydrological modelling in arid and semi-arid areas*.
WINTER, T. 1981. Uncertainties in estimating the water balance of lakes. *Water Resources Bulletin,* 17**,** 82-115.

WINTER, T., ROSENBERRY, D. O. & STURROCK, A. 1995. Evaluation of 11 equations for determining evaporation for small lakes in the north central United States. *Water Resources Research,* 31**,** 983-993.
WINTER, T. C. 1978a. Ground-water component of lake water and nutrient budgets. *SIL Proceedings, 1922-2010,* 20**,** 438-444.
WINTER, T. C. 1978b. Numerical simulation of steady state three-dimensional groundwater flow near lakes. *Water Resources Research,* 14**,** 245-254.
WINTER, T. C., BUSO, D. C., ROSENBERRY, D. O., LIKENS, G. E., STURROCK, A. J. M. & MAU, D. P. 2003. Evaporation determined by the energy-budget method for Mirror Lake, New Hampshire. *Limnology and Oceanography,* 48**,** 995-1009.
XIONG, J., WU, B., YAN, N., ZENG, Y. & LIU, S. 2010. Estimation and Validation of Land Surface Evaporation Using Remote Sensing and Meteorological Data in North China. *IEEE Journal of Selected Topics in Applied Earth Observations and Remote Sensing,* 3**,** 337-344.
XU, C.-Y., TUNEMAR, L., CHEN, Y. D. & SINGH, V. P. 2006. Evaluation of seasonal and spatial variations of lumped water balance model sensitivity to precipitation data errors. *Journal of Hydrology,* 324**,** 80-93.
XU, H. 2006. Modification of normalised difference water index (NDWI) to enhance open water features in remotely sensed imagery. *International Journal of Remote Sensing,* 27**,** 3025-3033.
YANG, X., WANG, N., CHEN, A. A., HE, J., HUA, T. & QIE, Y. 2020. Changes in area and water volume of the Aral Sea in the arid Central Asia over the period of 1960–2018 and their causes. *CATENA,* 191**,** 104566.
YAPIYEV, V., SAGINTAYEV, Z., VERHOEF, A., KASSYMBEKOVA, A., BAIGALIYEVA, M., ZHUMABAYEV, D., MALGAZHDAR, D., ABUDANASH, D., ONGDAS, N. & JUMASSULTANOVA, S. 2017. The changing water cycle: Burabay National Nature Park, Northern Kazakhstan. *WIREs Water,* 4**,** e1227.
YE, H. 2001. Quasi-Biennial and Quasi-Decadal Variations in Snow Accumulation over Northern Eurasia and Their Connections to the Atlantic and Pacific Oceans. *Journal of Climate,* 14**,** 4573-4584.
YE, H., CHO, H. R. & P.E., G. 1998. The Changes in Russian Winter Snow Accumulation during 1936-83 and Its Spatial Patterns. *Journal of Climate,* 11**,** 856-863.
YE, H. & MATHER, J. 1997. Polar snow cover changes and global warming. *International Journal of Climatology,* 17**,** 163-173.
YIHDEGO, Y. & KHALIL, A. 2017. Groundwater Resources Assessment and Impact Analysis Using a Conceptual Water Balance Model and Time Series Data Analysis: Case of Decision Making Tool. *Hydrology,* 4**,** 25.
ZEMLYANICYNA, L. A. 1970. Groundwater of lakes located in Ishim-Irtysh *Lakes of Semi-Arid Lakes in the USSR.* Leningrad: Nauka.
ZHANG, F., TIYIP, T., JOHNSON, V. C., KUNG, H., DING, J., ZHOU, M., FAN, Y., KELIMU, A. & NURMUHAMMAT, I. 2015. Evaluation of land desertification from 1990 to 2010 and its causes in Ebinur Lake region, Xinjiang China. *Environmental Earth Sciences,* 73**,** 5731-5745.
ZHANG, G., XIE, H., YAO, T., LI, H., D., S. 2014. Quantitative water resources assessment of Qinghai Lake basin using Snowmelt Runoff Mode. *Journal of Hydrology,* 519**,** 976-987.
ZHANG, J., XU, K., YANG, Y., QI, L., HAYASHI, S. & WATANABE, M. 2006. Measuring Water Storage Fluctuations in Lake Dongting, China, by Topex/Poseidon Satellite Altimetry. *Environmental Monitoring and Assessment,* 115**,** 23-37.
ZHANG, Q., LIU, J., SINGH, V. P., GU, X. & CHEN, X. 2016. Evaluation of impacts of climate change and human activities on streamflow in the Poyang Lake basin, China. *Hydrological Processes,* 30**,** 2562-2576.
ZHANG, X., HARVEY, K., W., H. & T., Y. 2001. Trends in Canadian Streamflow

Water Resources Research, 37**,** 987-998.
ZHOU, Y. & LI, W. 2011. A review of regional groundwater flow modeling. *Geoscience Frontiers,* 2**,** 205-214.

Appendix A – Water balance calculation spreadsheet

Excel spreadsheet example of the estimation of water balance parameters for 1986

Water balance estimations for 1986																		
month	Observed			ΔV	t	Input						Output					G_i-G_o (i) (10^6 m^3)	G_i-G_o (ii) (10^6 m^3)
	Lake level (m)	V (10^6 m^3)	A_L km^2			P (mm)	P_{rain} (10^6 m^3)	P_{snow} (mm)	P_{snow} (mil m^3)	SWE	Q_{snow}	E_{sub} (mm)	E_{sub} (10^6 m^3)	E_O (mm)	E_O (10^6 m^3)	Q_{abs}		
January	389.5	231.7	17.32		-12.9	20		20	0.4	170		2.5	0.0				0	
February	389.6	231.4	17.33	-0.30	-17.4	5		5	0.1	159		2.2	0.0				0	
March	389.9	232.1	17.33	0.64	-9.4	10		10	0.2	136		3.6	0.1					
April	389.6	232.2	17.34	0.11	5.1	5		5	0.1	71	2.3							
May	389.6	234.5	17.39	2.39	10	34	0.6							83	1.4			
June	389.6	233.7	17.37	-0.85	14.2	38	0.7							152	2.6			
July	389.6	231.7	17.32	-1.98	17.9	65	1.1							167	2.9			
August	389.6	229.9	17.28	-1.77	15.5	41	0.7							100	1.7			
September	389.5	228.9	17.26	-1.02	9.9	13	0.2							70	1.2			
October	389.4	227.9	17.24	-0.98	1.6	20	0.3							11	0.2			
November	389.4	228.1	17.24	0.16	-8.1	15		15	0.3	6		3.5	0.1				-0.51	
December	389.3	228.3	17.25	0.20	-17.2	12		12	0.2	28		2.5	0.0				-0.34	ΔV_{level}
						278	3.7	67	1.2		2.3	14	0.2	583	10.1	-		-3.35
						7.1						10.3					-0.85	-0.12
Total						ΔV≈-3.2											-4.1	-3.4

Appendix B – Evaporation modelling

Radiation computation

Extraterrestrial radiation (R_A)

Extraterrestrial radiation, Ra, is an input parameter required to estimate solar radiation as well as the parameter which is needed for the Penman equation (Penman, 1963), FAO-56 Penman-Monteith (Allen, 1998) and their simplified versions developed by Valiantzas (Valiantzas, 2006, Valiantzas, 2013).

Solar radiation received at the top of the earth's atmosphere on a horizontal surface is expressed as extraterrestrial radiation (R_A). It will change during the day and will be different at different latitudes and different seasons. As seasons change, the position of the sun, the length of the day and, hence Ra change as well.

For daily estimation of evaporation, it is necessary to calculate the daily value of these parameters. For this purpose, formulas from the widely recognised and considered as "standardised" - FAO-56 guidelines for computing crop water requirements for evaporation evaluation (Allen, 1998) were used, which represent more complex calculations of every input parameter separately on a daily basis.

$$R_A = \frac{24(60)}{\pi} G_{SC} d_r [\omega_S \sin(\varphi)\sin(\delta) + \cos(\varphi)\cos(\delta)\sin(\omega_s)] \quad \text{A.1}$$

where:

R_A - Extraterrestrial radiation in the hour (MJ m^{-2} day^{-1}),

G_{SC} - Solar constant, which is equivalent to 0.820 MJ m^{-2} min,

d_r - Inverse relative distance Earth-Sun,

w_s - Sunset hour angle,

φ - Latitude in radians,

$$J = Int(30.4 * M - 15) \quad \text{A.2}$$

where:

J - Julian days, where M-month (January=1)

$$\delta = 0.409 \sin(\frac{2\pi}{365} J - 1.39) \quad \text{A.3}$$

$$d_r = 1 + 0.033 \cos(\frac{2\pi}{365} J) \quad \text{A.4}$$

$$\omega_S = \frac{\pi}{2} - arctan\left[\frac{-\tan(\varphi)\tan(\delta)}{1-(\tan(\varphi)^2\tan(\delta)^2}\right] \quad \text{A.5}$$

$$N = \frac{24}{\pi}\omega_s \quad \text{A.6}$$

where:

δ - Solar decimation (eq.4a);

N - Maximum possible daylight hours.

Solar radiation (R_S)

According to FAO-56 guidelines (Allen, 1998) for daily evaporation estimation, if solar radiation (R_s) is not available it can be estimated using Angstrom equation which relates solar radiation to extraterrestrial radiation and relative sunshine duration expressed as:

$$R_S = \left(a_s + b_S\frac{n}{N}\right)R_A \quad \text{A.7}$$

where:

R_S- Solar radiation (MJ m day^{-1});

n - Measured sunshine duration per day (hours);

n/N - Relative sunshine duration;

a_S - Regression constant, expressing the function of extraterrestrial radiation reaching the earth on overcast days;

$a_S + b_S$ - Fraction of extraterrestrial radiation the earth on clear days (n=N).

FAO-56 guidelines suggest where no actual solar radiation data is available and no calibration has been accomplished, it is recommended to use values for a_S=0.25 and b_S=0.5 (Allen, 1998).

Relative shortwave radiation or $\frac{R_S}{R_{so}}$

The relative shortwave radiation is the ratio of solar radiation (RS) to the clear-sky solar radiation (Rso). Here, Rs is the solar radiation that actually reaches the earth's surface in a given period, while R_{so} is the solar radiation that would reach the same surface during the same period but under cloudless sky conditions.

The relative shortwave radiation is the ratio to express the cloudiness of the atmosphere, where cloudiness would result in a smaller ratio. As the net radiation (R_n) has never been measured directly in Shortandy, it was estimated by computing the relative shortwave radiation, which is required to determine the net longwave radiation. Consequently, the relative shortwave radiation could be computed through the following equation:

$$R_{so} = [0.75 + 2(Altitude)/100000]R_A$$

A.8

where:

R_{so} - clear-sky solar radiation, (MJ m^{-2} day^{-1})

Net solar radiation (R_{ns})

The R_{ns} is the fraction of the solar radiation that not reflected from the surface. This function for grass evapotranspiration could be obtained by following empirical expression:

$$R_{ns} = (1 - \alpha)R_s$$

A.9

where:

R_{ns} - Net solar radiation, (MJ $m^{-2}day^{-1}$);

α - Albedo or canopy reflection, which is equal to 0.23.

Net longwave radiation (R_{nl})

Net longwave radiation is the difference between incoming and outgoing longwave radiation. This relation is expressed by the Stefan-Boltzmann law. Due to the importance of humidity and cloudiness, the Stefan-Boltzmann law is corrected by these two factors (Allen, 1998). It can be estimated by the following equation:

$$R_{nl} = (\sigma T_{max} + \sigma T_{min})/2(0.34 - 0.14\sqrt{e_a})(1.35\frac{R_s}{R_{so}} - 0.35)$$

A.10

where:

R_{nl} - Net outgoing longwave radiation, (MJ m^{-2} day^{-1});

σ - Stefan-Boltzmann constant, 4.903 10^{-9}MJ $K^{-4}m^{-2}day^{-1}$;

T_{max} - Daily maximum air temperature expressed K;

T_{min} - Daily minimum air temperature expressed K;

e_s - Actual vapour pressure, (kPa);

$\frac{R_s}{R_{so}}$ - Relative shortwave radiation.

Net radiation (R_n)

Net radiation is the difference between incoming and outgoing radiation of both short and long wavelengths. It shows the balance between the energy absorbed, reflected and emitted by the surface. As a result, it could be estimated as follows:

$$R_n = R_{ns} - R_{nl}$$

A.11

Wind speed

Both simplified version of the classic Penman equation (Penman, 1948) and FAO-56 Penman-Monteith require wind speed measured at 2m above the surface. The wind speed sensor in Shortandy weather station is installed 10m above the ground. Wind speed records needed to adjust to the standard height of 2m. The following wind speed adjustment was estimated based on Allen (1998) equation which is described as follow:

$$u_2 = u_z \frac{4.87}{In(67.8z - 5.42)}$$

A.12

Where:

u_2 wind speed at 2m above ground surface (m s^{-1});

u_z wind speed at z above ground surface (m s^{-1});

z height of measurement above ground surface (m)

Air humidity

The energy from the sun and the surrounding air is the main force for vaporisation

The saturation vapour pressure is the pressure of vapour when it is in equilibrium with the liquid phase. It is entirely dependent on the temperature vaporisation of water, the change between the water vapour pressure at the evapo-transpiring surface and the encompassing air is the controlling component for the vapour replacement. Well-watered fields in hot, dry arid areas consume a large amount of water because of the abundance of energy and the drying up influence of the air. The daily actual vapour pressure, e_a is required. The actual vapour can be derived from maximum and minimum.

Mean saturation vapour pressure (e_s)

The saturation vapour pressure is related to air temperature. It can be estimated from the air temperature. The following relationship is described as follows:

$$e_S = \frac{e°(T_{max}) + e°(T_{min})}{2}$$

A.13

here:

$$e°(T_{max}) = 0.6108exp\left[\frac{17.27T_{max}}{T_{max} + 237.3}\right]$$

A.14

$$e^{\circ}(T_{min}) = 0.6108exp\left[\frac{17.27T_{min}}{T_{min} + 237.3}\right]$$

A.15

Actual vapour pressure (e_a)

Actual vapour pressure is a measurement of the amount of water vapour in a volume of air and increases as the amount of water vapour increases. It could be derived from dew point temperature:

$$e_a = 0.6108exp\left[\frac{17.27T_{dew}}{T_{dew} + 237.3}\right]$$

A.16

Appendix C – Snow sublimation modelling

Total monthly and total seasonal snow sublimation in mm from Shortandy Lake surface during the cold season from 1986 to 2015

Year	***Jan***	***Feb***	***Mar***	***Nov***	***Dec***	***Total***
1986	2.5	2.2	3.6	3.5	2.5	*14.3*
1987	2.5	3.2	4.7	2.4	3.6	*16.4*
1988	1.4	3.5	9.8	7.7	3.6	*26.0*
1989	2.5	2.2	10.1	4.5	3.6	*22.9*
1990	1.4	2.2	5.7	5.6	2.5	*17.4*
1991	2.5	2.2	3.6	7.7	2.5	*18.5*
1992	3.6	3.2	5.7	7.7	2.5	*22.7*
1993	3.6	3.2	5.7	2.4	1.4	*16.3*
1994	2.5	1.3	5.7	6.6	2.5	*18.6*
1995	2.5	3.2	9.0	8.7	1.4	*24.8*
1996	0.3	1.3	3.6	5.6	2.5	*13.3*
1997	1.4	2.2	6.8	4.5	2.5	*17.4*
1998	2.5	0.3	7.9	7.7	3.6	*22.0*
1999	2.5	5.2	4.7	6.6	4.5	*23.5*
2000	3.5	3.5	7.7	3.5	2.5	*20.7*
2001	3.6	3.2	9.0	7.7	3.6	*27.1*
2002	4.7	5.2	10.1	7.7	1.4	*29.1*
2003	3.5	2.4	6.6	7.7	4.7	*24.9*
2004	3.6	3.2	6.8	7.7	4.5	*25.8*
2005	4.5	2.4	9.8	6.6	4.7	*28.0*
2006	1.4	6.2	12.9	7.7	3.6	*31.8*
2007	2.5	2.2	6.6	8.7	1.4	*21.4*
2008	0.3	1.3	14.4	8.7	4.7	*29.4*
2009	3.6	2.2	11.2	4.5	1.4	*22.9*
2010	1.4	2.2	6.8	7.7	5.7	*23.8*
2011	2.5	2.2	2.5	4.5	3.6	*15.3*
2012	2.5	3.8	9.4	4.5	1.4	*21.6*
2013	1.4	2.2	5.7	9.8	2.5	*21.6*
2014	1.4	1.3	5.7	6.6	6.8	*21.8*

2015	5.3	6.9	9.5	5.2	6.8	*33.7*
Average	**2.6**	**2.9**	**7.4**	**6.3**	**3.3**	**22.4**

Appendix D – Runoff Modelling

The accuracy assessment of SRM, where D_V is volume difference between measured and simulated runoff volume in percentage and R^2Nash-Sutcliffe determination coefficient

Year	$D_v, \%$	R^2
1986	1.1	0.99
1987	1.5	0.98
1988	2.8	0.89
1989	2.6	0.91
1990	1.4	0.98
1991	1.0	0.99
1992	1.9	0.94
1993	0.3	1
1994	1.1	0.98
1995	0.9	0.99
1996	2.0	0.95
1997	1.3	0.98
1998	2.4	0.92
1999	0.8	0.99
2000	2.0	0.95
2001	1.2	0.98
2002	1.2	0.98
2003	1.2	0.98
2004	1.3	0.98
2005	0.8	0.99
2006	0.5	1
2007	0.7	0.99
2008	0.7	0.99
2009	1.2	0.98
2010	1.1	0.96
2011	1.3	0.97
2012	1.5	0.97
2013	0.4	1
2014	1.8	0.96

2015	1.5	0.97
2016	1.3	0.98
Average	**1.3**	**0.97**

Appendix E – Groundwater modelling

Groundwater flux (i)

Groundwater flux (i) by measured water levels model parameters and results,

where $V_{b.m}$ is water volume at the beginning of the cold month season estimated by measured water levels; $V_{e.m}$ is water volume at the end of the cold month season estimated by measured water levels; $G_i - G_o$is estimated groundwater flux by the equation 4.6.1

Year	***Month***	$V_{b.m}$, **10^6 m^3**	$V_{e.m}$, **10^6 m^3**	$G_i - G_o$, **10^6 m^3**
1986				***-0.1***
	January	231.8	231.9	0.2
	February	231.9	232.1	0.2
	March	232.1	232.1	0
	November	228.6	228.4	-0.2
	December	228.4	228.1	-0.3
1987				***-0.3***
	January	228.1	228.1	0
	February	228.1	228.1	0
	March	228.1	228.1	0
	November	226.1	226.1	0
	December	226.1	225.8	-0.3
1991				***0.7***
	January	211.45	211.8	0.35
	February	211.8	211.8	0
	March	211.8	212.1	0.3
	November	204.6	204.6	0
	December	204.6	204.6	0
1992				***-0.5***
	January	204.6	204.3	-0.3
	February	204.3	204	-0.3
	March	204	203.9	-0.1
	November	200.0	200.0	0
	December	200.0	200.2	0.2
1993				***-0.6***

	January	200.2	200.2	0
	February	200.2	200.0	-0.2
	March	200.0	200.0	0
	November	202.6	202.3	-0.3
	December	202.3	202.3	0
1994				***0.3***
	January	202.4	202.1	-0.3
	February	202.1	202.1	0
	March	202.1	202.1	0
	November	202.5	202.5	0
	December	202.5	203.2	0.7
1995				***0***
	January	203.2	203.2	0
	February	203.2	203.2	0
	March	203.2	203.2	0
	November	197.3	197.3	0
	December	197.3	197.3	0
1996				***0.2***
	January	197.3	197.5	0.2
	February	197.5	197.5	0
	March	197.5	197.5	0
	November	195.1	195.1	0
	December	195.1	195.1	0
1997				***-1.2***
	January	197.5	197.5	0
	February	197.5	197.5	0
	March	197.5	197.5	0
	November	188.4	187.2	-1.2
	December	187.2	187.2	0
1998				***0***
	January	187.2	187.2	0
	February	187.2	187.2	0
	March	187.2	187.2	0
2003				***-0.2***

	January	189.2	189.2	0
	February	189.2	189.0	-0.2
	March	189.0	189.0	0
	November	185.5	185.0	-0.5
	December	185.0	185.4	0.5
2004				***-1.0***
	January	185.4	185.2	-0.2
	February	185.2	185.2	0
	March	185.2	185.2	0
	November	179.8	179.0	-0.8
	December	179.0	179.0	0
2005				***1.0***
	January	179.0	179.3	0.3
	February	179.3	179.5	0.2
	March	179.5	179.5	0
	November	181.7	181.7	0
	December	181.7	182.2	0.5
2006				***1.1***
	January	182.2	182.9	0.7
	February	182.9	183.1	0.2
	March	183.1	183.3	0.2
	November	182	182	0
	December	182	182	0
2007				***-1.6***
	January	182	182.2	0.2
	February	182.2	182.7	0.5
	October	183.6	182.8	-0.8
	November	182.8	182	-0.8
	December	182	181.3	-0.7
2008				***-0.8***
	January	181.3	181.3	0
	February	181.3	181.6	0
	March	181.6	181.6	0
	November	178.8	178.3	-0.5

	December	178.3	178	-0.3
2009				***0.3***
	January	178	178	0
	February	178	178.3	0.3
	March	178.3	178.3	0
	November	176.8	176.6	-0.2
	December	176.6	176.8	0.2
2010				***2.1***
	January	176.8	176.3	0.5
	February	176.3	177.2	0.9
	March	177.2	177.7	0.5
	December	172.1	172.3	0.2
2011				***1.0***
	January	172.3	172.6	0.3
	February	172.6	172.8	0.2
	March	172.8	173.1	0.3
	November	171.6	171.6	0
	December	171.6	171.8	0.2
2012				***1.0***
	January	171.8	171.8	0
	February	171.8	172	0.2
	March	172	172	0
	November	167.6	167.6	0
	December	167.6	168.4	0.8
2013				***1.6***
	January	168.4	168.7	0.3
	February	168.7	169	0.3
	March	169	169.7	0.7
	December	171.4	171.7	0.3
2014				***0.8***
	January	171.7	172.2	0.5
	February	172.2	172.7	0.5
	March	172.7	173	0.3
	October	173.1	172.1	-1.0

	November	172.1	172.3	0.2
	December	172.3	172.6	0.3
2015				***1.3***
	January	172.6	173.1	0.5
	February	173.1	173.4	0.3
	March	173.4	173.7	0.3
	November	172.4	172.1	-0.3
	December	172.1	172.6	0.5
2016				***2.0***
	January	172.6	173.1	0.5
	February	173.1	173.4	0.3
	March	173.4	173.6	0.2
	November	173.9	174.2	0.3
	December	174.2	172.9	0.7
Average				***+0.29***

Groundwater flux (ii)

Groundwater model (ii) or water balance approach parameters and estimated groundwater flux,

where V_{begin} is the water volume of the lake estimated by measured water levels at the beginning of the year; V_{end} water volume estimated by measured lake level at the end of the year; I-O is the difference between input and output variables based on equation 4.1; $G_i - G_o$ estimated by equation 4.6.

Year	V_{begin}, $10^6 m^3$	V_{end}, $10^6 m^3$	$V_{begin} - V_{end}$, $10^6 m^3$	**I-O,** $10^6 m^3$	$G_i - G_o$, $10^6 m^3$
1986	231.6	228.3	-4.5	-3.4	-0.1
1987	228.3	226.0	-2.3	-2.3	0.1
1991	211.4	204.6	-6.8	-6.8	1.0
1992	204.6	200.2	-4.5	-4.5	0.2
1993	200.2	202.0	1.8	1.8	-0.6
1994	202.0	202.8	0.8	0.8	-1.1
1995	202.8	197.4	-5.4	-5.1	-0.6
1996	197.4	195.4	-2	1.5	-0.3
1997	195.4	188.7	-6.7	-6.7	-1.0
2003	189.2	185.5	-3.7	-3.7	0.3
2004	185.5	180.1	-5.4	-5.4	-1.0
2005	180.1	182.2	2.0	2.0	1.5
2006	182.2	182.0	-0.2	-0.2	1.5
2007	182.0	182.7	0.7	0.7	-1.5
2008	182.7	178.0	-4.7	-4.7	-1.4
2009	178.0	177.1	-0.9	-0.9	-1.2
2010	177.1	172.1	-5.1	-5.1	2.3
2011	172.1	171.6	-0.5	-0.5	1.4
2012	171.6	168.3	3.3	-3.3	1.5
2013	168.3	171.6	3.3	3.3	0.1
2014	171.6	173.1	1.5	1.5	1.2

2015	173.1	172.6	-0.5	-0.5	1.4
2016	172.6	174.9	1.9	1.9	3.3
Average					**+0.*16***

Appendix F - Interannual changes in net flux

Year-by-year annual relative contribution of water balance variables of Shortandy Lake from 1986 to 2016, where input variables are: warm-season months precipitation (P_{rain}), cold-season months precipitation (P_{snow}), snowmelt runoff (Q_{snow}), rainfall-runoff (Q_{rain}); output variables are: warm-season open lake evaporation (E_o), cold-season lake sublimation (E_o), water abstraction (W_{abs}) actual evapotranspiration from the lake catchment (E_{act}) ; and groundwater flux $G_i - G_o$

Relative contribution of input and output variables of Shortandy lake in 1986

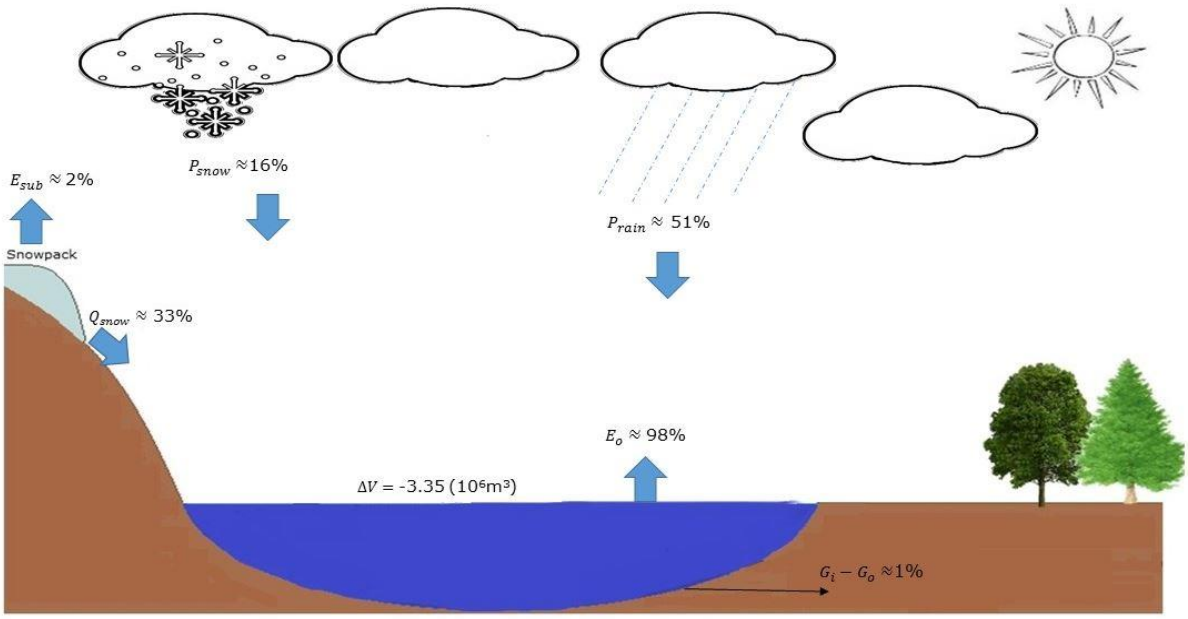

Relative contribution of input and output variables of Shortandy lake in 1987

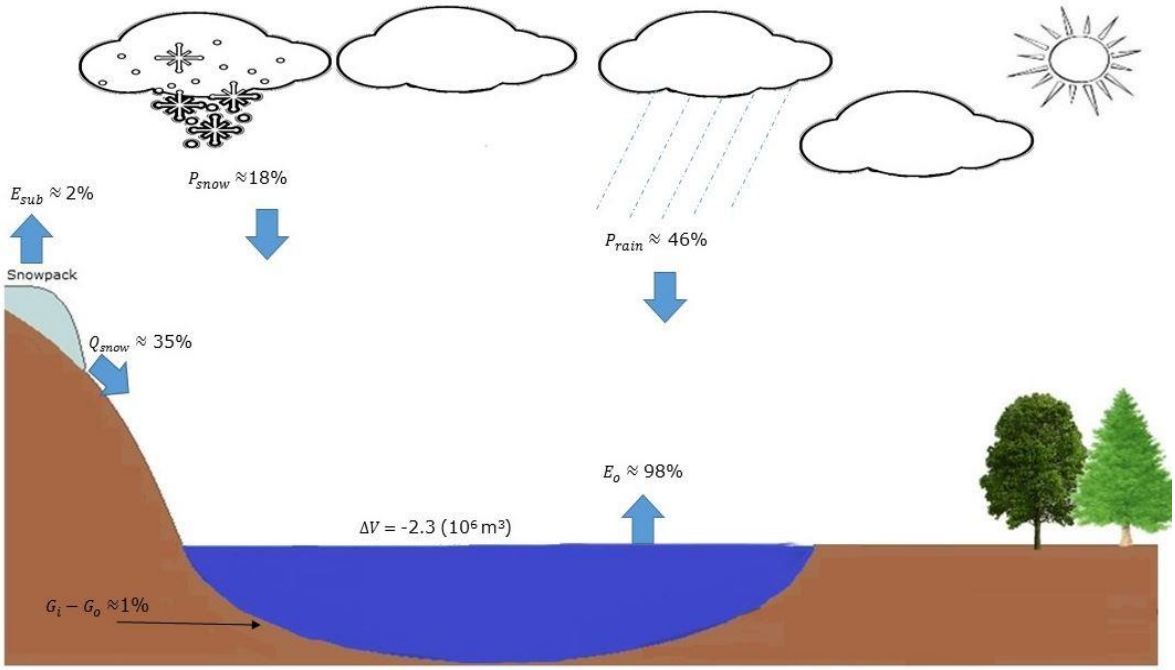

Relative contribution of input and output variables of Shortandy lake in 1988

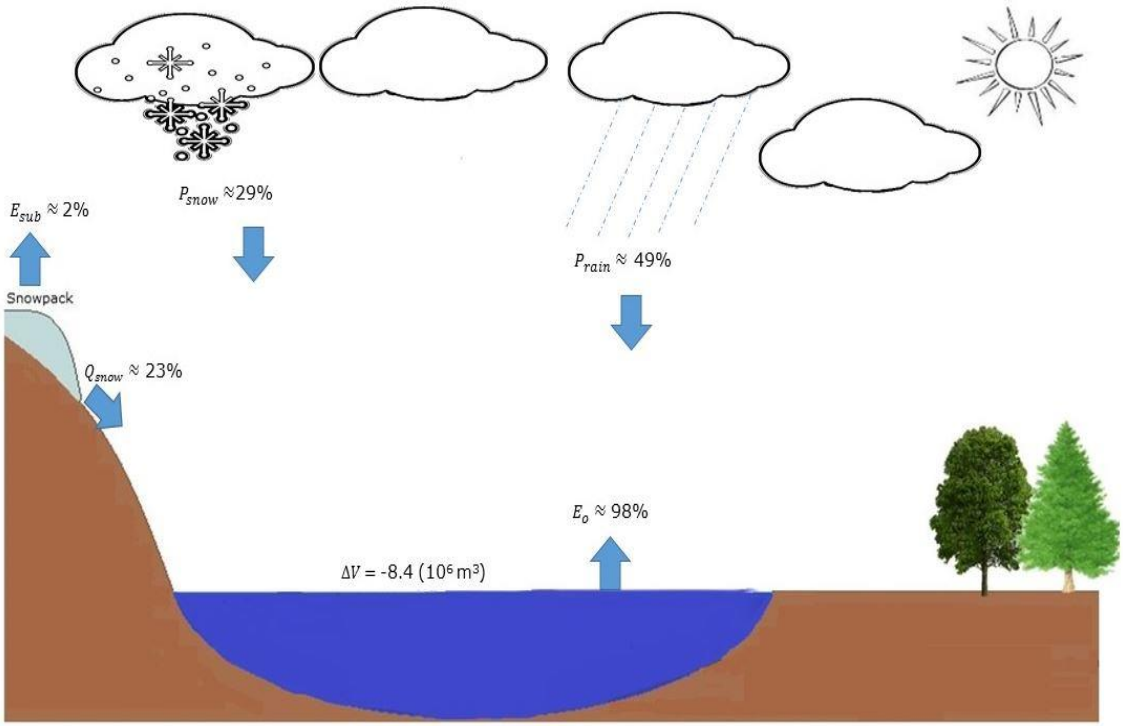

Relative contribution of input and output variables of Shortandy lake in 1989

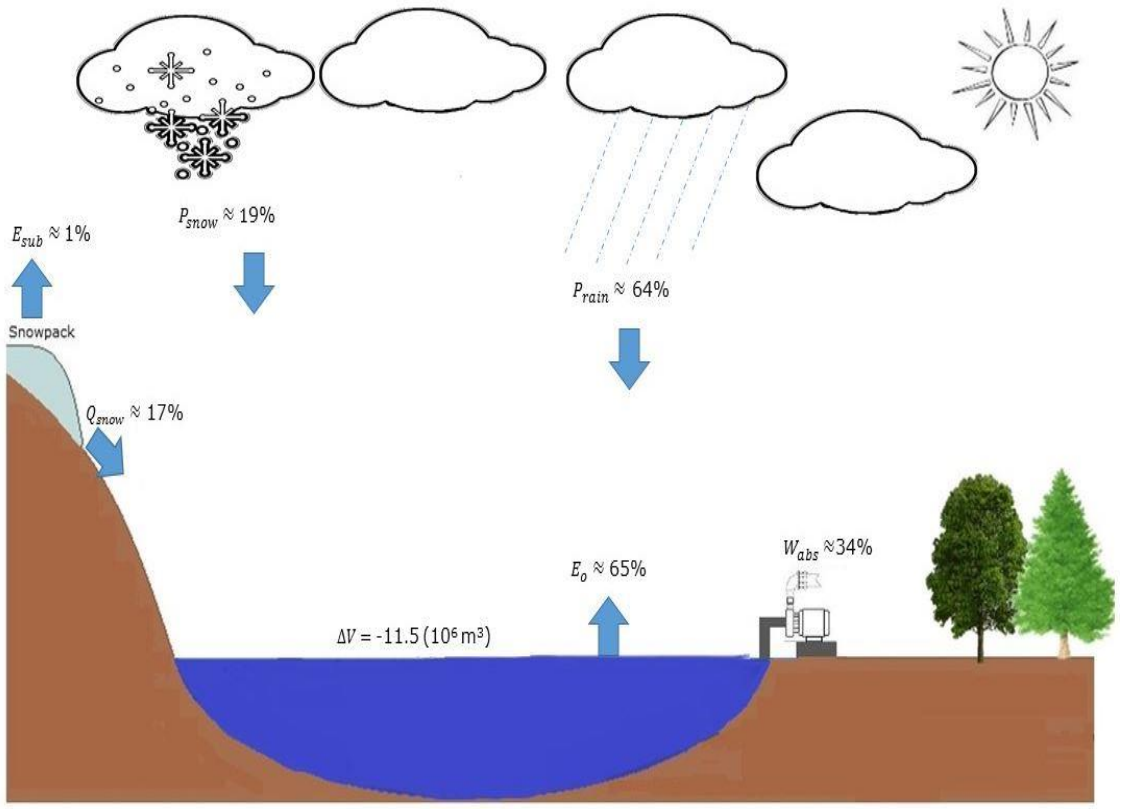

Relative contribution of input and output variables of Shortandy lake in 1990

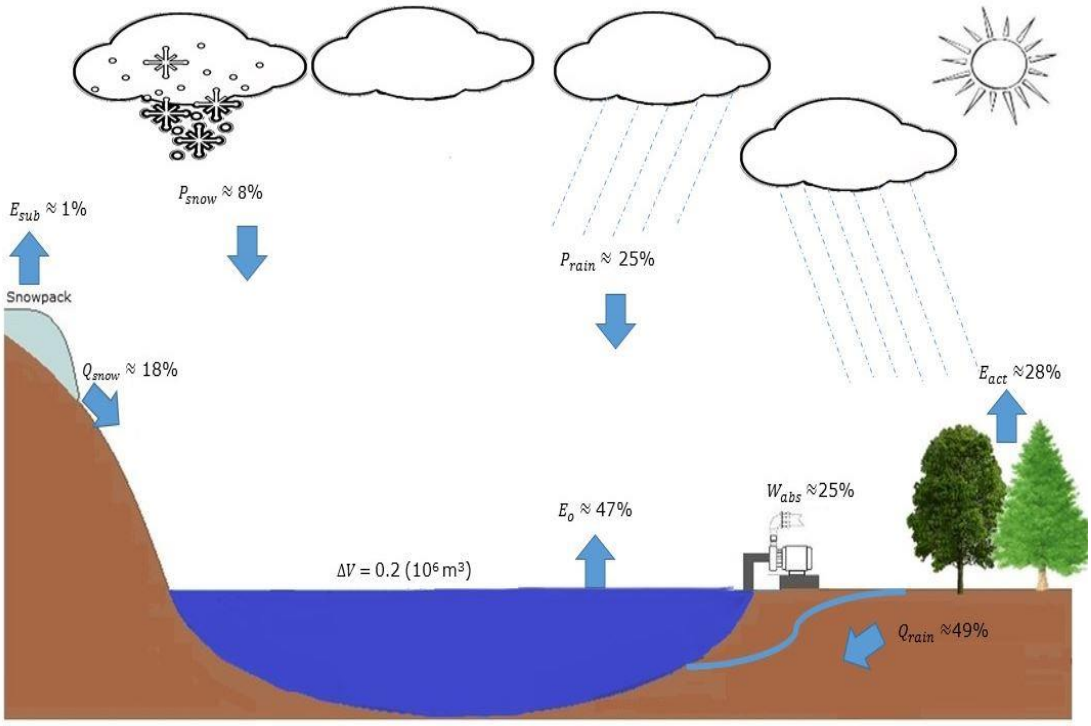

Relative contribution of input and output variables of Shortandy lake in 1991

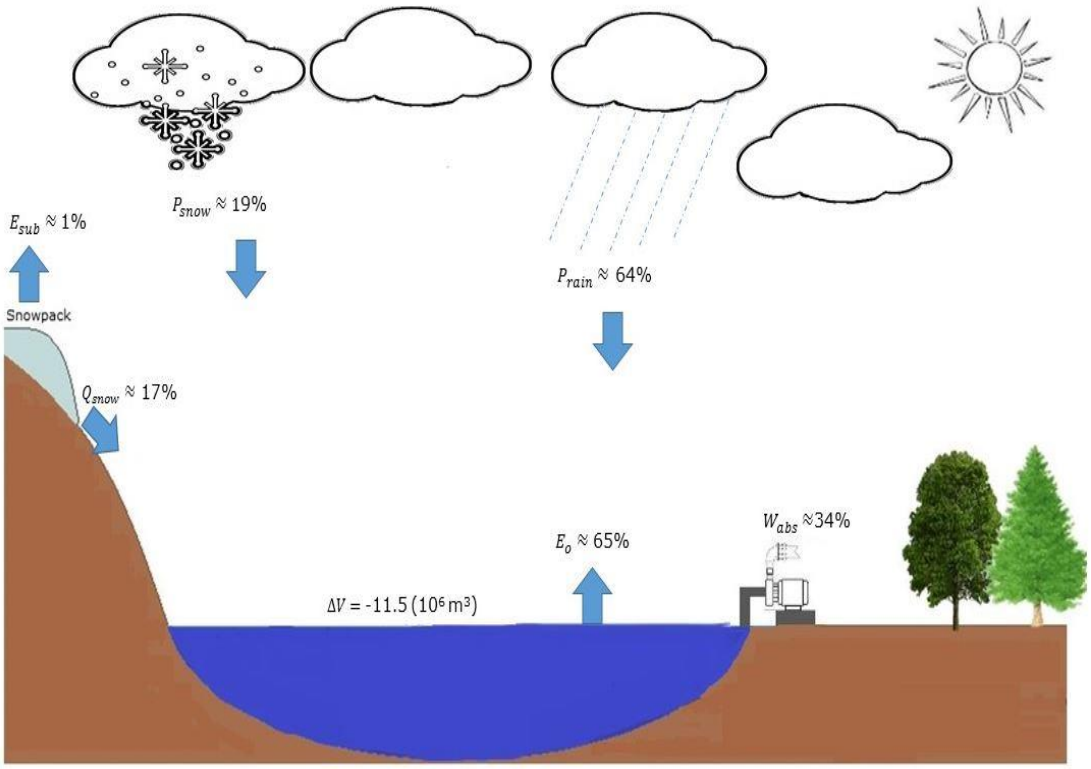

Relative contribution of input and output variables of Shortandy lake in 1992

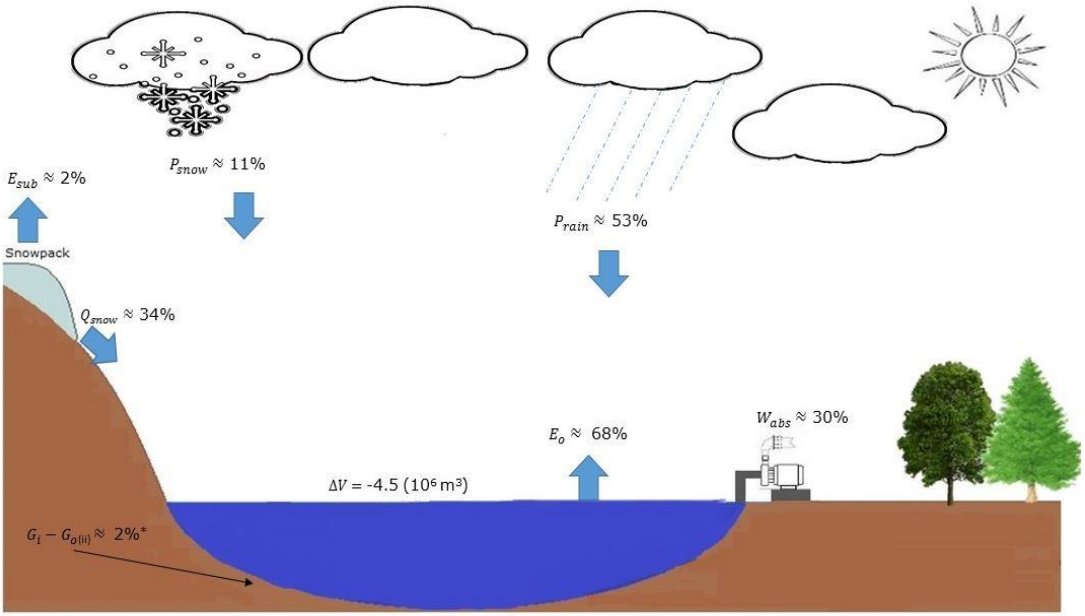

Relative contribution of input and output variables of Shortandy lake in 1993

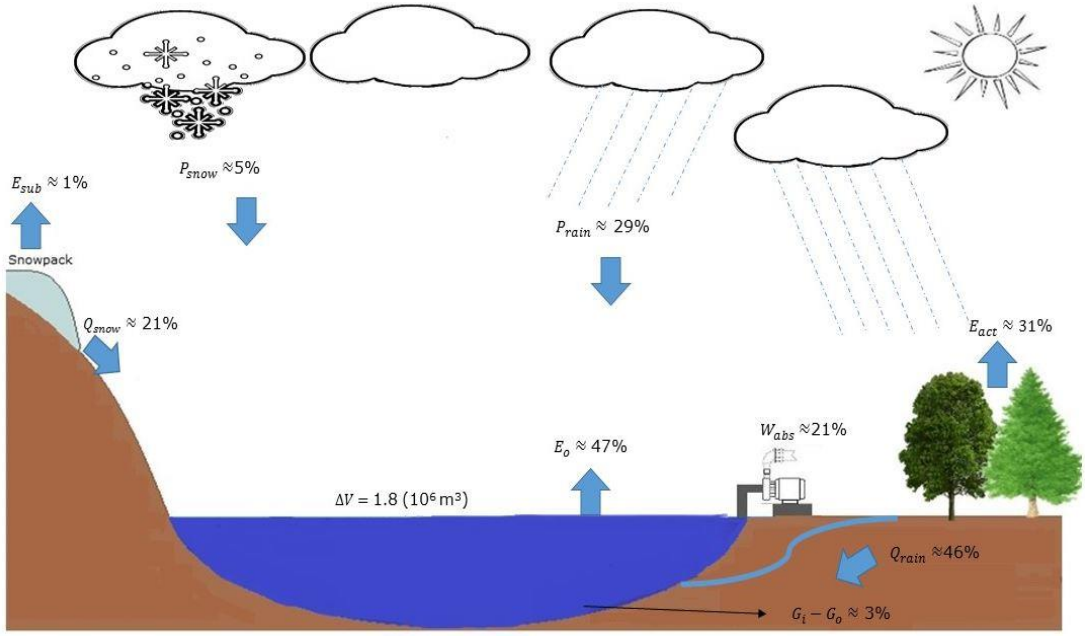

Relative contribution of input and output variables of Shortandy lake in 1994

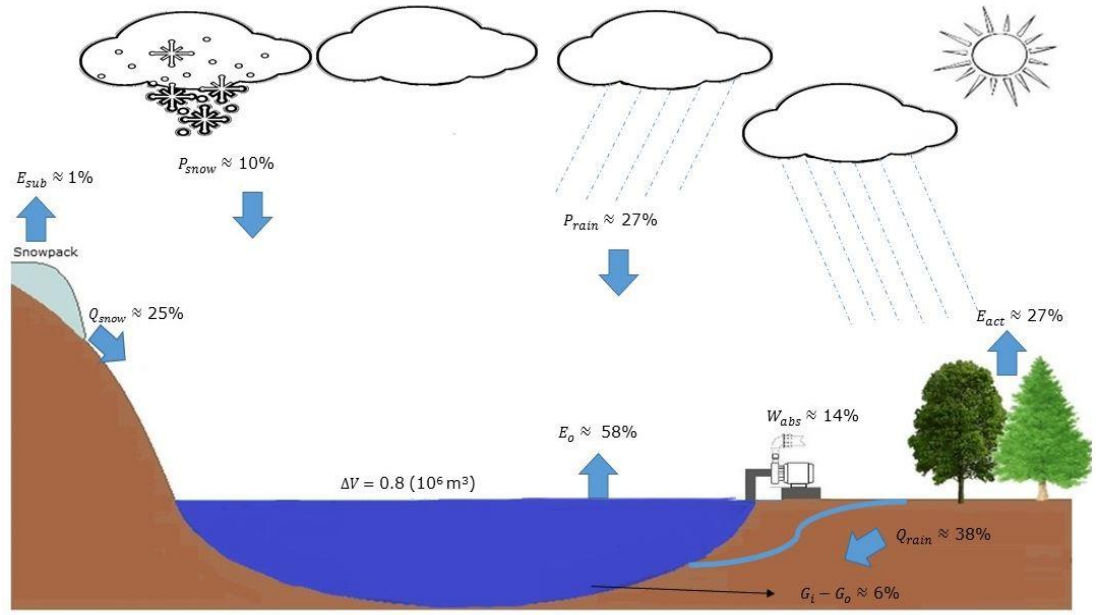

Relative contribution of input and output variables of Shortandy lake in 1995

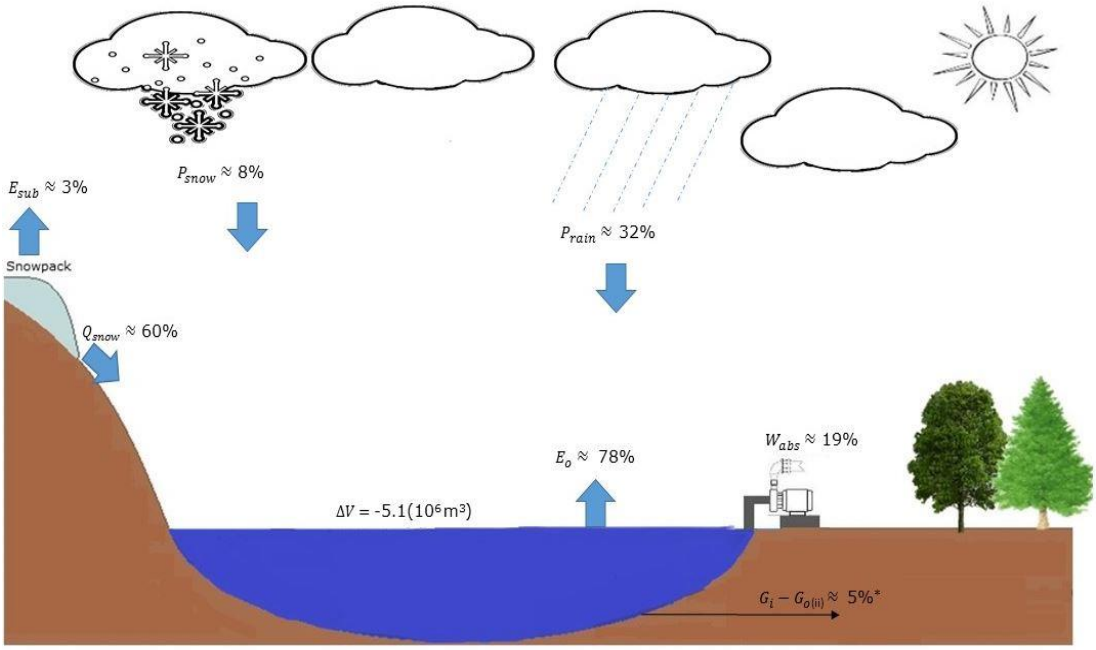

Relative contribution of input and output variables of Shortandy lake in 1996

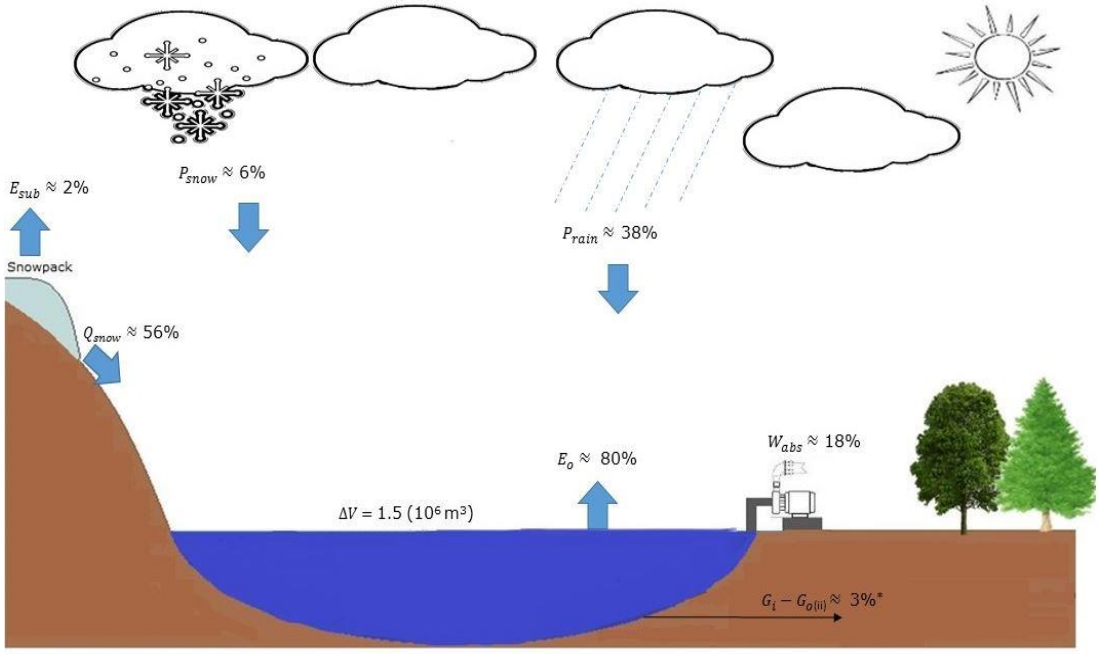

Relative contribution of input and output variables of Shortandy lake in 1997

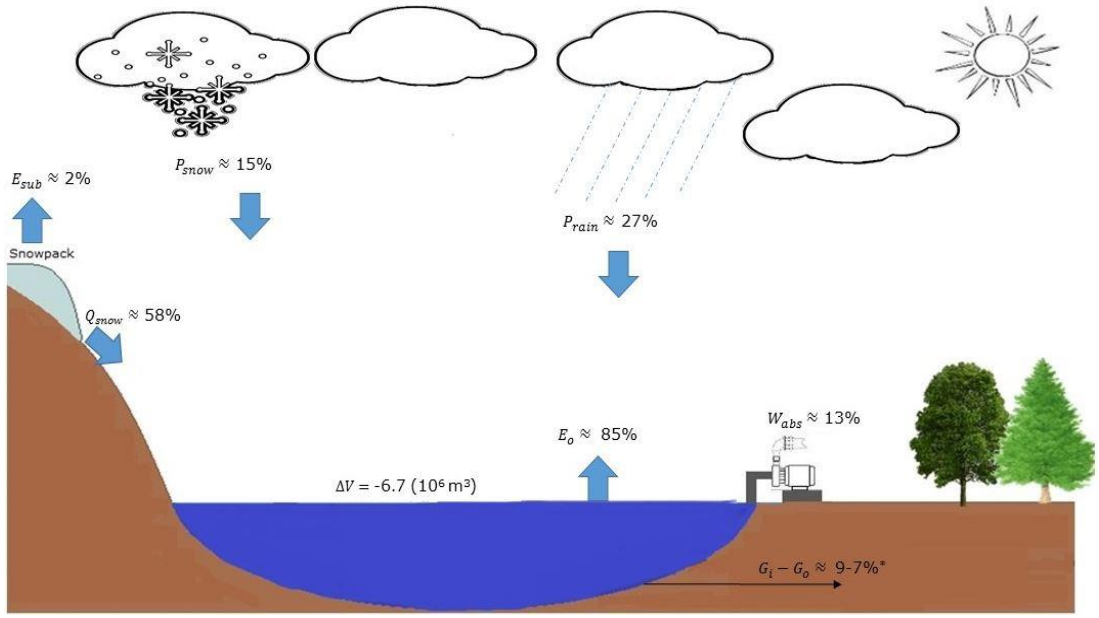

Relative contribution of input and output variables of Shortandy lake in 1998

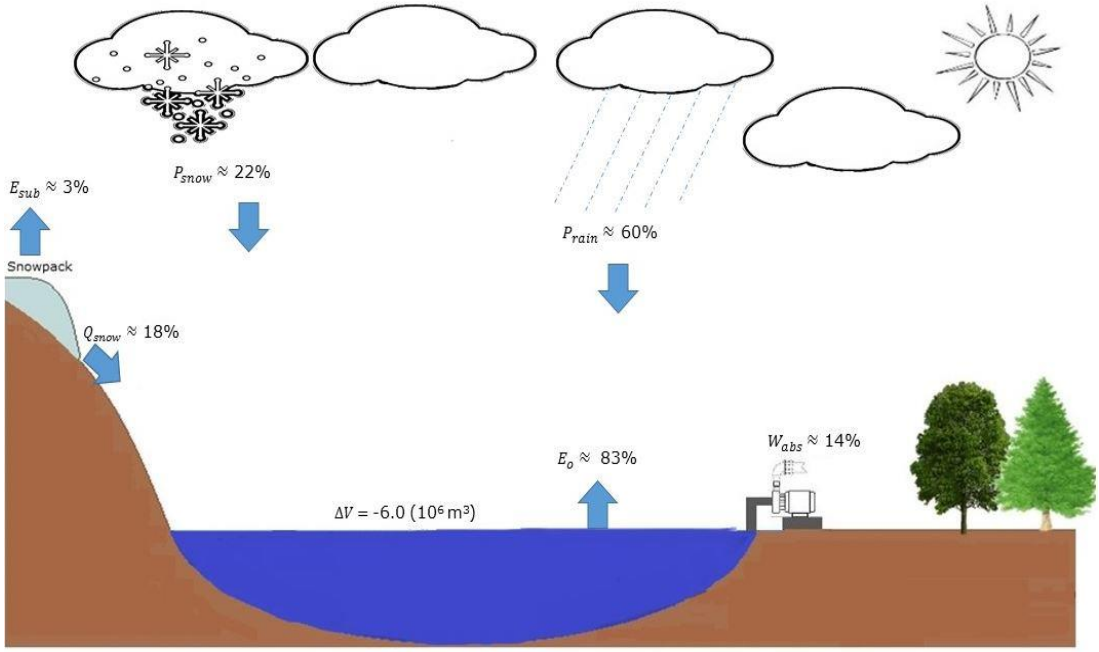

Relative contribution of input and output variables of Shortandy lake in 1999

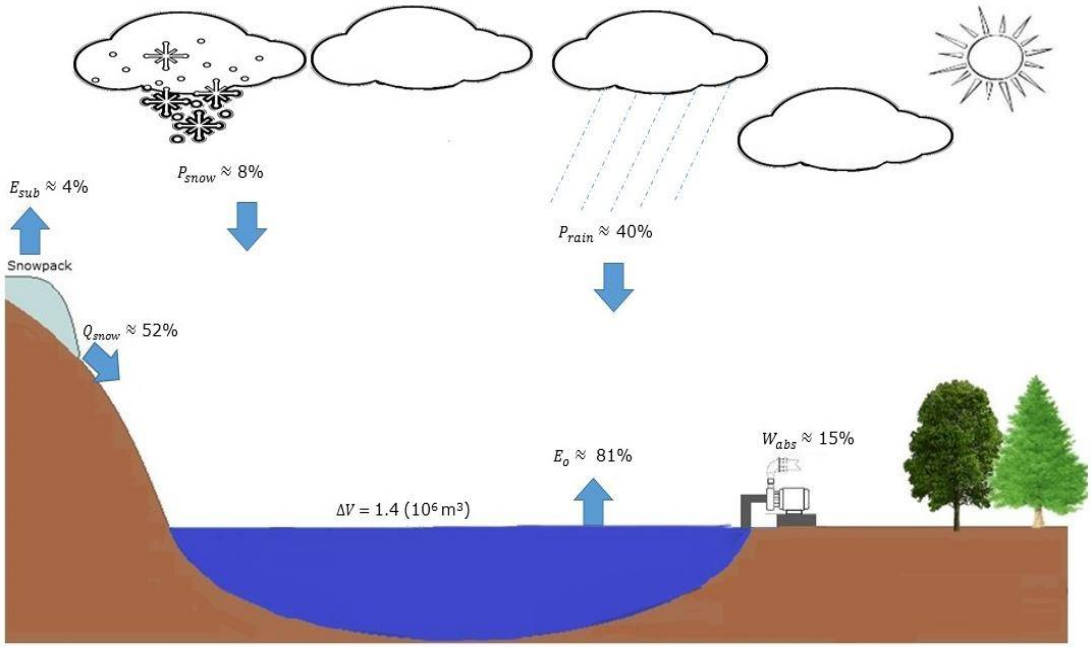

Relative contribution of input and output variables of Shortandy lake in 2000

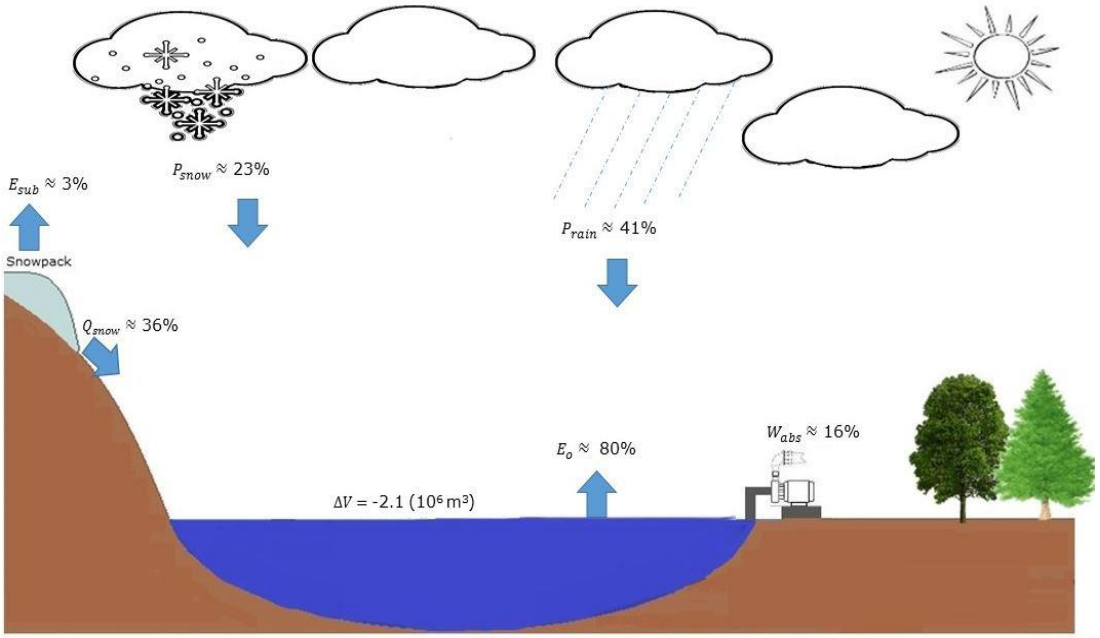

Relative contribution of input and output variables of Shortandy lake in 2001

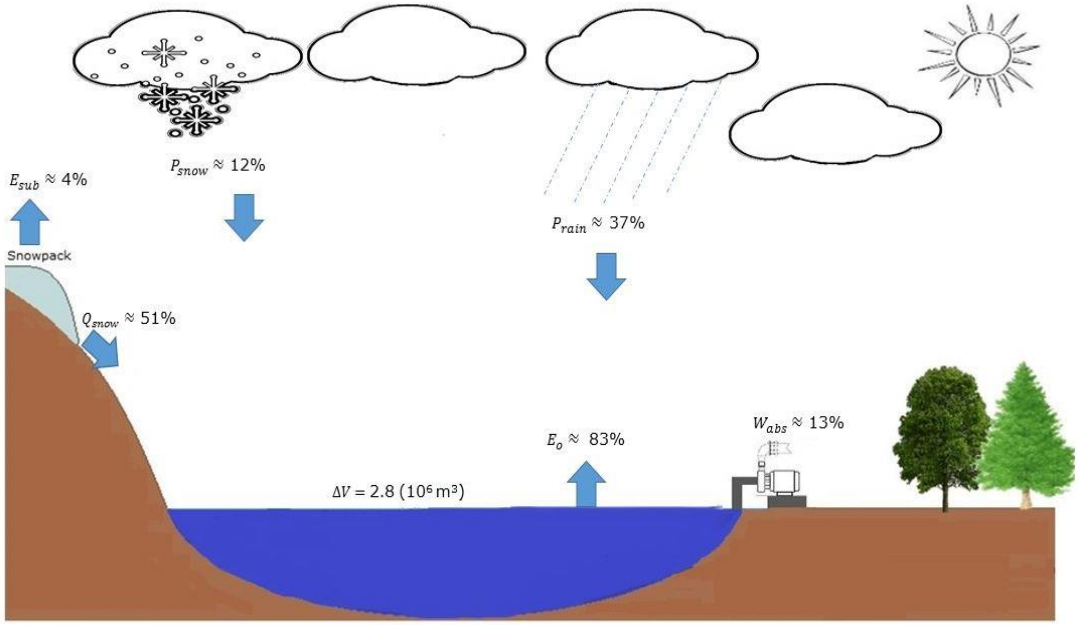

Relative contribution of input and output variables of Shortandy lake in 2002

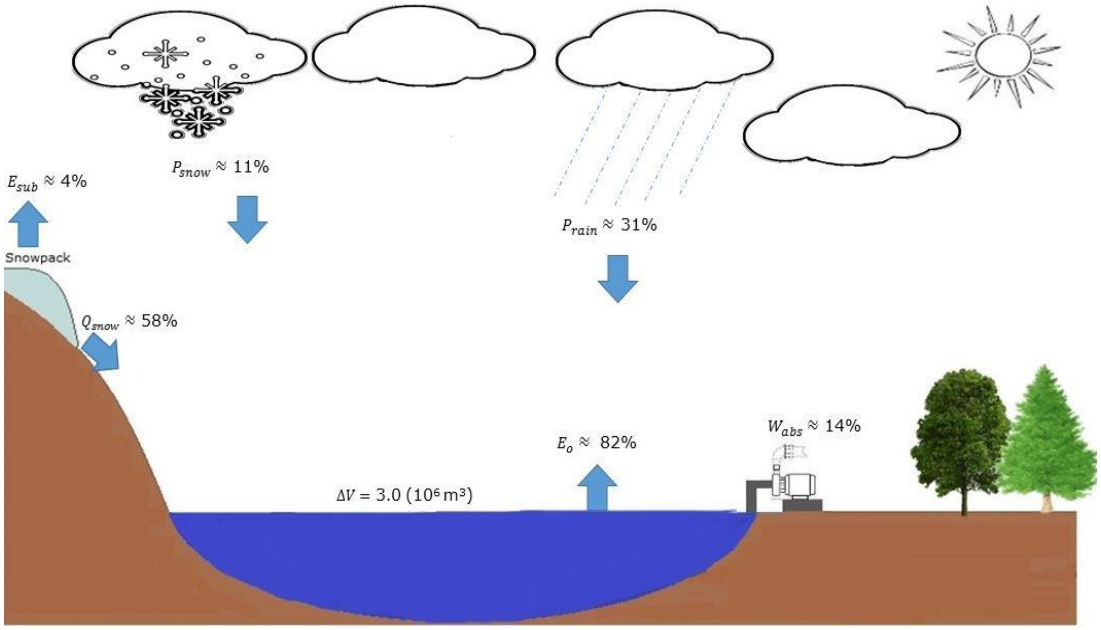

Relative contribution of input and output variables of Shortandy lake in 2003

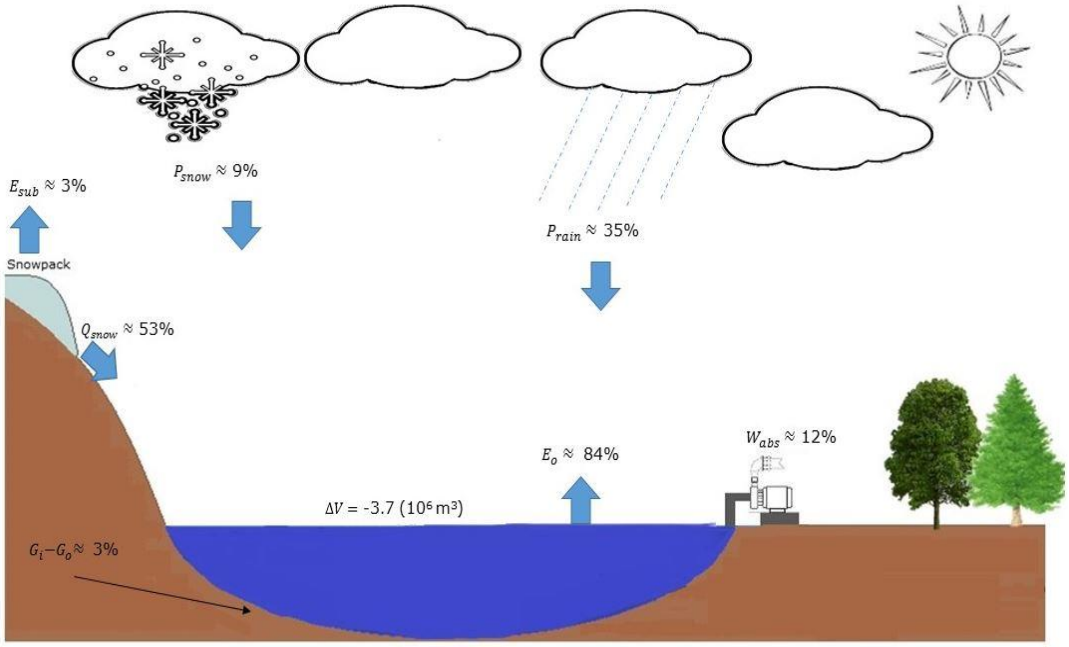

Relative contribution of input and output variables of Shortandy lake in 2004

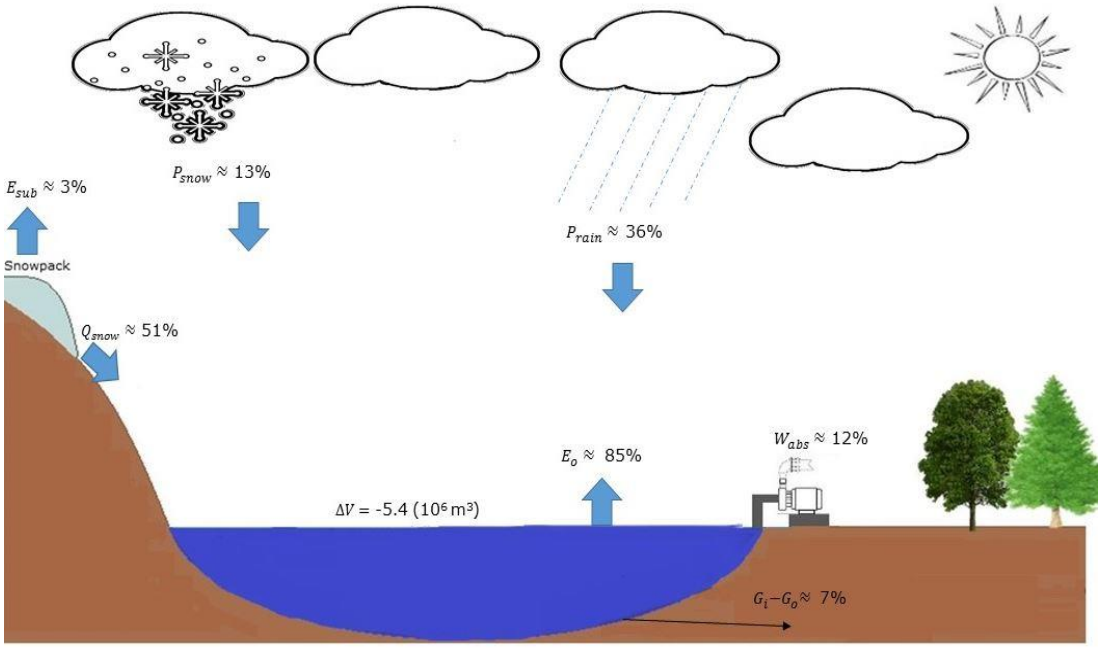

Relative contribution of input and output variables of Shortandy lake in 2005

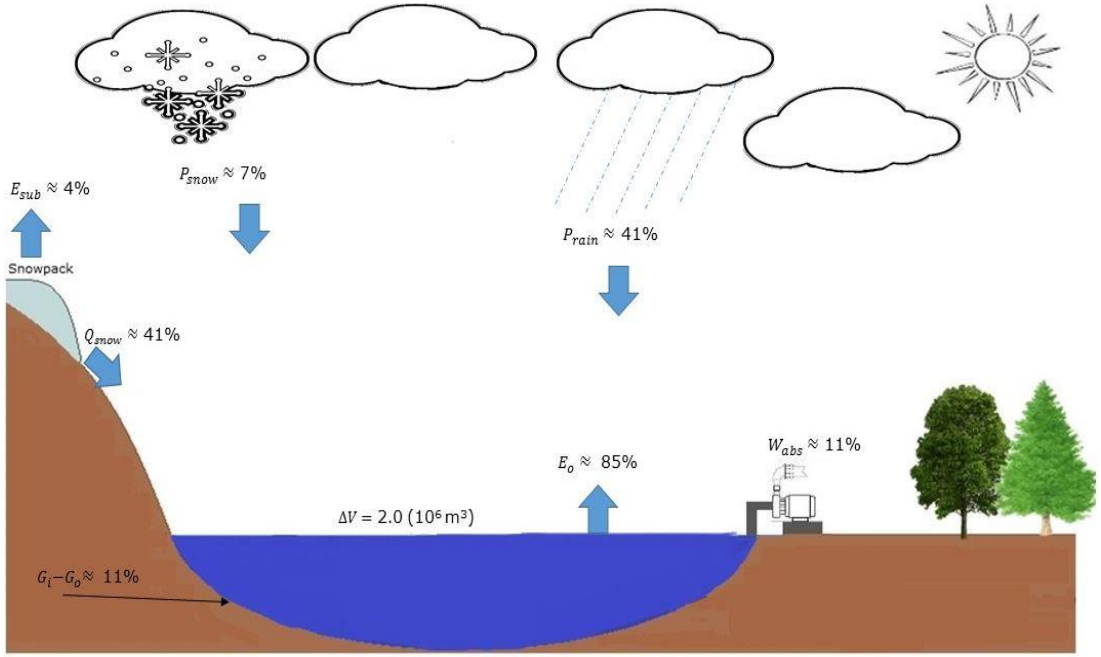

Relative contribution of input and output variables of Shortandy lake in 2006

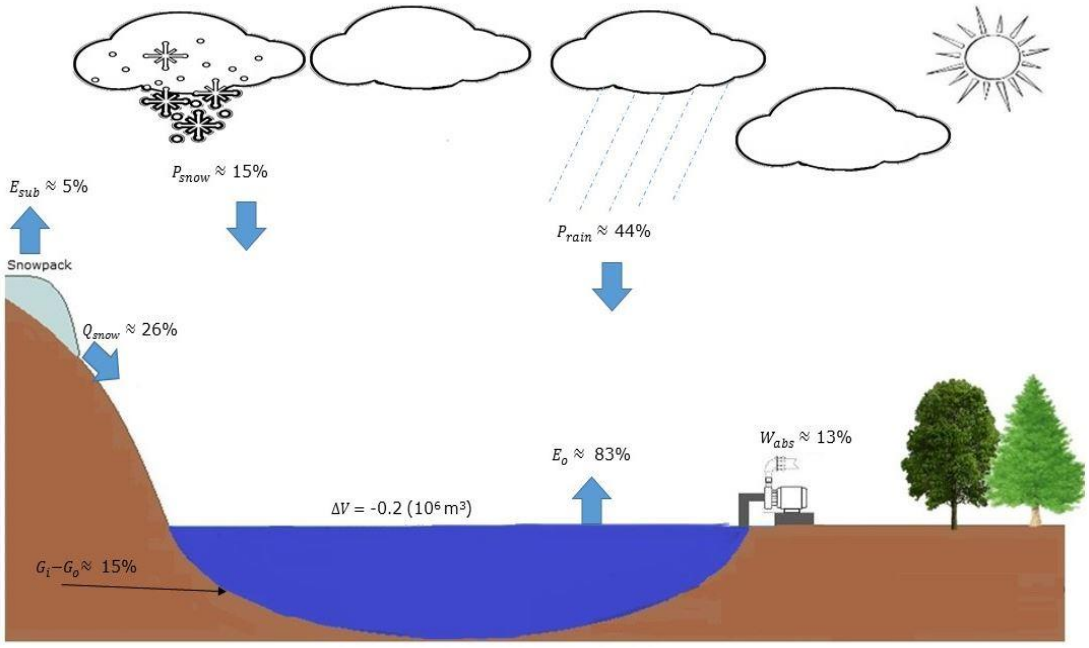

Relative contribution of input and output variables of Shortandy lake in 2007

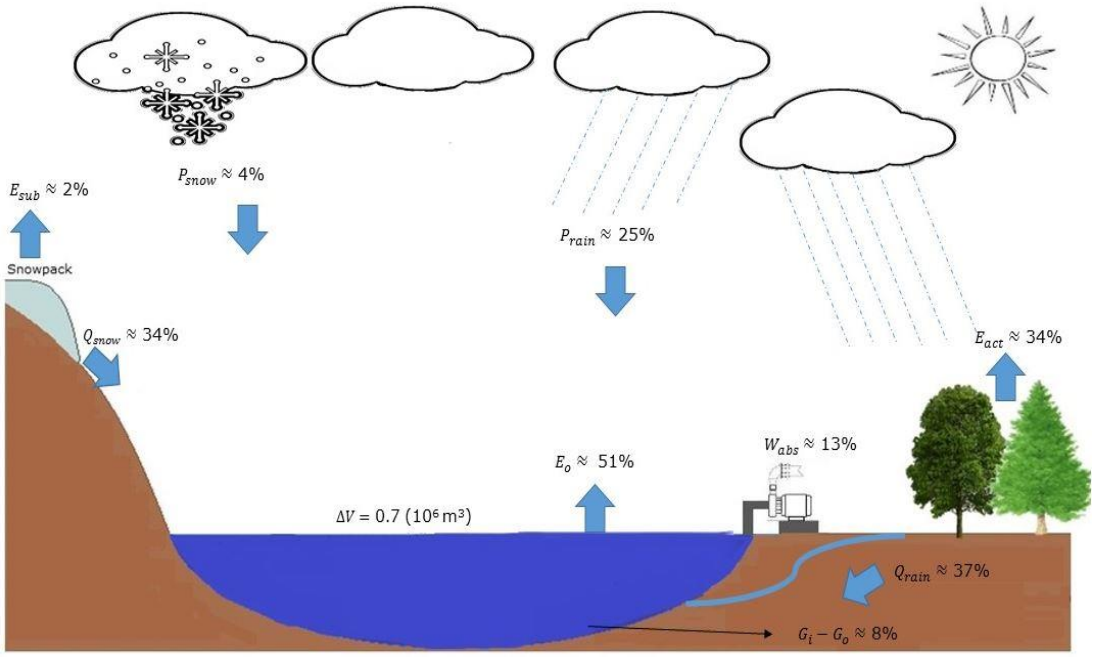

Relative contribution of input and output variables of Shortandy lake in 2008

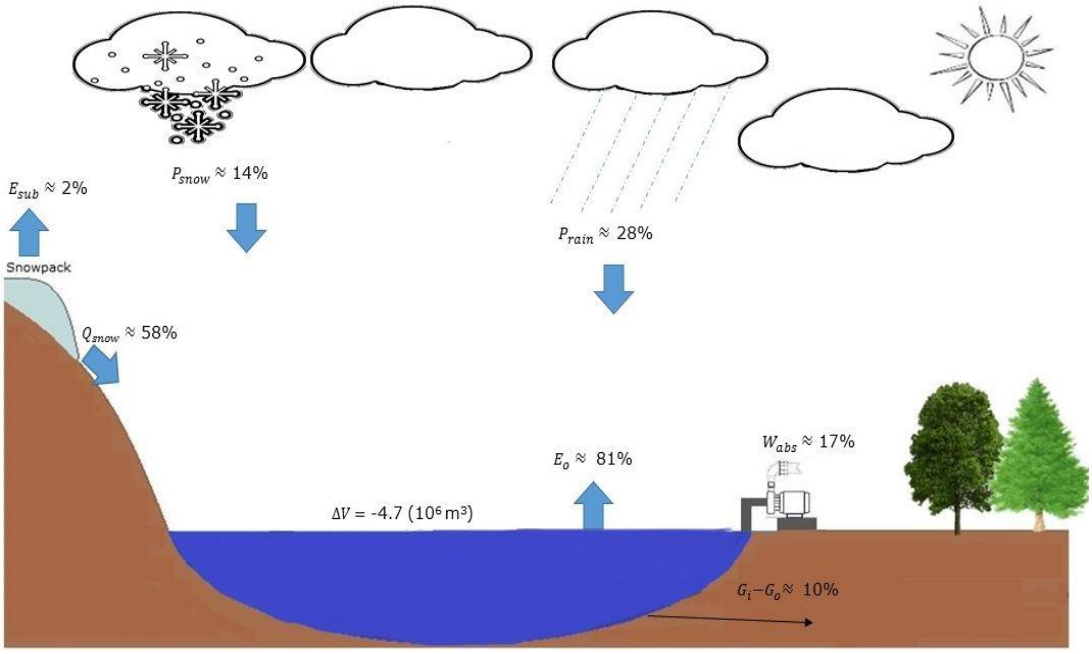

Relative contribution of input and output variables of Shortandy lake in 2009

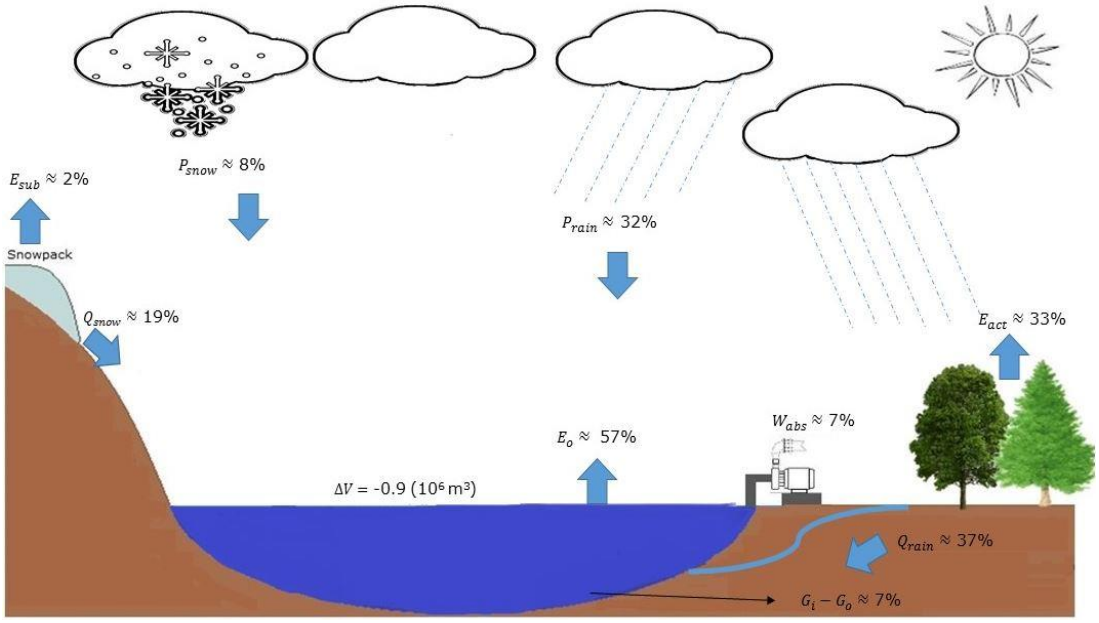

Relative contribution of input and output variables of Shortandy lake in 2010

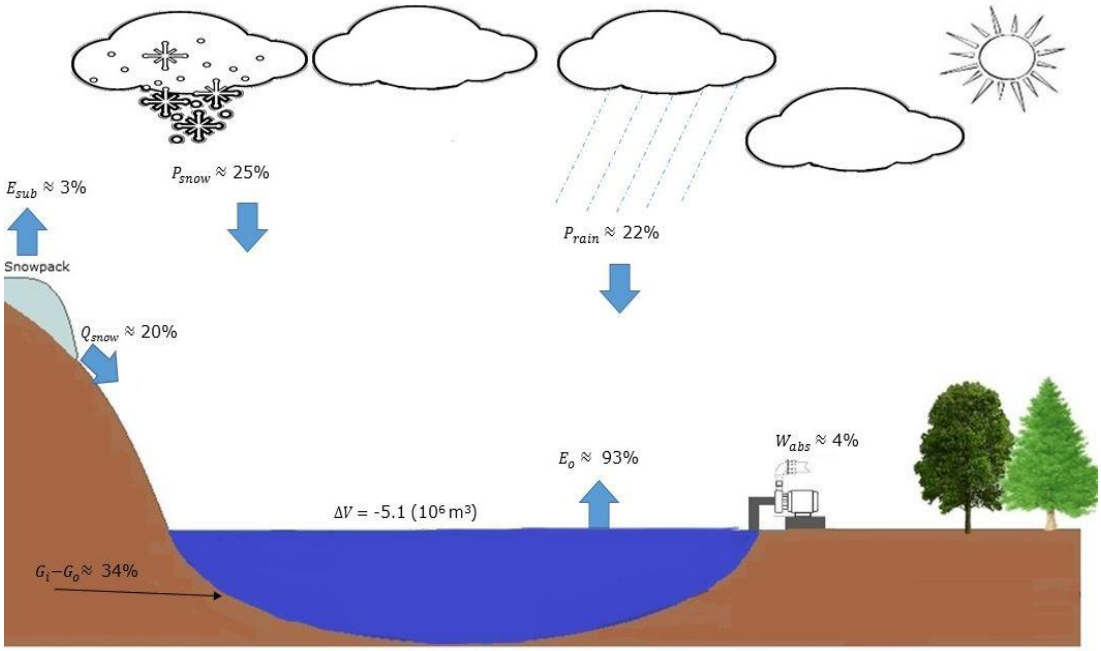

Relative contribution of input and output variables of Shortandy lake in 2011

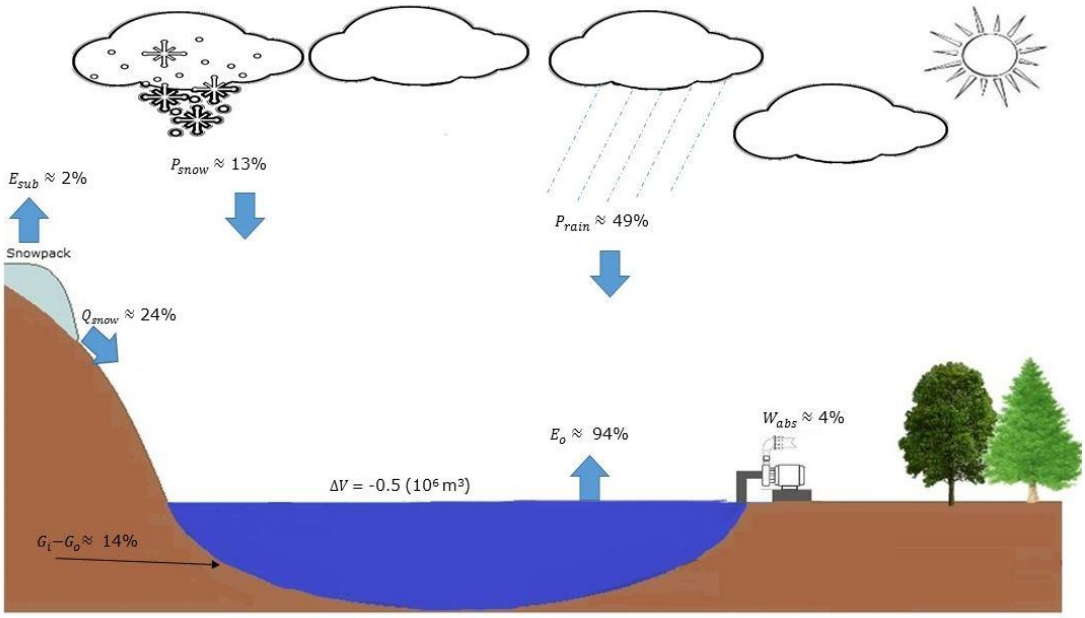

Relative contribution of input and output variables of Shortandy lake in 2012

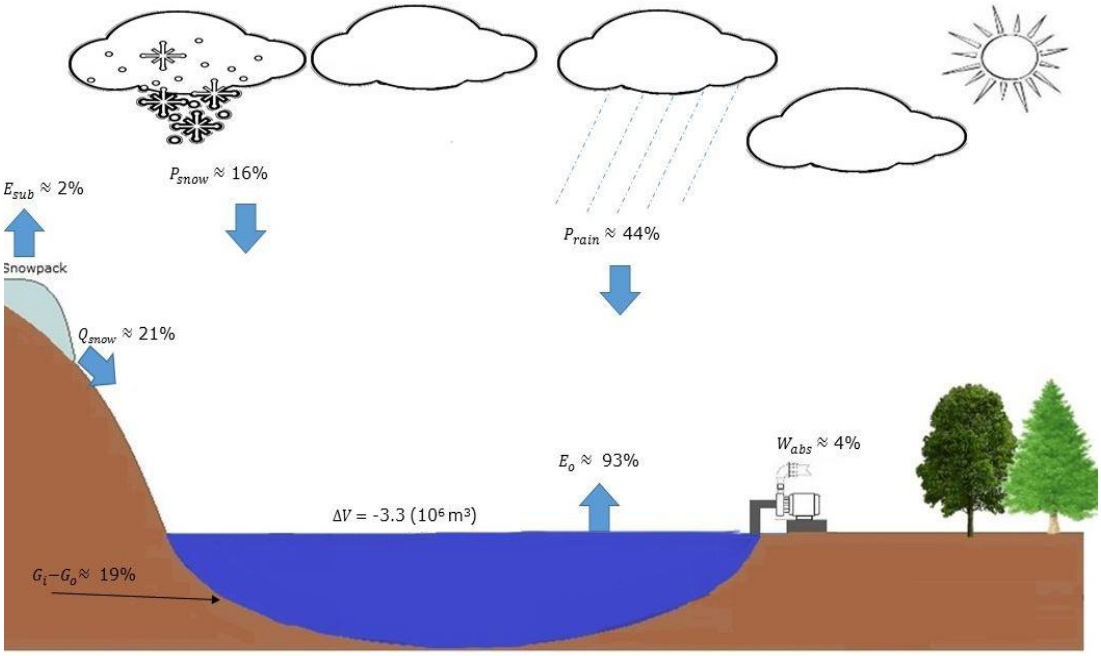

Relative contribution of input and output variables of Shortandy lake in 2013

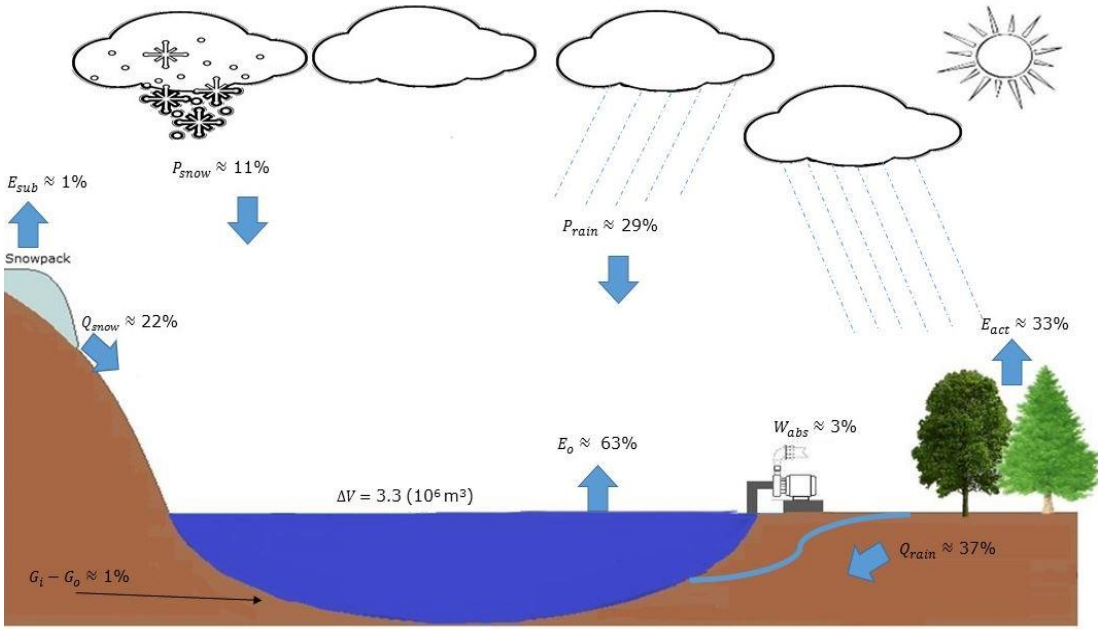

Relative contribution of input and output variables of Shortandy lake in 2014

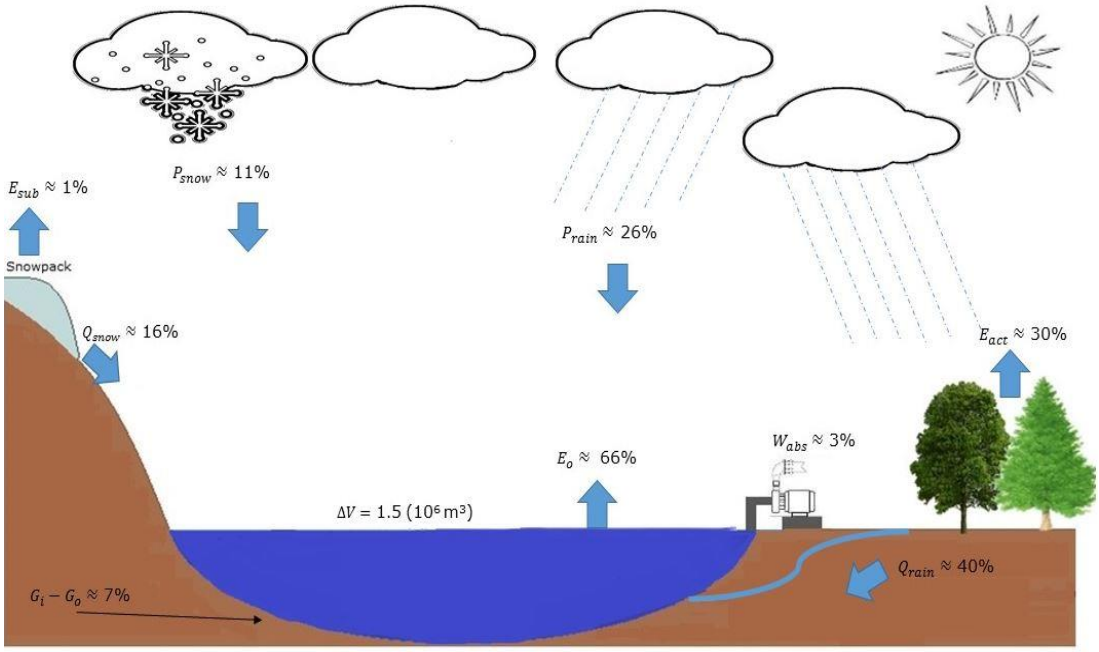

Relative contribution of input and output variables of Shortandy lake in 2015

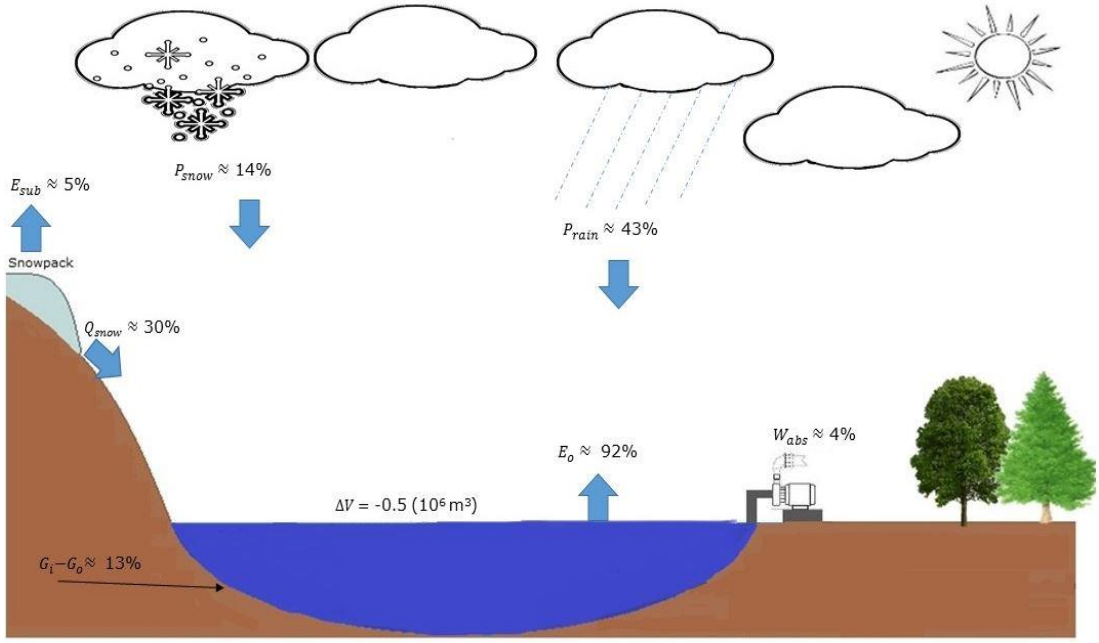

Relative contribution of input and output variables of Shortandy lake in 2016

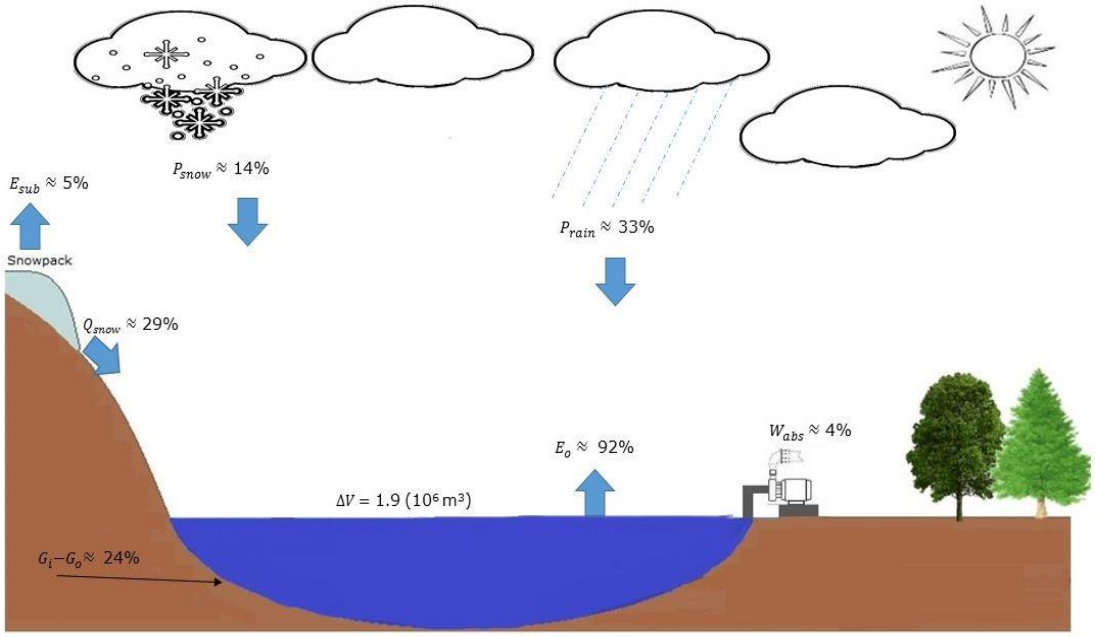

Appendix G – Future Climate Modelling

Hydrological periods in Shortandy based on future climate projections with the averages of water balance variables during those periods

RCP 2.6GFDL						
Hydrological period	P_{sum},mm	P_{snow}, mm	P_{rain}, mm	R_{snow},mm	R_{rain},mm	E_o, mm
dry	1979-1999					
	345	127	218	221	96	649
wet	2001-2007					
	452	147	306	229	208	591
dry	2008-2023					
	409	150	259	159	210	677
dry	2025-2061					
	432	157	275	180	252	718
wet	2061-2067					
	534	176	357	160	334	631
dry	2068-2090					
	446	151	295	180	272	707
wet	2091-2099					
	528	154	374	114	569	662
RCP6.0 GFDL						
dry	1979-1999					
	345	127	218	221	37	668
wet	2001-2007					
	474	147	147	222	255	593
dry	2008-2044					
	413	140	273	158	241	697
wet	2045-2048					
	529	137	392	120	928	635
dry	2051-2064					
	438	134	304	117	303	665
wet	2065-2082					
	487	145	333	89	362	696
dry	2083-2099					
	462	144	318	57	252	721
RCP2.6 IPSL						
dry	1971-1979					
	308	119	189	246	27	616
wet	1980-1985					
	480	145	335	312	287	517
dry	1986-2044					
	400	135	265	154	126	699
stable	2045-2068					

	447	144	302	201	270	741
dry	2069-2090					
	399	147	253	273	555	801
wet	2091-2099					
	485	154	331	430	363	742
RCP6.0 IPSL						
dry	1971-1979					
	308	119	189	246	27	616
wet	1980-1986					
	480	145	335	312	287	517
dry	1986-2040					
	378	128	250	163	127	705
wet	2041-2047					
	498	151	347	336	586	745
dry	2048-2099					
	403	139	264	274	394	817